

OPG's DEEP GEOLOGIC

# REPOSITORY

FOR LOW & INTERMEDIATE LEVEL WASTE

## Geosynthesis

March 2011

Prepared by: Nuclear Waste Management Organization

NWMO DGR-TR-2011-11

**nwmo**

NUCLEAR WASTE  
MANAGEMENT  
ORGANIZATION

SOCIÉTÉ DE GESTION  
DES DÉCHETS  
NUCLÉAIRES



OPG's DEEP GEOLOGIC

# **REPOSITORY**

FOR LOW & INTERMEDIATE LEVEL WASTE

## **Geosynthesis**

March 2011

Prepared by: Nuclear Waste Management Organization

NWMO DGR-TR-2011-11

**THIS PAGE HAS BEEN LEFT BLANK INTENTIONALLY**

**Document History**

<b>Title:</b>	Geosynthesis		
<b>Report Number:</b>	NWMO DGR-TR-2011-11		
<b>Revision:</b>	R000	<b>Date:</b>	March 2011
<b>Prepared by:</b>	T. Al (University of New Brunswick), R. Beauheim, R. Crowe, M. Diederichs (Queens University), R. Frizzell (AECOM Canada Ltd.), L. Kennell, T. Lam, A. Parmenter, B. Semec		
<b>Reviewed by:</b>	R.E.J. Leech (AECOM Canada Ltd.)		
<b>Approved by:</b>	M. Jensen		

**THIS PAGE HAS BEEN LEFT BLANK INTENTIONALLY**

## EXECUTIVE SUMMARY

Ontario Power Generation (OPG) is proposing the development of a Deep Geologic Repository (DGR) at the Bruce nuclear site located in the Municipality of Kincardine, Ontario for the long-term management of Low and Intermediate Level Waste (L&ILW) generated at OPG owned or operated nuclear generating facilities. The proposed DGR envisions the excavation of a repository at a depth of approximately 680 m in a limestone formation overlain by 200 m of low permeability shale. This Geosynthesis document provides an assessment of the Bruce nuclear site with respect to its geologic suitability for implementation of the DGR concept. The assessment is supported by a number of specific geoscience reports commissioned by NWMO as part of the geoscientific characterization program. In addition to these studies, this report has integrated the results of detailed site investigations of the Bruce nuclear site including drilling and borehole testing programs, laboratory analyses and geophysical surveys.

Geoscientific characterization was initiated in 2006. Since then a considerable amount of research has been conducted by the NWMO and its contractors including about 30 universities, specialized laboratories and consulting groups. The information generated from these programs is summarized in the Descriptive Geosphere Site Model (DGSM) and this report. These documents conclude that, from a geoscientific basis, the Cobourg Formation and the surrounding formations are suitable to safely host a DGR for the long-term management of L&ILW.

Seven key hypotheses that relate to geoscientific site attributes and characteristics, and are generally adopted internationally in nuclear waste programs, in some fashion, are used to demonstrate geoscientific site suitability. The scientific program developed to test these hypotheses was designed to provide regulators, the scientific community and other stakeholders with multiple lines of evidence to allow them to judge site suitability. The supporting information for the seven hypotheses follows.

### **Site Predictability: near-horizontally layered, undeformed sedimentary shale and limestone formations of large lateral extent**

- The occurrence of individual bedrock formations, facies assemblages, marker horizons, major mineralogy, and hydrocarbon and karst distributions are predictable and traceable at the site-scale.
- The thickness and orientation of bedrock formations encountered beneath the Bruce nuclear site are highly consistent. Within an area of approximately 1.5 km<sup>2</sup> enclosing the DGR footprint, information derived from the deep drilling and coring program confirms that Ordovician formation thickness variations are on the order of metres. Formation dips within the same chronostratigraphic sequence are uniformly 0.6° ( $\approx 10$  m/km) to the southwest towards the Michigan Basin.
- A 2D seismic reflection survey provided evidence for the traceable nature of the bedrock stratigraphy beneath the site. Inclined drilling and coring through interpreted sub-vertical structures showed no evidence of faulting or stratigraphic offset.
- Evidence supporting vertical fault displacement or the occurrence of steeply oriented linear and elongate hydrothermal dolomite (HTD) reservoirs within the Ordovician carbonate rocks is absent.
- Mapped faults are not known to penetrate Paleozoic sedimentary rocks younger than Ordovician age within the regional study area. This is consistent with the results of the detailed fracture mapping study, which found no evidence for complex fault structures or shear zones in the exposed bedrock proximal to the site.

**Multiple Natural Barriers: multiple low permeability bedrock formations enclose and overlie the DGR**

- The sedimentary sequence underlying the Bruce nuclear site comprises 34 near horizontally layered, laterally continuous bedrock formations. Within the Ordovician sediments that host and enclose the proposed DGR are numerous units characterized as aquicludes that possess extremely low rock mass permeabilities. The host Cobourg Formation has a very low horizontal hydraulic conductivity ( $K_H$ )  $\approx 10^{-14}$  m/s. The overlying > 200 m of Ordovician shales (3 formations) have  $K_H$  values of  $<10^{-13}$  m/s. The underlying 150 m of Ordovician carbonates (5 formations) have  $K_H$  values ranging from  $\approx 10^{-15}$  to  $10^{-10}$  m/s. The overlying Silurian sediments have  $K_H$  values which are on the order of  $<10^{-11}$  m/s.
- No geochemical evidence has been found for the infiltration of glacial or recent meteoric recharge water into the host or bounding formations. The stable water isotopes ( $^{18}\text{O}$  and  $^2\text{H}$ ) indicate that the maximum depth of glacial meltwater penetration is to the base of the Salina A1 carbonate aquifer.
- Numerical paleohydrogeologic simulations indicate: i) that glacial perturbations do not alter the governing solute transport mechanisms within the deep groundwater system; and ii) that single and multiple glaciation scenarios, when modelled using regional and site specific parameters, do not result in the infiltration of glacial meltwater into the deep groundwater system.
- The Appalachian Basin has gas traps below the Marcellus black shale that reach more than 70% of the overburden stress. The Marcellus black shale is also overpressured throughout the northern Appalachian Basin, leaving no doubt about its effectiveness as a regional seal. In a similar manner, the underpressured nature of the Ordovician shales beneath the Bruce nuclear site indicates that this sedimentary package represents a long-lived and stratigraphically controlled cap rock seal.
- Site-scale observations that provide further evidence for the long-term barrier integrity of the Ordovician shale cap rock include: i) sealed fractures filled with calcite, gypsum/anhydrite, and/or halite; ii) a low degree of thermal maturation, which inhibited the pervasive development of natural hydraulic fractures and commercial hydrocarbon accumulations; and iii) compartmentalization of the minor hydrocarbon phases.
- The Paleozoic succession beneath the Bruce nuclear site compares favourably with respect to the key physical parameters and geological attributes recognized internationally as necessary for a rock mass to successfully contain and isolate L&ILW for the long-term.

**Contaminant Transport is Diffusion Dominated: deep groundwater regime is ancient showing no evidence of glacial perturbation or cross-formational flow**

- Horizontal hydraulic conductivities ( $K_H$ ) within the Cobourg Formation (DGR host rock), the overlying Ordovician shales (Georgian Bay, Blue Mountain and Queenston formations, and the Collingwood Member of the Cobourg Formation), and underlying Ordovician limestones and dolostones (Sherman Fall, Kirkfield, Coboconk, Gull River, and Shadow Lake formations) are extremely low ( $\approx 10^{-15}$  to  $10^{-10}$  m/s). Vertical hydraulic conductivities within the same formations are lower. Such conditions are consistent with a diffusion dominated regime.
- The effective diffusion coefficient ( $D_e$ ) for HTO in the Ordovician shales is on the order of  $10^{-12}$  m<sup>2</sup>/s, and in the carbonates  $10^{-13}$  to  $10^{-12}$  m<sup>2</sup>/s.  $D_e$  values obtained with HTO are on average 1.9 times greater than  $D_e$  values obtained with an iodide tracer. This



difference is attributed to the influence of anion exclusion in lowering the tracer-accessible porosity for iodide. The low  $D_e$  values, coupled with the low hydraulic conductivities of the Ordovician sediments, indicate that solute migration is diffusion dominated in the deep groundwater system.

- The occurrence of isotopically distinct types of methane and helium in separate zones (one zone in the Upper Ordovician shale and another zone in the Middle Ordovician carbonates) indicates that there has been little to no cross-formational mixing (advective or diffusive) while these gases were resident in the system. The sharp isotopic gradients observed in both the methane and the helium in all DGR boreholes near the Cobourg Formation-Sherman Fall Formation contact, and the lack of apparent mixing of the respective solutes, suggests that a barrier to solute migration is present at that horizon.
- The radiogenic  $^{87}\text{Sr}/^{86}\text{Sr}$  ratios in the Middle and Upper Ordovician porewater are interpreted to result from a combination of water-rock interaction, in situ  $^{87}\text{Rb}$  decay, and diffusive transport upward from the shield. These mechanisms suggest extremely long residence times.
- The chemistries of the deep brines indicate that they were formed by evaporation of seawater, which was subsequently modified by fluid-rock interaction processes. The Cl/Br and Na/Cl ratios, as well as the stable water isotope data for the site, suggest that the deep groundwater system contains evolved ancient sedimentary brines at, or near, halite saturation. The nature of the brines, in particular the high salinities and the enriched  $\delta^{18}\text{O}$  values (enriched in  $^{18}\text{O}$  with respect to the GMWL) of the porewaters, indicate that the deep system is isolated from the shallow groundwater system and that the porewaters have resided in the system for a very long time.
- Illustrative hydrogeochemical modelling suggests that the currently measured natural tracer ( $^{18}\text{O}$ , Cl) profiles could evolve by diffusion from baseline conditions (evaporated seawater composition) in the timeframe of approximately 300 Ma.

### **Seismically Quiet: comparable to stable Canadian Shield setting**

- The Bruce nuclear site is located within the tectonically stable interior of the North American continent, which is characterized by low rates of seismicity. No earthquake exceeding magnitude 5 has been observed in the regional monitoring area in 180 years of record.
- A neotectonic remote-sensing and field-based study that analysed Quaternary landforms for the presence of seismically induced soft-sediment deformation concluded that the Bruce nuclear site has not likely experienced any post-glacial tectonic activity.
- No evidence has been found for the presence of structural features that would indicate a higher seismic hazard near the Bruce nuclear site than that estimated from the regional rate of earthquake occurrence.
- The micro-seismic monitoring network confirms the lack of low-level seismicity ( $> M1.0$ ), implying no seismogenic structures or faults within or in close proximity to the DGR footprint.
- A probabilistic seismic hazard assessment indicates far field/regional seismic sources are the dominant contributors to the hazard for the site at ground level. The estimated surface bedrock peak ground motions are 18.7 and 60.1%g for events of annual probabilities of  $10^{-5}$  and  $10^{-6}$ , respectively.

- Seismic analysis of a DGR emplacement room using ground motions of  $10^{-5}$  and  $10^{-6}$  annual probability events reveals that seismic shaking would not induce damage to the host rock other than dislodging already fractured rock mass around the opening.

**Geomechanically Stable: selected DGR limestone formation will provide stable, virtually dry openings**

- Precedent construction experience with the excavation of underground openings in southern Ontario reveals that excavated openings in the Ordovician shale and Ordovician limestone are mostly dry and stable.
- The laboratory testing of the Cobourg Formation core rock samples reveals a high strength argillaceous limestone with an average uniaxial compressive strength value of 113 MPa. These rock strength conditions compare favourably with other sedimentary formations considered internationally for long-term radioactive waste management purposes.
- No borehole breakouts observed in the deep DGR boreholes over a 24 month timeframe provide a constraint on the possible range of in situ stress magnitudes beneath the Bruce nuclear site. At the repository horizon, the range of stress ratios is estimated to be:  $\sigma_H/\sigma_V$  from 1.5 to 2.0;  $\sigma_T/\sigma_V$  from 1.0 to 1.2. Minor borehole deformation strongly suggests that the orientation of maximum horizontal stress is similar to that of the Michigan Basin, a NE to ENE direction.
- Numerical modelling results suggest that glacial loading has only a minor effect on the EDZ along the shaft. The maximum extent of the damage zone is less than 1.28 times the shaft radius.
- Numerical simulation of the lateral opening in the limestone Cobourg Formation which considered varied long-term rock mass properties and loading scenarios (i.e., glacial ice sheet, seismic ground motions and repository gas pressure) illustrate that the barrier integrity of the enclosing Ordovician bedrock formations is unaffected.

**Natural Resource Potential is Low: commercially viable oil and gas reserves are not present**

- No commercial oil hydrocarbon accumulations were encountered during site characterization. No structural, lithological, chemical or hydrological evidence suggests that the Bruce nuclear site is proximal to an ancient HTD reservoir system.
- The results of petroleum well drilling, the coring and testing of the deep boreholes at the Bruce nuclear site coupled with knowledge of the geologic setting strongly suggest that viable commercial oil and gas reserves do not exist within 40 km of the Bruce nuclear site.
- An average total organic carbon content of the Upper Ordovician shales of less than 1.0%, the recognition of low thermal maturity throughout the regional study, and the absence of natural gas shows during drilling of the DGR boreholes argues against the likelihood of commercial accumulations of either thermogenic or biogenic shale gas beneath the Bruce nuclear site.
- Lateral traceability between the Bruce nuclear site boreholes and other proximal dry wells (e.g., Union Gas #1 and Texaco #6) demonstrates that locally around the Bruce nuclear site (~7 km radius), no pockets of oil or gas hydrocarbon are likely to exist.
- A transition from fresh to saline groundwater is recorded through the shallow and intermediate hydrogeological systems with saline groundwater dominating below

depths of  $\approx 200$  mBGS. The porewater at the repository depth (680 mBGS) is not potable (TDS > 200 g/L) and the carbonate bedrock permeability is extremely low (hydraulic conductivities <  $10^{-14}$  m/s). This combination of extremely high salinities and low hydraulic conductivities at the proposed repository depth would discourage deep drilling for groundwater resources.

- No commercially exploitable base metal accumulations were encountered during site characterization activities.
- The Salina salt does not represent a commercial resource because it has been dissolved and removed beneath the Bruce nuclear site through natural processes in the Paleozoic.

### **Shallow Groundwater Resources are Isolated: near-surface groundwater aquifers are isolated from the deep saline groundwater system**

- Regionally, the hydrogeochemistry of the Michigan Basin defines two distinct groundwater regimes: i) a shallow bedrock system containing potable groundwater at depths above 200 m; and ii) an intermediate to deep saline system characterized by elevated TDS (> 200 g/L) and distinct isotopic signatures. A similar relationship is observed at the site-scale where a shallow potable water zone is defined down to approximately 170 mBGS.
- Groundwater resources in the vicinity of the Bruce nuclear site are obtained from shallow overburden or bedrock wells extending to depths of ca. 100 m into the permeable Devonian carbonates. At increasing depth, groundwater becomes brackish and then saline (non-potable) and yields decrease. This would prevent or discourage deep drilling for water resources.
- Evidence of modern karst is observed to a depth of approximately 180 mBGS. Conditions necessary to generate karst connections to the shallow groundwater system do not exist within the intermediate to deep groundwater system.
- Groundwater modelling illustrates that the Guelph Formation is the upper boundary for vertical radionuclide transport from the repository, whether by advection or diffusion; water-borne radionuclides would not reach the shallow groundwater system through the far field even after millions of years.
- Observed abnormal hydraulic heads in the Ordovician and Cambrian rocks and high vertical hydraulic gradients strongly suggest: i) extremely low rock mass hydraulic conductivities at formation scale; and ii) that vertical transmissive connectivity across bedrock aquitards/aquicludes is highly unlikely.

Multiple lines of evidence that support each of the site hypotheses indicate that the geologic setting beneath the Bruce nuclear site is suitable for the safe implementation of a DGR for L&ILW in the Cobourg Formation.

## ACKNOWLEDGEMENTS

This report encompasses the work of numerous individuals and organizations both prior to, and during, the site characterization program. First and foremost, the authors would like to thank Mark Jensen (NWMO), Robert (Bob) Leech (AECOM Canada Ltd.), and Ken Raven (Intera Engineering Ltd.<sup>1</sup>) for their instrumental work in managing all aspects of a project of this magnitude. Dylan Luhowy (NWMO) and Jim McLay (NWMO) are thanked for project management and general logistical support at the Bruce nuclear site during the site characterization program.

We are also grateful to the numerous contributing authors of the supporting technical reports, including John Avis (Intera Engineering Ltd.), Dr. Andrew Corkum (Itasca Consulting Group, Inc.), Dr. Ian Clark (University of Ottawa), Luigi Cotesta (Itasca Consulting Canada, Inc.), Dr. Alexander Cruden (Monash University), Dr. Branko Damjanac (Itasca Consulting Group, Inc.), Dr. Terry Engelder (Pennsylvania State University), Dr. Shaun Frape (University of Waterloo), Dr. Bernard Hallet (University of Washington), Dr. Dru Heagle (Intera Engineering Ltd.), Dr. Monique Hobbs (University of Bern), Dr. Richard Jackson (Intera Engineering Ltd.), Dr. William Lanyon (Fracture Systems Ltd.), Michael Melaney (Intera Engineering Ltd.), Dr. Stefano Normani (University of Waterloo), Dr. Richard Peltier (University of Toronto), Dr. Roseanne Perman (AMEC Geomatrix, Inc.), Dr. Orfan Shouakar-Stash (University of Waterloo), Shawn Slattery (Alberta Geological Survey), Sean Sterling (Intera Engineering Ltd.), Dr. Jon Sykes (University of Waterloo), Steve Usher (AECOM Canada Ltd.), Dr. Steve Worthington (Worthington Groundwater), Dr. Yong Yin (University of Waterloo), Dr. Robert Youngs (AMEC Geomatrix, Inc.). Their hard work made our work that much easier.

The quality of this report benefited from careful technical reviews by Derek Armstrong (Ontario Geological Survey), Dr. Gail Atkinson (University of Western Ontario), Dr. Dennis Bottomley, Dr. Mario Coniglio (University of Waterloo), Steven Davies (AECOM Canada Ltd.), Dr. Terry Engelder (Pennsylvania State University), Michael Lee (AECOM Canada Ltd.), Dr. Martin Mazurek (University of Bern), Dr. Dougal McCreath (Laurentian University), and Dr. Leslie Smith (University of British Columbia).

Advice and guidance during the site characterization and geosynthesis activities were provided by the Geoscience Review Group: Jacques Delay (ANDRA), Dr. Andreas Gautschi (NAGRA), Dr. Derek Martin (University of Alberta), and Dr. Joe Pearson (Ground-Water Geochemistry).

---

<sup>1</sup> Currently known as Geofirma Engineering Ltd.

**TABLE OF CONTENTS**

	<b><u>Page</u></b>
<b>EXECUTIVE SUMMARY .....</b>	<b>v</b>
<b>ACKNOWLEDGEMENTS .....</b>	<b>x</b>
<b>1. INTRODUCTION.....</b>	<b>1</b>
<b>1.1 BACKGROUND .....</b>	<b>1</b>
<b>1.2 DEEP GEOLOGICAL REPOSITORY CONCEPT.....</b>	<b>3</b>
<b>1.3 FUNDAMENTAL GEOSCIENCE ATTRIBUTES.....</b>	<b>3</b>
<b>1.4 REPORT STRUCTURE.....</b>	<b>5</b>
<b>2. GEOLOGICAL FRAMEWORK .....</b>	<b>6</b>
<b>2.1 INTRODUCTION .....</b>	<b>6</b>
<b>2.2 REGIONAL GEOLOGY.....</b>	<b>7</b>
2.2.1 Introduction .....	7
2.2.2 Geological Setting .....	7
2.2.3 Tectonic Evolution of Southern Ontario .....	14
2.2.3.1 Precambrian Tectonic History.....	15
2.2.3.2 Paleozoic Tectonic History.....	16
2.2.3.3 Mesozoic-Cenozoic Tectonic History.....	17
2.2.4 Basement Geology.....	18
2.2.4.1 Precambrian.....	18
2.2.5 Sedimentary Bedrock Geology .....	18
2.2.5.1 Regional Stratigraphy .....	18
2.2.5.2 3D Geological Framework .....	26
2.2.5.3 Michigan Basin Subsidence and Thermal History .....	29
2.2.5.4 Diagenesis .....	31
2.2.5.5 Karst and Paleokarst.....	32
2.2.6 Structural Geology .....	34
2.2.6.1 Structural Setting .....	34

---

2.2.6.2	Regional Faults - Overview.....	35
2.2.6.3	Regional Faults - Morphology.....	35
2.2.6.4	Regional Faults - Timing.....	36
2.2.6.5	Seismicity.....	37
2.2.6.6	Evolution of the Regional Stress Field.....	39
2.2.6.7	Regional Fracture Patterns.....	39
2.2.7	Quaternary Geology and Glaciation.....	42
2.2.7.1	Regional Quaternary Geology.....	42
2.2.7.2	Glacial Erosion.....	44
2.2.7.3	GIA of the Huron Basin.....	48
2.2.8	Economic Geology.....	50
2.2.8.1	Petroleum Geology.....	50
2.2.8.2	Ordovician Cap Rock Seal.....	55
2.2.8.3	Bedrock Resources.....	56
2.2.8.4	Surficial Sand and Gravel Resources.....	60
<b>2.3</b>	<b>SITE-SCALE GEOLOGY.....</b>	<b>60</b>
2.3.1	Introduction.....	60
2.3.2	Basement Geology.....	63
2.3.3	Sedimentary Bedrock Geology.....	64
2.3.3.1	Stratigraphic Descriptions.....	65
2.3.4	Site-scale Predictability of Ordovician Sedimentary Rocks.....	74
2.3.4.1	Lithofacies Analysis and Marker Beds.....	75
2.3.5	Rock Mineralogy and Geochemistry.....	81
2.3.5.1	Overview.....	81
2.3.5.2	Core Logging.....	83
2.3.5.3	Lithogeochemistry.....	84
2.3.5.4	Detailed Analysis of Ordovician Mineralogy.....	86
2.3.6	Hydrocarbon Occurrences.....	87

---

2.3.7	Halite Occurrences.....	89
2.3.8	Karst and Paleokarst Occurrences .....	91
2.3.9	Site-scale Structural Geology.....	92
2.3.9.1	Fracture Analysis .....	94
2.3.9.2	2D Seismic Reflection Survey.....	99
2.3.10	Summary.....	102
<b>3.</b>	<b>GEOMECHANICAL FRAMEWORK.....</b>	<b>105</b>
<b>3.1</b>	<b>INTRODUCTION .....</b>	<b>105</b>
<b>3.2</b>	<b>GEOMECHANICAL PROPERTIES .....</b>	<b>106</b>
3.2.1	Host Rock – MS Unit 4.....	108
3.2.1.1	Intact Rock Properties.....	108
3.2.1.2	Rock Mass Properties.....	117
3.2.1.3	Short-term Behaviour.....	117
3.2.1.4	Long-term Behaviour .....	122
3.2.2	Cap Rock – MS Unit 3.....	123
3.2.2.1	Intact Rock.....	124
3.2.2.2	Rock Mass Properties.....	128
3.2.2.3	Short-term Behaviour.....	131
3.2.2.4	Long-term Behaviour .....	132
3.2.3	MS Unit 2 – Upper Seals.....	132
3.2.3.1	Intact Rock.....	133
3.2.3.2	Rock Mass Properties.....	133
<b>3.3</b>	<b>IN SITU STRESS.....</b>	<b>137</b>
3.3.1	Orientations.....	138
3.3.2	Magnitudes.....	138
<b>3.4</b>	<b>SUMMARY .....</b>	<b>142</b>
<b>4.</b>	<b>HYDROGEOCHEMISTRY .....</b>	<b>146</b>
<b>4.1</b>	<b>INTRODUCTION .....</b>	<b>146</b>

---

<b>4.2</b>	<b>OBJECTIVES .....</b>	<b>147</b>
<b>4.3</b>	<b>MICHIGAN BASIN: EVIDENCE FOR FLUID MIGRATION AND SOLUTE TRANSPORT .....</b>	<b>147</b>
4.3.1	Ancient Events .....	151
4.3.2	Pleistocene and Post-Pleistocene Infiltration Events .....	153
4.3.3	Origin of Sedimentary Brines .....	153
4.3.4	Regional Summary.....	159
<b>4.4</b>	<b>HYDROGEOCHEMICAL DATA FROM THE BRUCE NUCLEAR SITE.....</b>	<b>159</b>
4.4.1	Natural Tracers .....	162
4.4.1.1	Water-rock Interaction.....	164
4.4.1.2	Fluid Mixing.....	165
4.4.2	Major Ions .....	165
4.4.3	Gas Characterization .....	167
4.4.3.1	Methane and Carbon Dioxide .....	167
4.4.3.2	Helium.....	172
4.4.4	Strontium Isotopes .....	173
4.4.5	Redox Conditions in the Ordovician Shale and Carbonate.....	176
4.4.6	Precambrian Porewater Composition .....	177
<b>4.5</b>	<b>ILLUSTRATIVE MODELLING OF THE BRUCE NUCLEAR SITE GEOCHEMISTRY.....</b>	<b>180</b>
4.5.1	Conceptual Model .....	180
4.5.1.1	The Ordovician Tracer Profiles: Diffusion-from-above.....	181
4.5.1.2	The Devonian and Silurian Profiles: Glacial Melt Water and Meteoric Water Infiltration.....	182
4.5.2	Numerical Modelling.....	182
4.5.2.1	Model Justification .....	182
4.5.2.2	Computational Model.....	183
4.5.2.3	Diffusion-from-above: Tracer Profiles in the Ordovician .....	183
4.5.2.4	Glacial Melt Water and Meteoric Water Infiltration: Tracer Profiles in the Silurian and Devonian.....	186



---

4.5.3	Modelling Summary .....	187
4.5.4	Cambrian Fluid Chemistry.....	187
<b>4.6</b>	<b>SUMMARY .....</b>	<b>188</b>
<b>5.</b>	<b>HYDROGEOLOGY .....</b>	<b>191</b>
<b>5.1</b>	<b>INTRODUCTION .....</b>	<b>191</b>
<b>5.2</b>	<b>FIELD STUDIES.....</b>	<b>191</b>
5.2.1	Shallow Bedrock Information .....	191
5.2.2	Straddle-packer Hydraulic Testing.....	193
5.2.2.1	Hydraulic Conductivity .....	193
5.2.2.2	Formation Pore Pressure.....	195
5.2.2.3	Test-zone Compressibility.....	195
5.2.3	Westbay Pressure Measurements in the DGR Boreholes .....	197
<b>5.3</b>	<b>LABORATORY STUDIES.....</b>	<b>199</b>
5.3.1	Porosity .....	200
5.3.2	Permeability .....	201
5.3.3	Fluid Saturations .....	201
5.3.4	Constitutive Properties and Specific Storage.....	202
5.3.5	Diffusion Properties.....	203
<b>5.4</b>	<b>HYDROGEOLOGICAL MODELLING .....</b>	<b>206</b>
5.4.1	Conceptual Models .....	207
5.4.2	Modelling Strategy .....	211
5.4.3	Computational Models .....	213
5.4.4	System Performance Measures.....	213
5.4.5	Regional-scale Model.....	214
5.4.5.1	Model Domain and Spatial Discretization .....	214
5.4.5.2	Model Parameters.....	219
5.4.5.3	Flow Boundary Conditions .....	225
5.4.5.4	Initial Conditions and Solution of Density-dependent Flow.....	226

---

5.4.5.5	Base-case Simulations .....	230
5.4.5.6	Alternative Simulations .....	234
5.4.5.7	Conclusions from Regional-scale Modelling .....	238
5.4.6	Regional-scale Paleoclimate Modelling .....	239
5.4.6.1	Climate Change and Glaciation .....	239
5.4.6.2	Glacial Meltwater .....	240
5.4.6.3	Linking to the UofT GSM.....	240
5.4.6.4	Paleoclimate Boundary Conditions .....	244
5.4.6.5	Paleoclimate Simulations.....	244
5.4.7	Site-scale Model.....	257
5.4.7.1	Model Geometry and Boundary Conditions .....	257
5.4.7.2	Model Parameters.....	260
5.4.7.3	Base-case Simulations .....	260
5.4.7.4	Alternative Simulations .....	265
5.4.7.5	Conclusions from Site-scale Modelling .....	271
5.4.8	Michigan Basin Cross-section Model .....	272
5.4.8.1	Model Domain and Mesh Generation .....	272
5.4.8.2	Flow Boundary and Initial Conditions.....	273
5.4.8.3	Hydraulic and Transport Parameters .....	274
5.4.8.4	TDS.....	274
5.4.8.5	Results from Michigan Basin Cross-section Model.....	275
5.4.8.6	Conclusions from the Michigan Basin Cross-section Analyses .....	276
5.4.9	1D Two-phase Model .....	277
5.4.9.1	Model Description .....	278
5.4.9.2	Model Parameters.....	278
5.4.9.3	Base-case Simulations .....	282
5.4.9.4	Alternative Scenario.....	284
5.4.9.5	Conclusions from 1D Two-phase Modelling .....	287

---

5.4.10	Conclusions from Hydrogeological Modelling Studies .....	287
<b>5.5</b>	<b>SUMMARY .....</b>	<b>289</b>
<b>6.</b>	<b>FUTURE EVOLUTION OF THE BRUCE NUCLEAR SITE .....</b>	<b>291</b>
<b>6.1</b>	<b>INTRODUCTION .....</b>	<b>291</b>
<b>6.2</b>	<b>LONG-TERM NATURAL EVOLUTION.....</b>	<b>292</b>
6.2.1	Climate Change (Glaciation) .....	292
6.2.1.1	Glacial Erosion.....	293
6.2.1.2	Glacial Loading .....	293
6.2.1.3	Permafrost Formation (Changes in Groundwater Recharge) .....	295
6.2.2	Geologic Disturbances .....	296
6.2.2.1	Seismicity and Seismic Hazard Assessment .....	296
6.2.2.1	Fault Rupture and Reactivation .....	303
6.2.2.2	Volcanism .....	304
<b>6.3</b>	<b>REPOSITORY-INDUCED DISTURBANCES .....</b>	<b>305</b>
6.3.1	EDZ .....	305
6.3.1.1	Definitions and Mechanisms .....	305
6.3.1.2	Long-term EDZ Behaviour: Self-sealing .....	309
6.3.2	Gas Generation.....	311
6.3.3	Repository Resaturation.....	311
<b>6.4</b>	<b>MODELLING OF REPOSITORY EVOLUTION.....</b>	<b>312</b>
6.4.1	Selection of Short-term and Long-term Strengths.....	313
6.4.2	Gas Generation and Its Effects .....	314
6.4.3	Shaft Seals and Long-term Performance.....	316
6.4.3.1	EDZ Prediction.....	317
6.4.3.2	Shaft Seal Geometry.....	318
6.4.3.3	Shaft Sequencing.....	321
6.4.3.4	Modelling Results.....	321
6.4.3.5	Modelling Results.....	326

---

6.4.4	Emplacement Room Stability: 2D Analyses .....	331
6.4.4.1	Long-term Strength Selection .....	332
6.4.4.2	Numerical Analyses .....	333
6.4.4.3	Lower Bound Long-term Strength.....	336
6.4.4.4	Multiple Glaciations.....	337
6.4.4.5	Potential for Hydraulic Fracturing.....	341
6.4.4.6	Seismic Analysis .....	343
6.4.4.7	Alternate Numerical Approach .....	344
6.4.5	Emplacement Panel: 3D Analyses.....	350
6.4.6	Geomechanical Modelling Results and Discussion .....	357
<b>6.5</b>	<b>SUMMARY .....</b>	<b>359</b>
<b>7.</b>	<b>ORDOVICIAN HOST AND BARRIER ROCK ATTRIBUTES .....</b>	<b>362</b>
<b>7.1</b>	<b>INTRODUCTION .....</b>	<b>362</b>
<b>7.2</b>	<b>FAVOURABLE GEOLOGICAL ATTRIBUTES OF THE ORDOVICIAN INTERVAL.....</b>	<b>362</b>
7.2.1	Host Cobourg Formation.....	369
7.2.2	Cap Rock Upper Ordovician Shales .....	370
7.2.3	Lower Bounding Ordovician Carbonates .....	372
<b>7.3</b>	<b>COMPARISON WITH INTERNATIONAL PROGRAMS .....</b>	<b>373</b>
<b>8.</b>	<b>SUMMARY AND CONCLUSIONS .....</b>	<b>376</b>
<b>9.</b>	<b>REFERENCES.....</b>	<b>382</b>
<b>10.</b>	<b>UNITS.....</b>	<b>412</b>
<b>11.</b>	<b>ABBREVIATIONS AND ACRONYMS.....</b>	<b>414</b>

**LIST OF TABLES**

	<b><u>Page</u></b>
Table 2.1: Overview of Referenced Databases Contributing to This Geological Synthesis.....	7
Table 2.2: Timetable of Major Tectonic Events in Southern Ontario.....	15
Table 2.3: Cobourg Formation (Lindsay Fm.) Descriptions from Southern Ontario Including the Bruce Nuclear Site.....	23
Table 2.4: Hydrocarbon Exploration Plays in Southern Ontario.....	51
Table 2.5: Summary of Economic Bedrock Units in the RSA .....	57
Table 2.6: Data Sources for Site Scale Geological Description .....	63
Table 2.7: Cambrian Borehole Log Description .....	66
Table 2.8: Middle Ordovician Borehole Log Descriptions .....	68
Table 2.9: Upper Ordovician Borehole Log Descriptions .....	69
Table 2.10: Lower Silurian Borehole Log Descriptions .....	71
Table 2.11: Middle Silurian Borehole Log Descriptions .....	72
Table 2.12: Upper Silurian Borehole Log Descriptions .....	72
Table 2.13: Devonian Borehole Log Descriptions.....	74
Table 2.14: Summary of Strike, True Dip, and Thicknesses of Ordovician Formations and Members Encountered in the DGR Boreholes.....	75
Table 2.15: Dips Calculated from Marker Beds .....	81
Table 2.16: Representative Estimates of Mineralogical Composition for All Stratigraphic Formations, Units and Members in All DGR Boreholes .....	82
Table 2.17: Summary of Occurrences of Fracture Infill, Vein and Other Secondary Mineralogy in DGR Boreholes.....	85
Table 3.1: Primary Sources of Information.....	105
Table 3.2: Shear Strength of the Cobourg and Sherman Fall Formations.....	116
Table 3.3: RQD Values for MS Unit 4 and Surrounding Rocks.....	119
Table 3.4: Summary of Brazilian Tension Test Results on MS Unit 3 Rocks .....	126
Table 3.5: Shear Strength of Georgian Bay and Blue Mountain Formations and the Collingwood Member .....	128
Table 3.6: RQD Values for MS Unit 3 from Boreholes DGR-2 to DGR-6 .....	129
Table 3.7: Joint Occurrences in MS Unit 3.....	130
Table 3.8: Proposed Concrete Bulkhead Seal Locations for Access and Ventilation Shafts in MS Unit 3 .....	133
Table 3.9: RQD Values for MS Unit 2 from Boreholes DGR-1 to DGR-6 .....	135
Table 3.10: Number of Joints Determined from Rock Core Logging of MS Unit 2.....	136
Table 3.11: Estimated Stress Ratios near Repository Depths .....	139
Table 3.12: Constraints on the Horizontal Stress Magnitude at Depths of 620, 680 and 700 mBGS, Assuming Various Scenarios for the Borehole Wall Strength .....	139
Table 3.13: Comparison of In Situ Stress Ratios at Various Horizons.....	142
Table 3.14: Summary of Laboratory Geomechanical Properties in MS Units 1 to 5.....	144
Table 4.1: Primary Sources of Information.....	147
Table 4.2: TDS, Water Type and pH with Depth in the Sedimentary Formations.....	161

---

Table 4.3:	Distribution of Diffusion Parameters Used in Diffusion Simulations .....	184
Table 5.1:	Summary of Horizontal Hydraulic Conductivities for Lucas, Amherstburg, Bois Blanc and Bass Islands Formations .....	192
Table 5.2:	Major Design Elements of MP55 Casing Systems Installed in DGR Boreholes .....	199
Table 5.3:	Specific Storage Estimates Derived from Laboratory Measurements on DGR Core .....	204
Table 5.4:	Iodide Effective Diffusion Coefficients .....	205
Table 5.5:	FRAC3DVS-OPG Model Layers and Corresponding Geologic Units .....	218
Table 5.6:	Base-case Hydrogeological Parameter Values for Regional-scale and Site- scale Modelling .....	222
Table 5.7:	Groundwater Transport Parameters for Regional-scale Modelling .....	224
Table 5.8:	Matrix of Regional-scale Simulations Performed .....	236
Table 5.9:	Mean Life Expectancy at the Location of the Proposed DGR for Alternative Modelling Scenarios .....	238
Table 5.10:	Péclet Numbers for the Cobourg from Regional-scale Analyses .....	239
Table 5.11:	Summary of Formation Parameters for Regional- and Site-scale Models Including the Presence of a Gas Phase .....	253
Table 5.12:	Parameters and Initial Conditions for Site-scale Analyses .....	266
Table 5.13:	Hydrogeologic and Two-phase Flow Properties for TOUGH2-MP Simulations .....	281
Table 6.1:	Seismic Zones and Their Seismogenic Probability .....	299
Table 6.2:	Summary of Seismic Hazard Analysis Results .....	301
Table 6.3:	EDZ Extent and Properties Observed from Underground Excavations .....	307
Table 6.4:	Overview of Self Sealing Potential of EDZ in Barrier Rocks .....	310
Table 6.5:	Summary of Properties Used and EDZ Estimates Obtained from 3D Models .....	323
Table 6.6:	Bedding-plane Strength Data .....	336
Table 6.7:	Material Parameters for the Panel-scale Models .....	352
Table 6.8:	Material and Stress Assumptions in the Blue Mountain Formation .....	353
Table 7.1:	Comparison of Bruce Nuclear Site Dataset for Host and Cap Rock Units with Those from International DGR Programs .....	363

## LIST OF FIGURES

	<u>Page</u>
Figure 1.1: Bruce Nuclear Site (DGR) Location .....	1
Figure 1.2: Organization and Project Interfaces within DGR Geoscientific Work Program .....	3
Figure 1.3: Conceptual Layout of the DGR below the Bruce Nuclear Site .....	4
Figure 2.1: Basement Tectonic Subdivisions of the Great Lakes Basin Region .....	8
Figure 2.2: Geological Features of Southern Ontario.....	9
Figure 2.3: Generalized Paleozoic Bedrock Geology Map of Southern Ontario .....	10
Figure 2.4: Geological Cross-section through the Michigan Basin.....	11
Figure 2.5: Interpreted Boundaries and Fault Contacts in Southern Ontario .....	12
Figure 2.6: Composite Seismic Section Showing Basement Geometry from the Lake Erie and Lake Ontario Regions .....	13
Figure 2.7: Phanerozoic Tectonic Cycles with Band Widths Representing Relative Tectonic Intensity .....	14
Figure 2.8: Paleozoic Stratigraphic Nomenclature of Southwestern Ontario .....	19
Figure 2.9: Ordovician Facies and Isopach Thickness Map of the Michigan and Appalachian Basin Regions .....	21
Figure 2.10: Distribution of Middle and Upper Silurian Carbonate Facies .....	25
Figure 2.11: Oblique (a) and Plan (b) Views of the RSA Bedrock Geology .....	28
Figure 2.12: Hypothetical Burial History Curves for Locations within the Michigan Basin .....	29
Figure 2.13: Karstified Near-surface Paleozoic Rocks in Southern Ontario.....	33
Figure 2.14: Seismicity in the Bruce Region from 1985 to 2010 Overlain with Mapped Faults in Southern Ontario .....	38
Figure 2.15: Joint Orientations in and around South-central Ontario .....	40
Figure 2.16: Quaternary Overburden Thickness in the RSA.....	43
Figure 2.17: Laurentide Ice Sheet Thickness at Last Glacial Maximum (-25 ka) .....	44
Figure 2.18: Photographs of Glacially Scoured Bedrock in the Bruce Peninsula Region .....	47
Figure 2.19: Reference Isostatic Response Surface for the Great Lakes Basin region Portraying Glacial Rebound Since 10.6 kaBP.....	49
Figure 2.20: Principal Oil and Natural Gas Producing Regions and Storage Pools.....	50
Figure 2.21: Schematic Representation of the Origin of Fracture-related HTD within the Ordovician Sequences of Ontario .....	53
Figure 2.22: Location Map for Economic Bedrock Resources Listed in Table 2.5.....	59
Figure 2.23: Geological Cross-section Through the RSA Beneath the Bruce Nuclear Site .....	61
Figure 2.24: Overview of the Bruce Nuclear Site .....	62
Figure 2.25: Subsurface Stratigraphy at the Bruce Nuclear Site.....	64
Figure 2.26: Core Sample of Argillaceous Limestone and Shale Interbeds, Sherman Fall Formation, 703.90 mBGS, DGR-2 .....	67
Figure 2.27: Core Sample of Argillaceous Limestone from the Proposed Repository Depth, Cobourg Formation, 669.81 mBGS, DGR-2.....	67
Figure 2.28: Core Sample of Interbedded Shale and Limestone, Georgian Bay Formation, 542.25 mBGS, DGR-2 .....	70

Figure 2.29: Core Sample of Green and Red Calcareous Shale, Upper Ordovician Queenston Formation, 454.82 mBGS, DGR-1.....	70
Figure 2.30: Lithostratigraphy, Natural Gamma Profiles and Major Mineralogy of the DGR Boreholes.....	77
Figure 2.31: Intervals Chosen for Facies Analysis from DGR-2, DGR-3, and DGR-4.....	79
Figure 2.32: Summary of Observed Hydrocarbon Occurrences and TOC Analyses from DGR-1/2, DGR-3, and DGR-4 Cores.....	88
Figure 2.33: Summary of Observations of Halite Presence in the DGR Cores.....	90
Figure 2.34: Potential or Active Karst and Paleokarst Beneath the Bruce Nuclear Site.....	92
Figure 2.35: Compilation of RSA and Site-scale Fault, Joint and Vein Data.....	95
Figure 2.36: Calcite-filled Veins Exposed along the Shoreline of Lake Huron near the Bruce Nuclear Site.....	96
Figure 2.37: Natural Fracture Orientations from Surface and Subsurface Datasets.....	98
Figure 2.38: 2D Seismic Line #1 with Interpreted Faults.....	101
Figure 3.1: Reference Stratigraphic Column Showing MS Units and Shaft Seal System at the Bruce Nuclear Site.....	107
Figure 3.2: Stress-strain Diagram Showing the Evolution of Crack Development of a Typical UCS Test.....	109
Figure 3.3: Uniaxial Compression Test Data for Collingwood, Cobourg and Sherman Fall: (a) UCS and (b) Elastic Modulus from Boreholes DGR-2 to DGR-6.....	110
Figure 3.4: MS Unit 4 UCS of the Cobourg – Site Specific and Regional Test Data.....	111
Figure 3.5: Distribution of (a) CD Stresses and (b) CI Stresses for the Collingwood Member and Cobourg and Sherman Fall Formations.....	112
Figure 3.6: Brazilian Tensile Strength of the Cobourg Formation.....	113
Figure 3.7: Hoek-Brown Failure Envelope for the Cobourg Formation.....	114
Figure 3.8: Direct Shear Test Results for the Cobourg Formation.....	115
Figure 3.9: Direct Shear Test Results for the Sherman Fall Formation.....	116
Figure 3.10: Stratigraphic Column Showing RQD, Fracture Frequency, and MS Units at the Bruce Nuclear Site.....	118
Figure 3.11: Variation with Depth of RQDs and Fracture Frequencies in MS Unit 4 from DGR-2, DGR-3 and DGR-4.....	119
Figure 3.12: Modulus Ratio Versus UCS.....	120
Figure 3.13: Long-term Envelopes for Lac du Bonnet Granite and Yucca Mountain Tuff.....	123
Figure 3.14: UCS of the Queenston Formation (a) and Georgian Bay Formation Shales (b).....	124
Figure 3.15: CI (filled symbols) and CD (unfilled symbols) Stresses of MS Unit 3.....	125
Figure 3.16: Triaxial Compressive Hoek-Brown Failure Envelope for Georgian Bay Shale.....	126
Figure 3.17: Triaxial Compressive Hoek-Brown Failure Envelope for the Collingwood Member.....	127
Figure 3.18: Direct Shear Test Results for Georgian Bay and Blue Mountain Shales.....	127
Figure 3.19: Direct Shear Test Results for the Collingwood Member.....	128
Figure 3.20: Variation with Depth of RQDs and Fracture Frequencies in MS Unit 3 from DGR-2, DGR-3 and DGR-4.....	130
Figure 3.21: Uniaxial Compression Test Results at the Bruce Nuclear Site.....	134



---

Figure 3.22: CI (filled symbols) and CD (unfilled symbols) Stresses of MS Unit 2.....	135
Figure 3.23: DGR Borehole Long Axis Orientation Histograms for Middle Ordovician Formations .....	138
Figure 3.24: Comparison of Calculated Maximum Horizontal In Situ Stress Profiles.....	141
Figure 4.1: (a) Timing of Paleozoic Orogenic Events and (b) $\delta^{18}\text{O}$ Variation in Deep Sea Sediment Core ODP-677 Depicting Recent Glacial Cycles.....	149
Figure 4.2: Conceptual Model Showing Ancient Brine at Depth, Cold-climate Water Infiltrated to Mid-depths, and Modern Meteoric Water near Surface .....	154
Figure 4.3: Chloride versus Bromide Concentrations for a) the UW Database, and b) Groundwater and Porewater Samples from the Bruce Nuclear Site.....	156
Figure 4.4: Hydrogen Versus Oxygen Isotopic Signatures for a) All Fluids Within the UW Database and b) Groundwater and Porewater Collected at the Bruce Nuclear Site.....	157
Figure 4.5: Sampling Locations for the UW Database .....	158
Figure 4.6: TDS versus Depth for DGR Boreholes .....	161
Figure 4.7: Vertical Depth Profiles for Natural Tracers $^{18}\text{O}$ and $^2\text{H}$ Determined in Porewater and Groundwater .....	163
Figure 4.8: Vertical Depth Profiles for Natural Tracers Cl and Br Determined in Porewater and Groundwater .....	164
Figure 4.9: Cl/Br Ratios versus Depth for DGR Boreholes .....	166
Figure 4.10: Concentration Distributions for $\text{CH}_4$ (mmol/kgw) versus Depth in DGR-3 and DGR-4, and Corresponding Distributions of $\delta^{13}\text{C}$ and $\delta^2\text{H}$ in $\text{CH}_4$ .....	168
Figure 4.11: Concentration Distribution for $\text{CO}_2$ (mmol/kgw) versus Depth (left), and Corresponding Distributions of $\delta^{13}\text{C}$ in $\text{CO}_2$ (right) .....	168
Figure 4.12: Discrimination Diagram Indicating Fields for $\text{CH}_4$ of Biogenic ( $\text{CO}_2$ Reduction and Fermentation) and Thermogenic Origin .....	170
Figure 4.13: TOC and $\text{CH}_4$ Concentrations with Depth in DGR-2, DGR-3, and DGR-4.....	172
Figure 4.14: Vertical Profiles of Helium Isotopic Ratios ( $^3\text{He}/^4\text{He}$ ) from DGR-2, DGR-3 and DGR-4.....	173
Figure 4.15: Depth Profiles for $^{87}\text{Sr}/^{86}\text{Sr}$ in Groundwater, Porewater and Host Rocks at DGR-2, DGR-3 and DGR-4.....	174
Figure 4.16: $^{87}\text{Sr}/^{86}\text{Sr}$ versus Sr Concentration for DGR Groundwaters and Porewaters .....	175
Figure 4.17: Back Scattered Electron Images Illustrating the Principal Solid Phases Involved in Sulphate Reduction Reactions.....	176
Figure 4.18: Compilation of Isotopic Data for Groundwater Samples from the Canadian Shield .....	178
Figure 4.19: $\delta^{18}\text{O}$ versus $\delta^2\text{H}$ for Ordovician and Cambrian Porewater from DGR-2, DGR-3 and DGR-4, and Groundwater Brine Samples from Ordovician Carbonates and Cambrian Sandstone Included in the UW Database .....	179
Figure 4.20: Profile of Deuterium Excess ( $d$ ) Versus Depth for Porewater and Groundwater from DGR Boreholes .....	180
Figure 4.21: Results of the Diffusion-from-above Modelling Scenario .....	185
Figure 4.22: Results of $\delta^{18}\text{O}$ Diffusion Simulation (dashed lines) Compared to Measured Porewater $\delta^{18}\text{O}$ Data .....	186

---

Figure 5.1:	Best-fit Interval Horizontal Hydraulic Conductivities from Borehole Straddle-packer Tests and Estimated Formation Average Values .....	194
Figure 5.2:	Formation Pressure Estimates and Uncertainty Ranges from Straddle-packer Tests in DGR-4.....	196
Figure 5.3:	Reference Fluid Density Profile and Formation Averages Based on US-8 and DGR Borehole Groundwater and Porewater Data .....	197
Figure 5.4:	Test-zone Compressibility Estimates from Straddle-packer Tests in DGR Boreholes .....	198
Figure 5.5:	Measured Westbay Pressures and Estimated Environmental Head Profile for Borehole DGR-4 .....	200
Figure 5.6:	Total Porosity Profiles from the DGR Borehole Cores .....	202
Figure 5.7:	Effective Diffusion Coefficients ( $D_e$ ) versus Depth .....	205
Figure 5.8:	Reference Stratigraphic Column Showing Hydrostratigraphic Units at the Bruce Nuclear Site .....	209
Figure 5.9:	Illustration of Life Expectancy Concept for an Idealized Cross-section .....	214
Figure 5.10:	Location of Proposed DGR Site, Regional-scale Modelling Domain, Land Surface Elevations and River Courses .....	215
Figure 5.11:	Block-cut View of FRAC3DVS-OPG Zone Identifiers for 33 Layers in Regional-scale Model.....	217
Figure 5.12:	Fence View of FRAC3DVS-OPG Zone Identifiers for 33 Layers in Regional-scale Model.....	217
Figure 5.13:	Block-cut View Showing Spatial Extent of the Cambrian (Yellow), Underlain by the Precambrian Basement (Pink), for the Regional Modelling Domain .....	220
Figure 5.14:	Block-cut View Showing Spatial Extent of the Middle Silurian (Top of the Niagaran Group) for the Regional Modelling Domain .....	220
Figure 5.15:	Block-cut View Showing Subcrop of the Bedrock Units Beneath Quaternary Drift Deposits for the Regional Modelling Domain .....	221
Figure 5.16:	Block-cut View of Initial TDS Concentration Distribution.....	227
Figure 5.17:	Fence View of Initial TDS Concentration Distribution .....	228
Figure 5.18:	Fence View of Steady-state Density-independent Freshwater Heads.....	228
Figure 5.19:	Fence View of Freshwater Heads that have Equilibrated to the Static TDS Distribution .....	229
Figure 5.20:	Fence View of Freshwater Heads that have Equilibrated at 1 Ma to the Temporally Varying TDS Distribution .....	229
Figure 5.21:	Fence View of TDS Concentration Distribution that has Equilibrated at 1 Ma to the Freshwater Heads.....	230
Figure 5.22:	Fence View of the Base-case Environmental Heads that have Equilibrated at 1 Ma to the Temporally Varying TDS Distribution .....	232
Figure 5.23:	Fence View of Base-case Porewater Velocity Magnitude.....	233
Figure 5.24:	Fence View of Base-case Mean Life Expectancy .....	234
Figure 5.25:	TIN Used to Interpolate Properties for the Regional-scale Spatial Domain .....	241
Figure 5.26:	Plots of Ice Thickness, Lake Depth, and Permafrost Depth versus Time for the nn9930 GSM Grid Block at the Bruce Nuclear Site .....	242
Figure 5.27:	Plots of Ice Thickness, Lake Depth, and Permafrost Depth versus Time for the nn9921 GSM Grid Block at the Bruce Nuclear Site .....	243

---

Figure 5.28: Fence View of Freshwater Heads at Present for the Base-case Paleoclimate Scenario .....	245
Figure 5.29: Fence View of Environmental Heads at Present for the Base-case Paleoclimate Scenario .....	245
Figure 5.30: Plot of Freshwater Head and Environmental Head Results from Paleoclimate Simulations .....	246
Figure 5.31: Fence View of TDS at Present for the Base-case Paleoclimate Scenario .....	247
Figure 5.32: Plot of TDS and Tracer Concentration versus Depth from Paleoclimate Simulations.....	248
Figure 5.33: Fence View of Pore Velocity Magnitude at Present for the Base-case Paleoclimate Scenario .....	249
Figure 5.34: Fence View of Tracer Concentrations at Present for the Base-case Paleoclimate Scenario .....	250
Figure 5.35: Regional-scale Discretization Showing Location of Site-scale Spatial Domain.....	258
Figure 5.36: Regional-scale Discretization Showing Site-scale Discretized Spatial Domain.....	259
Figure 5.37: Regional-scale Discretization Showing Vertical Details of Site-scale Discretized Spatial Domain .....	259
Figure 5.38: Fence View of Freshwater Heads for the Base-case Site-scale Analysis Shown in Figure 5.39 .....	261
Figure 5.39: Cross-sections of Freshwater Heads for the Base-case Site-scale Analysis with Equilibrated Regional-scale Heads as the Initial Condition .....	261
Figure 5.40: Fence View of Environmental Heads for the Base-case Site-scale Analysis Shown in Figure 5.41 .....	262
Figure 5.41: Cross-sections of Environmental Heads for the Base-case Site-scale Analysis with Equilibrated Regional-scale Heads as the Initial Condition.....	262
Figure 5.42: Cross-section View of the Spatial Distribution of a Tracer at 100 ka with Equilibrated Regional-scale Heads as the Initial Condition.....	263
Figure 5.43: Cross-section View of the Spatial Distribution of a Tracer at 1 Ma with Equilibrated Regional-scale Heads as the Initial Condition.....	264
Figure 5.44: Tracer-breakthrough Curves at the Niagaran Group and Cambrian for the Base-case Site-scale Model.....	265
Figure 5.45: Predicted Evolution of Environmental Heads with Base-case Black River Group Anisotropy of 0.001 .....	267
Figure 5.46: Predicted Evolution of Environmental Heads with Black River Group Anisotropy of 0.1 .....	268
Figure 5.47: Predicted Evolution of Environmental Heads with Black River Group Anisotropy of 0.01 .....	269
Figure 5.48: Tracer-breakthrough Curves at the Niagaran Group and Cambrian for Site-scale Simulations .....	269
Figure 5.49: Predicted Evolution of Environmental Heads with Fracture Zone 1 km from DGR .....	271
Figure 5.50: Stratigraphic Zones for the Michigan Basin Cross-section Model.....	273
Figure 5.51: Initial TDS Distribution.....	274
Figure 5.52: Equilibrium Environmental Heads for Defined TDS Distribution .....	275

---

Figure 5.53: Equilibrium Freshwater Heads for Defined TDS Distribution .....	276
Figure 5.54: Initial Conditions Base-case Two-phase Gas-water Flow Analysis: (a) Water Pressure, (b) Freshwater Head, (c) Gas Pressure, (d) Capillary Pressure.....	279
Figure 5.55: Initial Conditions Two-phase Gas-water Flow Analysis with Air Generation: (a) Water Pressure, (b) Freshwater Head.....	280
Figure 5.56: Capillary Pressure versus Saturation Relationships for the Two-phase Flow Analysis.....	280
Figure 5.57: Two-Phase Flow Analysis at 400 ka for Base-case Scenario: (a) Water Pressure, (b) Freshwater Head.....	282
Figure 5.58: Saturations for the Two-phase Flow Analysis at 400 ka for Base-case Scenario: (a) Gas Saturation Profile, (b) Water Saturation Profile.....	283
Figure 5.59: Two-phase Flow Analysis at 1.25 Ma for Base-case Scenario: (a) Water Pressure, (b) Freshwater Head.....	283
Figure 5.60: Saturations for the Two-phase Flow Analysis at 1.25 Ma for Base-case Scenario: (a) Gas Saturation Profile, (b) Water Saturation Profile.....	284
Figure 5.61: Two-Phase Flow Analysis at 300 ka with a Fracture Zone at 585 mBGS: (a) Water Pressure, (b) Freshwater Head .....	285
Figure 5.62: Saturations for the Two-phase Flow Analysis at 300 ka with a Fracture Zone at 585 mBGS: (a) Gas Saturation Profile, (b) Water Saturation Profile .....	285
Figure 5.63: Two-phase Flow Analysis at 1 Ma with Air Generation: (a) Water Pressure, (b) Freshwater Head .....	286
Figure 5.64: Two-phase Flow Analysis at 1 Ma with a Fracture Zone at 585 mBGS and Air Generation: (a) Water Pressure, (b) Freshwater Head.....	287
Figure 6.1: Factors Influencing the Future Evolution of the DGR.....	291
Figure 6.2: Simulated Evolution of Ice Sheet Load.....	294
Figure 6.3: Regional Source Zone Boundaries and Seismic Events used for the Probabilistic Seismic Hazard Assessment.....	298
Figure 6.4: Uniform Seismic Spectra for Surface Ground Motions on Hard Rock at the Bruce Nuclear Site .....	300
Figure 6.5: Total Mean Seismic Response Spectra of Horizontal Ground Motion Components with Probabilities of Exceedance of $10^{-5}$ per annum.....	302
Figure 6.6: Total Mean Seismic Response Spectra of Horizontal Ground Motion Components with Probabilities of Exceedance of $10^{-6}$ per annum.....	303
Figure 6.7: Schematic Illustration Defining EdZ, EDZ, and HDZ for an Unjointed Rock .....	306
Figure 6.8: Example of Typical EDZ Model Output Using Arbitrary Material Parameters.....	308
Figure 6.9: EDZ and HDZ Defined by Pseudo-continuum (Finite Element) Model .....	309
Figure 6.10: Depth of Water in the Repository .....	311
Figure 6.11: Repository Layout and Typical Emplacement Room Cross-section .....	313
Figure 6.12: Repository Gas Pressure Histories Used in Geomechanical Stability Analyses.....	316
Figure 6.13: Simplified 2D Analysis of Shaft and Potential Over-excavation (Seal) for the Cabot Head Formation.....	318
Figure 6.14: Details of the Three Concrete Bulkhead Geometries.....	319
Figure 6.15: Layout of Quarter-symmetrical FLAC3D Model of Over-excavated and Backfilled Access Shaft for B1 Seal.....	320

Figure 6.16: Yield State – Concrete Bulkhead B1: Time-dependent Strength Degradation – FLAC Yield States Coloured.....	322
Figure 6.17: EDZ and HDZ Estimates for Base-case.....	324
Figure 6.18: Pore Pressure Data (Base-case) at Various Distances from the Shaft Centre for Seal B1.....	325
Figure 6.19: Yield State – Concrete Bulkhead B1: Time-dependent Strength Degradation + Glacial Load + Pore Pressure .....	327
Figure 6.20: Volumetric Strain – Concrete Bulkhead B1 (Lions Head Formation): Time-dependent Strength Degradation + Glacial Load + Pore Pressure.....	328
Figure 6.21: Yielded Zones around the Shaft (Concrete Bulkhead B1) before and after 3 Seismic Events of $10^{-6}$ Annual Exceedance Frequency Were Applied.....	329
Figure 6.22: Distribution of Representative EDZ Extents in Specific Formations and Maximum Local EDZ Extents.....	330
Figure 6.23: Geometry of the Model for Panel-scale Parametric Analysis.....	332
Figure 6.24: Evolution of Plasticity Around Emplacement Rooms After 2 and 8 Glacial Cycles for Different Long-term Strengths.....	334
Figure 6.25: Geometries for the Emplacement Room Models (DGR Inverts at 683 mBGS and 679 mBGS).....	335
Figure 6.26: Evolution of Emplacement Room Outline and Pillar Damage with Lower Bound Strength, Gas and Pore Pressures.....	338
Figure 6.27: Evolution of Emplacement Room Outline and Pillar Damage, Representative Case for Four Glacial Cycles .....	339
Figure 6.28: Bulking Examples of Collapsed Limestone Cavern Roofs .....	340
Figure 6.29: Evolution of Pore Pressure (Pa) Around the Emplacement Room for 1 Ma Assuming One Glacial Cycle Starting at 60 ka .....	342
Figure 6.30: Opening of Bedding Planes (Horizontal Dashed Lines) Around an Emplacement Room at 100 ka Due to Extreme Gas Pressure History (15 MPa) .....	343
Figure 6.31: Emplacement Room Models Subjected to Shaking.....	344
Figure 6.32: EDZ and HDZ Determination from Finite-Element Results (Continuum with Bedding).....	345
Figure 6.33: Stresses Carried at the Spring-line Through the Pillar.....	346
Figure 6.34: Sensitivity Analysis of Discrete Fractures in Modelling HDZ Formation .....	347
Figure 6.35: Wall/Pillar Fractures in Underground Limestone Mines .....	348
Figure 6.36: Influence of In-plane Horizontal Stress Ratio, K .....	349
Figure 6.37: Influence of Strength Model for Bedding.....	349
Figure 6.38: Geometry of the Panel-scale Model.....	350
Figure 6.39: Model Panel Geometry Overlain with Repository Layout.....	351
Figure 6.40: Net Displacements (m) Induced by the Repository at the Peak of the Glacial Load: Case 1 with No Central Pillar .....	354
Figure 6.41: Yielding in the Blue Mountain Shale above the Repository for a) Case 1 and b) Case 2 with a Central Pillar in Place.....	355
Figure 6.42: Plastic Deformation at Peak of Glacial Load: Case 1 with No Central Pillar.....	356
Figure 6.43: Differential Displacements (cm) at the Lower Contact of the Georgian Bay Formation.....	356

Figure 6.44: Evolution of Emplacement Room Roof Stability.....	358
Figure 7.1: Summary Plot Indicating Key Physical Properties of the Ordovician Sedimentary Rock Interval Beneath the Bruce Nuclear Site.....	365
Figure 7.2: Cross-section Through the Paleozoic Succession Beneath the Bruce Nuclear Site.....	368
Figure 7.3: Relationship Between Porosity and Hydraulic Conductivity in Clays .....	374
Figure 7.4: Relationship Between Porosity and Effective Diffusion Coefficient for HTO (Normal to Bedding) in Low Permeability Rocks .....	375

## 1. INTRODUCTION

### 1.1 Background

Ontario Power Generation (OPG) is proposing the development of a Deep Geologic Repository (DGR) at the Bruce nuclear site for the long-term management of Low and Intermediate Level Waste (L&ILW) from OPG owned or operated nuclear generating facilities. Beneath the Bruce nuclear site (Figure 1.1), situated 225 km northwest of Toronto on the eastern shore of Lake Huron, is an 840 m thick sequence of Cambrian to Devonian age, near horizontally bedded, weakly deformed carbonate, shale, and evaporitic sedimentary rock of the Michigan Basin. Within this sedimentary sequence, the proposed DGR would be excavated within the low permeability argillaceous limestone Cobourg (Lindsay) Formation at depth of 680 mBGS, and overlain by 200 m of upper Ordovician shale formations.



Figure 1.1: Bruce Nuclear Site (DGR) Location

A key aspect of the DGR Safety Case is the integrity and long-term stability of the sedimentary sequence to contain and isolate L&ILW at timeframes of 1Ma. Early in the project, geoscientific studies that considered regional and site-specific public domain data sets indicated favourable geologic conditions for implementation of the DGR concept (GOLDER 2003, Mazurek 2004). In 2005, OPG initiated the process of developing a multi-phase Geoscientific Site Characterization Plan (GSCP) to support an Environmental Assessment for the project and submission of a site preparation and construction licence application. The site characterization program for the proposed DGR at the Bruce nuclear site was a four-year geoscientific endeavour focused on drilling, sampling, testing and monitoring of six continuously cored deep boreholes (DGR-series) and three shallow boreholes (US-series) in three phases (1, 2A and 2B) of site investigation. The Phase 1 GSCP, as well as a general overview of all planned Bruce nuclear site characterization work, is described by Intera Engineering Ltd. (INTERA 2006). Phase 2A and 2B GSCP activities are described by Intera Engineering Ltd. (INTERA 2008).

In general, the GSCP describes surface and sub-surface site characterization activities necessary to:

- Assess and reaffirm the technical suitability of the proposed DGR concept;
- Provide evidence on the geoscientific basis for repository safety at timeframes relevant to demonstrating DGR safety (i.e., stable rock formations; diffusion dominant transport regime);
- Yield information to support development of a site-specific engineered repository design;
- Provide a geoscientific basis for the Postclosure Safety Assessment; and
- Contribute to the development of an integrated DGR Safety Case describing the expected long-term safety and potential impacts of the DGR.

The activities described in the Phase 1, 2A and 2B GSCP were intended to support two key deliverables.

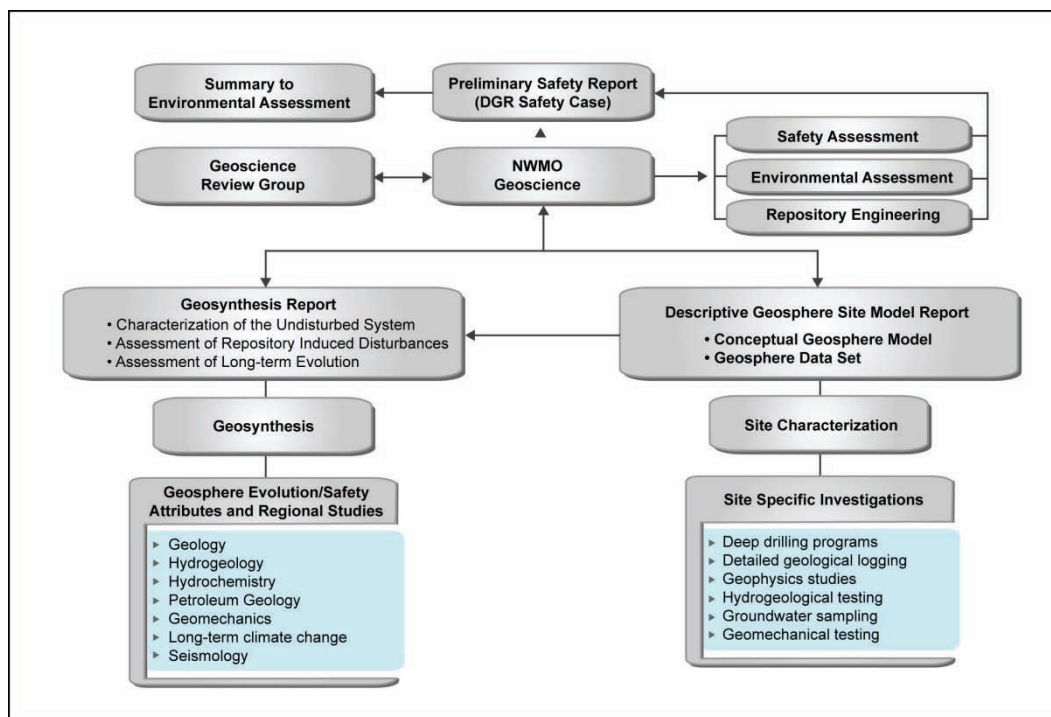
1. A geoscientific site characterization program to develop a Descriptive Geosphere Site Model (DGSM; INTERA 2011), which is an integrated, multi-disciplinary, geoscientific description and explanation of the undisturbed sub-surface environ as it relates to site-specific geologic, hydrogeologic and geomechanical characteristics and attributes.
2. A Geosynthesis, which is a geoscientific explanation of the overall understanding of site characteristics, attributes and evolution (past and future) as they relate to demonstrating long-term DGR performance and safety.

Figure 1.2 shows how the two key deliverables, Geosynthesis, and DGSM (INTERA 2011), relate to the overall DGR project from inception to approval. Results and discussion from the site characterization and geosynthesis programs are combined in this report as described in the Report Structure section below.

A Geoscience Review Group (GRG) of international geoscientists was established in order to assist in formulating the geoscience programs and to monitor progress in achieving objectives.

The results from the geoscientific investigations and the Geosynthesis are input to the repository engineering, environmental assessment and safety assessment programs. Together, all of these programs contribute to the DGR Safety Case, which is presented as part of the Preliminary Safety Report (OPG 2011a).





**Figure 1.2: Organization and Project Interfaces within DGR Geoscientific Work Program**

## 1.2 Deep Geological Repository Concept

The proposed DGR will be located at a depth of about 680 m below the surface near the Western Waste Management Facility (WWMF) at the Bruce nuclear site. The repository is located within the low permeability limestone Cobourg Formation, overlain by more than 200 m of low permeability shales. The repository, accessed via two vertical shafts, will require the excavation of nearly 649,700 m<sup>3</sup> of rock to accommodate an emplaced L&ILW volume of 200,000 m<sup>3</sup> within an approximate 27 ha repository footprint.

Figure 1.3 shows a conceptual diagram of the DGR facility. A full description of the proposed DGR can be found in the Preliminary Safety Report (OPG 2011a).

## 1.3 Fundamental Geoscience Attributes

Seven key geoscience attributes, or hypotheses, that relate to demonstrating the geoscientific suitability of the Bruce nuclear site were formulated and tested as part of the Geosynthesis program. The key geoscience arguments are organized around these fundamental hypotheses in order to demonstrate an understanding for regulators, the scientific community and other stakeholders and to allow them to judge site suitability. These scientific hypotheses were developed early in the project and were based on a preliminary understanding of the site provided by GOLDER (2003) and Mazurek (2004) and include:

- Site Predictability: near-horizontally layered, undeformed sedimentary shale and limestone formations of large lateral extent;

- Multiple Natural Barriers: multiple low permeability bedrock formations enclose and overlie the DGR;
- Contaminant Transport is Diffusion Dominated: deep groundwater regime is ancient showing no evidence of glacial perturbation or cross-formational flow;
- Seismically Quiet: comparable to stable Canadian Shield setting;
- Geomechanically Stability: selected DGR limestone formation will provide stable, virtually dry openings;
- Natural Resource Potential is Low: commercially viable oil and gas reserves are not present; and
- Shallow Groundwater Resources are Isolated: near-surface groundwater aquifers are isolated from the deep saline groundwater system.

Evidence gathered through site-specific investigation and Geosynthesis studies that contribute to the testing and understanding of these hypotheses is summarized in Chapter 8.

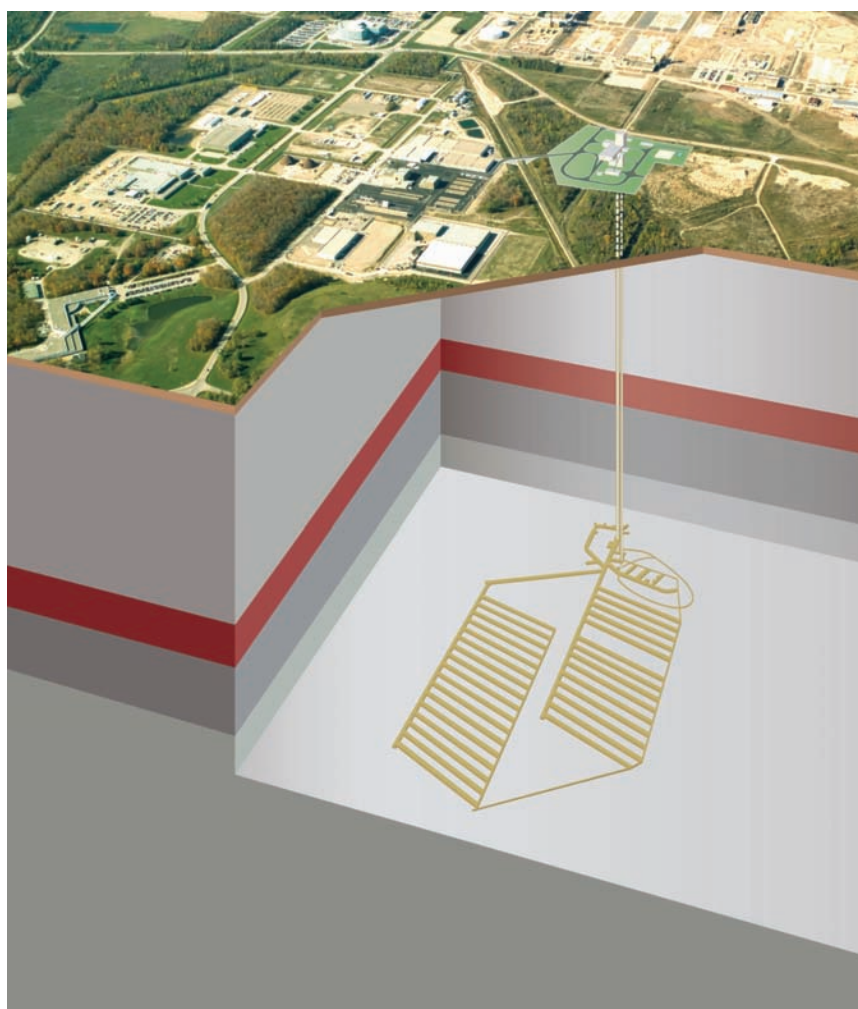


**Figure 1.3: Conceptual Layout of the DGR below the Bruce Nuclear Site**

## 1.4 Report Structure

This report is divided into nine (9) chapters, the details of which are summarized below.

- Chapter 1 provides an introduction to the DGR Project and the Geosynthesis program background and work scope;
- Chapter 2 provides a synthesis of the understanding of the deep sedimentary formations at the regional and site scale. Regional studies provide the framework for understanding and extrapolation of site conditions beyond the Bruce nuclear site boundary. Site geology includes results from the detailed programs carried out during the site characterization program.
- Chapter 3 presents a review and summary of regional and site specific geomechanical properties and in situ stress regime for the sedimentary sequence as it occurs in the Michigan Basin and at the Bruce nuclear site.
- Chapter 4 presents an understanding of the nature and timing of physical and chemical processes that have operated to define the chemical characteristics, including stable isotopes, of the natural water.
- Chapter 5 presents a numerical groundwater system analysis at basin, regional and Bruce nuclear site scales. The simulations performed examine issues surrounding parameter uncertainty, boundary condition uncertainty and realizations, variable groundwater density, glaciation, site-specific analogues (i.e., abnormal hydraulic heads) and 'what if' scenarios.
- Chapter 6 provides a prediction of the future evolution of the Bruce nuclear site and how the repository and surroundings will respond to: (i) repository induced disturbances, and (ii) externally induced disturbances over the next million years.
- Chapter 7 describes the attributes of the DGR host and bounding rock formations. The section draws together different lines of evidence as to why these rocks are a suitable host for the DGR. It describes the important attributes of: (a) the Cobourg Formation (host rock for the DGR), (b) the cap rocks (Ordovician shales), and (c) the lower bounding rocks (Ordovician sequence below the DGR horizon). Comparison is drawn to international repository programs.
- Chapter 8 presents the main findings and conclusions of the Geosynthesis program.
- Chapter 9 cites the references.
- Chapter 10 provides a list of the units used throughout the report.
- Chapter 11 provides a list of abbreviations and acronyms used throughout the report.

## 2. GEOLOGICAL FRAMEWORK

### 2.1 Introduction

This chapter describes the geological environment beneath the Bruce nuclear site at both the regional- and site-scales. The geological description presented in Section 2.2 provides a synthesis of the regional understanding of the deep sedimentary formations of southern Ontario and provides a framework for understanding and extrapolating site conditions beyond the Bruce nuclear site boundary. The site-scale geology presented in Section 2.3 describes the spatial distribution of all important geologic formations and structural features within the Paleozoic (Cambrian to Devonian) and Precambrian bedrock units at the site.

In 2004, the NWMO released a report titled Geoscientific Review of the Sedimentary Sequence in southern Ontario (Mazurek 2004). Although the purpose of this report was to complete an initial assessment of the suitability of the Paleozoic sedimentary rocks of the Michigan Basin within southern Ontario to host a DGR for long-term management of used nuclear fuel, the report's conclusions are equally applicable to a DGR for L&ILW. This assessment concluded that the sedimentary sequence in southern Ontario has favourable and predictable geometry, structure, hydrogeology, stress state (stability), and resistance to geological perturbations for hosting a DGR. Expanding on this work, a regional geology report (AECOM and ITASCA CANADA 2011) provided further support for Mazurek's (2004) assessment and focused on the geological suitability of the Bruce nuclear site to host a DGR for L&ILW. The regional geology report specifically examined aspects of the sedimentary rock relevant to demonstrating long-term repository safety, including host and cap rock predictability (geometry and lithology), structure and stability, and an assessment of economic geology for possible future human intrusion. Additional work programs were undertaken to further expand the geological understanding of the Bruce nuclear site, including assessments of: i) glacial erosion (Hallet 2011), ii) karst distribution (WORTHINGTON 2011), iii) neotectonism (Slattery 2011), iv) Ordovician shale cap rock integrity (Engelder 2011), v) outcrop-scale fractures (Cruden 2011), and integration of the results from all site investigation studies (INTERA 2011). A key outcome of the regional work program was the development of the regional 3D Geological Framework (3DGF) model (Section 2.2.5.2; ITASCA CANADA and AECOM 2011) for an area of approximately 35,000 km<sup>2</sup> surrounding the DGR and defined as the Regional Study Area (RSA) in Figures 2.1 and 2.3. These studies, along with the other data sources listed in Table 2.1 below, were the primary sources of information used to compile Section 2.2. The primary source for the site-scale description in Section 2.3 was the DGSM (INTERA 2011).

The information in this chapter is presented as evidence the Bruce nuclear site possesses key geological attributes which support its suitability to host a DGR, including:

- A predictable **geometry** which includes multiple natural barriers;
- A **seismically quiet** and tectonically stable location;
- A **resistance to geological perturbations** including glacial erosion and karstification; and
- A **low potential for natural resources**.

**Table 2.1: Overview of Referenced Databases Contributing to This Geological Synthesis**

Reference Study	Data Sources
<b>Regional Geology Southern Ontario</b>	<ul style="list-style-type: none"> <li>▶ Oil, Gas, and Salt Resources Library (OGSR) - Petroleum Wells Subsurface Database (OGSR 2004 and OGSR 2006) <ul style="list-style-type: none"> <li>• 299 of 341 wells identified within the RSA were used to build the 3DGF model</li> </ul> </li> <li>▶ Ontario Geological Survey (OGS) Digital Bedrock Geology of Ontario Seamless Coverage MRD 219 (Armstrong and Dodge 2007)</li> <li>▶ Michigan State Geological Survey mapping and Petroleum Well Database (MSGs 2007)</li> <li>▶ OGS Digital Bedrock topography and overburden thickness mapping, southern Ontario – Miscellaneous Data Release no. 207 (Gao et al. 2006)</li> <li>▶ National Oceanic and Atmospheric Administration (NOAA) digital bathymetry mapping of Lake Huron and Georgian Bay</li> <li>▶ An Assessment of Long-Term Climate Change (Peltier 2011)</li> <li>▶ An Assessment of the Cap Rock Integrity at the DGR (Engelder 2011)</li> <li>▶ An Assessment of the Maximum Amount of Future Glacial Erosion on the Bruce Peninsula (Hallet 2011)</li> <li>▶ An Assessment of Karst in Paleozoic Strata at the Proposed DGR (WORTHINGTON 2011)</li> <li>▶ An Assessment of Neotectonics near the Bruce nuclear site (Slattery 2011)</li> <li>▶ The remaining data sources were published literature, government reports (i.e., Geological Survey of Canada (GSC), Ontario Ministry of Natural Resources (MNR) and OGS, e.g., OGS 1991), and consulting reports. These data sources were useful for confirming lateral extent and predictability of geological units across the study area, as guidance for understanding detailed stratigraphic relationships in the subsurface, and for understanding current ideas on the tectonic evolution and setting of this portion of the Michigan Basin.</li> </ul>

## 2.2 Regional Geology

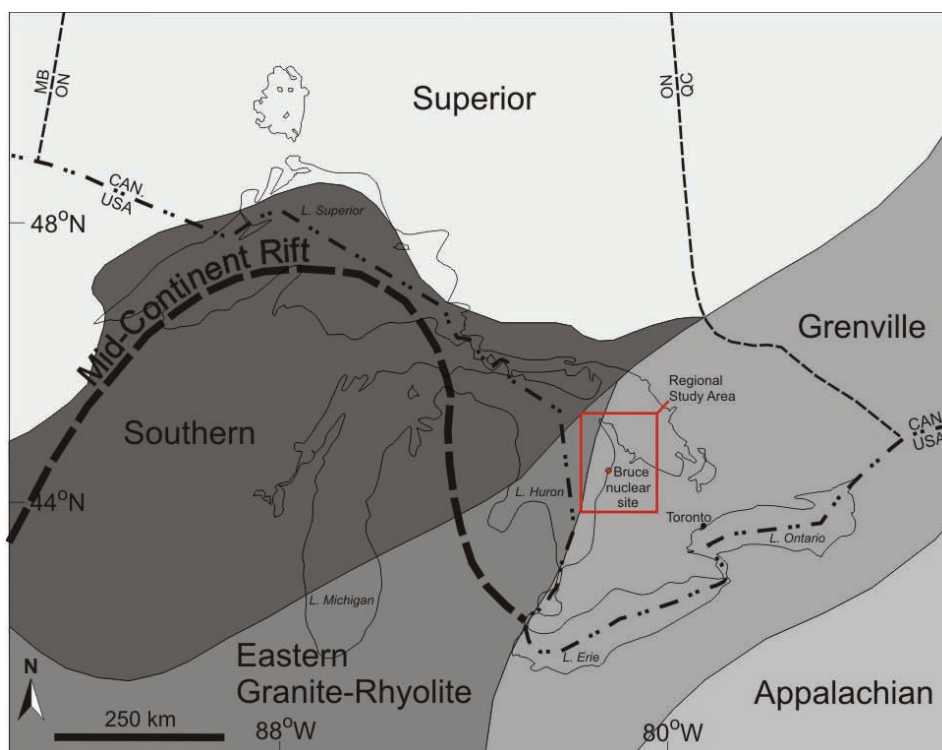
### 2.2.1 Introduction

The purpose of this section on regional geology is to present a synthesis of our understanding of the deep sedimentary formations and their underlying Precambrian basement foundation at the regional scale. In particular, this section describes the regional geologic setting surrounding the Bruce nuclear site in the context of its structural geology, tectonics, basin history, sedimentology, thermal history, depth of burial, economic resources, and glacial history – including erosion and isostatic rebound.

### 2.2.2 Geological Setting

Southern Ontario is underlain by Upper Cambrian (~510 Ma) to Devonian/Mississippian (354 Ma) sedimentary rocks resting unconformably upon Precambrian (ca. 1600 - 540 Ma) basement in the Great Lakes Basin region of North America (Figures 2.1 to 2.4). The basement beneath much of southern Ontario is characterized by gneisses and metamorphic rocks of the Grenville Province of the Canadian Shield (Carter and Easton 1990). Older Precambrian rocks occur to the north and west of the Grenville Province and are also projected, based on seismic

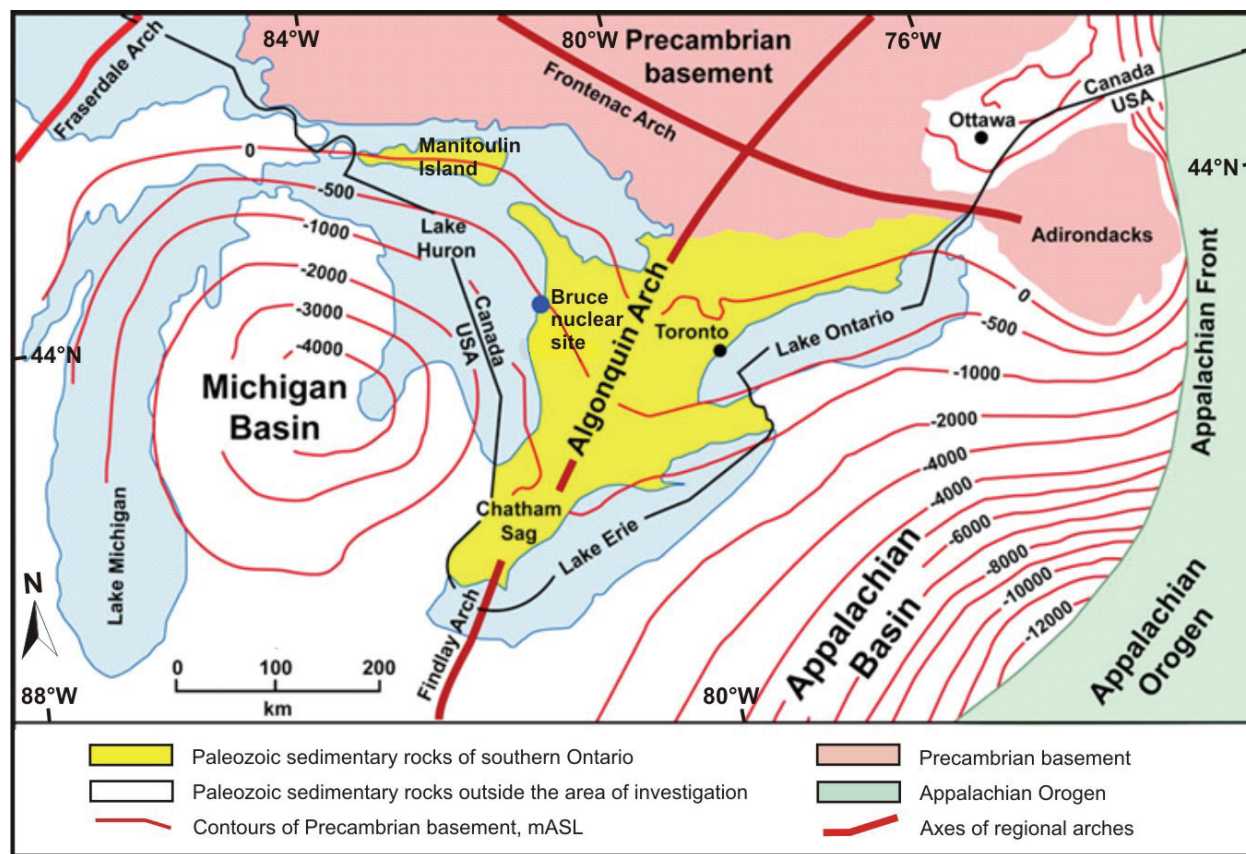
reflection studies, to extend beneath it to the base of the continental crust (e.g., Culotta et al. 1990, White et al. 2000).



Notes: Regional study area boundary and Bruce nuclear site location are also indicated. Figure is modified from Thurston (1991).

**Figure 2.1: Basement Tectonic Subdivisions of the Great Lakes Basin Region**

The overlying Paleozoic succession was deposited northwestward of the Appalachian Orogen (Figure 2.2), a mountain chain that formed during the protracted closure of the Iapetus Ocean and assembly of the Pangaeen Supercontinent (e.g., Williams and Hatcher 1982). Southwestern Ontario is underlain by two main paleo-depositional centres referred to as the Appalachian (Alleghenian) and Michigan Basins (Figure 2.2). The former is a foreland basin to the Appalachian orogen while the latter is a broadly circular intracratonic basin. These basins are separated by the northeast-trending Algonquin and Findlay arches which, along with the intervening east-southeast-trending Chatham Sag structural depression, define a regional basement high beneath southwestern Ontario (Figure 2.2). The Michigan Basin is also bounded, along its northwestern and northeastern flanks respectively, by the Fraserdale and Frontenac arches (Figure 2.2). These arches acted as structural and topographic controls on depositional patterns during the Paleozoic Era, rising and falling with respect to the Michigan and Appalachian Basins in response to vertical epeirogenic movements, horizontal tectonic forces, and subduction at the orogenic front (Quinlan and Beaumont 1984, Coakley and Gurnis 1995, Leighton 1996, Howell and van der Pluijm 1999, Nadon et al. 2000).

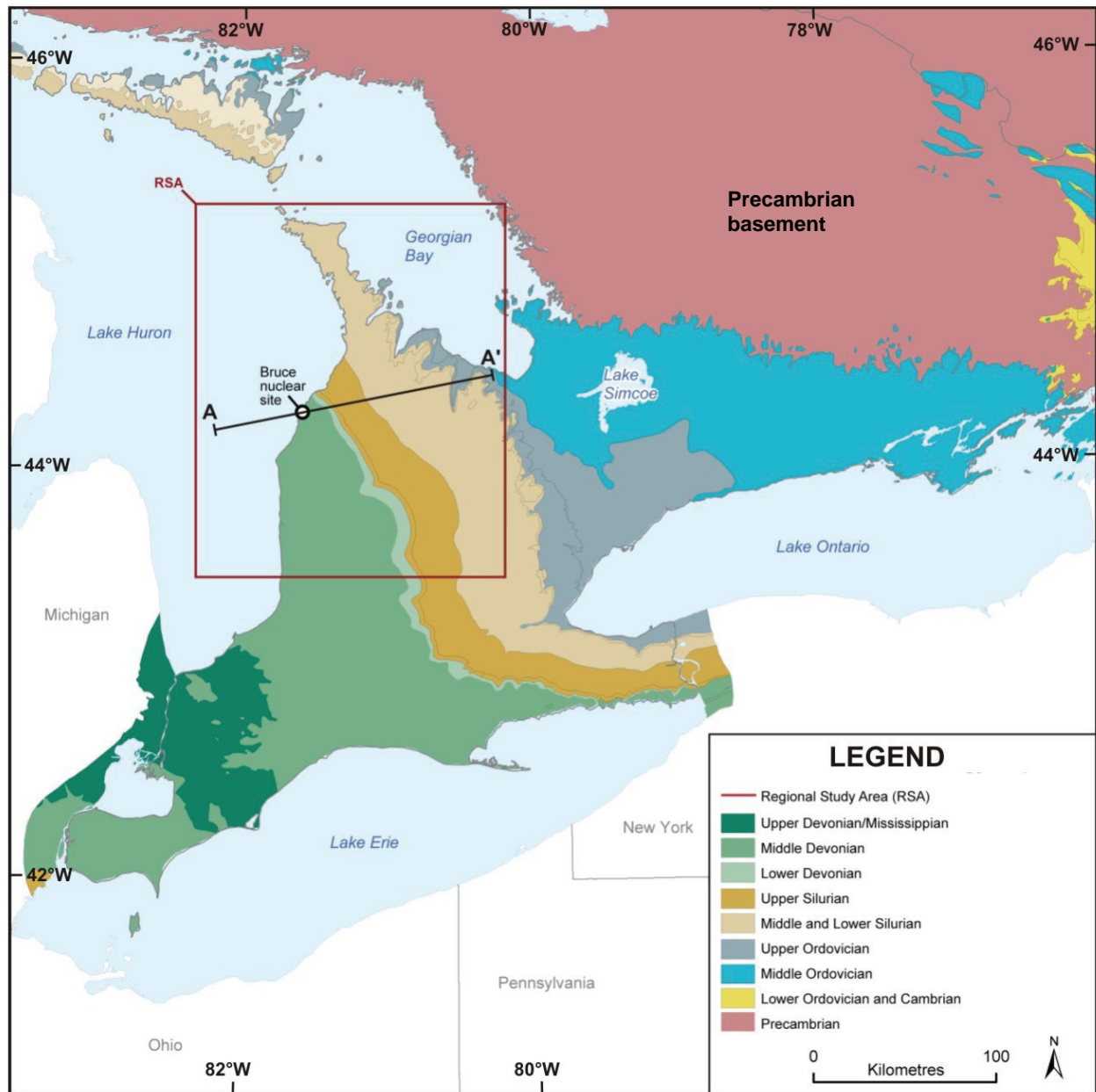


Notes: Figure is modified from Johnson et al. (1992).

**Figure 2.2: Geological Features of Southern Ontario**

The Paleozoic succession thins from a maximum of approximately 4,800 m at the centre of the Michigan Basin to approximately 850 m on the flank of the Algonquin Arch. In general, the strata dip very gently to the west or southwest throughout the region, with the oldest rocks cropping out against the Precambrian basement to the north and east and the youngest (Jurassic) rocks preserved in the basin centre (Figures 2.2 to 2.4). Figure 2.4 presents a geological cross-section through the Michigan Basin highlighting the west-southwesterly dip of the Paleozoic succession from the Niagara Escarpment in the east through the Bruce nuclear site to the west. Note that the vertical exaggeration, implemented in order to show the distribution of stratigraphy across the basin, also artificially exaggerates the dip magnitude. In reality, the Paleozoic succession throughout the RSA dips west-southwesterly at between 0.23 and 1° (e.g., Watts et al. 2009), as shown in the unexaggerated section in the lower inset of Figure 2.4.

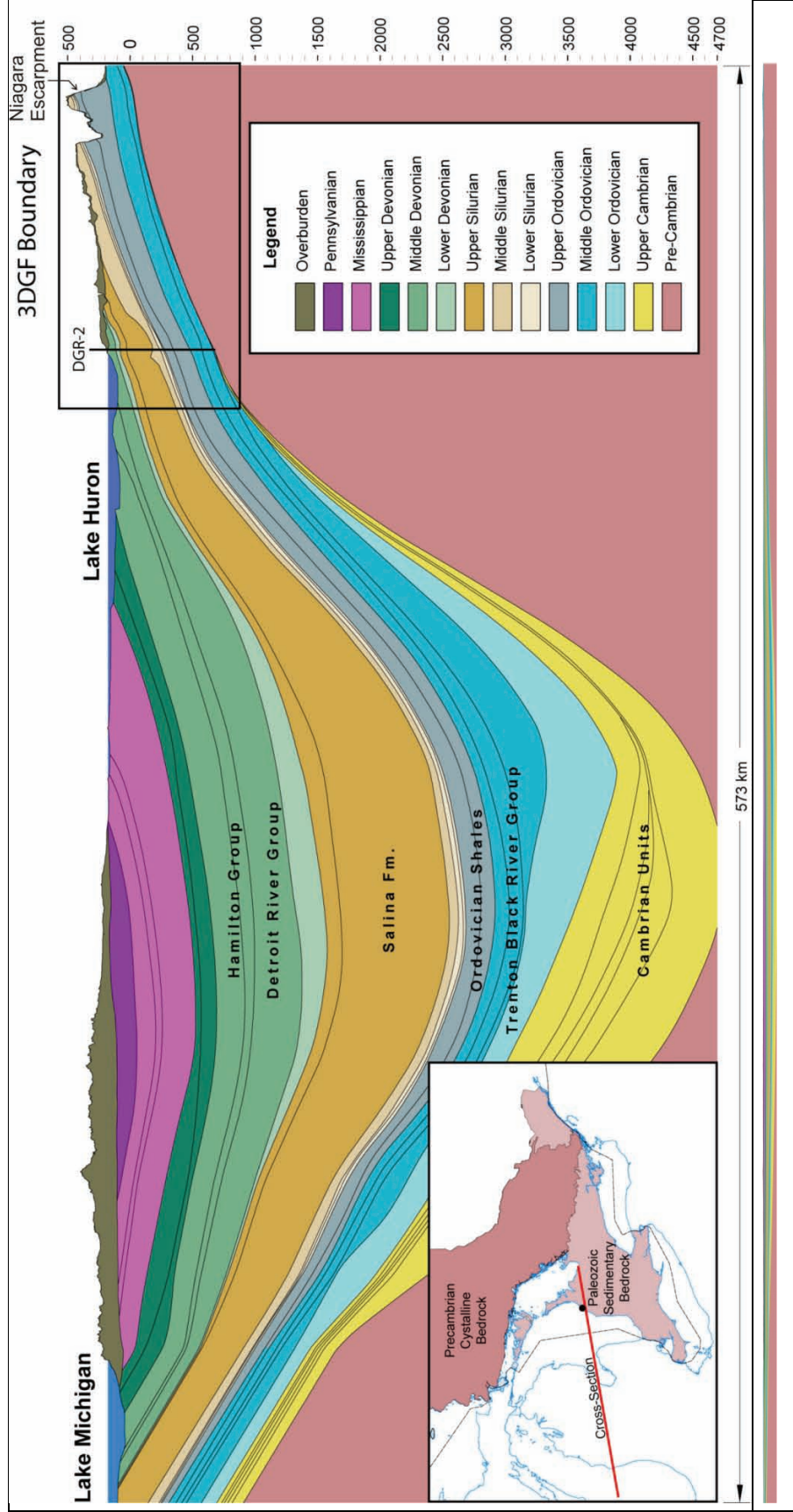
Major tectonic zones in southern Ontario are defined by extrapolation of exposed basement structural boundaries beneath the Paleozoic cover (Figure 2.5). The process is aided by seismic, aeromagnetic, and gravity map interpretation (e.g., Wallach et al. 1998, Boyce and Morris 2002), and by geochemical, geochronological, and petrographic analyses of samples recovered from drill cuttings and core (Carter and Easton 1990, Easton and Carter 1995, Carter et al. 1996).



Notes: Section along line A-A' is shown in Figure 2.23. See Figure 2.8 for detailed stratigraphic nomenclature of the mapped region. Modified from the OGS bedrock geology map (OGS 1991).

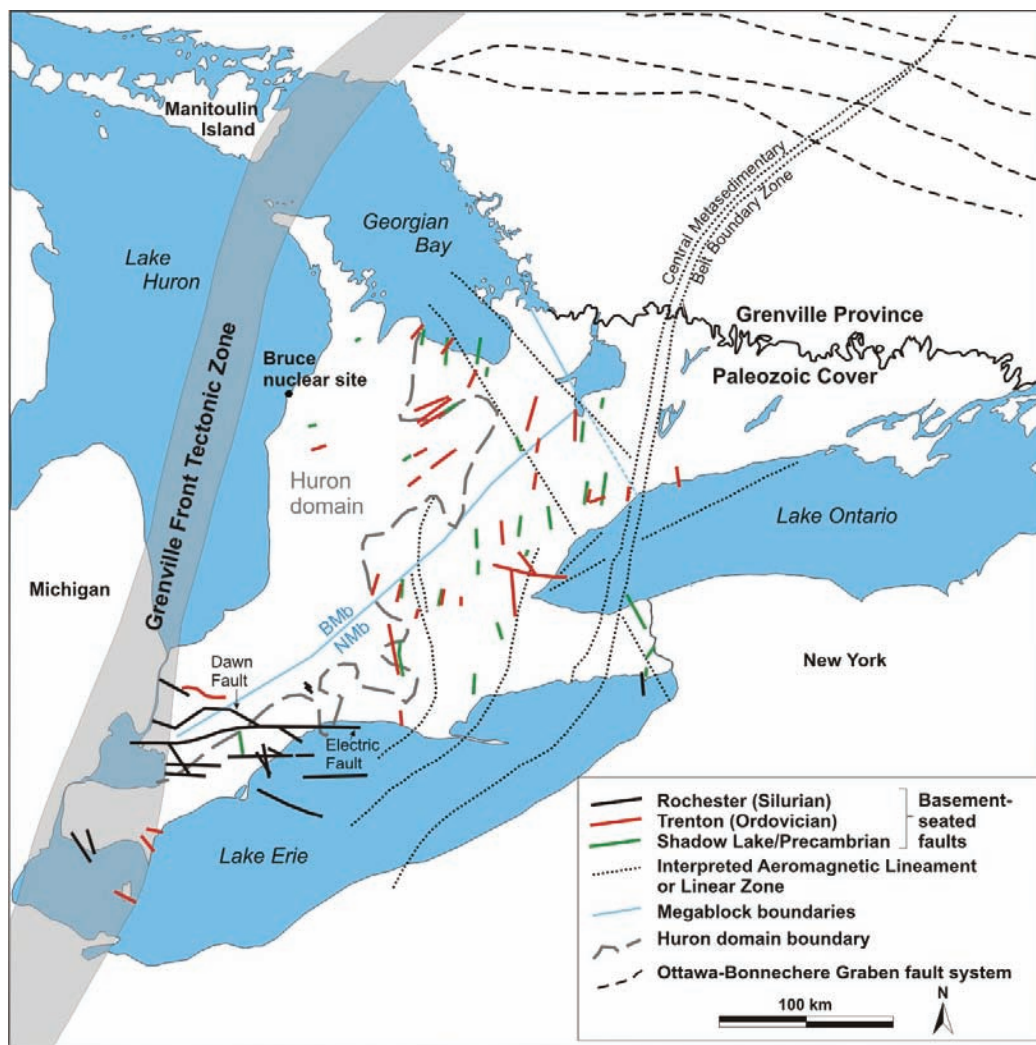
**Figure 2.3: Generalized Paleozoic Bedrock Geology Map of Southern Ontario**





Notes: Vertical axis is elevation measured in metres above sea level. Mesozoic rocks overlying the Pennsylvanian sediments are too thin and discontinuous to be shown on section. Location of borehole DGR-2 at the Bruce nuclear site is projected onto section. Upper right region within box indicates the approximate 3DGF boundary region shown in more detail in Figure 2.23. Lower left indicates the line of the cross-section. Vertical exaggeration is approximately 45x. Lower box shows the same cross-section with its geometry unexaggerated.

**Figure 2.4: Geological Cross-section through the Michigan Basin**

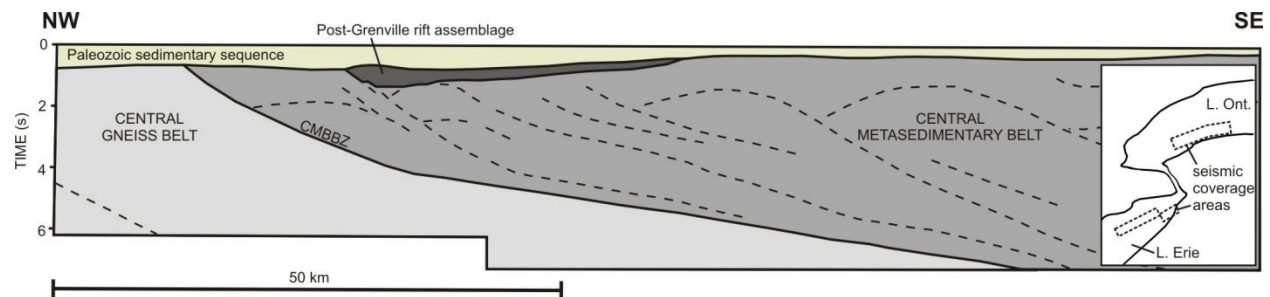


Notes: Contacts are based on field mapping and interpretations aided by subsurface drilling, borehole stratigraphic correlation, and aeromagnetic and gravity imaging (Liberty and Bolton 1971, and compiled from Brigham 1971, Bailey and Cochrane 1984a, Bailey and Cochrane 1984b, Sanford et al. 1985, Carter and Easton 1990, Sage 1991, Jacobi and Fountain 1993, Easton and Carter 1995, Carter et al. 1996, Wallach et al. 1998, Ketchum and Davidson 2000, Boyce and Morris 2002). AMB: Akron Magnetic Boundary; NPLZ: Niagara-Pickering Linear Zone; HLEL: Hamilton-Lake Erie Lineament; BTL: Burlington-Toronto Lineament; PL: Hamilton-Presqu'ile Lineament; GBLZ: Georgian Bay Linear Zone; EF: Electric fault; DF: Dawn fault; BMB - Bruce Megablock; NMB - Niagara Megablock.

**Figure 2.5: Interpreted Boundaries and Fault Contacts in Southern Ontario**

The most prominent aeromagnetic features are the southwestward continuation of the Grenville Front Tectonic Zone (GFTZ), which defines the westernmost boundary of the Grenville Province and the Central Metasedimentary Belt Boundary Zone (CMBBZ; Figure 2.5). The CMBBZ is an internal boundary within the Grenville Province that separates rocks of the Central Gneiss Belt to the northwest from rocks of the Central Metasedimentary Belt to the southeast (Carter and Easton 1990). The southwestward extension of the CMBBZ coincides with the Niagara-Pickering linear zone and the Akron-Magnetic boundary. It also parallels the Hamilton-Lake Erie lineament and is transected by the Burlington-Toronto and Hamilton-Presque Ile

lineaments, all of which are aeromagnetically interpreted features of the Precambrian basement (Boyce and Morris 2002; Figure 2.5). It should be noted that the GFTZ and CMBBZ are ancient (ca. 1000 Ma) tectonic boundaries. There is evidence that faults spatially coincident with the surface trace of the GFTZ in the area proximal to and south of the Findlay Arch (Figure 2.2) were active during Paleozoic orogenesis (Ramsey and Onasch 1999). However, in southern Ontario the basement structures appear to have remained relatively stable at least since the earliest Paleozoic (e.g., Figure 2.6; Milkereit et al. 1992).



Notes: Section is based on interpretation of seismic profiles from within the coverage areas shown in inset map. CMBBZ: Central metasedimentary belt boundary zone. Figure is modified from Milkereit et al. (1992).

**Figure 2.6: Composite Seismic Section Showing Basement Geometry from the Lake Erie and Lake Ontario Regions**

The RSA is underlain by the Huron domain of the Central Gneiss Belt (Carter and Easton 1990, Carter et al. 1996; Figure 2.5). This domain was defined based on analysis of drill cuttings and core samples from boreholes that penetrated the basement, as well as interpretation of geophysical datasets (Carter and Easton 1990). The irregularly shaped Huron domain boundary trends northeasterly and encloses a region characterized by a featureless Bouguer gravity signature and a broad low-intensity aeromagnetic pattern (Boyce and Morris 2002).

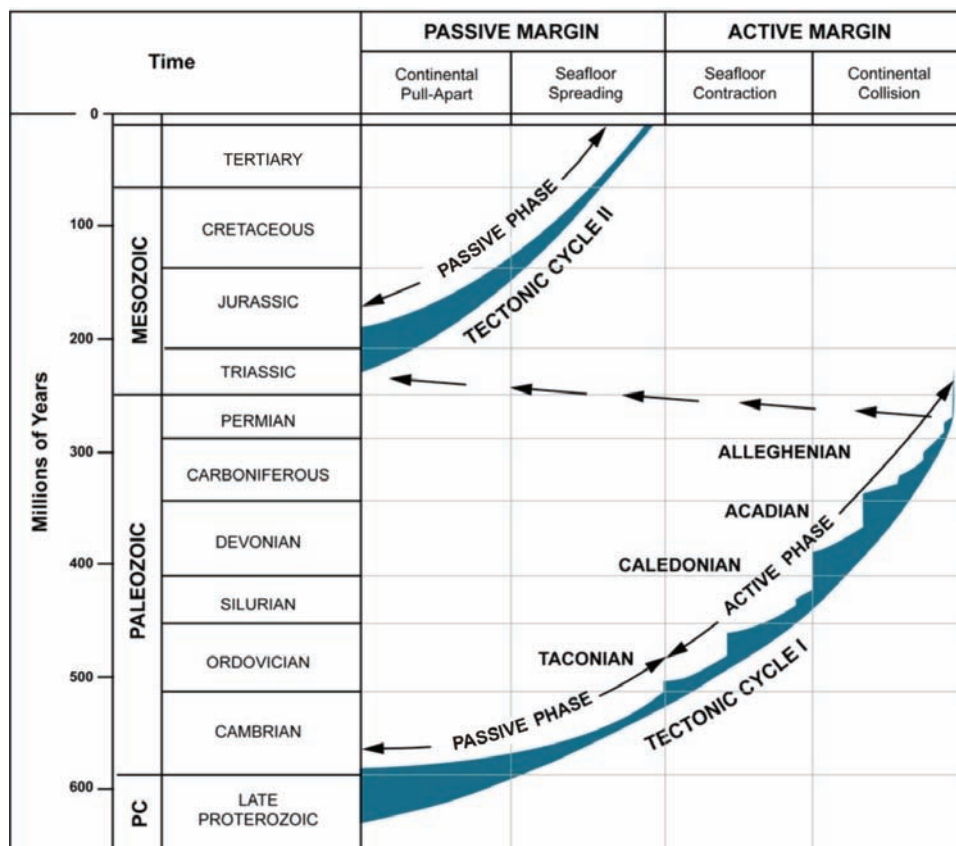
The Huron domain corresponds roughly with the triangular Bruce Megablock as defined by Sanford et al. (1985; Figure 2.5). In the conceptual model of Sanford et al. (1985) for southern Ontario, the Bruce Megablock was distinguished as a distinct tectonic unit with a simple ESE-trending fracture network controlled by re-activation of pre-existing basement faults. The megablock model was based on satellite lineament mapping of the Precambrian shield in conjunction with interpretation of subsurface data from southern Ontario. The tectonic significance of this megablock structure is unclear and the Grenville basement features described in the previous paragraph do not appear to exert a clear control on the distribution of the overlying sedimentary rocks within the RSA.

Regardless of the validity of the megablock concept of Sanford et al. (1985), present day and historical earthquake distribution data support the interpretation that the basement beneath the RSA is presently tectonically quiescent (Park and Jaroszewski 1994, van der Pluijm and Marshak 2004, Percival and Easton 2007). Tectonic complexity increases to the south of the RSA where the surface trace of the Paleozoic-aged Dawn and Electric faults, along with other unnamed brittle structures, are concentrated (Figure 2.5). Here, several orientations of basement fracture sets are interpreted to have imparted a significant control on the distribution

of Paleozoic faults (Sanford et al. 1985). Some of the largest hydrocarbon pools in southwestern Ontario are proximal to these faults and their eastern extension along the northeastern shoreline of Lake Erie (e.g., Legall et al. 1981, their Figure 3; OGSR 2004). This relationship suggests that basement relief and structure in this area exerted a controlling influence on the development of trapping mechanisms and reservoirs in the Paleozoic strata (Sanford et al. 1985, Carter et al. 1996). The distribution and movement history of faults throughout southern Ontario is discussed in further detail in Section 2.2.6.

### 2.2.3 Tectonic Evolution of Southern Ontario

The tectonic evolution of southern Ontario has occurred over the last approximately 1210 Ma. The first half of this period involved the development of the Precambrian basement. During this time, a series of tectonic events, structural uplift, erosion, burial, faulting, and intrusion occurred. The Phanerozoic stage of evolution was influenced by a complex history of Paleozoic to Mesozoic tectonism. Figure 2.7 and Table 2.2 summarize the stages of tectonic evolution for southern Ontario.



Notes: Figure is from Sanford et al. (1985).

**Figure 2.7: Phanerozoic Tectonic Cycles with Band Widths Representing Relative Tectonic Intensity**

**Table 2.2: Timetable of Major Tectonic Events in Southern Ontario**

<b>Time Interval Before Present (Ma)</b>	<b>Tectonic Activity</b>	<b>Reference</b>
1210 – 1180	Regional metamorphism in CMBBZ (proto-Grenville)	Easton 1992, Lumbers et al. 1990, Hanmer and McEachern 1992
1109 – 1087	Magmatism and formation of Midcontinent Rift	Van Schmus 1992
1030 – 970	Main phase of Grenville Orogeny	Carr et al. 2000, White et al. 2000
970 – 530	Extensional rifting and opening of the Iapetus Ocean	Thomas 2006
530 – 320	Subsidence of Michigan Basin and Uplift of Frontenac and Algonquin Arches (episodic)	Howell and van der Pluijm 1999, Sanford et al. 1985, Kesler and Carrigan 2002
470 – 440	Taconic Orogeny <ul style="list-style-type: none"> <li>E-W to NW-SE compression, uplift (Frontenac and Algonquin Arches)</li> </ul>	Quinlan and Beaumont 1984, Sloss 1982, McWilliams et al. 2007
410 – 320	Caledonian/Acadian Orogeny <ul style="list-style-type: none"> <li>E-W to NW-SE compression, uplift (Frontenac and Algonquin Arches)</li> </ul>	Gross et al. 1992, Marshak and Tabor 1989, Sutter et al. 1985, Kesler and Carrigan 2002
300 – 250	Alleghenian Orogeny <ul style="list-style-type: none"> <li>E-W to NW-SE compression</li> </ul>	Gross et al. 1992, Engelder and Geiser 1980
200 – 50	<ul style="list-style-type: none"> <li>opening of the Atlantic Ocean</li> <li>St. Lawrence rift system created</li> <li>reactivated Ottawa-Bonnechere Graben</li> <li>NE-SW extension</li> <li>uplift</li> </ul>	Kumarapeli 1976, 1985
50 – Present	<ul style="list-style-type: none"> <li>NE-SW compression (from ridge push)</li> <li>post-glacial uplift</li> </ul>	Barnett 1992

### 2.2.3.1 Precambrian Tectonic History

The Precambrian tectonic history of southern Ontario records events occurring since ca. 1210 Ma ago and culminating with the development and subsequent extensional collapse of the Grenville Orogen. Older tectonic events, including the 2.7 Ga Kenoran Orogeny, and the 2.0 - 1.7 Ga Trans-Hudson/Penokean Orogen, built the Laurentian (proto-North American) craton upon which Grenville deformation was imprinted. The earliest phase of Grenville orogenesis is associated with regional metamorphism in the CMBBZ, ca. 1210 to 1180 Ma (Easton 1992). This was followed by a continent-scale rifting event between ca. 1109 to 1087 Ma that generated voluminous magmatism in the form of intrusive mafic dykes and sills and extrusive basaltic flows now preserved in linked graben structures along the Midcontinent Rift system (Figure 2.1; Van Schmus 1992). Rifting was aborted by the onset of tectonic shortening during the main phase of the Grenville Orogeny ca. 1030 to 970 Ma (Table 2.2;

Carr et al. 2000, White et al. 2000). This widespread regional event was characterized in southern Ontario by thrusting of Grenville Province rocks northward upon the Superior and Southern provinces and formation of a Himalayan-style mountain belt on the southeastern margin of Laurentia (White et al. 2000, Percival and Easton 2007).

Post-Grenville extension associated with the initial opening of the Iapetus Ocean began approximately 750 Ma (Thomas 2006 and references therein). Rifting continued into the earliest Cambrian, eventually developing a passive margin along the northwestern edge of the ocean basin (the southeastern margin of Laurentia). At this time, compressional features were re-activated in extension and locally developed into large-scale rift zones, including the Ottawa-Bonnechere graben system (e.g., Thomas 2006; Figure 2.5). Apart from localized periodic reactivation of some of these rift structures during the Mesozoic Era (after 250 Ma), the Grenville Province in southern Ontario is presently considered to be a tectonically stable part of the North American craton (e.g., Percival and Easton 2007).

### 2.2.3.2 Paleozoic Tectonic History

Precambrian to Cambrian rifting marked the beginning of the passive phase of Paleozoic Tectonic Cycle I (Figure 2.7) and correlates with the initial episode of subsidence and deposition within the Michigan Basin (Sanford et al. 1985). This cycle was terminated in the early Middle Ordovician during regional uplift and development of the Knox unconformity which caused differential erosion of the basal cover rocks and locally exposed the underlying Precambrian basement. The variable surface geometry of the pre-existing basement, in combination with uplift and erosion, imparted an irregular topography to the paleosurface (e.g., Andjelkovic and Cruden 1998). In southern Ontario, the unconformity is overlain by rocks of Cambrian age, where they are preserved, or rocks of the early Middle Ordovician Black River Group where the Cambrian is absent (Armstrong and Carter 2006).

The Middle Ordovician to Devonian-Mississippian sedimentary succession preserved in southern Ontario reflects the complex interaction between regional-scale tectonic forces, sedimentation, and eustatic sea level fluctuations associated with the Appalachian-Caledonian orogen (Johnson et al. 1992, Sanford 1993). Three pulses of tectonic activity constitute the active phase of Tectonic Cycle I (Figure 2.7), including the Taconic (Ordovician), Caledonian/Acadian (Silurian-Devonian) and Alleghenian (Carboniferous-Permian) events (Sanford et al. 1985). They are contemporaneous with variations in regional depositional patterns within the episodically subsiding Michigan Basin and are linked to vertical movement of the Findlay-Algonquin arch system (Sanford et al. 1985; Howell and van der Pluijm 1990, 1999; Coakley and Gurnis 1995; Nadon et al. 2000). The Taconian Orogeny in particular played a dominant role in the development of the upper Middle to Upper Ordovician host, cap, and seal rocks of the proposed DGR. The Caledonian, Acadian, and Alleghenian orogenies are interpreted to have played an important role in diagenetic fluid migration (e.g., Bethke and Marshak 1990, Kesler and Carrigan 2002). In general, the regional maximum principal stress at that time is interpreted to have been northwesterly oriented in accordance with the direction of thrust motion along the Appalachian tectonic front and the pattern of loading in the orogenic foreland (Beaumont et al. 1988, NWMO and AECOM 2011).

The Taconic Orogeny is characterized by large-scale eastward-tilting of the Laurentian margin and departure of the depositional geometry of the Michigan Basin from its concentric, basin-centered pattern (Coakley et al. 1994, Coakley and Gurnis 1995, Howell and van der Pluijm 1999). This allowed for deposition of the laterally extensive Ordovician limestone and overlying shale successions. A regionally recognized bentonite layer

dated at ca. 454 Ma is interpreted as ash fall preserved from major (calc-alkaline) volcanic activity that occurred along the southeastern Laurentian margin during Taconic orogenesis (Huff et al. 1992, Kolata et al. 1998).

The Late Silurian (Caledonian phase of the) Acadian Orogeny (Figure 2.7), driven by the collision between the North American and African plates, rejuvenated the Algonquin-Findlay arch system and returned the Michigan Basin to its concentric geometry (e.g., Quinlan and Beaumont 1984, Howell and van der Pluijm 1990). Upper Silurian evaporites of the Salina Group were deposited at this time under restricted marine conditions (Johnson et al. 1992, Armstrong and Carter 2006). A major unconformity reflects emergent conditions at the end of the Silurian.

Foreland loading during the middle to late Devonian characterizes the main pulse of the Acadian event (Figure 2.7). Tectonism was concomitant with renewed platform margin subsidence that allowed another marine incursion into the Michigan Basin across the subdued arch system (Quinlan and Beaumont 1984, Armstrong and Carter 2006). Early Mississippian uplift of the arch system once again starved the Michigan Basin as it regained its concentric form (Quinlan and Beaumont 1984). The Alleghenian Orogeny was the last active tectonic event to stimulate significant sediment deposition in the Appalachian foreland during the Carboniferous, Permian, and likely early Mesozoic times. Thick coal deposits in the Appalachian foreland and in the centre of the Michigan Basin contrast with a lack of sediment accumulation over the arch axis in southern Ontario except proximal to the Chatham Sag.

### **2.2.3.3 Mesozoic-Cenozoic Tectonic History**

Active orogenesis throughout eastern North America during much of the Paleozoic Era transitioned to a passive margin extensional setting when the Atlantic Ocean began to open at the end of the Triassic Period approximately 200 Ma (Figure 2.7). Much of the resulting tectonic activity was concentrated near the continental margin, where Triassic and Lower Jurassic rift basin deposits record the onset of continent break-up (e.g., Lindholm 1978). Further inland, the majority of rift-related deformation and sediment deposition occurred in proximity to the trace of the Appalachian thrust front (Wheeler 1995). However, a thin seam of Late Jurassic sediments is preserved in the centre of the Michigan Basin.

Pre-existing faults, including those of the Neoproterozoic to Early Cambrian (Iapetan) St. Lawrence rift system and the Ottawa-Bonnechere Graben structure (Figure 2.5), were re-activated as a system of NE-striking extensional normal faults and WNW-striking transfer faults (Thomas 2006). These areas of re-activation, all greater than 150 km from the Bruce nuclear site, remain seismically active to the present day (Kumarapeli and Saull 1966, Adams and Basham 1991, see also Section 2.2.6.5 on regional seismicity).

Mesozoic magmatic activity in eastern North America is marked by kimberlites and other mafic intrusions within the Canadian Shield (Heaman and Kjarsgaard 2000), and the alkaline intrusion of the ca. 130-110 Ma Monteregian Hills and White Mountain magma series, which are the most prominent features of the New England-Quebec igneous province (McHone and Butler 1984), and the offshore basaltic New England Seamounts (McHone 1996). These magmatic events may record the Jurassic to Cretaceous northwesterly movement of North America as it passed above the Great Meteor Hotspot (e.g., Crough 1981, Legall et al. 1981, Morgan 1983, Heaman and Kjarsgaard 2000). Other magmatic activity includes Middle Jurassic ultramafic dykes dated at 173 Ma (K-Ar method; Barnett et al. 1984) which intrude Middle Ordovician strata in the Picton Quarry, Ontario. Dyke emplacement is believed to be related to fault reactivation and the

dykes are also interpreted to have been offset by E-trending brittle strike-slip faults (McFall 1990). Late Jurassic ultramafic dykes in the Finger Lakes region of New York State are spatially coincident with the Clarendon-Linden fault system to the south of Lake Ontario (Heaman and Kjarsgaard 2000). The majority of recognized Mesozoic magmatic activity is localized around pre-existing faults which are presently at a considerable distance away (> 150 km) from the RSA and the Bruce nuclear site in particular. No evidence exists that would suggest Mesozoic or younger magmatic activity has occurred within the RSA.

A Late Cretaceous to Eocene global-scale plate re-organization event resulted in the transition from northwesterly to west-southwesterly North American motion (Minster and Jordan 1978, Rona and Richardson 1978, Gordon and Jurdy 1986). Contemporaneous onset of southwest-northeast spreading in the North Atlantic may have initiated the east-northeast-oriented compressional stress field that controls the neotectonic evolution of eastern North America (Sbar and Sykes 1973, Zoback and Zoback 1989). A regionally persistent east-northeast-trending joint set is one possible manifestation of this contemporary stress (Engelder 1982). There is no indication, based on the present-day plate tectonic framework, that southern Ontario or the surrounding intraplate region will experience any major magmatic or volcanic activity over the next million years.

## **2.2.4 Basement Geology**

### **2.2.4.1 Precambrian**

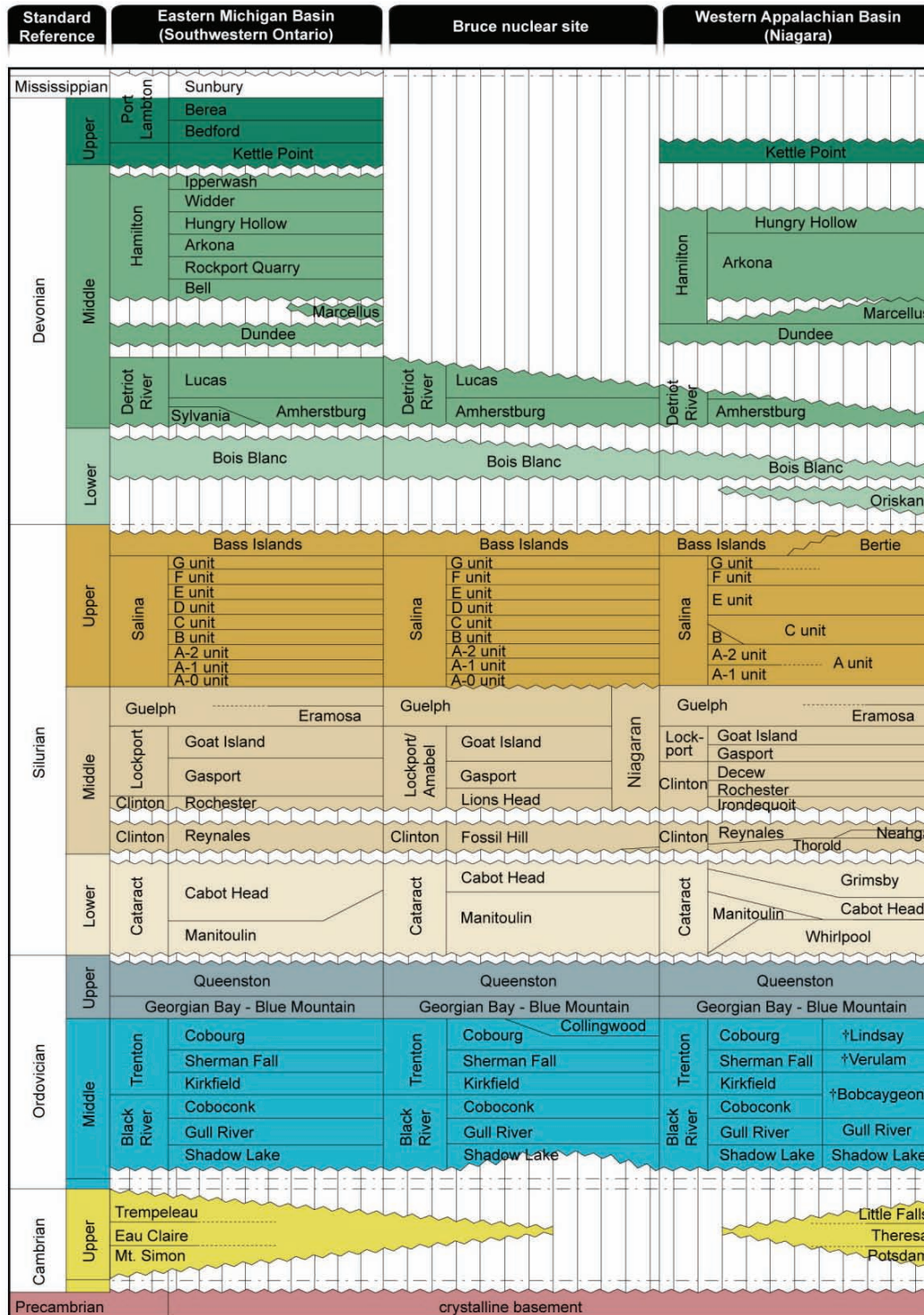
The Grenville Province forms the basement to the Paleozoic rocks in southern and eastern Ontario including beneath the DGR. It contains rocks that vary in age from 2690 to 990 Ma and were deformed and metamorphosed during the Grenville Orogeny (Percival and Easton 2007). Underlying the RSA is the Central Gneiss Belt (Easton and Carter 1995, Carter et al. 1996) (Figure 2.5) of the Grenville Province, which consists of upper amphibolite to granulite facies quartzo-feldspathic orthogneiss with subordinate metasedimentary gneiss (Carter and Easton 1990). This regional lithologic description is consistent with the Precambrian rock described at the DGR as granitic gneiss (see Section 2.3.2). The Central Gneiss Belt is bounded to the southeast by the CMBBZ and to the west-northwest by the GFTZ (Figures 2.5 and 2.6).

## **2.2.5 Sedimentary Bedrock Geology**

### **2.2.5.1 Regional Stratigraphy**

Figure 2.8 illustrates the Paleozoic stratigraphy of southern Ontario at locations within southwestern Ontario in the Appalachian Basin, the Bruce nuclear site, and the Michigan Basin. The oldest Paleozoic rocks in the RSA include a thin veneer of Late Cambrian clastic-dominated sediments unconformably overlying the Precambrian basement. These rocks, deposited during the initial development of the Michigan Basin, pinch out to the east of the RSA along the flank of the Algonquin Arch (e.g., Bailey and Cochrane 1984a, Bailey and Cochrane 1984b). The Cambrian units are unconformably overlain by Ordovician-aged sediments. The Ordovician stratigraphy in the RSA is essentially undeformed and dips gently to the southwest towards the centre of the Michigan Basin. Deposition occurred over a broad carbonate and clastic shelf and platform setting that extended from the eastern margin of the Appalachian Basin to the centre of the continent (Figure 2.9). Deposition during the Silurian, within the subsiding Michigan Basin, produced more complicated basin-centred assemblages which include for example, reef and evaporite facies.





Notes: Includes nomenclature from locations in the Michigan Basin (left), Bruce nuclear site (centre), and Appalachian Basin (right). † indicates outcrop nomenclature for southern and eastern Ontario. Figure is modified from Armstrong and Carter (2006) and based on Winder and Sanford (1972).

**Figure 2.8: Paleozoic Stratigraphic Nomenclature of Southwestern Ontario**

A total of 31 formations, members or units, from Cambrian sandstones at the base to dolostones of the Devonian Lucas Formation at the top, comprise the Paleozoic succession within the RSA proximal to the Bruce nuclear site (Figure 2.8). When the Salina A1, A2, and B units are further divided into evaporite and carbonate sub-units, a total of 34 stratigraphic entities are recognized (Armstrong and Carter 2006).

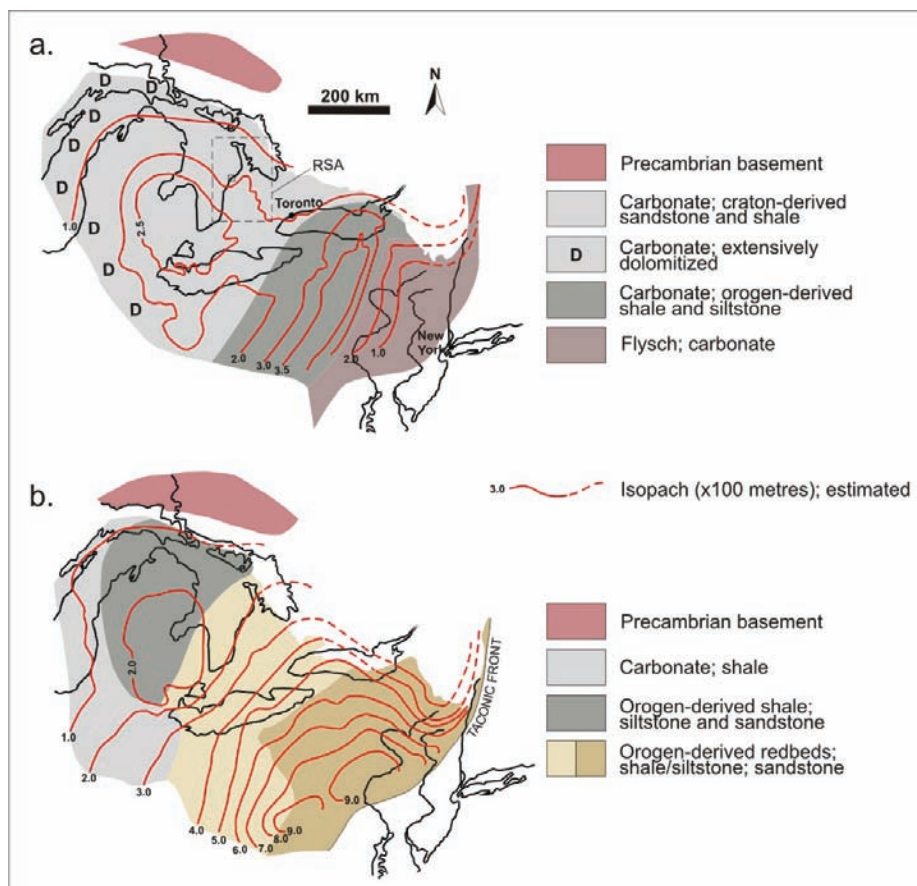
A recently published update of the Paleozoic stratigraphy of southern Ontario includes minor modifications to the terminology of reference ages for the strata as shown in Figure 2.8 (Armstrong and Carter 2010, their Table 3 and accompanying text). The Middle Silurian designation has been removed and now the Upper and Lower Silurian are separated at the top of the Eramosa Member of the Guelph Formation. In addition, the Black River and Trenton groups now comprise the lower portion of the Upper Ordovician Period. Acknowledging these recent re-interpretations, the descriptions below still follow the main sequence stratigraphic associations of Armstrong and Carter (2006) and Johnson et al. (1992) with the exception that herein the Silurian Gasport and Goat Island members of the Lockport Formation are considered to be formations as per Brett et al. (1995), as is the Lions Head Member.

### **Cambrian**

The lithology of the Cambrian units ranges from fine to medium crystalline dolostone, sandy dolostone, and argillaceous dolostone to fine to coarse quartzose sandstone (Hamblin 1999). The Cambrian in southwestern Ontario is dominated by white to grey quartzose, commonly porous sandstone (Armstrong and Carter 2006). In general, the Cambrian deposits are considered to be a succession of marine sandstone and dolostone resulting from transgressive Cambrian seas that flooded across the broad platform of the Algonquin Arch and into the subsiding Michigan Basin (Hamblin 1999). Cambrian deposits extend from the Appalachian Basin to the Michigan Basin but have largely been eroded over the Algonquin Arch (Bailey and Cochrane 1984a, Bailey and Cochrane 1984b, Bailey 2005). Well logs from the MNR petroleum well database and interpretations from Bailey and Cochrane (1984a, 1984b) as well as Carter et al. (1996) suggest that the Cambrian does pinch-out against the Precambrian surface to the east of the Bruce nuclear site. A regional scale unconformity separates the Cambrian sediments from overlying rocks of Middle Ordovician and younger age.

### **Middle Ordovician Carbonates**

In the subsurface of southern Ontario, including the Bruce nuclear site, the Middle Ordovician carbonate-dominated sedimentary package is divided into the Black River and overlying Trenton groups. The Black River Group includes three formations (in ascending order), the Shadow Lake Formation, the Gull River Formation, and the Coboconk Formation, while the Trenton Group is composed of the Kirkfield Formation, the Sherman Fall Formation, and the Cobourg Formation (Figure 2.8). The Cobourg Formation is also known as the Lindsay Formation in surface mapping nomenclature but, with the exception of Table 2.3, this alternate terminology is not used throughout the remainder of the report. The Cobourg Formation is further subdivided based on lithological variation, into an upper unit comprising organic-rich calcareous shale with fossiliferous interbeds termed the Collingwood Member, and a Lower Member comprising argillaceous limestone. Except for Chapter 6, all references to the Cobourg Formation, or simply Cobourg, throughout this report imply reference to the argillaceous limestone Lower Member of the Cobourg Formation only. The Cobourg is the host formation for the proposed DGR project.



Notes: a) Middle Ordovician carbonate-dominated facies (Bruce nuclear site location is marked by black open square within RSA boundary); and b) Late Ordovician facies showing clastic influx into the Michigan Basin during the Taconic Orogeny. Figure is modified from Sanford (1993).

**Figure 2.9: Ordovician Facies and Isopach Thickness Map of the Michigan and Appalachian Basin Regions**

A major marine transgression was responsible for deposition of the Black River and Trenton groups. Facies assemblages generally characterize a succession from supratidal and tidal flat clastics/carbonates to lagoonal carbonates and offshore shallow water and deep shelf carbonates (Coniglio et al. 1990). During deposition of the Black River and Trenton groups eastern North America formed a southeastward-facing shelf passive margin (ramp) (Melchin et al. 1994) located at paleogeographic latitude of approximately  $15^{\circ}$  (Van der Voo 1982). During this period, the Algonquin and Frontenac arches had a very subdued relief caused by subsidence of the Appalachian and Michigan basins. Figure 2.9a presents interpreted regional lithofacies distributions, with isopach thicknesses, of the Middle Ordovician units (Sanford 1993).

The facies model (tropical, arid shelf and ramp depositional environment) used to explain the Black River and Trenton limestone is well understood from modern carbonate-forming environments, which provide an understanding of the lateral and horizontal extent of large-scale facies assemblages (lithology changes at formation scales) within the Ordovician rocks. This lateral extent is confirmed by outcrop and well data across Ontario. Brookfield and Brett (1988)

describe the Arabian (Persian Gulf) and Sahul (Southeast Asia) shelves as two modern examples closest to the Black River and Trenton seas. Deposition of the Middle Ordovician Trenton carbonates was in response to the collision of the passive Laurentian margin with an island arc system during the onset of the Taconic Orogeny (Figure 2.7). This event resulted in foreland loading and eastward tilting at the continental margin which in turn caused flooding and then eventual submergence of the platform of the Trenton Group (Quinlan and Beaumont 1984, Hamblin 1999). Eastward tilting of the Michigan Basin and northwesterly migration of the Taconic structural front led to the progressive inundation of the Trenton carbonates by Upper Ordovician clastic sediments from the evolving orogen (Hamblin 1999).

The rock types described for the succession of Ordovician carbonates in Ontario range from coarse-grained bioclastic limestone to carbonate mudstone and dolostone with interbedded calcareous and non-calcareous shale. Individual facies exhibit vertical and lateral variability. However, the facies assemblages are predictable in range of lithology and general thickness trends, and well documented regionally (AECOM and ITASCA CANADA 2011). Although small-scale lithofacies changes occur everywhere, major lithologies of the key DGR units are described consistently over large lateral distances. The following sections briefly overview the formation-scale lithology of the Black River and Trenton groups.

The Shadow Lake Formation, at the base of the Black River Group, is characterized by poorly sorted, red and green sandy shales, argillaceous and arkosic sandstones, minor sandy argillaceous dolostones and rare basal arkosic conglomerate (Armstrong and Carter 2006). The lower part of the overlying Gull River Formation consists mainly of light grey to dark brown limestones and the upper part of the formation is very fine grained. Thin shale beds and partings may be present (Armstrong and Carter 2006). The Coboconk Formation, at the top of the Black River Group, is composed of light grey-tan to brown-grey, medium to very thick bedded, fine to medium grained bioclastic limestones. A distinctive bentonite marker horizon, or set of closely spaced horizons of variable thickness and representing altered volcanic ash, is commonly observed near the top of the Coboconk Formation across a broad region of eastern Laurentia (Huff et al. 1992, Kolata et al. 1998).

The lowest interval of the Trenton Group is the Kirkfield Formation. It is characterized by fossiliferous limestones with shaley partings and locally significant thin shale interbeds. The overlying Sherman Fall Formation ranges in lithology from dark grey argillaceous limestones interbedded with calcareous shales, found lower in the formation, to grey to tan bioclastic, fossiliferous limestones that characterize the upper portions of the unit.

The overlying Cobourg Formation is described regionally (Table 2.3) as a grey, fine-grained limestone to argillaceous limestone with coarse-grained fossiliferous beds and a nodular texture (Hamblin 2003, Armstrong and Carter 2006, and INTERA 2011). Minor variation in appearance occurs at the top of the Cobourg Formation in southwestern Ontario where the uppermost portion of the unit has been dolomitized and is referred to as the "Cap Dolomite" (Sanford 1961). Additionally, the relative proportion of bioclastic zones, or thickness of shale stringers, etc., may change laterally and vertically; however, the key lithological properties are consistent and enable straightforward correlations of this stratigraphic unit across southern Ontario. It should be noted that the terms muddy and mudstone in Table 2.3 describe both carbonate and clastic mud. Beneath the Bruce nuclear site, and in accordance with the regional description, this formation is described as mottled light to dark grey, very fine- to coarse-grained, fossiliferous argillaceous limestone (INTERA 2011).

The overlying Collingwood Member consists of dark grey to black, calcareous shales with increased organic content and distinctive fossiliferous limestone interbeds. The Collingwood Member is relatively restricted in its distribution and is typically found in a zone from Oshawa, Ontario, west to Lake Huron and north to Manitoulin Island (Johnson et al. 1992). The Collingwood Member is associated with the underlying Cobourg Formation based on its calcareous nature. The overlying Blue Mountain Formation shales are distinctly non-calcareous.

**Table 2.3: Cobourg Formation (Lindsay Fm.) Descriptions from Southern Ontario Including the Bruce Nuclear Site**

<b>Cobourg/Lindsay Fm. (Hamblin 2003)</b>	<b>Location</b>
<b>Mottled light to dark grey, very fine- to coarse-grained</b> , fossiliferous argillaceous limestone. Irregular to wavy to diffuse shale interbeds found over bottom few metres (INTERA 2011).	Bruce nuclear site – Bruce County
<b>Grey very fine to fine crystalline limestone</b> , bioclastic, thin bedded, abundant muddy partings, thicker mudstone beds toward top, bioclastic stringers.	Corbetton
<b>Pale grey fine crystalline limestone</b> , argillaceous, nodular, mottled, thick bedded, separated by burrowed muddy laminae.	Clarkson
<b>Pale grey fine to medium crystalline fossiliferous limestone</b> , beds up to 20 cm thick separated by thin dark grey mudstone partings which increase upward - abundant vertical and horizontal burrows, abundant fossils.	Courtwright
<b>Grey fossiliferous limestone</b> with dark grey mudstone partings, bioturbated, nodular, medium bedded, fine crystalline.	Port Stanley
<b>Pale grey fine crystalline limestone</b> , medium bedded, bioclastic, nodular, argillaceous, numerous thin muddy burrowed zones, numerous thin sharp based bioclastic beds.	Nobleton
<b>Armstrong and Carter 2006 (southern Ontario standard description)</b>	
The Cobourg Formation consists of very fine- to coarse-grained, fossiliferous, bluish-grey to grey-brown limestones and argillaceous limestones.	

### **Upper Ordovician Shales**

The continuity, thickness and distribution of the Upper Ordovician shale units supports the interpretation of Quinlan and Beaumont (1984) that eastward tilting at the Taconic front subdued the circular Michigan Basin and largely incorporated it, across the Algonquin Arch, into the Appalachian Basin (Figure 2.9b). Figure 2.9b illustrates the interpreted broad platformal tectonic setting which developed during the Upper Ordovician, and the regional distribution of the shale facies which is pervasive across the RSA (Sanford 1993). Modern equivalent depositional environments include the Gulf of California and the western coast of Australia (AECOM and ITASCA CANADA 2011).

The extensive Upper Ordovician shale, siltstone, and carbonate sequences are composed of the Blue Mountain, Georgian Bay, and Queenston formations, which underlie southern Ontario including the Bruce nuclear site. The Blue Mountain Formation is characterized by uniform soft and laminated (Hamblin 1999), grey non-calcareous shale with minor siltstone and minor impure carbonate (Johnson et al. 1992). The facies within the Blue Mountain Formation are primarily open marine (grey shale). Restricted marine facies are found only in the lower portion of the formation (Hamblin 1999). The overlying Georgian Bay Formation is composed of blue-grey shale with intermittent centimetre-scale siltstone and limestone interbeds. Facies within this formation are consistent with a shallowing-upward storm-dominated shelf succession (Johnson et al. 1992). The Queenston Formation is characterized by maroon, with lesser green, shale and siltstone with varying amounts of carbonate. The carbonate content increases regionally to the northwest. Gypsum is found locally as small nodules and thin subhorizontal fracture fillings. In general, the Queenston Formation deposits are considered to be non-marine in the southeast (closer to the clastic sediment source) and marine in the northwest toward Manitoulin Island.

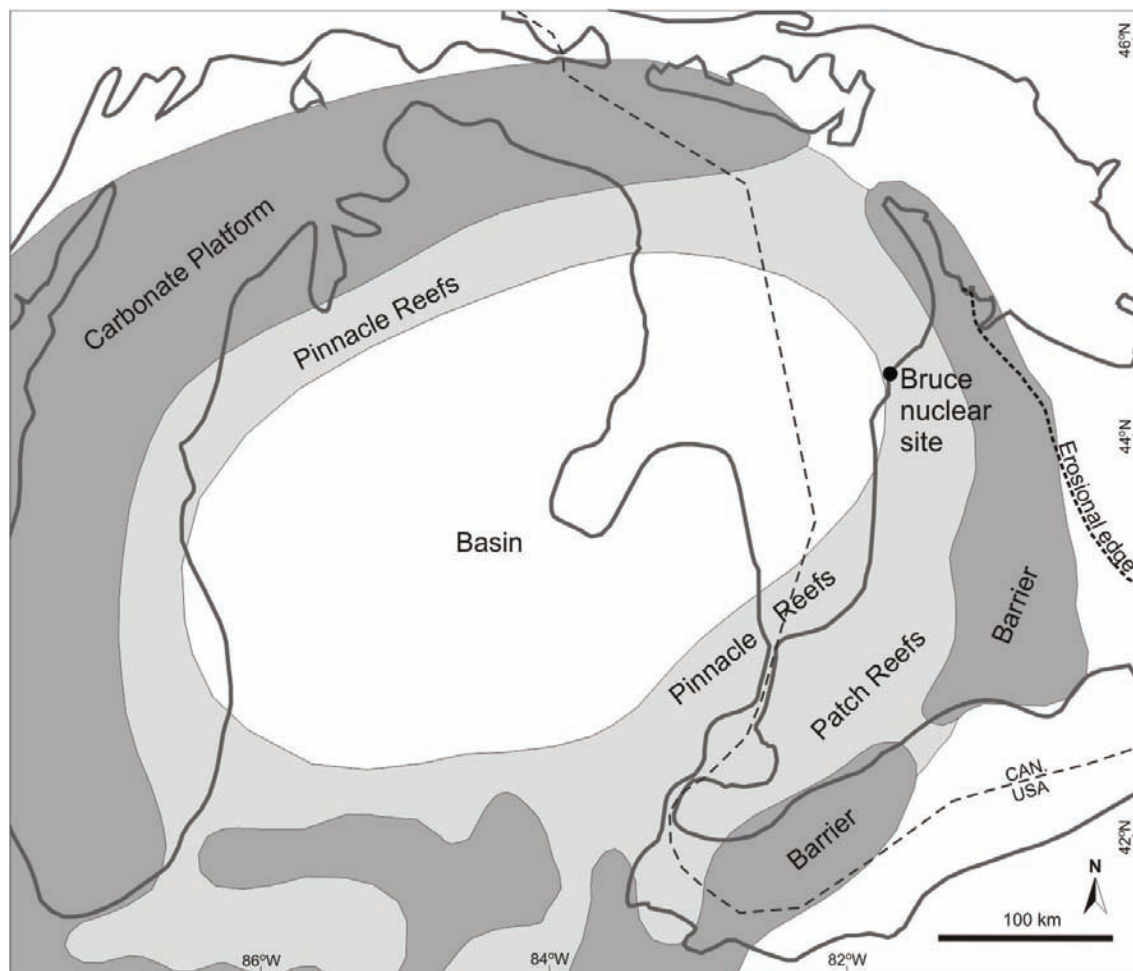
### **Lower Silurian Carbonates and Shales**

The Lower Silurian Manitoulin Formation unconformably overlies the Queenston Formation shales across the RSA. The Manitoulin Formation consists of grey argillaceous dolostone and minor grey-green shale, as well as bioherms on Manitoulin Island and the northern Bruce Peninsula. This unit was deposited in a shallow carbonate ramp setting (Armstrong and Carter 2006). The overlying Lower Silurian Cabot Head Formation consists of grey to green to maroon noncalcareous shales with minor sandstone and carbonate interbeds (Armstrong and Carter 2006). The depositional environment is interpreted as offshore basinal or marginal marine setting.

### **Middle Silurian Carbonates**

The Middle Silurian rocks beneath the DGR consist of the Fossil Hill, Lions Head, Gasport, Goat Island, and Guelph formations. The Fossil Hill Formation is composed of thin to medium bedded, very fine to coarse grained fossiliferous dolostone. The top of the Fossil Hill Formation is a regional disconformity and records a marine regression during the Middle Silurian. Uplift along the Algonquin Arch is responsible for erosion and the development of an angular unconformity moving away from this high-relief feature (Johnson et al. 1992). The marine transgression that followed this erosion was responsible for deposition of extensive carbonates of the Lions Head, Gasport, Goat Island, and Guelph formations. These Middle Silurian carbonates have been grouped collectively as the Niagaran within the regional 3DGF model (ITASCA CANADA and AECOM 2011) and for the purposes of hydrogeologic modelling (Chapter 5 and Sykes et al. 2011). The concentric form of the Michigan Basin during this interval is recognizable from the pattern of carbonate facies deposition (Figure 2.10).

The Lions Head Formation is a light grey to grey-brown, finely crystalline, thin to medium bedded, sparingly fossiliferous dolostone with minor chert nodules. The Gasport Formation is blue-grey, fine to coarse grained, thick bedded to massive dolostone which locally contains minor dolomitic limestone. The Goat Island is lithologically very similar to the Lions Head but is more argillaceous and may contain vugs filled with gypsum, calcite, or fluorite. Deep water basinal facies characterize the Middle Silurian carbonates in the Michigan Basin, while the margin of the basin and Algonquin Arch are characterized by shallow low-energy restricted facies and shallow high-energy facies (Armstrong and Goodman 1990).



Notes: Figure is modified from Johnson et al. (1992).

**Figure 2.10: Distribution of Middle and Upper Silurian Carbonate Facies**

The Guelph Formation lithology varies from reefal to inter-reefal dolostones (Armstrong and Goodman 1990). Reefal facies represent pinnacle, patch, and barrier reefs and their distribution defines the key aspects of the paleogeography during their deposition (Figure 2.10). The widespread inter-reefal dolostones are typically sucrosic, dark brown to black dolo-mudstones with pebble-size fragments lithologically similar to the underlying Goat Island Member (Armstrong and Carter 2006). Within the RSA, the Guelph Formation is characterized by facies deposited between the basinward pinnacle reef belt and the basin margin barrier reef complex (Johnson et al. 1992; Figure 2.10).

### **Upper Silurian Carbonates, Shales, and Evaporites**

The Upper Silurian package includes the Salina Group and the Bass Islands Formation. Deposition of carbonate, evaporites, and argillaceous sediments within both the Appalachian Basin and Michigan Basin characterize the Salina Group. The lithology of the Salina Group

units, as encountered beneath the Bruce nuclear site, include the A0 (carbonate), A1 (evaporite), A1 (carbonate), A2 (evaporite), A2 (carbonate), B (evaporite), B (carbonate), C (carbonate, shale and evaporite), D (carbonate and evaporite), E (carbonate and shale), F (carbonate, shale, and evaporite), and G (carbonate, shale, and evaporite) units. Salina units vary cyclically in lithology, grading upwards from basal carbonates to anhydrites to halite (evaporites), with the tops of each evaporite cycle often marked by shaley strata (Armstrong and Carter 2006).

The Bass Islands Formation is a microcrystalline commonly bituminous dolostone, and contains evaporite mineral clasts. This formation represents a return to more open marine conditions in contrast to the cyclical evaporite- and carbonate-forming conditions of the Salina Group. The contact with the overlying Devonian carbonates is a major unconformity characterized by subaerial exposure (Uyeno et al. 1982).

### **Devonian Carbonates**

The Devonian carbonates include the Bois Blanc Formation and the Detroit River Group. The Bois Blanc Formation is primarily a cherty dolostone unit within the RSA, grading laterally into limestones towards the Michigan Basin centre and interfingering with mixed carbonate clastic units within the Appalachian Basin (Hamilton 1991). Deposition of the Bois Blanc represents a major marine transgression after a long period of exposure at the end of the Silurian (Uyeno et al. 1982).

Overlying the Bois Blanc Formation are the mixed limestones and dolostones of the Detroit River Group (Amherstburg and Lucas formations). Similar to the Bois Blanc, this unit is primarily limestone towards the basin centre, and locally dolomitized along the Algonquin Arch (Sanford 1968). Local reef development within the Amherstburg Formation is commonly also known as the Formosa Limestone. The Lucas Formation conformably overlies the Amherstburg Formation (Johnson et al. 1992) and is characterized by fine-grained dolostone and limestone. The Lucas and Amherstburg formations form the bedrock surface beneath the overburden at the Bruce nuclear site and the Lucas Formation crops out extensively along the shores of Lake Huron in the vicinity of the site.

#### **2.2.5.2 3D Geological Framework**

Itasca Consulting Canada, Inc. was retained by OPG to work with AECOM in developing the 3DGF model (ITASCA CANADA and AECOM 2011). The model was designed using Gocad™ software, an earth modelling and scientific visualization program capable of displaying three-dimensional configurations of individual stratigraphic layers, as well as partial or entire stratigraphic sequences. The model generated for the RSA was based on observations and re-interpretation of Ministry of Natural Resources well records. The primary data source for the model construction was the Oil, Gas, and Salt Resources Library (OGSR) Petroleum Wells Subsurface Database (OGSR 2004 and OGSR 2006). This data set includes geological formation tops, logging records, and oil/gas/water intervals for thousands of petroleum wells throughout Ontario. The vast majority of these wells are located in southwestern Ontario along the shore of Lake Erie extending towards Sarnia/Lambton County. At the time of model development, the RSA contained a total of 341 wells, from which 299 wells were determined useful through a data validation process (ITASCA CANADA and AECOM 2011, AECOM and ITASCA CANADA 2011).



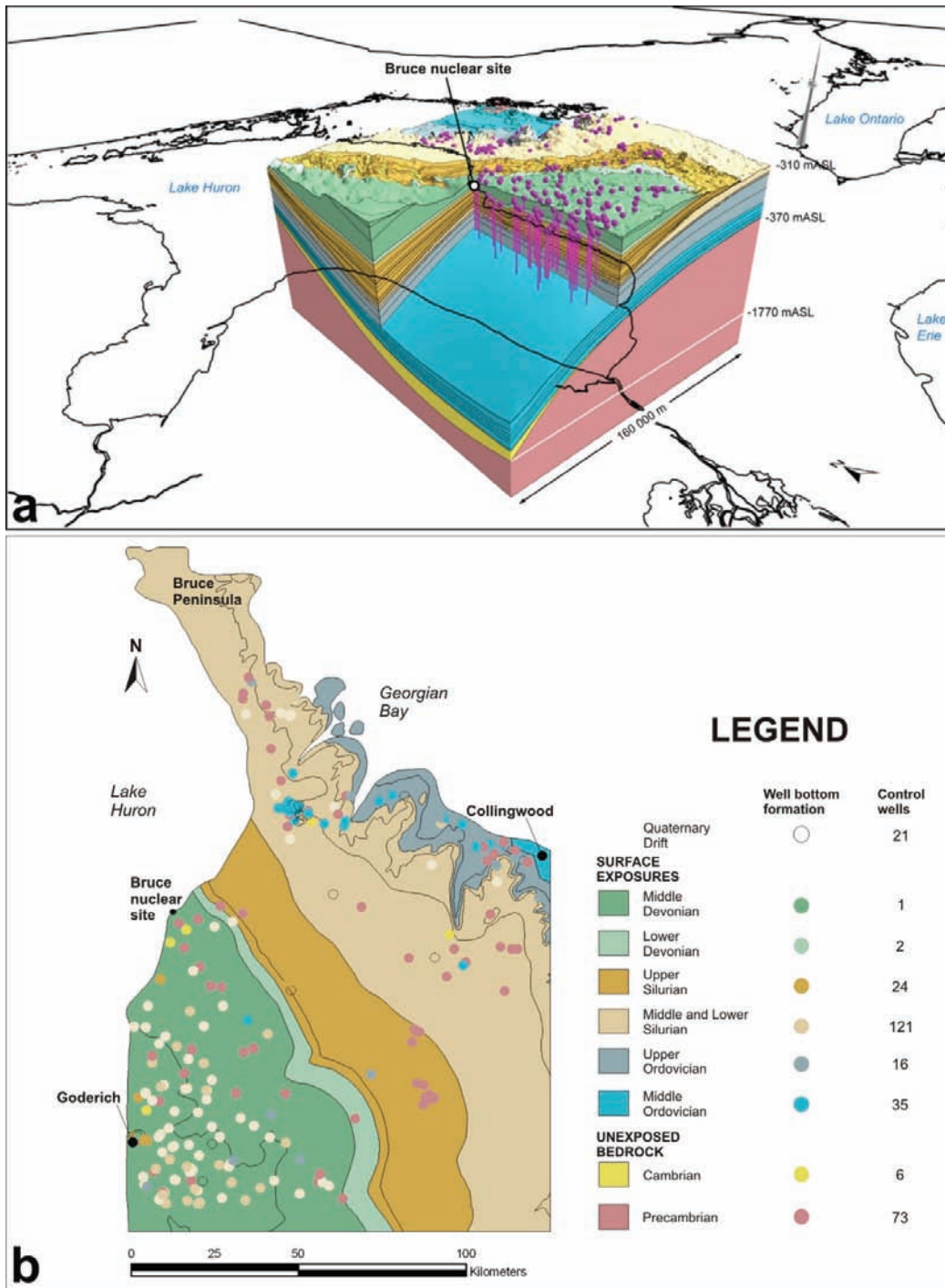
Development of the 3DGF stratigraphic model allows both geostatistical and manual interpretation to recognize plausible geologic structures (e.g., pinnacle reefs, erosional features, faults) and enables an assessment of formation spatial variability and uncertainty. Geological cross-sections were used to constrain model layers between well picks to ensure that known stratigraphic relationships were honoured in the model. It is noteworthy that development of the 3DGF would not have been possible using geostatistical techniques alone. The stratigraphic relationships and knowledge of basin evolution and structure were required for the model to remain consistent with contemporary understanding. Examples include the following:

- The separation of bedrock formations that were grouped together in the database;
- Obvious errors on inspection of the database in which formation contacts and/or elevations were incorrectly reported. Identification of such errors was typically made possible by adjacent borehole data and/or well established regional stratigraphic relationships;
- Corrections for known geologic features such as pinnacle or barrier reef geometry; and
- The location of erosional features and stratigraphic pinch-outs, particularly in association with the Cambrian sediments in the RSA.

Where formation contacts were not reliably or consistently identified, the formations were grouped together within the 3DGF. The groupings observed are as follows: 1) the Salina B Unit and the C Unit were combined; 2) the A0 Unit was not identified in the regional database; 3) the Guelph, Goat Island, Gasport, and Lions Head Formations were combined as the Niagaran, and 4) the Georgian Bay and Blue Mountain formations and the Collingwood Member were combined. The geological framework forms the basis of the hydrostratigraphic model domain used for the hydrogeologic modelling described in Chapter 5. An oblique map view of the geological framework within the RSA boundary is provided in Figure 2.11a with borehole control points indicated. The framework extends from Collingwood, Ontario in the east to the midpoint of Lake Huron in the west, south to Goderich, Ontario, and north to the Bruce Peninsula (Figure 2.11b). Figure 2.11b shows a plan view of the DGR location relative to the bedrock stratigraphy and the well control within and proximal to the RSA used to develop the 3DGF model. The Gocad™ platform allows various means to illustrate the formation geometry. Structure and isopach contour maps generated from the model (see appendices in ITASCA CANADA and AECOM 2011) are able to illustrate spatial variability of formation elevations and thicknesses, and to identify potential structural features (e.g., faults).

Other key sources of data used to help construct the model included downhole geophysics (used to verify well contacts/picks), acquired from the OGSR for select wells within the RSA, and Ontario Geological Survey (OGS) Open File Report 6191, "An updated guide to the Paleozoic stratigraphy of southern Ontario" (Armstrong and Carter 2006). Reference wells used by Armstrong and Carter (2006) to generate a series of representative geological cross-sections through the subsurface of southern Ontario were also used in the 3DGF as a verification tool (compare stratigraphic correlations) and to provide consistency with the accepted Ontario geological nomenclature and scientific understanding. Other important data used to constrain the geological layers within the 3DGF include:

- 1:50,000 OGS Digital Bedrock Geology of Ontario Seamless Coverage ERLIS Data Set 6 and MRD219 (Armstrong and Dodge 2007);
- Michigan State Geological Survey mapping and Petroleum Well Database;



Notes: (a) is a three-dimensional representation of surface and sub-surface geological units surrounding the Bruce nuclear site with a cut-away exposing the top of the Cobourg Formation (approximately 40x vertical exaggeration). Control point wells used to build the 3DGF model are shown as pink pins and dots. In (b), the same control points are colour-coded to indicate the lowermost geological unit encountered in each well.

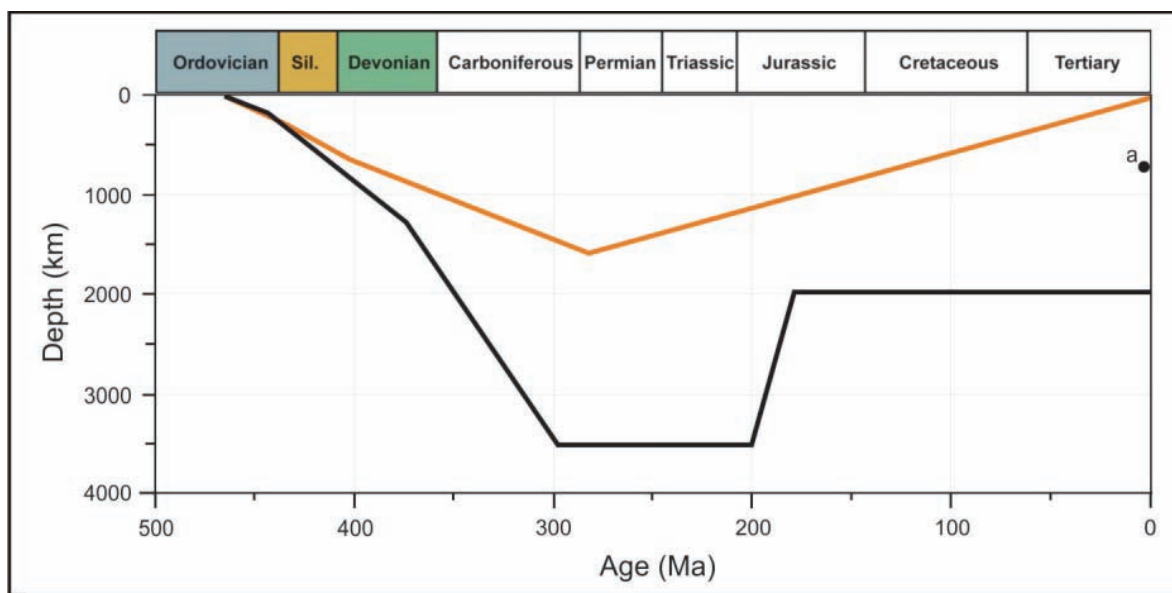
**Figure 2.11: Oblique (a) and Plan (b) Views of the RSA Bedrock Geology**

- OGS Digital Bedrock topography and overburden thickness mapping, southern Ontario – Miscellaneous Data Release no. 207 (Gao et al. 2006); and
- National Oceanic and Atmospheric Administration (NOAA) digital bathymetry mapping of Lake Huron and Georgian Bay (NOAA 2007).

The bathymetry mapping was used to correlate submerged scarp faces in Lake Huron with the stratigraphic data extrapolated from subsurface well data and bedrock maps. Since no well data exist from within Lake Huron, geological maps and selected petroleum well data from the State of Michigan were used to provide some guidance in extrapolating beneath the lake. The remaining data sources include published literature, government reports (i.e., MNR and OGS), and consulting reports.

### 2.2.5.3 Michigan Basin Subsidence and Thermal History

Figure 2.12 shows maximum burial-erosion curves for carbonate rocks of Middle Ordovician age from two different locations within the Michigan Basin. The orange curve in Figure 2.12 was included in a study of Ordovician diagenesis (Coniglio and Williams-Jones 1992) and was drawn primarily based on stratigraphic information and data from Cercone (1984).



Notes: Interpretations are based on data collected from Middle Ordovician carbonate sedimentary rocks. Orange curve is from Coniglio and Williams-Jones (1992) after Cercone (1984). Black curve is from Wang et al. (1994). (a) Indicates the present day burial depth of approximately 675 m for the middle of the Ordovician sedimentary succession at the Bruce nuclear site. See text for further discussion.

**Figure 2.12: Hypothetical Burial History Curves for Locations within the Michigan Basin**

Coniglio and Williams-Jones (1992) estimate that a minimum of 1500 m of compacted Paleozoic sediment has been eroded from the Manitoulin Island region since Permo-Carboniferous peak burial. An analysis of regional apatite fission track dates from around the south-central portion of the Michigan Basin, focused more directly on understanding the complete burial-erosion history (black line in Figure 2.12), was completed by Wang et al. (1994). Wang et al. (1994)

studied apatite fission tracks within Carboniferous sediments and document a similar late Carboniferous to early Permian timing for peak burial of ~3500 m of sediment at this south-central location within the basin, and determined that a maximum of 1500 m of sediments had been eroded. Given that the top of the Ordovician succession exposed at Manitoulin Island is encountered at 450 mBGS beneath the Bruce nuclear site (INTERA 2011), and the Bruce nuclear site is located slightly closer to the basin centre, it is reasonably estimated that a maximum of approximately 1000 m of sediment has been eroded from above the existing Paleozoic succession at the site.

Based on the above discussion, we can calculate an approximate peak burial in situ temperature for the top of the Trenton Group limestones, at the top of the Collingwood Member of the Cobourg Formation (~650 mBGS), assuming no other factors are involved. Ziegler et al. (1977) and Morel and Irving (1978) both define a position for southwestern Ontario at around 10°-15° south of the Equator during the Ordovician which allows for a mean annual surface temperature of 25°C at this time. Geothermal gradients of 20-30°C/km (Legall et al. 1981) and ~23°C/km (Hogarth and Sibley 1985) are suggested for the central and northern parts of the basin, respectively. An additional 1000 m of sediment at the Bruce nuclear site would have placed the Trenton Group (Collingwood Member) top at approximately 1650 mBGS resulting in an in situ temperature of 63.0°C using a 23°C/km estimate, 66.3°C using a 25°C/km estimate, and 74.5°C using a 30°C/km estimate, respectively, for the geothermal gradient. Therefore 70°C is considered a reasonable conservative maximum in situ burial temperature for the top of the Trenton Group beneath the Bruce nuclear site.

The resulting in situ temperatures, and therefore the maximum burial estimates in Figure 2.12, are consistent with results from Legall et al. (1981) which characterize two thermal alteration facies in the Paleozoic strata of southern Ontario using primarily a conodont alteration index (CAI). The first, from the top of the Paleozoic to the mid-Ordovician Trenton Group limestones, represents an organically immature to marginally mature facies that attained a maximum temperature of approximately 60°C. The second facies extends from the mid-Ordovician downwards to the base of the Paleozoic sequence. This group would comprise predominantly the Black River Group in the RSA where the Cambrian is very thin or nonexistent. These rocks attained maximum burial temperatures of 60-90°C (Legall et al. 1981). Samples taken approximately 80 km east of the DGR indicate a CAI of 1.5, representing Ordovician burial temperatures of approximately 75-85°C (Legall et al. 1981). Legall et al. (1981) also designate a third maturation facies in eastern Ontario and southern Quebec. Paleozoic sediments in this region attained much higher maximum burial temperatures of 90-120°C as a result of proximity to the path of the Great Meteor Hotspot (Heaman and Kjarsgaard 2000).

The regional CAI estimate of 1.5 (Legall) represents a burial temperature of around 75°C with a possible error range of approximately ±15°C. This large error could potentially mask any localized low-level heating by hydrothermal fluids, which could have migrated into the region from the basin centre. Occurrences of thin planar dolomite horizons are found within the Ordovician shales beneath the Bruce nuclear site (INTERA 2011) and may represent the results of percolation and horizontal migration of warm fluids from deeper in the basin.

Powell et al. (1984) suggest that the alteration facies designation devised by Legall et al. (1981) would indicate a very limited potential for in situ petroleum generation in rocks as deep as the Middle Ordovician Trenton Group in southern Ontario in general. Importantly, this interpretation is consistent with the observation that the same rocks beneath the Bruce nuclear site only barely reached the oil window in terms of thermal hydrocarbon maturation (e.g., INTERA 2011, their Section 3.7.5 and Section 2.3.7 herein). This is consistent with the observed transition

from immature to mature hydrocarbons across the Georgian Bay – Blue Mountain sequence beneath the Bruce nuclear site (INTERA 2011).

The two burial curves in Figure 2.12 are considered to be suitable for constraining maximum peak burial conditions for rocks within the RSA, including the Bruce nuclear site. They vary, however, in their interpretation of the timing and rate of erosion. While the orange curve depicts a constant erosion rate since peak burial until the present day, the black curve indicates a non-constant erosion rate where much of the 1500 m was removed prior to the Middle Jurassic. This timing constraint is justified by the observation of a regional unconformity that separates Middle Jurassic sandstones from Pennsylvanian sandstones within the centre of the basin (Wang et al. 1994, Dickinson et al. 2010). Given that this unconformable relationship is regional in scale (e.g., Sloss 1963), and that the Bruce nuclear site shares a common geological history with the Michigan Basin, it is reasonable to suggest that much of the missing 1000 m of Paleozoic rocks at the Bruce nuclear site were eroded during the same (pre-Mid Jurassic) time interval. A late Paleozoic to early Mesozoic timing for the majority of the erosion at the Bruce nuclear site therefore coincides with the waning of the Alleghenian stage of the Appalachian Orogeny, the break-up of Pangaea and opening of the Atlantic Ocean.

#### **2.2.5.4 Diagenesis**

A number of diagenetic processes have influenced or altered the Paleozoic rocks of southern Ontario since Cambrian times (Coniglio and Williams-Jones 1992). As introduced above, the most significant of these is dolomitization whereby calcite or aragonite is converted to dolomite by the replacement of calcium ions by magnesium ions. The primary dolomitization mechanisms are reportedly: a) sabkha type, b) mixed-water aquifer, c) seepage reflux, d) burial compaction, and e) hydrothermal (Morrow 1990). The timing of dolomitization events ranged from during or shortly after marine carbonate deposition during the Ordovician (a and b above) to the Late Paleozoic/Early Mesozoic and/or corresponding to maximum burial compaction (c, d, and e above). Hydrothermal dolomitization selectively altered the Paleozoic rocks along and adjacent to discrete fracture systems in response to tectonic events during the Paleozoic and Early Mesozoic. The conditions that led to dolomitization within the RSA region of the Michigan Basin (i.e., basinal groundwater flow, fracture-related tectonically driven flow, and hydrothermal dolomitization) have not existed for the last approximately 200-250 Ma (e.g., Coniglio and Williams-Jones 1992).

Coniglio and Williams-Jones (1992) argue that hydrothermal dolomitization may have involved percolation of fluids much warmer (ca. 100 to 200°C) than would be expected due to burial alone. In some cases, this mechanism of dolomitization was associated with the development of large hydrocarbon deposits, generally where a structural control also dominated, for example the fault-related Albion-Scipio hydrocarbon field in southern Michigan described by several authors (e.g., Prouty 1988, Hurley and Budros 1990, Davies and Smith 2006). Several studies indicate that when hydrothermal fluids are included as a component of the system, wide ranging peak temperature conditions are likely to prevail at the basin scale (e.g., Hurley and Budros 1990, Coniglio and Williams-Jones 1992, Davies and Smith 2006). In turn this suggests that the extent or volume of hydrothermal dolomitization can also vary along with its morphology. Instances of dolomitization, formed both in situ due to compaction under ambient conditions of burial, and/or hydrothermal due to percolation of hot fluids, appear to have developed at all scales in the Michigan Basin. Regional studies (e.g., Legall et al. 1981) suggest that low burial temperatures prevailed throughout much of the RSA. The peak temperature estimates from the previous section suggest that any addition of a hydrothermal fluid component within the Ordovician sediments beneath the site was (in the absence of additional data) indiscernible from the temperature effects of burial.

The key post-dolomitization diagenetic phases are all volumetrically minor and include late stage calcite cements, Mississippi Valley Type (MVT) mineralization, and late stage anhydrite and gypsum (Budai and Wilson 1991, Coniglio et al. 1994). These phases do not include those related to modern surface exposure in the near-surface rocks of the Michigan Basin, which are not discussed here. Other diagenetic events include salt dissolution and subsequent collapse features (Upper Silurian and Devonian stratigraphy), clay alteration at the Precambrian-Paleozoic boundary, and hydrocarbon migration and emplacement.

Salt dissolution is typically identified at the margin of the Michigan Basin in a zone extending from the Bruce Peninsula south along Lake Huron and into southwestern Ontario. This process occurred primarily during the Late Silurian to Devonian Caledonian Orogeny. A second major salt dissolution event occurred during the Late Devonian-Mississippian Acadian Orogeny (Sanford et al. 1985; Figure 2.7). Salt dissolution is interpreted to have occurred via fluid migration through regional fractures and faults (Sanford et al. 1985). Removal of salt from the subsurface is interpreted to have created collapse features (e.g., breccia) and initiated faulting within the overlying Upper Silurian and Devonian strata. The zones affected by this dissolution are brecciated and characterized by an evaporite cement filling (gypsum and/or anhydrite) enclosing dolostone clasts. The pervasive cementation and fracture infilling has resulted in very low measured hydraulic conductivities in the Silurian rocks (INTERA 2011).

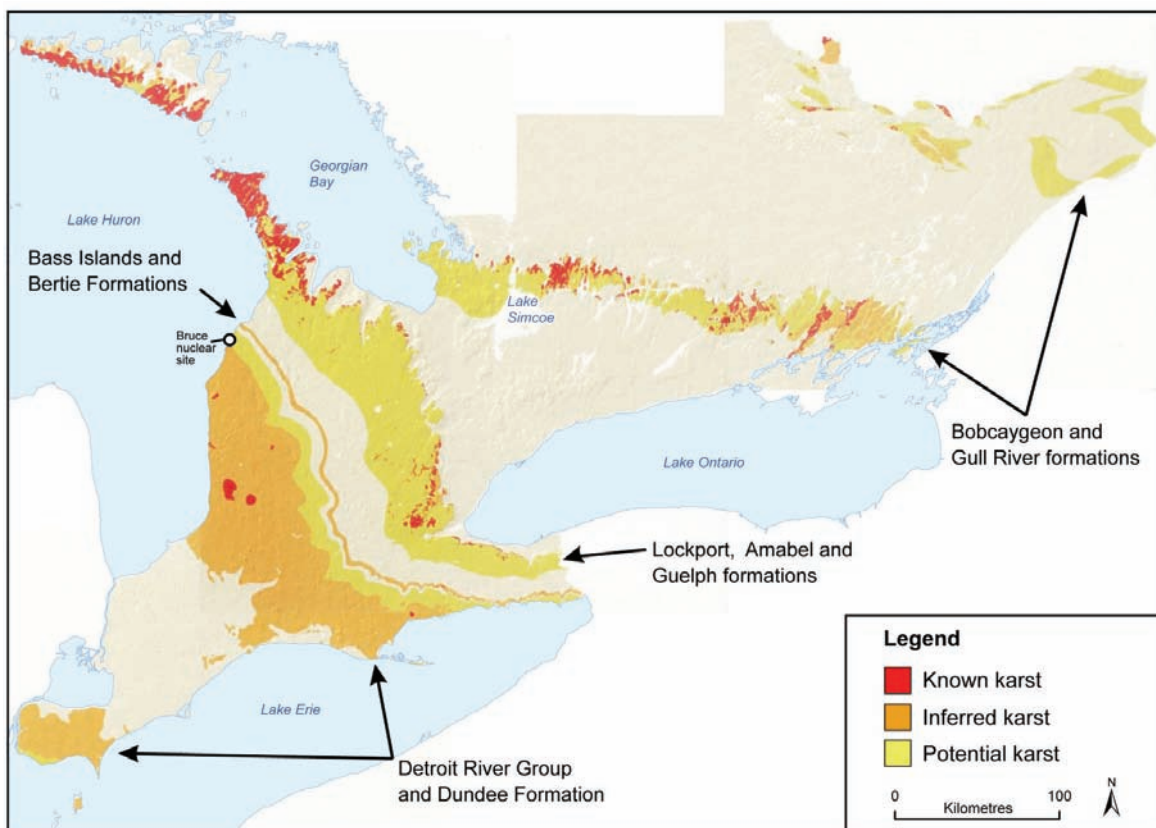
#### **2.2.5.5 Karst and Paleokarst**

Rocks such as carbonates and evaporites are eroded principally by dissolution. At shallow depths below the surface, most of the permeability in these rocks is created by dissolution, part of the process of karstification. This process, to a great extent, is a function of the flux of water through an aquifer and the chemical undersaturation of that water. Consequently, karstification tends to be most pronounced in the upper parts of soluble rock aquifers. A key property of karst aquifers is that the high-permeability channels resulting from karstification become interconnected to form a network (WORTHINGTON 2011). This constitutes a major difference that distinguishes karst aquifers from fractured-rock aquifers.

Dissolution is most active in the shallow subsurface, usually < 200 m depth in southwestern Ontario, and potentially reaching 300 mBGS in the Devonian carbonates in southern Huron County and western Perth County. Middle Silurian carbonates are unlikely to have been affected and the deeply buried Ordovician carbonates are unaffected by modern karstification processes (WORTHINGTON 2011).

A map of karst distribution in Paleozoic strata throughout southern Ontario (Brunton and Dodge 2008; Figure 2.13) indicates karst occurrences in the shallow subsurface of Ordovician, Silurian, and Devonian age rocks in the Bruce Peninsula region and around the periphery of the RSA. Areas of mapped karstification include: the Ordovician carbonates cropping out to the south of the Canadian Shield that extend into eastern Ontario (e.g., Gull River Formation, Lower Bobcaygeon Formation); Silurian Formation carbonates exposed along the escarpment; the aquifer formed by the Amabel - Lockport and Guelph formations in some locations such as Guelph; evaporite units of the Salina Group (Singer et al. 2003); and, Devonian carbonates in southwestern Ontario, particularly in areas where there is a deep unsaturated zone (> 100 m). Regional-scale karst inventories suggest that large-scale karstification occurs both proximal to significant escarpment or cuesta margins and/or laterally within a few hundred metres of incised river systems (Brunton and Dodge 2008). This is not surprising given that karst development requires an active groundwater flow system in proximity to a recharge zone to provide meteoric water that is undersaturated with respect to carbonate.

Modern karstification of carbonates is likely to occur almost exclusively in shallow freshwater zones. This increases permeability by several orders of magnitude to typical values of  $10^{-6}$  to  $10^{-4}$  m/s (WORTHINGTON 2011). The depth of penetration of freshwater from the outcrop or subcrop belt is dependent on flow path length and also the salinity (density) of the water at depth. Freshwater is unlikely to penetrate to significant distances down dip into the Silurian or Ordovician units, as the freshwater would have to displace high-density saline brines which characterize these rocks at depth.



Notes: Figure is modified from Brunton and Dodge (2008).

**Figure 2.13: Karstified Near-surface Paleozoic Rocks in Southern Ontario**

Paleokarst is essentially a rock that has been karstified and subsequently buried by later deposition. As with modern karst, paleokarst zones can display enhanced porosity and permeability. In most cases, including at the Bruce nuclear site, the paleokarst porosity has been infilled with younger sediments, such as evaporites (salt, gypsum, and anhydrite), that destroy the porosity and permeability of the original karst. In southwestern Ontario, some interpreted paleokarst zones that have not been occluded by cements or evaporites form hydrocarbon reservoirs. The paleokarst zones are most extensive at large breaks in the sedimentary record that record regional unconformities (e.g., Silurian - Devonian boundary, Brunton and Dodge 2008; below and above the Reynales/Fossil Hill Formations and below and above the Detroit River Group; AECOM and ITASCA CANADA 2011). Typical examples of paleokarst fabrics at the Bruce nuclear site are described in Section 2.3.9.

## 2.2.6 Structural Geology

The primary materials reviewed in preparation of the structural geology section were: a detailed structural analysis of the Bruce nuclear site and surrounding region (Cruden 2011); a report evaluating the cap rock integrity at the DGR (Engelder 2011); and a recent regional geological synthesis by Mazurek (2004). Regional analyses by Sanford et al. (1985) that introduced the “block” concept for southern Ontario, publications by Easton and Carter (1995) and Carter et al. (1996) on the basement structure and evidence for Paleozoic faulting in southern Ontario, and the Ontario Geological Survey synthesis report on the Paleozoic geology of Ontario (Johnson et al. 1992) were also incorporated. Additional materials included publications on neotectonics (Wallach et al. 1998), jointing and pop-up structures (Rutty and Cruden 1993, Andjelkovic et al. 1996 and 1997, Andjelkovic and Cruden 1998) in southern Ontario, and reports and publications on the structure and depositional history of the intraplate basins of North America, including the Michigan Basin (Howell and van der Pluijm 1990, 1999, Leighton 1996, van der Pluijm et al. 1997, Wood and Harrison 2002 and references therein), and selected papers from a special issue in the journal *Tectonophysics* (v. 353, 2002) that focused on neotectonics and seismicity in the eastern Great Lakes region. A synthesis of regional joint measurement data, compiled by OPG and AECOM was also made available (NWMO and AECOM 2011).

### 2.2.6.1 Structural Setting

The RSA is underlain by Paleozoic sedimentary rocks that unconformably overlie the Precambrian Grenville basement along the southern edge of the Canadian Shield (e.g., Figures 2.2 and 2.3). This part of North America is generally considered to have been relatively tectonically stable since the Paleozoic (e.g., Park and Jaroszewski 1994, van der Pluijm and Marshak 2004, Percival and Easton 2007). Post-Paleozoic tectonic stability throughout southern Ontario is suggested by the relatively undisturbed sequence of Ordovician and younger sedimentary rocks overlying the Precambrian basement, as interpreted from seismic reflection data (Milkereit et al. 1992), and the recognition that the youngest strata transected by basement-seated faults in southern Ontario are Silurian in age (Armstrong and Carter 2010).

Figure 2.5 shows the various interpretations of structural subdivisions of the Precambrian basement in southern Ontario based on work by Carter et al. (1996), and aeromagnetic lineament analysis detailed in Wallach et al. (1998), and based on a conceptual model of Sanford et al. (1985). As noted previously, two major basement features, the Grenville Front Tectonic Zone (GFTZ) and the Central Metasedimentary Belt Boundary Zone (CMBBZ), can be traced from their surface exposure northwest and east of Georgian Bay beneath the Paleozoic cover to the southwest (Figure 2.5). Apart from localized low-level seismicity near the subsurface trace of the CMBBZ, there is no evidence for significant neotectonic activity along these ancient boundaries (Percival and Easton 2007). The Georgian Bay Linear Zone (GBLZ; Figure 2.5) is defined by an interpreted aeromagnetic anomaly trending at a high angle to the GFTZ and CMBBZ (Wallach et al. 1998). Wallach et al. (1998) argue that the GBLZ may be collinear with a region of anomalous recent seismic activity (see also Boyce and Morris 2002). In a review of Wallach’s interpretation, Roest (1995) states that the existence of the GBLZ south of Georgian Bay is questionable based on the gravity and aeromagnetic dataset. A more recent analysis of the neotectonics stress field in southern Ontario does not include the GBLZ as a tectonic element (Baird and McKinnon 2007).



### 2.2.6.2 Regional Faults - Overview

Sanford et al. (1985) introduced a conceptual fracture framework for southwestern Ontario based on hand contouring of selected Silurian unit isopachs and structure contours on the top of the Silurian Rochester Formation from within southwestern Ontario. This work suggested that Silurian units contain ENE- to ESE-trending normal faults, depending on location throughout southern Ontario, with ~10 km spacing. Such a systematic fault pattern is not observed in structural contours on the top of the Precambrian basement surface, nor is it consistent with known or interpreted mapped faults that displace this surface (Bailey and Cochrane 1984a, Carter et al. 1996, Armstrong and Carter 2010). Furthermore, it is difficult to reconcile the fracture model of Sanford et al. (1985) with the known and mapped joint distribution data for southern Ontario, Michigan, and northern New York (Holst 1982, Parker 1942, Nicholson and Hough 1967, Scheidegger 1977, Gross and Engelder 1991, Andjelkovic et al. 1996, 1997, Andjelkovic and Cruden 1998). Johnson et al. (1992) note that although fractures may exist, the extensive fracture framework conceptualized by Sanford et al. (1985), which includes an ordered and densely spaced set of faults offsetting Silurian strata, is not recognized. Although borehole density is low in the Bruce region, the closest interpreted fault structure is > 25 km away from the DGR footprint and it is overlain by undisturbed Ordovician strata (Armstrong and Carter 2010; Figure 2.5). There is nothing apparent in the sediment cover, either from correlation studies (regional cross-sections in Armstrong and Carter 2006), interpreted 2D seismic data (Watts et al. 2009), or from detailed field studies (Slattery 2011, Cruden 2011), that would suggest that faults with major (> 10 m) offsets are likely to occur in the subsurface proximal to the DGR. Information to support this statement is found in Section 2.3 below.

Carter et al. (1996) and Armstrong and Carter (2010) document all faults known to displace the Proterozoic/Paleozoic unconformity in southwestern Ontario. This analysis is based on geophysical and borehole data and compilations by Brigham (1971) and Bailey and Cochrane (1984b; in Carter et al. 1996; Figure 2.5). Within southeastern Ontario, where there is an abundance of subsurface data available, these faults have been mapped with a high degree of confidence. The faults are grouped based on observation of the youngest stratigraphic unit that is offset (Figure 2.5). The oldest faults only offset Cambrian strata and rocks of the immediately overlying Ordovician Shadow Lake Formation. Another group of faults offset rocks as young as the Ordovician Trenton Group limestones. The youngest faults in southern Ontario offset rocks of the Silurian Rochester (Lions Head equivalent) Formation (e.g., Armstrong and Carter 2010, their Figure 25 and Figure 2.5 herein).

Within the RSA where subsurface data are sparse these features are inferred by subsurface structure contouring and isopach mapping with limited well-control or through seismic interpretation. As a result these faults are poorly constrained in terms of location and movement history and are mapped with a low degree of confidence. Based on the limited dataset no mapped faults within the RSA are interpreted to be younger than the limestones of the Ordovician Trenton Group (Armstrong and Carter 2010). This is consistent with the results of the 2D seismic survey, discussed below in Section 2.3.9.2, which indicate that no faults have breached the Upper Ordovician shale rock beneath the Bruce nuclear site. This is also consistent with the observed present day tectonic stability of the RSA in general.

### 2.2.6.3 Regional Faults - Morphology

Mapped faults within southern Ontario (Figure 2.5) are shown as < 10 to ~40 km long segments, with one exception that is > 100 km in length. The faults are generally interpreted to be nearly

vertical in attitude, exhibit normal and/or strike-slip motion, and cluster into two main orientations, ENE- to SE- and N- to NNE-trending (Figure 2.5). Displacements on all faults range from a few metres up to a maximum of 100 m (Brigham 1971, Carter et al. 1996).

Where faults strike easterly, the predominant offset is south-side-down. This fault orientation is most common near the Chatham Sag in southwestern Ontario where a marked concentration of faults occur along and south of the contact between the Niagara and Bruce megablocks and are approximately coincident with the interpreted southeastern boundary of the lithotectonic Huron domain (Carter et al. 1996; Figure 2.5). Two named faults in the area, Dawn and Electric, coincide with the Chatham Sag structure (Carter et al. 1996; Figure 2.5). These structures may be part of a system of wrench structures formed during regional transtensional (normal and strike-slip) conditions and whose distribution is controlled by pre-existing basement structure (see below; Prouty 1988, Colquhoun 2004, Colquhoun and Johnston 2004, Smith 2006, Davies and Smith 2006).

NNE-striking faults are mostly mapped to the north and east of the Chatham Sag around the margins of the Algonquin Arch and near the head of Georgian Bay (Figure 2.5). These faults occasionally exhibit east-side-down offset (Carter et al. 1996). Significantly, sparse well control here renders the existence of many of these fault structures highly speculative. Further to the southeast into the Appalachian Basin, the NNE-trending Clarendon-Linden Fault system in upstate New York is interpreted as a recently active seismic feature (Fakundiny and Myers 1978). This structural zone may also represent a reactivated Iapetus normal fault system (e.g., Wheeler et al. 1995) and may define the northwesternmost boundary of present-day continental margin seismicity in the region. The Picton Fault system (Liberty 1960) in the northeastern Lake Ontario region and also within the Appalachian Basin, has been interpreted as a possible northeastward continuation of the Clarendon-Linden Fault system (McFall and Allam 1989).

#### **2.2.6.4 Regional Faults - Timing**

Paleozoic basin development throughout central North America is interpreted to be linked directly to the activation of pre-existing basement faults (e.g., Marshak and Paulsen 1996). The discussion of a Precambrian basement control on the location and activity of Paleozoic faulting in southern Ontario was presented by Sanford et al. (1985). In support of this argument, Carter and Easton (1990) and Easton and Carter (1995) noted a correlation between the location of the Huron lithotectonic domain and the Bruce Megablock. The bimodal (NNE and ESE) distribution of regional fault trends described above is similar to the orientations of early Cambrian extension-related faults observed throughout the midcontinent region described by Marshak and Paulsen (1996). It is therefore likely that at least some of the mapped basement faults in southern Ontario were active in the Precambrian during the initial extension and rifting (ca. 760 to 650 Ma) associated with the opening of the Iapetus Ocean (e.g., Wheeler 1995, Thomas 2006 and references therein).

Basement-controlled fracture systems are characterized by a regional pattern of similarly oriented sets of discontinuities (e.g., Thomas 2006) that have experienced slip. If fault activation post-dates deposition of the overlying cover rocks, they will fracture by jointing or faulting depending on the amount of slip and according to the nature of the fault (Engelder 2011). Hydrothermal dolomite (HTD) hosted natural gas pools within the Middle Ordovician Black River Group in south-central New York are formed adjacent to basement-rooted and steeply dipping wrench faults that die out in the overlying Trenton Limestone and Utica Shale (Coniglio et al. 1994, Smith 2006). The wrench fault systems are interpreted to be

transtensional in nature. In cross-section, perpendicular to the strike of the surface fault trace, the fault systems exhibit a characteristic geometry with a central downwarping of strata bounded by steeply inward-dipping fractures. This geometry is referred to as a 'negative flower structure'.

This fracture system morphology is recognized in the dolomitized hydrocarbon reservoirs in Michigan. The associated fractures do not transect the Upper Ordovician shale cap rock suggesting that the majority of these wrench faults, which appear throughout southwestern Ontario (Colquhoun 2004), ceased to be active by the end of the Taconic Orogeny. Only a limited number of faults in southern Ontario exhibit post-Trenton movement activity, indicated by fault disruption of the overlying Silurian formations (Figure 2.5). The lack of post-Trenton faulting throughout the RSA supports the argument that the shale cap rock at the Bruce nuclear site has maintained its integrity since prior to the Silurian period. This interpretation is reinforced by the recognition of a regularly oriented joint set pattern observed in the exposed Devonian section near the Bruce nuclear site and whose genesis is attributed to middle Devonian basin-centred subsidence (Cruden 2011), and the seismic interpretation of a relatively undisturbed Ordovician sedimentary succession throughout southern Ontario as discussed by Milkereit et al. (1992) and shown in Figure 2.6.

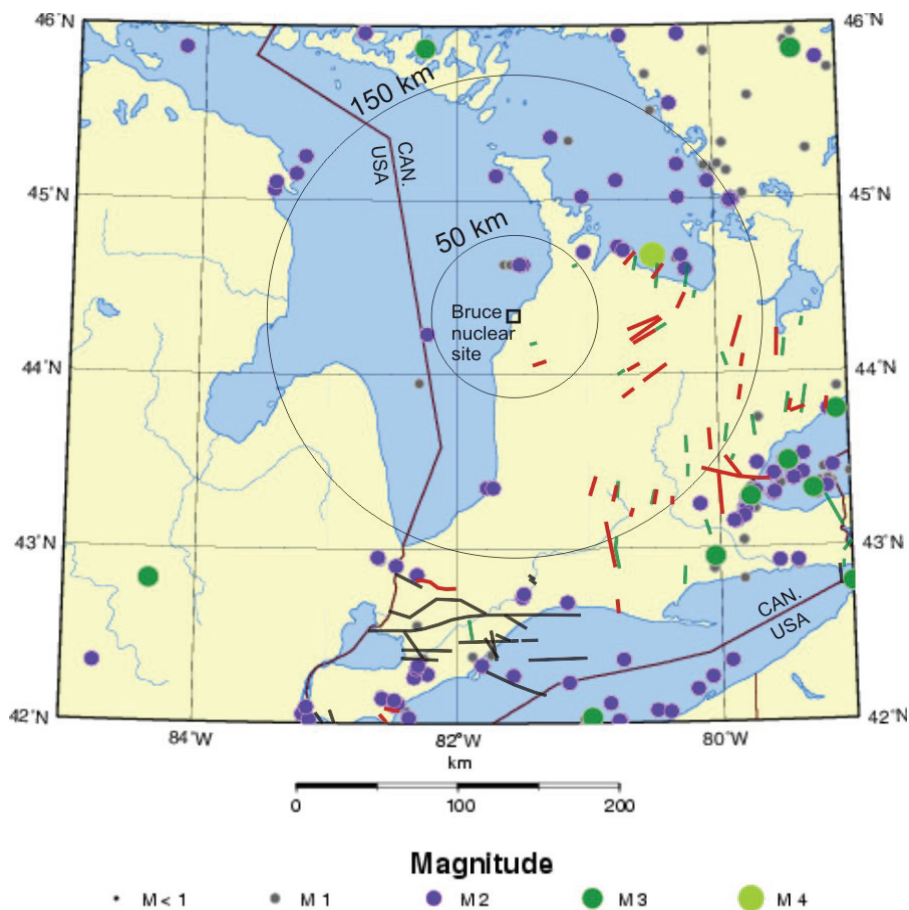
#### **2.2.6.5 Seismicity**

The RSA is within the tectonically stable interior of the North American continent. This region is characterized by low rates of seismicity with historical records since the late 1800's. Figure 2.14 shows all known earthquakes in the region between 1985 and 2010 (Hayek et al. 2010), overlain with the mapped faults in southern Ontario from Figure 2.5. Figure 2.14 shows that the Bruce region experiences sparse seismic activity, with no apparent concentrations of activity that might delineate regional active faults or other seismogenic features. Most recorded events have a magnitude of less than M3 (Nuttli Magnitude: the primary local magnitude scale used for reporting in the region), with rare occurrences of larger events within a 150 km radius from the Bruce nuclear site. Twenty-six events have been detected in this region since 1952 with a maximum of M4.3 (focal depth of about 11 km). This seismic event was located 99 km northeast of the Bruce nuclear site (15 km north of Meaford, ON) (Dineva et al. 2004, Hayek et al. 2010). The historical record is considered to be relatively complete for events of about  $M > 3.5$ . It has become more complete for lower magnitude events over the last 10 years owing to the increased station density in the region (Hayek et al. 2008).

The historical seismic monitoring record is considered to be relatively complete for events of about  $M > 3.5$  since the early part of this century. The detection threshold in the region has been reduced to M2.0 with the expanded POLARIS (Portable Observatories for Lithospheric Analysis and Research Investigating Seismicity) network in 2002. This threshold was further lowered to M1.0 after installation of three borehole microseismic monitoring stations approximately 40 km from the Bruce nuclear site during the summer of 2007. An objective of this new array is to capture microseismic events in the immediate area for the delineation of seismogenic features deep in the bedrock.

The historical dataset suggests that, in general, the RSA experiences sparse seismic activity and there is no indication of the existence of major seismogenic features or active faults of concern. Mapped faults throughout southern Ontario only locally appear to be spatially associated with seismic event locations (Figure 2.14). Also, a recently completed remote sensing and field-based study looked at landforms within 50 km of the Bruce nuclear site and

found no evidence for neotectonic activity associated with the most recent glacial cycle within the RSA (Slattery 2011).



Notes: Fault data are from Armstrong and Carter (2010). Refer to legend of Figure 2.5 for detailed information on fault ages. All seismic events are plotted in local magnitude (M=Nuttli Magnitude) and were compiled from [www.EarthquakesCanada.ca](http://www.EarthquakesCanada.ca). The circles around the Bruce nuclear site represent 50 km and 150 km radii.

**Figure 2.14: Seismicity in the Bruce Region from 1985 to 2010 Overlain with Mapped Faults in Southern Ontario**

Currently, Canadian Hazards Information Services (CHIS) of the Geological Survey of Canada (GSC) monitors and reports on seismic activity in the immediate region of the Bruce nuclear site on an annual basis (Hayek et al. 2008, Hayek et al. 2009, Hayek et al. 2010). CHIS (Hayek et al. 2008) reviewed historical seismicity for the Bruce area and noted that only three earthquakes have historically been detected within 50 km of the Bruce nuclear site prior to 2007. These three events occurred in Lake Huron about 20 km northwest of Southampton with M1.7 to M2.1. The current and historical monitoring data confirm that the Bruce nuclear site is located in a seismically quiet area with only one event in each of the last two years (see Section 6.2.2.1, AMEC GEOMATRIX 2011).

### 2.2.6.6 Evolution of the Regional Stress Field

The mean of the current maximum principal stress orientation in central and eastern North America, based on the World Stress Map (Zoback 1992) is N63°E +/- 28°. This orientation coincides roughly with both the absolute and relative plate motions of North America (Zoback 1992, Baird and McKinnon 2007).

The current stress regime in southern Ontario has its origins in the opening of the Atlantic Ocean in the Jurassic and subsequent establishment of sea floor spreading along the mid-Atlantic ridge (NWMO and AECOM 2011). The eastern margin of North America transitioned into a passive margin tectonic setting at this time (Figure 2.7). Initially oriented east-southeasterly at approximately 200 Ma, the maximum regional principal stress has since rotated counter-clockwise into its present-day east-northeasterly orientation (e.g., Heidbach et al. 2007), controlled by the present tectonic configuration of the North Atlantic spreading ridge (Sbar and Sykes 1973). This configuration has likely been consistent at least since the most recent Paleocene-Eocene plate reorganization (Rona and Richardson 1978, Gordon and Jurdy 1986). Paleostress analyses on stylolites and fault striations indicate that intraplate stress orientations and magnitudes change on a timescale of a few million years (e.g., Letouzey 1986, Csontos et al. 1991). Therefore, within the current tectonic regime, the Michigan Basin is considered to be tectonically stable (e.g., Park and Jaroszewski 1994, van der Pluijm and Marshak 2004). This stability is likely to persist beyond the requisite 1 Ma timeframe of the DGR safety case.

Since the Quaternary Period, these far field tectonic stresses have interacted with vertical and flexural loads associated with continental glaciation and deglaciation events, culminating in the retreat of the Wisconsin ice sheet 12,000 years ago, to produce a variety of small-scale structures, such as open field pop-ups (Karrow and White 2002) and offset glacially striated surfaces.

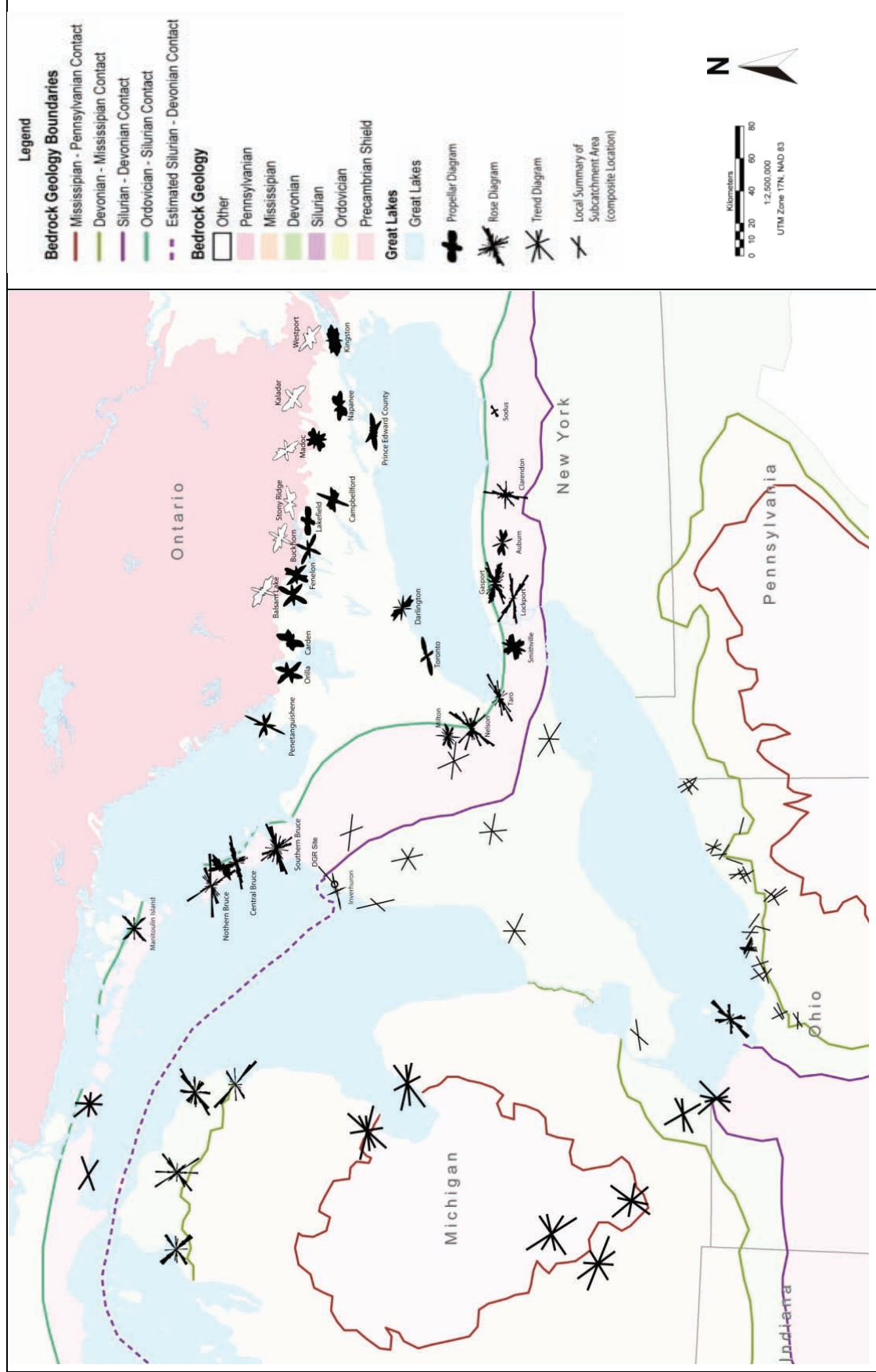
### 2.2.6.7 Regional Fracture Patterns

Perhaps the best gauge of the history of tectonic forces in southern Ontario are the regionally consistent, systematic fractures which have formed in response to loading or unloading of the rock mass. The majority of fractures observed in southern Ontario exhibit no measureable slip or dilation at the scale of observation and are therefore joints (e.g., Hancock 1985). The Regional Geomechanics Report (NWMO and AECOM 2011) provides a review of the literature with respect to joint orientation and location both regionally and through geologic time. The following section summarizes the results of this work.

Joint planes develop normal to the minimum principal stress either due to pure tension, or extension due to compression. Three possible geological processes are implicated as the mechanism of joint formation in southern Ontario, including:

- a. Vertical compaction under conditions of high pore fluid pressure;
- b. Tectonic loading events; and
- c. Unloading and isostatic rebound.

Andjelkovic et al. (1996, 1997) and Andjelkovic and Cruden (1998) measured ~7,000 fracture orientations from outcrops and quarries between Georgian Bay and Kingston (Figure 2.15), predominantly within Ordovician formations and the exposed crystalline Precambrian basement.



Notes: Joint orientations are plotted as Gaussian contoured and smoothed rose diagrams. Figure is from NWMO and AECOM (2011).

**Figure 2.15: Joint Orientations in and around South-central Ontario**

These studies recognized three regionally persistent joint sets oriented NNE, E, and SE. The results were supported by analysis of thousands of lineaments detected from Landsat TM and Radarsat SAR images of the same area. A fourth major set trending ESE (090°-120°) becomes important along the northeastern flank of the Michigan Basin and higher in the stratigraphy (Figure 2.15).

Rutty and Cruden (1993) conducted a study of fractures in the Balsam Lake area east of Orillia (Figure 2.15), where Ordovician rocks of the Bobcaygeon and Sherman Fall formations are exposed. Using a similar outcrop measurement and remote sensing approach to Andjelkovic et al. (1996 and 1997), they determined that fractures in the area have peak trends oriented 027°, 091° and 152° (NNE, E, SSE, respectively). Post-glacial (i.e., < 12,000 year) pop-up structures in the same area are predominantly oriented 118°, and have nucleated on a subset of the E-trending fracture set. These pop-ups are interpreted to have formed during rapid release of high in situ tectonic stress shortly after the retreat of the Laurentian ice sheet.

Joints measured in Silurian strata exposed in quarries and excavations in the Smithville (Niagara) area have peak orientations of 018°, 082°, 132°, and 152° (Gartner Lee Limited 1996). These results are generally similar to those determined by Rutty and Cruden (1993) and Andjelkovic et al. (1997) but with a subtle shift of the ENE set from 082° to 091°, and the NNE set from 018° to 027°. Joint set orientations from upstate New York exhibit a subtle shift of about 050° from NNE in the east to NNW in the west (Figure 2.15).

Andjelkovic et al. (1996, 1997) and Andjelkovic and Cruden (1998) have proposed the following interpretations for the formation of the major systematic vertical joint sets in south-central Ontario, in chronological order.

1. ***NNE-trending set***: these joints track the orientation of the structural grain of the underlying Precambrian basement with remarkable consistency. They are interpreted to have formed due to differential compaction of Paleozoic sediments over a structurally controlled "corrugated" basement-cover interface under conditions of high pore fluid pressure (i.e., Process (a) above).
2. ***SE-trending set***: most likely formed due to high in-plane stresses transmitted into the foreland of the Appalachian Orogeny (i.e., Process (b) above).
3. ***ESE-trending set***: formed due to regional crustal extension that affected all of eastern North America during the Jurassic opening of the Atlantic Ocean (i.e., Process (b) above).
4. ***ENE-trending set***: may be neotectonic in origin. This set may have formed during the current tectonic stress regime which is attributed to a ridge push mechanism that has remained approximately constant since the late Cretaceous (i.e., Process (b) above).

Alternatively, recent fracture mapping by Cruden (2011) suggests that the ENE-trending set near the Bruce nuclear site is contemporaneous with a N-striking fracture set and that both likely formed late during the Middle Devonian Period during subsidence and sediment burial under conditions of high pore fluid pressure (i.e., Process (a) above).

On a larger regional scale, Holst (1982) measured fracture orientations in Paleozoic strata from the northern and northwestern flanks of the Michigan Basin. Holst determined that there were four dominant orientations of vertical joints that define two sets of orthogonal joints oriented NW-SE and NE-SW, and N-S and E-W, respectively. A systematic variation in this dataset indicates that a significant control on dominant joint orientation may be related to position along the margin of the Michigan Basin. For example, the NE-SW striking joint set is dominant in the domain covering the northwestern margin of the basin while E-striking joints dominate along the

northern margin (Holst 1982, Figures 1 and 4 therein). A similar conclusion was reached by Cruden (2011) who suggested that radial tensile stress generated during Middle Devonian basin-centered subsidence (Howell and van der Pluijm 1999) may have produced a basin concentric fracture set. At the Bruce nuclear site, this fracture set is one of two dominant sets and strikes NNW in accordance with the position of the site along the east-northeastern margin of the basin.

## **2.2.7 Quaternary Geology and Glaciation**

### **2.2.7.1 Regional Quaternary Geology**

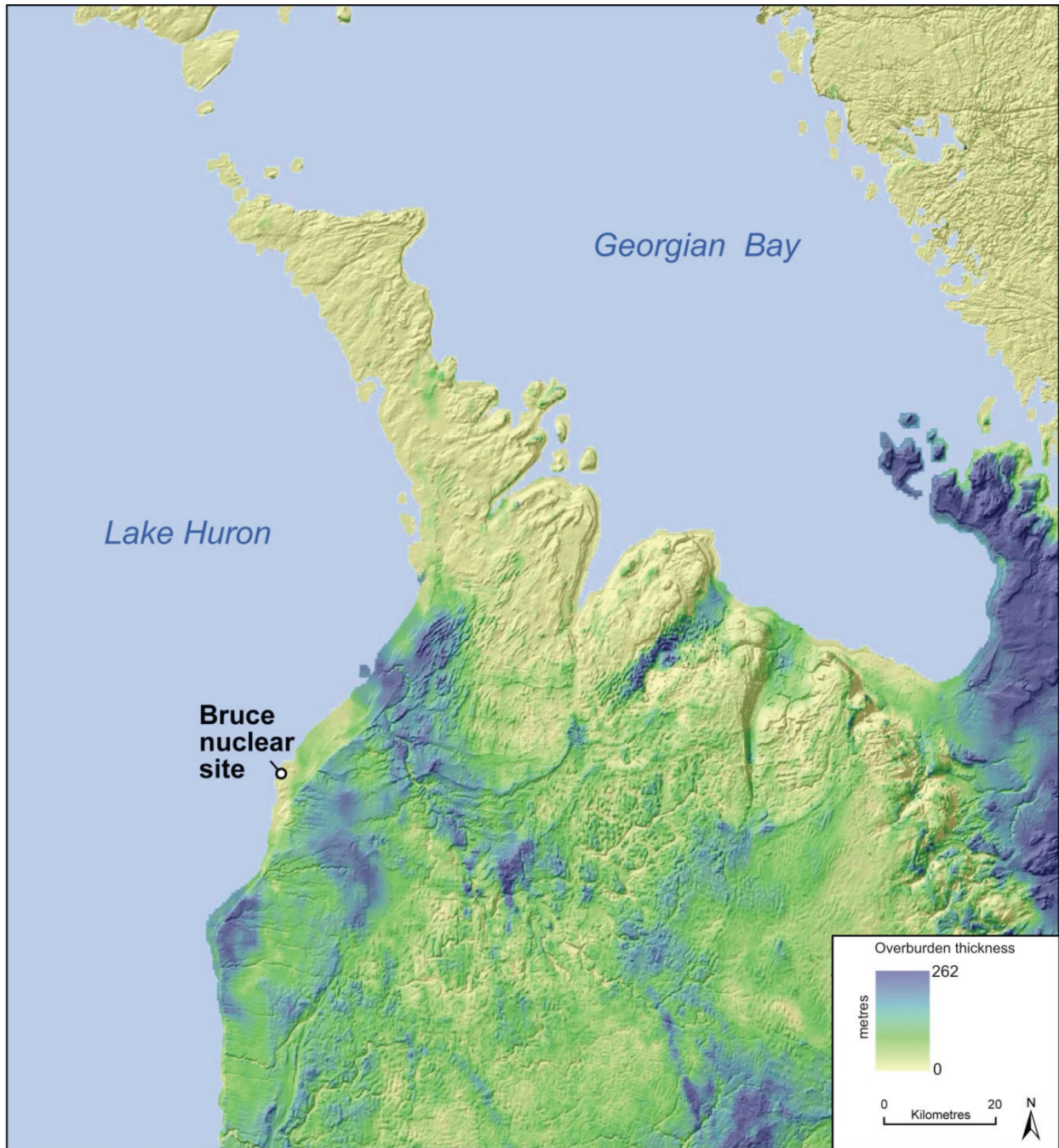
The Quaternary Period represents the last 2.588 million years of geologic history. In the last million years, the North American continent has endured nine glacial events (Peltier 2011). The thickness of Quaternary sediments in the DGR study area is shown in Figure 2.16 and described in AECOM and ITASCA CANADA (2011). The unconsolidated materials consist mainly of the following: (a) ground moraine or glacial till laid down directly by the ice; (b) glaciofluvial deposits, the sand and gravel deposited by water from the melting glacier; (c) glaciolacustrine deposits, the clays, silts, and sands deposited in glacial lakes; and (d) ice contact deposits formed at the margin of the glacier. Quaternary sediment thicknesses vary across the Bruce nuclear site from about 1 m at the lakeshore to 20 m in the southeastern part of the site and overlying the Palaeozoic rocks at the DGR drill sites (INTERA 2011).

The past glacial events, which markedly altered the landscape and physiography of southern Ontario, created significant external perturbations on the sedimentary sequence and regional groundwater flow systems. Peltier (2011) provides a detailed account of the glacial process and a series of constrained numerical simulations of recent glacial history using the University of Toronto Glacial Systems Model (UofT GSM) as an analogue to predict future glacial conditions as they may affect the Bruce nuclear site.

The Late Pleistocene Laurentide Ice Sheet that developed in the Arctic and advanced over most of Canada into the United States began approximately 120,000 years ago (Peltier 2011). At last glacial maximum (LGM), approximately 25,000 years ago (-25 ka), the Laurentide Ice Sheet (LIS) surpassed 2,800 m in thickness over the most glaciated regions of the continent (Figure 2.17). Within the Great Lakes region, as the ice sheet retreated 14,000 years ago, glacial melt waters from the retreating ice filled erosional depressions that evolved into the modern day Great Lakes Basin (GLB). The weight of the ice sheet depressed the surface of the earth by approximately 600 m (Peltier 2011). After the ice retreated, the earth's surface has rebounded. This process is known as glacio-isostatic adjustment (GIA) and is still occurring today. In the Great Lakes region, the magnitude of GIA increases northward with uplift rates of about 1.5 mm/a. Conversely, GIA induces subsidence to the south of the GLB at about the same rate, thus the continent is tilting slightly upward in the north (Peltier 2011).

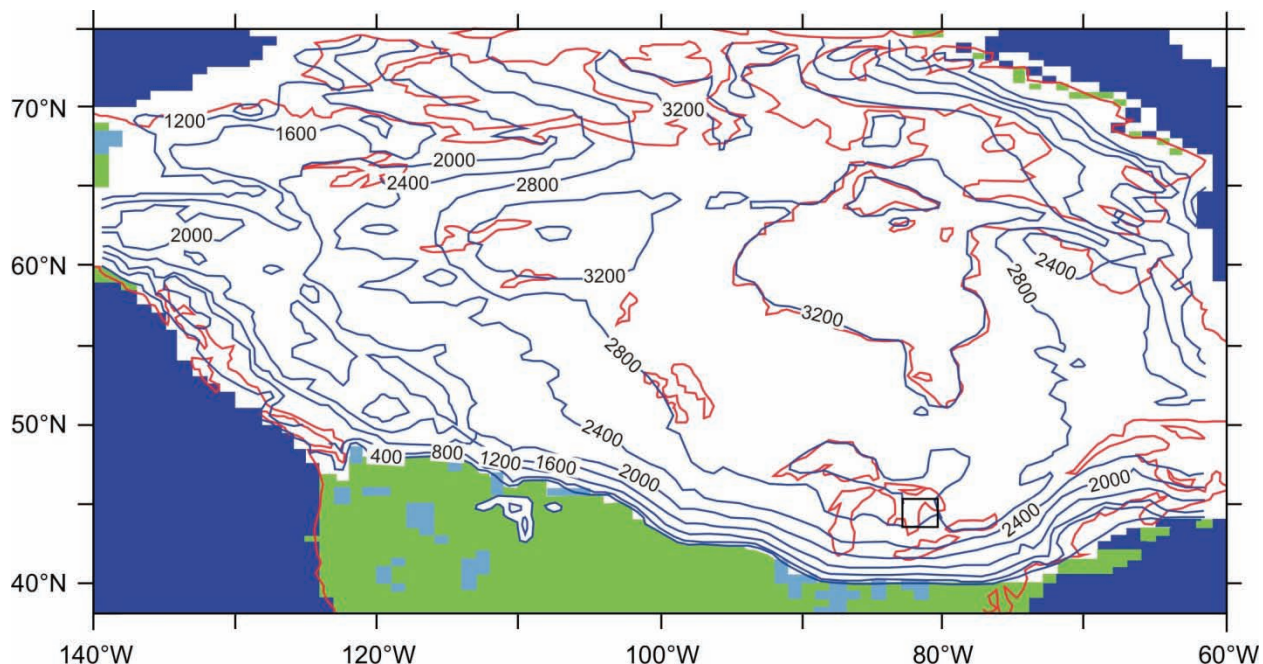
Evidence for each single glacial period is derived, in part, from isotopic analysis of undisturbed deep-sea cores. The determination of relative concentrations of  $^{16}\text{O}$  and  $^{18}\text{O}$  in pore fluids at different depths within the cores yields a high-resolution quality proxy for understanding continental ice-sheet volume. The lighter  $^{16}\text{O}$  isotope is evaporated preferentially and precipitated to build up the northern ice sheets; confirmation is obtained from ice cores collected in modern day glaciers. Another source of evidence includes relative sea level histories that provide a direct measure of the transfer between oceanic and land ice, for example in the Caribbean (Peltier and Fairbanks 2006, Peltier 2011).





Notes: Image is from Google Earth with OGS Quaternary thickness data.

**Figure 2.16: Quaternary Overburden Thickness in the RSA**



Notes: Contour interval is in metres. Figure is from model nn9921 of Peltier (2011).

**Figure 2.17: Laurentide Ice Sheet Thickness at Last Glacial Maximum (-25 ka)**

The UofT GSM (Peltier 2011) was applied to simulate glacial ice-sheet and ground surface conditions at the Bruce nuclear site during the Laurentide glaciation. Among other states, the GSM provided time series predictions of normal stress (ice-sheet thickness), permafrost depth, basal ice-sheet temperatures, crustal depression and uplift, and glacial melt water production. It is evident from the simulations that three periods of glacial advance and retreat across the Bruce region occurred with maximum ice sheet thickness approaching 2.5 km at last glacial maximum approximately 25,000 years ago (-25 ka). The model has been calibrated against multiple data sets including relative sea level curves, ground surface uplift rates, and radiocarbon-dated ice-sheet margins during retreat to yield a series of glaciation scenarios. Peltier (2011) also points out that it will be approximately 60,000 years before conditions are suitable for the next advance of a continental scale glaciation.

In Section 6.2, the glacial scenario is discussed further; the UofT GSM results are coupled to transient simulations of groundwater system response and perturbation in order to assess repository stability with respect to glacial events. It is noteworthy that the accumulation of greenhouse gases in the atmosphere has created uncertainty with respect to the timing of the next glacial onset. Regardless, the GSM predictions provide a conservative basis to understand glacial-induced perturbations on the repository and groundwater system necessary to demonstrate repository safety.

### 2.2.7.2 Glacial Erosion

As part of this study, an investigation was commissioned to evaluate the possible impact of erosion at the Bruce nuclear site over the lifetime of the Bruce DGR. The study reports are presented in Hallet (2011). Estimates of erosion were based on the rates of erosion that

occurred during the Quaternary Period. The long-term climate-change study (Peltier 2011) suggested that the region will be subjected to major glaciations, recurring every approximately 100,000 years.

The study looked at a number of independent estimates of total erosion spanning decades of research pertaining to erosion. These earlier studies covered the following four broad areas of study:

- Available geological studies from the Laurentide Ice Sheet (LIS) area (Hallet 2011);
- Studies of glacial erosion in diverse areas beyond the LIS area (e.g., alpine glaciers, Antarctica);
- Direct geological observations from the Bruce Peninsula and other nearby areas in southern Ontario; and
- Glacial erosion at the Bruce nuclear site based on the UofT GSM.

Pertinent results of each of these areas of study are provided in the following subsections.

### **Glacial Erosion Estimates from Studies of the LIS area**

Glacial erosion can occur by abrasion, quarrying, and mechanical erosion by melt water. Regardless of the mechanism, evacuation of debris can be limited because excavation is possible until water and sediment can no longer be evacuated due either to an insufficient hydraulic head gradient to drive subglacial water out of the basin, or the lack of adequate subglacial pathways for water. In terms of erosion at a local level, the basal sliding velocity is the primary factor controlling the rate of erosion. However, rapid basal velocity does not necessarily correlate with rapid erosion at the base of the glacier and may be decoupled from the bedrock surface by a thin layer of basal melt water.

A number of studies have produced estimates of the amount of erosion by the LIS and Fennoscandian ice sheets with a wide range of results. Geomorphic studies indicate many examples where the pre-glacial regoliths or river valleys have been preserved and most workers suggest that total erosion during the Quaternary did not exceed 10 m to 40 m for both the LIS and Fennoscandian ice sheets (Sugden 1976, Lidmar-Bergstrom 1997).

Other studies have estimated the amount of erosion based on sediment volumes produced from the ice sheet. There have been a number of studies in this area since the 1940s with varying results ranging from 120 m over 3 Ma (Bell and Laine 1985) to 18 to 30 m over the last glacial cycle (~100,000 years) (Elverhøi et al. 1995).

Estimates of erosion have also been provided by studies looking at the current location and bathymetry of the GLB. The origin of the lakes is thought to be from a combination of focused glacial erosion and pre-glacial bedrock valley systems (Larson and Schaetzl 2001). The deep excavation of the GLB, especially Lake Superior, suggests that during the Quaternary, erosion of bedrock by the Laurentide Ice Sheet may have exceeded 600 m locally and represents a maximum erosion scenario. Assuming that all of this erosion took place over the last 2 million years, this suggests a rate of differential erosion of 0.33 mm/a, which would be a maximum for the region. However, Hallet (2011) concludes that it is highly unlikely that a similar glacial excavation could occur at the Bruce nuclear site because the exceptional erosion at Lake Superior represents a rare condition. Further, there is a tendency for ice lobes and interlobate areas to occur at generally the same locations in successive glaciations and so the general configuration of the bedrock surface may have been established in pre-Pleistocene times (Hallet 2011). Hence, the topographic high at the Bruce nuclear site, and other topographically

elevated areas, tend to have limited erosion relative to the erosion that occurred in the adjacent lake basins.

An important study by Hildes et al. (2004) provides the results for a large-scale physically based model of subglacial processes in which the cumulative erosion of a full glacial cycle (approximately 120,000 years) for the LIS were calculated. The model predicted an average ranging from 0.41 m to 0.58 m of total erosion and a maximum of 1.63 m of total erosion. The authors of the report point out a number of ways in which the erosion may have been underestimated; however, the results convincingly suggest that a great deal of erosion did not occur.

Cosmogenic nuclide studies have also been used to assess erosion rates. Cosmic rays hitting the earth surface produce distinct nuclides (e.g.,  $^{10}\text{Be}$ ,  $^{26}\text{Al}$ , and  $^{36}\text{Cl}$ ) in rocks and surficial sediments. As soon as ice retreat exposes the bedrock surface to cosmic ray bombardment, cosmogenic nuclides build up over time and decrease with depth, becoming insignificant at 1 to 2 m below the rock surface. Using the cosmogenic nuclide technique, Colgan et al. (2002) studied a number of sites near the southern margin of the LIS during the LGM and concluded that it was unlikely that erosion at any of the sites was more than 10 to 30 m during the Quaternary.

### **Other Studies of Glacial Erosion**

Recent study of glacial erosion in contemporary high-latitude and tectonically active mountain range settings has yielded the highest known rates of glacial erosion in the world. These high rates are often associated with high-altitude coastal mountain ranges, where very erosive valley glaciers occur. In coastal Alaska, for example, glacial erosion rates are estimated to range from 1 to 15 mm/a, although higher rates (38 mm/a) have been noted for short periods of time (Koppes and Hallet 2006). The range of 1 to 15 mm/a translates to a range of 100 m to 1,500 m of erosion over 100 ka, assuming steady-state conditions. With tectonic uplift rates on the order of only 1 mm/a (Diraison et al. 1997), the erosion rate cannot be sustained over the long-term, otherwise the alpine setting would be flattened in one glacial episode. As a result, it is thought that there must be short-lived periods of rapid erosion, which are typically associated with glacial retreat.

The empirical upper limit of total erosion is provided by a few well-studied examples. The Lambert glacier system in Antarctica has a very thick ice sheet. It drains a major portion of the East Antarctic ice sheet and has been under ice cover for the last 34 Ma. Despite its size and longevity, the inferred glacial and preglacial erosion rates range from only 1 to 2 m/Ma (0.001 - 0.002 mm/a; Jamieson et al. 2005). Catastrophic floods associated with glacial terrains have also been known to be very erosive, particularly in localized areas. Widespread erosion by catastrophic floods from the former Lake Missoula and Pend'Oreille are well documented examples (e.g., Baker 1973, Atwater 1986) where repeating catastrophic flood events were capable of producing narrow areas (e.g., Lake Missoula and Pend'Oreille) of focused bedrock erosion of 300 – 400 m in depth. While catastrophic flood events have been documented in southern Ontario (e.g., Kor et al. 1991, Kor and Cowell 1998, Shaw 2002), they typically covered vast, low-relief areas rather than narrow channels. As such, the total depth of glacial erosion related to catastrophic outburst floods was estimated to be on the 1 to 30 m scale.

### **Direct Geological Observations from the Bruce Peninsula**

There is abundant and unequivocal field evidence in southern Ontario of intense glacial erosion of bedrock by ice or subglacial melt water. Many researchers have attributed these features to catastrophic melt water floods (e.g., Shaw 2002, Kor et al. 1991). The French River area, north of the Bruce Peninsula, has been well studied (Kor et al. 1991) and provides many good examples of subglacial melt water erosional features on bedrock, such as potholes, sculpted and elongated s-forms, flutes, etc. Kor and Cowell (1998) documented suites of erosional marks on the bedrock surface on the Bruce Peninsula down gradient of the French River area. All of these features reflect pervasive bedrock scouring under the LIS across the Bruce Peninsula. However, although large-scale subglacial flooding and/or sliding ice sculpted the bedrock surface distinctly, the total erosion of bedrock was limited to, at most, a few tens of metres over tens of kilometres, roughly transverse to the southwesterly-oriented flow direction (Hallet 2011).

A large number of distinct reentrants in the Niagara Escarpment have attracted attention, and have been interpreted as demonstrating large-scale erosion by ice (Straw 1968) or by melt water floods (Kor and Cowell 1998). Based on an assessment of depth and length of the reentrants in the Owen Sound area, as well as a consideration of the possible westward retreat of the Escarpment, 200 to 330 m of erosion is thought to be necessary to create the reentrants. Several factors are likely to be responsible for the differential erosion that created the reentrant. Erosion was presumably localized because pre-existing topography funnelled the ice and subglacial water to these sites or the bedrock was more pervasively fractured in the reentrants. Therefore, the amount of erosion related to catastrophic melt water floods or glacial scouring is very likely considerably less than this 200 to 330 m estimate.

In terms of small-scale features, there are numerous examples of relatively fresh exposures of glacially abraded bedrock proximal to the site and along the Bruce Peninsula suggesting that relatively little bedrock was removed via glacial erosion. Figure 2.18 shows several field photographs which indicate the preservation of multiple generations of cross-cutting striations on the bedrock surface (Hallet 2011).



Notes: All photos (Hallet 2011) are viewed down the former ice flow direction (highlighted with white arrows). (a) Weathered flutes on naturally exposed surface near the northern tip of the peninsula. (b) Freshly exposed limestone surface entirely covered with long, distinct striations, Adair Quarry. (c) Freshly exposed southwest trending shallow striations (solid arrow) crossing older and deeply scoured striae (broken arrow).

**Figure 2.18: Photographs of Glacially Scoured Bedrock in the Bruce Peninsula Region**

Several important conclusions regarding the extent of bedrock erosion across the RSA can be drawn based on the examples shown in Figure 2.18, including:

- The preservation of multiple episodes and varying direction of basal flow suggests that significant bedrock erosion (> 1 to 10 mm) did not occur;
- Many continuous and long striae, relatively distinct yet shallow striae, and only very rare observances of friction cracks and lunate fractures suggests that the contact forces between the glacier and the bed were modest; and
- Pervasively striated surfaces typically have low relief (< 1 m), similar to the underlying bedding surfaces, which would not likely be the case if significant erosion of the bedrock had occurred.

### **Numerical Estimates of Glacial Erosion at the Bruce Nuclear Site**

The UofT GSM provides a quantitative framework for assessing glacial erosion rates as it includes a number of variables that relate to glacial erosion. For this study, erosion rates were calculated using the UofT GSM results that define: the duration of ice cover and temperate basal conditions; and the rate of basal melting, which is expected to control erosion rates. The model predicted that for most of the LGM, the LIS did not cover the Bruce nuclear site; on average the site was only covered roughly 25% of the time (Peltier 2011).

Glacial erosion was therefore calculated only when the site was ice covered. The most conservative estimate was made by using the highest known rates of erosion worldwide for the time that the model predicted the site was ice covered. This approach yields a result of 62 m and 201 m of erosion over the last 100 ka. This erosion rate is unlikely, however, because it is not reasonable to use the fastest known rates of glacial erosion in the world because they occur in a very different setting than the LIS. Taking into account site-specific factors, the total realistic erosion estimates at the site range from 2 m to 33 m, averaging 14 m (Hallet 2011).

Overall, the study by Hallet (2011) concluded that although uncertainties remain in ice sheet reconstructions and estimates of erosion by ice and melt water, all lines of study indicate that, at the Bruce nuclear site, glacial erosion would not exceed a few tens of metres in 100 ka with a conservative site-specific estimate of erosion of 100 m per 1 Ma. This conclusion is supported in the literature, by field investigations, and using numerical modelling.

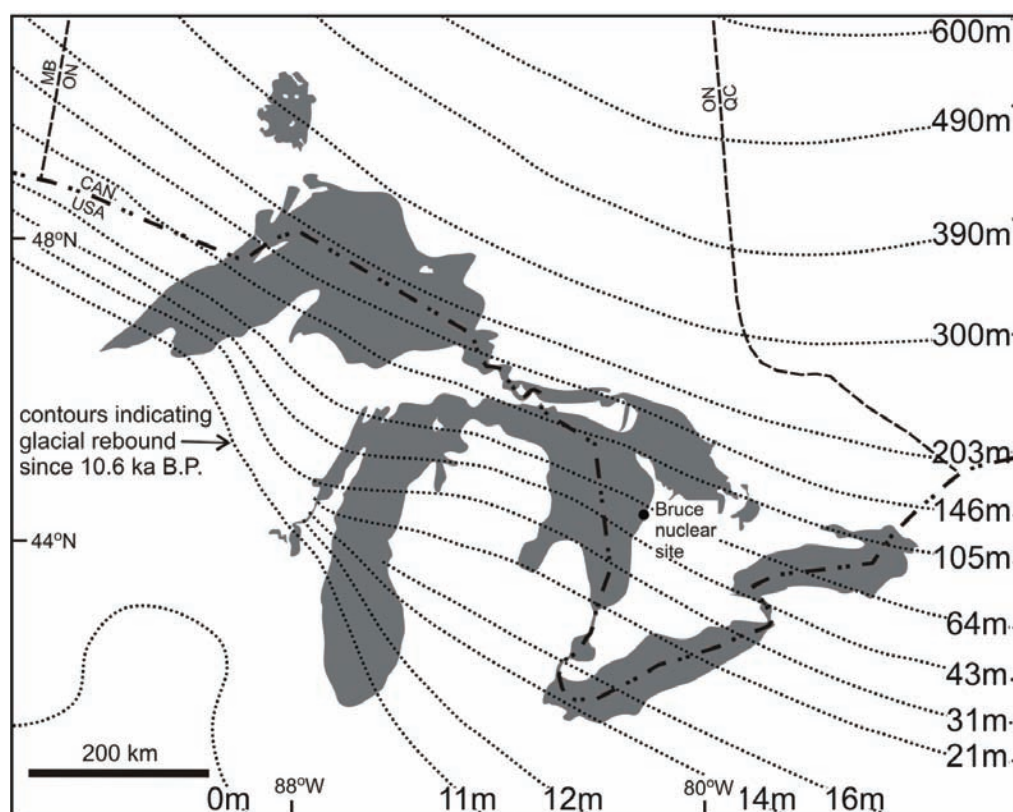
### **2.2.7.3 GIA of the Huron Basin**

Deglaciation of the GLB occurred as the ice margin of the LIS retreated generally in a northeasterly direction in a series of pulses, first exposing the Lake Erie basin approximately 15.5 ka ago and finally the Lake Superior basin at about 9.5 ka ago (Dyke et al. 2003, Slattery et al. 2007). During this retreat, a series of ice-marginal and proglacial lakes formed shorelines of different ages that are upwarped today toward the north-northeast in the direction of thicker and longer lasting ice. This upwarping is the cumulative effect of GIA of the Earth's crust following the removal of the former ice sheet load. This differential rebound or adjustment proceeded throughout ice-marginal retreat and postglacial time at decelerating rates of uplift. Lake level measurements obtained from lake gauges located between the south and north shores of the GLB indicate that isostatic adjustment is still occurring at present within the GLB (Co-ordinating Committee on Great Lakes Basic Hydraulic and Hydrologic Data 1977, Tushingham 1992, Mainville and Craymer 2005).

Differential GIA in the Huron Basin has long been recognized from the observed deformation of raised shorelines, particularly those associated with the Algonquin series of glacial lakes

(12.0-10.5 kaBP) and the postglacial Nipissing Great Lakes (Goldthwait 1907, Leverett and Taylor 1915, Hough 1958, Lewis and Anderson 1989, Schaetzl et al. 2002). From Nipissing time, ~5.5 kaBP to present day, lake levels dropped in the northern Huron – Georgian Bay region as the basin upwarped and drainage outlets in the southern portion of Lake Huron were activated. Surface drainage patterns varied markedly throughout the GLB during the deglaciation (see Figure 21.56 of Barnett 1992).

Figure 2.19 presents a paleo-elevation model for the GLB relative to an area SW of Lake Michigan beyond the leading edge of the last glacial advance. This figure was compiled by subtracting modern digital elevation data from reference uplift contours to generate a paleo-elevation model. Isobases related to GIA are typically defined by the elevations of differentially uplifted shorelines and beach ridges of a former lake plane (Goldthwait 1907, Leverett and Taylor 1915, Hough 1958, Lewis and Anderson 1989, Schaetzl et al. 2002). This model shows that the Bruce nuclear site has rebounded approximately 55 m since 10.6 kaBP.



Notes: Isostatic rebound is measured relative to an area southwest of Lake Michigan and beyond the southern limit of glacial advance during the last glaciation (modified from Lewis et al. 2005).

**Figure 2.19: Reference Isostatic Response Surface for the Great Lakes Basin region Portraying Glacial Rebound Since 10.6 kaBP**

## 2.2.8 Economic Geology

### 2.2.8.1 Petroleum Geology

Commercial accumulations of oil and gas hydrocarbons have been found in more than a dozen stratigraphic units throughout the Paleozoic sedimentary cover of southwestern Ontario (Figure 2.20). The main hydrocarbon exploration play types for the region are listed in Table 2.4.



Notes: Base map is from Ontario Ministry of Natural Resources Pool data supplied by the Oil, Gas and Salt Resources Library and the Ontario Ministry of Natural Resources. All pool boundaries are accurate as of October 2006. Pool boundaries are interpretive and approximate. Production boundaries are modified from Carter (1990).

**Figure 2.20: Principal Oil and Natural Gas Producing Regions and Storage Pools**



**Table 2.4: Hydrocarbon Exploration Plays in Southern Ontario**

<b>Play</b>	<b>Reservoir Rocks</b>	<b>Trapping Mechanism</b>	<b>Geographic Distribution</b>
Cambrian (CAM)	<ul style="list-style-type: none"> <li>Middle/Upper Cambrian-Middle Ordovician shallow marine sandstones and dolostones</li> </ul>	<ul style="list-style-type: none"> <li>Pools controlled by faulting and tilting (juxtaposition against low-permeability limestones of the Black River Group) or as permeability pinch outs around the edges of the Algonquin Arch</li> </ul>	<ul style="list-style-type: none"> <li>Mainly along the erosional boundary of the Cambrian along a line connecting Windsor and Hamilton.</li> <li>No active economic reservoirs known on the Michigan Basin side.</li> </ul>
Middle Ordovician Hydrothermal Dolomite (ORD)	<ul style="list-style-type: none"> <li>Hydrothermal dolostones within shallow marine carbonates of the Black River and Trenton groups</li> </ul>	<ul style="list-style-type: none"> <li>Occur as narrow, linear, vertically oriented, fault-related hydrothermal dolomitization zones in the vicinity of rejuvenated faults along which spatially limited dolomitization took place (permeability pinch-out). Upper Ordovician shales act as cap rocks</li> </ul>	<ul style="list-style-type: none"> <li>Southwest end of southern Ontario (London - Windsor area). Limited potential (not exploited) in the whole Niagara Megablock, low potential in the Bruce Megablock (3 small gas pools; low density of reservoirs expected because of less dense faulting and/or limited dolomitization).</li> </ul>
Lower to Middle Silurian Sandstones (CLI)	<ul style="list-style-type: none"> <li>Sandstones (Whirlpool, Grimsby/Thorold (Medina) formations) and dolomites (Irondequoit Formation) of the Appalachian Basin</li> </ul>	<ul style="list-style-type: none"> <li>Permeability pinch-out due to internal heterogeneity of the host formations (spatially variable cementation)</li> </ul>	<ul style="list-style-type: none"> <li>Occurrence of the sandstones and pools mainly along the north shore of Lake Erie (Appalachian Basin, Niagara Megablock)</li> </ul>
Middle/ Upper Silurian (Niagaran) Reefs (SAL)	<ul style="list-style-type: none"> <li>Reef limestones of the Guelph Formation, carbonates of the Salina Group (A1, A2)</li> </ul>	<ul style="list-style-type: none"> <li>Related to patch and pinnacle reefs in Guelph Formation</li> <li>All reservoirs are sealed by surrounding thick evaporite deposits of the Salina Group</li> </ul>	<ul style="list-style-type: none"> <li>Along the edge of the Michigan Basin (from Lake St. Clair north along the shore of Lake Huron)</li> </ul>
Middle Devonian (DEV)	<ul style="list-style-type: none"> <li>Shallow marine platform carbonates of Dundee Formation and Detroit River Group</li> </ul>	<ul style="list-style-type: none"> <li>Structural traps generated by dissolution of underlying salt</li> </ul>	<ul style="list-style-type: none"> <li>Southwestern Ontario (Chatham Sag)</li> </ul>

Notes: Modified from Mazurek 2004, Sanford 1993b, Carter (ed.) 1990, Lazorek and Carter 2008, Hamblin 2008.

Early hydrocarbon production was derived from shallow (120 m) Devonian carbonate reservoirs. After more discoveries in shallow Devonian reservoirs, commercial quantities of liquid

hydrocarbons were found in deeper Silurian rocks. Current exploration interest is focussed on targets in the southwestern tip of Ontario in Middle Ordovician carbonates and Upper Cambrian sandstones at depths of 800 to 1,000 m (GOLDER 2005). The majority of exploration is concentrated within the geographic triangle between London, Sarnia, and Chatham-Kent (AECOM and ITASCA CANADA 2011).

Given the potential for hydrothermal dolomitization within Ordovician rocks, these potential reservoirs are explored in further detail, including an evaluation at the site scale (see below and Section 2.3.6.2).

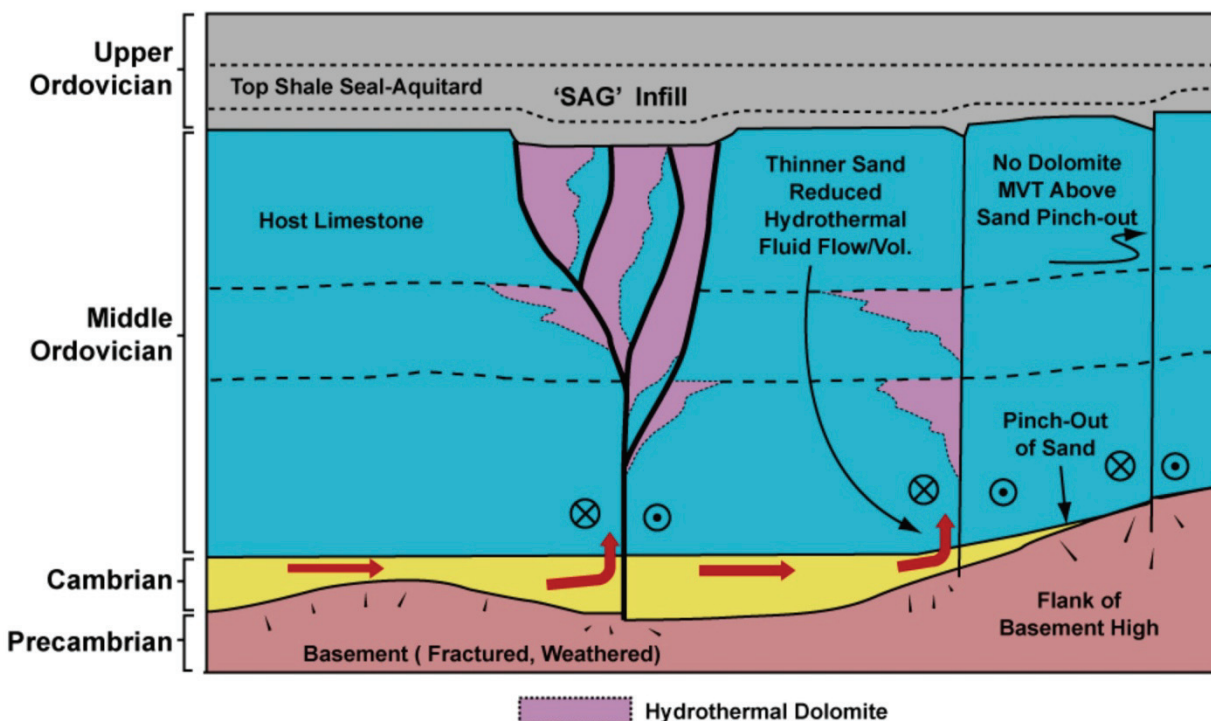
### **Ordovician HTD Reservoirs**

Studies of Middle Ordovician oil and gas fields in southwestern Ontario, Michigan, Ohio, and New York provide conceptual models of fault structure and associated reservoir development for HTD plays (Colquhoun 2004, Colquhoun and Johnston 2004, Smith 2006, Davies and Smith 2006). A comparison of Bruce nuclear site data with these conceptual models in Section 2.3.6.2 is used to evaluate the potential for Ordovician HTD reservoir rocks to occur at or adjacent to the DGR.

Recent work by Davies and Smith (2006) describes the mechanism for hydrothermal fluid flow and dolomitization in the Middle Ordovician as horizontal flow through the basal Cambrian and vertical flow along steeply-dipping strike-slip faults (Figure 2.21). In this model, the permeable basal sandstone focuses fluids from external sources to vertical fractures or fracture damage zones (commonly related to basement highs). The overlying Ordovician shale acts as an aquitard, inhibiting fluid flow. The “sag” feature commonly found above HTD facies in seismic reflection surveys (Figure 2.21) is generally interpreted to result from transtensional subsidence along a wrench fault system (Davies and Smith 2006). The reservoir is created within the dolomitized zones between faults. This structurally controlled model appears consistent with examples of HTD reservoirs from southern Ontario (Davies and Smith 2006, Carter et al. 1996, Bailey 2005).

Bailey (2005) speculated that without the presence of the porous Cambrian sandstone underlying the Ordovician limestones, the probability of developing a hydrothermal reservoir in those rocks would be poor. Davies and Smith’s (2006) schematic model shown in Figure 2.21 incorporates this idea by showing that regions with thinner Cambrian sands are associated with reduced volumes of HTD up-dip along a fault. This model also suggests that HTD may potentially be absent in areas above the Cambrian pinchout.

HTD reservoirs are variable in size, ranging from a few kilometres upwards to, for example, the Albion- Scipio field in central Michigan, which is some 58 km in length (Prouty 1988, Hurley and Budros 1990).



Notes: Hydrothermal fluid flow is focused along the basal Cambrian sandstone through transtensional strike-slip faults. Fluid flow is decreased as the Cambrian thins and HTD is absent above the Cambrian pinchout. Symbols inside circles indicate relative transcurrent movement towards (circles) and away from (crosses) the reader. This model may also apply to MVT mineralization. Figure is modified from Davies and Smith (2006).

**Figure 2.21: Schematic Representation of the Origin of Fracture-related HTD within the Ordovician Sequences of Ontario**

Only small hydrocarbon occurrences have been found within the RSA and adjacent areas (Figure 2.20). A total of 12 documented active and abandoned petroleum pools were identified within the boundaries of the RSA. Petroleum production within the RSA has been primarily natural gas from Ordovician HTD and Silurian reef or carbonate traps. The only actively producing Ordovician pool in the RSA is the Arthur Pool (Black River Group), which has produced 33,871,600 m<sup>3</sup> of natural gas between 1968 and 2006. This pool; however, is situated southeast of the crest of the Algonquin Arch in the Appalachian Basin (Sanford 1961). Small amounts of crude oil have been produced from Silurian reef pools within the RSA. Cumulative natural gas production totals amount to approximately 200 million m<sup>3</sup> or less than 0.1% of the cumulative southern Ontario natural gas production. Crude oil production amounts to a negligible 1,441.7 m<sup>3</sup>, or approximately 0.01% of the cumulative production in Ontario.

### **Conceptual Plays**

Recent advances in petroleum exploration have identified a number of possible new conceptual plays within the Lower and Middle Paleozoic sequences of southern Ontario (Hamblin 2008). These conceptual plays include:

- The Cambrian sandstone/sandy dolostone play around the edges of the Algonquin Arch into the Michigan Basin and possibly even onto the erosional surface of the arch (Bailey 2005);

- The basal Middle Ordovician Shadow Lake sandstone where it overlaps, and may be in communication with, the Cambrian (Lazorek and Carter 2008, Hamblin 2008);
- The Upper Ordovician shoreline-related sandstones and carbonates at the tops of shallowing-upward sequences in the Georgian Bay and Queenston Formations (Hamblin 2003);
- The discontinuous Lower Devonian Oriskany and Springvale sandstones (Hamblin 2008); and
- Shale gas (thermogenic and/or biogenic) produced from shales of the Upper Ordovician Collingwood and Blue Mountain (Utica-equivalent) formations; the late Middle Devonian Marcellus Formation; and the Upper Devonian Kettle Point Formation, where they are overlain by glacial till (Hamblin 2006, Hamblin 2008, Engelder 2011).

From an evaluation of existing literature (AECOM and ITASCA CANADA 2011), the probability of future identification of potential economic oil and/or gas resources adjacent to the proposed Bruce nuclear site is low. Although porous Cambrian sediments have been identified in core within the RSA, no oil or gas shows have been encountered during drilling.

Ordovician HTD reservoirs have been shown to occur in porous and permeable zones in the vicinity of rejuvenated major faults with intersecting fracture systems. As a result, the geological investigations and 2D seismic study specifically evaluated the potential for this petroleum play at the Bruce nuclear site. The results discussed in Section 2.3.6.2 do not support the presence of a commercial HTD reservoir at, or directly adjacent to, the Bruce nuclear site.

Silurian natural gas pools have been identified within this area of the RSA at depths of 490 to 580 m; however, none of the reefs adjacent to the DGR, as shown in the 3DGF, encountered commercially viable resources. In addition, the Bruce nuclear site is located within an inter-reef lithology (AECOM and ITASCA CANADA 2011). Minor oil showings in the Silurian Guelph Formation from the DGR core are associated with similarly non-commercial hydrocarbon accumulations (INTERA 2011).

The potential for Devonian hydrocarbon resources to occur throughout the RSA is low and restricted to the southwest quadrant where the oil-hosting Dundee and Lucas Formations are underlain by Salina Group evaporites. The probability of commercial quantities of hydrocarbons occurring in these Devonian units northeast of the Kincardine-Wingham area is substantially reduced because of the absence of overlying Hamilton Group limestones and shales to provide an adequate seal.

### **Ordovician Shale Gas**

A study by Engelder (2011), which included an evaluation of shale gas potential, concluded that the likelihood of commercial shale gas at the Bruce nuclear site would be low for a number of reasons related to gas genesis. Primarily, this is due to the Total Organic Carbon (TOC) content of even the darkest shale reaching a maximum of only 2.5% in the Collingwood Member of the Cobourg Formation in the DGR boreholes (INTERA 2011, their Figure 3.14). When this observation is combined with the low thermal maturity around the Bruce Peninsula, which barely reached the oil window (Legall et al. 1981, Obermajer et al. 1996, Engelder 2011), there is little chance of encountering commercial accumulations of in situ generated hydrocarbons.

The low degree of thermal maturation in the vicinity of the Bruce nuclear site is consistent with the recognition that the methane encountered at depth within the Ordovician shale has a biogenic rather than thermogenic origin (INTERA 2011, their Section 4.6.7.1). Economic

biogenic gas shales exhibit very high TOC values, are encountered at very shallow depths, and are extensively fractured. For example, the highly prospective Devonian Antrim shale yields 5 to 15% TOC, over a thickness of approximately 48 m at depths ranging between 150 and 760 m. The natural fracture network distributed throughout this gas play is critical to its productivity (Curtis et al. 2009). In this manner, some near-surface examples of the exposed (i.e., shallow) Upper Devonian Kettle Point Formation shale in southwestern Ontario, with TOC values of up to 15%, might represent good candidate biogenic shale gas plays (e.g., Beland-Otis 2010). However, the Kettle Point Formation has been eroded away within the RSA. A maximum TOC of only 2.5% encountered over a less than 10 m thick interval at the top of the Collingwood Member (INTERA 2011 their Figure 3.15) argues against any economical concentration of shale gas at the Bruce nuclear site.

The absence of remarkable natural gas shows during drilling of the DGR boreholes is consistent with the argument against commercial accumulations of either thermogenic or biogenic shale gas hosted by the Ordovician shales beneath the Bruce nuclear site (INTERA 2011).

### **2.2.8.2 Ordovician Cap Rock Seal**

Geosynthesis investigations included an assessment of the cap rock integrity and seal potential of the cap rock at the Bruce nuclear site based upon evaluation of petroleum traps in the Appalachian and Michigan basins (Engelder 2011). The purpose of this study was to explore whether the thick package of Upper Ordovician shale rocks at the DGR would provide a natural barrier to migration of fluids. A good cap rock is capable of maintaining a gas-pressure differential against hydrostatic pressure (pressure in a free column of water) for significant lengths of time. Commonly this stack consists of gas over petroleum over water, trapped for a long enough time that equilibrium is established with each fluid at its own hydrostatic gradient (Engelder 2011). The cap rock seal includes the Collingwood Member, the Blue Mountain Formation, the Georgian Bay Formation, and the Queenston Formation, totalling 211 m of low-permeability shale rocks overlying the proposed DGR (INTERA 2011). The clay content of the Blue Mountain Formation is also high, relative to that observed in economically productive gas shales in the Appalachian Basin. This high clay content can lead to more effective sealing of minor displacement faults or fractures that could exist within the cap rock (Engelder 2011).

Several Devonian and Ordovician shale sequences are known to provide effective hydrocarbon seals within the Appalachian and Michigan basins and are suitable natural analogues to the cap rock at the Bruce nuclear site. A comparison of these known seal rocks to the Ordovician shale at the Bruce nuclear site is made possible because the seal rocks correlate stratigraphically with Upper Ordovician shales across the Appalachian and Michigan basins. The Devonian section of the Appalachian Basin contains two black shales (Marcellus and Genesee), which, like the Ordovician sequence at the Bruce nuclear site, were the product of a tectonically induced sea level rise and therefore share the same mechanism for the generation of accommodation space. In addition, the Blue Mountain Formation in Ontario correlates with a number of formations across the Appalachian-Ouachita Stratigraphic Sequence (A-OSS) that include the Utica (MI, NY, PA), Antes (PA), Pleasant Point (OH), Reedsville (PA), and Martinsburg (PA) formations (Engelder 2011).

These formations form hydrocarbon seals across the Michigan and Appalachian basins throughout a variety of different tectonic and stratigraphic settings. The Ordovician cap rocks at the Bruce nuclear site contain many favourable attributes that compare well to these analogues within the A-OSS. These include formation scale underpressures, low permeability, comparable rock density, similar electric log properties and low thermal maturity, which in turn will

significantly reduce the occurrence of natural hydraulic fracturing. While individually none of these formations provide an identical (one to one) analogue for the cap rock at the Bruce nuclear site, they do, however, when examined and combined together, contain a wide ranging set of favourable properties that are directly comparable and demonstrate that long-term integrity of the Upper Ordovician cap rock at the Bruce nuclear site will be maintained for geologic time periods.

A potential natural analogue for the DGR shale cap rock is the Devonian Marcellus black shale of the Appalachian Basin, where gas traps below the Marcellus reach more than 70% of the overburden stress and are therefore overpressured. The Marcellus black shale is also overpressured throughout the northern Appalachian Basin, leaving no doubt about its effectiveness as a seal. Underpressured compartments in layered sediments also indicate effective sealing qualities. Examples of this type of behaviour are found within the southern portion of the Appalachian Basin and within the shale seal rock at the Bruce nuclear site.

Gas generation can lead to extensive and pervasive natural hydraulic fracturing (NHF). However, the integrity of the seal rock at the DGR was protected by the low concentration of TOC and a low degree of thermal maturation, and is consistent with the long-lived formation underpressures. The major structural mechanism which could potentially disrupt the seal integrity at the DGR is probably basement related faulting that penetrates upward into the seal rock. Seismic evidence may suggest that some basement faults exist proximal to the Bruce nuclear site (INTERA 2011), however, no such faults appear to penetrate the Upper Ordovician shale aquitard above the DGR aquiclude. This may reflect the fact that these faults have been inactive since the deposition of the seal rocks (i.e., greater than 400 Ma ago), or that the high clay content of the cap rock at the DGR acted to promote self-sealing of the basement-related faults at the DGR. A regional compilation of brittle subsurface faults (Armstrong and Carter 2010) suggest that the youngest strata affected by basement-seated faults are the Ordovician-aged Trenton Group limestones (Figure 2.5). Therefore if any faults exist proximal to the proposed DGR, they are ancient and inactive.

The lack of any appreciable volume of HTD observed during site characterisation activities (INTERA 2011 and Section 2.3.6.2 herein) argues against the likelihood of a major Paleozoic fault system having been active in the vicinity of the Bruce nuclear site. The presence of strong hydraulic gradients across the Cambrian and Ordovician, and results of hydraulic testing and geochemical analysis (INTERA 2011) suggest that any possible faults are completely sealed and do not represent permeable pathways (refer to Chapter 4 and Chapter 5 for further discussion). The shale cap rocks at the Bruce nuclear site represent a natural > 200 m thick seal that has long-term integrity and the capability to prevent migration of oil and gas over geological time (Engelder 2011). Similarly, the shale cap rock is well suited to act as a primary barrier to contaminant transport in the subsurface. This conclusion is supported by the hydraulic and petrophysical testing of the shales (INTERA 2011) and hydrogeological modelling (Chapter 5).

### **2.2.8.3 Bedrock Resources**

Many of the Paleozoic rocks identified at the Bruce nuclear site have been exploited elsewhere in the RSA (Figure 2.22) and across Ontario for their aggregate potential, for building stone, and brick manufacture. Generally, for these industries to be economic, the rock source must be close to the surface, less than 8 m deep, and be of mineable thickness. Most bedrock extraction operations are developed in areas where the overburden thickness is 3 m or less. Therefore, most of the rock aggregate is extracted in quarries along the Niagara Escarpment or

areas of shallow overburden in Bruce County. Boreholes DGR-1 and DGR-2 encountered approximately 20 m of overburden at the site, whereas bedrock is exposed to the west on the lake shoreline (INTERA 2011).

Table 2.5 summarizes the various economic bedrock units and their locations (Figure 2.22) in the RSA. Current quarrying activities in the RSA are almost exclusively limited to Middle Silurian dolostones, which are extracted for building stone, landscaping stone, and aggregate.

Massive dolostones of the Warton-Colpoy Bay Member of the Amabel Formation are currently actively quarried for aggregate and dimension stone products in the southern and central Bruce Peninsula on or near the Niagara Escarpment in Albemarle and Sydenham Townships in Bruce County (Derry Michener Booth and Wahl, and Ontario Geological Survey 1989).

**Table 2.5: Summary of Economic Bedrock Units in the RSA**

Age	Group/Formation	Type	Potential Usage	Location in RSA	Quarried in RSA?
Mid Upper Ordovician	Lower Lindsay Formation (Cobourg Formation)	Limestone	Aggregate	Collingwood area	Past producer
Mid Upper Ordovician	Lindsay Formation (Collingwood Member)	Calcareous shale	Oil Shale	Collingwood area	Past producer
Upper Ordovician	Blue Mountain Formation	Noncalcareous shale	Structural clay products, pottery	Collingwood – Georgian Bay	Past producer
Upper Ordovician	Georgian Bay Formation	Limestone and shales	Manufacture of bricks	Collingwood area – Georgian Bay shore	Past Producer
Upper Ordovician	Queenston Formation	Shale	Brick Making	Bruce Peninsula/ Base of Niagara Escarpment	Past Producer
Lower Silurian	Whirlpool Formation	Sandstone	Building stone	Niagara Escarpment.	No
Lower Silurian	Manitoulin Formation	Dolomitic limestone	Landscaping and building stone, aggregate	Niagara Escarpment St. Vincent and Sarawak Counties	Yes
Lower Silurian	Cabot Head Formation	Shales	Aggregate potential/brick, tile	Niagara Escarpment	No
Middle Silurian	Dyer Bay Formation	Dolostone	None	Northern Bruce Peninsula	No
Middle Silurian	Wingfield Formation	Shale/ dolostone	None	Northern Bruce Peninsula	No
Middle Silurian	St. Edmund Formation	Dolostone	Fill, crushed stone, asphalt and concrete suitable	Northern Bruce Peninsula	No

Age	Group/Formation	Type	Potential Usage	Location in RSA	Quarried in RSA?
Middle Silurian	Warton/Colpoy Bay Member of the Amabel Formation	Massive dolostone	Industrial mineral use (glass manufacturing), dimension stone, dolomitic lime, crushed stone, concrete aggregate and building stone	On or near Niagara Escarpment to end of Bruce Peninsula (Grey County, Bruce County - Albemarle Twp., Sydenham Twp.), Manitoulin Island	Yes
Middle Silurian	Guelph	Thickly bedded dolostone	Dolomitic lime, crushed stone, concrete aggregate and building stone	Bruce County – Amabel Twp.	Yes
Middle Silurian	Guelph (Eramosa Member)	Thinly bedded bituminous dolostone	Building and landscaping stone (flag, paving, ashlar, and polished dimension stone)	Bruce County – Albemarle Twp., Amabel Twp. – Grey County – Keppel Twp.	Yes
Upper Silurian	Salina Group	Evaporite	Salt, brine	Southwestern ON: Windsor, Goderich, Sarnia, North Wellington Cty. Only in subsurface.	Yes
Middle Devonian	Detroit River Group (Amherstburg (Formosa Reef) and Lucas Formations)	Limestone	Cement manufacture, high purity and used by the steel, cement and chemical industries	southern Grey and northern Wellington Counties	Past producer
Middle Devonian	Anderdon Member limestone of the Lucas Formation	Limestone	Aggregate, building stone, armour stone, lime and cement	Southwest quadrant	No

Notes: Twp = township. Data are from a recent aggregate resources inventory report (OGS 2004).

An economically important bedrock resource in the RSA is the thinly bedded bituminous dolostone Eramosa Member of the Guelph Formation, which is currently quarried for a variety of building stone products from numerous quarries in the southern and central Bruce Peninsula (Armstrong and Meadows 1988). A number of presently abandoned Eramosa quarries also exist in the northwest (Bruce County) portion of the RSA. The dolostones of the Manitoulin Formation are quarried intermittently along the Niagara Escarpment in St. Vincent and Sarawak Townships for aggregate. The Georgian Bay Formation and Queenston Formation shales have been used in the past for brick making.

The Upper Silurian Salina Group is characterized by dolomite, shale, gypsum, and salt. This formation has little value as a source for crushed stone aggregate but salt is extracted to the south of the RSA at Goderich. Rock salt has been mined continuously since 1959 at depths



approaching 500 m. The Salina salt has been dissolved and removed over most of the RSA and beneath the Bruce nuclear site through natural geologic processes. The limestones of the Middle Devonian Detroit River Group (Amherstberg and Lucas formations) occur in the southwestern corner of the RSA. The Formosa Reef Limestone, which has a thickness of up to 26 m of high-purity limestone, is a member of the Middle Devonian Amherstburg Formation and subgroups in the southwest of the RSA.

Sphalerite concretions within Silurian dolomite on the Bruce Peninsula have attracted some base metal exploration interest for potential MVT deposits (e.g., Sangster and Liberty 1971). Evidence of historical exploration (e.g., shafts, trenches) exists on the peninsula; however, no commercial MVT deposits have been found within Ontario.

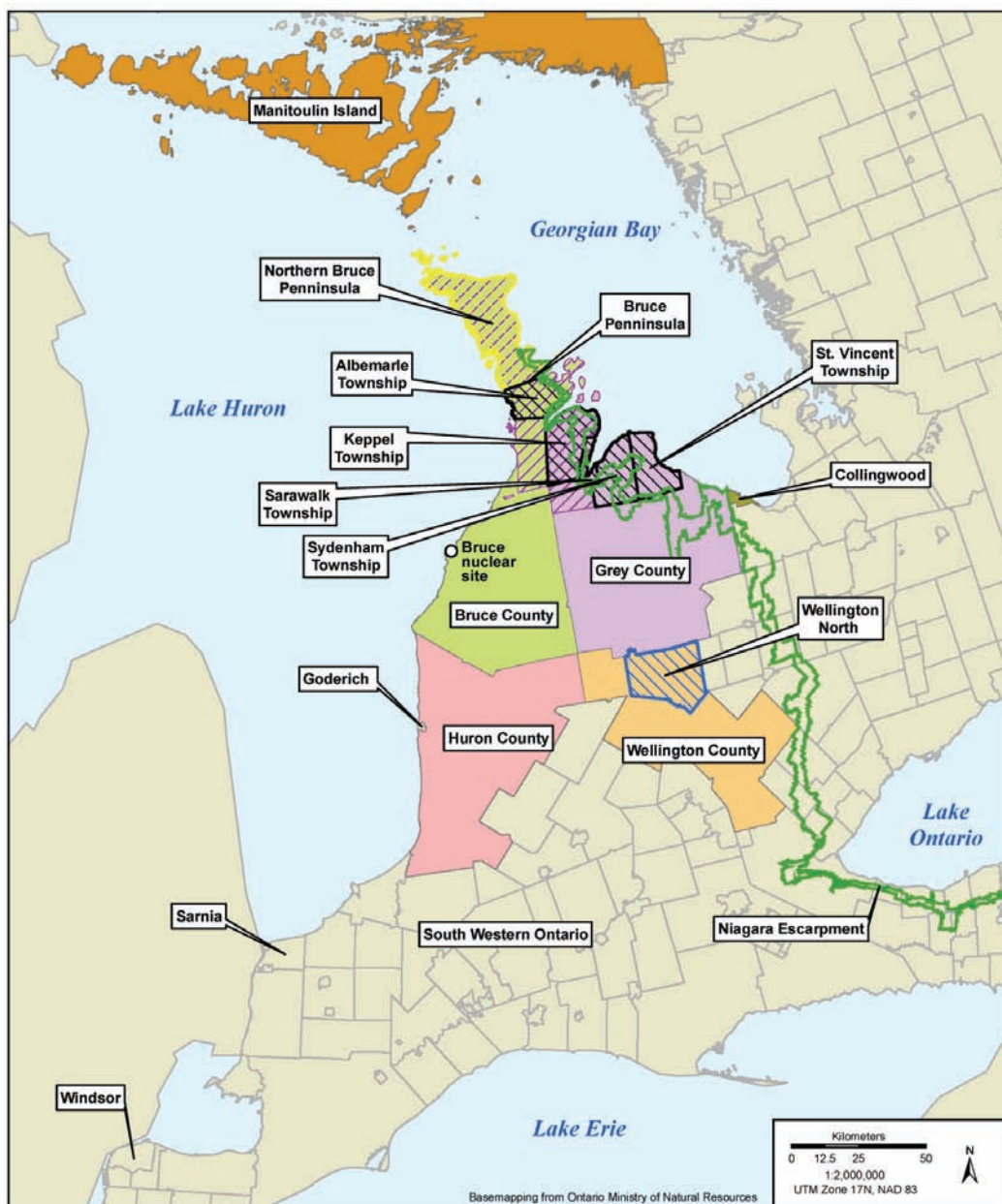


Figure 2.22: Location Map for Economic Bedrock Resources Listed in Table 2.5

#### 2.2.8.4 Surficial Sand and Gravel Resources

The Regional Geology Report (AECOM and ITASCA CANADA 2011) summarizes the aggregate resources of the RSA and Huron, Grey, Wellington, Perth, and Bruce counties. These resources comprise sand and gravel esker, glaciofluvial outwash, ice-contact, and glaciolacustrine beach deposits. A number of areas have been identified by the Ontario Geological Survey and Ministry of Natural Resources as containing significant resources of sand and gravel. These resources have been organized around the physiographic regions identified by Chapman and Putnam (1984).

- In the Huron Slope, glaciolacustrine and beach sand or sand and gravel occurs as thin beds or low ridges on a flat to undulating plain trending parallel to Lake Huron from the Bruce Peninsula to the southern limit of the RSA.
- In the Port Huron Moraine, the most significant concentration of primary aggregate deposits occurs as 2 to 15 m thick networks of spillway outwash deposits in a north-northeast trending belt parallel to the shore through the RSA.
- In the Teeswater Drumlin Field, resources occur as sandy to silty stony till with a large distribution of outwash sand and gravel.
- In the Stratford Till Plain, resources are identified in the small eskers that frequently occur.

Sand and gravel pit operations within the study area are located within the Lake Algonquin bluff. Many of these pits are now abandoned due to resource exhaustion (Slattery 2011). No other primary sand or gravel resources have been identified within 20 km of the Bruce nuclear site (OGSR 2004).

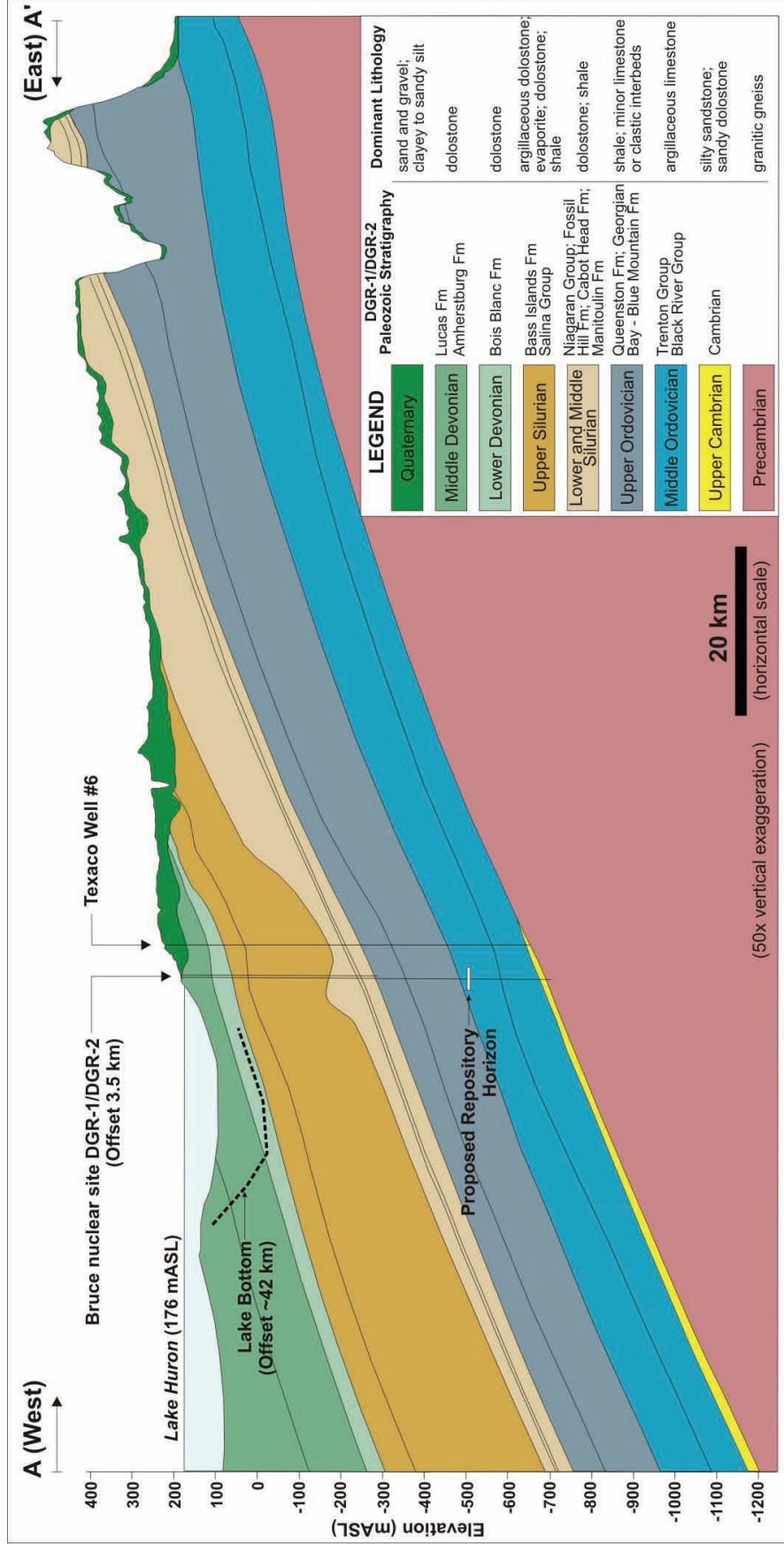
### 2.3 Site-scale Geology

#### 2.3.1 Introduction

The following sections present an overview of the site-scale geological framework at and beneath the Bruce nuclear site (Figures 2.23 and 2.24). These descriptions provide a basis for our understanding of the current geological framework of the site, its past evolution, and likely future natural evolution over the period of interest for Safety Assessment of the proposed DGR. The 3D spatial distribution of all geologic formations and the occurrence of all important geologic structural features within the Paleozoic (Cambrian to Devonian) and Precambrian bedrock units encountered at the Bruce nuclear site are discussed. The data support the conclusion that the site geology is suitable for hosting and enclosing the proposed DGR.

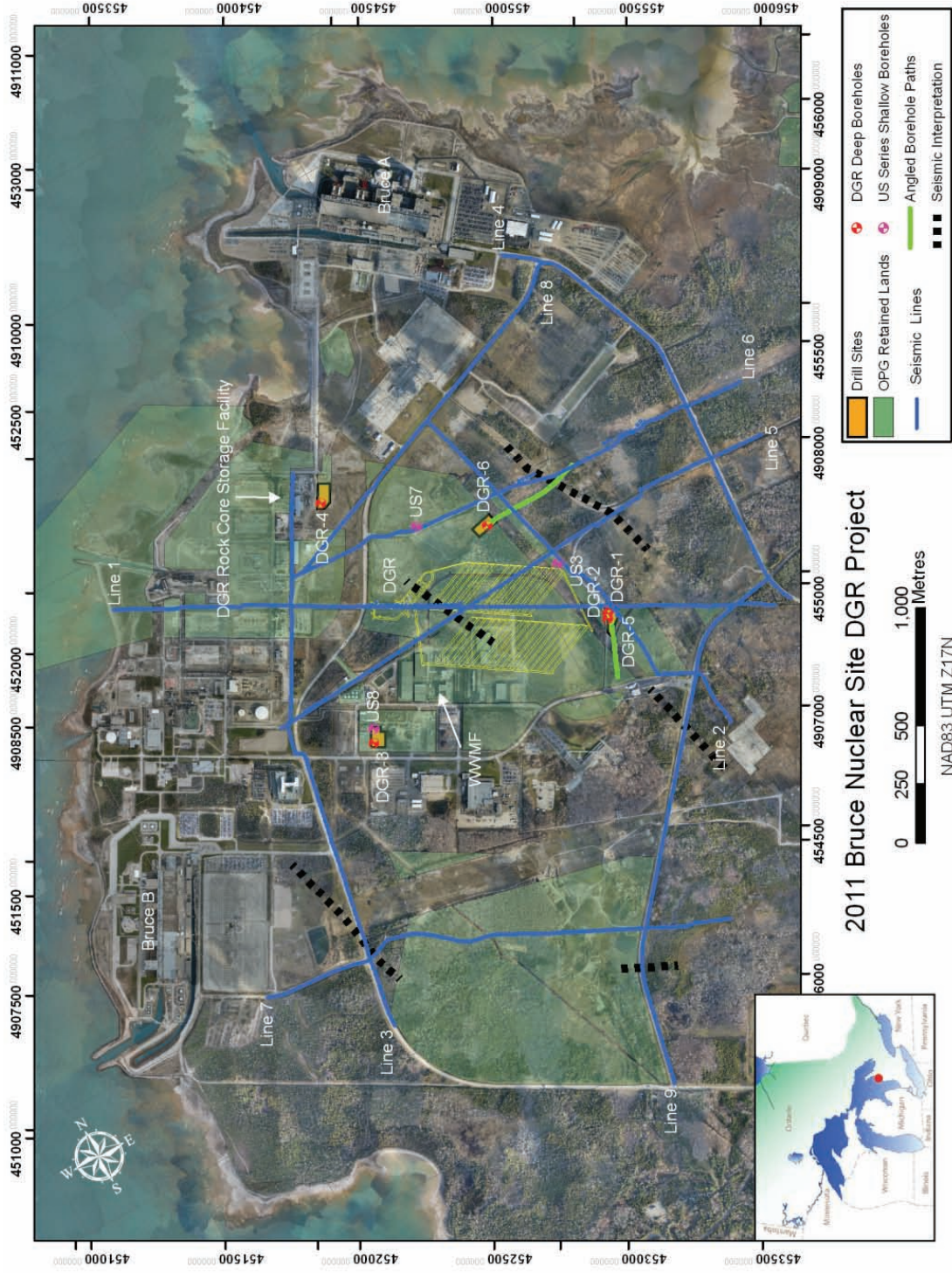
Organization for Economic Co-Operation and Development Nuclear Energy Agency (OECD 2010) lists three main factors that contribute to the suitability of a site for waste disposal. These factors are listed below along with the corresponding sections in this report that relate to each factor.

- Explorability or the ability to characterize the rock with sufficient lateral extent at any stage of the project to a degree that is adequate to support a decision to proceed. Sections 2.3.2 through 2.3.5 present data on the predictability of geological units (2.3.2, 2.3.3), uniform formation thickness (2.3.4), large lateral extent and homogeneity of both lithofacies (2.3.4) and rock geochemistry (2.3.5).
- Long-term geological stability of the geosphere. The main discussions include the structural setting and consistency of joint/fracture data (2.3.6). Further information regarding the geological stability of the site is found in the section on regional seismicity (2.2.6.4).



Notes: Location of cross-section line A-A' is shown in Figure 2.3. The subsurface trace of boreholes DGR-1/DGR-2 and Texaco #6 have been projected onto the cross-section. Simplified lithological descriptions are from INTERA (2011). Detailed stratigraphic nomenclature for the cross-section is shown in Figure 2.8 and discussed in Sections 2.2.5.1 and 2.3. Dashed line indicates maximum depth of lake bottom from a location ~42 km north of the site. Fm = Formation; mASL = metres above sea level.

**Figure 2.23: Geological Cross-section Through the RSA Beneath the Bruce Nuclear Site**



Notes: Figure indicates the position of the proposed DGR footprint, all DGR- and US-series boreholes, the Western Waste Management Facility (WWMF), and the 9-Line (19.7 km) seismic survey array (blue lines).

**Figure 2.24: Overview of the Bruce Nuclear Site**

- Absence of, low likelihood of, or insensitivity to perturbations, including climatic and geological events and processes, and future human intrusion. From a site-scale perspective, possible perturbations include neotectonic faulting (Section 2.3.6), karst development (Section 2.3.7), and erosion (Section 2.2.6).

Table 2.6 lists the relevant data sources used to compile the site-scale geological description of the Bruce nuclear site and used for the descriptive geological site model presented in INTERA (2011).

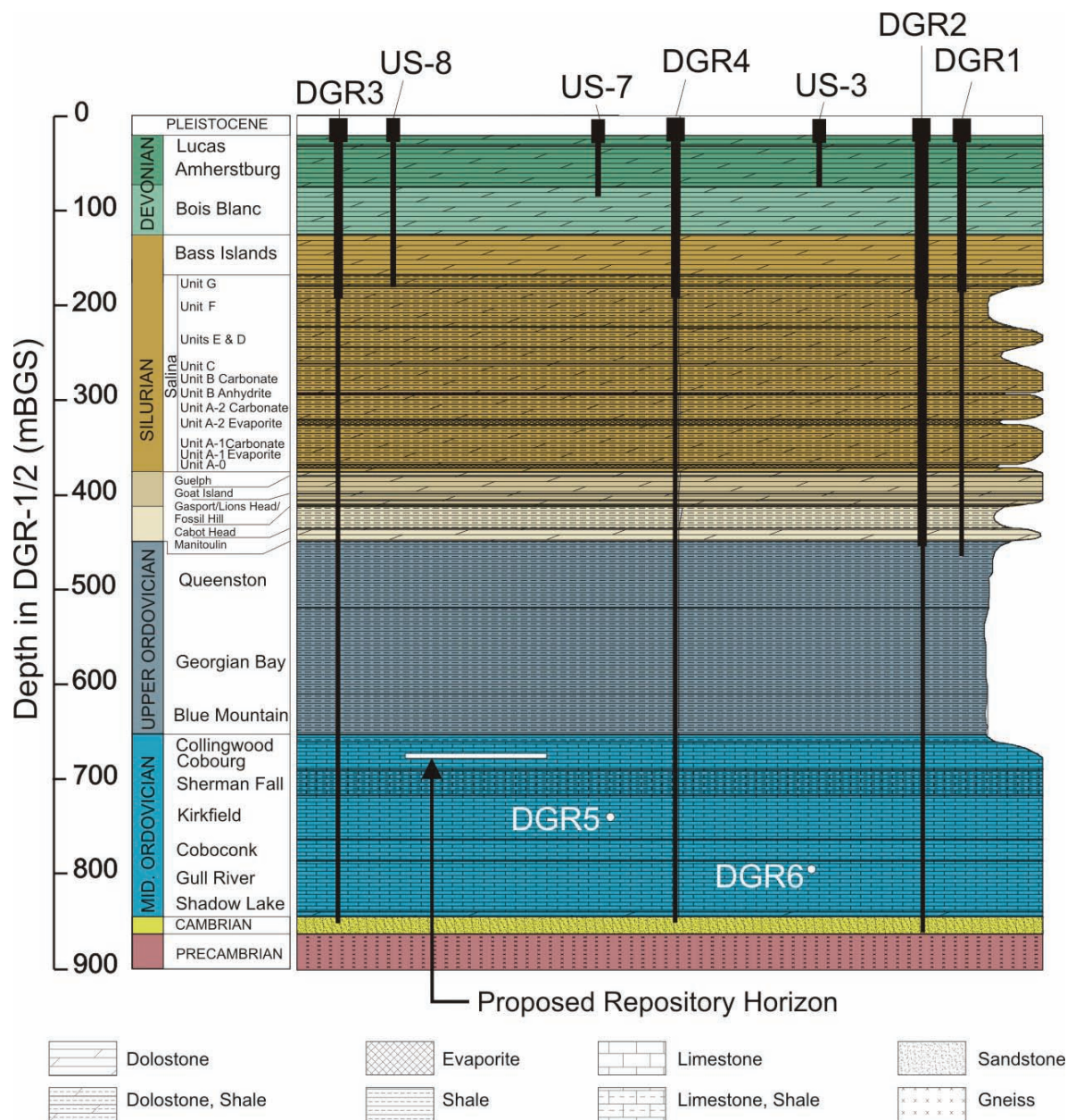
**Table 2.6: Data Sources for Site Scale Geological Description**

- |  |
|--|
| <ul style="list-style-type: none"> <li>➤ Drilling and core logging of new boreholes DGR-1, DGR-2, DGR-3, DGR-4, DGR-5 and DGR-6 (Sterling 2010a, Sterling 2010b, Figures 2.24 and 2.25 herein).</li> <li>➤ Borehole geophysical logging of DGR-1 through DGR-6 (Pehme and Melaney 2010a, 2010b, 2011; e.g., Figure 2.30 herein).</li> <li>➤ Laboratory geochemical, mineralogical, and petrographic analyses of DGR-1, DGR-2, DGR-3, and DGR-4 core (Schandl 2009, Skowron and Hoffman 2009a, Skowron and Hoffman 2009b, Koroleva et al. 2009; e.g., Figure 2.30 herein).</li> <li>➤ Drilling and core logging of boreholes US-1 and US-3 to US-7 (Lukajic 1988).</li> <li>➤ Drilling, chip sampling and borehole geophysical logging of new borehole US-8 (Briscoe 2009).</li> <li>➤ Borehole geophysical logging of US-3 and US-7 (Melaney 2009).</li> <li>➤ 2D seismic reflection surveys (Watts et al. 2009; Figures 2.24, 2.35 and 2.36).</li> <li>➤ Regional Geology – Southern Ontario report (AECOM and ITASCA CANADA 2011).</li> <li>➤ 3DGF model report (ITASCA CANADA and AECOM 2011).</li> <li>➤ Outcrop Fracture Mapping report (Cruden 2011).</li> <li>➤ Assessment of Cap Rock Integrity report (Engelder 2011).</li> </ul> |
|--|

### 2.3.2 Basement Geology

The Precambrian basement beneath the proposed Bruce nuclear site was intersected by borehole DGR-2 at a depth of 860.7 mBGS (Figures 2.23 and 2.25). A total of 1.55 m was sampled and, at this location, the basement is described as a pink to grey, fine- to medium-grained, felsic granitic gneiss with a well-defined penetrative foliation. Petrographic analysis of a sample from 861.90 mBGS yielded a granitic gneiss composition predominated by quartz, K-feldspar and biotite, with minor muscovite alteration and traces of rutile and pyrite (INTERA 2011).

Some weathering alteration of the Precambrian gneiss is evident in the upper 1.2 m of the 1.55 m cored interval. This alteration zone at the top of the Precambrian basement is observed regionally and extends, on average, 2 to 5 m beneath the Precambrian/Cambrian unconformity (Carter and Easton 1990, Di Prisco and Springer 1991). The alteration zone is characterized by secondary mineralization associated with regional brine migration (e.g., Ziegler and Longstaffe 2000a). In DGR-2, the observed red (k-feldspar +/- hematite), green (sericite +/- epidote +/- carbonate) and black (possibly chlorite) staining of the Precambrian gneiss is consistent with other basement descriptions throughout the Huron domain of Carter and Easton (1990). Uranium-lead dating of four zircons in a basement sample from DGR-2 yielded ages of 1526 to 1371 Ma which are within the range expected for the Huron domain (Easton 2008). This supports the conclusion that the basement geology described at the site scale is consistent with our current understanding of the basement geology at the regional scale.



Notes: Vertical borehole penetration depths are indicated by vertical black lines. White dots indicate approximate depth of penetration for angled boreholes DGR-5 and DGR-6. Figure was developed based on information from INTERA (2011).

**Figure 2.25: Subsurface Stratigraphy at the Bruce Nuclear Site**

### 2.3.3 Sedimentary Bedrock Geology

Drilling, logging, and testing of boreholes DGR-1 to DGR-6 at the Bruce nuclear site led to the identification of 34 distinct Paleozoic bedrock formations, members, or units of approximately 840 m cumulative thickness beneath a thin veneer (7 to 20 m) of Pleistocene overburden and

unconformably overlying the aforementioned Precambrian granitic gneiss (Figure 2.25). The surface and subsurface distribution of Paleozoic formations in the RSA are shown in Figures 2.3 and 2.23, respectively. The locations of the DGR-series boreholes and shallow existing US-series wells are shown on Figure 2.24. A schematic site stratigraphy is presented in Figure 2.25 which shows a stratigraphic column and contact depths for the US- and DGR-series boreholes. The angled boreholes DGR-5 and DGR-6 are indicated by dots corresponding to their maximum depth of penetration within the succession.

The Pleistocene overburden at the Bruce nuclear site typically comprises 1 to 3 m of surficial fill and sand and gravel interpreted as former beach deposits overlying 5 to 21 m Elma-Catfish Creek till, a clayey silt to sandy silt glacial deposit (Sharpe and Edwards 1979). The till is underlain by 0 to 2 m of basal gravel deposited at the weathered bedrock surface.

### 2.3.3.1 Stratigraphic Descriptions

The Paleozoic stratigraphic sequence encountered at the site is consistent in distribution, scale and character with the regional stratigraphic framework described in detail by Armstrong and Carter (2006; Figure 2.25). All the recognized subdivisions are consistent, and have been logged in accordance with the stratigraphic nomenclature of Armstrong and Carter (2006), with the following exceptions. Herein the Silurian Gasport and Goat Island members of the Lockport Formation are promoted to formation status as per Brett et al. (1995), as is the Lions Head Member. As in the regional stratigraphic description, any mention of the Cobourg Formation below implies reference to the argillaceous Lower Member only, and similarly the upper Collingwood Member is described as a separate stratigraphic entity.

The reference Paleozoic sequence, based on core logging of the DGR-1 and DGR-2 boreholes, comprises 16.9 m of Cambrian sandstone, 5.2 m of Ordovician siltstone and sandstone, 179.1 m of Middle Ordovician argillaceous limestone, 211.8 m of Upper Ordovician shale, 323.7 m of Silurian dolostone, argillaceous dolostone, shale and evaporite and 104.0 m of Devonian dolostone. The DGR underground facilities will be located within the Middle Ordovician argillaceous limestone of the Cobourg Formation (Figures 2.23b and 2.25). Detailed descriptions of each stratigraphic unit are provided in Tables 2.6 through 2.12 and Figures 2.26 to 2.29 based on the site characterization work of INTERA (2011). The following discussion reviews the stratigraphy from Bruce nuclear site drilling investigations based on the detailed site model of INTERA (2011, their Chapter 3) and provides a comparison with the regional descriptions presented in Section 2.2 above. Note that all thickness data are referenced to DGR-2 values.

#### **Cambrian**

The Cambrian unit, where fully intersected, is 16.9 m thick and found at depths of 843.8 to 860.7 mBGS at the site. It is characterized lithologically as sandstone to dolostone (Table 2.7). Cambrian unit thickness and lithology are consistent with the position of the Bruce nuclear site to the west of the Cambrian erosion front against the Algonquin Arch as described in Section 2.2.5 (Bailey and Cochrane 1984a, Carter et al. 1996, AECOM and ITASCA CANADA 2011). The interpreted pinch out of the Cambrian carbonates and siliciclastics against the Algonquin Arch is based both on the distribution as noted in the literature (e.g., Carter et al. 1996) and the borehole distribution from the Ontario Oil, Gas and Salt Resources database (OGSR 2004, OGSR 2006, AECOM and ITASCA CANADA 2011).

**Table 2.7: Cambrian Borehole Log Description**

Geological Unit	Stratigraphic Description	Thickness
<b>Cambrian</b>	Grey, tan, brown, white, pinkish-orange, medium-grained sandstone that is locally abundantly pyritic and glauconitic, and is interbedded with brown to light grey dolostone and sandy dolostone in places. Fractures filled with quartz, calcite, and pyrite.	16.9 m

Notes: Data are from INTERA (2011).

### **Ordovician**

The Ordovician section is characterized by a succession of shale-dominated Upper Ordovician rocks overlying carbonate-dominated Middle Ordovician rocks. This vertical (temporal) lithological variation is consistent with an increase in clastic input derived from the east during the evolving Taconic Orogeny. The transition begins at the top of the Black River Group where the less argillaceous Coboconk Formation is overlain by the more argillaceous Kirkfield Formation at the base of the Trenton Group. This same lithological transition is observed regionally (e.g., Armstrong and Carter 2006). An approximately 10 cm thick weathered and fissile soft shale zone observed near the top of the Coboconk Formation is interpreted to represent an altered volcanic ash bed marking the onset of the Taconic event. This marker bed along with other distinct facies intervals from within the Ordovician formations will be described in greater detail as part of the lithofacies analysis presented in Section 2.3.4 (also see Wigston and Heagle 2009) which discusses the high degree of predictability encountered at the site.

DGR drilling intersected approximately 190 m of Middle Ordovician carbonates dominated by argillaceous limestones of the Cobourg, Sherman Fall, and Kirkfield formations (Trenton Group), and limestones of the Coboconk and Gull River formations (Black River Group). The Shadow Lake Formation at the bottom of the Middle Ordovician Black River Group ranges from sandstone to argillaceous dolostone. Figure 2.26 shows a core photo of the shaly Sherman Fall Formation which underlies the host Cobourg. Figure 2.27 shows the characteristic mottled argillaceous limestone of the Cobourg Formation. Table 2.8 provides unit thicknesses and descriptions from DGR core logging of the Middle Ordovician units.

The thicknesses and lithologies described by INTERA (2011) for these formations are consistent with thickness ranges, lithologies, and interpreted facies described by Johnson et al. (1992), and Armstrong and Carter (2006) for the subsurface of southern Ontario.

Zones described as petroliferous or containing minor seeping oil are found within the Ordovician limestone units (Table 2.8). Hydrocarbons occur in thin discrete zones such as the approximately 0.5 m thick dolomitized intervals in the Coboconk and Gull River formations or associated with stylolites, shale partings, or organic-rich shale beds in the argillaceous limestones and Collingwood Member shales.





Figure 2.26: Core Sample of Argillaceous Limestone and Shale Interbeds, Sherman Fall Formation, 703.90 mBGS, DGR-2

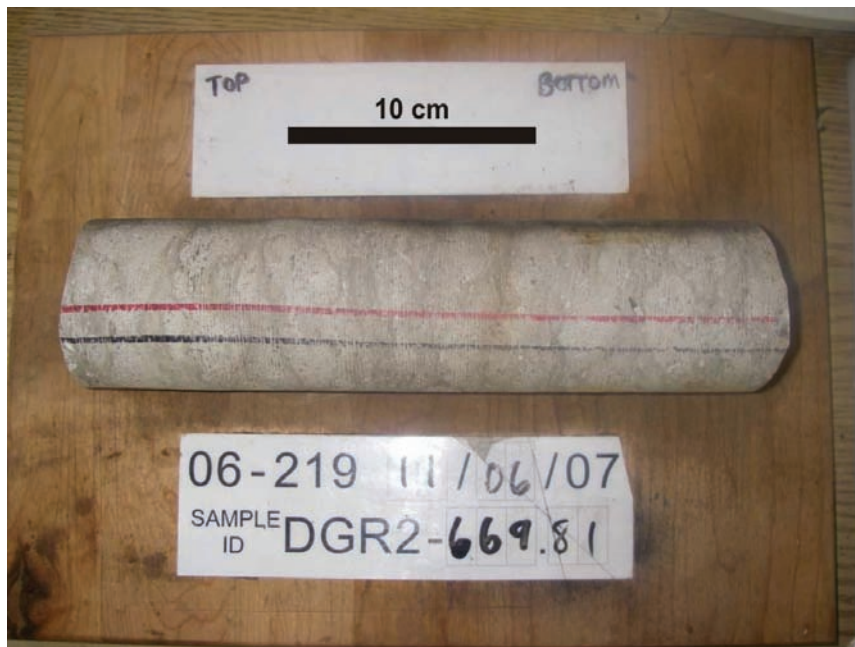


Figure 2.27: Core Sample of Argillaceous Limestone from the Proposed Repository Depth, Cobourg Formation, 669.81 mBGS, DGR-2

**Table 2.8: Middle Ordovician Borehole Log Descriptions**

<b>Geological Unit</b>	<b>Stratigraphic Descriptions</b>	<b>Thickness</b>
<b>Collingwood Member</b>	Dark grey to black, organic-rich, calcareous shale interbedded with grey, very fine- to coarse grained, fossiliferous (brachiopods, crinoids, shell fragments), locally bioturbated, hard limestone. Petroliferous odour. Limestone is locally mottled grey to dark brown-grey, very fine grained, fossiliferous, argillaceous and seeps hydrocarbons. Irregular cm-scale thick bed of phosphate nodules at top.	7.9 m
<b>Cobourg Formation</b>	Mottled light to dark grey, very fine- to coarse-grained (i.e., packstones and grainstones), very hard, fossiliferous (crinoids, brachiopods, shell fragments) argillaceous limestone. Petroliferous odour and hydrocarbons seep from rock in places. Olive-brown to green-brown shale stringers noted in bottom part of formation. Irregular to wavy to diffuse shale interbeds found over bottom few metres.	28.6 m
<b>Sherman Fall Formation</b>	Light grey to grey, medium- to coarse-grained, transitioning to fine- to medium-grained with depth, argillaceous limestone. Coarse-grained beds are bio- and intraclastic grainstones; fossils include brachiopods and other shell fragments. Grey-green, irregular shale laminae and beds are interbedded and interlaminated with the limestone and increase in abundance with depth to typically around 20% by volume. Formation is locally mottled with depth (nodular bedding). Petroliferous odour over upper few metres.	28.0 m
<b>Kirkfield Formation</b>	Grey, fine- to medium-grained argillaceous, fossiliferous (brachiopods) limestone interbedded with dark grey-green irregular to planar bedded shale that locally constitutes up to 50% by volume of the rock. Some shale beds contain limestone clasts. Formation has petroliferous odour.	45.9 m
<b>Coboconk Formation</b>	Grey to tan-grey, mostly fine-grained with subordinate medium- and coarse-grained beds, fossiliferous, bioturbated limestone with irregular mottled bituminous shale laminae. Locally contains horizons of brown and black chert nodules and rare calcite-filled vugs. Formation is petroliferous and locally weeps hydrocarbons.	23.0 m
<b>Gull River Formation</b>	Light grey to grey, as well as tan-brown with depth, very fine-grained to medium-grained, locally bioturbated and fossiliferous limestone with brown to black bituminous shale laminae, beds, and stringers. Limestone is locally arenaceous in middle of formation. Stylolites are locally common and the formation is commonly petroliferous and locally weeps hydrocarbons.	53.6 m
<b>Shadow Lake Formation</b>	Interbedded grey-green sandy shale and grey to light green-grey-brown pyritic and glauconitic siltstone and sandstone.	5.2 m

Notes: Data are from INTERA (2011).

Table 2.9 describes the Upper Ordovician Queenston, Georgian Bay (Figure 2.28), and Blue Mountain (Figure 2.29) formations which comprise < 200 m of blue-grey, non-calcareous shale with minor limestone interbeds, sandstone interbeds, and red/maroon-green calcareous shales

to non-calcareous shales with limestone interbeds. As with the Middle Ordovician carbonates, the Upper Ordovician shale thicknesses, lithologies, and associated facies interpretations are consistent with regional information. For example, minor bioclastic limestone interbeds within the Queenston Formation are predicted from regional information (e.g., Brogly 1990, Johnson et al. 1992, Armstrong and Carter 2006) based on the geographic location of the DGR near the base of the Bruce Peninsula.

**Table 2.9: Upper Ordovician Borehole Log Descriptions**

<b>Geological Unit</b>	<b>Stratigraphic Descriptions</b>	<b>Thickness</b>
<b>Queenston Formation</b>	Red to maroon shale. The shale is calcareous to non-calcareous and contains subordinate amounts of grey-green shale and grey to brown dolostone, limestone, and siltstone. Locally contains gypsum and anhydrite nodules and halite-filled fractures. Green shale in middle of the formation is interbedded with cm- to dm-thick grey to dark grey, fossiliferous (brachiopods) limestone beds.	70.3 m
<b>Georgian Bay Formation</b>	Interbedded shale and limestone. Green to blue-grey shale interbedded with light grey, fossiliferous (crinoids, brachiopods, shell fragments, and trace fossils), moderately hard limestone beds and grey, calcareous siltstone beds. Few filled fractures, commonly with halite; pyrite mineralization on fractures surfaces less common. Rare anhydrite and gypsum nodules. Fossiliferous limestone beds decrease in abundance with depth from few to rare. Petroliferous and sulphurous odour noted with depth. Core dinking common.	90.9 m
<b>Blue Mountain Formation</b>	Green-blue to grey-blue and transitioning to grey to dark grey with depth, fossiliferous (crinoids, brachiopods) shale interbedded over upper part of formation with cm-thick grey siltstone and fossiliferous limestone beds. Shale has a petroliferous and sulphurous odour. Locally contains calcite-filled fractures with pyrite mineralization on fracture surfaces. Pyritization of fossils locally common. Core dinking common.	38.1 m
<b>Blue Mountain Formation - lower member</b>	Grey to dark grey shale with few siltstone laminae and petroliferous odour. Core dinking common. Interbedded with mottled grey, fine- to medium-grained, fossiliferous, hard limestone with depth.	4.6 m

Notes: Data are from INTERA (2011).



**Figure 2.28: Core Sample of Interbedded Shale and Limestone, Georgian Bay Formation, 542.25 mBGS, DGR-2**



**Figure 2.29: Core Sample of Green and Red Calcareous Shale, Upper Ordovician Queenston Formation, 454.82 mBGS, DGR-1**

## **Silurian**

The Lower Silurian Manitoulin and Cabot Head formations at the Bruce nuclear site comprise a combined total of 37 m of dolostone with minor non-calcareous shale, and non-calcareous shale with minor dolostone, respectively (Table 2.10; INTERA 2011). As predicted from regional information, the Lower Silurian Whirlpool sandstone, which commonly overlies the Queenston Formation in southern Ontario, pinches out at the eastern margin of the RSA, and is not present beneath the site.

**Table 2.10: Lower Silurian Borehole Log Descriptions**

<b>Geological Unit</b>	<b>Stratigraphic Descriptions</b>	<b>Thickness</b>
<b>Cabot Head Formation</b>	Shale grading with depth to interbedded shale and limestone. Shale is diffusely banded or mottled red and maroon; filled mud cracks tentatively identified. Limestone is grey, coarse-grained (wacke- to packstone) dolomitic limestone with bituminous laminae and contains variable amounts of green shale.	23.8 m
<b>Manitoulin Formation</b>	Dolostone, shale, and argillaceous dolostone. Dolostone is mottled grey-blue to grey-tan, fine- to coarse-grained, fossiliferous, and contains variable amounts of grey-green calcareous shale laminae and beds, black organic-rich laminae, and stylolites. Argillaceous dolostone is mottled grey-green to grey-blue, medium- to coarse-grained, slightly fossiliferous (brachiopods), is variably argillaceous, and locally contains few light grey-tan cm-thick chert layers.	12.8 m

Notes: Data are from INTERA (2011).

The Middle Silurian Fossil Hill, Lions Head, Gasport, Goat Island, and Guelph formations are mainly dolostone which is locally fossiliferous (Table 2.11). Across the site, this package of rock units exhibits a consistent total thickness of between 35.9 and 36.5 m based on borehole logging, which suggests deposition in an inter-reef basinal-slope zone within the broader pinnacle and patch reef depositional environment characteristic of this age (Figure 2.10). This geometry contrasts with the character of some temporally equivalent reef strata (particularly the Guelph and Gasport-Goat Island formations) in the RSA where total interval thickness may exceed 100 m. The Middle Silurian Rochester shale is absent at the site, consistent with the regional dataset that predicts it pinching out at the southern margin of the RSA (Sanford 1969, and Armstrong and Carter 2006).

The Upper Silurian Salina Group beneath the Bruce nuclear site is composed of approximately 250 m of alternating carbonates, shales, and evaporites (Table 2.12). The occurrence, thickness, and lithology of the individual units within Salina Group and the overlying Bass Islands Formation at the Bruce nuclear site are consistent with the regional descriptions as summarized in Armstrong and Carter (2006).

**Table 2.11: Middle Silurian Borehole Log Descriptions**

<b>Geological Unit</b>	<b>Stratigraphic Descriptions</b>	<b>Thickness</b>
<b>Guelph Formation</b>	Brown to grey-brown, very fine- to medium-grained (i.e., sucrosic) petroliferous dolostone with grey-brown bituminous shale laminae and beds. Formation grades downwards from vuggy to non-vuggy. Few anhydrite nodules within upper part of formation.	4.1 m
<b>Goat Island Formation</b>	Light grey to brown, very fine grained, massive, hard dolostone with stylolites and common dark grey irregular to wavy bituminous laminae.	18.8 m
<b>Gasport Formation</b>	Light to dark grey-brown, very fine- to fine-grained dolomitic limestone with pits and vugs that are filled with pyrite and calcite. Also contains tan-grey mottled, diffuse shale laminae.	6.8 m
<b>Lions Head Formation</b>	Mottled light grey to tan-grey, very fine-grained dolostone with few shale and siltstone clasts and laminae	4.4 m
<b>Fossil Hill Formation</b>	Mottled light grey to tan-grey, very fine-grained dolostone with few shale and siltstone clasts and laminae, stylolites, and medium- to coarse-grained interbeds.	2.3 m

Notes: Data are from INTERA (2011).

**Table 2.12: Upper Silurian Borehole Log Descriptions**

<b>Geological Unit</b>	<b>Stratigraphic Descriptions</b>	<b>Thickness</b>
<b>Bass Islands Formation</b>	Light grey to brown to tan, very fine- to fine-grained dolostone with common to rare shale and bituminous laminae and intervals. Argillaceous dolostone intervals are grey-blue with shale and dolostone intraclasts. Vuggy in very few places, with vugs filled with calcite. Rare evaporite mineral moulds. Few zones are fractured with calcite fill. Few anhydrite layers and filled fractures in bottom part of formation.	45.3 m
<b>Salina Group G Unit</b>	Grey-blue to grey-green, very fine- grained, soft, argillaceous dolostone with common to abundant white to pink-orange anhydrite veins and layers throughout. Tan to brown, very fine-grained, hard, dolostone near middle of formation.	9.3 m
<b>Salina Group F Unit</b>	Dolomitic shale and subordinate dolostone. Dolomitic shale is grey-green to grey-blue with rusty brown-red mottling and diffuse staining with abundant cm-thick white and pink-orange anhydrite veins and layers throughout; anhydrite nodules are less common. Dolostone found near bottom of the formation and is light grey to light brown, very fine grained, hard, and contains rare to few anhydrite nodules and veins and locally contains dark grey to black bituminous laminae.	44.4 m
<b>Salina Group E Unit</b>	Interbedded dolostone, dolomitic shale, and argillaceous dolostone. Dolostone is grey tan to brown, very fine grained,	20.0 m

Geological Unit	Stratigraphic Descriptions	Thickness
	massive, and with dark grey to black bituminous laminae and few anhydrite veins. Dolomitic shale is grey to grey blue, soft, with abundant anhydrite veins and layers. Argillaceous dolostone is tan-brown, very fine grained, hard, massive, and contains few anhydrite veins and layers. Formation is locally brecciated.	
<b>Salina Group D Unit</b>	Light grey-blue, fine-grained dolostone with abundant anhydrite as veins and blebs; locally slightly vuggy.	1.6 m
<b>Salina Group C Unit</b>	Dolomitic shale grading downwards to shale. Dolomitic shale is grey-blue with diffuse rusty-red staining in lower part, and is massive to laminated with few anhydrite layers. Shale is mottled greyish green and red, massive, and contains few anhydrite veins, layers, and nodules.	15.7 m
<b>Salina Group B Unit</b>	Dolomitic shale and argillaceous dolostone grading downwards to dolostone near base of unit. Upper metre contains a zone of brecciated tan, fine-grained dolostone with anhydrite (B marker bed of Armstrong and Carter 2006). Dolomitic shale is grey-green with abundant anhydrite veins, layers, and nodules. It is locally brecciated with dolostone clasts. Dolostone is tan-brown, very fine grained with abundant white anhydrite nodules and veins, and abundant dark brown-black laminae.	30.9 m
<b>B Unit Evaporite</b>	Interbedded light to dark grey dolostone and bluish-grey anhydrite, grading to mottled dolostone and anhydrite with depth.	1.9 m
<b>Salina Group A2 Unit</b>	Dolostone with subordinate dolomitic shale and shale. Dolostone, dolomitic shale, and shale are locally interbedded. Dolostone is tan to grey, very fine to fine grained, laminated to massive, locally with dark brown to black bituminous laminae and less common anhydrite layers; strong sulphur odour in places. Dolomitic shale is grey-brown with trace anhydrite and pyrite flecks and has sulphurous odour when broken. Shale is brown to dark grey, soft and friable, and locally contains dolostone clasts and distorted bedding.	26.6 m
<b>A2 Unit Evaporite</b>	Mottled grey-blue, very fine-grained, laminated to massive dolostone with abundant anhydrite veins and blebs. Locally slightly vuggy.	5.8 m
<b>Salina Group A1 Unit</b>	Grey to tan-grey argillaceous dolostone with common to abundant dark grey, petroliferous shale laminae, beds, and shale-rich intervals, and few to common anhydrite veins and layers. Dolostone and anhydrite are locally brecciated.	41.5 m
<b>A1 Unit Evaporite</b>	Interlaminated to interbedded to massive and mottled brown dolostone and bluish-grey anhydrite.	3.5 m
<b>Salina Group A0 Unit</b>	Grey-brown to black, fine-grained, thinly laminated, dolostone with abundant black bituminous laminae.	4.0 m

Notes: Data are from INTERA (2011).

### **Devonian**

The Lower Devonian Bois Blanc Formation at the Bruce nuclear site is composed of approximately 49 m of cherty and fossiliferous limestone/dolostone (Table 2.13). Johnson et al. (1992) suggested a range of 4 to 50 m thickness for the Bois Blanc, with thickness increasing towards the centre of the Michigan Basin. The Amherstburg Formation (approximately 45 m thick) is described by INTERA (2011) as a fossiliferous (coral) dolostone. Approximately 10 m of Lucas Formation overlies the Amherstburg Formation at the site. Regional descriptions that characterize the Amherstburg Formation as dolostone/limestone with abundant reef building corals (Johnson et.al. 1992, and Armstrong and Carter 2006) are consistent with the Bruce nuclear site description.

**Table 2.13: Devonian Borehole Log Descriptions**

<b>Geological Unit</b>	<b>Stratigraphic Descriptions</b>	<b>Thickness</b>
<b>Lucas Formation</b>	Brownish grey, grey, and brown, fine-grained, hard, dolostone locally with abundant bituminous laminae (stromatolitic laminations). Formation is locally very vuggy with partial calcite fill. Shaley layers with subordinate dolomite in few places. Formation has brecciated appearance in few spots due to light coloured dolostone fragments in matrix of grey calcite. Rock becomes cherty with depth. Rock also becomes fossiliferous near bottom of formation, including stromatolite, brachiopods, and corals.	10.4 m
<b>Amherstburg Formation</b>	Light brown to grey, fine- to coarse-grained, hard, fossiliferous (stromatolite, corals, brachiopods), cherty dolostone with abundant bituminous shale laminae and zones. Locally vuggy with secondary calcite, pyrite and quartz mineralization in places and locally extensively fractured with fractures commonly filled with calcite and pyrite.	44.6 m
<b>Bois Blanc Formation</b>	Light to dark grey to brown to tan, fine- to medium-grained, hard, fossiliferous (corals, brachiopods) cherty dolostone with intermittent bituminous shale laminae. Chert is abundant and is found as light grey to white nodules and less commonly as up to 10 cm thick layers, some with dolostone clasts. Shale laminae are absent near the base of the formation. Slightly vuggy in places. Extensively fractured in few zones with calcite and, less commonly, pyrite found on fracture surfaces. Calcite stringers common throughout.	49.0 m

Notes: Data are from INTERA (2011).

#### **2.3.4 Site-scale Predictability of Ordovician Sedimentary Rocks**

An important attribute of the Bruce nuclear site is the predictability of the Ordovician sedimentary rock units across distances of 1.5 km (site scale) or greater. The Regional Geology Report (AECOM and ITASCA CANADA 2011) concluded, based on a review of the



stratigraphy across the RSA and a preliminary assessment of site geology that the lithology (shale, evaporite, carbonate, and clastic content) defining broad facies assemblages are well predicted by the regional data of Armstrong and Carter (2006, 2010). The following sections build a case for site-scale predictability based on the consistency of Ordovician unit thicknesses and lithofacies and mineralogical distributions (e.g., Figure 2.30, Table 2.14 and Table 2.16), and the recognition of distinct marker bed horizons, within the DGR borehole framework (Figure 2.31).

Intersection of the Ordovician bedrock formations by the deep DGR boreholes (DGR-1 only intersected as deep as the top of the Queenston Formation as shown in Figure 2.25) allows for an assessment of the uniformity in formation thickness and attitude (strike and dip). The formation thicknesses were calculated from formation top picks based on a combination of core and borehole geophysical logging and the integration of interpretations emerging from two core workshops, which involved experts from the MNR, OGS and GSC. Table 2.14 shows a comparative list of formation thicknesses based on the information from the deep DGR boreholes, as well as their strike and dip calculated by three-point analysis from formation tops. Immediately apparent is the marked consistency in formation thickness and attitude.

**Table 2.14: Summary of Strike, True Dip, and Thicknesses of Ordovician Formations and Members Encountered in the DGR Boreholes**

Ordovician Formation/Member	Strike	Dip	Thickness (m)				
			DGR-2	DGR-3	DGR-4	DGR-5	DGR-6
Queenston	N24°W	0.41°SW	70.3	74.4	73.0	70.3	69.3
Georgian Bay	N17°W	0.61°SW	90.9	88.7	88.7	88.6	88.2
Blue Mountain	N23°W	0.51°SW	42.7	44.1	45.1	45.1	45.0
Collingwood Member	N14°W	0.56°SW	7.9	8.7	8.4	8.6	6.5
Cobourg	N14°W	0.60°SW	28.6	27.8	27.5	27.1	28.5
Sherman Fall	N17°W	0.57°SW	28.0	28.9	28.3	29.3	28.8
Kirkfield	N18°W	0.63°SW	45.9	45.8	45.7	-	46.8
Coboconk	N19°W	0.63°SW	23.0	23.7	23.8	-	22.4
Gull River	N16°W	0.66°SW	53.6	51.7	52.2	-	-
Shadow Lake	N19°W	0.56°SW	5.2	4.5	5.1	-	-
Total Ordovician Thickness			396.1	398.3	397.8	-	-

Notes: Strike and true dip values are based only on data from the vertical boreholes, DGR-2 to DGR-4 (DGR-1 only intersected the top of the Queenston Fm and therefore is not included in this analysis, see Figure 2.25). Dashes (-) are required where DGR-5 and DGR-6 did not intersect the entire Ordovician interval (see Figure 2.25). Data are from Table 3.1 and Table 3.2 of INTERA (2011).

#### 2.3.4.1 Lithofacies Analysis and Marker Beds

In order to fully assess the degree of predictability of individual lithofacies at the site scale, an evaluation of the lateral (horizontal) homogeneity and vertical variation of lithofacies within key intervals was conducted. Borehole coverage around the periphery of the DGR footprint provides the data control for this analysis. Facies variation is caused by the changing dynamics

of the depositional environment, and can potentially alter the hydrogeological and mechanical properties of the rock mass. If sufficient homogeneity exists, then the important geophysical, geomechanical, and hydrogeological datasets may be associated to specific lithologies. A positive correlation of intraformational facies changes between the boreholes would, therefore, allow for confident interpolation of the lithostratigraphy across the DGR footprint. The specific targets for this analysis were portions of the cap rock shales (Queenston and Georgian Bay formations) and the host rock (Cobourg Formation) for the proposed DGR.

The analysis was carried out in three parts.

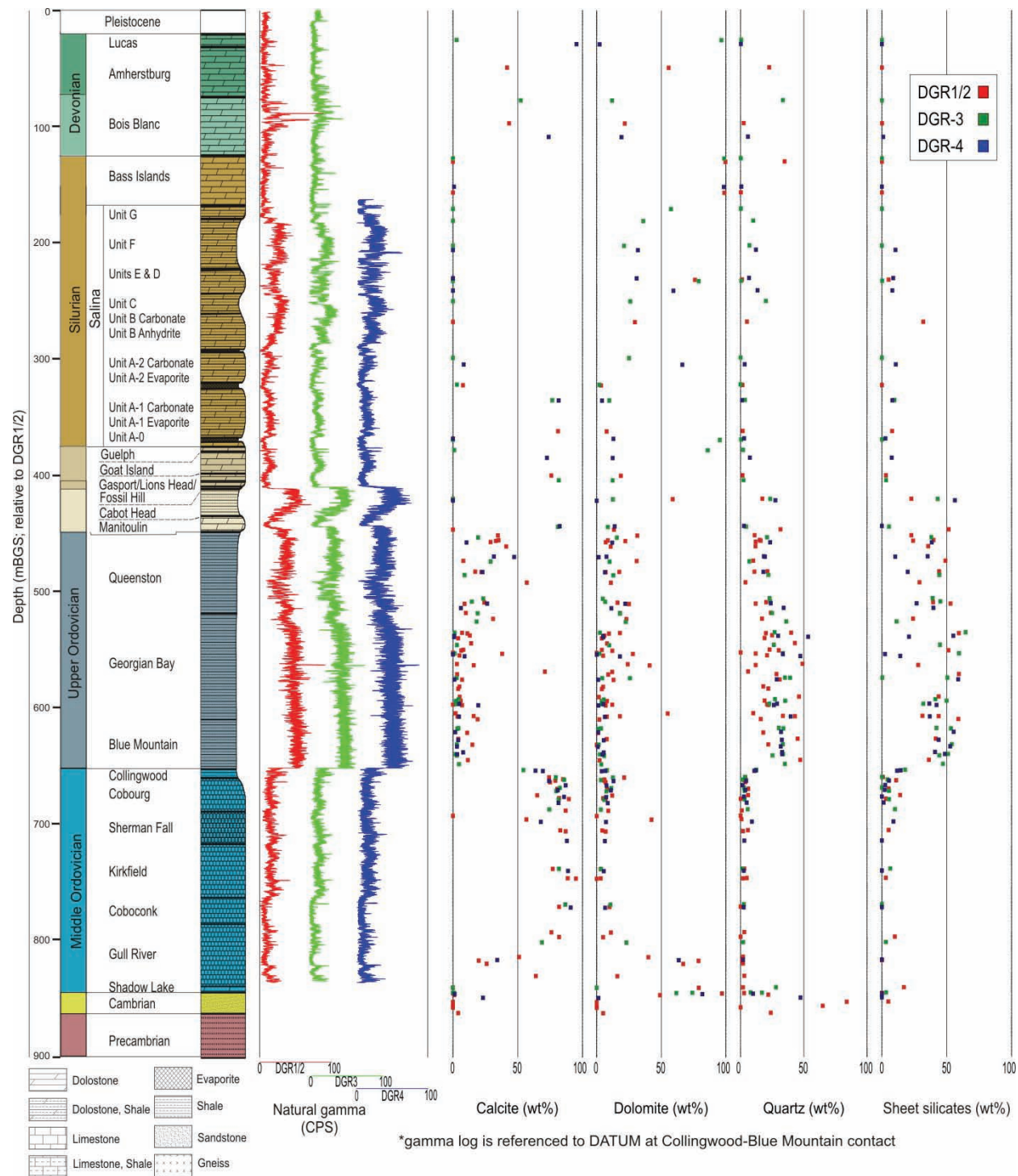
- A comparison of the Natural Gamma Ray borehole logs (Pehme and Melaney 2010a, 2010b) from the Middle and Upper Ordovician sections of all three vertical holes was undertaken to assess the degree of correlation. Gamma ray measurements distinguish major lithological differences by detecting the variation in natural radioactivity based on changes in concentration of potassium, thorium, and uranium. Potassium, which is found in sheet silicate minerals, is the most common source of natural gamma radiation in sedimentary rocks. The gamma profile is measured in counts per second (CPS) with higher values indicating higher sheet silicate content (see also Table 3.16 and Figure 2.30). Therefore, the alternating sheet silicate-rich shale and sheet silicate-poor carbonate layers, as well as concentration of sheet silicates within the carbonate-rich horizons, can be qualitatively compared.
- This comparison showed that 1 dm to 1 m thick beds could be readily correlated between boreholes. Small-scale lithological variation of mm to cm thick beds could not typically be confidently matched and this is evidenced by minor variation of the gamma ray profiles between boreholes (Figures 2.30 and 2.31). This is not unexpected given the nature of the carbonate shelf depositional environments characteristic of the Middle Ordovician (e.g., Lehmann et al. 1995) and the clastic-dominated shallow prograding coastal plain and deltaic depositional environment characteristic of the Upper Ordovician (Brogly et al. 1998).
- An approximate 20 to 30 m thick interval was chosen from each of the Queenston, Georgian Bay, and Cobourg formations. The gamma ray signature for each interval was compared among the three boreholes and matched to the core descriptions. The hypothesis, based on a thorough review of regional and site data (DGR-series boreholes) as presented in the Regional Geology report (AECOM and ITASCA CANADA 2011), was that the lithofacies would generally be predictable and continuous across the site in these key formations.

#### **Comparison of Natural Gamma Ray Profiles for DGR-2, DGR-3, and DGR-4**

The Natural Gamma Ray profiles, including the Ordovician section, from each of DGR-1/2, -3, and -4 are plotted in Figure 2.30. Formation tops at the Bruce nuclear site were selected based on these profiles, core logging, correlation with regional data, and scientific consensus (Wigston and Heagle 2009). The general similarity of all three profiles supports the assessment of uniform unit thicknesses and structurally simple geometry (Wigston and Heagle 2009).

Immediately apparent in all three gamma ray profiles is a bimodal distribution of CPS values separating the high count and shale-rich Upper Ordovician from the low count and carbonate-rich Middle Ordovician. Another interesting quality of all three profiles is that the Middle Ordovician carbonate-rich section can be further separated into a relatively sheet silicate-poor Black River Group (Shadow Lake, Gull River and Coboconk formations) overlain by a relatively sheet silicate-rich Trenton Group (Kirkfield, Sherman Fall, and Cobourg formations). These variations are consistent with an increase in clastic input derived from the east during the

evolving Taconic Orogeny. These broad lithological variations are also recognized regionally (e.g., Armstrong and Carter 2006).



Notes: Figure is based on data from INTERA (2011).

**Figure 2.30: Lithostratigraphy, Natural Gamma Profiles and Major Mineralogy of the DGR Boreholes**

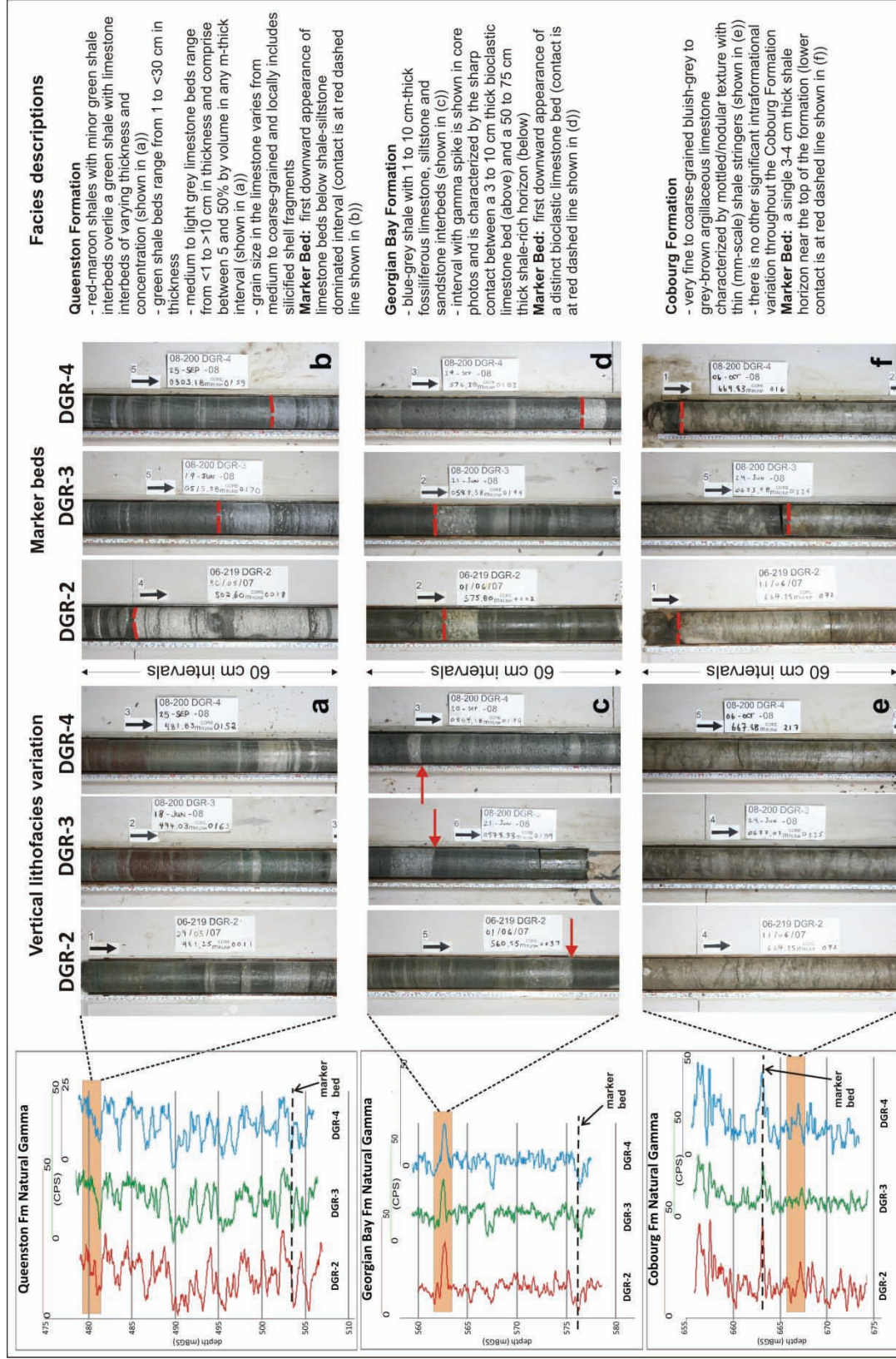
An interval from within each of the three Ordovician units was chosen for comparison across all three gamma profiles. The main consideration in deciding which approximate 20 to 30 m interval to select was to find a section of the DGR-2 gamma profile that showed variations reflecting lithology changes, which could then be compared with the other two profiles (Figures 2.30 and 2.31). The interval length was selected to be coincident with the hydraulic packer testing intervals used in the site hydrogeological investigations. Using the DGR-2 profile as a baseline was arbitrary; however, a similar pattern in all three profiles suggests lateral homogeneity. An example of a facies transition from each interval is also shown in Figure 2.31 to highlight the scale at which the homogeneity occurs. The results indicate that the Ordovician stratigraphy at the Bruce nuclear site is laterally homogeneous and predictable at the decimetre to metre scale, suggesting that interpolation of the borehole correlations across the DGR footprint is valid. The following sections give detailed descriptions of the style and scale of facies variation within the three formations examined.

### Queenston Formation

The interval chosen for analysis (Figure 2.31, top left) is from the lower middle interval of the Queenston Formation. It is approximately 25 m thick and distinguished by abundant cm to dm scale green shale and siltstone beds interlayered with medium to coarse grained, < 1 to > 10 cm thick, limestone beds commonly containing silicified shell fragments (Figure 2.31a and b). This interval exhibits a more erratic gamma profile with distinct metre scale segments that correspond to changes in thickness and concentration of the limestone beds. Comparison of the three profiles highlights the fact that these metre scale variations are traceable between boreholes. In core, the upper part of this facies transition corresponds to the appearance of millimetre to centimetre thick medium to coarse grained limestone beds over a 25 to 35 cm thick horizon within the green shale (Figure 2.31a). The core photos highlight the fact that the facies change is evident in all boreholes at small scale (millimetre to centimetre scale typically) and individual limestone beds are not directly traceable. The consistency is in the decimetre to metre scale transitions from shale and siltstone to more carbonate-rich intervals.

### Georgian Bay Formation

The upper third of the Georgian Bay Formation is characterized by interbedded shale with fossiliferous limestone. The lower two thirds are characterized predominantly by dark shale, a variation which is seen in the gamma ray log (Figure 2.30). The interval chosen for analysis (Figure 2.31, middle left) spans the transition through the lower middle part of the formation. It is an approximately 20 m-thick interval within which dark grey/green/blue shale is interbedded with 1 to 10 cm thick light grey fossiliferous limestone, siltstone, and fine-grained sandstone beds (Figure 2.31c). Of particular interest is the presence of a marked CPS spike in the middle of the gamma profile at the same stratigraphic depth in the Georgian Bay Formation in all boreholes (Figures 2.30 and 2.31). Visual core inspection confirmed that this spike is lithologically controlled and defined by the sharp transition from a distinct 3 to 15 cm thick fossiliferous limestone bed into underlying dark shale (Figure 2.31c, red arrows). Several other metre scale CPS trends can be confidently traced between all three profiles even though individual spikes are sometimes too fine to match between holes. The centimetre scale thickness variations reflect the small-scale lithological differences due to locally varying conditions of deposition. However, this sharp lithofacies transition is observed in all boreholes and therefore suggests, as with the Queenston above, that the Georgian Bay Formation is laterally predictable, exhibiting vertically consistent variations at the decimetre to metre scale.



Notes: Intervals chosen for analysis are highlighted in orange in left column of figure. Accompanying photographs of representative facies variations and marker beds are shown in 60 cm intervals. Each of (a) to (f) includes the same approximate stratigraphic interval from DGR-2, DGR-3, and DGR-4 for comparison. Photographs are not stratigraphically aligned.

Figure 2.31: Intervals Chosen for Facies Analysis from DGR-2, DGR-3, and DGR-4

### Cobourg Formation

The Cobourg Formation is a very fine- to coarse-grained bluish-grey to grey-brown argillaceous limestone unit, locally divided by thin shaley interbeds. Much of the formation at the Bruce nuclear site, including the proposed repository depth, is characterized by a nodular fabric and bioturbated bedding surfaces with minor intraformational variation (Figure 2.31e). The minor facies variation is evident in the generally consistent low CPS pattern on the three profiles (Figures 2.30 and 2.31). The most distinct marker bed identified in this study in the Cobourg Formation is a single 3 to 4 cm thick shale marker bed in the upper section of the formation (discussed further in the next section; Figure 2.31f). The lithological and geophysical similarity of the majority of the Cobourg section suggests that this formation is laterally homogeneous and is predictable at the decimetre to metre scale across the DGR footprint. Vertically there is an increase in CPS in all boreholes consistent with increasing argillaceous material towards the base of the formation.

The lithofacies study and the results presented in INTERA (2011) and Regional Studies (AECOM and ITASCA CANADA 2011) demonstrate that interpolation of the borehole correlations across the DGR footprint is valid and that the lithostratigraphy is consistent and predictable at the site scale. Lithofacies changes within the DGR footprint (between boreholes) in the host and bounding formations are likely to occur as minor small-scale (cm to dm) conformable changes in quantities of shale, siltstone, or limestone. Hydraulic testing of these lithofacies (Chapter 5.0) demonstrates that regardless of the small-scale vertical lithofacies, the hydraulic conductivities remain extremely low and vertically consistent throughout the unit.

### **Marker Beds**

Each of the three stratigraphic intervals described above also includes at least one distinct marker bed. These marker beds were identified during the detailed core logging and used to aid in stratigraphic correlation between the boreholes (Figure 2.31 herein; Wigston and Heagle 2009). The markers are all < 20 cm thick beds and are lithologically distinct horizons that are laterally continuous and common to all boreholes. The marker for the Queenston Formation is the top of a distinct medium to coarse grained bioclastic limestone horizon (Figure 2.31b). This marker represents a distinct conformable facies transition recognizable as a low CPS spike on all three gamma profiles (Figure 2.31, top left). The marker for the Georgian Bay Formation is a single 6 to 10 cm thick coarse grained bioclastic limestone bed within grey shale with minor siltstone interbedded facies (Figure 2.31d). This marker also represents a distinct conformable facies transition recognizable as a low CPS spike on all three gamma profiles (Figure 2.31, middle left). The marker for the Cobourg Formation is a single 3 to 4 cm thick horizon of shale that contrasts sharply with the nodular and bioturbated limestone fabrics that characterize the formation (Figure 2.31f). The shale bed is characterized by a thin high CPS spike which is observed in all three profiles (Figure 2.31, lower left). A distinct dolostone marker bed and a volcanic ash layer were also identified from within the Coboconk Formation, well below the proposed repository level (Wigston and Heagle 2009). That these isolated marker beds can be readily traced across the site strongly suggests that major lateral changes in depositional setting occurred at a scale larger than that of the Bruce nuclear site and reinforces the notion of site-scale predictability based on the borehole data of INTERA (2011).

The marker bed study also provides further indication of the formation lateral continuity and traceability at the site-scale, as shown in Table 2.15. See Section 3.9 in INTERA (2011) for further discussion.

**Table 2.15: Dips Calculated from Marker Beds**

Marker Bed Fm.	Marker	True dip of marker (°)	True dip of formation (°)	Dip Direction (azimuth°)
Queenston	Limestone bed in shale	0.61	0.41	246
Georgian Bay	Fossiliferous limestone bed in shale	0.59	0.61	253
Cobourg	Shale bed in limestone	0.52	0.60	256
Coboconk A	Volcanic ash layer	0.55	0.63	251
Coboconk B	Tan dolostone bed in limestone	0.54	0.63	248

Notes: Includes data from Tables 3.2 and 3.12 of INTERA (2011).

The regular and consistently very shallow dip magnitude of all layers through the Ordovician section, and their lateral traceability across the site, reduces the probability that basement-rooted normal faults with any significant (metre scale or greater) offset exist within this DGR footprint. The only fault geometry which could possibly remain undetected is a strike-parallel transcurrent offset; however, no evidence exists either locally or regionally from surface or subsurface data to suggest that faults of this nature are present (e.g., Cruden 2011).

### 2.3.5 Rock Mineralogy and Geochemistry

Core samples recovered from the DGR boreholes were subjected to a suite of laboratory tests to determine the intact rock mineralogy and litho-geochemistry (e.g., Figure 2.30) as well as confirm or modify the stratigraphy and lithology of the bedrock sequence as described by Armstrong and Carter (2006). Laboratory testing included thin-section petrography with electron microscope analyses, whole rock and sheet silicate fraction X-ray diffraction (XRD) testing, scanning electron microscope/energy dispersive spectral (SEM/EDS) analyses, trace element inductively coupled plasma mass spectrometry (ICP-MS) analyses, elemental oxide analyses by ICP optical emission spectrometry, carbon and sulphur infrared spectroscopy analyses, and chloride by instrumental neutron activation analyses (e.g., INTERA 2011, Wigston and Jackson 2010a, Wigston and Jackson 2010b). Representative estimates of the mineralogical composition of all formations, members and units, based on analysis of all DGR boreholes, are listed in Table 2.16 and illustrated for the four major minerals (calcite, dolomite, quartz, sheet silicates), determined from the vertical boreholes only, in Figure 2.30.

#### 2.3.5.1 Overview

There are clear mineralogical associations or trends which can be summarized based on the laboratory analyses. Devonian and Upper Silurian carbonate sequences are predominantly dolostone with minor limestone-rich layers, minor illite, and quartz (present as chert). Gypsum and anhydrite, as indicated in Table 2.16, were abundant in samples collected from the Salina Group F, A2, and A1 Evaporite units, and gypsum composed 42% of the sample collected from the Salina G Unit. Middle Ordovician carbonates are primarily limestone and dolomite while sheet silicates, dolomite, and quartz compose the majority of the Cabot Head Formation. The Upper Ordovician shales are dominated by sheet silicates, with increasing amounts of quartz

with depth and moderate amounts of calcite and dolomite, particularly in the Queenston Formation, and decreasing in percentage with depth. The Blue Mountain and Georgian Bay formations show a marked decrease in calcite and dolomite content at less than 15%. The Middle Ordovician limestone-dominated formations consist of typically greater than 80% calcite, with the remainder being composed of varying minor amounts of dolomite, quartz and sheet silicates. The exception is the Gull River Formation, which has an increased percentage of dolomite, consistent with the visual evidence of dolomitized horizons (INTERA 2011). The Cambrian rock samples were dominated by dolomite, quartz, and orthoclase (Figure 2.30).

**Table 2.16: Representative Estimates of Mineralogical Composition for All Stratigraphic Formations, Units and Members in All DGR Boreholes**

Model Layer	Major Mineralogy (%)					Trace Mineralogy
	Calcite	Dolomite	Quartz	Sheet Silicates	Other	
Clay till overburden	-	-	-	-	-	-
Lucas	49	49	0.4	0	0	Sp
Amherstburg	42	56	2	0	0	Py
Bois Blanc	56	20	14	1	0	Ch, Py, He
Bass Islands	1	88	6	0	5-Gy	Ce, Py
Salina G Unit	0	57	1	0	42-Gy/An	An, Py, Sa
Salina F Unit	0	30	10	16	44-Gy/An	An, Py, O
Salina E Unit	0	61	6	8	23-Gy	An, Py, O, Sa
Salina D Unit	0	20	0	0	80-An/Gy	An
Salina C Unit	0	26	20	44	0	An, Sa, Ha
Salina B Unit - Carb	10	30	5	32	15-An/Gy	Ha
Salina B Unit - Evap	0	10	0	0	90-An/Gy	-
Salina A2 Unit - Carb	10	60	5	10	10-Gy/An	Ha, Py, Ce, O
Salina A2 Unit - Evap	5	3	1	0	90-An	Gy
Salina A1 Unit - Carb	79	7	2	10	0	Py, O, Gy, An
Salina A1 Unit 0 Evap	0	30	2	2	66-An	Py, Sa
Salina A0 Unit	15	75	2	2	0	Py, An
Guelph	1	86	2	0	10-Ha	Py
Goat Island	73	12	7	8	0	Py
Gasport	79	15	2	3	0	An, He, Py
Lions Head	79	15	2	3	0	An, He
Fossil Hill	79	15	2	3	0	An, Py
Cabot Head	0	25	25	40	6-Go/O	Gy, An, Ha, Py, Ce
Manitoulin	54	12	13	19	0	An, Gy, Ha, Py, He
Queenston	24	14	17	40	0	Gy, An, Ha, He, Go
Georgian Bay	9	11	29	41	9-O	Ha, Gy, An, Py, Ce



Model Layer	Major Mineralogy (%)					Trace Mineralogy
	Calcite	Dolomite	Quartz	Sheet Silicates	Other	
Blue Mountain	6	3	32	49	10-O/Mi	Ha, Py
Collingwood Member	73	9	7	10	0	M, O, Py
Cobourg	81	8	3	6	0	Mi, Py, Ha, An
Sherman Fall	75	10	3	2	6-Mi	An, Ha, Py
Kirkfield	86	3	3	5	3-O/Mi	Py, Ma
Coboconk	86	9	2	2	0	An, Py
Gull River	53	38	2	6	0	An, Py
Shadow Lake	0	40	15	35	9-Kf	Gl, Py, Ce
Cambrian	3	40	30	4	12-O/Mi	Py, Ma, Gy, Ha, An
Upper Precambrian	4	5	24	23	40-Kf	Py

Notes: An = Anhydrite, Ce = Celestite, Ch = Chalcopyrite, Gy = Gypsum, Go = Goethite, Gl = Glauconite, Ha = Halite, He = Hematite, Kf = K Feldspar, O = Orthoclase, Ma = Marcasite, Mi=Microcline, Py = Pyrite, Sa = Sanidine, Sp= Sphalerite. Data are from INTERA (2011, their Table 3.18)

Dolomitization is evident in varying proportions in parts of the Cabot Head, Queenston, Georgian Bay, Blue Mountain, Shadow Lake, and lower Gull River formations, the Collingwood Member and the Cambrian unit (Figure 2.30). Formation sheet silicate content plotted in Figure 2.30 ranges from trace for the Devonian and Upper Silurian dolostones to 25 to 70% within the Ordovician shales of the Queenston, Georgian Bay, and Blue Mountain formations. In all cases, the major sheet silicate mineral is illite and the minor phase is chlorite (INTERA 2011). The sheet silicate content of the Ordovician limestones is typically less than 20%. The sheet silicates within the Precambrian basement are predominantly the micaceous minerals biotite and muscovite. In the Salina above the B Unit, illite occurs as a component in the sheet silicate-rich matrix that encompasses brecciated dolostone created by dissolution of the former B Unit salt and collapse of overlying formations.

The sheet silicate fraction of the Upper Ordovician shale-rich units was analysed as part of a larger study investigating the organic geochemistry of these shales (Jackson 2009). The results indicate that illite + mica together represent > 50% of the sheet silicate mineral constituents, followed by chlorite at 20-45% and with minor kaolinite and interstratified illite-smectite. The interstratified illite-smectite is predominantly illite, with only 5-10% smectite layers. Therefore, smectite is interpreted to represent only approximately 1% of all sheet silicate minerals. Typically, these Ordovician shales also contain about 20-30% quartz and highly variable amounts of carbonate minerals (Figure 2.30). Pyrite is the principal iron mineral throughout the entire Paleozoic interval, although hematite is observed in the Cabot Head and Queenston formations.

### 2.3.5.2 Core Logging

Logging of recovered core identified secondary mineral phases preserved within filled fractures (veins), vugs, and nodules. The infilling mineral phases include quartz, calcite, pyrite, anhydrite, Fe oxide/hydroxide, sheet silicate, halite, and gypsum. Anhydrite is frequently observed from the Bass Islands Formation to the Coboconk Formation. Gypsum was observed in the Salina G

to A2 units. Differentiation of anhydrite from gypsum was done in the field based on hardness and colour; both anhydrite and gypsum are present in many samples. Calcite and pyrite are observed from the Amherstburg Formation to the Shadow Lake Formation. Halite is observed throughout the Upper Ordovician shales and into the Cobourg Formation. Its distribution will be discussed in more detail in Section 2.3.7.

### **Fracture Filling**

Self-sealing by a precipitating mineral phase is a naturally occurring time-dependent process that leads to a reduction in the hydraulic transmissivity of a fracture. When fully self-sealed, the fracture is not a preferential pathway for fluid migration. If partially self-sealed, the fracture may act as a pathway but at a lower transmissivity than when it was open.

Infilled fractures observed during core logging and by petrographic analysis may be of hydrothermal origin or result from mineral precipitation during diagenesis. The vast majority of these secondary mineral phases occur within healed discontinuities in the otherwise intact host rock (Table 2.17). Unlike the surface exposures, which only appear to host calcite veins (e.g., Figures 2.33a and 2.33b), a varied mineralogy is observed throughout the borehole sections. Devonian cherty dolostone contains quartz and chert veins within shale interbeds. Silurian dark shales include both gypsum and anhydrite veins and iron-stained illite veins were recorded in the fossiliferous dolostones. Shales from the upper Queenston Formation contain prominent millimetre thick halite-filled fractures bounded by a carbonate mineral lining the fracture wall. The Queenston Formation also displays calcite, anhydrite, celestite, and gypsum veins. Georgian Bay Formation shales include illite and calcite-filled veins and one ~0.15 mm thick halite vein was observed in thin section. Pyrite and illite veins are observed in shales of the Blue Mountain Formation. Middle Ordovician limestones exhibit dolomite veins and other infill material including iron oxide, pyrite, calcite, anhydrite, and occasionally halite (INTERA 2011).

### **2.3.5.3 Litho geochemistry**

Major elemental oxide data provide confirmation of the dominant mineral composition of the Paleozoic strata. The CaO and MgO data show that most of the Devonian and Silurian carbonates are dolomitic, that the Queenston shale is calcareous, and that the Cabot Head shale has undergone dolomitization. Ca- and Mg-carbonate are minor constituents (< 15%) of the Georgian Bay and Blue Mountain shales. Ca-carbonates dominate the Middle Ordovician units although there is a trend downwards from the top of the Gull River Formation into the Cambrian unit of decreasing CaO and increasing MgO. The data show that the Ordovician carbonates are indeed dominantly limestone with minor dolomite.

Elevated SiO<sub>2</sub> and Al<sub>2</sub>O<sub>3</sub> data (INTERA 2011) confirm the presence of clay minerals sporadically in the Silurian formations and throughout the Ordovician shales. The Fe<sub>2</sub>O<sub>3</sub> content is generally depleted (< 1.5%) in the Devonian and Silurian formations, relatively uniform at about 4 to 8% in the Cabot Head, Queenston, Georgian Bay, and Blue Mountain formation shales, and depleted again in the Ordovician limestones. Most of the detected Fe<sub>2</sub>O<sub>3</sub>, especially in the deeper Ordovician formations, is present as a sulphide phase (e.g., pyrite).

Chloride content varies with depth from generally low (< 0.2 wt%) in the Devonian and through to the top of the Cabot Head Formation, and then increasing to 0.45 to 0.6 wt% in the Cabot Head and through the Queenston, Georgian Bay, and Blue Mountain formation shales. Chloride content then drops significantly to < 0.3 wt% throughout the lower Ordovician to Cambrian

interval. Elevated chloride contents of 0.81 and 1.38% were measured at the top of the Queenston Formation where halite has been observed in core samples by petrographic analysis.

**Table 2.17: Summary of Occurrences of Fracture Infill, Vein and Other Secondary Mineralogy in DGR Boreholes**

Formation	Core Logging	Petrography/XRD/SEM
Lucas + Amherstburg	Calcite, pyrite, Fe staining	Calcite, quartz
Bois Blanc	Calcite, pyrite, chert	Quartz, chert, calcite, pyrite
Bass Islands	Calcite, pyrite, anhydrite, Fe staining	Calcite, gypsum, pyrite, celestite
Salina G+F	Anhydrite, gypsum	Gypsum, anhydrite
Salina E+D	Anhydrite, gypsum	Gypsum, anhydrite, calcite, halite, celestite
Salina C+B	Anhydrite, gypsum, halite	Quartz, chert, halite
Salina A2	Anhydrite, gypsum, clay, halite	Anhydrite, gypsum, calcite
Salina A1+A0	Anhydrite, gypsum, calcite, pyrite	Calcite, pyrite, halite, anhydrite, gypsum
Guelph to Fossil Hill	Calcite, anhydrite, pyrite	Fe-stained illite, halite
Cabot Head + Manitoulin	Chert, quartz, halite, anhydrite	anhydrite, gypsum, quartz, halite, celestite, clays
Queenston	Halite, gypsum, anhydrite, pyrite, Fe staining	Halite, calcite, gypsum, anhydrite, celestite, pyrite
Georgian Bay	Halite, anhydrite, gypsum, pyrite	Illite, calcite, halite, anhydrite, celestite, pyrite, sphalerite
Blue Mountain	Calcite, pyrite, halite, clay	Illite, calcite, pyrite, halite
Cobourg	Anhydrite	Dolomite, Fe-stained illite, pyrite, halite, marcasite, calcite
Sherman Fall	Clay, anhydrite, halite	Calcite, Fe-hydroxide, pyrite, anhydrite, halite, illite
Kirkfield	Calcite	Calcite, pyrite, marcasite
Coboconk	Anhydrite, calcite	Pyrite, calcite
Gull River	Calcite, celestite, aragonite	Fe-staining, pyrite, calcite, dolomite, anhydrite, halite
Shadow Lake	Glauconite, calcite, pyrite, celestite	Pyrite
Cambrian	Calcite, quartz, pyrite, glauconite, Fe staining	Calcite, quartz, pyrite, marcasite, halite, green chlorite
Precambrian	-	Muscovite, rutile, pyrite

Notes: Data are from Table 3.13 of INTERA (2011).

TOC and total sulphur ( $S_{Tot}$ ) are generally low (< 0.75 wt%) throughout the entire Paleozoic section, with a few notable exceptions.  $S_{Tot}$  of up to 4 wt% is measured in the Salina E unit and decreases to trace levels below the Goat Island Formation. The lower Georgian Bay and Blue Mountain formations exhibit TOC and  $S_{Tot}$  of up to 1.0 and 1.25 wt%, respectively, with the largest values encountered at the base of the latter. TOC reaches a peak of 2.5 wt% within a

discrete interval at the top of the Collingwood Member. TOC is discussed in association with noted hydrocarbon occurrences in Section 2.3.6.

#### **2.3.5.4 Detailed Analysis of Ordovician Mineralogy**

A more detailed mineralogical description is included below for the host and bounding formations which include the Queenston, Georgian Bay/Blue Mountain, Cobourg, and Sherman Fall formations. In the following sections, semi-quantitative ranges (wt%) of constituent minerals are grouped into one of four categories: major (> 30 wt%), moderate (10-30 wt%), minor (2-10 wt%), and trace (< 2 wt%). These compositional ranges were defined using X-ray diffraction (XRD) analysis. In most cases, scanning electron microscopy (SEM) analysis identified the same principal components in corresponding samples as compared to the XRD data. Minor differences were found in the matrix content of halite and sheet silicate/quartz in the Queenston Formation (e.g., Wigston and Jackson 2010a, DGR-3 samples). The results of the ActLabs XRD analysis are presented in Figure 2.30 and show the major mineralogy associated with samples at depth from the DGR vertical boreholes.

##### **Queenston Formation Mineralogy**

The Queenston Formation is a thick shale unit with a moderate amount of carbonate throughout in the form of centimetre-thick limestone beds. Three samples from the Queenston shale yielded clays (sheet silicates) as a major component, with moderate amounts of quartz, calcite, and ankerite. Dolomite, orthoclase, and hematite were minor constituents while anatase and pyrite were found in trace amounts. Similar results were obtained from SEM analysis. Halite was observed to commonly comprise void/vein infillings along calcite-dolomite grain contacts. Halite also occurs as the primary component within the silicate and carbonate groundmass, highly irregular interconnected grains, or as veins and stringers. Pore space is characterized by micron-scale irregularly shaped voids. The distribution of halite in the DGR cores will be discussed in more detail in Section 2.3.7.

##### **Georgian Bay and Blue Mountain Formation Mineralogy**

The Georgian Bay Formation was sampled at five depth intervals. This formation is characteristically clastic (shale) rich and dominated by major and moderate amounts of clay and quartz, respectively (INTERA 2011). The clay was identified as illite in three of these samples (INTERA 2011). Orthoclase, dolomite (locally minor), and albite occur in moderate amounts and exhibit a somewhat varying percentage between sampled intervals. Minor phases include pyrite, calcite, and ankerite with trace anatase. Halite in the Georgian Bay Formation mostly occurs as irregular veins, as interstitial disseminated grains within the carbonate and silicate matrix, or as discontinuous rims around carbonate grains. Pore space is characterized by micron-scale irregularly shaped voids.

Petrographic analyses from the upper member of the Blue Mountain Formation show the samples to be very fine-grained, laminated calcareous shale and siltstone. In one sampled interval from the upper portion of this formation, illite, chlorite, and quartz were identified as major mineral constituents with minor dolomite, calcite, feldspar, and pyrite.

Petrographic analyses from the lower member of the Blue Mountain Formation show the samples to be very fine-grained, calcareous shale. The lower Blue Mountain was sampled at one interval. Quantitative XRD analysis of this sample identified the major minerals as illite, chlorite, and quartz with minor dolomite, calcite, feldspar, and pyrite, and with trace halite

(0.5%). Both sub-rounded and elongated coarse-grained halite and irregular discontinuous rimmed halite around silicates were noted in some parts of the lower member of the Blue Mountain Formation.

### **Cobourg Formation Mineralogy**

Five samples from the Cobourg Formation – Lower Member were analysed for mineralogy. Calcite is the dominant major mineral phase by a broad margin, constituting greater than 74% in all samples, and as great as 85.9% locally. The remaining mineral phases, including dolomite, ankerite, orthoclase, and quartz, are present in minor amounts. Halite in the Cobourg Formation is found within the carbonate-dominated matrix as thin cavity-filling stringers, disseminated grains, networks of irregular cavity fillings, or as wider veins. Pore spaces are disseminated and form irregular discontinuous vein-like networks and are commonly filled by halite and less commonly by pyrite.

### **Sherman Fall Mineralogy**

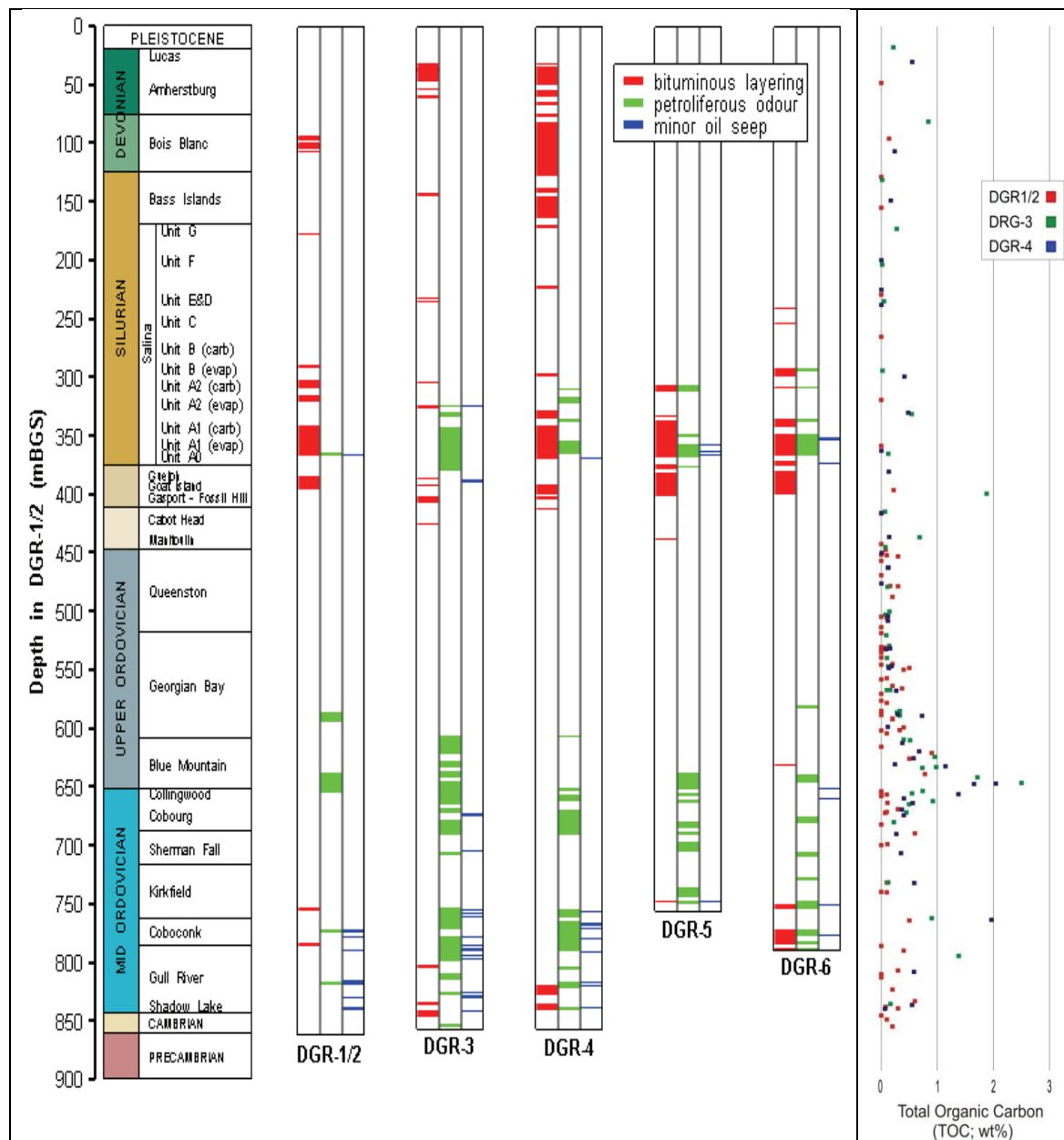
Petrographic analysis of core collected from the Sherman Fall Formation shows the samples to be fine-grained fossiliferous limestone with varying amounts of fossil fragments, pyrite, and iron staining of the calcareous clay matrix. Quantitative XRD analyses of 1 to 2 samples in each DGR core within the Sherman Fall identified the major mineral as calcite with minor dolomite, illite, and quartz, and trace pyrite and anhydrite.

### **2.3.6 Hydrocarbon Occurrences**

Although there is no indication of economic accumulations of hydrocarbon resources at the Bruce nuclear site (INTERA 2011, Engelder 2011), visual inspection of the DGR core and detailed laboratory analysis of selected samples does show the presence of discrete hydrocarbon occurrences (Jackson 2009, Sections 3.7.4 and 3.7.5 of INTERA 2011). Hydrocarbon is observed in the DGR cores primarily as thin bituminous layering, indirectly as a prominent petroliferous odour, and as minor localized seeping or oozing of oil from vugs, fractures, and dolomitized sedimentary horizons. Figure 2.32 shows hydrocarbon distribution from the vertical DGR boreholes. The hydrocarbon bearing intervals are concentrated into three main horizons which correspond in general to zones of elevated TOC within the Paleozoic stratigraphic sequence (Figure 2.32). A shallow interval of prominent petroliferous odour and minor oil seeping is observed at the top of the Silurian Guelph Formation and into the overlying basal Salina units (Figure 2.32). An intermediate interval corresponds to the base of the Upper Ordovician shales where maximum TOC values of up to 2.5 wt% are measured within the Collingwood Member (Figure 2.32). A deep interval comprises isolated hydrocarbon occurrences throughout the Black River Group and includes the base of the Kirkfield Formation of the overlying Trenton Group (Figure 2.32).

DGR core samples from locations within the Upper Ordovician shales were also evaluated by Rock-Eval pyrolysis in order to characterize their thermal maturity and kerogen source (e.g., Jackson 2009). Shales from the Collingwood Member and Blue Mountain Formation are thermally mature and of marine origin, tending to form oil rather than gas. Most of the Georgian Bay Formation and Queenston Formation shales contain kerogen derived from a terrestrial source and are more gas prone. In situ temperatures of between 70 to 130 °C have been estimated during thermal maturation and development of oil hydrocarbon within the Collingwood Member and Blue Mountain Formation shales (Jackson 2009), and at 75 to 85°C for the deeper Black River Group based on a regional CAI analysis (e.g., Legall et al. 1981). The peak burial

temperature estimate of 70°C for the Collingwood Member (top of Trenton Group) at the site (see Section 2.2.5.3) suggests that the actual temperature was towards the lower end of the range given by Jackson (2009). This is consistent with the field observation of only minor visible oil staining and seeping in the cores at this stratigraphic horizon (Figure 2.32; INTERA 2011).



Notes: Hydrocarbon occurrences are based on core log descriptions from Sterling (2010a) and Sterling (2010b). TOC data are from INTERA (2011).

**Figure 2.32: Summary of Observed Hydrocarbon Occurrences and TOC Analyses from DGR-1/2, DGR-3, and DGR-4 Cores**

### 2.3.7 Halite Occurrences

Halite was specifically targeted for identification and distribution analysis because of its high solubility (~6000 mmol/kgw) and its role as a groundwater tracer. The presence of halite within a formation or group of formations is a strong indicator that there has been no flow of fresh, or halite-undersaturated, water through that rock sequence since the halite was precipitated.

Halite was detected visually during core logging, and via optical microscope, XRD, and SEM/EDS analyses (Figure 2.33; INTERA 2011 and references therein). Halite occurrences include: 1) mineral infilling of subhorizontal and steeply-dipping fractures; 2) voids and cavities; 3) a grain-boundary mineral phase within a matrix dominated by gypsum, dolomite, calcite, or silicate minerals; and, 4) as disseminated grains and irregular, discontinuous stringers. Halite was found within several Silurian units, in abundance throughout the Upper Ordovician shales, as a minor mineral phase throughout the Cobourg, Sherman Fall, and Gull River formations, and the Cambrian (Figure 2.33; INTERA 2011, Koroleva et al. 2009). Whole-rock and clay-mineral XRD analyses yielded average halite concentrations of 0.7 wt% and 0.6 wt% in DGR-3 and DGR-4, respectively. Maximum halite concentrations were recorded in the Blue Mountain Formation with concentrations ranging from 0.5 to 1.4 wt%.

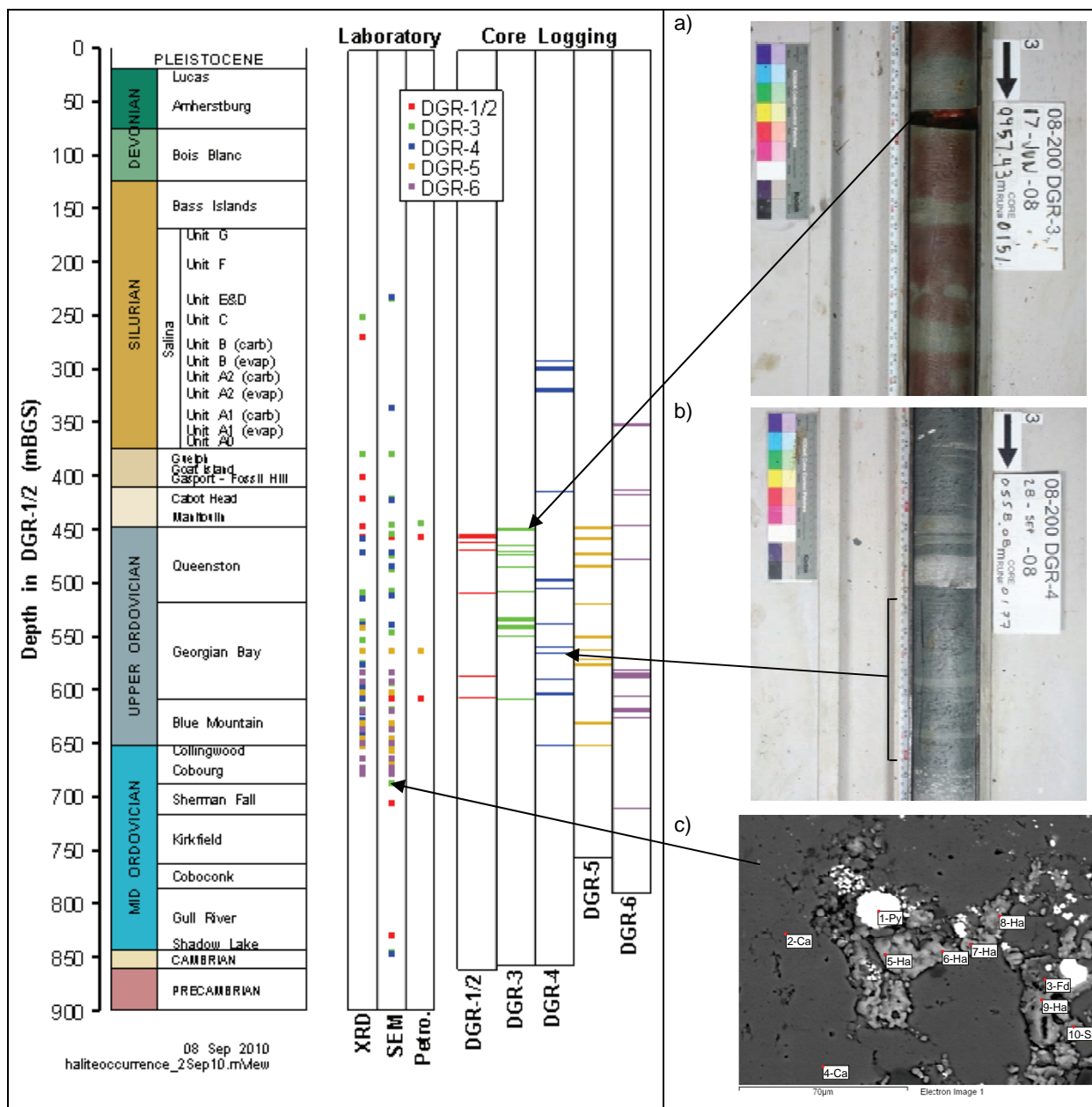
Halite was most commonly observed infilling millimetre-scale to hairline thickness fractures throughout the Upper Ordovician shales (e.g., Figures 2.33a and b). There is visual evidence that drilling fluids locally dissolved some of the vein halite (e.g., Figure 2.33a), but where this occurred there was generally enough preserved for positive identification. In the deeper limestones, including the Cobourg Formation, a lack of open fractures is consistent with halite only being recognized as a mineral phase at the micron scale. In these instances it was commonly observed as the dominant mineral phase within networks of irregular cavities between larger calcite grains (e.g., Figure 2.33c, SEM backscatter image of DGR-3-699.62).

Halite saturation index calculations, using porewater chemistry results for the Ordovician limestones and the Cambrian sandstone, are presented in Section 4.6 of INTERA (2011). Only three core samples from the Ordovician limestones had calculated halite saturation or supersaturation (DGR-3-702.54, DGR-4-669.18 and DGR-4-772.19), and the Ordovician shales are uniformly undersaturated (see Section 4.6.3 of INTERA 2011). These lower than saturation porewater concentration estimates may be due to release of clay-bound water during laboratory heating (Section 4.6.3 of INTERA 2011) and/or anion exclusion processes (Section 4.6.4 of INTERA 2011).

Similar calculations, and the opportunistic groundwater analyses, indicate that the Cambrian sandstone samples are also undersaturated with respect to halite. These results, which suggest that halite should not be present in the Cambrian, are inconsistent with its identification in one Cambrian sample (DGR-3-856.28) using SEM/EDS. An SEM feasibility study (Herwegh and Mazurek 2008) exposed a sample from the Cambrian sandstone (DGR-2-852.39) to air and examined the minerals formed on the surface of the core. Halite and Ca-sulphate minerals (likely gypsum or anhydrite) formed on the core due to the evaporative concentration of the porewater.

These results suggest that a small amount of halite and Ca-sulphate may be produced by the evaporation of cores during sample preparation for mineral identification, and this may explain the halite presence in the Cambrian. This is clearly not the case in the Cobourg sample where the SEM backscatter image (Figure 2.39c) shows halite grains completely surrounding pyrite grains in the irregular voids between the larger calcite crystals, indicative of a primary halite occurrence, or further up in the section where halite is common as a fracture infill.

The highest calculated concentrations of chloride and sodium in porewater are observed throughout the Upper Ordovician shales and into the Sherman Fall Formation (Section 4.6.5 of INTERA 2011). The distribution of halite occurrences observed during core logging and the various laboratory analytical techniques exhibits a definite depth correlation with the porewater analytical results.



Notes: Observed halite distribution is based on core log descriptions, XRD, SEM, and petrographic analysis of the DGR cores (INTERA 2011 and references therein). Arrows indicate location of each of (a), (b) and (c). (a) Sub-horizontal halite-filled fracture in the Queenston Formation. (b) Sub-vertical halite-filled fracture in the Georgian Bay Formation. (c) SEM backscatter image of pore-filling halite in the Cobourg Formation. Spot mineral analyses are indicated by red dots: 1. Pyrite, 2. Calcite, 3. Feldspar, 4. Calcite, 5. Halite, 6. Halite, 7. Halite, 8. Halite, 9. Halite, 10. Silica (Quartz).

**Figure 2.33: Summary of Observations of Halite Presence in the DGR Cores**



### 2.3.8 Karst and Paleokarst Occurrences

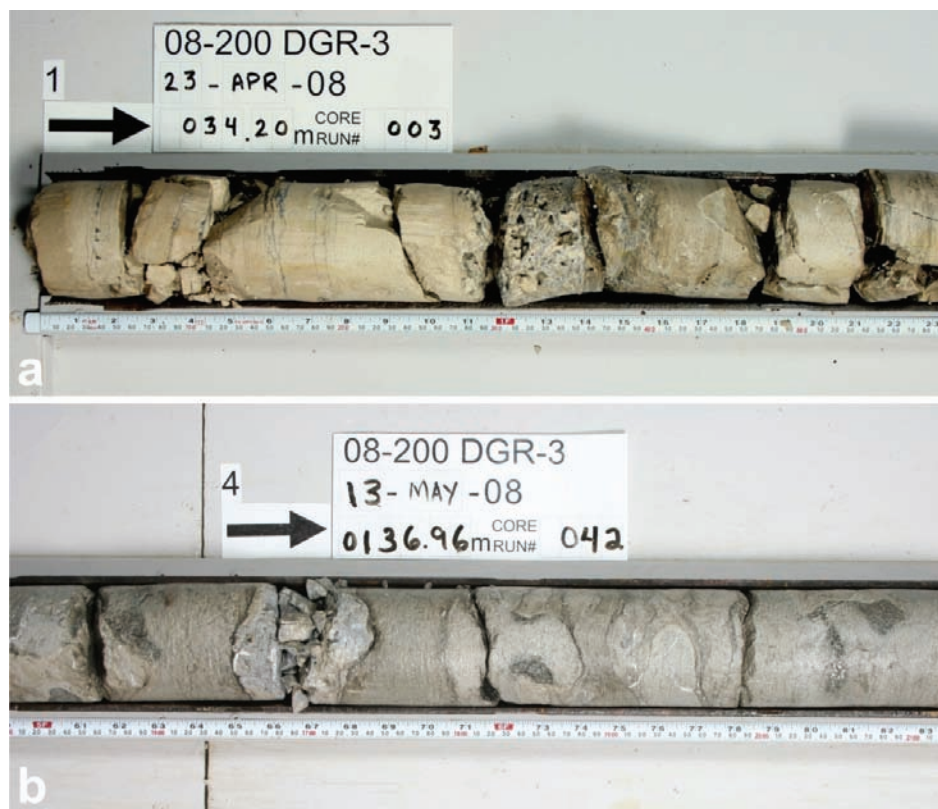
An evaluation of the distribution of karst beneath the Bruce nuclear site was undertaken in order to aid in understanding the shallow groundwater system at the Bruce nuclear site (WORTHINGTON 2011). Modern karstification is on-going today, while the term paleokarst refers to karst that was formed at an earlier time and subsequently buried and rendered inactive by later deposition of sediments or by changes in groundwater flow conditions. Paleokarst is therefore ancient and most likely to have been most extensive at the largest unconformable breaks in the sedimentary record. At the site, and regionally, similar breaks are recognized at the top of the Bass Islands Formation (e.g., Brunton and Dodge 2008), below and above the Reynales/Fossil Hill formations, below and above the Detroit River Group, and at the top of the Guelph Formation. The lateral extents of these high-permeability zones were a few kilometres at most (WORTHINGTON 2011), consequently, this localized karstification is unlikely to contribute significantly to modern regional groundwater flow. Though karst features are preserved at such paleokarst horizons, subsequent deposition and diagenesis would have occluded much of the karstic function (i.e., enhanced permeability) of such strata.

The pertinent conclusions of the karst study are summarized below. These are based on the interpretation of several independent data sets collected during site characterization and compiled in Figure 4.1 of the Karst Assessment report (WORTHINGTON 2011).

- The top approximately 180 mBGS of bedrock at the Bruce nuclear site down to the Salina G Unit is recognized as a zone of modern karst development. This zone is characterized by higher hydraulic conductivity than is found in the deeper units, and groundwaters that range in Total Dissolved Solids (TDS) from fresh (< 0.5 g/L) to brackish (approximately 5.0 g/L) near the bottom of this groundwater zone.
- Higher hydraulic conductivity intervals at depths of about 326 to 329 mBGS (Salina A1 dolostone) and 375 to 379 mBGS (Guelph Formation) also show isolated evidence of potential karstification. However, these zones are characterized by Na-Cl waters with TDS values of 29 g/L and 371 g/L, respectively.
- The Ordovician carbonates are unaffected by modern karstification processes.

These conclusions are supported by the results of the hydraulic testing which indicate uniformly very low hydraulic conductivities throughout the deep Ordovician interval. The site-scale distribution of TDS, and formation-scale hydraulic conductivities are discussed in more detail in Chapters 4 and 5, respectively.

Examples of modern karst and potential paleokarst from beneath the Bruce nuclear site are shown in Figure 2.34. Shallow Devonian carbonates are characterized by modern karst features such as solution-enhanced joints and stained/weathered fractures (Figure 2.34a). Groundwater in the shallow bedrock system may preferentially flow along paleokarst horizons where modern karstification has dissolved cement infilling. An example is observed near the bottom of the Bois Blanc Formation (Figure 2.34b) which overlies the unconformity at the top of the Bass Islands Formation.



Notes: Arrow points downhole towards stratigraphic bottom in all photographs. (a) Core photo from shallow Devonian Lucas Formation carbonates. This interval is characterized by karst features such as solution-enhanced joints, stained/weathered fractures, and vuggy porosity. (b) Core photo from near the base of the Devonian Bois Blanc Formation where present-day groundwater flow may be concentrated along a remnant paleokarst horizon.

**Figure 2.34: Potential or Active Karst and Paleokarst Beneath the Bruce Nuclear Site**

### 2.3.9 Site-scale Structural Geology

The proposed DGR site is near the eastern shoreline of Lake Huron on the east-northeastern flank of the intracratonic Michigan Basin (e.g., Figures 2.2, 2.22, and 2.23). The interpretation of minimal structural complexity in this area is reinforced by observations of the consistently oriented and extremely shallow-dipping attitude of the Paleozoic strata. Rocks in outcrop, and in the subsurface, dip gently southwestward at between 4 and 17.5 m/km, or 0.23° to 1° toward the basin depocentre in central Michigan (Liberty and Bolton 1971, Watts et al. 2009, Wigston and Heagle 2009; Tables 2.13 and 2.14). Bedding dips reported from the southern Bruce Peninsula by Armstrong (1993) and formation top dips (e.g., Wigston and Heagle 2009) and marker bed dips (Section 2.3.4.2; Table 2.14), based on information in the DGR borehole database, all fall within this range (INTERA 2011).

Further evidence for a lack of structural complexity is reflected by the fact that stratigraphic units recognized in the DGR cores fit well into the regional stratigraphic framework, and their thicknesses are similar to those of reference wells proximal to the site (Watts et al. 2009). The

Middle and Upper Ordovician sections, in particular, exhibit a remarkably consistent total thickness within and outside of the DGR footprint. As indicated in Table 2.13, total thickness of the Ordovician section in the DGR wells was determined to range from 396.2 to 398.2 m. Moving outside of the DGR footprint, interpreted stratigraphic contacts for the Kincardine #1 Union Gas and the Texaco #6 boreholes yield total Ordovician thicknesses of 393.5 and 393.1 m, respectively. A regional cross-section that includes DGR-1/2, DGR-3, and Texaco #6 highlights this remarkable consistency. Three-point solutions based on data that include Texaco #6 formation top picks define planar bedding geometries nearly identical to those determined from the DGR boreholes (Table 2.13). Although a site-scale 2D seismic survey identified several potential basement-seated faults (Watts et al. 2009), these site-scale and broader stratigraphic correlations suggest that no significant metre-scale fault offset is likely to be present within or proximal to the DGR footprint. DGR 6 was targeted at one such interpreted fault from seismic lines 5 and 6. Analysis of core from DGR 6 demonstrated that no such feature existed and that the seismic anomaly was an artefact of signal processing.

Other independent results are consistent with a lack of significant evidence for faulting at the Bruce nuclear site.

- Preliminary results from the drilling program, which specifically targeted one potential feature and the possible extension of another, as identified by the 2D seismic survey, did not yield any evidence of a fault zone through the targeted intervals in any of the recovered core.
- A detailed shoreline surface mapping and structural analysis study of Devonian bedrock exposed at the Bruce nuclear site found that only 10 out of 610 measured fractures exhibited any offset (ranging from 26 to 150 mm), supporting the likelihood that fault movement was minor. The systematic nature of the jointing pattern observed in the Devonian-aged outcrops also suggests that no major post-Paleozoic tectonic event has disturbed these rocks (Cruden 2011).
- A neotectonic remote-sensing and field-based study that analysed Quaternary landforms for the presence of seismically induced soft-sediment deformation concluded that the Bruce nuclear site has not likely experienced any post-glacial tectonic activity (Slattery 2011).

Faults throughout the broader RSA region were interpreted and mapped by correlation of historical well logging records based on a sparse borehole dataset (Bailey and Cochrane 1984a, Bailey and Cochrane 1984b; Figure 2.35a). Of the 30 interpreted faults within the RSA boundary, 18 have 3 or more well control points to provide confidence in their interpretation. These 18 faults, highlighted in yellow on Figure 2.35a, and plotted in the rose diagram in Figure 2.35c-1, exhibit a bimodal distribution of N- and ENE-trending sets which is consistent with joint measurements from throughout the RSA (Figures 2.35). The remaining faults should be considered as speculative features only. From the 10 boreholes drilled nearest to the site, only one kilometre-scale ENE-striking fault was indicated. It is located greater than 25 km from the site and is included in the speculative (black lined) subset (Figure 2.35a). The results from a more recent study that produced contoured formation top surfaces for the Paleozoic units generally support the interpreted regional fault distribution (AECOM and ITASCA CANADA 2011). A conceptual model, comprising a system of regularly spaced ESE-trending normal faults that control regular sedimentary thickness changes (Sanford et al. 1985), is not supported by the regional data set.

No borehole breakouts were observed during the course of the multi-year drilling program. However, a systematic SE-trending elongation was noted during borehole cross-section shape analysis (Valley and Maloney 2010). The orientation of the borehole elongation falls within the trend expected based on the broadly oriented (N63°E +/- 28°; Zoback 1992) compressional

stress field that persists regionally (e.g., Sbar and Sykes 1973, Zoback and Zoback 1989, Baird and McKinnon 2007). Seismic activity is minimal at the Bruce nuclear site because it falls within the stable cratonic region of the North American continent, as discussed in Section 2.2.6.5.

### 2.3.9.1 Fracture Analysis

A detailed fracture mapping study was undertaken near the Bruce nuclear site with the objective of collecting brittle fracture orientation data, including a systematic examination of joint, vein, and fault features (Figures 2.35b, 2.35c-3 and 2.35c-4; Cruden 2011). The results of this analysis are presented below and will be integrated with the borehole datasets (INTERA 2011), and the structural framework of the RSA, in order to provide a more complete understanding of the brittle deformation history at the site scale.

Fracture analyses were undertaken focusing both on shoreline exposures of the Devonian Lucas Formation (Figure 2.35b; Cruden 2011), and for the entire bedrock interval intersected by the DGR boreholes (INTERA 2011). The following sections review the important features of each. It is confirmed that the surface data are generally consistent with the subsurface data, and further, that both are broadly consistent with the regional dataset.

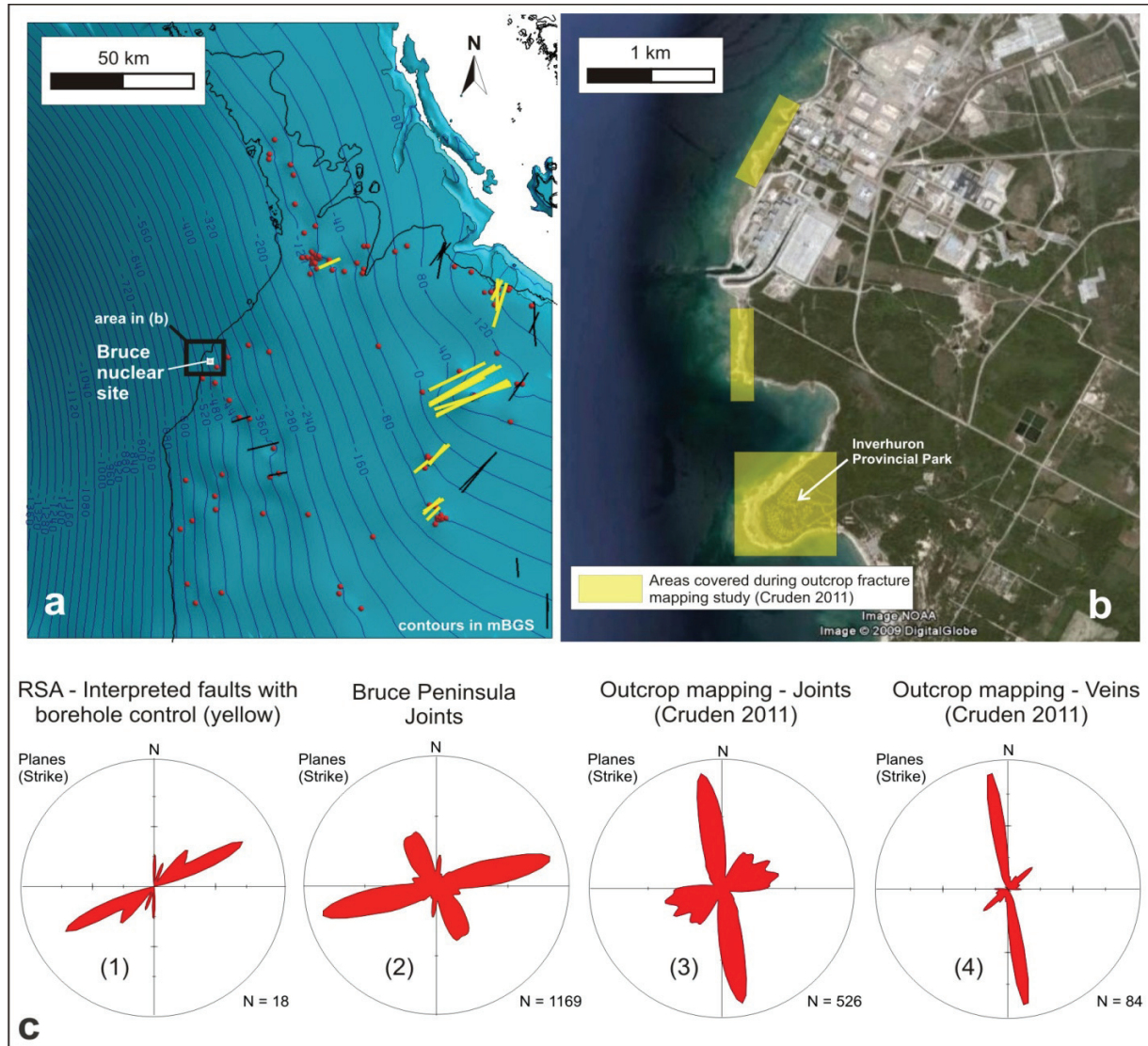
#### Outcrop Data

Bedrock outcrop near the proposed Bruce nuclear site is restricted to fine- to medium-grained, light grey limestone and dolostone of the Devonian Lucas Formation. This rock is observed as discontinuous pavements along the shoreline of Lake Huron immediately adjacent to the Bruce nuclear site and further to the south around Inverhuron Provincial Park (Figure 2.35b). The bedrock dips at less than 1° towards the SW, in accord with both regional values and those determined from formation top picks and a marker bed study (above). Bedding attitude is locally deflected due to sediment compaction over the top of 1 to 2 m diameter stromatolite mounds. At a larger scale, aerial photograph interpretation of surface bedding traces indicates that bedding layers are locally deflected into 40 to 100 m diameter dome and basin features (Cruden 2011).

Only systematic joint sets were documented for the study, and their observable characteristics are as follows (Cruden 2011):

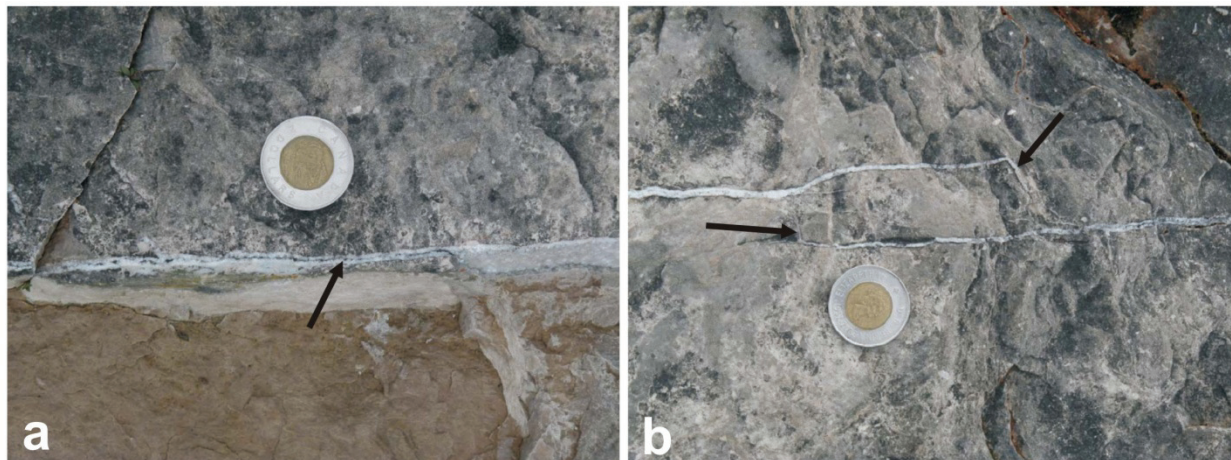
- Joint frequency is linked to grain size where thin beds of fine-grained micritic limestone host fractures spaced 1 to 20 cm apart, while thicker beds of medium-grained limestone host fractures spaced 20 cm to 2 m apart;
- Most joints do not exceed 5 m in horizontal length while vertical joint height could not be measured accurately due to the sub-horizontal nature of the outcrop;
- Most joints are closed and tight and those with measurable aperture have been widened by solution processes (karst) or creep;
- Joints only exhibit carbonate mineral infilling (Figures 2.36a and b), with no iron oxide filling or coatings, indicating a lack of groundwater penetration along joint surfaces;
- Only one joint had plumose structure, a N-striking sub-vertical feature with sub-horizontal median line, and no other lineation pattern was observed throughout the area;
- Both joint and vein sets share common orientations with subtle variations; two main sets are distinguished, one trending ENE and the other NNW (Figures 2.35c-3 and 2.35c-4);
- Only 10 of the 610 measured joints and veins displayed horizontal offsets with both sinistral and dextral displacement, ranging from 2 mm to 150 mm, observed on both the ENE- and N-striking sets with no systematic distribution noted; and

- No significant brittle faults or evidence of ductile shear zones in the rocks were observed in the study area.



Notes: North orientation is the same in both (a) and (b). Base map in (a) depicts the Cobourg Formation subsurface contour map (in metres above sea level) and control wells used to define it. Fault distribution data in (a) are compiled from Bailey and Cochrane (1984a) and Bailey and Cochrane (1984b). Faults with sufficient well control to allow for confidence in their interpreted existence and distribution are drawn in yellow in (a) and plotted in (c1). Plan view photograph in (b) indicates areas covered during detailed outcrop fracture mapping analysis (Cruden 2011). Rose diagrams of fault and joint data collected throughout the RSA are shown in (c1-4). Data in (c2) are from Armstrong (1993). Data in (c3) and (c4) are from Cruden (2011).

**Figure 2.35: Compilation of RSA and Site-scale Fault, Joint and Vein Data**



Notes: Photographs are from outcrop fracture mapping study by Cruden (2011). In (a), the vein trends  $119^\circ$  and is filled with calcite. A thin dark discontinuous seam of wall rock occurs in the centre of the vein (indicated by arrow), indicating its crack-seal nature. Overlapping veins with Interacting (bridging) tips (indicated by arrows) are shown in (b). Tip Interaction shown in (b) indicates that the veins likely propagated as fluid-pressurized cracks (hydrofractures). Coin for scale in both photos.

**Figure 2.36: Calcite-filled Veins Exposed along the Shoreline of Lake Huron near the Bruce Nuclear Site**

In several places, fracture propagation and mineral precipitation are interpreted to have been synchronous based on the occurrence of crack-seal veins (Figures 2.36a and b). This type of vein formation is associated with multiple cycles of hydraulic fracturing and mineral precipitation, and curved and branching vein tips (Figures 2.36a and b). Such features are indicative of fracture propagation under conditions of elevated pore fluid pressure. Given that both joints and veins share common orientations, it is likely that most fractures observed in the Lucas Formation formed under conditions of elevated pore fluid pressure (Cruden 2011). Elevated pore fluid pressure conditions were likely experienced during either Acadian or Alleghenian orogenesis, possibly associated with a topographically driven flow system (e.g., Engelder 1990).

The measured joint population is dominated by a major set with a peak orientation of  $350^\circ$  (NNW) and ranging between  $336^\circ$  and  $006^\circ$  (Figure 2.35c-3; Cruden 2011). A second population of fractures defines a broad peak trending ENE with range between  $025^\circ$  and  $098^\circ$  and four sub-peaks at  $041^\circ$ ,  $060^\circ$ ,  $075^\circ$ , and  $088^\circ$  (Figure 2.35c-3). The vein population is dominated by a major set with a peak orientation of  $350^\circ$ , and a secondary trend of  $048^\circ$  (Figure 2.35c-4). The former bisects the range of the NNW-striking joint set and the latter bisects the  $041^\circ$  and  $060^\circ$  sub-peaks of the NE-striking joint set (Figure 2.35c). This geometric relationship suggests that the NNW-striking joints and some of the NE-striking joints are conjugate hybrid fractures, formed contemporaneously, and bisected by extensional veins (Cruden 2011). These sets overshadow a very minor third set of SE-striking joints and veins.

Taking a closer look at the vein and joint set data from within the RSA it is observed that both joint and vein populations are dominated by sub-vertical ( $> 85^\circ$ ) dip attitudes but range as low as  $20^\circ$ . Statistically, these shallower planes therefore define either a domal or basinal arrangement with dips  $\sim 50^\circ$  in all directions. This configuration is interpreted to have resulted from sediment compaction over algal mounds as discussed above.

The two main joint and vein set orientations determined from this outcrop-scale analysis are broadly consistent with joint orientations as determined from studies throughout the RSA and elsewhere in southern Ontario (compare Figures 2.15 and 2.35c-2 with Figures 2.35c-3 and 2.35c-4), including data from the Bruce Peninsula collected by Armstrong (1993). The local joint and vein data are also similar to the regional fault trend dataset which includes all of the fault traces mapped throughout southern Ontario (e.g., Figure 2.5). Figure 2.35a includes all interpreted faults within the RSA (black and yellow lines) and highlights (yellow lines only) those faults which are proximal to at least three boreholes (see also rose diagram of Figure 2.35c-1). The existence of the other interpreted faults (black lines) is much more speculative. Nevertheless, the NE- and N-trending fault trends are generally consistent with the two main joint/vein orientations recognized by Cruden (2011).

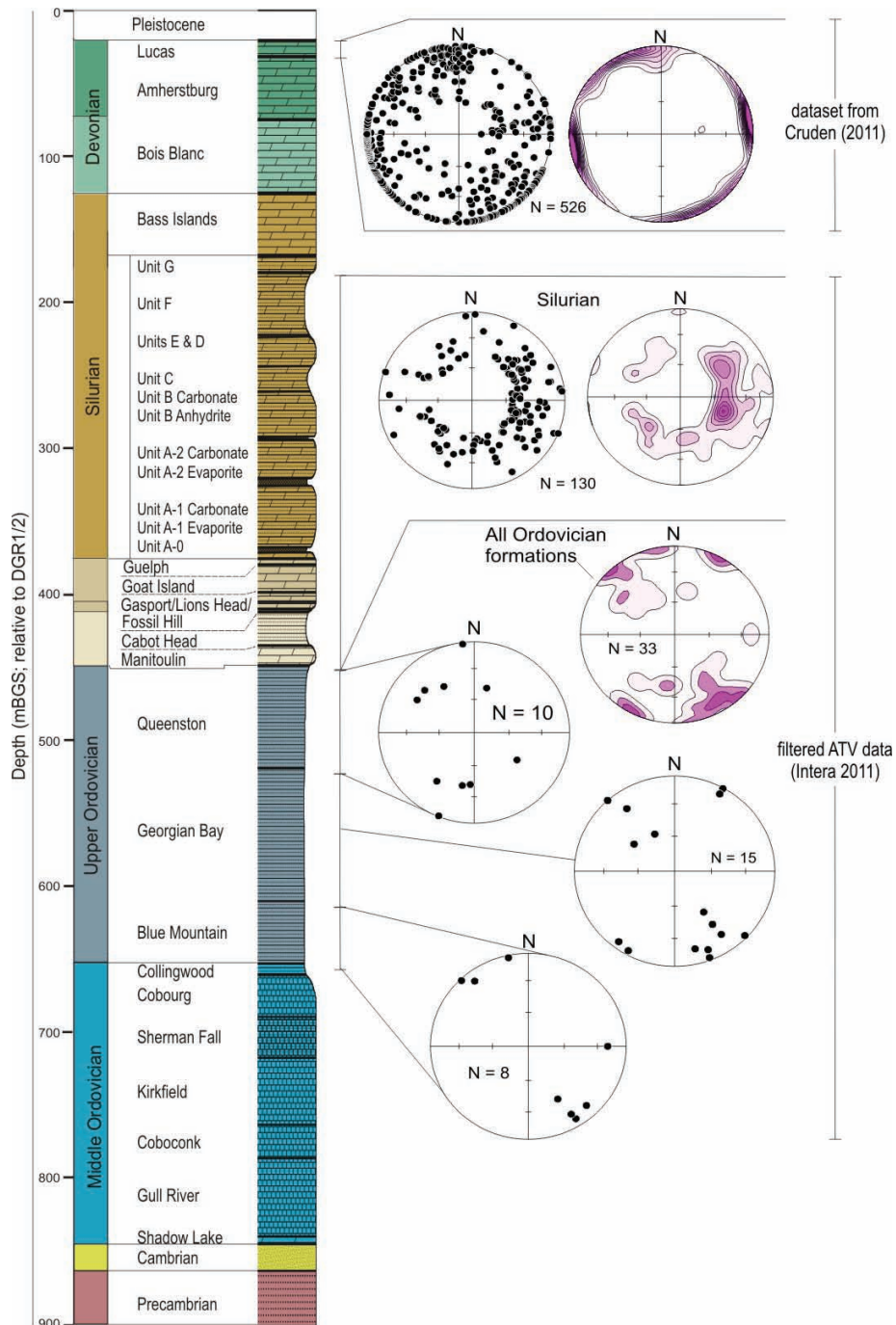
These NNW- and ENE-trending fracture sets appear to be part of the regional fracture system in the Silurian and Devonian strata of the Bruce Peninsula, Manitoulin Island, and northern Michigan. In particular, the NNW-trending set is concentric with respect to the outline and structure contours of the Michigan Basin (e.g., Figure 2.2). A broad basin-centred subsidence event coincided with deposition of the Middle Devonian Dundee Formation and Traverse Group strata in the Michigan Basin (Howell and Van der Pluijm 1999). Cruden (2011) suggests that radial tensile stresses generated during this event provide a plausible mechanism for developing the basin-scale concentric fracture set in general, and the NNW-trending fracture set in the study area in particular.

The geometrical relationships discussed above suggest a contemporaneous late Paleozoic age for formation of the NNW- and ENE-trending fracture sets. A neotectonic origin for the ENE-trending fractures (e.g., Holst 1982, Gross and Engelder 1991) is difficult to reconcile with an interpreted late Paleozoic timing for formation of the NNW-trending fractures given that detailed fracture mapping suggests these two sets formed contemporaneously. Recent work re-analysing the paleo-stress field of the Appalachian Basin suggests that some of these ENE-trending joint sets distributed throughout the basin are actually late Paleozoic (Pennsylvanian-Permian) in age (Engelder and Whitaker 2006). They now simply share a common orientation with a prominent neotectonic joint set (Hancock and Engelder 1989). Therefore there is no genetic significance to the similarity in orientation between the ENE-trending fracture population and the present in situ maximum horizontal stress. The origin of the vein filling material and the timing of the main fracture forming event, for both the NNW and ENE fracture sets, is best interpreted as late Paleozoic in age (Cruden 2011).

### **Vertical Borehole Results**

Boreholes DGR-1, DGR-2, DGR-3, and DGR-4 were drilled to approximate depths of 462, 862, 869, and 857 mBGS, respectively, and are subvertical, never exceeding tilts of 1.5°, 1°, 4.5°, and 4°, respectively. Details of the borehole layout at the site are given in Figure 2.24. Core logging and acoustic televiewer (ATV) images represent the primary means of structural data collection. The former gives information primarily on occurrence and approximate dip of fractures while the latter can quantify both occurrence and orientation through the analysis of the elliptical traces of fractures on the borehole wall. Figure 2.37 shows a plot of ATV-derived fracture data with depth, separated by formation, as well as data compiled by Cruden (2011) from surface mapping. The ATV data have been filtered to only include features that dip > 35° from horizontal (INTERA 2011). INTERA (2011) also noted bedding sub-parallel discontinuities throughout the DGR cores. These structures may include natural fractures which are predominantly mineral-filled veins, mechanical breaks, and lithological layering. In the latter case, many examples exist in the DGR cores where fractures are localized in, or along, the

contact of thin shale-rich beds, which occur within more massively layered limestone. These have the appearance of mechanical breaks.



Notes: Orientation data are plotted on equal-area lower hemisphere projections. Surface dataset is from Cruden (2011) and subsurface dataset is from ATV logging of DGR-2, DGR-3, DGR-4, DGR-5 and DGR-6 (INTERA 2011).

**Figure 2.37: Natural Fracture Orientations from Surface and Subsurface Datasets**



The borehole data for the Ordovician are sparse with 33 total measurements across all formations (Figure 2.37). Peak orientations trend NE, N, and E generally with dips of 50° or more (Figure 2.37). A much larger dataset for the Silurian section (130 measurements) exhibits similar peaks, except that in this case, a steeply dipping and SE-trending fracture set appears to dominate. The fracture orientations, as determined by Cruden (2011), are also similar to the Ordovician dataset in general, although there is an obvious bias against steeply dipping structures when determined from a vertical borehole investigation.

### **Inclined Borehole Results**

As noted above, vertical boreholes have an inherent sampling bias against steeply dipping structural features. Inclined boreholes DGR-5 and DGR-6 (Figure 2.24) were drilled so that a statistically meaningful lateral section of rock could be sampled for quantification of the joint and vein distribution within the subsurface. The majority of steeply inclined joints within the Ordovician section occur in the Georgian Bay and Blue Mountain formations, with only three in the Collingwood and none in the Upper or Lower Cobourg and Sherman Fall formations. All of the observed joints appear to be planar with smooth surfaces, particularly in the shales. Joint surfaces tend to be rougher in the limestone beds. Some joints are discontinuous, terminating abruptly in the core. Occasional very thin (< 1 mm thick) halite or calcite joint infilling is observed. Refer to Sections 3.2.1.2 and 3.2.2.2 for a detailed description of the rock mass properties, including joint spacing.

The inclined-drilling program was also designed to test for the existence of NNW-striking vertical faults proximal to the DGR. DGR-5 was oriented such that it would potentially intersect a northward extension of one such fault structure which was interpreted from the 2D seismic survey (see Section 2.3.9.2 below) on seismic line 9 (Figure 2.24). DGR-6 was oriented such that it would transect a similarly oriented structure at depth which transects seismic line 6 (Figure 2.24). Continuous core retrieved from both inclined boreholes showed no indication of the existence of either one of these potential faults. There was no evidence of shear zones, slickensides, cataclasites, fault gouge, or a fault-related offset in the stratigraphy within the core recovered from the targeted intervals. The following section discusses the methodology, limitations, results, and conclusions of the 2D seismic survey.

### **2.3.9.2 2D Seismic Reflection Survey**

A two-dimensional (2D) seismic survey including nine survey lines totalling 19.7 km was conducted on the Bruce nuclear site as part of the geoscientific investigation for the proposed DGR (Figure 2.24; INTERA 2011). The purpose of this 2D seismic survey was to obtain preliminary deep bedrock geological, stratigraphic, and structural information for the Bruce nuclear site, and to assess the predictability and continuity of the host rock for the DGR (Cobourg Formation) and the “potential” location of faults and fault zones in the subsurface within the Paleozoic bedrock. The bedrock units of primary interest were the shales and argillaceous limestones at depths of about 400 to 800 m. These strata include the Middle Ordovician limestones (Cobourg, Sherman Fall, Kirkfield, Coboconk, and Gull River formations) and overlying Ordovician shales (Queenston, Georgian Bay, and Blue Mountain formations). In general, the seismic survey imaged horizontal reflections interpreted to represent traceable bedrock stratigraphy across the entire survey area shown in Figure 2.24 (Watts et al. 2009).

Conventional oil and gas exploration techniques and expertise were used to acquire and process the data with the intent to mitigate environmental noise and obtain the best achievable data quality. However, seismic data quality was affected by poor seismic energy coupling

between the heterogeneous glacial drift and underlying bedrock, as well as by anthropogenic and natural background noise. As a result, the data quality is not good enough to determine with a high degree of confidence, the orientation of interpreted faults, or whether some features tentatively identified as faults are instead persistent noise artefacts remaining after data processing.

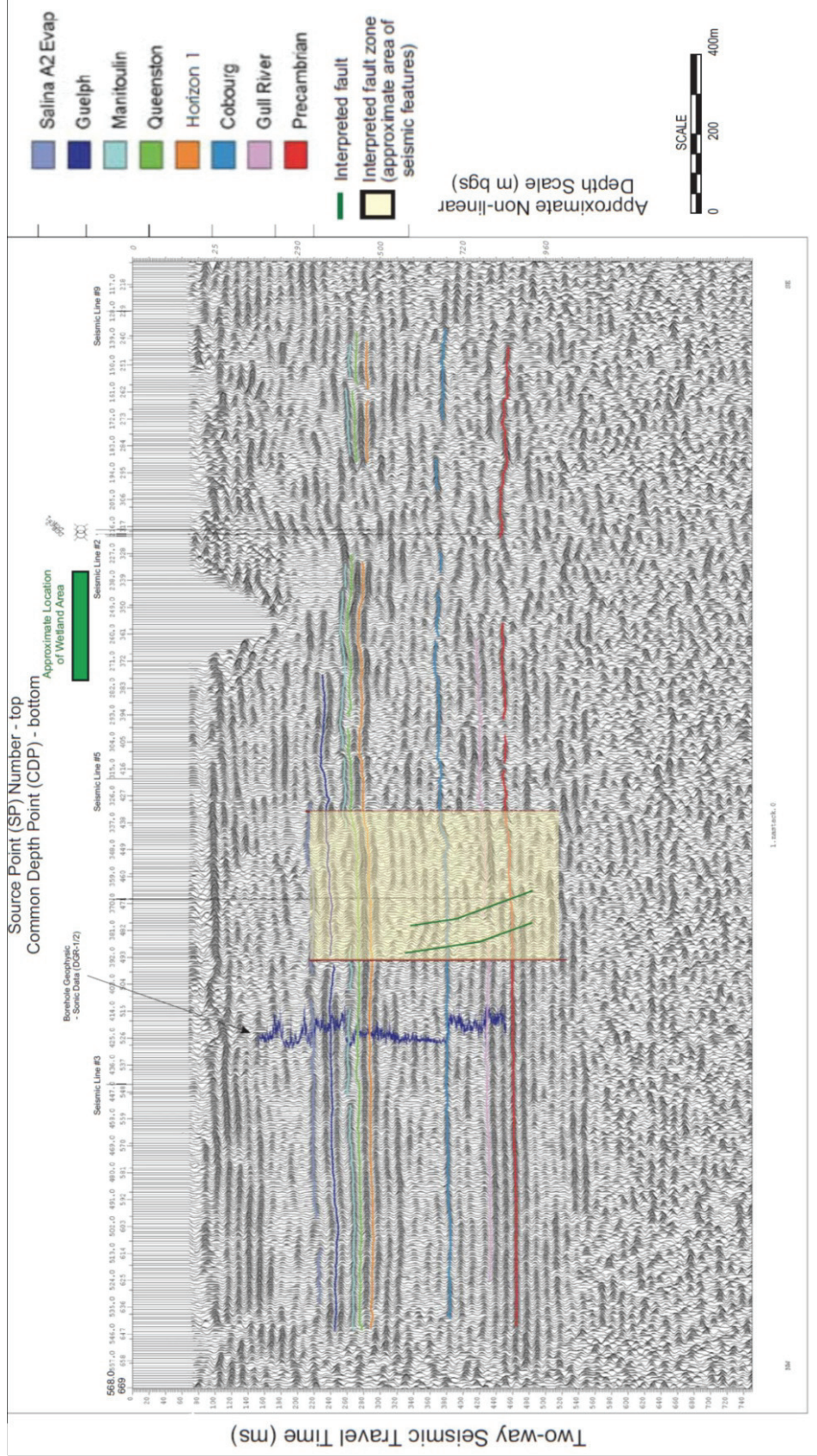
Despite such limitations, interpretation of the dataset indicates the possible presence of some key structural features.

- Within the DGR footprint, an apparent north-trending basement structural high with as much as 10 m of relief is imaged in Line 1 (Figures 2.24 and 2.38) as well as lines 5 and 6. The basement high is interpreted to be bounded on its eastern flank by a steeply dipping normal fault and on its western flank by several distinct elevation lows within the Ordovician succession which may represent a graben-type structure.
- Another basement high, which may be an extension of the feature interpreted from lines 1, 5, and 6, is bounded by a steeply dipping NNW-trending fault that crosses Line 9 (Figure 2.24).
- A NNW-trending and steeply dipping fault structure, possibly with normal-sense displacement, crosses Line 7 approximately 1.25 km southwest of the repository footprint (Figures 2.24). This interpreted fault bounds a basement high to the east and is interpreted to terminate within the Ordovician shales. It is therefore constrained to a pre-Silurian movement history, if it exists.

INTERA (2011) notes that the seismically interpreted faults within and proximal to the DGR footprint (Figure 2.24) are not consistent with known geometry, size, and seismic profiles of faults normally associated with a HTD reservoir (see Figure 2.21 and associated discussion in Section 2.2.8.2). HTD-related sag structures are related to transtensional (strike slip and extensional) shear zones, with the structural lows being the expression of negative flower structures where strata have been faulted downward. No faults of this nature, nor related sagging of the Ordovician units or basement rock, are recognized at the Bruce nuclear site within the resolution of the 2D seismic data. This assessment is supported by the uncertainty related to the identification of minor faulting along lines 1, 5, 6, and 9 (INTERA 2011) and the associated absence of measureable offsets in the local stratigraphic succession. An interpreted basement high of 10 m and an equivalent fault offset in the overlying stratigraphy is also not supported by the triangulated borehole structural analysis (INTERA 2011).

As noted above continuous core retrieved from both of the inclined boreholes showed no indication of the potential fault structure interpreted on seismic line 6, or the extension of the interpreted feature on seismic line 9 (Figure 2.24; INTERA 2011). The 2D seismic results also confirm the lateral continuity of the various bedrock units across the site.

There is also no evidence in the borehole drilling and testing program for widespread hydrothermal dolomitization, as indicated by the presence of only minor dolomite occurrences throughout much of the Ordovician strata (INTERA 2011). Pervasively dolomitized zones in the Middle Ordovician appear to be restricted to two thin (0.3 to 0.7 m) dolomite beds; one found in the Coboconk Formation more than 100 m below the proposed DGR, and the other in the Gull River Formation approximately 150 m below the proposed DGR.



Notes: Modified from Figure 16a of the 2D seismic survey report (Watts et al. 2009)

Figure 2.38: 2D Seismic Line #1 with Interpreted Faults

Both the Coboconk and Gull River formations also contain trace quantities of residual oil (INTERA 2011). These are thin and planar, stratiform horizons of large lateral extent and which extend across the borehole footprint. They also lack the vertical continuity of the commonly accepted conceptual HTD reservoir model (Figure 2.21) which further argues against the likelihood of a major fault system in the subsurface at the Bruce nuclear site. The limited vertical distribution and scarcity of similar dolomitized zones suggests that the ancient fluid flow associated with these dolomite zones was minor.

It is clear from the strong overpressures maintained in the Cambrian sediments (Chapter 5.0) that even minor faults or fractures associated with Paleozoic fluid flow are no longer transmissive pathways. Hydraulic and petrophysical testing of the Ordovician limestone rocks show hydraulic conductivities less than  $10^{-11}$  m/s, permeabilities in the range of  $10^{-21}$  to  $10^{-19}$  m<sup>2</sup>, and matrix porosities of approximately 1.5% (Chapter 5.0). These values demonstrate that, apart from the two confined, thin dolostone layers, the Ordovician limestones are not reservoir-quality rocks.

### 2.3.10 Summary

The synthesis of geological information, as presented in the regional and site scale sections above, support the assessment of Mazurek (2004) regarding the suitability of the Bruce nuclear site to host a DGR. The Paleozoic sequences are predictable with respect to geometry and lithology, have within their succession multiple natural barriers, have a favourable structural setting, and demonstrate resistance to geological perturbations, including karst and glacial erosion. The Bruce nuclear site, and its surrounding areas, also exhibits low natural resource potential, thus limiting the effects of possible future human intrusion. In general, uncertainty relating to understanding the geology at the Bruce nuclear site is very low. The following is a summary of the key geological attributes of the Bruce nuclear site organized according to the hypotheses outlined in Chapter 1.

- **Predictable (Geometry, Thickness and Lithology)**

- The stratigraphic formation thicknesses and lithologies of the primary geological units relevant to demonstrating DGR suitability and safety (Ordovician units) are predictable at site scale (~1.5 km) or greater. These Ordovician units are present throughout the RSA as a result of deposition over broad carbonate and clastic shelf paleo-environments, which extended from the eastern margin of the Appalachian Basin to the centre of the continent.
- The geology encountered in the DGR boreholes is consistent with the regional geology as described in this report (Chapter 2.2) and presented in the 3DGF model (ITASCA CANADA and AECOM 2011). The formation thickness and lithological properties such as shale, evaporite, carbonate, and clastic content, and dolomite versus limestone distribution, are predicted by regional data for a site located at the margin of the Michigan Basin. The Bruce nuclear site displays approximately 400 m of continuous limestone and shale represented by the Middle Ordovician Trenton and Black River groups, and the Upper Ordovician Blue Mountain, Georgian Bay and Queenston formations along with an additional 190 m of argillaceous dolostones and evaporites of the Upper Silurian Salina Group (INTERA 2011).
- Formation thicknesses of the Middle and Upper Ordovician units are remarkably consistent with variation less than 5% across the Bruce nuclear site, and beyond (Texaco #6 and Union Gas – Kincardine #1 wells).
- Lithofacies within the key DGR units are laterally homogenous. Results of downhole geophysical analysis and core logging suggest that lithofacies changes occur primarily

as small-scale conformable variations in quantities of shale, siltstone, or limestone over the centimetre to decimetre scale. Therefore, no significant lithofacies variations are predicted between boreholes.

- Major mineral distribution is generally similar and therefore predictable between boreholes. This consistency is expected due to lithofacies homogeneity. The geochemical data also confirm that the Ordovician cap rocks are dominated by clay minerals, while the host and lower bounding rocks are primarily limestone with lesser shale and minor dolomite.
- **Multiple Natural Barriers**
  - Barrier quality is shown by distinction of three separate hydrocarbon horizons separated by > 200 m of low permeability shale cap rock with halite throughout (see Figure 2.32 and 2.33).
  - Maximum sediment burial at the end of the Paleozoic Era only induced a peak temperature of approximately 70°C at the top of the Trenton Group. This estimation is consistent with the interpretation that these sediments barely reached the oil window, and is also consistent with the observed lack of pervasive natural hydraulic fractures whose development would have been limited by the low degree of thermal maturation (see discussion in Section 2.2.5.3).
- **Favourable Structural Setting (stability)**
  - The RSA is essentially undeformed and presently tectonically quiescent with no known active faults within the Precambrian basement or overlying Paleozoic sedimentary succession. The Paleozoic strata dip gently between 0.28° and 1.0° towards the centre of the Michigan Basin to the southwest. Three principle fracture (joint) sets, oriented NNW, ENE, and ESE, are recognized throughout the Paleozoic succession of the RSA. The NNW- and ENE-trending sets were also recognized at the site indicating a general consistency in this dataset at all scales. The regional consistency in joint set orientation suggests that no major post-Paleozoic tectonic complexity (i.e., faulting) has overprinted these rocks.
  - The site is located in a stable tectonic regime with low seismicity and no evidence of neotectonic faulting. Field investigations included outcrop mapping (Cruden 2011) and analysis of neotectonic seismically-induced sedimentary features (Slattery 2011).
  - Marker bed analysis and inclined-drilling results demonstrate that the site is structurally simple and undeformed, with no significant offset in Paleozoic strata. Ordovician marker beds and formation tops dip consistently at approximately 0.6° to the southwest. This predictable geometry can be extended beyond the DGR footprint to the nearest borehole control points (Texaco #6 and Kincardine #1) outside of the Bruce nuclear site.
  - Fracture data from site-scale surface mapping and regional observations exhibit an orthogonal geometry consisting of two major subvertical joint sets oriented ENE and NNW, which are consistent with a regionally concentric pattern. These data trends are broadly comparable with joint set orientations measured at depth within the vertical boreholes, where Silurian joints trend approximately N-S and Ordovician joints trend in ENE and ESE directions.
  - Vein infilling and geometrical relationships suggest that the fracture sets were most likely formed during the Paleozoic, and that no significant post-Paleozoic tectonic activity has occurred in the region.

- **Resistance to Perturbations**

- An evaluation of karst at the regional scale suggests that karst is not observed below the uppermost Silurian and processes are typically active only at depths < 200 m in southwestern Ontario (~180 mBGS).
- Diagenetic events that have altered the Paleozoic rocks, excluding shallow bedrock water-rock interactions, occurred during the Paleozoic or early Mesozoic more than 200 million years ago. Major diagenetic processes coincided with large-scale tectonic events acting at the margin of the North American plate and/or with maximum burial and compaction.
- An evaluation of existing literature and results from DGR drilling suggest that the probability of future identification of potential economic oil and/or gas resources at or adjacent to the proposed Bruce nuclear site is low.
- Systematic joint patterns at surface which exhibit no significant joint offsets (faults) or evidence of fault gouge suggest a lack of glacially-induced faulting proximal to the Bruce nuclear site.
- Predicted rates of erosion are insignificant at timescales related to DGR safety. An assessment of past and potential glacial erosion combined with numerical simulations suggest erosion at the Bruce nuclear site will be on the order of 10's of metres per hundred thousand years.

- **Natural Resource Potential is Low**

- No commercial oil hydrocarbon accumulations were encountered during site characterization activities as discussed in Section 2.3.6 and in INTERA (2011). No structural, lithological, chemical or hydrological evidence suggests that the Bruce nuclear site is proximal to an ancient HTD system as discussed in Sections 2.2.8.2 and 2.3.9.2 and in INTERA (2011).
- Lateral traceability between the Bruce nuclear site boreholes and other proximal dry wells (e.g., Union Gas #1 and Texaco #6) as discussed in Section 2.3.9 (and see also discussion in Chapter 7), demonstrates that locally around the Bruce nuclear site (~7 km radius), no pockets of oil or gas hydrocarbon are likely to exist (INTERA 2011).
- An average TOC content for the Upper Ordovician shales of less than 1.0% (Section 2.2.8.1; INTERA 2011), the recognition of low thermal maturity throughout the RSA which indicates that these sedimentary rocks only reached the lower threshold of the oil window as discussed in Section 2.2.5.3, and the absence of natural gas shows during drilling of the DGR boreholes (INTERA 2011) argues against the likelihood of commercial accumulations of either thermogenic or biogenic shale gas beneath the Bruce nuclear site (see also Engelder 2011).

### 3. GEOMECHANICAL FRAMEWORK

#### 3.1 Introduction

The geomechanical characteristics presented in this chapter provide a synthesis of the understanding of the rock strength properties relevant to the construction and long-term performance of the DGR. The geomechanical descriptions provide a framework for the discussions on ground response to short-term construction and waste emplacement, and long-term repository evolution, which are presented in Chapter 6. Geomechanics in the context of this report refers to the strength of a rock mass and its behaviour when subjected to stresses. The term “rock mass” describes an assemblage of intact blocks or layers of rock material, and discrete fractures at varying scales. The geomechanical properties presented herein provide a synthesis of our understanding of the behaviour of the rocks beneath the Bruce nuclear site in terms of three broad categories of data analysis.

- **Laboratory rock strength and deformation properties** comprising uniaxial compressive strength (UCS), stress thresholds for the onset of damage, tensile strength, triaxial compressive strength, shear strength, slake durability, swelling potential, rock material abrasiveness, long-term rock strength degradation due to stress corrosion, and properties deduced from dynamic measurements based on the testing of intact cores.
- **Rock mass properties** comprising rock quality designation (RQD), natural fracture frequency, and bulk properties (i.e., density, dynamic deformation properties, etc.) from rock core and geophysical logging.
- **In situ stress state** at the site based on modelling, wellbore characterization, and comparison with regional information.

The overall objective of this chapter is to provide an assessment of the short- and long-term geomechanical properties of the Bruce nuclear site to host the DGR. Short term reflects a time period relevant to the construction and waste-emplacement stages measured in decades. Long-term reflects a time period relevant to demonstrating the performance and safety of the DGR. For the purpose of the DGR safety case, this is defined nominally as 1 Ma. Table 3.1 outlines the primary sources of information used to define the site geomechanical properties of the Paleozoic sedimentary formations.

**Table 3.1: Primary Sources of Information**

Reference Study	Data Sources
<b>Regional Geomechanics</b>	<ul style="list-style-type: none"> <li>➤ Regional Geomechanics of Southern Ontario study (NWMO and AECOM 2011)</li> <li>➤ Low level waste geotechnical feasibility study (GOLDER 2003)</li> </ul>
<b>Site Geomechanics</b>	<ul style="list-style-type: none"> <li>➤ Site scale geological and structural (bedrock joint/fracture system) mapping of bedrock outcrops (Cruden 2011)</li> <li>➤ DGSM (INTERA 2011)</li> <li>➤ Observations during drilling, logging, and sampling of boreholes DGR-1 to DGR-6 (Sterling 2010a, 2010b, Briscoe et al. 2010a, 2010b, Sterling et al. 2011)</li> <li>➤ Bedrock Formations in DGR-1 to DGR-6 (Sterling and Melaney 2010)</li> <li>➤ Oriented Core Logging of DGR-5 and DGR-6 (Gaines et al. 2011)</li> <li>➤ Field geomechanical testing of DGR-1 to DGR-6 core (Gaines and Sterling 2009a, 2009b)</li> </ul>

Reference Study	Data Sources
	<ul style="list-style-type: none"> <li>▶ Laboratory geomechanical strength testing of DGR-1 to DGR-6 core (Gorski et al. 2009a, 2009b, 2010a, 2010b, 2010c, Murphy and Heagle 2010)</li> <li>▶ Laboratory abrasiveness testing of DGR-2 to DGR-4 core (Maloney 2010, Maloney and Bahrani 2009)</li> <li>▶ Borehole geophysical logging of DGR-1 to DGR-6 (Pehme and Melaney 2010a, 2010b, 2011)</li> <li>▶ Laboratory swell testing of DGR-2 to DGR-4 core (Micic and Lo 2009, 2010)</li> <li>▶ Laboratory long-term strength degradation testing of DGR-2 to DGR-4 core (Gorski et al. 2009b, 2010b)</li> </ul>
<b>Site In Situ Stress</b>	<ul style="list-style-type: none"> <li>▶ Field in situ stress measurements in MS Unit 1 from US-6 (McKay 1989)</li> <li>▶ Analyses of DGR-1, DGR-2, DGR-3, and DGR-4 borehole images for Stress Characterization (Valley and Maloney 2010)</li> </ul>

### 3.2 Geomechanical Properties

This section provides a site-scale summary of the geomechanical properties of the Paleozoic sedimentary formations that are relevant to the DGR concept. This includes the Cobourg and Sherman Fall formations (host rock and shaft seals), the Queenston, Georgian Bay and Blue Mountain formations (cap rocks and shaft seals), and the upper Ordovician and Silurian formations intersecting other shaft seals (Figure 3.1).

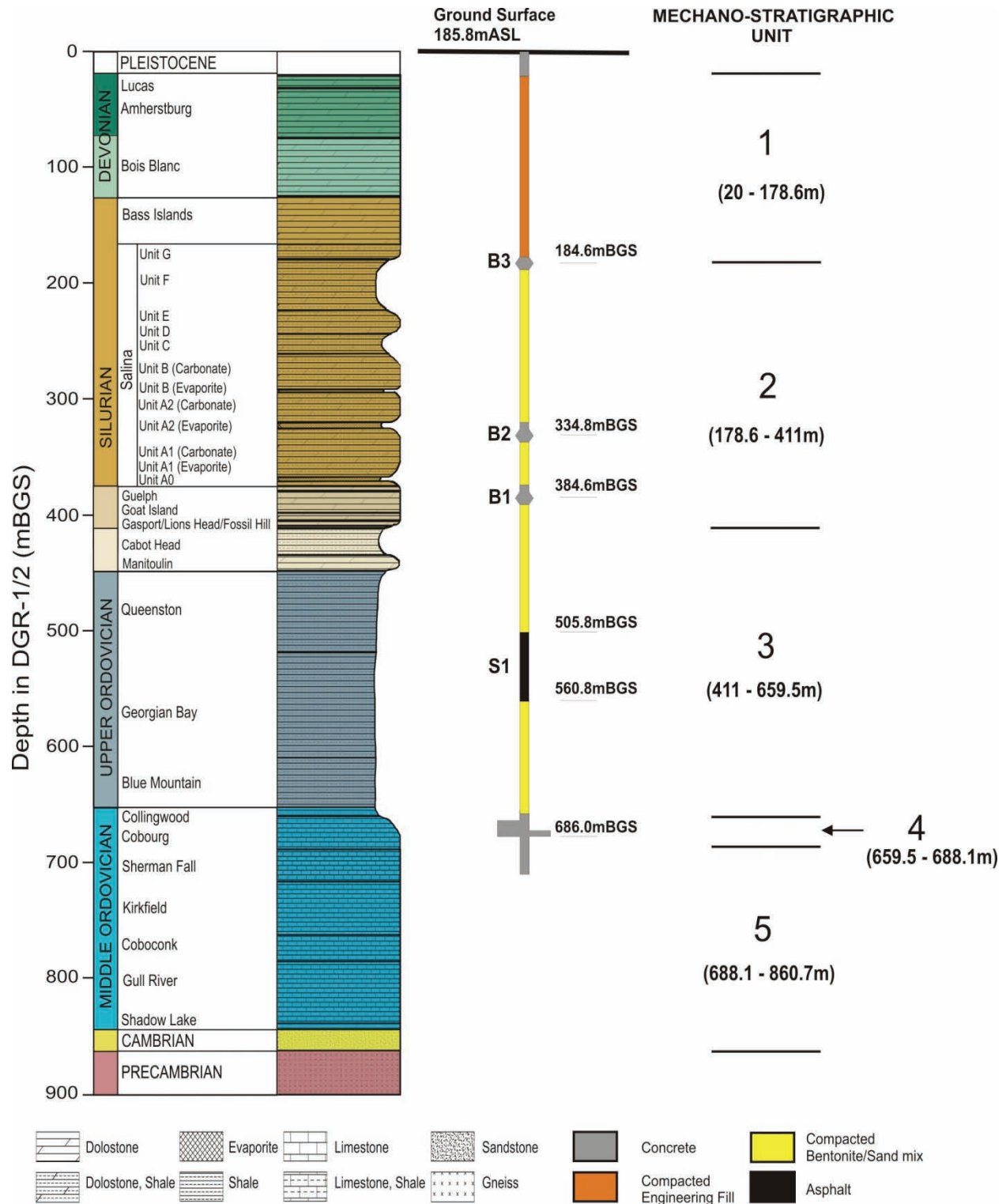
Geomechanical analyses were conducted using site-specific field and laboratory testing techniques on core samples from the DGR series of boreholes (Figure 2.24). These comprehensive site-specific tests provided quantitative best estimates of the physical properties that will control the geomechanical behaviour of the rock mass. A detailed description of the types of tests and corresponding results from boreholes DGR-1 to DGR-6 are presented in various Intera Technical Reports (TRs; see Table 2.1 of INTERA 2011) and summarized in the DGSM (INTERA 2011).

The DGSM also subdivides the Paleozoic stratigraphy into five distinct mechano-stratigraphic (MS) units, as shown on Figure 3.1. Listed depths of these MS units are based on boreholes DGR-1 and DGR-2 stratigraphy with unit thickness variations taken from boreholes DGR-1 to DGR-6. The simplified MS units are not intended to be a “classification”, but instead represent a brief summary/guide to the geomechanical testing program solely as a means of convenience to provide a broad grouping and an overall picture of the geomechanical properties encountered in the sub-surface. All detailed data from every geological unit tested is available in the appropriate TR and is summarized in this geosynthesis report.

The following sub-sections focus on:

- MS Unit 4 and the adjacent upper portion of MS Unit 5 and lower portion of MS Unit 3, including the Collingwood Member, the Cobourg Formation (MS Unit 4), and the underlying Sherman Fall Formation;
- MS Unit 3, the Upper Ordovician shale cap rock; and
- MS Unit 2 and upper MS Unit 3, the locations of the upper shaft seals.





Notes: Figure is modified from INTERA (2011).

**Figure 3.1: Reference Stratigraphic Column Showing MS Units and Shaft Seal System at the Bruce Nuclear Site**

The descriptions of the rocks at selected shaft seal locations are discussed in the context of the Excavation Damaged Zone (EDZ) together with the evolution and extent of the EDZ in Section 6.3.

### **3.2.1 Host Rock – MS Unit 4**

MS Unit 4 comprises the Cobourg Formation which is the argillaceous limestone host rock for the proposed DGR (Figure 3.1). The thickness of the Cobourg Formation is fairly consistent in all DGR boreholes, ranging from 27.5 to 28.6 m. This discussion also includes the Collingwood Member comprising interbedded shale and limestone. The Collingwood Member was included in MS Unit 3 in the DGSM by INTERA (2011), however, its mechanical behaviour is more akin to the Cobourg Formation than to the shaley formations of the rest of MS Unit 3. The geomechanical properties of the Collingwood Member are presented herein and in Section 3.2.2. The Sherman Fall Formation, which underlies the Cobourg Formation, is also included in the discussion herein because of its potential influence on repository stability.

#### **3.2.1.1 Intact Rock Properties**

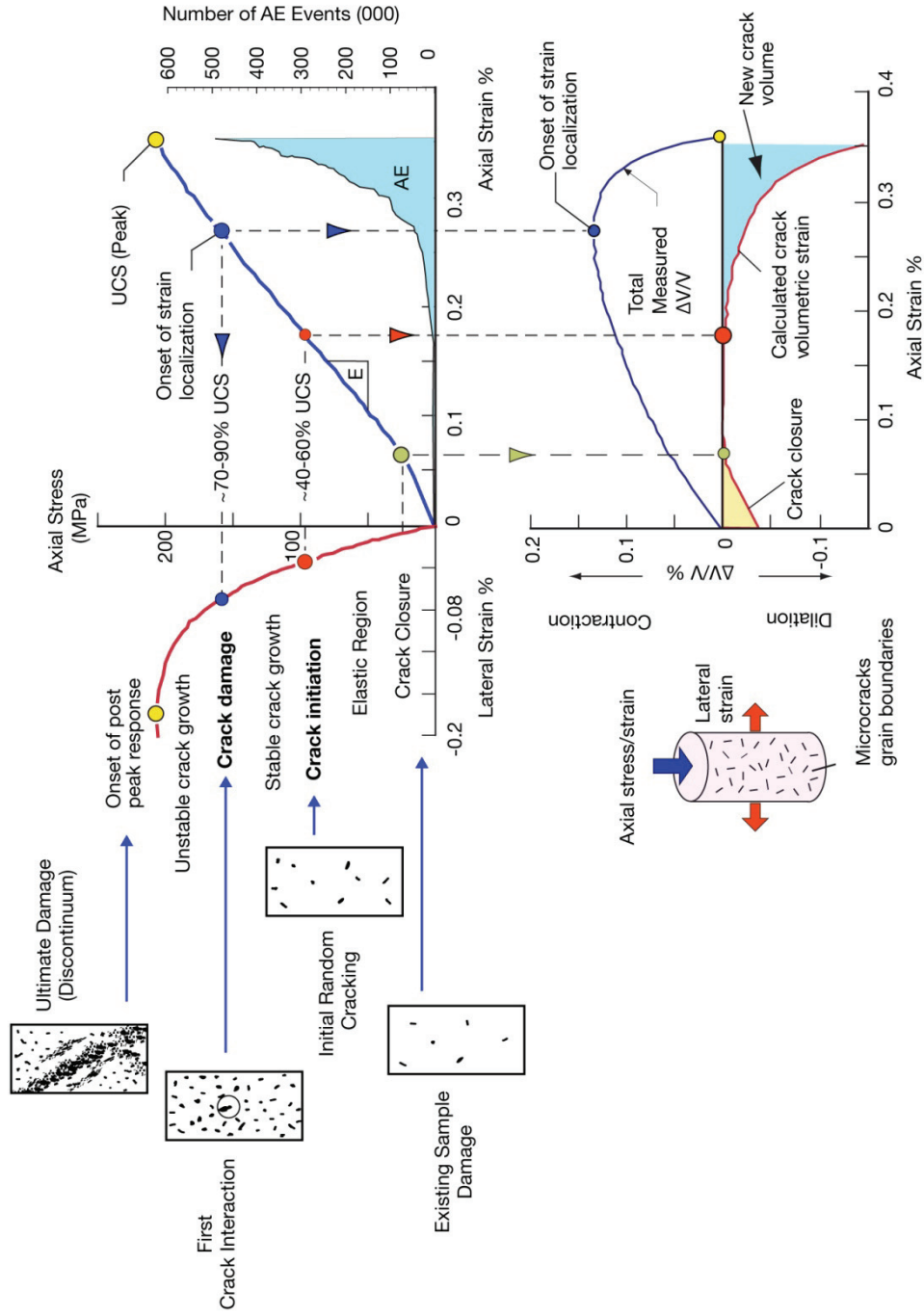
The uniaxial compression test is the most widely performed test for classifying rock and determining the rock strength to be used in the analysis and design of underground openings. It provides the basis parameters of an intact rock such as UCS, modulus of elasticity (E) and Poisson's ratio ( $\nu$ ). The test can also allow examination of the damage development of the rock as it provides insight to the in situ rock mass behaviour. Other important parameters are determined from the tension and triaxial compression tests. Together with the UCS data, rock mass strength criteria can be developed.

#### **UCS**

A common laboratory test conducted on intact rock to determine its strength and deformation parameters is the uniaxial compression test which measures the UCS of the rock. The evolution of crack damage development within a uniaxially loaded rock sample is illustrated using a typical stress-strain diagram in Figure 3.2. This figure demonstrates that unique material characteristics of a fracturing rock element or specimen can be measured by various critical stress states along the path of the stress-strain curves.

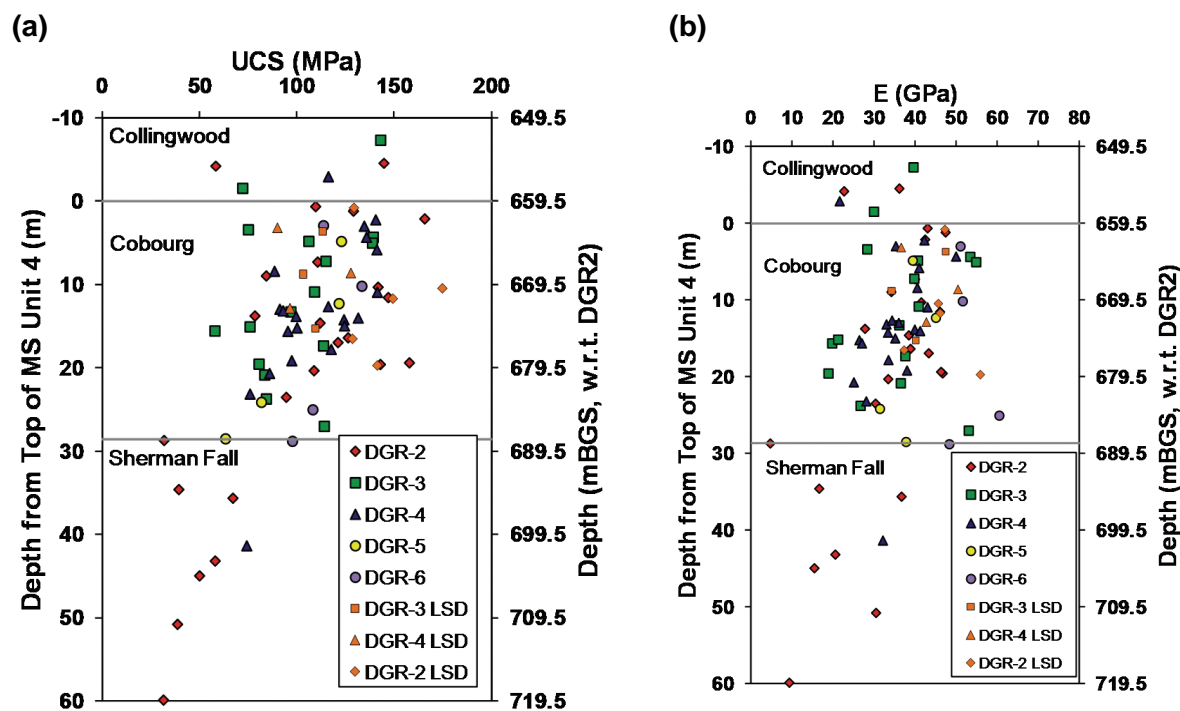
The peak UCS of the Cobourg Formation (MS Unit 4), based on the results of 67 samples, ranges from 58 to 175 MPa (Figure 3.3a) with an arithmetic mean of 113 MPa and a standard deviation of 25 MPa. The corresponding elastic modulus has a mean value of 39 GPa (Figure 3.3b). These results indicate that the limestones of MS Unit 4 can be classified as high strength with an average modulus ratio (Lam et al. 2007). Thus, the results indicate a high degree of stability for deep underground excavations at the DGR horizon.

Figure 3.3 shows the distribution and range of the UCS results from boreholes DGR-2 to DGR-6 within the formation plotted versus depth. The variation in strength noted in the UCS test results is due to the variation in material properties within the formation, pre-existing damage as a result of sampling (unloading) from great depth, and local platen interference or other boundary effects during laboratory testing.



Notes: AE = acoustic emissions. Figure is modified from Martin and Chandler (1994).

**Figure 3.2: Stress-strain Diagram Showing the Evolution of Crack Development of a Typical UCS Test**



Notes: LSD = Long-term Strength Degradation.

**Figure 3.3: Uniaxial Compression Test Data for Collingwood, Cobourg and Sherman Fall: (a) UCS and (b) Elastic Modulus from Boreholes DGR-2 to DGR-6**

A comparison of site versus regional UCS results for the Cobourg Formation (NWMO and AECOM 2011) reveals that the former have a considerably higher average peak strength value (Figure 3.4). This strength increase is likely attributed to different sampling depths, mineralogical variation (i.e., clay fraction), improved sample preservation methods, and/or the quality of the laboratory testing. Also, the UCS values appear to be uniform across the Bruce nuclear site.

Because of the close proximity of the Sherman Fall Formation to the DGR nominal invert level at 680 mBGS, eight uniaxial compression tests were carried out on core retrieved from boreholes DGR-2 and DGR-4. The results are also summarized on Figure 3.3 and indicate a best estimate mean peak UCS for the Sherman Fall Formation of 49 MPa, which is therefore considerably weaker than the Cobourg. For the overlying Collingwood Member, the mean UCS based on testing of 5 samples is 107 MPa. The distribution of UCS results within these formations is shown on Figure 3.3. The large variation in strength values derived from the Sherman Fall Formations is likely attributed to the same factors as discussed above.

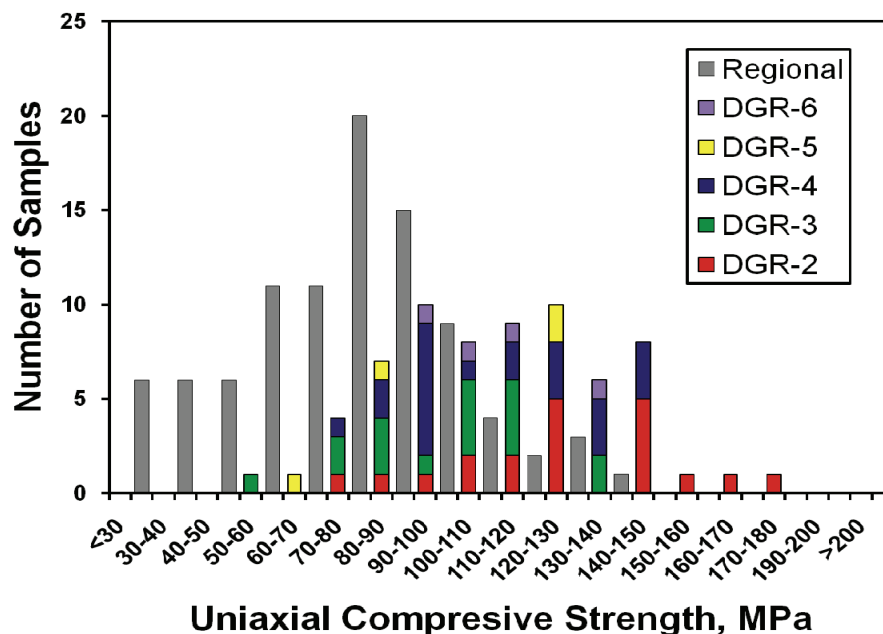


Figure 3.4: MS Unit 4 UCS of the Cobourg – Site Specific and Regional Test Data

### **Crack Initiation and Damage Stresses**

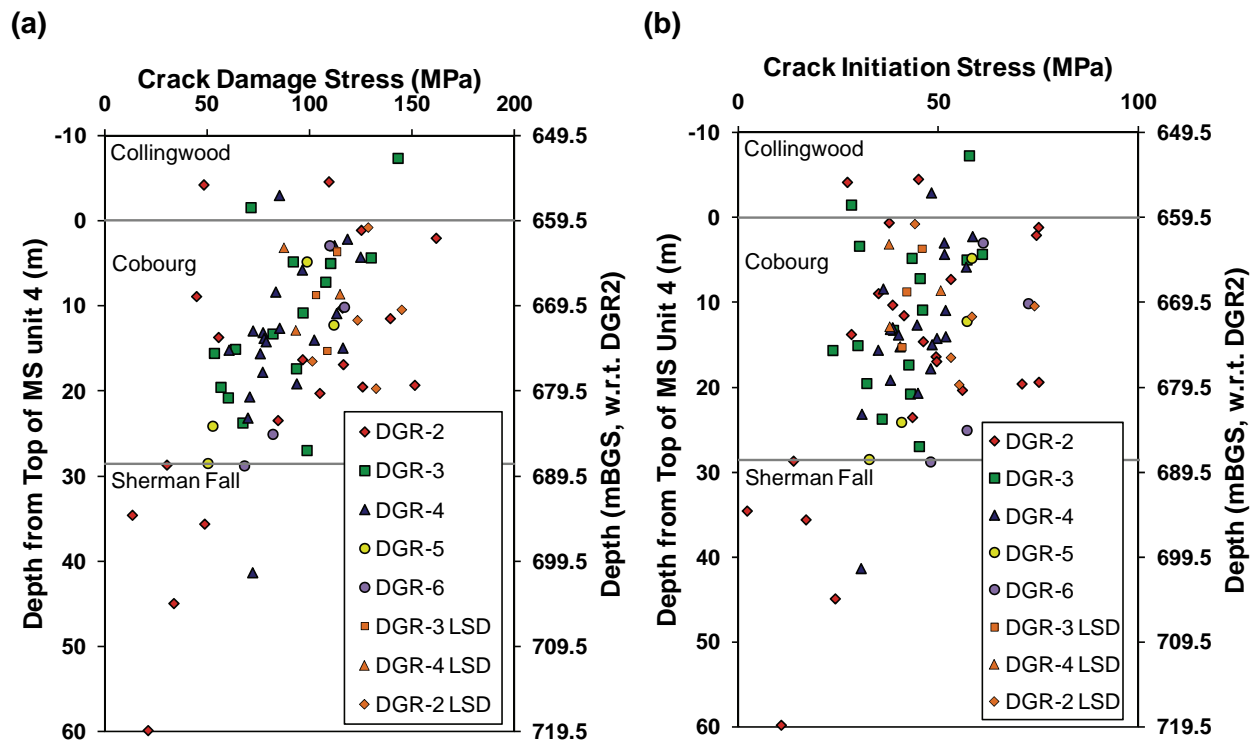
As shown in Figure 3.2, two other important parameters, the crack initiation (CI) and crack damage (CD) stresses can also be obtained from the results of a uniaxial compression test. Martin and Chandler (1994) determined that the peak failure strength of rock is highly dependent on its loading conditions. Using laboratory data of the Lac du Bonnet granite, Martin and Chandler (1994) demonstrated the use of these two critical stress states, CI and CD, to better characterize rock strength.

The CI and CD stresses mark the onset of two stages in crack development in a sample subjected to a compressive load (Figure 3.2). CI is identified as the point where the lateral strain curve of the test sample departs from linearity (Figure 3.2) and represents the threshold of stable, grain-scale distributed cracking. Martin and Chandler (1994) suggested that CI in laboratory samples was a unique material property independent of scale and loading rate, and Andersson et al. (2007) found CI was insensitive to anisotropy. Andersson et al. (2007) suggested that CI based on uniaxial compression tests could be used to estimate the lower bound in situ rock mass spalling strength. More recently Damjanac and Fairhurst (2010) proposed that laboratory CI values could also be used as a lower bound estimate for the long-term strength of rock over geological time when the rock is unconfined. The underlying premise for proposing CI as a lower bound estimate for in situ stress-driven failure is that if the maximum stress around an excavation boundary is less than CI, the in situ rock remains essentially elastic.

Further loading leads to unstable crack growth at the CD stress threshold. This point corresponds to macroscopic or sample-scale yield during which a coalescence of propagating cracks develops. In uniaxial testing, the onset of CD stresses is characterized by a volumetric strain reversal (Figure 3.2). Bieniawski (1976) suggested that this stress level represents the

long-term strength (measured in days) of laboratory samples. This definition is also consistent with the long-term strength of concrete (Desayi and Viswanatha 1967). A detailed description of cracking/damage observed in laboratory compression testing is presented in Bieniawski (1976) and Martin and Chandler (1994).

Based on the UCS testing, CI and CD stresses for the Cobourg range from 24 to 75 MPa (mean = 47 MPa) and 45 to 162 MPa (mean = 97 MPa), respectively (Figure 3.5a and Figure 3.5b). For the Collingwood Member, the average CI and CD thresholds are 41 MPa and 92 MPa. For the Sherman Fall Formation, the average CI and CD stress levels are 16 MPa and 37 MPa, respectively. Figure 3.5a and Figure 3.5b show the distribution of the CD and CI stresses normalized to UCS and based on all test samples of these formations recovered from boreholes DGR-2 to DGR-6. Although the UCS and CD thresholds scatter throughout the formations, the CI stress is consistently at about 40% of the peak UCS (Figure 3.5). Because of the slight dip of the sedimentary sequence toward the southwest direction, all plots of strength profiles with depths are adjusted to a datum at the top of the Cobourg for comparison.



Notes: LSD = Long-term Strength Degradation. Results determined from intact DGR core.

**Figure 3.5: Distribution of (a) CD Stresses and (b) CI Stresses for the Collingwood Member and Cobourg and Sherman Fall Formations**

### Tensile Strength

Tensile failure is the primary cause of stress-induced spalling around excavation openings and is also associated with roof instability in underground openings in sedimentary rock masses. Thus, the determination of the tensile strength is of prime importance for evaluating the potential

overstressing developed along the soffit of a horizontally bedded emplacement room roof. Eight laboratory specimens from boreholes DGR-2 to DGR-4 were tested to determine the Brazilian or indirect tensile strength of the Cobourg (INTERA 2011; Figure 3.6). All but one test sample experienced tensile diametral failure resulting in a best estimated average indirect tensile strength of 6.5 MPa (INTERA 2011). The test results of the Brazilian tensile strength fall within the range of the regional database (NWMO and AECOM 2011). However, the tensile strength of a rock mass is substantially smaller approaching a tensionless state because of the presence of much weaker bedding partings.

The Brazilian tension test is probably the most commonly performed geomechanical test to determine the tensile strength of rock. However, because of the presence of shaley interbeds causing material anisotropies in the rock encountered at the Bruce nuclear site, the tensile strength measured from this test does not necessarily correspond to the lowest strength measured by the direct tension test. For intact rock material between bedding partings, Brazilian tests may overestimate tensile strength by 30 to 40% in comparison to direct tension test data (INTERA 2011).

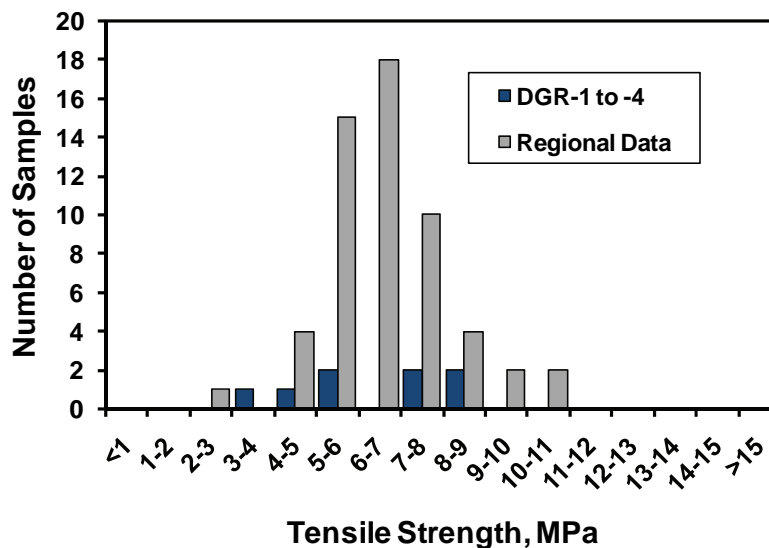


Figure 3.6: Brazilian Tensile Strength of the Cobourg Formation

### Triaxial Compressive Strength

In this study, the Hoek-Brown Criterion (Hoek et al. 2002) is used to estimate the strength and deformability of the rock mass. With the 12 triaxial compression tests conducted on core samples retrieved from boreholes DGR-3 and DGR-4, the triaxial compressive strength of the Cobourg Formation was determined. Combining these test results with the aforementioned UCS data allows for determination of the strength parameters for the Hoek-Brown failure criterion by means of a regression analysis (Figure 3.7). This failure criterion applies to intact rock blocks such as occur between bedding planes. The Hoek-Brown strength parameters, for the intact material ( $s = 1$ ) in the Cobourg, are:

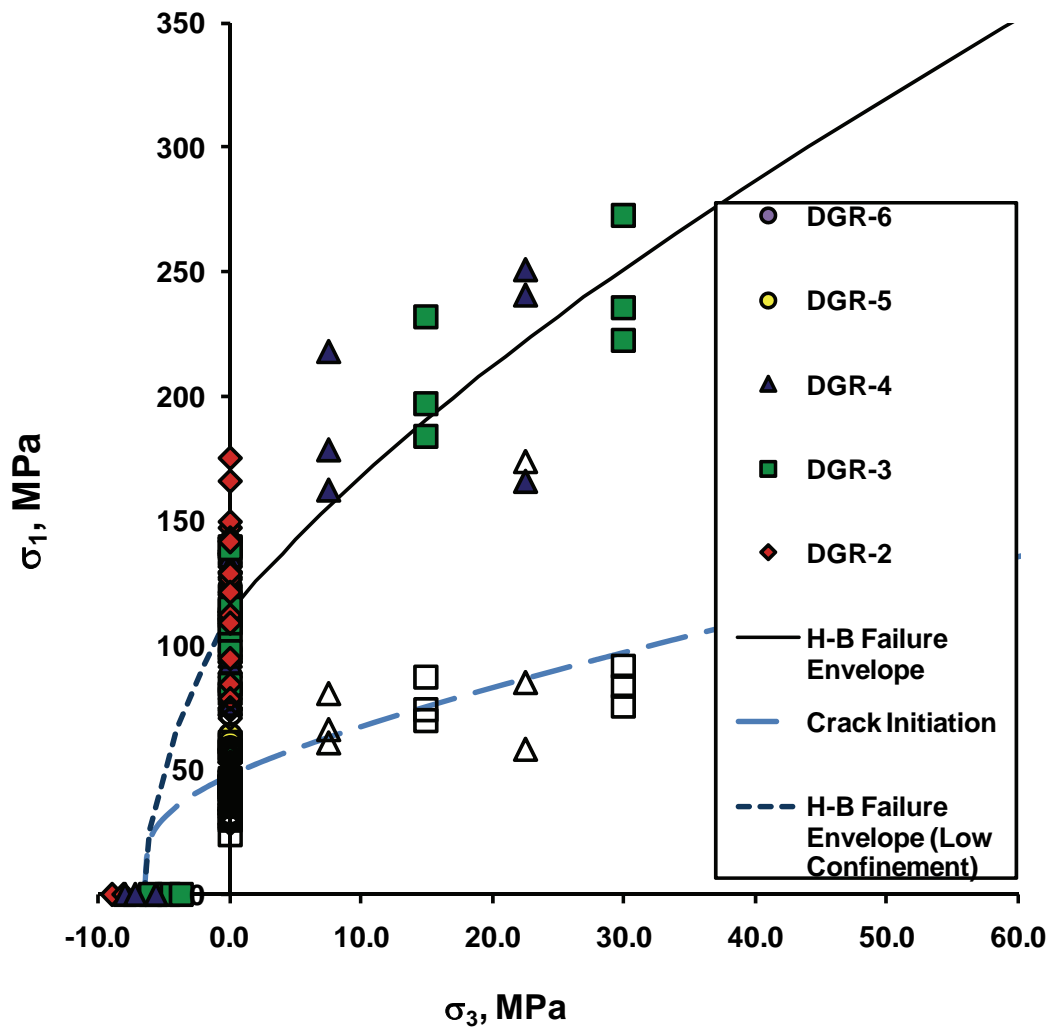
$$\sigma_{ci} = 113 \text{ MPa}, m_i = 10.6 \text{ and } a = 0.5 \quad (3.1)$$

Where ( $\sigma_{ci}$ ) is the UCS of intact rock and ( $m_i$ ) and ( $a$ ) are material constants which depend on the composition and structure of the rock. This strength envelope characterizes the rock element well beyond the surface of excavation under confining stresses. However, near the excavation surface, the rock is subjected to low confinement and the Hoek-Brown failure envelope should be expressed using the following set of strength parameters:

$$\sigma_{ci} = 113 \text{ MPa}, m_i = 17.4 \text{ and } a = 0.5 \tag{3.2}$$

The CI stresses determined from the uniaxial and triaxial compressive tests on these Cobourg specimens are also plotted against the failure criterion in Figure 3.7. These results demonstrate the dependency of confinement stress on the CI behaviour on the rock. The Hoek-Brown parameters for this strength envelope are:

$$\sigma_{ci} = 113 \text{ MPa}, m_i = 0.2 \text{ and } a = 0.2 \text{ (s=0.013)} \tag{3.3}$$



Notes: Filled symbols = peak strength and unfilled symbols = CI stress.

Figure 3.7: Hoek-Brown Failure Envelope for the Cobourg Formation



### **Shear Strength of Rock and Thin Shaley Bedding Planes**

The Cobourg Formation is described as a very fine to coarse-grained argillaceous limestone with poorly defined thin shaley interbeds. Because of low confinement near the excavated openings, the behaviour of the rock mass may be governed by the shear strength and sliding deformability of these thin shaley beds.

Direct shear tests of the thin shaley beds were performed to determine the shear strength of these planes of potential weakness. Ten intact samples and two samples with a detachment along the shaley bedding surfaces from the Cobourg Formation were selected for testing. All samples generally exhibited poorly defined undulatory shaley beds within the mottled or nodular limestone texture (e.g., Figure 2.27). The peak shear strengths parallel to shaley partings were measured under various contact pressures ranging between 0.6 MPa and 3.1 MPa before running multiple staged shear tests at several incremental normal stress levels to determine the residual strength of the shear surface. For residual strength parameters, the test results indicate the shaley partings have a residual strength that appears to be relatively consistent with zero apparent cohesion and a base friction of  $39^\circ$ . For intact material, the tests subjected to confined normal pressures ranging from 0.6 to 3 MPa yielded an apparent cohesion of 1.3 MPa and a rather high friction angle of  $77^\circ$  (Figure 3.8 and Table 3.2). Because this additive resistance is active at low or zero confinement, there will be a tendency to shear through the stronger limestone “asperities”. On the same figure, the CI strength envelope was plotted showing the rock is likely to commence fracturing through limestone asperities as it approaches a normal stress of 3 MPa.

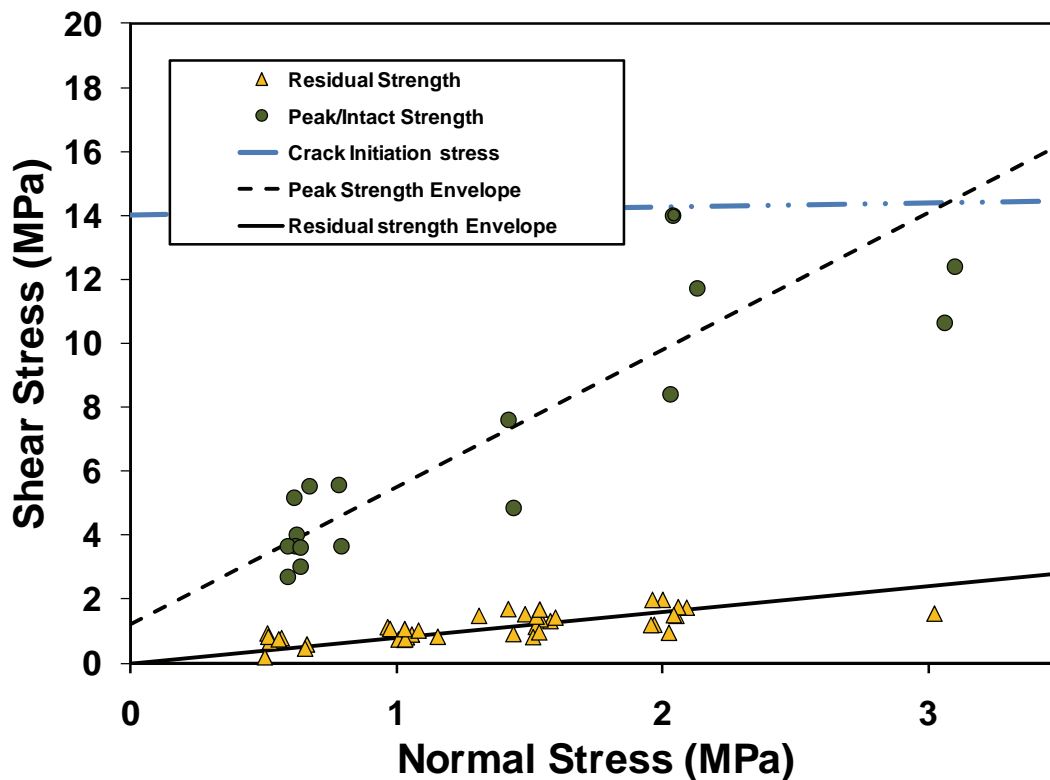
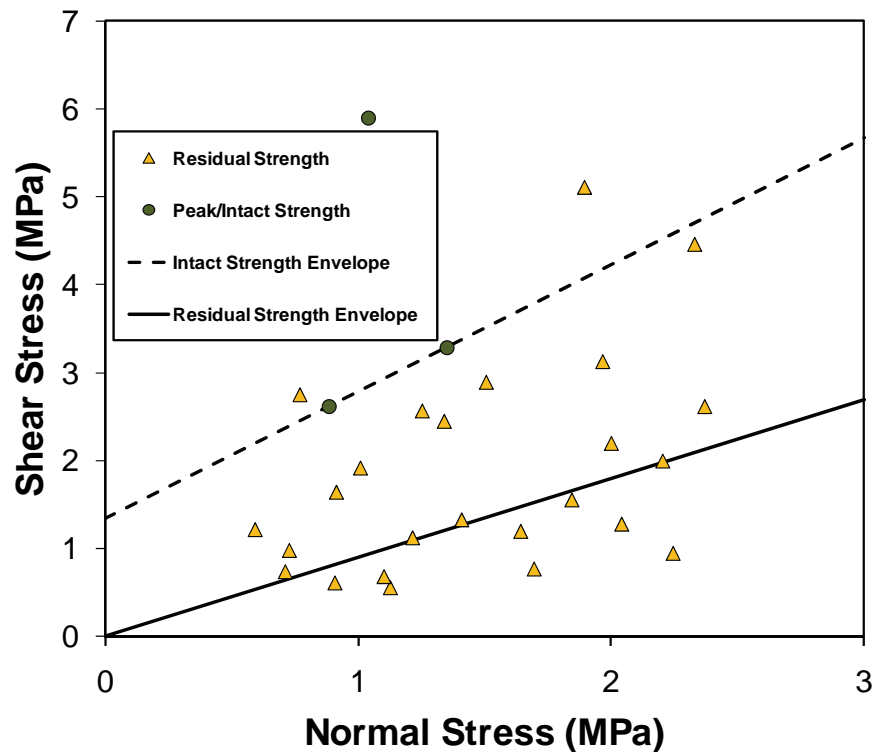


Figure 3.8: Direct Shear Test Results for the Cobourg Formation

**Table 3.2: Shear Strength of the Cobourg and Sherman Fall Formations**

Formation	Apparent Cohesion Intercept (MPa)	Apparent Friction Angle (Deg.)	Residual Cohesion (MPa)	Residual Friction Angle (Deg.)
Cobourg	1.3	77	0	39
Sherman Fall	1.2	55	0	42

Figure 3.9 and Table 3.2 present the results of direct shear tests of intact core and open bedding/fractures of the Sherman Fall Formation. Because of the interbedded nature of the shale and limestone rock (see Figure 2.26), a large scattering of results was observed. This is likely due to the shearing of different rock material. The shearing of intact rock resulted in an apparent cohesion of 1.2 MPa and a friction angle of 55°, which is rather high for sedimentary rock. The best-fit line for the residual shear strength indicates zero apparent cohesion, but a relatively high base friction angle of 42°.



**Figure 3.9: Direct Shear Test Results for the Sherman Fall Formation**

### 3.2.1.2 Rock Mass Properties

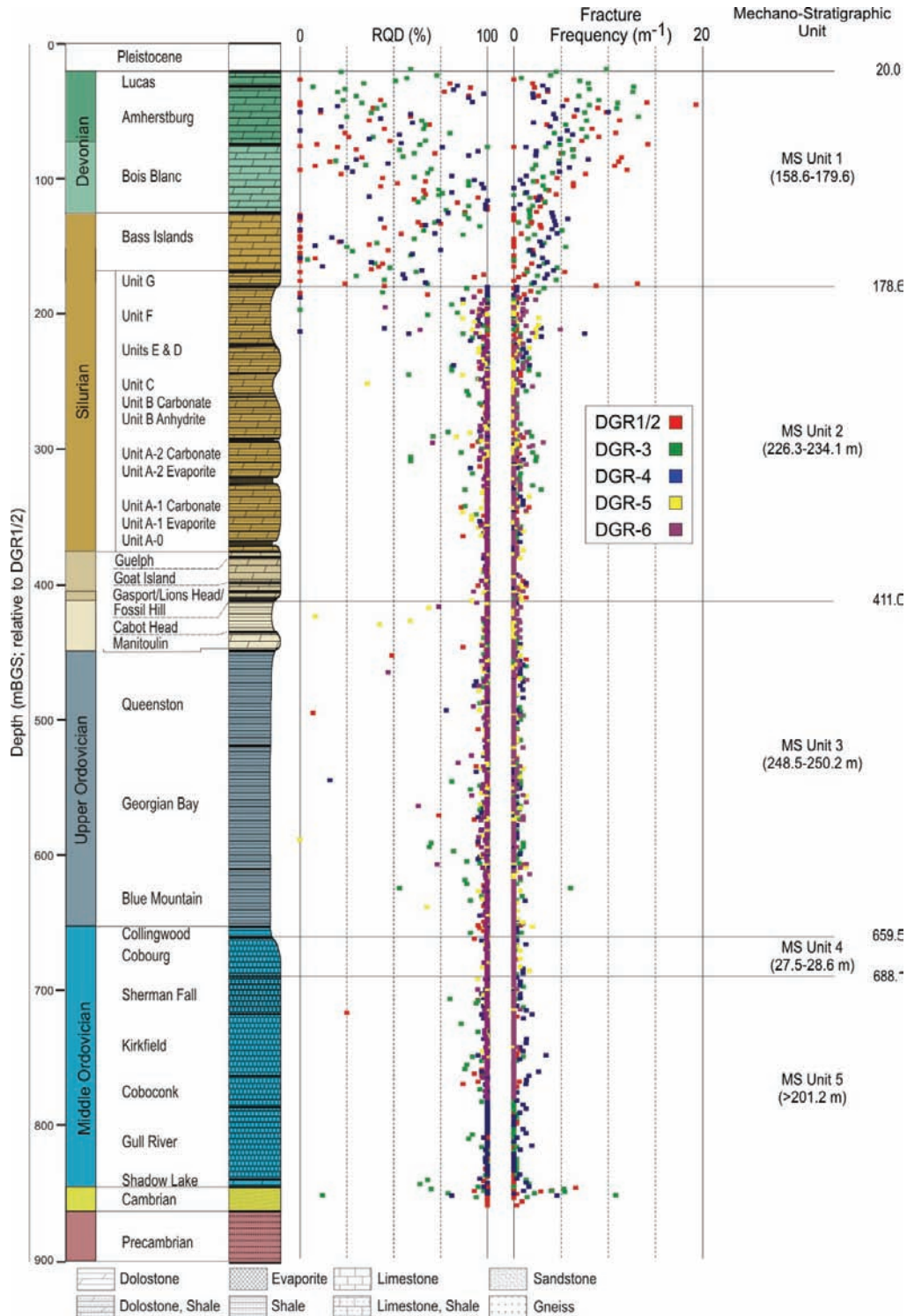
The drilling of the DGR boreholes and examination of the rock cores provide an opportunity for a preliminary characterization of the rock mass. Basic rock mass properties such as rock core recovery, RQD, fracture frequency, and joint spacing for the Collingwood Member, Cobourg and Sherman Fall formations have been determined and are discussed below. It must be noted that during rock core logging of sedimentary rocks it may not be possible to clearly distinguish all natural discontinuities from fractures induced by drilling or core retrieval procedures. Therefore, where there was any doubt regarding the cause of a fracture, a certain amount of such fractures may have been included in the RQD and fracture frequency values, thus introducing a measure of conservatism.

Core recovery, RQD (Deere et al. 1967), and fracture frequency results from six boreholes are summarized in Table 3.3, and the results from boreholes DGR-2 to DGR-6 are plotted versus depth in Figure 3.10 and Figure 3.11. In summary, the Collingwood Member, the Cobourg Formation and Sherman Fall Formation have a rock mass designation of excellent with RQD generally ranging between 90 and 100%. The fracture frequency in all three is comparable, and the Collingwood and Sherman Fall fracture frequencies are slightly higher than that of the Cobourg (Figure 3.11). It is estimated that the spacing of bedding sub-parallel discontinuities is 3 m or greater with possible local zones of closer spacing occurring, particularly in the Collingwood Member and Sherman Fall Formation. Only three vertical joints were encountered in the Collingwood Member; two in borehole DGR-3 and one in DGR-4. No vertical to oblique joints were encountered in the underlying Cobourg or the Sherman Fall formations in any of the boreholes. One completely healed joint (strongly cemented, solid rock core), evident only by a partial planar trace of trace amounts of oil seeping from the core, was encountered in the Cobourg in borehole DGR-6 at about 745.8 mBGS along the borehole incline. Inclined boreholes DGR-5 and DGR-6 have a lateral coverage of 7.0 m and 19.1 m, respectively, in the Cobourg Formation and 6.3 m and 17.4 m, respectively, in the Sherman Fall Formation. Based on the above observations, the spacing of vertical/subvertical joints at the DGR level is most likely greater than 10 m. The fracture frequency from borehole logging in the Cobourg and Sherman Fall formations (Figure 3.11) is entirely due to bedding sub-parallel discontinuities, since no oblique or vertical joints have been identified in any of the boreholes.

### 3.2.1.3 Short-term Behaviour

#### **Anisotropy**

Rocks of sedimentary origin often possess an inherent anisotropy due to well-defined layering or bedding fabric. Extensive studies on cross-anisotropic behaviour of sedimentary rocks from southern Ontario have been carried out (Lo and Hori 1979, Lo et al. 1979 and Ontario Hydro 1991). The studied carbonates represent those from the Silurian Lockport Formation and the Ordovician Trenton Group. Aside from some shaley limestone (probably of the Gasport Member of the Lockport Formation), the limestones and dolostones of the Lockport Formation and Trenton Group do not exhibit significant anisotropic behaviour. Conversely, the Georgian Bay and Collingwood shale specimens do indicate significant mechanical anisotropy (Lo and Hori 1979).



Notes: MS unit thickness ranges, determined from DGR-1 to DGR-4 only, are noted in brackets (INTERA 2011).

**Figure 3.10: Stratigraphic Column Showing RQD, Fracture Frequency, and MS Units at the Bruce Nuclear Site**

**Table 3.3: RQD Values for MS Unit 4 and Surrounding Rocks**

Rock Formation	Borehole No.	Core Recovery (%)	RQD (%)	Natural Fracture Frequency* (Fractures/m)	Classification Based on RQD
Collingwood	DGR-2	96-98 (97)	95-98 (96)	0-0.7 (0.2)	Excellent
	DGR-3	100	91-100 (97)	0-0.8 (0.4)	Excellent
	DGR-4	100	100	0-1.0 (0.4)	Excellent
	DGR-5 (~77°)	100	98-100 (99)	0-2.0 (1.0)	Excellent
	DGR-6 (~57°)	100	98-100 (99)	0	Excellent
Cobourg (DGR horizon)	DGR-2	90-100 (99)	90-100 (99)	0-0.3 (0.03)	Excellent
	DGR-3	100	100	0-0.3 (0.1)	Excellent
	DGR-4	100	97-100 (100)	0-1.3 (0.3)	Excellent
	DGR-5 (~77°)	100	98-100 (99)	0-0.7 (0.3)	Excellent
	DGR-6 (~57°)	100 *	99-100 (100)*	0	Excellent
Sherman Fall	DGR-2	100	100	0	Excellent
	DGR-3	80-100 (97)	80-100 (97)	0-1.0 (0.4)	Excellent
	DGR-4	97-100 (100)	97-100 (99)	0-1.3 (0.7)	Excellent
	DGR-5 (~77°)	100	95-100 (99)	0-1.6 (0.2)	Excellent
	DGR-6 (~57°)	100	95-100 (99)	0-0.3 (0.03)	Excellent

Notes: Average values are shown in brackets (). All boreholes orientations are vertical unless noted by inclination. Fracture frequency includes all joints and bedding plane breaks. RQD terminology based on Deere et al. (1967). \*Poor values due to drilling problems are not included.

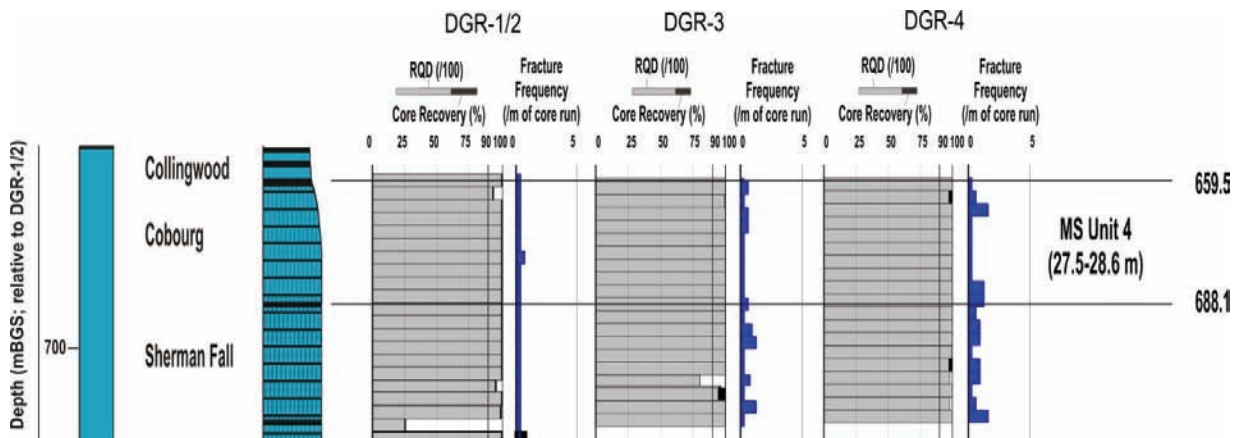
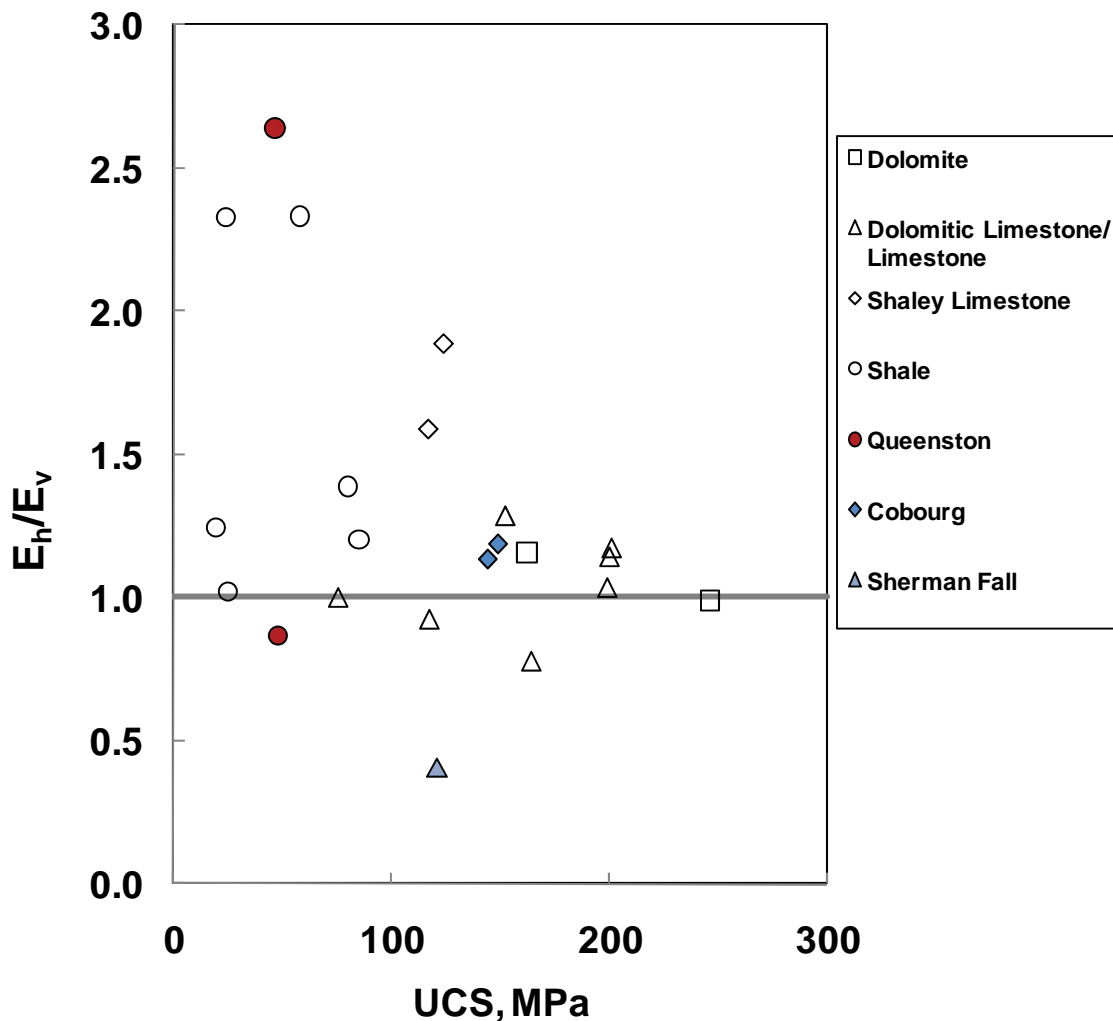


**Figure 3.11: Variation with Depth of RQDs and Fracture Frequencies in MS Unit 4 from DGR-2, DGR-3 and DGR-4**

Cross-anisotropic uniaxial compression tests were carried out on DGR core samples of the Cobourg and Sherman Fall formations. Both vertical and horizontal 24.6 mm diameter samples, 60 mm in length, were obtained by subcoreing of the 75 mm diameter core retrieved from boreholes DGR-3 and DGR-4. The testing method to determine the rock cross-anisotropic properties is described in Gorski et al. (2010a). Figure 3.12 summarizes the test results. The UCS and elastic modulus of samples from the Cobourg Formation are similar in the vertical and horizontal directions, suggesting slight anisotropic rock behaviour. The results are generally inconclusive based on two test samples. A more extensive off-site cross-anisotropic testing at Darlington (Lo and Lukajic 1984) revealed ratios of 0.8 (horizontal:vertical) and 1.2 (horizontal:vertical) for strength and stiffness anisotropies, respectively.



Notes: Unfilled symbols are based on data from Lo and Hori (1979).

**Figure 3.12: Modulus Ratio Versus UCS**

Figure 3.12 shows that the cross-anisotropic behaviour of a rock appears to diminish as the sample becomes stronger, which is consistent with the findings of Lo and Hori (1979). Samples from the Sherman Fall interbedded limestone and the overlying Queenston shale from MS Unit 3, are also plotted in Figure 3.12. The results show that the Sherman Fall Formation could behave anisotropically. These results are also presented in the discussion of MS Unit 3 in Section 3.2.2.3.

### **Swelling**

Upon the completion of an excavation, tunnel convergence or creep continues in weak shales and shaley formations in southern Ontario as a result of the relaxation of the surrounding highly stressed rock mass. Shales, anhydrites, and rock salts are susceptible to time-dependent deformation under stress changes which may affect both tunnel serviceability and integrity.

Swelling of sedimentary rock in southern Ontario has been extensively studied by Lo (1989) and Lo et al. (1978). The swelling potential of a rock was found to be influenced by the clay and calcite content in the rock. The clay contents in the Cobourg and Sherman Fall limestones are found to be moderately low at about 5 to 20% and 10 to 35%, respectively, while their calcite content generally exceeded 70% (INTERA 2011). Time-dependent swelling deformation of the Cobourg and Sherman Fall Formation was studied by subjecting rock specimens to free swell tests by submerging them in both fresh and highly saline formation water. The amount of swelling was then evaluated based on a swelling potential measured as the percentage of strain that occurs per log cycle of time (Lo et al. 1978). All tests in fresh and formation water showed zero vertical and horizontal swelling potential, which agrees with the observations by Lo et al. (1978) that the swelling phenomenon is primary related to ion exchange between the rock pore fluid and the surrounding environment and that the severity of swelling diminishes as the calcite content of rock increases. In addition to the effects on swelling due to the composition of the formation water to which the rock is exposed, Hawlader et al. (2002) show applied stresses can also effectively reduce the swelling potential.

### **Rock Mass Behaviour**

In practice, the strength of a rock mass cannot be solely estimated from UCS data. It also depends on: i) the fracture frequency of the rock mass; ii) the degree of rock interlocking; iii) the state of ground stress; and iv) the hydraulic conditions. A discussion of the fracture frequency at the DGR level is presented in Section 3.2.1.2. Studying the analog of excavation in similar formations allows acquired knowledge of sub-surface rock mass behaviour and excavation design to be extrapolated from one engineering project to another. In this section, tunnelling case histories within the Paleozoic rocks of Ontario and Ohio are reviewed to gain insight into expected rock mass behaviour at the Bruce nuclear site.

GOLDER (2003) compiled existing rock mass information from shallow tunnelling projects in similar rock as that of the host and cap rocks at the Bruce nuclear site. Based on measurements from site investigation work at the Darlington Nuclear Generating Station, overall rock quality for the Cobourg Formation was classified to be good. The integrity of the rock mass was demonstrated by two precedent 8 m and 10.4 m span tunnel excavations in this formation: the 925 m long Darlington cooling water intake tunnel, and the 470 m long oil storage cavern access tunnel at the Wesleyville Generating Station. The Darlington tunnel is completely located in the Cobourg Formation beneath Lake Ontario, whereas the Wesleyville tunnel intersects both this formation and the underlying Sherman Fall Formation. Drill and blast techniques were used to construct both tunnels with no significant construction problems related

to rock stability or overbreak during the course of either project. Further, there was no sign of seepage inflow from the rock units and the tunnels remained completely dry. This observation demonstrates the low bulk hydraulic conductivity of the intersected formations, which is consistent with observations at the Bruce nuclear site.

Rock mass properties are primarily governed by the strength of the intact rock and by the presence of discontinuities within the rock mass. The rock mass at the repository depth is anticipated to be stronger, and in a less disturbed state, with a much higher rock mass rating than at shallow depths; preliminary findings on the host rock from boreholes DGR-1 to DGR-6 appear to confirm this. This observation is also supported by the high RQD values (Figure 3.10) indicating competent rock with massive beds and more than 10 m wide spacing between vertical to subvertical joints. This evidence of generally high quality rock mass bodes well with respect to emplacement room stability.

Another underground excavation analog in limestone similar to that of the Cobourg Formation is the Norton Mine in Barberton, Ohio. This mine is located more than 380 km south of the Bruce nuclear site and was developed at a depth of 670 m within the 75 m thick massive and fossiliferous Devonian-aged Columbus Limestone. Similar to the Bruce nuclear site, the limestone is overlain by an approximately 580 m thick shale cap. Room-and-pillar mining was used with room and entry dimensions of 9.7 m wide and 5.2 m high. In situ overcoring stress measurements at the 670 m depth revealed high horizontal stresses at about twice that of the vertical component. Detailed information on the mine and in situ stress measurements are described in Obert (1962) and Bauer et al. (2005). Mine production was halted in 1976 but the facility was kept in an active standby state. Since then, the mine has remained completely dry with no evident damage or instability to openings even at sectors of the mine that have been abandoned since the late 1940's. Because of the similar geological characteristics between Columbus Limestone and the Cobourg Formation limestone, this analog provides a relevant example of the longevity of a development in a massive limestone formation at depth.

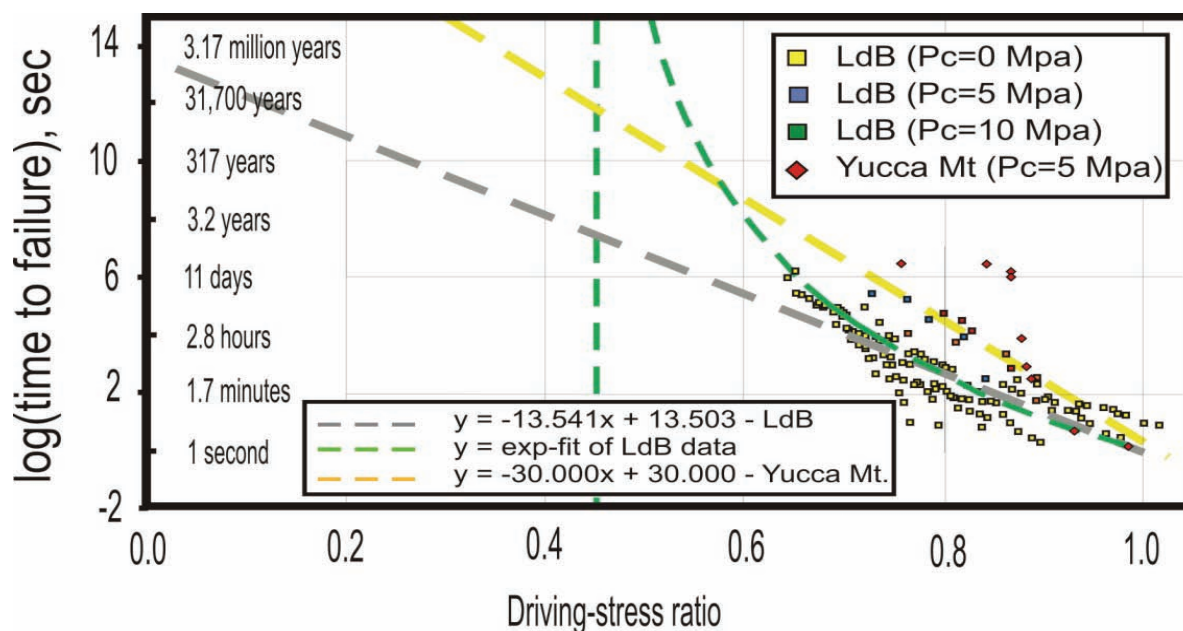
#### **3.2.1.4 Long-term Behaviour**

One task of this geosynthesis is to predict the likelihood of rockfall and changes to the repository emplacement rooms in the Cobourg Formation due to long-term degradation of rock strength as a result of time-dependent processes associated with the current geological regime and to future perturbations. Long-term rock behaviour is generally investigated using laboratory static-fatigue testing which examines the time-to-failure of a material at a particular driving-stress (deviatoric stress) ratio. Various researchers have shown that the laboratory strength of small-diameter confined and unconfined cylindrical samples subjected to these tests decrease with time. Figure 3.13 shows the static-fatigue curves of Lac du Bonnet granite (Schmidtke and Lajtai 1985, Lau et al. 2000) and of Yucca Mountain welded tuff (BSC 2004). Both datasets appear to have similar trends confirming the time-dependent behaviour. However, the duration of these laboratory experiments is generally less than 50 days. Therefore, use of the data to extrapolate strength degradation to long time periods of thousands of years could be problematic.

Based on Figure 3.13, the time-dependent process continues until the driving-stress ratio decreases to very low values approaching zero over geological time. This notion, however, is not supported by any field evidence (Damjanac and Fairhurst 2010). The assumption that time-dependent processes continue over the repository service life is extremely conservative and unrealistic; otherwise, all rock would essentially collapse under its own weight (ITASCA 2011). Evidence from laboratory static-fatigue tests, tectonic data, analytical predictions, and time-dependent numerical modelling suggests that a stress threshold exists in rock, below which no



creep occurs (Damjanac and Fairhurst 2010). A non-linear extrapolation of the Lac du Bonnet granite data reveals such a finite threshold at a driving-stress ratio of about 0.45 (Figure 3.13). This coincides with the CI stress of the rock at about 45% of UCS. Also, from static-fatigue testing of laboratory intact rock samples, no failure was observed below a driving stress ratio of about 0.65 (Figure 3.13). This indicates that time-dependent processes are not observed in laboratory tests below this stress state (0.65 UCS), and below the CI stress (0.45 UCS) the rock response to loading is entirely elastic.



Notes: Lac du Bonnet (LdB) data are from Schmidtke and Lajtai (1985) and Lau et al. (2000). Tuff data are from Martin et al. (1997). Modified from Potyondy (2007).

**Figure 3.13: Long-term Envelopes for Lac du Bonnet Granite and Yucca Mountain Tuff**

Long-term Strength Degradation (LSD) tests were carried out for the Cobourg Formation. The results of the LSD tests did not indicate that any strength degradation had occurred for samples that had been statically loaded for 100 days to stress levels that averaged 70% (range from 43 to 100%) of the CI stress level or 20 to 57% of UCS (see Figure 5.22 in INTERA 2011).

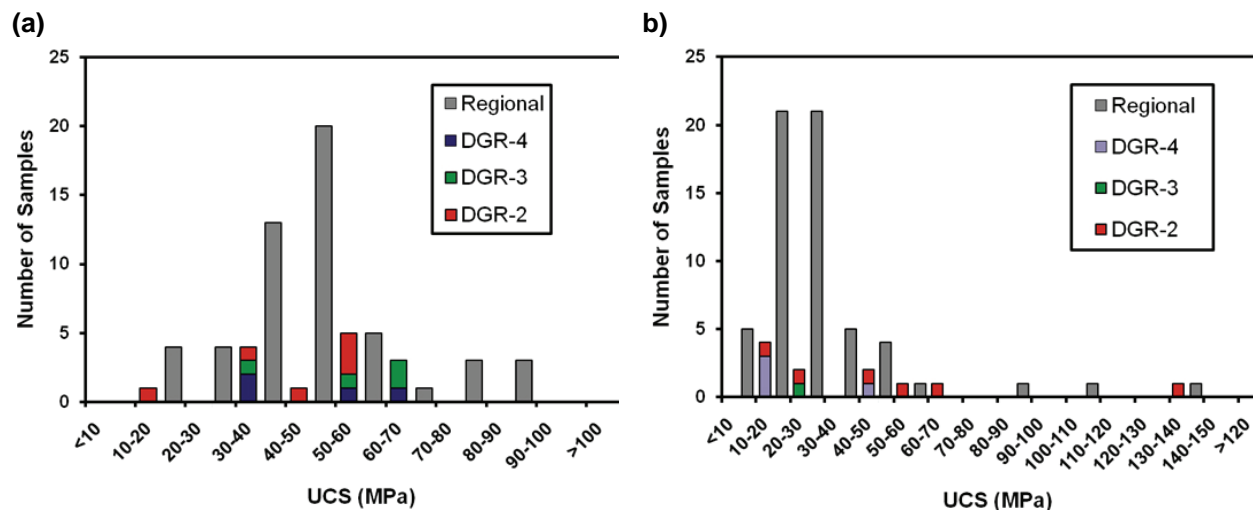
### 3.2.2 Cap Rock – MS Unit 3

The Upper Ordovician barrier shale unit at the Bruce nuclear site incorporates most of the formations of the MS Unit 3 (Figure 3.3), including the Cabot Head, Manitoulin, Queenston, Georgian Bay and Blue Mountain formations (mostly shale) and the Collingwood Member. This shale-dominated sequence is 248.5 to 250.2 m thick and directly overlies the repository host rock of the Cobourg Formation, the mechanical properties of which were described above. Only the major units (Queenston and Georgian Bay formations) are described in detail below. For relatively thin formations like the Blue Mountain, a review of all geomechanical testing is presented in the DGSM (INTERA 2011).

### 3.2.2.1 Intact Rock

#### UCS

To determine the intact strength of the cap rock, uniaxial compression testing was carried out on a total of 14 Queenston and 11 Georgian Bay samples from boreholes DGR-2 to DGR-4. Tests were also conducted on the Collingwood Member, as described in Section 3.2.1.1 for MS Unit 4. From these tests, key parameters such as the peak UCS, CI and CD stresses, the corresponding elastic modulus, and Poisson's ratio were measured. Results plotted in Figure 3.14 show that the shales have a moderate strength with estimated mean values of 48 MPa and 32 MPa for the Queenston and Georgian Bay formations, respectively. Regional UCS data of both rock formations are also presented in Figure 3.14 and it is clear that both data sets lie within the same range (NWMO and AECOM 2011). Based on the limited data, the values across the site appear to be uniform.



Notes: Data are from the regional compilation (NWMO and AECOM 2011) and boreholes DGR-2, DGR-3 and DGR-4 (INTERA 2011).

**Figure 3.14: UCS of the Queenston Formation (a) and Georgian Bay Formation Shales (b)**

There is no clear distribution trend in strength with depth other than variability due to differences in rock composition and the sensitivity of the shale materials to moisture changes after retrieval from drilling. As noted from the laboratory test results reported in Gorski et al. (2009a, 2010a) a few uniaxial compressive test failures are in mixed modes rather than in extensile mode. This could partially explain the strength variance with depth in MS Unit 3.

Similar to the regional data (NWMO and AECOM 2011) the site-specific UCS of the Georgian Bay Formation is lower than that of the Queenston Formation. Like the regional test results, the outliers in Figure 3.14b represent hard layers. Excluding these test results, the average strength of the shale would be reduced to approximately 32 MPa.

**CI and CD Stresses**

CD stress determinations show a large variability ranging from 43 to 100% of UCS based on testing of MS Unit 3 formations (Figure 3.15). Despite this high variation in the UCS and CD stresses, the CI stress determinations from all tests are very consistent, remaining at about 40% of UCS. This is similar to the results from the Cobourg and Sherman Fall formations of MS Unit 4.

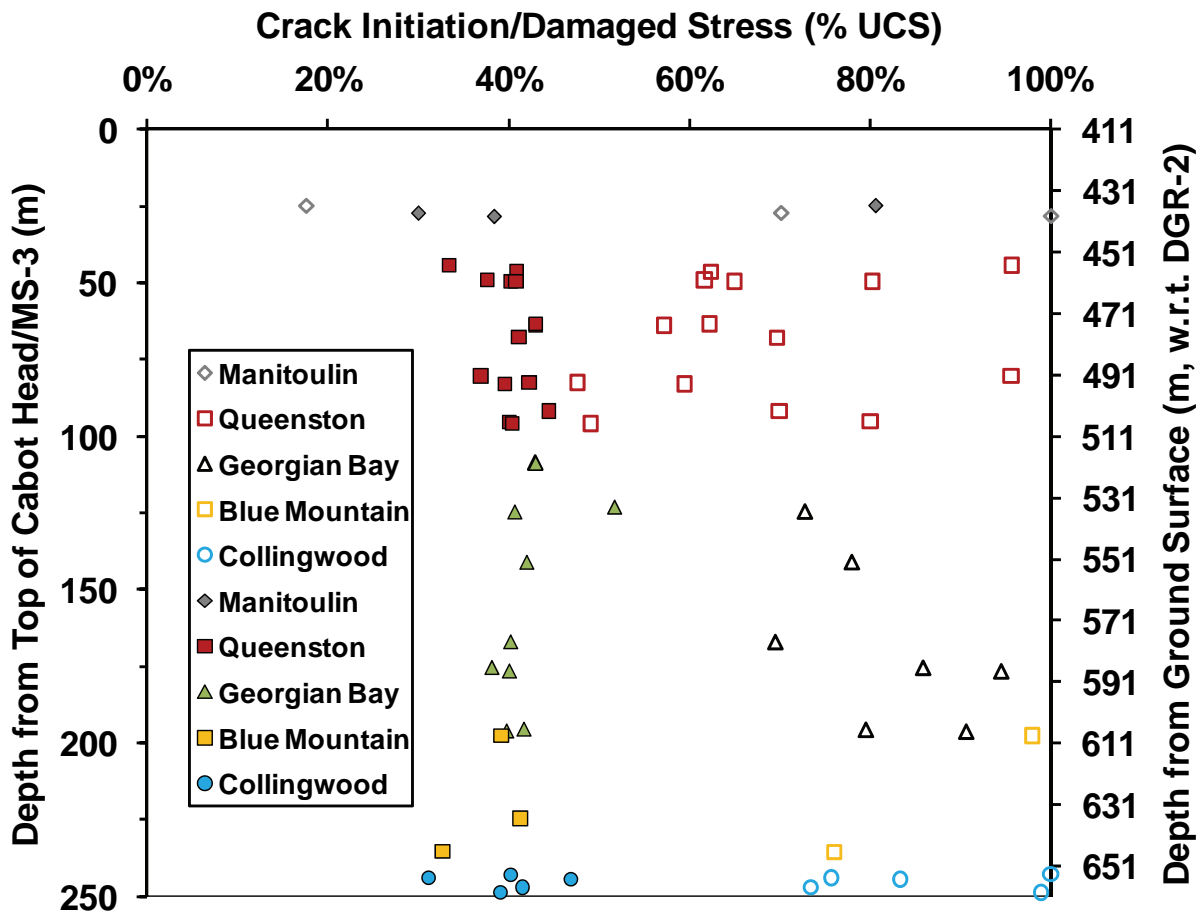


Figure 3.15: CI (filled symbols) and CD (unfilled symbols) Stresses of MS Unit 3

**Tensile Strength**

In addition to the UCS and triaxial testing, Brazilian tension tests were carried out on samples of the Queenston, Georgian Bay and Blue Mountain shales, and the Collingwood Member. Table 3.4 summarizes the Brazilian tensile strength of these rocks and the limited regional database (NWMO and AECOM 2011).

**Table 3.4: Summary of Brazilian Tension Test Results on MS Unit 3 Rocks**

Formation	Site Specific		Regional	
	Number of Valid Tests	Best Estimated Split Tensile Strength (MPa)	Range	Mean Split Tensile Strength (MPa)
Queenston	2	3.0	2.2/3.8	3.4
Georgian Bay	2	7.3	5.6/9.1	
Blue Mountain	3*	1.5	0.9 – 2.6	
Collingwood	1	5.6	5.6	

Notes: (\*) indicates mixed diametrical and slabbing mode failure.

**Triaxial Compressive Strength**

Two sets of triaxial compression tests of intact samples of the Georgian Bay Formation and the Collingwood, taken from each of boreholes DGR-2 to DGR-5, were carried out under confining pressures of 5 to 15 MPa. The results of these tests were accompanied by results from uniaxial compression testing in order to construct a complete failure envelope (Figure 3.16 and Figure 3.17). Regression analysis gives Hoek-Brown parameters for the intact rock (s=1) in these formations as:

$$\sigma_{ci} = 32 \text{ MPa}, m_i = 8 \text{ and } a = 0.5 \text{ (Georgian Bay Formation); and} \tag{3.4}$$

$$\sigma_{ci} = 107 \text{ MPa}, m_i = 18.2 \text{ and } a = 0.5 \text{ (Collingwood Member)} \tag{3.5}$$

At low confining pressures, these parameters can be considered as conservative values.

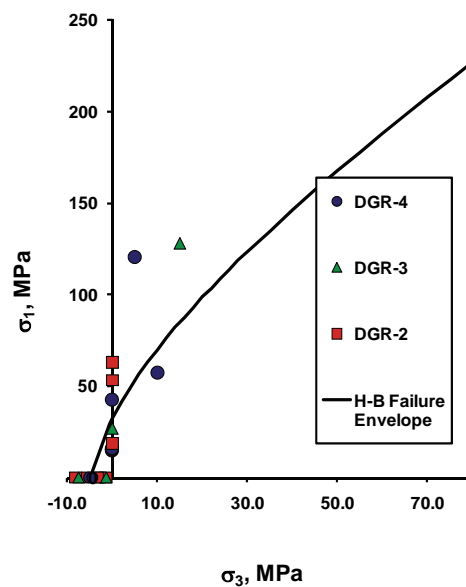


**Figure 3.16: Triaxial Compressive Hoek-Brown Failure Envelope for Georgian Bay Shale**

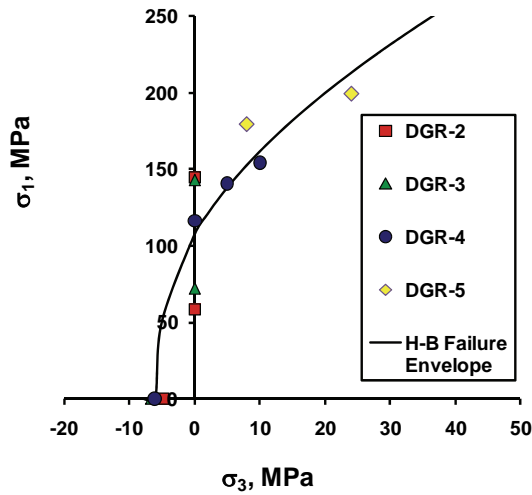


Figure 3.17: Triaxial Compressive Hoek-Brown Failure Envelope for the Collingwood Member

**Shear Strength of Rock and Bedding Planes**

Direct shear testing was performed on open bedding planes and intact samples from the Georgian Bay and Blue Mountain formations and from the Collingwood Member. The results are summarized in Figures 3.18 and 3.19, respectively, and in Table 3.5.

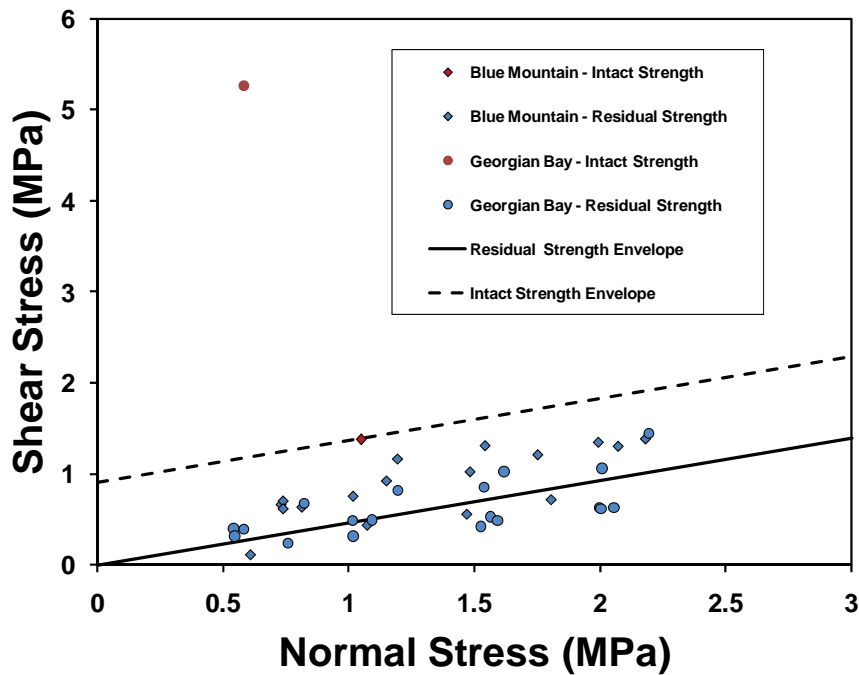


Figure 3.18: Direct Shear Test Results for Georgian Bay and Blue Mountain Shales

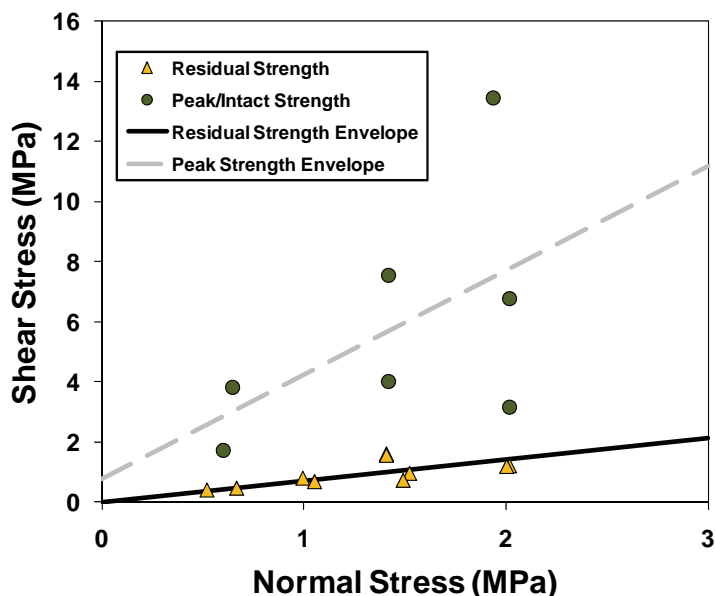


Figure 3.19: Direct Shear Test Results for the Collingwood Member

Based on the above results, the apparent cohesion and friction angle of intact material in the Georgian Bay and Blue Mountain formations are 0.9 MPa and 25°, assuming conservatively that the internal angle of friction is the same as the residual friction angle and the apparent residual shear strength is zero (Figure 3.18). For the Collingwood Member, both peak and residual strength envelopes were constructed using direct shear test data measured under contact pressures between 0.6 and 2.1 MPa. The shearing of intact rock resulted in an apparent cohesion of 0.8 MPa and a high friction angle of 74°. The best-fit line for the residual shear strength reveals zero apparent cohesion and a base friction angle of 36° (Figure 3.19).

Table 3.5: Shear Strength of Georgian Bay and Blue Mountain Formations and the Collingwood Member

Formation/Member	Apparent Cohesion Intercept (MPa)	Apparent Friction Angle (Deg.)	Residual Cohesion (MPa)	Residual Friction Angle (Deg.)
Georgian Bay and Blue Mountain	0.9	25	0	25
Collingwood	0.8	74	0	36

### 3.2.2.2 Rock Mass Properties

The following section describes the rock core recovery, RQD, fracture frequency, and joint spacing properties of MS Unit 3 with a focus on the Queenston, Georgian Bay, and Blue Mountain formations.

These rock mass properties are summarized in Table 3.6 and plotted versus depth in Figure 3.20. As can be seen from the table, the rock mass designation, based on RQD (Deere et al. 1967), for all of the formations is generally excellent (RQD of 90 to 100%) with occasional local zones of lower quality. A few localized areas of poor core recovery are most likely a result of drilling rather than the condition of the rock itself and have not been included. The measured fracture frequency is similar in all of the formations in MS Unit 3 and ranges from 0 to 1.7 fractures per metre, with an average value of generally less than 0.3 fractures per metre. The fractures appear to be very tight and well sealed. Some of the shale rock core from the Georgian Bay and Blue Mountain formations is fissile and breaks up into disc-like portions during handling and storage.

**Table 3.6: RQD Values for MS Unit 3 from Boreholes DGR-2 to DGR-6**

Rock Formation	Borehole No.	Core Recovery (%)	RQD (%)	Fracture Frequency (Fractures/m)	Classification Based on RQD
Queenston	DGR-2	95-100 (100)*	7-100 (100)*	0-0.7 (0.1)	Excellent
	DGR-3	95-100 (100)	95-100 (100)	0-1.3 (0.3)	Excellent
	DGR-4	96-100 (100)	78-100 (98)	0-1 (0.4)	Excellent
	DGR-5 (~72°)	98-100 (100)	96-100 (99)	0-0.7 (0.2)	Excellent
	DGR-6 (~67°)	80-100 (99)	47-100 (97)	0-1.4 (0.1)	Excellent
Georgian Bay	DGR-2	95-100 (100)	74-100 (99)	0-1.0 (0.1)	Excellent
	DGR-3	87-100 (100)	70-100 (96)	0-1.0 (0.3)	Good-Excellent
	DGR-4	94-100 (99)*	96-100 (99)*	0-0.7 (0.1)	Excellent
	DGR-5 (~73°)	97-100 (100)*	97-100 (99)*	0-1.3 (0.2)	Excellent
	DGR-6 (~57°-66°)	90-100 (100)	63-100 (97)	0-1.3 (0.2)	Excellent, locally Fair
Blue Mountain	DGR-2	91-100 (99.7)	91-100 (100)	0	Excellent
	DGR-3	100	53-100 (94)	0-0.6 (0.6)	Excellent, locally Fair
	DGR-4	100	100	0-1.2 (0.1)	Excellent
	DGR-5 (~77°)	100	68-100 (97)	0-0.6 (0.1)	Excellent, locally Fair
	DGR-6 (~57°)	100	73-100 (98)	0-1.7 (0.2)	Excellent, locally Fair

Notes: Average value in brackets ( ) and all boreholes are vertical unless noted by inclination. \* Poor values due to drilling problems are not included. RQD terminology is based on Deere et al. (1967).

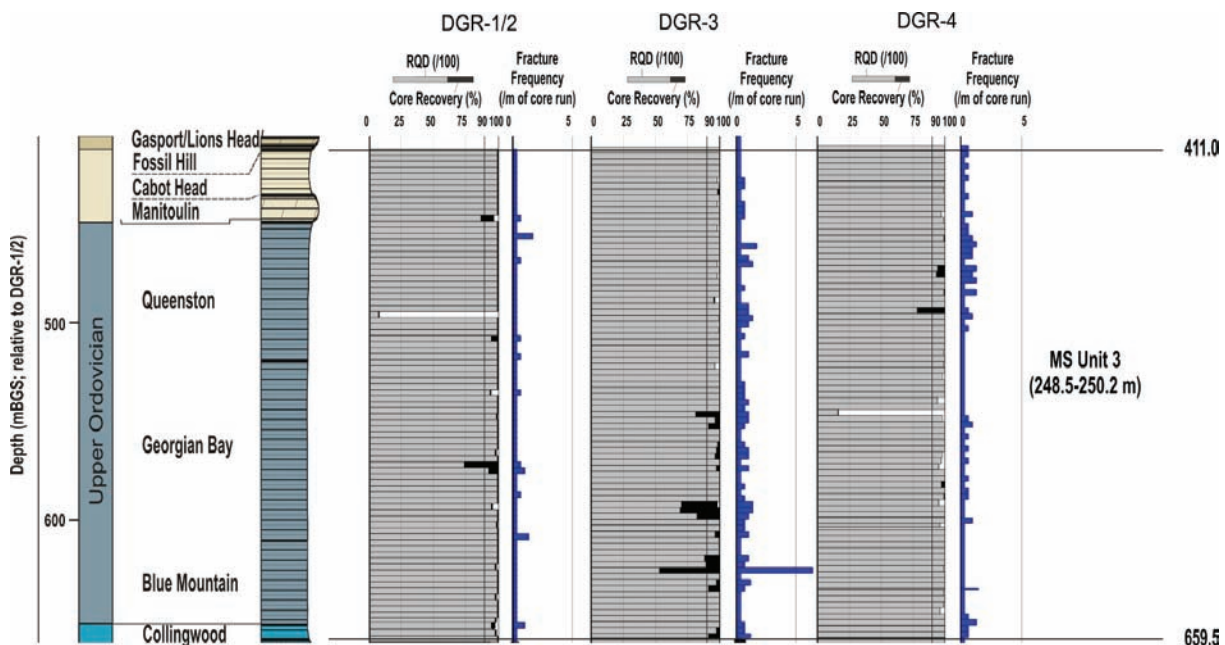


**Figure 3.20: Variation with Depth of RQDs and Fracture Frequencies in MS Unit 3 from DGR-2, DGR-3 and DGR-4**

Table 3.7 summarizes the number of oblique to vertical joints in MS Unit 3 determined by core logging of the DGR boreholes and does not include bedding sub-parallel discontinuities. Based on these data, the Georgian Bay and Blue Mountain formations appear to have larger joint populations than the Queenston Formation. Based on core logging (Briscoe et al. 2010) there may be a local concentration of joints in the Blue Mountain Formation in borehole DGR-3 at a depth of 637.1 - 639.5 m (18 joints). The majority of these are not vertical, as might be expected, but dip at 30° - 60°. All of these joints are most likely tight and sealed in situ, as none were identified by the acoustic televiewer (ATV) log. Based on data from inclined boreholes, DGR-5 and DGR-6, the average joint spacing is estimated to be > 10 m (locally down to 4 m) in the Queenston Formation, > 10 m (locally down to 1.5 m) in the Georgian Bay Formation, and about 7 m (locally down to 0.3 m) in the Blue Mountain Formation. These spacing's should be considered as preliminary as they are based solely on the two inclined boreholes. Inclined boreholes DGR-5 and DGR-6 have lateral coverage of about 61 m and 98 m, respectively, through MS Unit 3.

**Table 3.7: Joint Occurrences in MS Unit 3**

Rock Formation	Borehole No.	Number of Joints	Angle with Core Axis (°)	True Dip (°)
Queenston	DGR-2	3	20-40 [3]	--
	DGR-3	7	25-35 [2], 60-70 [5]	--
	DGR-4	10	0-10 [6], 30-55 [4]	--
	DGR-5	8	--	42-57 [3], 65-89 [5]
	DGR-6	4	--	67-90 [4]



Rock Formation	Borehole No.	Number of Joints	Angle with Core Axis (°)	True Dip (°)
<b>Georgian Bay</b>	DGR-2	3	10-23 [3]	--
	DGR-3	19	0-20 [14], 25-60 [5]	--
	DGR-4	3	0-10 [3]	--
	DGR-5	10	--	42-45 [2], 79-85 [8]
	DGR-6	18	--	30-58 [6], 63-89 [12]
<b>Blue Mountain</b>	DGR-2	1	15	--
	DGR-3	23	0-15 [5], 30-60 [18]	--
	DGR-4	0	--	--
	DGR-5	9	--	74-89[9]
	DGR-6	10	--	39-54 [4], 74-84 [6]

Notes: Data exclude bedding sub-parallel discontinuities. All data were determined during core logging investigations. [x] = number of joints measured.

### 3.2.2.3 Short-term Behaviour

#### **Anisotropy**

The cross-anisotropic behaviours of the Queenston and Georgian Bay formations from MS Unit 3 were determined by testing samples as described and summarized above in Section 3.2.1.3 and in Gorski et al. (2010a). The testing on the Queenston and Georgian Bay samples reveals signs of anisotropic behaviour. Also from the field testing, the ratios of diametral-to-axial Point Load Test data of MS Unit 3 indicate signs of strong anisotropic behaviour. As mentioned in Section 3.2.1.3, the cross-anisotropic behaviour of rock appears to diminish as the sample becomes stronger (Figure 3.12), which is consistent with the findings of Lo and Hori (1979).

#### **Swelling**

The time-dependent swelling deformation of the shaley rock formations in MS Unit 3 was studied by subjecting rock specimens to free swell and semi-confined tests. The swelling in these formations was determined based on tests that measured the percentage of strain that occurs per log cycle of time (Lo et al. 1978). As noted previously, the swelling phenomenon is primarily related to ion exchange between the rock pore fluid and the surrounding environment and calcite content can be used as an indicator of the severity of swelling (Lo et al. 1978). It is clear that the low calcite content of MS Unit 3 makes it susceptible to fresh water swelling (Micic and Lo 2009); however, when exposed to formation water, which is very saline, the swelling potential for all these rocks is essentially zero regardless of mineralogy. Based on Figure 5.18 of the DGSM report (INTERA 2011), it appears that, even when submerged in fresh water, only rock cores sampled from several horizons in MS Unit 3 indicated high vertical and horizontal swelling potentials.

#### **Rock Mass Behaviour**

Information of a preliminary nature used for the rating of the rock mass classification was obtained from investigations associated with the Niagara Hydroelectric Development (Acres Bechtel Canada 1993). The rock mass classification for the Queenston shale revealed good

quality rock. A good example of tunnel construction in rock of this quality is the 13.5 m diameter enlargement of the development's test adit. Mechanical excavation was employed by means of a road header. There was no major instability of the rock following excavation except some slabbing at the crown and on the sidewalls. This surficial spalling only occurred at areas where primary bedding planes exist (Acres Bechtel Canada 1993). Also, it is known that the shale tends to be susceptible to swelling upon exposure. Rock reinforcement was required to control slabbing and slaking. Despite this condition, the rock encountered was of better quality than was anticipated. The tunnel was essentially dry except at local bedding planes where minor seepage was observed (GOLDER 2003).

The following example provides a case history example of rock mass behaviour from the Dufferin Creek Tunnel. The tunnel (Lo 1989, Morton et al. 1975) is located in the region of Durham, Ontario, and was constructed in the mid 1970's in Ordovician shale of the Blue Mountain Formation (formerly designated as Collingwood). The tunnel is an outfall tunnel for the West Dufferin Treatment Plant. It was excavated with a tunnel boring machine, has an excavated diameter of 3.66 m, a finished diameter of 3.0 m, and a length of 1.1 km. A vertical shaft, also with a finished diameter of 3 m, is located at one end and has a length of 37.6 m. The shale consists of interlayered black shale and grey mudstone. Free swell tests on the black shale indicate no swelling, however, the grey mudstone has a horizontal swelling potential of 0.07% and a vertical swelling potential of 0.45%. Cracking of the tunnel lining occurred nine months after construction along the springline in a 280 m long section of tunnel located primarily in grey mudstone. Of interest, the vertical shaft also crosses the same grey mudstone as the tunnel with no recorded lining deformation, indicating that the effects on the swelling are different for vertical and horizontal openings in this rock. Based on this observation, the effects of swelling on the DGR shafts would be expected to be minimal.

#### **3.2.2.4 Long-term Behaviour**

There are no data available for the cap rocks in MS Unit 3 on LSD testing. However, Figure 3.15 shows that the relative CI stresses for all rock units are remarkably consistent at approximate 40% of the UCS values. It is considered reasonable to apply the same assumption that the CI stress threshold can represent the lower bound on the long-term rock strength for MS Unit 3 as was done for the Cobourg Formation (MS Unit 4).

#### **3.2.3 MS Unit 2 – Upper Seals**

Figure 3.1 shows the proposed seal arrangement of the DGR main and ventilation shafts along with the bedrock stratigraphy. A detailed description of the shaft seal is described in the Preliminary Safety Report (OPG 2011a). The following section will focus on the description of the rock formation properties of the upper seals in MS Unit 2 above the cap rock (above 557.7 mBGS). For seals located within the formations of the cap and host rock horizons, the information discussed in previous sections will apply and will not be repeated here. Based on the proposed shaft seal arrangement, there are three concrete bulkheads located in the upper MS-2 Unit, as presented in Table 3.8.

**Table 3.8: Proposed Concrete Bulkhead Seal Locations for Access and Ventilation Shafts in MS Unit 3**

Formation(s)	Seal	Interval (mBGS)
Salina F Unit	B3	178.6 - 190.6
Salina A2 Evaporite and A1 Carbonate	B2	322.8 - 340.8
Salina A0, Guelph, and Goat Island Dolostones	B1	372.6 - 390.6

### 3.2.3.1 Intact Rock

#### UCS

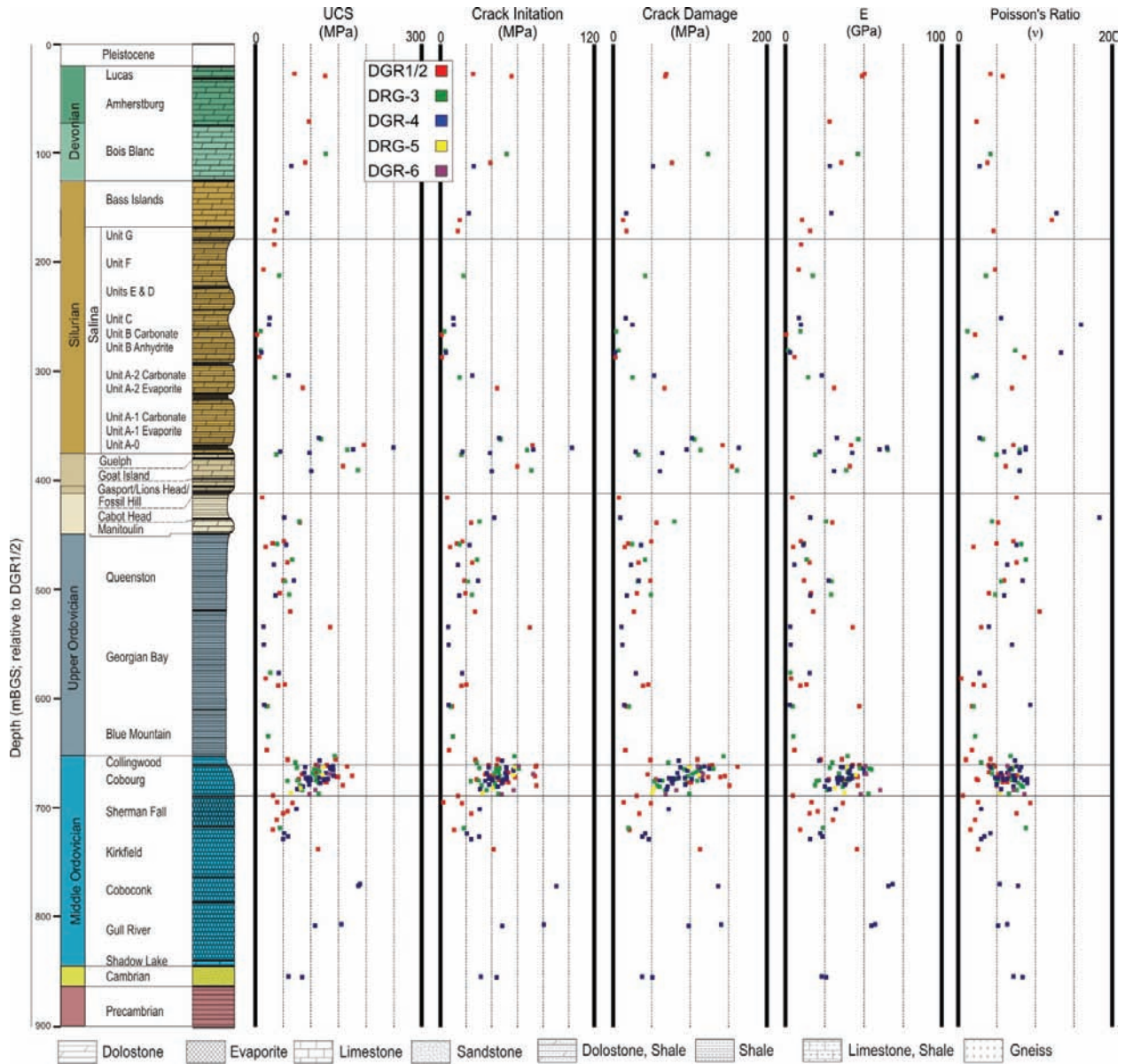
To obtain the geomechanical properties of rock in formations encountered by the upper shaft seals, limited core samples were retrieved from boreholes DGR-1, DGR-3 and DGR-4 for mechanical testing. All cores were tested for UCS only. Key results of the testing are summarized in Figure 3.21. Because of the heterogeneous nature of the rock in MS Unit 2, which contains interbedded anhydrite/gypsum and shale within any given rock specimen, some of the testing of the samples from the upper 115 m measured lower strength. This effect is less prevalent in the lower dolostone, such as the Salina A units and the underlying Middle and Lower Silurian rocks (Figure 3.21). Figure 3.21 also reveals a large variation in Poisson's ratio. Therefore, judgment should be exercised in the selection of design parameters.

#### CI and CD Stresses

Despite the observed variations of the UCS measurement, the relative stress magnitudes at which cracks initiate show remarkable consistence, at about 40% of the UCS (Figure 3.22). There are no data available for the rocks in MS Unit 2 regarding possible relationships between short-term strength and the stress threshold at which long-term strength degradation may commence.

### 3.2.3.2 Rock Mass Properties

The core recovery, RQD, and fracture frequency of MS Unit 2 encountered in boreholes DGR-1 to DGR-6 are summarized in Table 3.9 and plotted versus depth in Figure 3.21. As can be seen from the table, the rock mass designation, based on RQD (Deere et al. 1967), for the listed formations, is generally excellent (RQD of 90 to 100%) except for the Salina F Unit where it ranges from good to excellent with occasional local zones of lesser quality. The rock core recoveries are also lower in the Salina F Unit than in the underlying units. The greatest fracture frequencies are observed in the Salina F unit and range from 0 to 4.9 fractures per metre based on data from boreholes DGR-1 to DGR-6. The Salina A1 Carbonate has a comparable fracture frequency, ranging from 0 to 2.9 fractures per metre. These rocks also have numerous thin subhorizontal gypsum/anhydrite filled veins which have generally not been included in the fracture frequency. Throughout the remainder of MS Unit 2, the fracture frequency ranges from 0 to 1.0 fractures per metre. A few localized areas of poor core recovery are probably a result of drilling rather than the condition of the rock.



Notes: MS units are separated by horizontal black lines. Figure is based on data from INTERA (2011).

**Figure 3.21: Uniaxial Compression Test Results at the Bruce Nuclear Site**

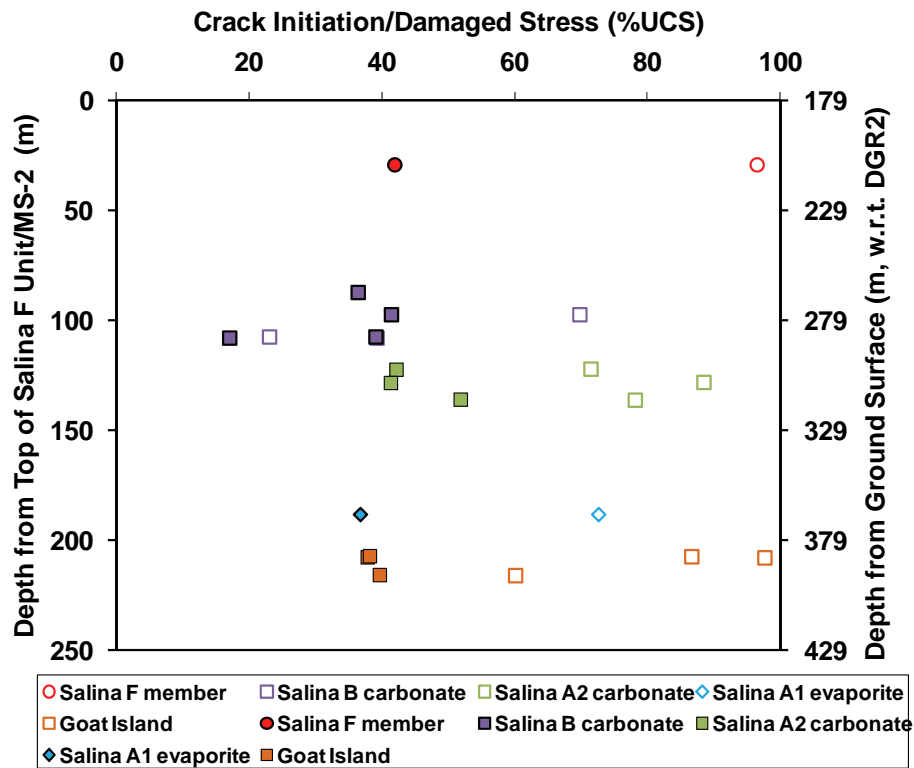


Figure 3.22: CI (filled symbols) and CD (unfilled symbols) Stresses of MS Unit 2

Table 3.9: RQD Values for MS Unit 2 from Boreholes DGR-1 to DGR-6

Rock Formation	Borehole No.	Core Recovery (%)	RQD (%)	Fracture Frequency (Fractures/m)	Description
Salina F Unit	DGR-1	0-100 (94)	0-100 (91)	0-1.8 (0.2)	Good to Excellent
	DGR-3	0-100 (94)	0-100 (92)	0-0.7 (0.1)	Good to Excellent
	DGR-4	0-100 (84)	0-100 (81)	0-2.9 (1.2)	Good to Excellent
	DGR-5 (~72°)	87-100 (98)	76-100 (92)	0-2.6 (1.1)	Good to Excellent
	DGR-6 (~67°)	25-100 (91)	0-100 (84)	0-4.9 (1.4)	Poor to Excellent
Salina A2 Evaporite	DGR-1	100	100	0	Excellent
	DGR-3	100	100	0.6-2.0 (1.1)	Excellent
	DGR-4	100	100	0	Excellent
	DGR-5 (~73°)	100	100	0	Excellent
	DGR-6 (~57°-66°)	100	100	0	Excellent
Salina A1 Carbonate	DGR-1	96-100 (100)	86-100 (98)	0-1.6 (0.2)	Excellent
	DGR-3	93-100 (100)	88-100 (99)	0-2.9 (0.7)	Excellent

Rock Formation	Borehole No.	Core Recovery (%)	RQD (%)	Fracture Frequency (Fractures/m)	Description
	DGR-4	96-100 (100)	96-100 (100)	0-1.0 (0.2)	Excellent
	DGR-5 (~77°)	99-100 (100)	92-100 (97)	0-1.6 (0.4)	Excellent
	DGR-6 (~57°)	100	97-100 (100)	0-1.3 (0.3)	Excellent
<b>Salina A0 Unit</b>	DGR-1	100	100	0	Excellent
	DGR-3	100	100	0	Excellent
	DGR-4	100	100	0	Excellent
	DGR-5 (~77°)	100	100	0	Excellent
	DGR-6 (~57°)	100	100	0	Excellent
<b>Guelph</b>	DGR-1	100	100	0.3	Excellent
	DGR-3	100	100	0-0.3 (0.2)	Excellent
	DGR-4	100	100	0-0.3 (0.2)	Excellent
	DGR-5 (~77°)	100	100	0.3-1.0 (0.7)	Excellent
	DGR-6 (~57°)	100	100	0-0.3 (0.2)	Excellent
<b>Goat Island</b>	DGR-1	95-100 (99)	95-100 (99)	0-1.0 (0.2)	Excellent
	DGR-3	100	98-100 (100)	0	Excellent
	DGR-4	98-100 (99)	98-100 (99)	0-0.3 (0.03)	Excellent
	DGR-5 (~77°)	100	98-100 (100)	0-0.7 (0.1)	Excellent
	DGR-6 (~57°)	100	98-100 (100)	0-0.3 (0.1)	Excellent

Notes: Average value in brackets () and all boreholes are vertical unless noted by inclination in degrees. RQD terminology based on Deere et al. (1967).

Table 3.10 summarizes the number of joints in MS Unit 2 upper seal locations as determined by core logging of the DGR boreholes. Joint density is highest in the Salina F unit, with the greatest concentration in borehole DGR-4. Most of these joints are oblique. Joints in the deeper underlying units tend to be subvertical to vertical. The Salina A2 Evaporite, Salina A0 Unit, and the Guelph and Goat Island formations have none to very few joints (Table 3.10).

**Table 3.10: Number of Joints Determined from Rock Core Logging of MS Unit 2**

Rock Formation	Borehole No.	Number of Joints	Angle with Core Axis (°)	True Dip (°)
<b>Salina F Unit</b>	DGR-1	2	30 & 50	--
	DGR-3	5	25-55 [5]	--
	DGR-4	16	0 (5), 20-50 [11] --	--
	DGR-5	10	--	54 [6], 77-89 [4]
	DGR-6	10	--	39-40 [3], 50-79 [7]

Rock Formation	Borehole No.	Number of Joints	Angle with Core Axis (°)	True Dip (°)
<b>Salina A2 Evaporite</b>	DGR-1	0	--	--
	DGR-3	0	--	--
	DGR-4	0	--	--
	DGR-5	0	--	--
	DGR-6	0	--	--
<b>Salina A1 Carbonate</b>	DGR-1	3	5,10 & 40	--
	DGR-3	1	0	--
	DGR-4	6	0-15 [4], 45 [2]	--
	DGR-5	10	--	33-44 [2], 68-90 [8]
	DGR-6	11	--	31-53 [3], 74-89 [8]
<b>Salina A0 Unit</b>	DGR-1	0	--	--
	DGR-3	1	5	--
	DGR-4	0	--	--
	DGR-5	0	--	--
	DGR-6	0	--	--
<b>Guelph</b>	DGR-1	0	--	--
	DGR-3	0	--	--
	DGR-4	0	--	--
	DGR-5	4	--	42, 61, 71 & 85
	DGR-6	0	--	--
<b>Goat Island</b>	DGR-1	0	--	--
	DGR-3	0	--	--
	DGR-4	1	0	--
	DGR-5	0	--	--
	DGR-6	0	--	--

Notes: Data exclude apparent bedding discontinuities. All data determined during core logging investigations. [x] = number of joints measured.

### 3.3 In Situ Stress

There are great challenges in obtaining, with confidence, the in situ stress magnitude and orientations at the depths of interest from a surface-based exploratory borehole. This is particularly true in horizontally bedded formations where the vertical stress is less than the horizontal stresses, as hydrofracture techniques cannot be used with confidence in this situation (Evans and Engelder 1989). While traditional strain-relief methods (e.g., overcoring) are suitable for relatively shallow measurements, such testing from within an exploration borehole at the ~680 m depth of the DGR has not been successfully demonstrated. Consequently, no measurements of the in situ stresses at the depth of the proposed repository at the Bruce nuclear site were undertaken during the site characterization investigations. Nonetheless there was adequate information from regional in situ stress data, behavior of the borehole core and walls during site characterization, and numerical modelling of the sedimentary sequence to develop a preliminary stress model for the site (INTERA 2011). In situ stress measurements

are planned for the next phase of field activities, during geoscientific data verification from the vertical shafts and lateral development at the repository horizon.

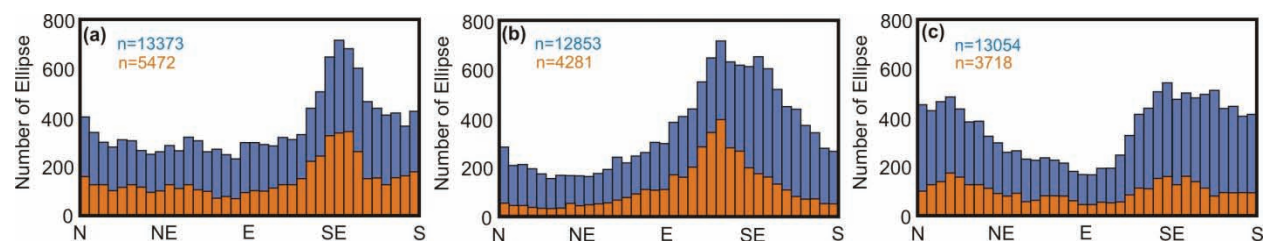
### 3.3.1 Orientations

As discussed in Chapter 2, Section 2.2.6.5, the principal sources for estimating regional in situ stress orientations are the database compiled for the World Stress Map project (Heidbach et al. 2007) and the regional in situ stress database as described in Section 5 in the Regional Geomechanics report (NWMO and AECOM 2011). In brief, the regional maximum horizontal in situ stress is consistently oriented in a northeasterly to east-northeasterly direction (NWMO and AECOM 2011).

Acoustic televiewer (ATV) logs from DGR-1 to DGR-4 utilized ellipticity detection analyses to fit ellipses on borehole sections measured from the acoustic travel time logs over 10 cm intervals. From the analysis, the lengths of the ellipse's long and short axes, as well as their orientation, were determined. The results reveal the length difference between the ellipse axes is typically less than 0.5%. The orientations of the long axis of the ellipses are erratic for most of the borehole length in DGR-1, DGR-2, and DGR-4, except in the Cobourg, Sherman Fall, and Kirkfield formations (660 – 760 mBGS) where the orientations are systematically in a SE direction (138° in DGR-1 & 2 and 131° in DGR-4). The same systematic southeast (141°) borehole elongation in the Ordovician limestones was observed in borehole DGR-3. Figure 3.23 shows the histograms of the orientation of the ellipse long axis for all boreholes. It appears that the systematic SE borehole elongation could possibly be stress related (i.e., the direction of the maximum horizontal stress is NE). This orientation is consistent with the regional trend.

### 3.3.2 Magnitudes

The regional in situ stress data indicate the presence of relatively high horizontal compressive stresses in the Appalachian and Michigan basins, characteristic of a thrust fault regime ( $\sigma_v < \sigma_h < \sigma_H$ ). Table 3.11 summarizes the possible ranges of the maximum and the minimum horizontal stresses, respectively, expressed as a ratio of the vertical (gravity) stress based on the regional database from different in situ stress measuring techniques (NWMO and AECOM 2011).



Notes: (a) DGR-1 and DGR-2, (b) DGR-3, and (c) DGR-4. Peak values are interpreted to indicate the orientation of the minimum horizontal in situ stress for all orientations (blue) and for axis ratios greater than 1.0025 (orange).

**Figure 3.23: DGR Borehole Long Axis Orientation Histograms for Middle Ordovician Formations**



**Table 3.11: Estimated Stress Ratios near Repository Depths**

Depth Range	665 to 700 mBGS		650 to 715 mBGS	
Type	Hydrofracturing	Overcoring*	Hydrofracturing	Overcoring
$\sigma_H/\sigma_v$	2.0 to 2.2	1.6	1.7 to 2.5	1.6 to 1.9
$\sigma_h/\sigma_v$	1.0 to 1.2	1.3	1.0 to 1.2	1.0 to 1.3
$\sigma_H/\sigma_h$	1.8 to 2.0	1.3	1.5 to 2.1	1.3 to 1.9

Notes: Results are subdivided by measurement method and based only on southern Ontario regional in situ stress data. (\*) indicates only one set of measurements in interval. Table is from NWMO and AECOM (2011).

At the site scale, borehole core and televiwer data from DGR-1 to DGR-4 were analyzed to determine the physical response of these deep boreholes to the surrounding stress field. The objective of such review was to back-calculate the in situ stress magnitudes that were consistent with the measured stability of the borehole wall. Valley and Maloney (2010) assessed the possible range of the maximum in situ stress magnitudes that could exist without inducing failure of the borehole wall. Assessing the lack of borehole wall failure must assume a strength value for the borehole wall strength. Valley and Maloney (2010) assumed strength values that ranged from 30% to 150% of the laboratory UCS values given in Table 3.12. Strength and stiffness profiles were created by averaging UCS strength and elasticity modulus over a 30 m moving window along the borehole. Assuming a 100% of UCS threshold rock strength with the characteristic of no failure observation along borehole walls, the maximum allowable horizontal stress could be estimated for each section of the borehole and the results are summarized in Figure 3.24. The 100% UCS threshold, which represents no failure, is shown on the figure by a green line.

**Table 3.12: Constraints on the Horizontal Stress Magnitude at Depths of 620, 680 and 700 mBGS, Assuming Various Scenarios for the Borehole Wall Strength**

Formation and Depth	Assumed Borehole Wall Strength	~Vertical Stress, $\sigma_v$ (MPa)	Bounding Horizontal Stress Values		Maximum Ratio $\sigma_H/\sigma_v$
			Maximum Value of $\sigma_H$	Range: Minimum to Maximum Value of $\sigma_h$	
Blue Mountain 620 mBGS	1.5 UCS	16.4	16	8-16	0.98
	UCS (20 MPa)	16.4	13	8-13	0.80
	0.75 UCS	16.4	11	8-11	0.68
	0.5 UCS	16.4	10	8-10	0.61
	0.3 UCS	16.4	10	8-10	0.61
Cobourg 680 mBGS	1.5 UCS	18.0	42	9-42	2.33
	UCS (107 MPa)	18.0	30	9-30	1.67
	0.75 UCS	18.0	24	9-24	1.33
	0.5 UCS	18.0	18	9-18	1.00

Formation and Depth	Assumed Borehole Wall Strength	~Vertical Stress, $\sigma_v$ (MPa)	Bounding Horizontal Stress Values		Maximum Ratio $\sigma_H/\sigma_v$
			Maximum Value of $\sigma_H$	Range: Minimum to Maximum Value of $\sigma_h$	
	0.3 UCS	18.0	14	9-14	0.78
Sherman Fall 700 mBGS	1.5 UCS	18.5	25	9-25	1.36
	UCS (70 MPa)	18.5	19	9-19	1.03
	0.75 UCS	18.5	16	9-16	0.86
	0.5 UCS	18.5	13	9-13	0.71
	0.3 UCS	18.5	11	9-11	0.60

Notes: Vertical stress at repository depth (680 mBGS) is about 18 MPa. Table is from INTERA (2011).

During the site-scale investigations, replacement of the Westbay casings in boreholes DGR-2 and DGR-3 provided two opportunities to re-inspect their borehole walls. ATV inspection detected no evidence of borehole breakouts or drilling-induced tension fractures over a 24 month period for DGR-2 and a 6 month period for DGR-3. This supplements previous observations that found no evidence of drilling-induced tension fracturing or borehole breakouts in these holes.

A model of the DGR stratigraphy was also constructed using *FLAC3D* to further evaluate the vertical distribution of in situ stress within the sedimentary succession in the subsurface below the Bruce nuclear site (ITASCA 2011). The model simulates the stiffness variability of individual rock formations oriented in the direction of the maximum horizontal principal stress. The model was strained horizontally in both directions to simulate tectonic strains observed at the Norton mine, in Ohio, which has a similar depth horizon and stratigraphy. The results indicate that stiffness contrasts in adjacent rock units play a significant role governing formation-specific in situ stress distributions. Similar findings were reported by Cartwright (2007) for the sedimentary rocks in the United Kingdom. A comparison between the estimated maximum horizontal in situ stress from the modelling and the constraints deduced from the analysis based on the observed lack of borehole breakouts, and using 100% UCS as the borehole wall strength, is given in Figure 3.24.

At the repository horizon (about 680 mBGS) with  $\sigma_v$  assumed equal to the approximate gravity load of superincumbent materials,  $\sigma_H/\sigma_v$  is estimated to range from 1.5 to 2.0 and  $\sigma_H/\sigma_h$  from 1 to 1.2 (INTERA 2011).

A summary of the constraints for the maximum horizontal stress and the modelling results is shown in Table 3.13.



**Table 3.13: Comparison of In Situ Stress Ratios at Various Horizons**

Depth (mBGS)	Formation	$\sigma_v$ (MPa)	Borehole Back-analysis		FLAC3D Model	
			Upper Bound $\sigma_H/\sigma_v$	Lower Bound $\sigma_H/\sigma_v$	Average $\sigma_H/\sigma_v$	Average $\sigma_H/\sigma_v$
200-228	Salina F	5.3-6.0	0.9-1.9 (1.3)	0.5	1.7-1.8 (1.8)	1.2-1.4 (1.3)
228-379	Salina E to A0	6.0-10.0	0.5-4.0 (1.8)	0.5	2.0-3.2 (2.3)	1.6-2.6 (1.9)
379-415	Guelph to Fossil Hill	10.0-10.9	1.3-3.3 (2.4)	0.5	1.2-3.2 (3.0)	1.0-2.6 (2.4)
415-612	Cabot Head to Georgian Bay	10.9-16.1	0.5-1.6 (1.0)	0.5	0.6-1.2 (1.1)	0.6-1.0 (0.9)
612-656	Blue Mountain	16.1-17.3	0.5-1.0 (0.6)	0.5	0.6-1.5 (0.7)	0.6-1.1 (0.6)
656-665	Collingwood	17.3-17.5	1.0-2.3 (1.6)	0.5	1.44-1.45 (1.5)	1.11-1.12 (1.1)
665-693	Cobourg	17.5-18.2	1.2-2.4 (1.8)	0.5	1.86-1.92 (1.9)	1.51-1.55 (1.5)
693-720	Sherman Fall	18.2-19.0	1.0-1.2 (1.0)	0.5	1.01-1.04 (1.0)	0.77-0.79 (0.8)

Notes: Average value in brackets ( ). Data are compiled from ITASCA (2011) and Valley and Maloney (2010).

### 3.4 Summary

This section provides an overview of the geomechanical rock properties of the sedimentary sequence, including the host rock, the Cobourg Formation, in MS Unit-4 and its cap rock in MS Unit-3, as determined by the laboratory testing of rock core samples from the DGR deep boreholes and correlating these test results with regional data. Based on this, the following conclusions can be made:

- The geomechanical site characterization data reveal a uniform and laterally continuous stratigraphic section of rock formations beneath the site. The RQD and natural fracture frequencies observed from boreholes DGR-1 to DGR-6 indicate the Devonian and Upper Silurian dolostones are in poor to fair condition and are moderately fractured. Many of the low RQD values in these formations are attributed to the blocky nature of the rock created by core grinding under difficult drilling conditions. Below these units, the rock encountered in the boreholes is generally in very good condition and sparsely fractured.
- Table 3.14 summarizes the laboratory geomechanical properties from uniaxial compression testing for the Upper and Lower Ordovician, Silurian, and Devonian units.
- The Cobourg argillaceous limestone host rock at the Bruce nuclear site is found to be very competent and massive with high RQD and UCS values.

- The values of geomechanical parameters determined from site specific testing agree favourably with the regional database assembled, with the exception of the UCS, which is significantly higher than the regional values for the Cobourg. Laboratory testing gave an average UCS value of 113 MPa compared to 72 MPa from the regional database. The strength increase is likely attributed to different sampling depths, mineralogical variation, improved sample preservation methods, and/or the quality of the laboratory testing.
- Based on acoustic emission measurements on samples of the Cobourg, the average CI and damaged stresses are 47 MPa and 97 MPa, respectively. The CI stress level appears very consistent at about 40% of the peak UCS.
- The Hoek-Brown failure criterion could give good prediction of the peak strength for the Cobourg over the tested stress range. An empirical expression can be developed to describe the spalling behaviour around the excavation by using dimensionless parameters of  $m_i = 17.4$ ,  $s = 1$  and  $a = 0.5$ .
- The average indirect/Brazilian tensile strength of the Cobourg is about 6.5 MPa. All tension test data lie within the range of that of the regional data set. No direct tension test of the rock was performed during the current study.
- Based on limited cross-anisotropic deformation testing, the Cobourg Formation appears to behave near anisotropically.
- No oblique or vertical joints were encountered in the Cobourg or Sherman Fall formations. The spacing of the vertical joints in these formations is likely on the order of 10 m. Whereas, the spacing of bedding sub-parallel discontinuities in the Cobourg Formation is estimated to be also greater than about 3 m.
- The Upper Ordovician barrier shales, the Queenston, Georgian Bay and Blue Mountain formations also have a very high RQD indicating rock of excellent quality, with local fair to good quality zones, are slightly more fractured with more numerous bedding sub-parallel discontinuities and a lower UCS than the Cobourg. The strength parameters for these rocks are within the range of the regional values.
- The free-swell test results reveal that swelling of the sedimentary sequence is only observed when shale samples were submerged in fresh water. There was no observation of swelling in highly saline formation water. Tests of Cobourg and Sherman Fall samples do not show any swelling in either formation fluids or fresh waters.
- Based on the ellipticity detection analysis using ATV measurements from the DGR boreholes, the orientation of maximum horizontal stress at the Bruce nuclear site appears to be similar to the stress orientation in the Michigan Basin, a NE to ENE direction. This conforms to the general trend of in situ stresses in Eastern North America.
- Stress analyses to estimate horizontal in situ stress magnitudes were carried out, assuming that one principal stress is vertical. The absence of breakouts observed in the DGR boreholes permits the setting of an upper bound on the allowable maximum horizontal stress magnitude of the formation sequence.
- Numerical modelling suggests that the stiffness contrasts between the different stratigraphic units may be significant in controlling the magnitude of the horizontal in situ stress within the sedimentary sequence.
- At the repository horizon (about 680 mBGS) with  $\sigma_v$  assumed equal to the approximate gravity load of superincumbent materials,  $\sigma_H/\sigma_v$  is estimated to range from 1.5 to 2.0 and  $\sigma_H/\sigma_h$  from 1 to 1.2.

**Table 3.14: Summary of Laboratory Geomechanical Properties in MS Units 1 to 5**

Rock Formation/Unit		UCS (MPa)	Brazilian Tensile Strength (MPa)	Elastic Modulus (GPa)	Poisson's Ratio
Amherstburg (3)	Mean	98		43	0.21
	Range	71 - 126		28 - 51	0.12 - 0.29
Bois Blanc (3)	Mean	94		37	0.18
	Range	65 - 127		28 - 46	0.14 - 0.21
Bass Islands (3)	Mean	43		19	0.23(1)
	Range	34 - 58		11 - 29	-
Salina F Unit (3)	Mean	31		12	0.21 (2)
	Range	15 - 43		8 - 18	0.18 - 0.24
Salina C (3)	Mean	20		9	0.17
	Range	9.6 - 26		9 - 10	0.06 - 0.28
Salina B Unit (4)	Mean	8		3	0.40
	Range	3 - 11		0.5 - 6	0.11 - 0.67
Salina A2 Unit (2)	Mean	48		19	0.11
	Range	35 - 60		15 - 23	0.10 - 0.12
Salina A1 Carbonate (3)	Mean	143.1		41	0.23
	Range	115 - 196		33 - 47	0.14 - 0.36
Salina A0 (3)	Mean	197.6		63	.43
	Range	166 - 250		60 - 65	0.40 - 0.44
Guelph (3)	Mean	60		28	0.32
	Range	38 - 98		19 - 43	0.25 - 0.40
Goat Island (3)	Mean	148		37	0.37
	Range	101 - 185		31 - 41	0.31 - 0.40
Cabot Head (1)	Mean	13		4	0.38
	Range	-		-	-
Manitoulin (3)	Mean	66		23	0.24(2)
	Range	52 - 80		16 - 30	0.22 - 0.26
Queenston (14)	Mean	48	40 (6)	15	0.31
	Std. Deviation	14.6	-	8	0.09
	Range	19 - 70	2.2 - 8.3	5 - 25	0.09 - 0.44
Georgian Bay (11)	Mean	32	5.6 (8)	12	0.23

Rock Formation/Unit		UCS (MPa)	Brazilian Tensile Strength (MPa)	Elastic Modulus (GPa)	Poisson's Ratio
	Std. Deviation	17.4	-	8.1	0.18
	Range	15 - 63	1.4 - 9.1	3 - 18	.02 - 0.5
Blue Mountain (3)	Mean	21	1.5 (3)	5	0.10
	Range	21 - 24	0.9 - 2.6	5 - 6	0.09 - 0.11
Collingwood (5)	Mean	107	6.2 (5)	30	0.27(4)
	Range	58 - 145	4.8 - 7.8	22 - 40	0.15 - 0.37
Cobourg (67)	Mean	113	6.5 (8)	39	0.3
	Std. Deviation	25.6	-	6.8 (8)	.07
	Range	58 - 175	3.7 - 8.9	19 - 56	0.1 - 0.45
Sherman Fall (8)	Mean	49	4.9 (7)	23(7)	0.22
	Range	32 - 75	3.2	9 - 27	0.08 - 0.47
Kirkfield (5)	Mean	64		26	0.2
	Range	44 - 113		14 - 46	0.11 - 0.44
Coboconk (2)	Mean	188		68	0.33
	Range	186 - 189		67 - 68	0.32 - 0.33
Gull River (2)	Mean	132		56	0.27
	Range	109 - 156		54 - 58	0.24 - 0.29
Cambrian (2)	Mean	72		23	0.33
	Range	60 - 85		21 - 24	0.29 - 0.36

Notes: (x) = number of measurements. Data are from Gorski et al. (2009a, 2009b, 2010a, 2010b and 2010c) and Murphy and Heagle (2010).

## 4. HYDROGEOCHEMISTRY

### 4.1 Introduction

Hydrogeochemical studies seek to understand the nature and timing of physical and chemical processes that have operated to define the chemical characteristics of natural water. The term hydrogeochemistry refers to the chemistry of water as it is affected by a variety of chemical reactions with components of soil, sediment, rocks and minerals, and by various physical processes such as advection, evaporation and diffusion. In general, hydrogeochemistry may involve the study of water in the atmosphere, surface water such as rivers and lakes, and groundwater. In most cases, these would be considered low-temperature systems (somewhat arbitrarily defined as  $< 100^{\circ}\text{C}$ ), but there is much interest in hydrogeochemistry of higher temperature systems ( $> 100^{\circ}\text{C}$ ; commonly referred to as hydrothermal systems) because of their importance in the formation and accumulation of economically important deposits of mineral and hydrocarbon resources.

In the context of the Deep Geological Repository (DGR), and assessing the long-term integrity of the enclosing rock mass to contain and isolate low and intermediate level waste, hydrogeochemical evidence provides direct insight into two of the seven fundamental geoscience hypotheses.

- **Solute Transport is Diffusion Dominated:** deep groundwater regime is ancient showing no evidence of cross-formational flow or glacial perturbation.
- **Multiple Natural Barriers:** multiple low-permeability bedrock formations enclose and overlie the DGR.

Physical controls on the movement of groundwater and associated solutes, and the timing of such movements, represent the principal themes of these hypotheses. Groundwater movement and solute transport are commonly the subject of hydrogeochemical studies that focus on exploitation and protection of water resources. These types of investigations generally employ field methods designed to directly or indirectly measure flow rates and solute velocities. Hydrogeochemical studies that focus on water resources are restricted to active flow systems that can be easily exploited for water supply. It is common practice to make direct measurements of flow rate, flow direction, and solute velocity in active systems. In contrast, investigations of low-permeability geologic systems are limited by very low advection rates and solute velocities, which cannot be detected within the time available for measurements. Consequently, studies of porewater movement and solute transport in low-permeability geologic systems rely, in part, on hydrogeochemistry in order to elucidate: 1) the age (i.e., residence time) and origin of the porewater, 2) the processes responsible for observed spatial variations in porewater chemistry, and 3) the mechanisms controlling transport of solutes.

The term “groundwater” is commonly used to represent all water contained in geologic formations below the Earth surface, but in the present context, it is useful to distinguish between groundwater that is unconstrained by low-permeability media and therefore free to flow under the influence of hydraulic gradients, and groundwater that is contained in the pores of low-permeability rocks and effectively immobile. In the remainder of this chapter, we use the term “groundwater” to represent water that can flow under the influence of hydraulic gradients. This includes water within the connected pore space between mineral grains in unconsolidated sediment or in a fractured or porous rock matrix, as well as water in permeable, connected structures in the subsurface. Operationally, groundwater is water which flows into and can be sampled from boreholes, typically over time scales of days to months. We use the term



“porewater” to describe water within the connected pore space between mineral grains in low-permeability sediments or rocks in which flow under the influence of hydraulic gradients is inhibited. Operationally, porewater is water which cannot flow into and be sampled from surface-drilled boreholes over time scales of days to months. Laboratory techniques are required to extract porewaters from the sediment or rock matrix.

## 4.2 Objectives

There is a significant body of hydrogeochemical research within the Michigan Basin in both Canada and the United States, and the data collected during the course of previous research, in part, provides a basis for the current understanding of the origin and residence time of the water contained in the sediments of the basin. In addition, site-specific research activities have been ongoing at the Bruce nuclear site since 2006 in order to characterize the geoscientific properties of the underlying sedimentary rocks relevant to the implementation of a DGR (INTERA 2011).

The objective of this chapter is to integrate data from the geoscience characterization activities at the Bruce nuclear site with data obtained from previous research in and around the Michigan Basin. The purpose of this integration is to develop an understanding of the origin and residence time of the groundwater and porewater, and of the mechanisms that cause migration of solutes in rocks that underlie the Bruce nuclear site. The primary sources of information used to characterize the regional and site hydrogeochemistry are listed in Table 4.1.

**Table 4.1: Primary Sources of Information**

Reference Study	Data Sources
<b>Regional Hydrogeochemistry</b>	<ul style="list-style-type: none"> <li>➤ Regional Hydrogeochemistry – Southern Ontario report (Hobbs et al. 2011a)</li> </ul>
<b>Site Hydrogeochemistry</b>	<ul style="list-style-type: none"> <li>➤ DGSM (INTERA 2011)</li> <li>➤ Laboratory diffusion testing of DGR cores: DGR-1 through DGR-4 (Al et al. 2010a, Van Loon 2010, Al et al. 2010b)</li> <li>➤ Field and laboratory analyses of groundwater and porewater chemistry (major ions, trace elements, isotopes, radioisotopes) for DGR-1 through DGR-6 (Koroleva et al. 2009, Jackson and Heagle 2010, Clark et al. 2010a, 2010b, Heagle and Pinder 2010, Clark and Herod 2011, Clark et al. 2011, Hobbs et al. 2011b)</li> <li>➤ Laboratory analyses of DGR cores: mineralogy, petrography (Schandl 2009, Skowron and Hoffman 2009b, Jackson 2009)</li> <li>➤ Investigation of laboratory methods (Clark et al. 2010c)</li> </ul>

## 4.3 Michigan Basin: Evidence for Fluid Migration and Solute Transport

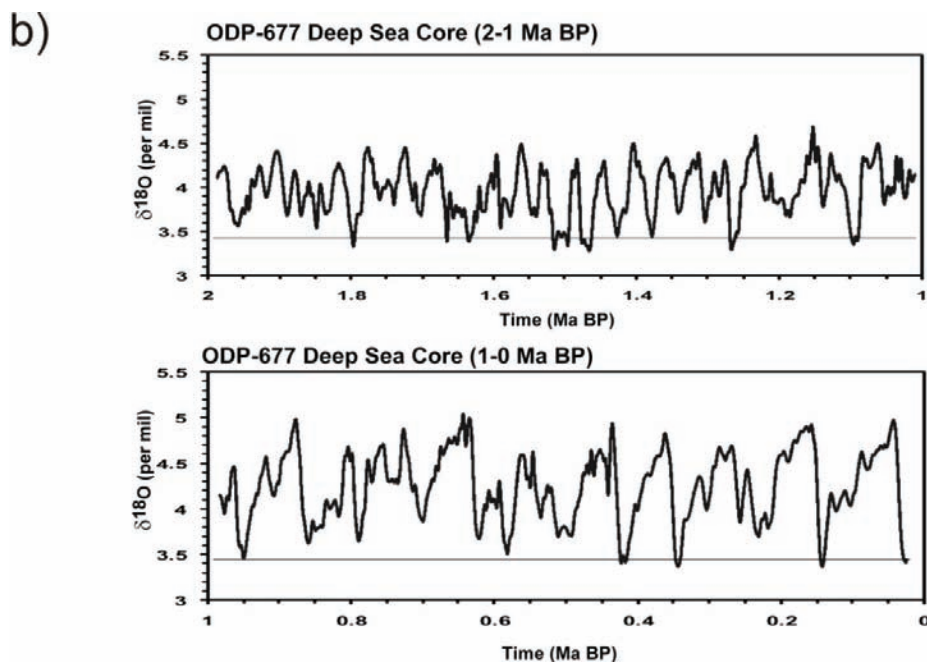
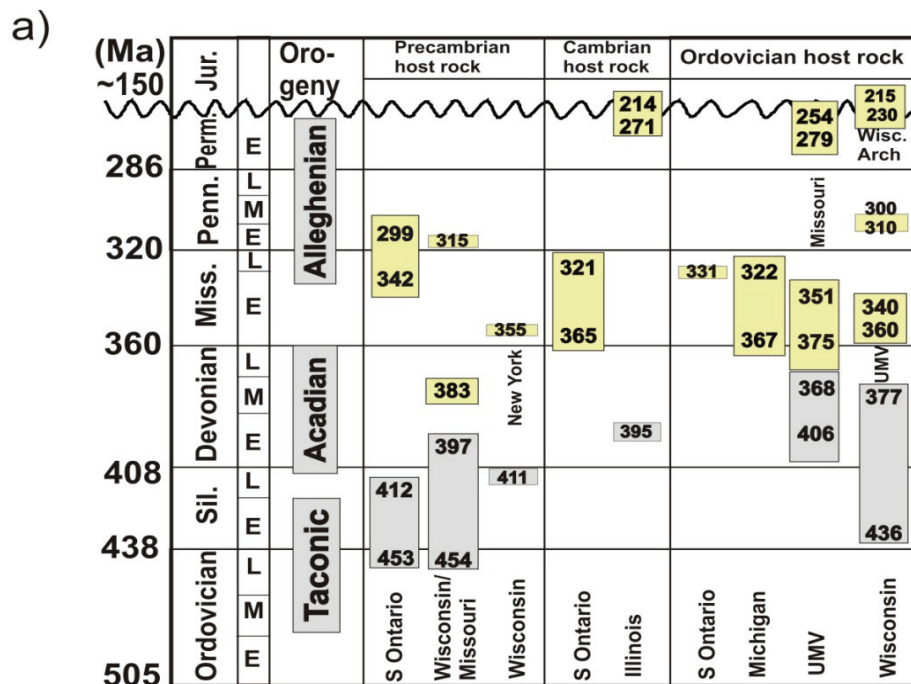
It is important to distinguish between the concepts of flow and solute transport by noting that solute transport results from the combined influence of advection and diffusion. Consequently, solute transport can occur in the absence of advection (flow) provided there is a concentration gradient to drive diffusion. Tectonic activity and glaciation are known to cause significant hydrological disturbances to groundwater systems, and Figure 4.1(a, b) summarizes the timing of tectonic and glaciation events that may have influenced groundwater flow and solute

transport in the Michigan Basin. With reference to the timing of events shown in Figures 2.7 and Figure 4.1(a, b), expectations for fluid migration, solute transport, and the resulting geochemical evolution in the Michigan Basin, are described within this section.

### Possible Fluid Migration Processes

The possible driving forces for fluid migration within the context of the geologic history of the Michigan Basin are summarized below.

- The Taconic Orogeny (Middle Ordovician-Lower Silurian) may have resulted in basin-scale westward migration of fluids in the more permeable Paleozoic stratigraphic units (Cambrian sandstones, dolomitized Ordovician carbonates). How far inland, toward the Michigan Basin, the hydraulic influence of the Taconic Orogeny reached is not certain, but there is evidence for Taconic fluid movement at the Precambrian-Cambrian boundary in the Appalachian Basin in southern Ontario (Harper et al. 1995, Ziegler and Longstaffe 2000a, 2000b). HTD-hosted oil and gas reservoirs in southern Ontario and Michigan in the Black River and Trenton groups are presumed to have formed as a result of brine migration during this time period (Davies and Smith 2006).
- Episodes of sea water evaporation, particularly during the Silurian and Devonian periods, would have created an unstable high salinity brine layer in the upper stratigraphic levels of the basin. Although the Silurian is underlain by low-permeability Upper Ordovician shale, localized fracture and fault systems may have provided the opportunity for dense brine to migrate downward and invade relatively permeable regions within the underlying Ordovician, Cambrian and Precambrian rocks (Coniglio et al. 1994, Davies and Smith 2006). This is a model similar to that proposed by Bottomley and others who suggest that dense evaporated-seawater brine migrated from sedimentary basins into adjacent shield flow systems, forming the precursor to present-day brines in the Canadian Shield (Bottomley et al. 1999, 2003, 2004, 2005, Greene et al. 2008). In the absence of localized fracturing, the resulting concentration gradients between the underlying sedimentary porewaters and the hypersaline fluids would have resulted in the downward diffusion of solutes.
- Fluid migration would have occurred within permeable sedimentary units in response to hydraulic gradients and crustal motion related to Acadian (Devonian) and Alleghenian (Early Mississippian-Lower Permian) orogenesis. Ziegler and Longstaffe (2000a, 2000b) present evidence for illite formation during this time period along the Precambrian-Paleozoic unconformity in the western Appalachian Basin (Figure 4.1a). The light yellow and grey boxes in Figure 4.1a represent the estimated timeframes for secondary mineral formation in the respective geographic areas based on the radiogenic (K-Ar) dating of secondary illite (light yellow) and K-feldspar (grey).
- High fluid pressures at the base of glacial ice sheets are potentially able to drive the infiltration of glacial melt water to depth. Although glacial events are recognized periodically throughout geologic history, there are no known events that would have affected the Michigan Basin between Upper Silurian and Pleistocene time (Price 1999). The Pleistocene cycles of glacial and interglacial periods during the timeframe of 2 million years before present (MaBP) to 1 MaBP are not clear from data presented in Figure 4.1b, but there were clearly, at least, 9 recognizable glacial – interglacial cycles since 1 MaBP (Peltier 2011).
- Fluid migration can also occur in response to pressure gradients formed by tilting of the basin during differential isostatic rebound following deglaciation. Data presented by Harrison (1972) suggest that the north rim of the Michigan Basin at Little Current, Ontario, has undergone approximately 110 m of post-glacial differential uplift relative to the Bruce nuclear site.



Notes: In (a), the duration of secondary mineralization is indicated by number ranges within the yellow (illite) and grey (K-feldspar) boxes plotted in relation to the main pulses of Paleozoic orogenesis (from Ziegler and Longstaffe (2000b)); UMV = Upper Mississippi Valley; S. Ontario samples are from the Appalachian Basin). In (b), glacial advance-retreat cycles for the past 2 Ma are indicated by the saw-tooth patterned oxygen isotope curve (from Peltier (2011)).

**Figure 4.1: (a) Timing of Paleozoic Orogenic Events and (b)  $\delta^{18}\text{O}$  Variation in Deep Sea Sediment Core ODP-677 Depicting Recent Glacial Cycles**

Based on the possible mechanisms and events capable of driving fluid migration presented here, it follows that there may have been a long period of time (approximately 200-250 MaBP to 2 MaBP) when the hydraulic regime in the Michigan Basin was relatively static.

#### Processes Controlling the Initial Porewater Geochemistry and the Geochemical Evolution of Groundwater and Porewater in the Michigan Basin

- During the Cambrian, shallow marine sediments covered the Canadian Shield east and west of the Algonquin Arch. It is likely that seawater infiltrated the groundwater system in the upper several hundred meters of the underlying shield.
- A major marine transgression during the Middle Ordovician resulted in deposition of the Black River Group and Trenton Group carbonates in a normal marine setting. During this period, the underlying shield and overlying Paleozoic sediments were in contact with normal marine seawater. These conditions lasted through the deposition of the Upper Ordovician shale. The Georgian Bay to Queenston succession, however, records a shallowing-upward sequence, and the upper Queenston shale contains gypsum and occasional halite hopper casts interpreted to have formed in a near-shore mud flat environment under arid conditions (Brogly et al. 1998).
- The first occurrence of restricted marine conditions, leading to formation of hypersaline brines, is in the Silurian (resulting in deposition of the Salina Group). Syndepositional processes, such as dolomitization and evaporite mineral precipitation, would have been operative at the surface and in the shallow subsurface during this period.
- A great variety of post-depositional diagenetic reactions have been ongoing to the present day in response to variations in temperature, pressure, and reaction rates. These reactions include: dolomitization, feldspar albitization, maturation of organic carbon, gas generation, sulphate reduction-sulphide precipitation, smectite to illite transformation, and isotopic exchange.
- Fluid migration processes and geochemical evolution are intimately coupled, and the compositions of groundwaters and porewaters at specific locations in the basin are affected by solute transport processes.
  - Advective transport is expected to cause changes in fluid chemistry within relatively permeable stratigraphic units, and in faults and fractures. Advective transport would have been most influential in the early history of the basin when tectonic forces could have created large hydraulic gradients capable of driving brine migration. One such example is the formation of localized HTD reservoirs in the Trenton Group and Black River Group limestone formations of the Michigan and Appalachian basins. Davies and Smith (2006) propose a model whereby HTD formed from fluids that migrated laterally within the underlying Cambrian sandstone aquifer and were able to penetrate vertically upwards into the overlying limestones along preferential pathways associated with wrench faults.
  - Diffusive transport operates to minimize chemical concentration gradients in space. Diffusion would be the dominant transport mechanism in low-permeability units and may also dominate transport in relatively high permeability units when extremely low hydraulic gradients persist. Diffusion would be influential over the entire history of the basin, and likely was the dominant mechanism for solute transport during the time period from the end of the Alleghenian Orogeny to the Pleistocene (approximately 250 MaBP to 2 MaBP), a period for which there are no identified driving mechanisms that could have resulted in advective transport.

Paleozoic tectonic activity and Pleistocene glaciation are notable driving forces that could have caused movement of dense brines within the Michigan Basin. There is evidence to indicate the occurrence of cross-formational mixing within the Michigan Basin in deep bedrock formations up to the late Paleozoic. There is also evidence of cross-formational mixing in the shallow bedrock sequences in southern Ontario during the Pleistocene due to glacial melt water infiltration. The following sub-sections discuss these events and the origin of the sedimentary brines.

#### 4.3.1 Ancient Events

The presence of hypersaline brines in the sediments should result in a gravitationally stable system, and fluid flow would not be expected without a large pressure perturbation to the system. In a review of fluids in sedimentary basins, Kyser and Hiatt (2003) note that fluids in sedimentary basins do not flow without changes to hydraulic gradients, most of which are tectonically induced. The principal tectonic influences on the Michigan Basin occurred during the Paleozoic Era during Appalachian mountain building, and were intimately linked to the processes of subsidence and sedimentation (Howell and van der Pluijm 1999).

Hydrocarbons are obvious examples of fluids that have migrated within the sedimentary rocks of the Michigan Basin. Powell et al. (1984) conducted geochemical characterization of hydrocarbons in southwestern Ontario. They demonstrated the occurrence of Cambro-Ordovician oils in two Silurian reservoirs, indicating cross-formational flow between the source-rock regions and the reservoirs. Similarly, Barker and Pollock (1984) used chemical and isotopic evidence to demonstrate that Silurian, Ordovician, and Cambrian formations hosting natural gas are not sufficiently mature to have provided a source for the gas. They suggested that the natural gas accumulated by lateral migration into southwestern Ontario from more mature source rocks deeper in the Michigan and Appalachian basins. Barker and Pollock (1984) noted that the natural gas chemistries in samples from the Michigan Basin were distinct from the natural gas chemistries within the Appalachian Basin, indicating that there has been no significant migration of gases between the basins.

Sherwood-Lollar et al. (1994) characterized natural gas from Ordovician and Cambrian strata using isotopic and compositional indicators. They found that the gases in these formations are thermogenic in origin, which is consistent with data from the Ordovician sediments at the Bruce nuclear site (see Section 4.4.3.1). Gas samples collected from wells where the sedimentary rocks are in direct contact with the Precambrian basement strata had anomalously high helium (He) concentrations. Based on the elevated He concentrations and  $^3\text{He}/^4\text{He}$  ratios, Sherwood-Lollar et al. (1994) suggested that the gas that resides within the respective formations could be a mixture of in situ gas (sourced within the Cambrian and Ordovician strata) and a He-enriched end-member that was derived from deep within the Precambrian basement. Based on 1) the structural interpretation of the Chatham Sag, 2) the identification of pinch-out structures in oil and gas reservoirs (Sanford et al. 1985, Carter et al. 1996), and 3) data on the temperature of emplacement and maturity of the hydrocarbons, Sherwood-Lollar et al. (1994) concluded that only the hydrocarbons to the southeast of the Algonquin Arch/Cambrian pinch-out boundary display elevated thermal maturities that would support migration from the Appalachian Basin. Gas in reservoirs in the Michigan Basin do not display such elevated maturities, suggesting that they are not sourced from the Appalachian Basin and that there has been no detectable migration of gas between the basins.

Mississippi-Valley-Type (MVT) lead-zinc sulphide mineralization occurs in the Middle Silurian dolomites in southern Ontario. On the basis of geographic and mineralogical differences, sulphide mineralization was classified into two groups: i) occurrences in the Bruce District,

which is northwest of the Algonquin Arch along the eastern margin of the Michigan Basin, and ii) occurrences in the Niagara District, which is southeast of the Algonquin Arch along the western margin of the Appalachian Basin (Farquhar et al. 1987). Sulphide mineralization is most prevalent in the Niagara District, with only sparse occurrences in the Bruce District (Farquhar et al. 1987). Lead (Pb) isotope ratios ( $^{207}\text{Pb}/^{204}\text{Pb}$  and  $^{208}\text{Pb}/^{204}\text{Pb}$ ) for the Bruce District galena (PbS) suggest that the Pb was derived from a crustal source distinct from the Pb in galena samples from the Niagara District (Farquhar et al. 1987). Similarly, results of Pb and strontium (Sr) isotopic analyses of brines from producing oil and gas wells (McKenna et al. 1992), and brines from gas wells and dry wells (Dollar 1988, Dollar et al. 1991), indicate that groundwaters in Ordovician formations within the Michigan Basin have a different origin than fluids in the Appalachian Basin. McNutt et al. (1987) measured the Sr isotopic composition of oil-field brines from the Michigan Basin and observed that brines obtained near the eastern edge of the basin in Ontario have Sr isotopic compositions that are very similar to samples from deeper within the Michigan Basin. They suggest that this is evidence for intra-basin fluid migration over distances of hundreds of kilometres. Although these brines have migrated internally within the basins, the Pb and Sr isotope data do not indicate mixing between Michigan Basin and Appalachian Basin fluids. Results from studies of the hydrocarbon geochemistry are consistent with the Pb and Sr isotopic data in that they indicate intra-basin, but not inter-basin, fluid migration for the Michigan and Appalachian basins.

There are several studies that provide evidence for tectonically induced fluid migration in Paleozoic rocks of southern Ontario, although most focus on data from the Appalachian Basin rather than the Michigan Basin because petroleum exploration and development activities on the Appalachian Basin side of the Algonquin Arch provide greater opportunity for data collection. The comprehensive studies of fluid-related mineral alteration by Harper et al. (1995) and Ziegler and Longstaffe (2000a, 2000b) provide the best available information on fluid composition and the timing of fluid migration. They studied alteration at the Precambrian-Paleozoic unconformity in the Appalachian and Michigan basins in southwestern Ontario. Based on their measurements of stable oxygen (O) and hydrogen (H) isotopes in secondary chlorite, and K-Ar geochronology on secondary K-rich feldspar from the Appalachian Basin, they proposed a conceptual model in which westward migration of hot sedimentary basin brine was responsible for forming secondary minerals. The paragenetic sequence and estimated crystallization temperatures suggest that chlorite formed first at  $\geq 150^\circ\text{C}$  and subsequent cooling of the brine caused formation of secondary K-feldspar at temperatures  $\geq 100^\circ\text{C}$ . They suggested that evaporated sea water, trapped in Paleozoic formations, was driven westward under the influence of Taconic orogenesis and that flow was focused along the Precambrian-Paleozoic unconformity.

Dolomite in Middle and Upper Ordovician strata in Ontario, including the Trenton Group and Black River Group, the Blue Mountain Formation, and the Georgian Bay Formation (Manitoulin area) was studied by Coniglio and William-Jones (1992), Middleton et al. (1993), and Coniglio et al. (1994). Two types of dolomite were identified by Coniglio et al. (1994): 1) a ferroan 'cap' dolomite that overlies the Trenton Group near Manitoulin Island, and 2) dolomite that occurs in proximity to fractures or faults. Coniglio et al. (1994) and Taylor and Sibley (1986) report that the fracture dolomite post-dates the ferroan cap dolomite. Middleton et al. (1993) measured homogenization temperatures ranging between 100 and  $220^\circ\text{C}$  in primary fluid inclusions from the fracture-related dolomite in oil and gas fields in the Chatham Sag region of southern Ontario (refer to Figures 2.2 and 2.20). These temperatures are substantially higher than those likely to be generated during peak burial of the sedimentary sequence, leading Coniglio et al. (1994) to suggest that the data reflect the influence of hydrothermal fluids; the heat source, however, was not identified.

On the basis of carbon and strontium isotope data, Coniglio et al. (2003) suggest that sea water-derived fluids are responsible for regional-scale dolomitization in the Middle Silurian Guelph Formation. Based on examination of primary fluid inclusions, the temperatures ranged between 65 and 130°C (Coniglio et al. 2003, after Zheng 1999), indicating that the fluids were hydrothermal in nature as suggested by Coniglio et al. (1994) for dolomite in Ordovician strata in Ontario. Several authors suggest that fracture-related dolomitization and hydrocarbon migration in the Michigan Basin likely occurred during the Late Paleozoic to Early Mesozoic (Prouty 1988, Hurley and Budros 1990, Budai and Wilson 1991). These authors compared fracture-related dolomite in the Michigan Basin with mineral alteration associated with MVT deposits in the central and eastern United States. These fluid-driven processes are considered to be contemporaneous, and were likely the result of the Alleghenian deformation and thrusting events taking place in the east.

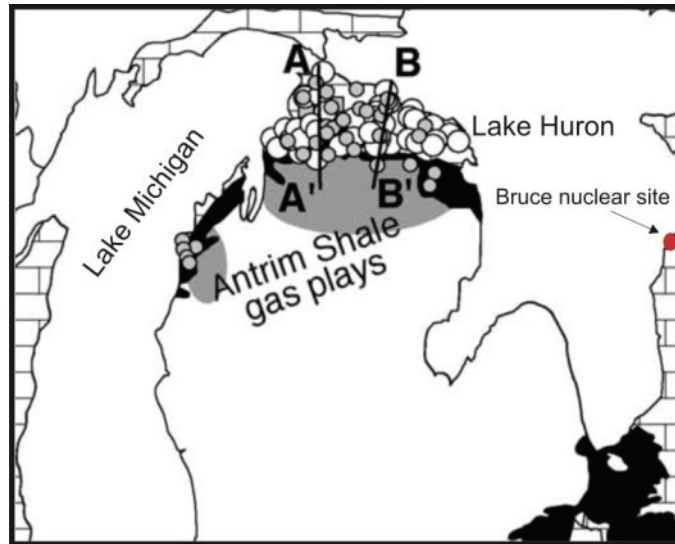
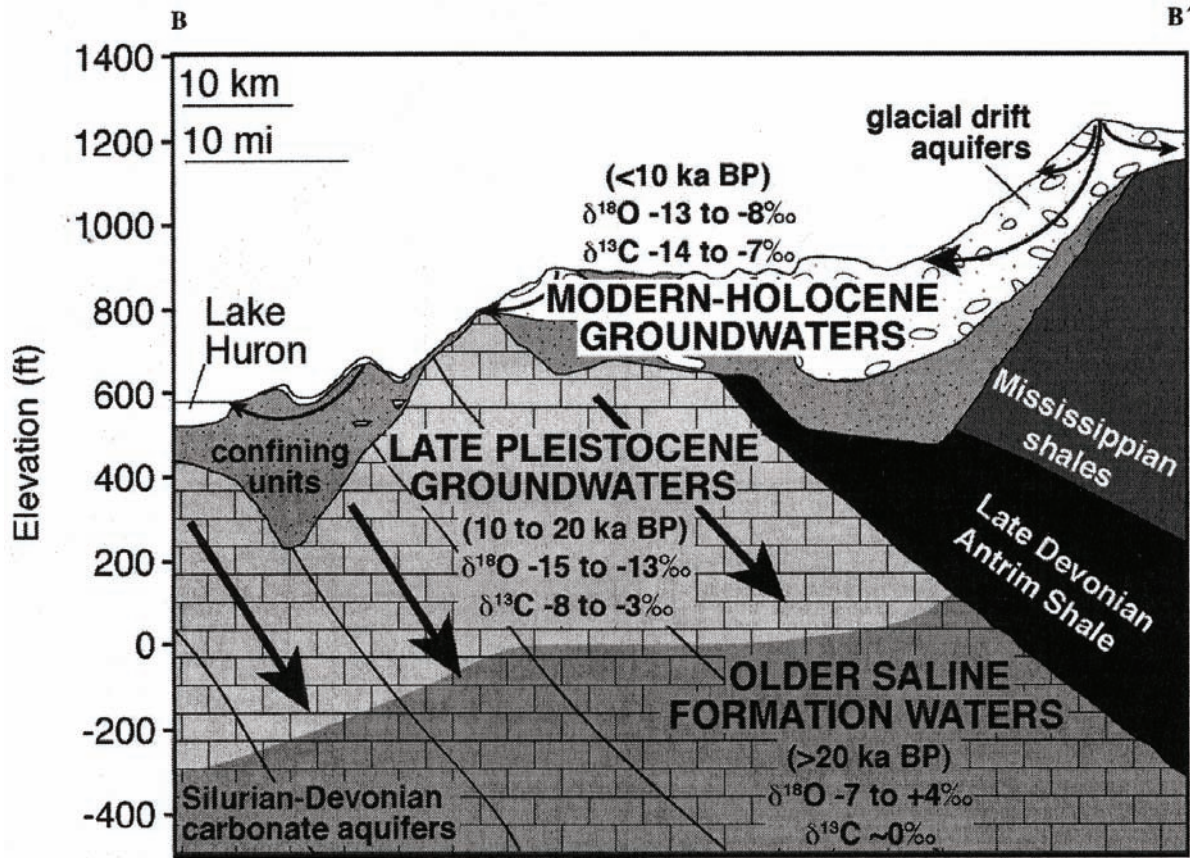
#### **4.3.2 Pleistocene and Post-Pleistocene Infiltration Events**

The widespread occurrence of ancient brines in the Michigan Basin demonstrates that, under conditions prevalent since the Paleozoic, it has not been possible for hydraulic heads generated in freshwater aquifers at the top boundary of the basin to displace the deep basin brines. Glacial melt water, however, which can be pressurized beneath continental ice sheets during interglacial periods to levels in excess of ambient heads, has been driven to depths of several hundred metres in Paleozoic aquifers around the periphery of the Illinois and Michigan basins (see McIntosh and Walter 2005, 2006; Person et al. 2007 and references therein). Stable O isotope data provide the best evidence for infiltration of glacial melt water, which displays strongly depleted  $\delta^{18}\text{O}$  values (between -25 and -11‰), and this cold-climate water can be distinguished from: i) hypersaline basinal brines which have  $\delta^{18}\text{O}$  values ranging between -6 and +5‰ (Wilson and Long 1993a) and ii) modern recharge in southwestern Ontario which has  $\delta^{18}\text{O}$  values typically ranging between -11 and -7.5‰. In addition,  $^{14}\text{C}$  analyses suggest that the  $^{18}\text{O}$ -depleted waters infiltrated during the Pleistocene (McIntosh and Walter 2005, 2006).

Although stable O and H isotopic data demonstrate that fresh glacial melt water has infiltrated around the periphery of the Michigan Basin, the composition of the water has been significantly altered by mixing with ancient hypersaline brines and by dissolution of evaporite minerals. Evidence for these changes in water chemistry is reviewed in detail by McIntosh and Walter (2005, 2006) who use major ion chemistry to interpret the degree of mixing and the nature of mineral-water interactions that have influenced the chemistry of the Pleistocene water. The conceptual model developed by McIntosh and Walter (2006) for Pleistocene infiltration around the margins of the Michigan Basin is presented in Figure 4.2. Their research suggests that glacial melt water has penetrated to depths up to 200-300 m in Silurian-Devonian carbonate aquifers in northern Michigan on the northern margin of the Michigan Basin.

#### **4.3.3 Origin of Sedimentary Brines**

The brines in the Michigan Basin are considered to have originated by evaporation of ancient sea water (Wilson and Long 1993a, b) and deviations from the sea water evaporation curve (McCaffrey et al. 1987) on a plot of chloride (Cl) versus bromide (Br) can aid in the interpretation of processes that have influenced the evolution of the brine compositions through time.



Notes: Developed by McIntosh and Walter (2006).

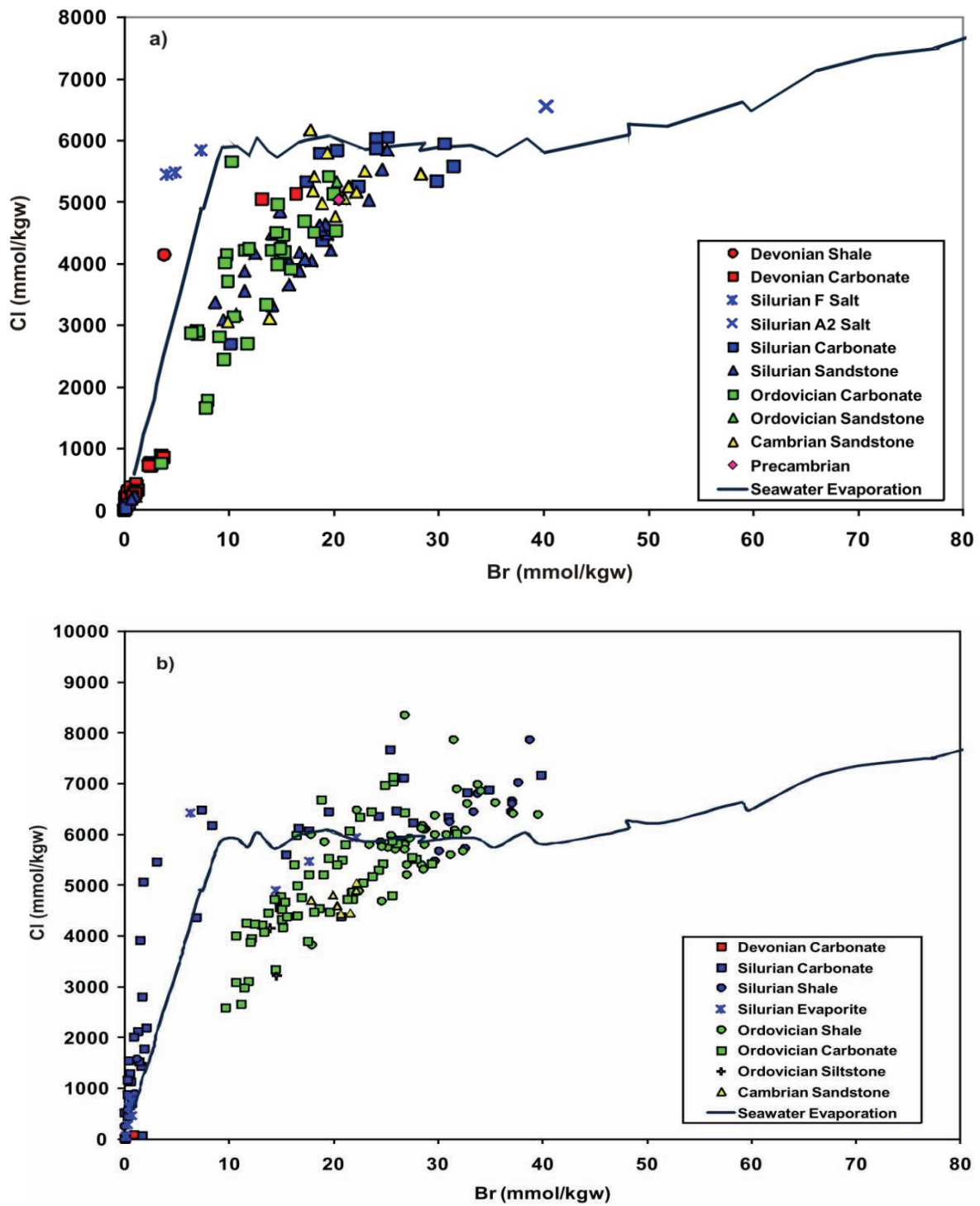
**Figure 4.2: Conceptual Model Showing Ancient Brine at Depth, Cold-climate Water Infiltrated to Mid-depths, and Modern Meteoric Water near Surface**



Utilizing hydrogeochemical data for oilfield brines in southwestern Ontario (UW database; presented in Hobbs et al. 2011a), the Cl-Br plot (Figure 4.3a) displays trends that indicate: i) dilution of brines by lower salinity water, and ii) dissolution of halite. Dilution is indicated for samples that plot below the sea water evaporation curve on a trend toward the origin, and dissolution of halite is indicated for samples that plot above the sea water evaporation trend. Mixing with lower salinity water, such as meteoric water, glacial melt water, normal sea water, or water of hydrothermal origin, could contribute to the observed dilution trends. The origin of water contributing to dilution cannot be determined from the Cl-Br plot. Figure 4.3b shows the Cl and Br data from groundwater and porewater collected during site characterization activities at the Bruce nuclear site. The trends in the data are very similar to the regional data, suggesting an evaporated seawater origin for the brine, with subsequent modification by processes such as dilution, halite dissolution, and water-rock interaction.

Stable O and H isotopic signatures of groundwater from the Paleozoic rocks of the Michigan Basin (Figure 4.4a), mostly from southern Ontario, provide additional insight into the origin of lower salinity water that contributed to dilution. A number of the shallowest samples, from depths of 140 m or less in Devonian and Silurian formations, have depleted  $\delta^{18}\text{O}$  values that are typical of present-day meteoric water and plot along the Global Meteoric Water Line (GMWL). Some data for the Silurian sandstones, and for one group of groundwater samples from the Ordovician carbonates, plot between the meteoric water line and brine end members, consistent with a trend toward depletion of  $^2\text{H}$  and  $^{18}\text{O}$  that would result from mixing of meteoric water with brine. The Ordovician carbonates described above are from the Appalachian Basin and represent the shallowest Ordovician fluids obtained on the northwestern shores of Lake Ontario (see Figure 4.5). There are a small number of samples from the Devonian and Silurian formations that display highly depleted  $\delta^{18}\text{O}$  values and plot along the GMWL in the range of glacial melt waters; this is indicative of mixing with cold-climate water. These waters were sampled from Devonian- or Silurian-aged formations at depths of less than 100 m. The majority of the Devonian fluid stable isotopic signatures are indicative of mixing with glacial melt water and/or meteoric water.

Figure 4.4b is a cross-plot of the  $\delta^{18}\text{O}$  and  $\delta^2\text{H}$  data from groundwaters and porewaters collected from DGR boreholes at the Bruce nuclear site. The data collected from the Bruce nuclear site (Figure 4.4b) display the same general distribution patterns as the regional data. The shallow formations (including the Bois Blanc, Bass Islands, and some fluids from the Salina Group) have depleted  $\delta^{18}\text{O}$  and  $\delta^2\text{H}$  signatures ( $\delta^{18}\text{O} = -7.5$  to  $-11\text{‰}$ ;  $\delta^2\text{H} = -50$  to  $-70\text{‰}$ ) relative to modern precipitation and plot on the GMWL, suggesting that they have been influenced by cold-climate waters. The Salina Group samples that plot in the glacial melt water range on Figure 4.4b are from the A1 Unit carbonate aquifer, which represents the maximum depth to which glacial melt water infiltration is evident at the Bruce nuclear site (325.5 to 328.5 mBGS). The location of the Bruce nuclear site relative to the majority of the regional wells along the Michigan Basin margins for which data have been collected (see Figure 4.5) suggests that the shallow sedimentary formations (Devonian and Silurian) at the Bruce nuclear site may show more evidence of mixing with glacial and/or meteoric water(s) (see Figure 4.4b) due to their shallower depth relative to the same sedimentary formations nearer to the Chatham Sag (refer to Figure 2.2). The majority of the deep formation fluids (Ordovician shales, Ordovician carbonates and Cambrian) have enriched  $\delta^{18}\text{O}$  signatures, plotting to the right of, and below, the GMWL, suggesting long timeframes for water-rock interaction.



Notes: The sea water evaporation trend is from McCaffrey et al. (1987).

**Figure 4.3: Chloride versus Bromide Concentrations for a) the UW Database, and b) Groundwater and Porewater Samples from the Bruce Nuclear Site**

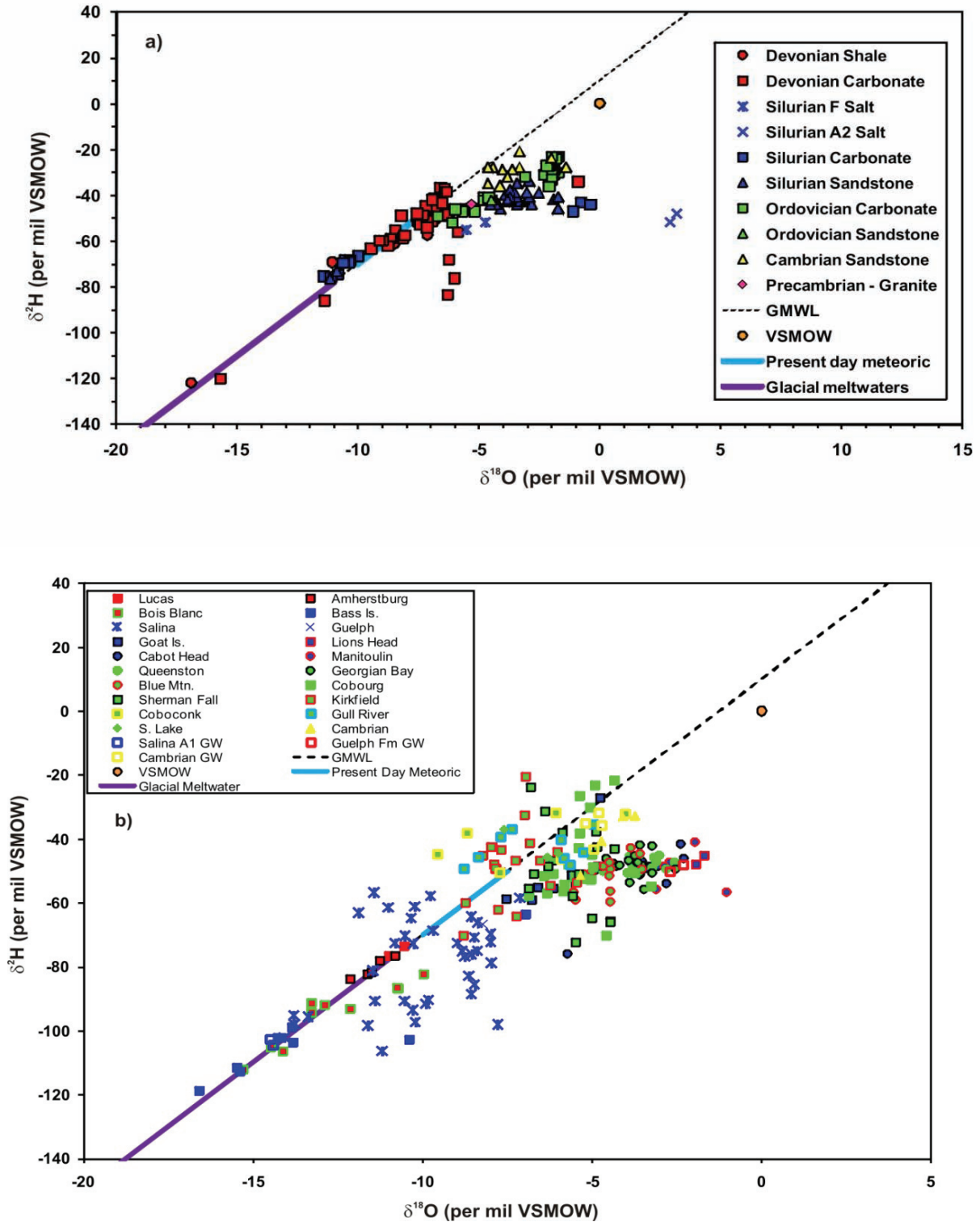


Figure 4.4: Hydrogen Versus Oxygen Isotopic Signatures for a) All Fluids Within the UW Database and b) Groundwater and Porewater Collected at the Bruce Nuclear Site

The Salina Group samples that show enriched  $\delta^2\text{H}$  values and plot above the GMWL in Figure 4.4b are presumed to have been shifted towards more depleted values for  $\delta^{18}\text{O}$  due to the release of mineralogically bound waters in gypsum during analysis and are not considered representative of the true porewater compositions (INTERA 2011). Water that is bound in the gypsum structure has been shown to have widely varying isotopic composition depending on whether it is derived from the “original” evaporative brine, or from a subsequent hydration or exchange process (Sofer 1978). A number of samples from the Trenton and Black River groups (Cobourg, Kirkfield, Sherman Fall, Coboconk, Gull River and Shadow Lake formations) have apparent isotopic signatures that plot on or above the GMWL relative to the majority of the porewaters collected from the Ordovician carbonates. The possible causes of the  $^{18}\text{O}$ -depletion and  $^2\text{H}$ -enrichment in the porewater from these Ordovician carbonates, most evident within the Black River Group, are discussed in Section 4.4.1.

The stable isotope data presented in Figure 4.4 (a, b) are consistent with the Cl-Br data presented in Figure 4.3 (a, b) in that they indicate mixing has occurred in the shallow formations between saline brines and more dilute water(s). Most of the samples that display evidence of mixing with meteoric water are from Devonian and Silurian formations, which, in southern Ontario, occur at shallow depths and are commonly overlain by unconsolidated glacial overburden. These formations are therefore directly exposed to waters of Pleistocene and younger age. The deep sedimentary formations of Ordovician and Cambrian age plot primarily to the right of, and below, the GMWL, indicative of long time periods of water-rock interaction.

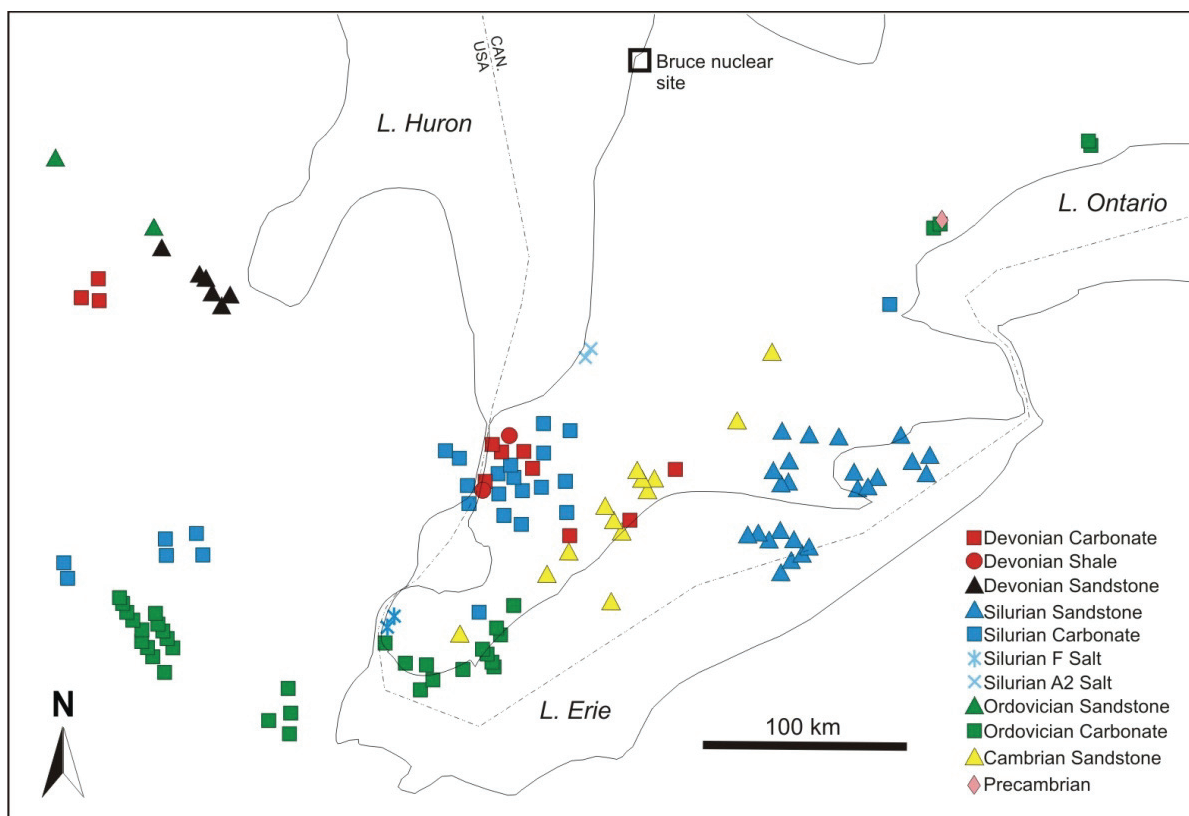


Figure 4.5: Sampling Locations for the UW Database

#### 4.3.4 Regional Summary

The preceding sections provide a preliminary comparison of the regional data compiled in the UW database (and presented in the Regional Hydrogeochemistry – Southern Ontario report (Hobbs et al. 2011a)) with the data collected at the Bruce nuclear site for characterization purposes. The site-specific geochemical data are consistent with regional values, suggesting a common origin and evolution of the sedimentary fluids. The primary conclusions of the regional evaluation are presented below. The site-specific geochemical data collected from the Bruce nuclear site are discussed in detail in Section 4.4.

- Paleozoic tectonic activity is associated with fluid migration (e.g., hydrothermal) within the Michigan Basin, and is indicated to be the only significant driver for the movement of saline brines at depth. Based on the thermal and evolutionary history of the Michigan Basin, the last stage(s) of orogenesis occurred in the late Paleozoic to early Mesozoic eras and the region has remained relatively stable for approximately the last 200-250 Ma.
- Pb and Sr isotopic data, as well as natural gas characterization data from the Michigan and Appalachian basins, indicate intra-basin, but not inter-basin, fluid migration.
- The presence of thermogenic gas in the Ordovician and Cambrian sediments within the Michigan Basin is consistent with data collected at the Bruce nuclear site (see Section 4.4.3.1).
- On a regional scale, glacial melt water and meteoric infiltration have been observed to maximum depths of 300 mBGS along the northern margins of the Michigan Basin. The depth of glacial melt water infiltration at the Bruce nuclear site is consistent with the regional data, with the maximum depth of glacial melt water infiltration at approximately 328.5 mBGS in the thin Salina A1 Unit aquifer.
- The sedimentary brines at the Bruce nuclear site are chemically (Cl, Br) and isotopically ( $\delta^{18}\text{O}$ ,  $\delta^2\text{H}$ ) similar to brines in the regional dataset, and are consistent with an evaporated sea water origin for the fluids and subsequent modification resulting from mixing and/or dilution of sedimentary brines, halite dissolution, and water-rock interaction.

#### 4.4 Hydrogeochemical Data from the Bruce Nuclear Site

Hydrogeochemical site characterization activities at the Bruce nuclear site have focused on the collection of data that could:

- Assist in identifying the residence time and origin of the porewater and groundwater underlying the Bruce nuclear site;
- Provide evidence of meteoric water and/or glacial melt water infiltration;
- Allow for estimation of the redox conditions present in the Ordovician shale and limestone formations; and
- Provide constraints on the processes and timing of solute transport, particularly in the Ordovician rocks.

It should be noted that all references to the 'Cobourg Formation' within this section are in regard to the Lower Member carbonate of the Cobourg Formation, the proposed host rock for the DGR. The upper member is explicitly discussed as the Collingwood Member.

The TDS distribution with depth for all DGR boreholes is presented in Figure 4.6. The TDS values increase with depth from the bottom of the Devonian (Bois Blanc Formation) to the

Silurian Guelph Formation. Below the Guelph Formation, TDS values are relatively stable within the Lower Silurian carbonates and the Upper Ordovician shales (Queenston Formation to Collingwood Member). TDS values decrease with depth in the Middle Ordovician carbonates (Cobourg to Gull River formations). At the base of the profile, within the Shadow Lake and Cambrian formations, TDS values increase slightly, but are still lower than the values measured within the Ordovician shales. The high TDS value measured at the base of the Queenston Formation (~423 g/L) is not considered to be representative of the porewater TDS in this interval and is, instead, interpreted to be the result of mineral salt dissolution during the porewater extraction process.

Table 4.2 shows the average values of TDS (mg/L) for the porewater in sedimentary formations, as well as the characteristic water type of the formations determined from the major ion chemistry. The sedimentary units are grouped in Table 4.2 (as in INTERA 2011; their Table 4.17) based on their classification as an aquifer, aquiclude, or aquitard (as defined in Section 5.4.1), and are described below.

- The overburden (consisting of glacial till of Pleistocene age) is considered to be an aquitard.
- The Devonian formations (Lucas, Amherstburg, and Bois Blanc), as well as the Silurian Bass Islands Formation are classified as aquifers.
- The Salina units and underlying Middle to Lower Silurian carbonates and shales are classified as aquitards, with the exception of the high conductivity Salina A1 Unit (carbonate) and the Guelph Formation, which are classified as aquifers.
- The Upper Ordovician shales (Queenston through Blue Mountain) and the Middle Ordovician Trenton Group carbonates (Cobourg through Kirkfield) are classified as aquicludes based on the low horizontal hydraulic conductivities of these units (see Figure 5.1).
- The Middle Ordovician Black River Group carbonates (Coboconk and Gull River) are classified as aquitards.
- The Cambrian and the overlying Shadow Lake Formation siltstone are classified as aquifers due to their horizontal hydraulic conductivities on the order of  $10^{-9}$  to  $10^{-6}$  m/s (Figure 5.1).
- The underlying Precambrian shield is classified as an aquitard.

The hydrogeochemical characteristics of the porewaters and groundwaters that underlie the Bruce nuclear site are obtained by direct sampling in the case of groundwater (Jackson and Heagle 2009, Heagle and Pinder 2010), and by use of leaching/extraction techniques for estimation of porewater composition in low-permeability rocks (Clark et al. 2010a, 2010b, Koroleva et al. 2009). Stable isotope data ( $\delta^{18}\text{O}$  and  $\delta^2\text{H}$ ) are determined by vacuum distillation on samples that have been coarsely crushed and heated under vacuum to 150°C for 6 hours. The water yield from each sample during the distillation is recorded. Following the vacuum distillation step, the dried rock samples remaining are used to estimate the major ion concentrations by leaching with distilled water, and the mass of solutes leached is normalized to the water content of the individual samples determined during the distillation. The reader should bear in mind that, although referred to as porewater concentrations, the data are more properly considered leachate concentrations. There are uncertainties that relate to: 1) differences between the volume of water extracted by distillation compared to the volume in which the salts were dissolved in situ; and 2) the influence of reaction processes during the leaching step, such as the dissolution of soluble salts originally present in the rocks, and the gain or loss of mass on cation exchange sites. Therefore, the leachate solution concentrations should not be considered exactly equivalent to porewater concentrations.

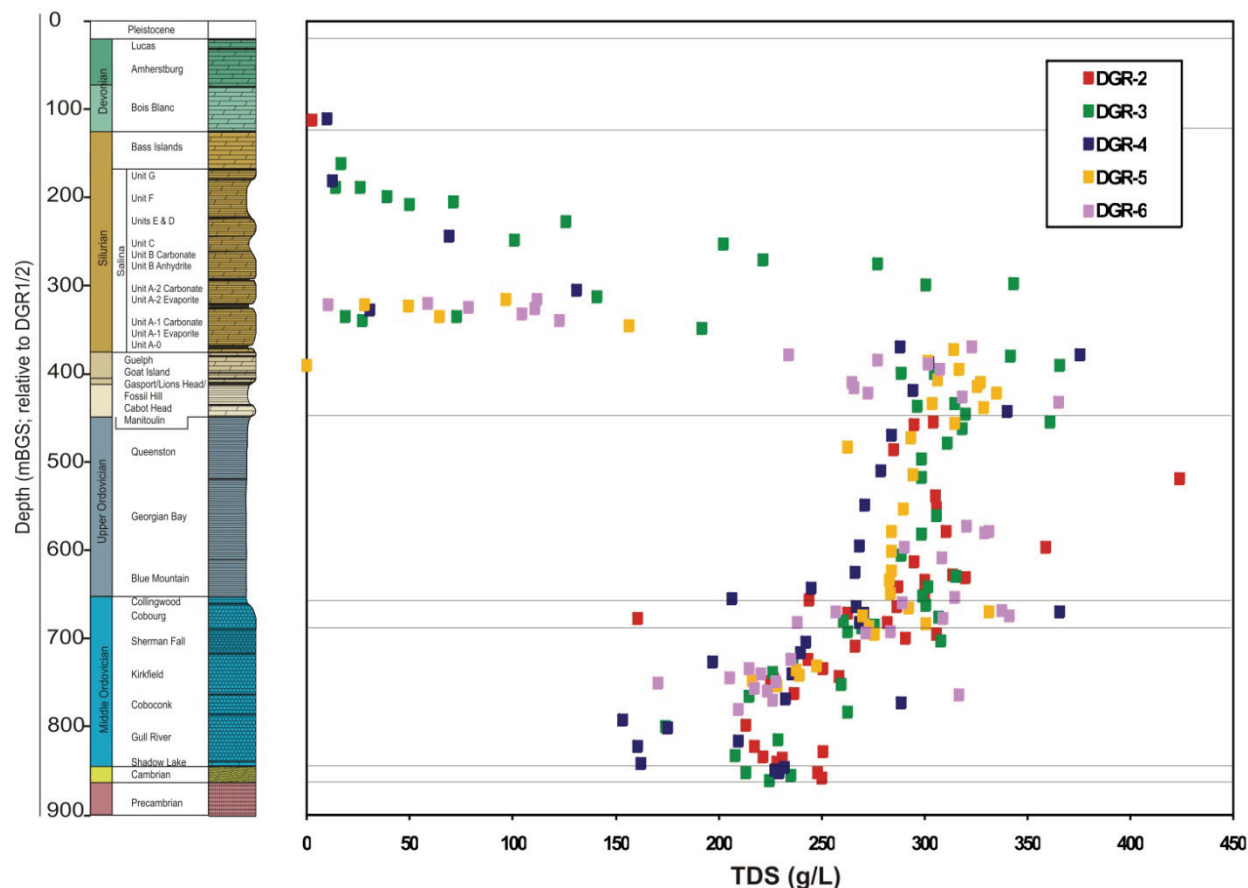


Figure 4.6: TDS versus Depth for DGR Boreholes

Table 4.2: TDS, Water Type and pH with Depth in the Sedimentary Formations

HS Unit	Depth (mBGS)	TSD (mg/L)	Water Type	pH
1: Overburden Aquitard	0-20	<500	Ca, Na-HCO <sub>3</sub>	7-8
2: Dolostone Aquifer	20-169.3	500 to 5000	Ca,Mg-HCO <sub>3</sub> to Ca-SO <sub>4</sub>	7-8
3: Silurian Aquitards	169.3-447.7	10,000 to 350,000	Ca-SO <sub>4</sub> to Na-Cl	7
4A: Silurian Aquifer	325.5-328.5	30,000	Na-Cl	7.1
4B: Silurian Aquifer	374.5-380.0	370,000	Na-Cl	6.8
5: Ordovician Shale Aquiclude	447.7-659.5	300,000	Na-Cl	
6: Ordovician Carbonate Aquiclude	659.5-762.0	230,000 to 270,000	Na-Cl	
7: Ordovician Carbonate Aquitard	762.0-838.6	200,000 to 230,000	Na-Cl	
8: Cambrian Aquifer	838.6-860.7	225,000 to 235,000	Na,Ca-Cl	6-7
9: Precambrian Aquitard	>860.7	50,000 to 350,000	Ca,Na-Cl	6

Notes: Modified from Table 4.17 of INTERA (2011).

#### 4.4.1 Natural Tracers

One of the principal objectives in obtaining site-specific geochemical data for the groundwater and porewater is to place constraints on the residence time of the water and the processes that contribute to solute transport. From this perspective, naturally occurring tracers have great value, particularly when it can be reasonably assumed that the tracers behave conservatively. Although it is unlikely that there is such a thing as a perfectly conservative tracer, those that are expected to approach conservative character are the stable isotopes of water ( $^{18}\text{O}$ ,  $^2\text{H}$ ) and Br. In most systems, Cl would also be considered conservative; however, Cl may not behave conservatively in the Michigan Basin waters because of precipitation-dissolution reactions involving halide minerals, particularly halite. Profiles of the stable water isotopic data below the Bruce nuclear site are presented in Figure 4.7 and the Cl and Br profiles are presented in Figure 4.8. The analytical precision for Br analyses is lower for samples from DGR-2 compared to samples from DGR-3 through DGR-6, which explains the greater scatter in the DGR-2 Br data. Bromide in DGR-2 samples was determined using ion chromatography, and precision was improved for analysis of porewaters from DGR-3 through DGR-6 by using inductively coupled plasma mass spectrometry (ICP-MS).

Trends in the data should be considered in terms of deviations from some initial baseline condition. For these tracers, that condition could be considered to be their respective concentrations in the ancient evaporated sea water from which the Michigan Basin brines are thought to have been derived (Wilson and Long 1993a, b). The range of tracer values in the Upper Ordovician Queenston and Georgian Bay shales are a reasonable approximation for evaporated sea water that has been modified somewhat by diagenetic processes. The Upper Ordovician shale porewater values for  $\delta^{18}\text{O}$  (-3 to -4‰) are more depleted than might be expected, perhaps due to water-rock interaction processes, and the baseline  $\delta^{18}\text{O}$  is probably better represented by a value closer to -2‰ for all of the sedimentary formations (Graf et al. 1965, Dollar 1988, Wilson and Long 1993a, b). An initial Cl concentration of 6 to 7 mol/kgw is proposed for the Silurian and Devonian fluids to represent evaporated sea water, and an initial Cl concentration of 0.6 mol/kgw is suggested for the Ordovician and Cambrian formation fluids as a representation of normal marine sea water. The baseline values are assigned to maintain consistency with the evolutionary history of the Michigan Basin, as outlined in Section 4.3. The tracer data include the following features:

- There is a large decrease for all tracers from the Guelph Formation upward through the Silurian;
- There is a persistent trend toward depleted  $\delta^{18}\text{O}$  values, reduced Cl and Br concentrations, and a minor increase in  $\delta^2\text{H}$  values with depth below the Ordovician shale; and
- The trends with depth toward depleted  $\delta^{18}\text{O}$  values, and reduced Cl and Br concentrations, below the Ordovician shale, are interrupted at the Cambrian where the tracer values become more enriched relative to the overlying Black River Group fluids.



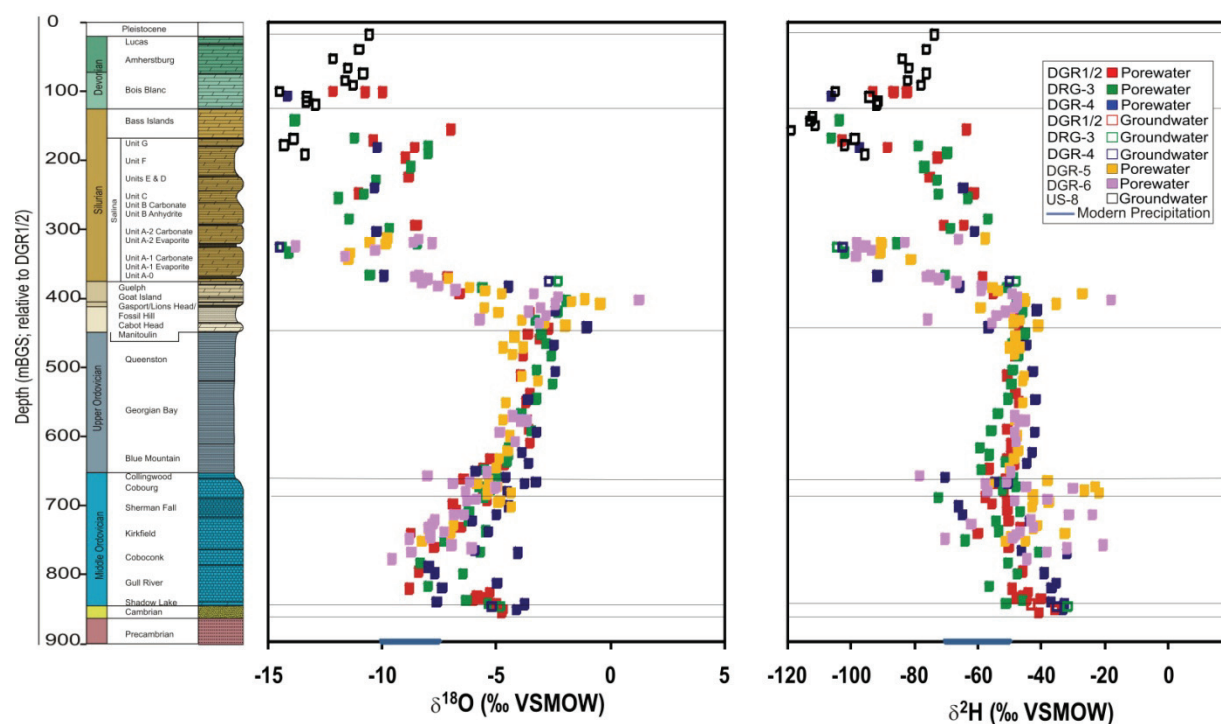


**Figure 4.7: Vertical Depth Profiles for Natural Tracers  $^{18}\text{O}$  and  $^2\text{H}$  Determined in Porewater and Groundwater**

The  $\delta^{18}\text{O}$  and  $\delta^2\text{H}$  profiles in the Silurian and Devonian stratigraphic units provide evidence for infiltration of some combination of glacial melt water and warmer climate water during glacial and interglacial periods, presumably during the Pleistocene. The occurrence of  $^{18}\text{O}$ - and  $^2\text{H}$ -depleted water ( $\delta^{18}\text{O}$  of  $-14.5$  and  $\delta^2\text{H}$  of  $-110$ ‰, respectively) in a thin aquifer at approximately 328.5 m depth in the Silurian Salina A1 carbonate unit (Figure 4.7) is indicative of the presence of glacial melt water and represents the maximum depth of glacial melt water infiltration observed at the Bruce nuclear site. The presence of high hydraulic conductivity ( $K_H$ ) zones in the Silurian (see Figure 5.1), and the corresponding abrupt variations in tracer profiles with depth through the Silurian sediments, suggest that dilution may have occurred by a combination of advective mixing and diffusion. Little is known about the erosion rate and timing of exposure of the Devonian rocks in southern Ontario to infiltrating surface water. If something close to the present-day erosion level was exposed during the Pleistocene, then the cyclic nature of glacial-interglacial periods in the past 1 to 2 Ma (Figure 4.1b) would have resulted in repeated infiltration events in the Devonian (and possibly Silurian) stratigraphy of southern Ontario, with subsequent diffusive equilibration of the formation waters in the low- $K_H$  sediments with fresh water during interglacial periods. These processes may explain the depletion trends for  $\delta^{18}\text{O}$  and  $\delta^2\text{H}$ , and the decreased Cl and Br concentrations (salinity) that are observed above the Silurian Guelph Formation (Figure 4.8).

With increasing depth, the general trend in the data in the Middle Ordovician is toward a gradual decrease in  $\delta^{18}\text{O}$  values and decreasing salinity. Coincident with the decreasing  $\delta^{18}\text{O}$  values, there is a minor increase in  $\delta^2\text{H}$  values (Figure 4.7). In contrast with the tracer profiles in the

Silurian, the very low  $K_H$  values in the Ordovician limestone (see Figure 5.1), and the smooth nature of the downward depletion trends, suggest that diffusion dominates in the Ordovician. The time period required to form such trends in the profiles by diffusion is expected to be on the order of tens to hundreds of millions of years, and is discussed in more detail in Section 4.5.

The profiles change in the groundwater and porewater within the Cambrian sandstone, where tracer concentrations shift back toward values similar to Cambrian groundwater sampled from southwestern Ontario oilfields (Figures 4.3a and 4.4a). Further discussion of the chemical signature in the Cambrian at the Bruce nuclear site is presented in Section 4.5.4.

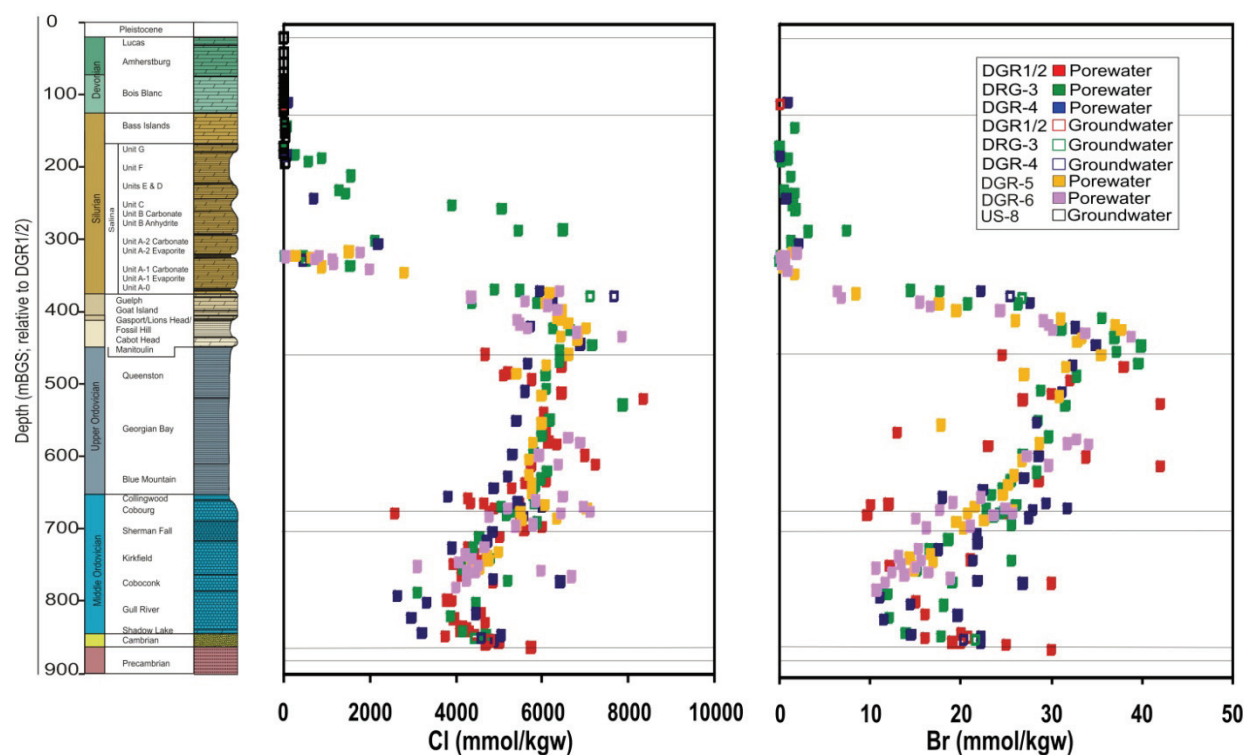


**Figure 4.8: Vertical Depth Profiles for Natural Tracers Cl and Br Determined in Porewater and Groundwater**

#### 4.4.1.1 Water-rock Interaction

Water-rock interaction must be considered as a possible explanation for the observed  $\delta^{18}\text{O}$  and  $\delta^2\text{H}$  profiles versus depth. At elevated temperatures, reactions with calcite and illite-smectite clays could lead to an increase in  $\delta^{18}\text{O}$  values (as is commonly observed in sedimentary basin brine), but such reactions cannot easily explain the decrease in  $\delta^{18}\text{O}$  to values as low as  $-8.78\%$  in the Middle Ordovician carbonates. INTERA (2011; their Figure 3.5) demonstrates that the dolomite content in the Middle Ordovician limestone increases versus depth, coincident with the decrease in  $\delta^{18}\text{O}$  values versus depth. If we assume that the porewater in the system is static, a very long porewater residence time is available and it may be possible that the observed  $\delta^{18}\text{O}$  profiles have evolved in response to isotopic equilibration with dolomite. Using  $\delta^{18}\text{O}$  values for Middle Ordovician dolomite provided by Coniglio and Williams-Jones (1992) and dolomite-water

fractionation factors from Vasconcelos et al. (2005) and Chacko and Deines (2008), the isotopic composition of porewater in equilibrium with dolomite can be calculated over a reasonable temperature range (25 to 45°C). Results of these calculations indicate that equilibration with dolomite could result in porewater  $\delta^{18}\text{O}$  values from -13.1 to -2.7‰. These results suggest that isotopic equilibration with dolomite might explain the observed decrease in  $\delta^{18}\text{O}$  values versus depth.

Although water-rock interaction might provide an explanation for the decrease in the  $\delta^{18}\text{O}$  profile, it is not apparent that water-rock interactions could explain the observed  $^2\text{H}$ -enrichment versus depth in the Middle Ordovician. It is well known that  $^2\text{H}$  partitions preferentially to the fluid during mineral hydration reactions (e.g., feldspar to clay transformations) (Clark and Fritz 1997) and this fractionation may have operated throughout the Ordovician units as detrital feldspars were altered to clay minerals. However, mass-balance requirements suggest that any resulting  $^2\text{H}$  enrichment of the porewater should be proportional to the ratio of sheet-silicate content to porosity. INTERA (2011; their Figure 3.7) presents analyses of illite and chlorite content, and there is no significant increase in sheet-silicate content versus depth in the Middle Ordovician as would be expected if mineral hydration reactions were responsible for the observed  $^2\text{H}$  enrichment in the porewater.

#### 4.4.1.2 Fluid Mixing

In contrast to water-rock interaction, the Middle Ordovician trends for all tracer profiles could result from one or more mixing events with water at depth that is relatively depleted in  $^{18}\text{O}$ , has low Cl and Br concentrations, and is enriched in  $^2\text{H}$ . This could not be the brine that is currently contained in the Cambrian sandstone because it has a higher salinity and more enriched isotopic composition than the porewater in the Middle Ordovician carbonates (Figures 4.7 and 4.8). However, the relatively high permeability in the Cambrian sandstone could have allowed changes in the groundwater composition at some point in the geologic past, provided the appropriate driving mechanism(s) for fluid migration were present.

The question arises as to whether groundwater in the Cambrian aquifer, or groundwater in the underlying shield, could have provided a suitable end member to generate these mixing trends. The current state of knowledge regarding groundwater in the Precambrian shield is discussed in Section 4.4.6.

#### 4.4.2 Major Ions

The major ion data are affected by several artifacts which limit the ability to present sound interpretations. INTERA (2011) demonstrates that the results of major ion analyses from the crush and leach method underestimate porewater concentrations in shale-rich samples, possibly a result of ion exclusion effects. The magnitude of this artifact is likely different for each rock core sample, making it difficult to correct the porewater concentrations within the shales. Also, the reported concentrations of the major ions from all sedimentary fluids account for mineral dissolution for calcite and anhydrite only, which may neglect other major mineral phases and their relative effects on solubility, dissolution, and equilibrium states (i.e., dolomite).

Dissolution of anhydrite and calcite contribute excess calcium (Ca) and sulphate ( $\text{SO}_4$ ) to the porewater, and geochemical modelling has been used to correct the porewater concentrations by calculating the reduction in Ca and  $\text{SO}_4$  concentrations necessary to bring the solutions to equilibrium with respect to anhydrite and calcite. There are also indications in the leach data that the concentration of potassium (K) is overestimated, probably as a result of ion exchange

processes operating during the leaching process. Magnesium (Mg) porewater and groundwater concentrations are similar in the Salina Upper A1 Unit, the Guelph Formation, and the Cambrian permeable horizons. However, there is considerable scatter observed in Mg concentration profiles for the Ordovician limestones. The scatter may be due to the assumption that the porewaters are in equilibrium with calcite and not Mg-bearing calcite or dolomite. Using only calcite as the equilibrium phase does not correct for Mg added to the leach water during the porewater characterization process, which may overestimate the Mg concentrations. Confidence in Ca, Mg, K and SO<sub>4</sub> data is judged to be low due to potential effects of dissolution of anhydrite, gypsum and celestite, interaction with clays, and oxidation of pyrite during leaching experiments. These artifacts suggest that the data for Ca, Mg, K and SO<sub>4</sub> should be interpreted with caution and these data will not be discussed further in this hydrogeochemical synthesis. Discussion of these major ion data, as they relate to data quality, data use, and porewater characterization, is presented in the DGSM (INTERA 2011).

Contribution of solutes from soluble minerals to the leachable ion fraction is an artifact that affects the ability to interpret the major ion data. Halite dissolution is evident in several locations, particularly in the Georgian Bay and Queenston formations, where anomalously high Na and Cl concentrations occur.

With the exception of those limited cases where halite dissolution has influenced the leach data, the Cl/Br ratios should be reliable. The relatively constant Cl/Br ratios in the Ordovician and Cambrian rocks suggest that halite dissolution does not have a significant influence on the Cl concentration in the porewater (Figure 4.9). The elevated Cl/Br ratios in the Salina Group suggest that these porewaters have been influenced by halite dissolution.

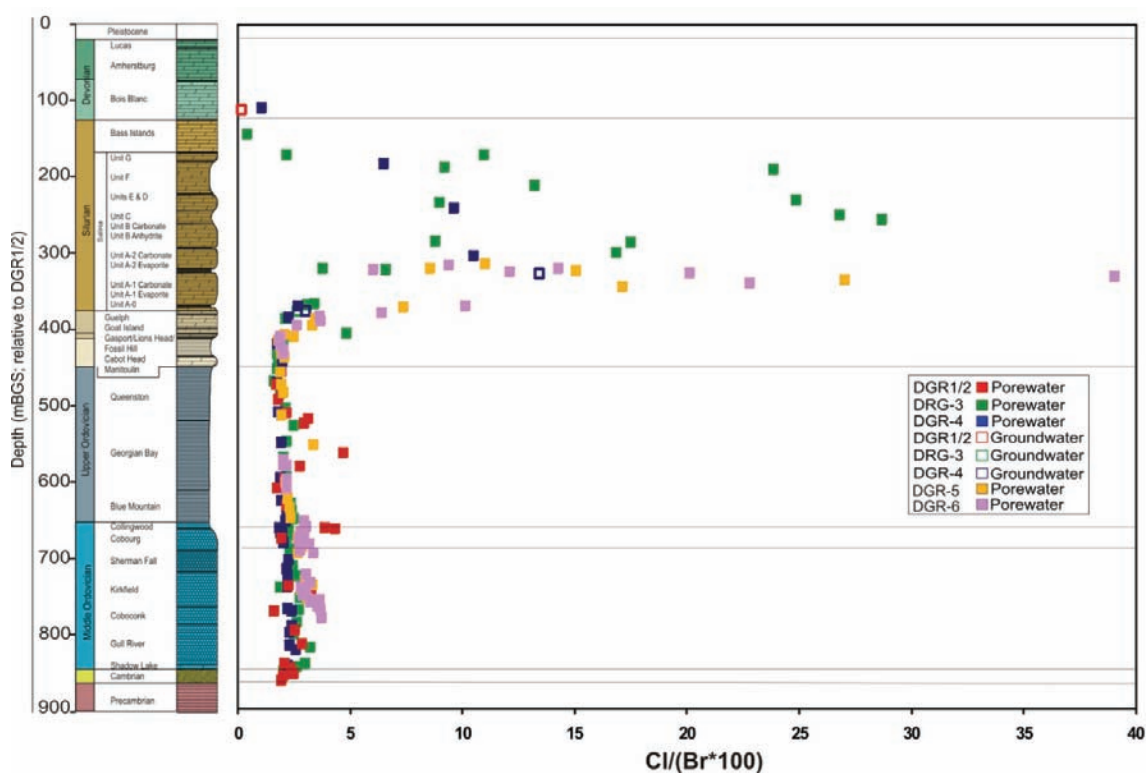


Figure 4.9: Cl/Br Ratios versus Depth for DGR Boreholes

INTERA (2011) reports sporadic occurrences of halite within the Ordovician core below the Cobourg Formation. They suggest that much, if not all, of the halite detected in the Middle Ordovician samples could have precipitated as a result of porewater evaporation during sample preparation. At least one halite occurrence in the Gull River Formation (Herwegh and Mazurek 2008), however, is thought to be naturally occurring and unrelated to sample preparation. The presence of halite suggests that hypersaline brine was present at depth within the Middle Ordovician at some time in the geologic past.

#### 4.4.3 Gas Characterization

Methane (CH<sub>4</sub>), carbon dioxide (CO<sub>2</sub>) and helium (He) were extracted from samples of groundwater and core for highly permeable and less permeable sections, respectively, of the stratigraphy below the Bruce nuclear site (Clark et al. 2010a, 2010b). The isotopic ratios  $\delta^{13}\text{C}$  (CH<sub>4</sub> and CO<sub>2</sub>),  $\delta^2\text{H}$  (CH<sub>4</sub>) and  $^3\text{He}/^4\text{He}$  were determined for the gases. In the cases where the gases were extracted from core, the gas concentration data could be presented in terms of: 1) the mass of gas per mass of porewater, or 2) the mass of gas per mass of rock. The former approach is generally preferred, and was adopted for normalization of the DGR concentration data, because it accounts for variable porosity in the rocks and provides a concentration measure that can be useful to assess the potential for diffusive transport. The approach of normalizing the total mass of extracted gas to the porewater content does not provide an accurate measure of dissolved gas content in cases where gas occurs in other forms, such as in a separate gas phase, dissolved in liquid hydrocarbons, or sorbed to solid forms of organic carbon. However, concentrations expressed as mass of gas per mass of water can be compared to the solubility limits for the gases in brine; values in excess of the solubility limits provide evidence for the presence of either a separate gas phase or gas in association with solid organic carbon or liquid hydrocarbons.

##### 4.4.3.1 Methane and Carbon Dioxide

The CH<sub>4</sub> and CO<sub>2</sub> data are reported in units of mmol/kgw but, as discussed in Section 4.4, they should not be considered to be exactly equivalent to porewater aqueous concentrations. The concentrations of CH<sub>4</sub> and CO<sub>2</sub>, and the respective stable isotopic data, are presented in Figures 4.10 and 4.11. There are a number of features observed consistently in the CH<sub>4</sub> data from the DGR drill cores.

- Low CH<sub>4</sub> concentrations are observed near the surface and down to a depth of approximately 300 mBGS, which corresponds to the top of the Upper Silurian Salina A2 Unit.
- Elevated CH<sub>4</sub> concentrations occur in proximity to the hydrocarbon-containing Guelph Formation (375 to 410 mBGS; Obermajer et al. 2000). The overlying Salina A1 and A2 units may represent a low-permeability barrier to gas transport upward from the Guelph Formation. Core samples of the dolomite, argillaceous dolomite, and anhydritic dolomite from the Salina A1 and A2 units are described as being “unfractured to sparsely fractured with excellent core quality” (INTERA 2011).
- The CH<sub>4</sub> concentration increases gradually downward through the Ordovician Queenston Formation shale and then remains at a near constant value through the Georgian Bay Formation shale.
- There is a pronounced increase in the CH<sub>4</sub> concentration in the interval represented by the Blue Mountain Formation shale and the Collingwood Member (617 to 660 mBGS).

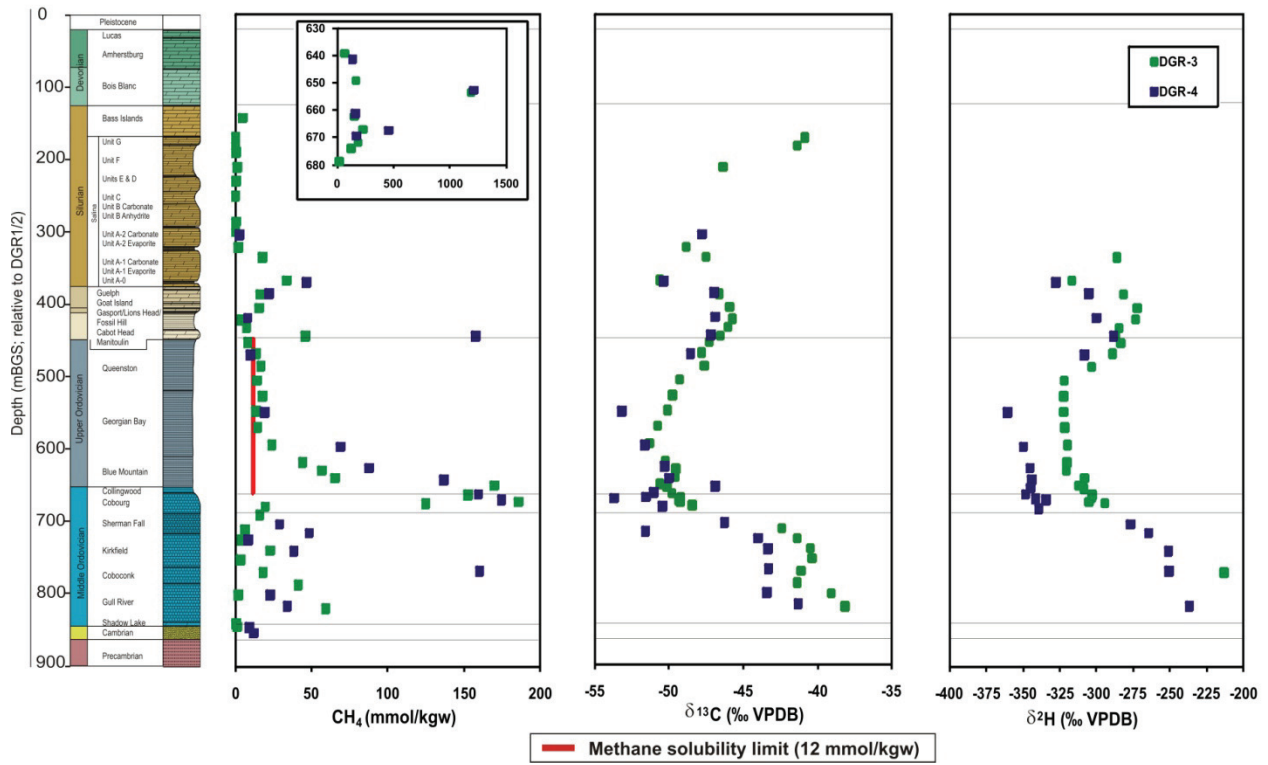


Figure 4.10: Concentration Distributions for CH<sub>4</sub> (mmol/kgw) versus Depth in DGR-3 and DGR-4, and Corresponding Distributions of δ<sup>13</sup>C and δ<sup>2</sup>H in CH<sub>4</sub>

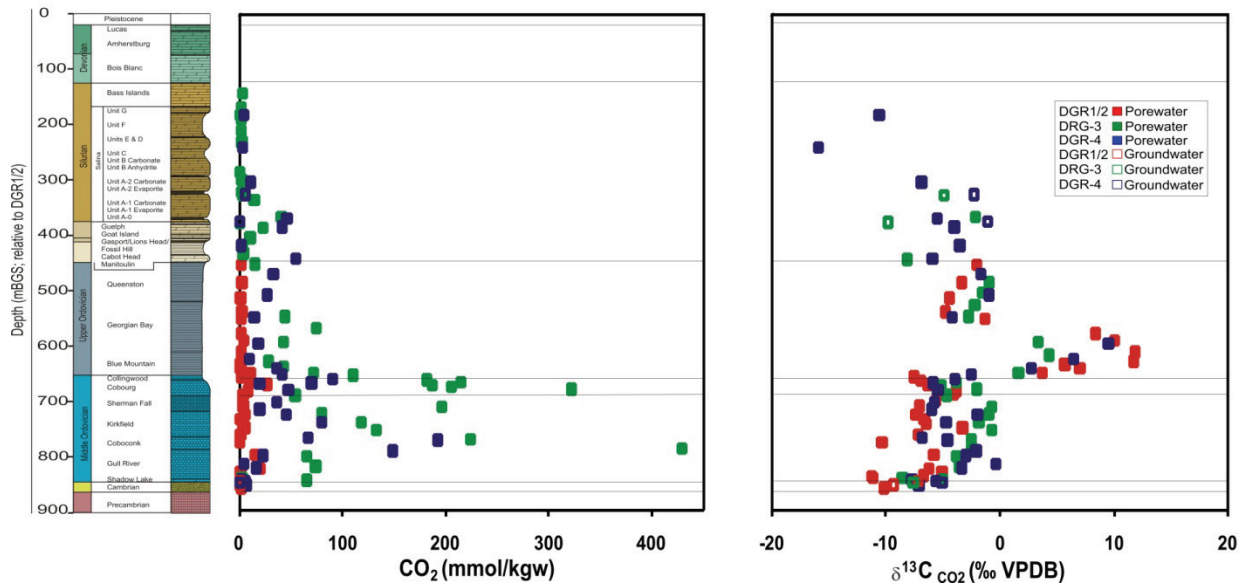


Figure 4.11: Concentration Distribution for CO<sub>2</sub> (mmol/kgw) versus Depth (left), and Corresponding Distributions of δ<sup>13</sup>C in CO<sub>2</sub> (right)

- The CH<sub>4</sub> concentration in the Middle Ordovician limestones and the underlying Cambrian sandstone is low relative to the overlying Blue Mountain shale and the Collingwood Member, but there are localized zones with elevated CH<sub>4</sub> content similar to that observed in the Silurian Guelph Formation.

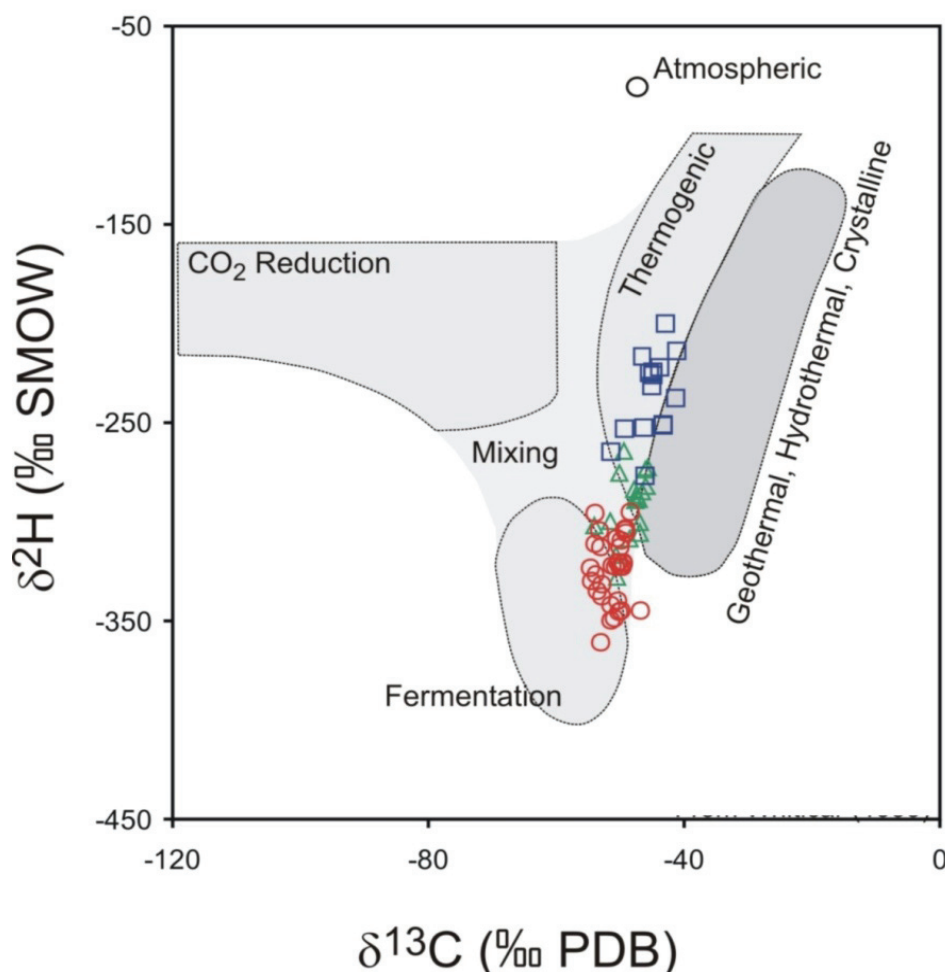
The CO<sub>2</sub> data (Figure 4.11) display a step-wise increase, with the lowest concentrations occurring from surface downward to the Guelph Formation, intermediate concentrations from the top of the Guelph Formation down to the bottom of the Blue Mountain Formation shale, and highest concentrations in the Middle Ordovician carbonates.

The stable isotope data provide important insight into the origin of the CH<sub>4</sub>. The  $\delta^{13}\text{C}$  and  $\delta^2\text{H}$  data for CH<sub>4</sub> display a clear separation between the Upper Ordovician shales and the Middle Ordovician carbonates (Figure 4.10). This type of systematic variation has been used to distinguish between biogenic and thermogenic origins for CH<sub>4</sub> (Whiticar 1999). The stable isotope data from CH<sub>4</sub> have been plotted on the variation diagram from Whiticar (1999) and they define two fields: one field represents CH<sub>4</sub> of biogenic origin in the Upper Ordovician shales and the Cobourg Formation, and a second field represents CH<sub>4</sub> of thermogenic origin in the remainder of the Middle Ordovician carbonates (Figure 4.12). These indications that CH<sub>4</sub> in the Upper Ordovician shales and Cobourg Formation is of biogenic origin are supported by the  $\delta^{13}\text{C}$  data for CO<sub>2</sub> (Figure 4.11). The CO<sub>2</sub> residual in a system following biogenic CH<sub>4</sub> generation is expected to be enriched in  $\delta^{13}\text{C}$ , and the zone of enriched  $\delta^{13}\text{C}$  in CO<sub>2</sub> observed in the Blue Mountain Formation shale (Figure 4.11) corresponds closely to the zone of biogenic CH<sub>4</sub> formation that is inferred from the stable-isotope composition of CH<sub>4</sub> (Figures 4.10 and 4.12).

The generation of thermogenic gas requires temperatures in excess of 70°C (Hunt 1996), and such a condition has probably not prevailed since maximum burial in the Carboniferous. It is therefore likely that the thermogenic gas is very old, and could be of in situ or allochthonous origin, or a combination of both. The age of the biogenic CH<sub>4</sub> contained in the Ordovician rocks is unknown, but some insight can be gained by considering two alternative interpretations:

- All of the extracted gas was originally dissolved in the porewater; or,
- A fraction of the extracted gas was dissolved in the porewater and the remainder was present as a discrete gas phase, and/or sorbed to solid organic carbon, and/or dissolved in petroleum hydrocarbons.

If the system is 100% brine saturated and all of the gas was dissolved in the porewater, the profile would be interpreted in terms of large CH<sub>4</sub> concentration gradients directed upward and downward from the Blue Mountain. These gradients would drive diffusion of biogenic CH<sub>4</sub> upward and downward from the source region in the Blue Mountain shale. Under these conditions, the biogenic production would be relatively recent or the large CH<sub>4</sub> peak (Figure 4.10) would have been attenuated by diffusion over time. In addition, if the biogenic gas is young, or perhaps even accumulating via methanogenesis at the present time, then there should be viable and active methanogens in the Blue Mountain shale. The presence of active methanogens is highly unlikely due to the high salinities and low water activities (0.6 to 0.7) measured in the Ordovician sediments. A preliminary microbiological investigation did not find evidence of active methanogens within the Ordovician sediments (Stroes-Gascoyne and Hamon 2008), suggesting that microbes, if present within the sediments at depth, are most likely in a dormant state. It should be noted that only two samples were analyzed for the microbiological study - one from the Queenston Formation above the methanogenic zone, and one from the Cobourg Formation limestone.



Notes: Green triangles represent data from the Queenston Formation and above, red circles from the Cobourg, Blue Mountain and Georgian Bay formations, and the blue squares from below the Cobourg Formation. From Whiticar (1999).

**Figure 4.12: Discrimination Diagram Indicating Fields for CH<sub>4</sub> of Biogenic (CO<sub>2</sub> Reduction and Fermentation) and Thermogenic Origin**

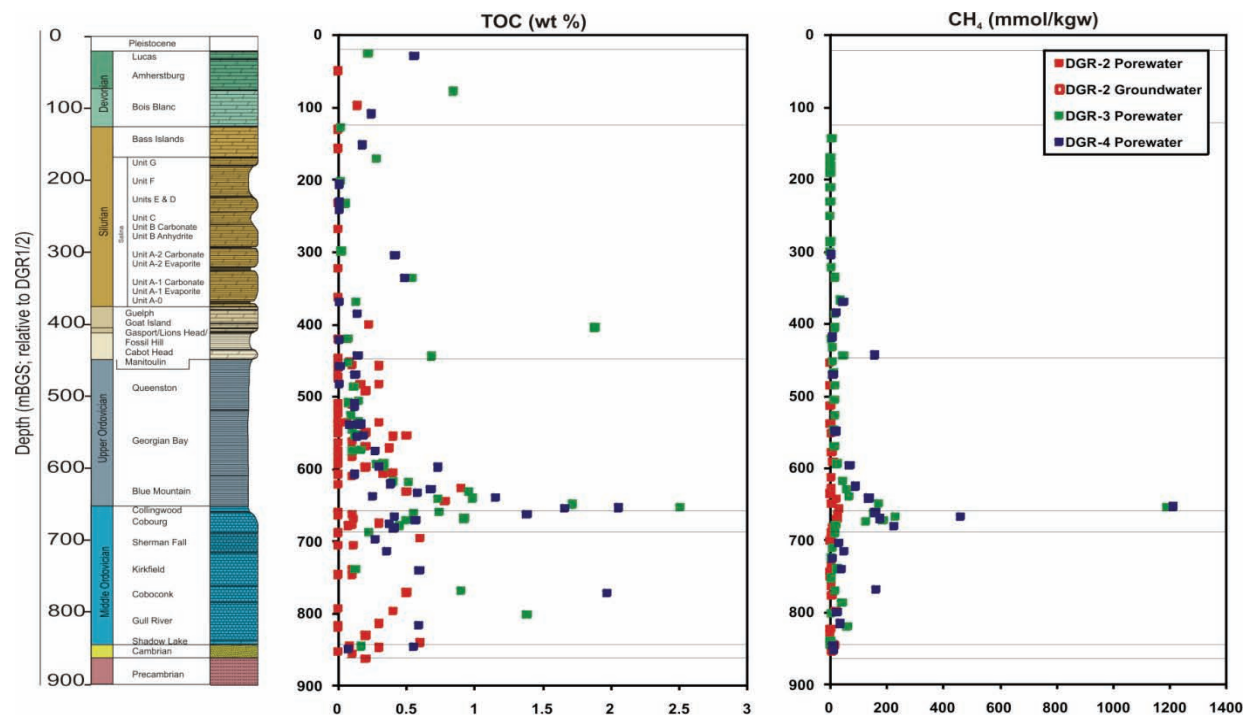
The alternative interpretation, that the biogenic gas is relatively old and immobile, is supported if it can be shown that the aqueous CH<sub>4</sub> concentrations are at saturation in the porewater throughout the Ordovician, in which case there is no vertical concentration gradient to drive migration of gas by diffusion. This is possible if sections of the profiles with elevated CH<sub>4</sub> content can be explained either by the presence of a discrete gas phase, or by the partitioning of CH<sub>4</sub> into solid organic carbon or liquid hydrocarbons. The solubility limit for CH<sub>4</sub> in brine as a function of pressure and temperature has been investigated by Duan and Mao (2006). Their calculations indicate a solubility of 12 mmol/kgw at 5.0 MPa and 30°C in 6 mol NaCl/kgw. These conditions are representative of the Blue Mountain Formation where the current pressure and temperature are approximately 5.5 MPa and 20-25°C and the porewater is near saturation with respect to halite. Therefore, 12 mmol/kgw can be considered as an upper limit on CH<sub>4</sub> solubility, and where the CH<sub>4</sub> concentrations exceed 12 mmol/kgw, CH<sub>4</sub> may occur in a



separate gas phase or in association with organic carbon or liquid hydrocarbons. The  $\text{CH}_4$  concentrations exceed 12 mmol/kgw in the Collingwood Member, the Blue Mountain Formation shale, and, in most samples obtained from the Georgian Bay Formation shale and the lower portion of the Queenston Formation shale (Figure 4.10). INTERA (2011) reports solid organic carbon contents equal to or less than 0.5 wt% in Ordovician units, with the exception of the Blue Mountain Formation and the Collingwood Member where the organic carbon content increases to 2.5 wt%. Considering the  $\text{CH}_4$  data, as well as the distribution of solid organic carbon (Figure 4.13) and the results of petrophysical analyses (INTERA 2011), it appears that the elevated  $\text{CH}_4$  concentrations can be explained by a combination of sorption on organic carbon and localized occurrences of a separate gas phase. Therefore, equilibrium partitioning between the aqueous, sorbed and gas phases is expected and the porewater should be saturated with respect to  $\text{CH}_4$ . Under such conditions, the aqueous concentration gradient goes to zero and there is no driver for diffusion of aqueous  $\text{CH}_4$ .

Although the diffusion of aqueous  $\text{CH}_4$  may be limited due to the absence of a vertical concentration gradient, vertical gradients in the  $^{13}\text{C}$  and  $^2\text{H}$  isotopic compositions do exist (Figure 4.10) and would be expected to drive diffusion in the vertical direction. There are at least two possible explanations for the apparent retardation of diffusive transport.

- Sorption and dissolution/exsolution reactions between  $\text{CH}_4$  and solid organic carbon, or liquid hydrocarbons, respectively, cause a decrease in apparent diffusion coefficients ( $D_a$ , which include a retardation term for sorption/dissolution/exsolution processes; Choi and Oscarson 1996). Schloemer and Krooss (1997, 2004) report that  $D_a$  for  $\text{CH}_4$  in shale is strongly dependent on organic carbon content and temperature. At 150°C, they report a ten-fold decrease in  $D_a$  for  $\text{CH}_4$  between shale with essentially no organic matter and shale with 5% organic content. At 90°C, the effect is stronger, with a decrease of two orders of magnitude between shale with essentially no organic matter and shale with 2.2% organic content. This temperature effect reflects the temperature dependence of the partitioning coefficient for  $\text{CH}_4$  between water and organic carbon. As noted above, INTERA (2011) reports a maximum solid organic carbon content of approximately 2.5 wt% in the Collingwood Member (Figure 4.13). The temperature at this depth is approximately 20-25°C, and based on the results from Schloemer and Krooss (1997, 2004), a decrease in  $D_a$  of at least two orders of magnitude compared to an organic-free shale is expected in the Collingwood Member.
- Infill of porosity in the Cobourg Formation by precipitation of secondary minerals would also act to inhibit solute transport. It is possible that at some point in the geologic past, fluid mixing within the Cobourg Formation and overlying shales resulted in secondary mineral precipitation. The mixing of fluids could have occurred following compaction of the shales, for example, during periods of basin subsidence; saline fluids expelled from the shales would have mixed with the carbonate porewater(s). During mixing, saturation can be exceeded with respect to minerals such as anhydrite and halite, and the resulting secondary minerals formed occlude porosity and lower the rock permeability as well as  $D_e$ . This hypothesis is consistent with results of mineralogical analyses which indicate that halite is present within the matrix and pore spaces in the Ordovician shales as well as the Cobourg Formation limestone (see Section 2.3.7).



Notes: There is a correspondence between peak TOC and elevated  $\text{CH}_4$  in the Blue Mountain Formation and in the Collingwood Member.

**Figure 4.13: TOC and  $\text{CH}_4$  Concentrations with Depth in DGR-2, DGR-3, and DGR-4**

The observed separation of biogenic gas above, from thermogenic gas below, provides evidence that there has been little or no cross-formational mixing by advection while the gas was resident in the system. It appears that neither the biogenic nor the thermogenic gas is mobile, at least in the vertical direction, and this immobility may reflect slow accumulation over a very long period of time. Given that high salinities and low water activities appear to inhibit microbial activity within these sediments, it may be that the biogenic gas is of Paleozoic age.

#### 4.4.3.2 Helium

Profiles of  $^3\text{He}/^4\text{He}$  for DGR-2, DGR-3 and DGR-4 are presented in Figure 4.14. The data are presented as the isotope ratio in the sample ( $R_s$ ) normalized to the isotope ratio in air ( $R_a$ ) such that  $xR_a = R_s/R_a$ . The data are remarkably consistent among the three drill cores, and they define two distinct regions of differing isotope ratio separated at the base of the Cobourg Formation, with  $xR_a$  of approximately 0.02 within and above the Cobourg Formation, and  $xR_a$  of approximately 0.035 below. Consistent with observations from the  $\text{CH}_4$  and  $\text{CO}_2$  data, the clear separation between regions of differing He isotope composition indicates that there has been very little cross-formational mixing of helium between the Middle Ordovician limestones and the Upper Ordovician shales.

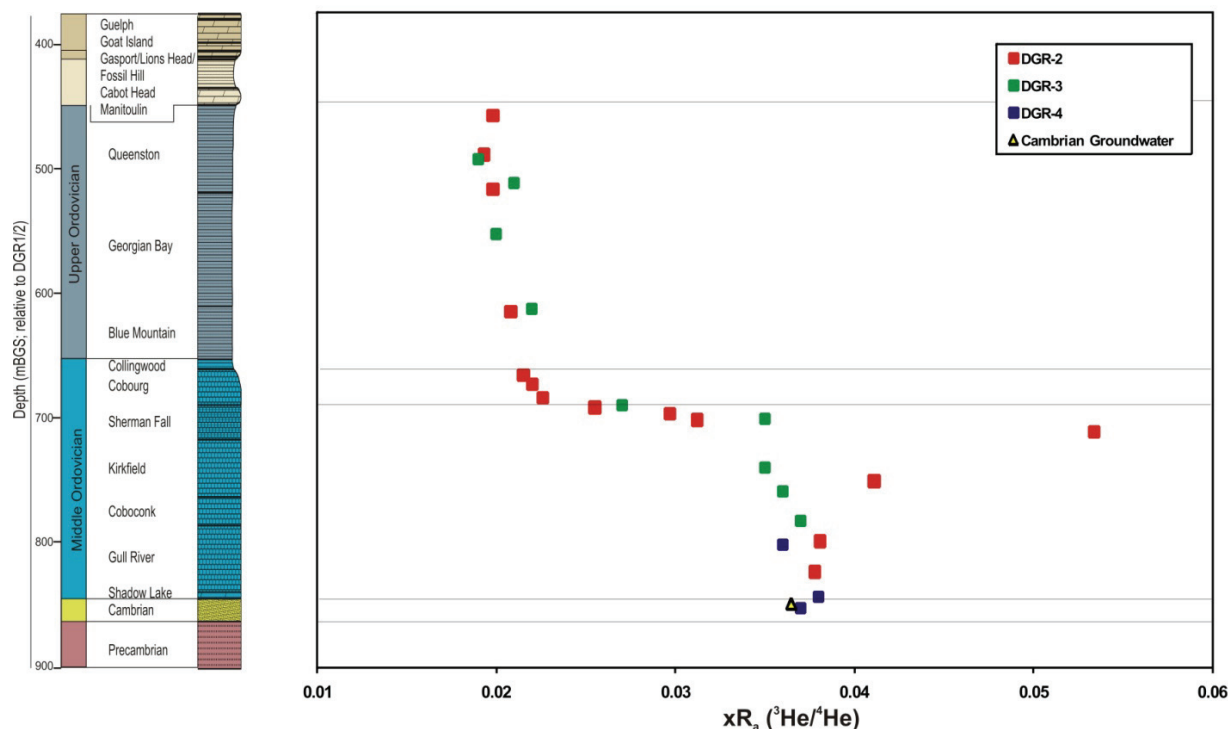


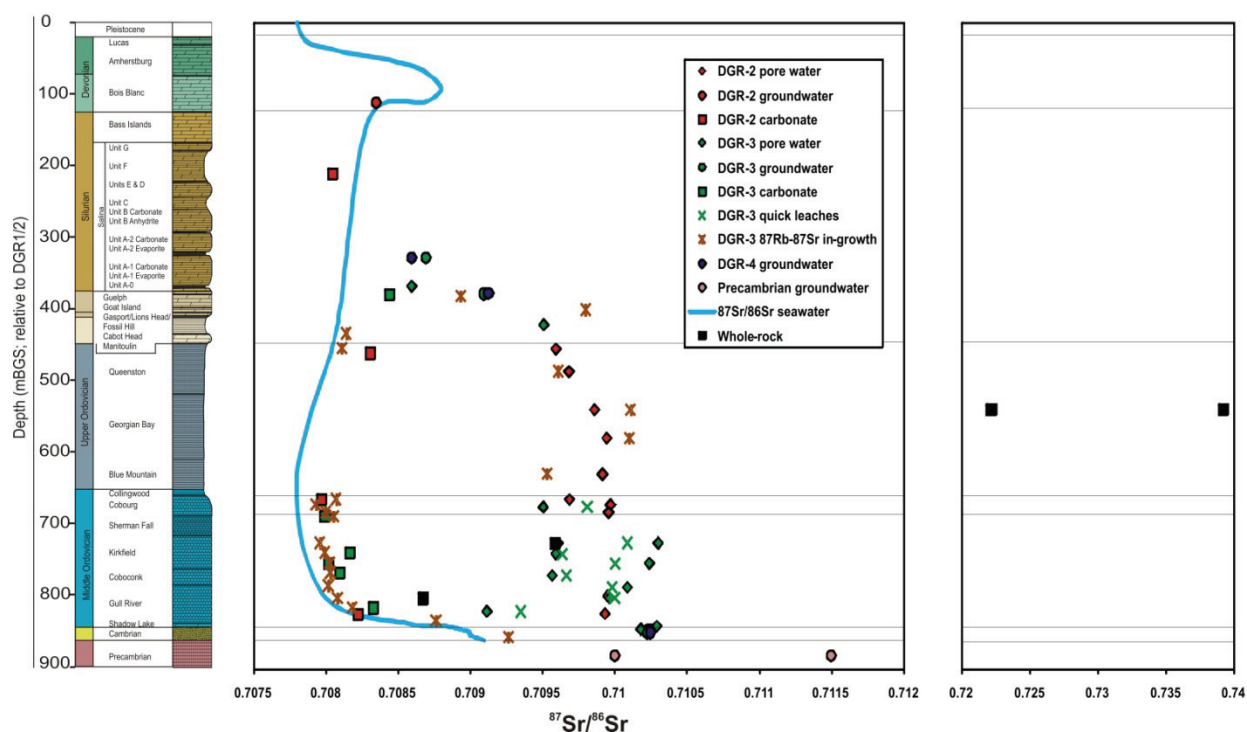
**Figure 4.14: Vertical Profiles of Helium Isotopic Ratios ( $^3\text{He}/^4\text{He}$ ) from DGR-2, DGR-3 and DGR-4**

Similar to the inferences made above regarding  $\text{CH}_4$  mobility, the apparent lack of vertical mixing between He of differing isotopic compositions may in part be due to the lack of a vertical concentration gradient for He in the porewater. However, there is a gradient in the isotope concentrations, so isotopic diffusion is expected. Unlike the argument for  $\text{CH}_4$  retardation due to sorption on organics, He is considered to be a highly conservative tracer (Simon and Brusseau 2007) and its diffusion should not be significantly retarded by sorption processes. The solubility of He in crude oils, however, is higher than in water, and approximately 15 times higher than in high-TDS brine (Kharaka and Specht 1988). If liquid hydrocarbons are present (INTERA 2011), it is possible that dissolution of He in hydrocarbons causes retardation of diffusive transport. In addition, occlusion of pores by secondary mineral precipitation, as discussed in the previous section (Section 4.4.3), could also be responsible for the lack of He isotope transport.

#### 4.4.4 Strontium Isotopes

The  $^{87}\text{Sr}/^{86}\text{Sr}$  ratios in the porewater and the host rocks were determined by Clark et al. (2010a, 2010b). Sampling and analytical methods are presented and discussed by Clark et al. (2010a, 2010b). Consistent with the results for strontium (Sr) isotopic analysis of oilfield groundwater from the Michigan Basin reported by McNutt et al. (1987), the  $^{87}\text{Sr}/^{86}\text{Sr}$  ratios from Cambrian groundwaters and from the Ordovician porewaters at the Bruce nuclear site are more radiogenic than the Paleozoic seawater curve (Figure 4.15). With the exception of the Ordovician shale units, the  $^{87}\text{Sr}/^{86}\text{Sr}$  signatures of the porewater are more radiogenic than those of the host rocks. There are three possible explanations for the  $^{87}\text{Sr}$  enrichment in the porewater:

- Ingrowth of  $^{87}\text{Sr}$  from  $^{87}\text{Rb}$  decay since the Ordovician;
- Leaching of  $^{87}\text{Sr}$  from old shield-derived siliciclastic material in the shales and the argillaceous component of the limestones; and
- Transport of Sr upward from an  $^{87}\text{Sr}$ -enriched brine source in the underlying Precambrian shield.



Notes: The seawater  $^{87}\text{Sr}/^{86}\text{Sr}$  curve from Veizer and MacKenzie (2005) is shown for reference.

**Figure 4.15: Depth Profiles for  $^{87}\text{Sr}/^{86}\text{Sr}$  in Groundwater, Porewater and Host Rocks at DGR-2, DGR-3 and DGR-4**

Calculations suggest that the enriched  $^{87}\text{Sr}/^{86}\text{Sr}$  ratios observed in the porewater of the Ordovician shales could be derived by ingrowth via  $^{87}\text{Rb}$  decay, but only if all of the  $^{87}\text{Sr}$  was released to the porewater, which is unlikely. Whole-rock analyses of the Ordovician shales indicate that they are highly enriched in radiogenic  $^{87}\text{Sr}$  (Figure 4.15), suggesting that leaching of  $^{87}\text{Sr}$  from old shield-derived siliciclastic material contributes to  $^{87}\text{Sr}$  enrichment in the porewater.

The Rb content of the argillaceous carbonates is too low to explain the  $^{87}\text{Sr}$  enrichment in the Middle Ordovician porewater by ingrowth alone. A combination of ingrowth and leaching of  $^{87}\text{Sr}$  from shield-derived siliciclastic material is possible, but the  $^{87}\text{Sr}$  enrichment that would result might be expected to be proportional to the siliciclastic content of the enclosing rocks, and therefore the degree of enrichment in the argillaceous carbonate porewater should be lower than in the Upper Ordovician shale porewater. The  $^{87}\text{Sr}$  enrichment in the argillaceous

carbonates is quite variable (Figure 4.15) but it is not significantly lower than in the porewater in the shale. In fact, some of the limestone porewater samples from DGR-3 display the same degree of enrichment as the groundwater from the underlying Cambrian aquifer – the most enriched samples in the dataset. Highly radiogenic Sr signatures have been measured in Canadian Shield brines, and upward transport of  $^{87}\text{Sr}$  may have contributed to the observed enrichment in the Cambrian aquifer and in the porewater of the overlying Middle Ordovician carbonates. The observed  $^{87}\text{Sr}$  enrichment in the Ordovician must have resulted from some combination of the three processes described above, but the respective contributions cannot be resolved quantitatively. In any case, the presence of radiogenic Sr throughout the Ordovician indicates extremely long time periods for water-rock interaction and/or diffusive transport of radiogenic Sr upward from the shield.

Above the Guelph Formation aquifer, the  $^{87}\text{Sr}/^{86}\text{Sr}$  ratios for Silurian porewater and groundwater at the Bruce nuclear site approach the values of the enclosing host rock and the seawater curve. The convergence demonstrates the dominance of the Silurian sea water  $^{87}\text{Sr}/^{86}\text{Sr}$  signature in the evaporite minerals (anhydrite) and non-argillaceous limestones of the Salina Group. A significant decrease in Sr concentrations in the Upper Silurian and Devonian formations (Bois Blanc, A1 carbonate) is also observed (Figure 4.16), further demonstrating that the shallow groundwaters have been diluted, most likely due to the influx of glacial melt water and/or meteoric water in these relatively high permeability zones.

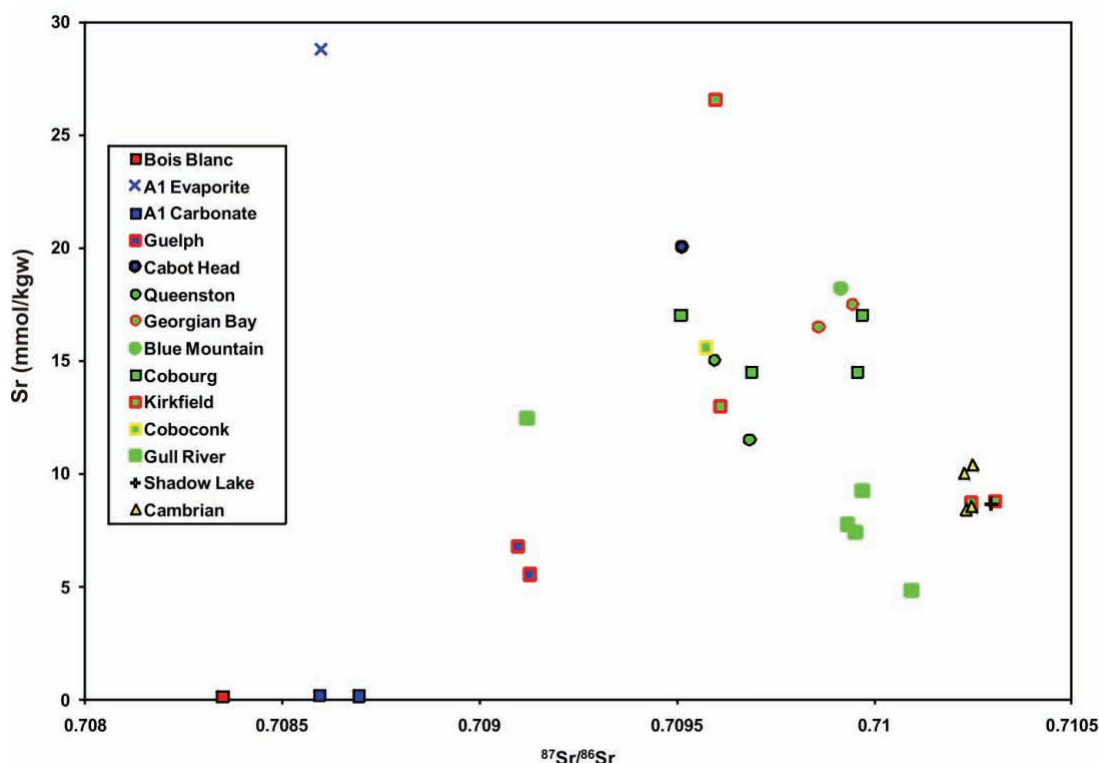
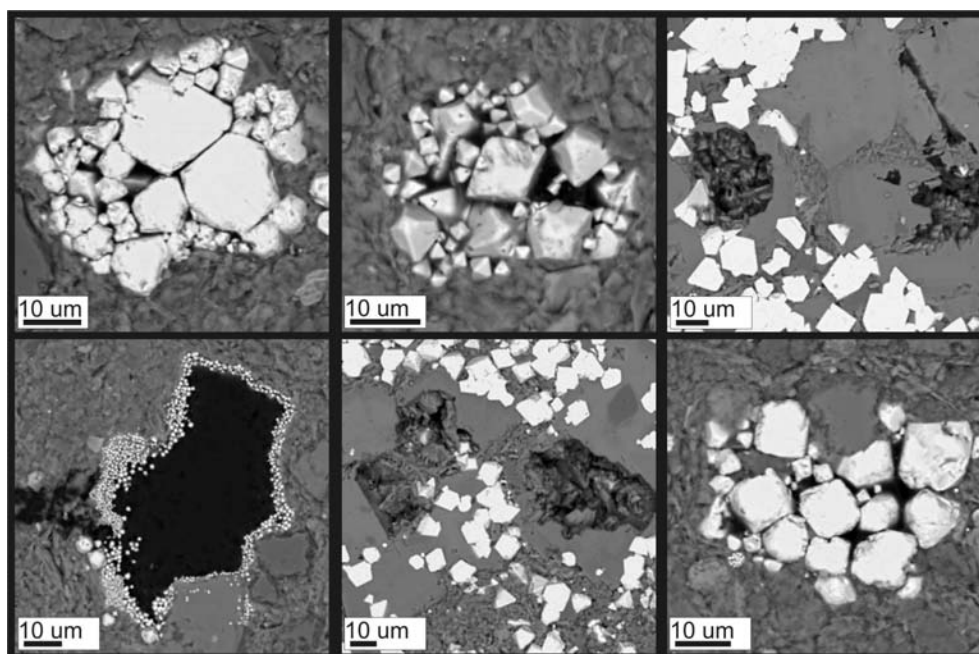


Figure 4.16:  $^{87}\text{Sr}/^{86}\text{Sr}$  versus Sr Concentration for DGR Groundwaters and Porewaters

#### 4.4.5 Redox Conditions in the Ordovician Shale and Carbonate

Redox conditions can be defined in terms of the principal redox couples that reflect the oxidation state at a given depth (e.g.,  $\text{Fe}^{3+}/\text{Fe}^{2+}$ ;  $\text{SO}_4^{2-}/\text{S}^{2-}$ ;  $\text{CO}_2/\text{CH}_4$ ). It is commonly possible to determine the dominant redox couple by analysis of dissolved gases, stable carbon isotope ratios, and the distribution of redox-sensitive minerals. Mineralogical and geochemical evidence (Schandl 2009, Skowron and Hoffman 2009b) indicates that sulphide minerals (predominantly pyrite) and organic carbon are common throughout the stratigraphic sequence, particularly below the Silurian (Figure 4.17). The presence of these materials suggests that redox conditions range from sulphate reducing to methanogenic.



Notes: Pyrite (light grey to white crystals), organic carbon (black). Calcite (medium grey crystals) is a secondary product of sulphate reduction.

**Figure 4.17: Back Scattered Electron Images Illustrating the Principal Solid Phases Involved in Sulphate Reduction Reactions**

The  $\text{CH}_4$  concentration is relatively low in the porewater of the Queenston Formation shale. The Queenston shale unit is commonly red, indicating the presence of fine-grained hematite, which suggests that the redox state of the Queenston Formation is less reducing than that of the Georgian Bay and Blue Mountain shales. However, detailed petrographic investigations of the Queenston Formation shale (Schandl 2009) indicate that fine-grained pyrite is common, suggesting that the redox state is in the realm of iron- or sulphate reduction.

Analyses of the concentration and stable carbon isotopic ratios for  $\text{CO}_2$  and  $\text{CH}_4$  were conducted on gases extracted from core samples (Clark et al. 2010a, 2010b). As noted above, there is a prominent zone of elevated  $\text{CH}_4$  content extending downward from the lower Georgian Bay Formation shale, through the Blue Mountain Formation shale, and into the Collingwood Member, and secondary zones of elevated  $\text{CH}_4$  content in the Silurian Guelph Formation and

the Middle Ordovician limestones. Stable isotopic data indicate that CH<sub>4</sub> in the Upper Ordovician shales and in the Guelph and Cobourg formations is of biogenic origin, while CH<sub>4</sub> in the majority of the Middle Ordovician carbonates is thermogenic. The presence of CH<sub>4</sub> suggests that the redox conditions are strongly reducing throughout most of the Ordovician. One caveat is that the CH<sub>4</sub> may be of Paleozoic age and it cannot be stated for certain that present-day redox conditions are in the realm of methanogenesis.

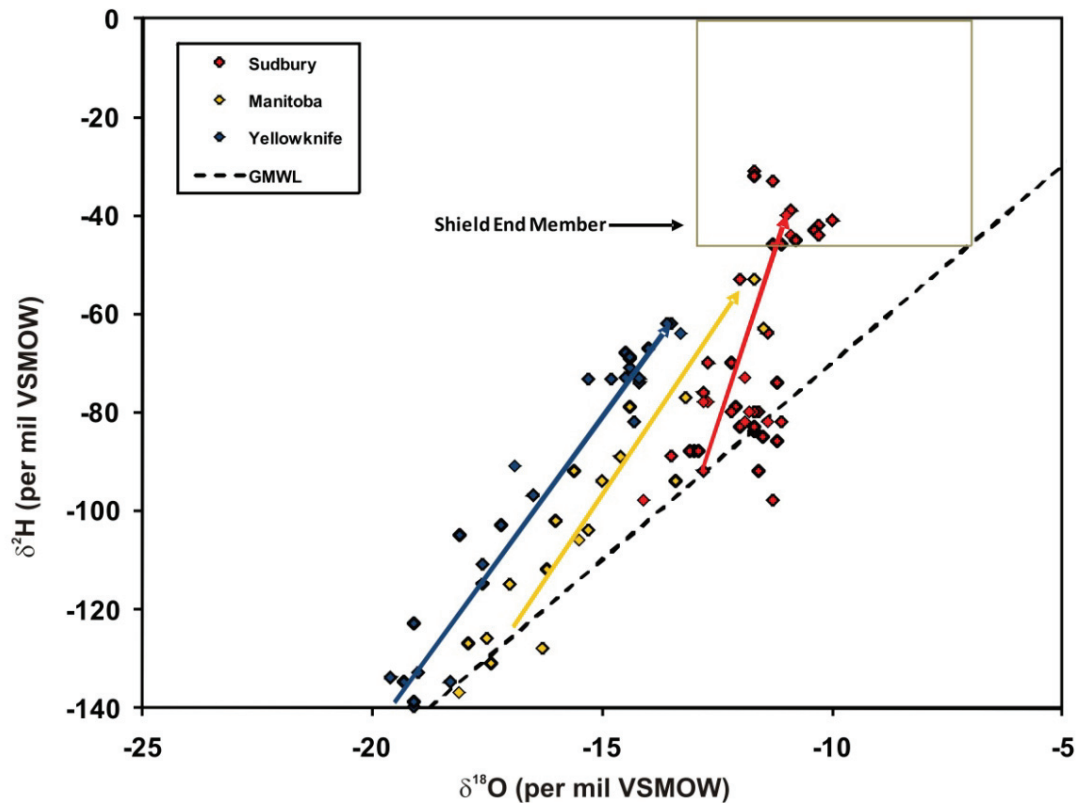
Based on the data collected at the Bruce nuclear site, INTERA (2011) conclude that the Ordovician sediments are reducing, most likely in the realm of iron- or sulphate reduction or methanogenesis, with E<sub>h</sub> values estimated at -150 mV for the whole of the Ordovician sedimentary sequence.

#### 4.4.6 Precambrian Porewater Composition

The composition of groundwater in the Precambrian below the Michigan Basin is not known, but there has been considerable effort extended to develop an understanding of Precambrian shield groundwater elsewhere in Canada, and around the world, which may be relevant (Fritz and Frape 1982, Frape et al. 1984, Frape and Fritz 1987, Pearson 1987, Bottomley et al. 1999, Bottomley et al. 2003, 2004, 2005, Greene et al. 2008). Considering present-day shield brines collected in various locations across Canada, the hypothesis developed by Bottomley and others suggests that these waters originated as sedimentary basin brines formed by evaporation of sea water, which subsequently infiltrated the underlying and adjacent shield during the Devonian in regions where the shield rock is relatively shallow or exposed.

One would expect that the water present in the Michigan Basin during the Cambrian and Ordovician (normal marine seawater, or perhaps even evaporated seawater brine) would have invaded the underlying shield to some extent. The salinity of groundwater in the underlying shield might then be expected to have been somewhere between normal marine and saline brine. With regard to the ionic tracers, Cl and Br, however, there is significant uncertainty about the salinity of the groundwater present in the shield below the Michigan Basin and it is not possible to make inferences about the Cl and Br concentrations in the shield groundwater in terms of an end member for mixing.

In contrast to the salinity, reasonable inferences can be made to constrain the isotopic composition of Precambrian groundwater or porewater below the Michigan Basin. Previous research on present-day shield brines provides knowledge of geochemical modifications to the stable isotope composition of groundwater that result from diagenetic reactions in shield settings (Frape et al. 1984, Pearson 1987). This knowledge can be helpful toward developing expectations for the  $\delta^{18}\text{O}$  and  $\delta^2\text{H}$  composition of shield groundwater below the Michigan Basin that could represent an end member for mixing with basin brines. Stable isotope data collected by Fritz and Frape (1982), Frape and Fritz (1987), Bottomley et al. (1999), Douglas et al. (2000), Bottomley et al. (2003, 2005) and Greene et al. (2008) from shield settings in Canada are shown in Figure 4.18.



Notes: Data are from Fritz and Frape (1982), Frape and Fritz (1987), Bottomley et al. (1999), Douglas et al. (2000), Bottomley et al. (2003, 2005), Greene et al. (2008). The data display isotopic enrichment of  $^2\text{H}$  relative to  $^{18}\text{O}$  that is characteristic of shield brine, with trends moving above the GMWL. The rectangle represents the proposed range of values for a Precambrian shield groundwater end member (see text).

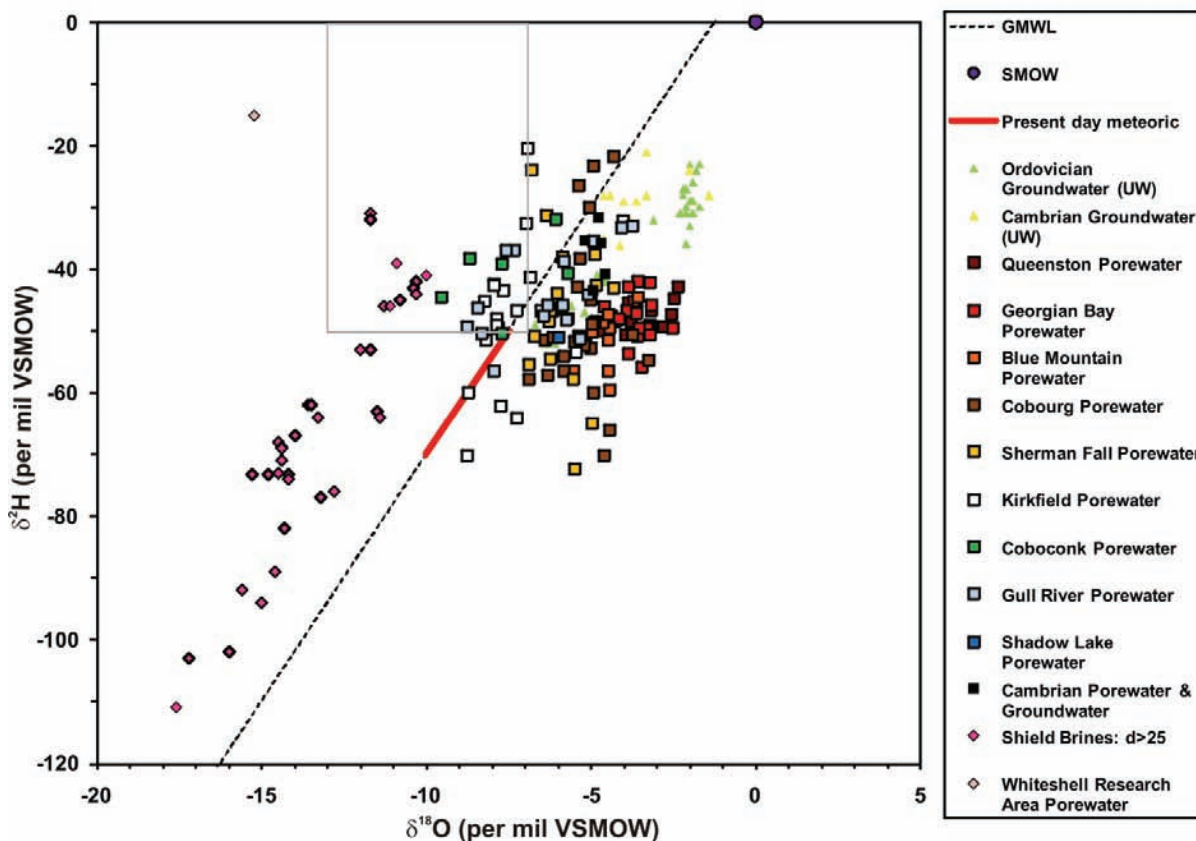
**Figure 4.18: Compilation of Isotopic Data for Groundwater Samples from the Canadian Shield**

The samples from specific locations each define a trend that is interpreted to represent mixing between local meteoric water (i.e., the  $\delta^{18}\text{O}$  and  $\delta^2\text{H}$  precipitation signatures in the respective geographic locations) and a hypothetical shield-brine end member (Figure 4.18). The proposed shield-brine end member responsible for the observed mixing trends plots to the left of the GMWL, and the  $^2\text{H}$  enrichment that is required to cause this shift is thought to occur as a result of water-rock interactions over long periods of geologic time. The observed  $^2\text{H}$  enrichment, coupled with  $^{18}\text{O}$  depletion, are consistent characteristics of old groundwater in a shield setting, and the residence time for groundwater in the shield below the Michigan Basin has certainly been long enough for the water to acquire such a signature.

Various authors have proposed isotopic compositions for a hypothetical shield groundwater end member based on mixing trends such as those observed in Figure 4.18, and they range from  $\delta^2\text{H} = -50$  to  $-20\text{‰}$  and  $\delta^{18}\text{O} = -13$  to  $-7\text{‰}$  (Fritz and Frape 1982, Frape et al. 1984, Pearson 1987, Bottomley et al. 1999). The characteristic  $^2\text{H}$  enrichment observed in shield groundwater data can be represented by a parameter called deuterium excess ( $d$ ; where  $d = \delta^2\text{H} - 8 \times \delta^{18}\text{O}$ ). The range of values presented above for a hypothetical shield end member correspond to  $d$



between 54 and 76, and present-day shield groundwaters shown in Figure 4.19 display  $d$  values up to 62.6.



Notes: Precambrian shield brines from Figure 4.18 that display values for  $d > 25$  are also shown. The red to black transition in porewater symbols represents increasing depth. The grey box represents the proposed range of composition for a hypothetical shield end member.

**Figure 4.19:  $\delta^{18}\text{O}$  versus  $\delta^2\text{H}$  for Ordovician and Cambrian Porewater from DGR-2, DGR-3 and DGR-4, and Groundwater Brine Samples from Ordovician Carbonates and Cambrian Sandstone Included in the UW Database**

The deuterium excess profile for the Bruce nuclear site data is shown in Figure 4.20. The profiles show steady increase in the  $d$  values with depth. Given that the porewater and groundwater in the shield underlying the Michigan Basin is likely to be at least as old as, and perhaps several hundred million years older than, shield groundwater studied in exposed regions of the Canadian Shield, it is expected that the isotopic composition of shield brines underlying the basin would be characterized by strong  $^2\text{H}$  enrichment, depleted  $\delta^{18}\text{O}$  values, and  $d$  values on the order of 60 or higher. It may be that the isotopic composition could approach that of the most  $^2\text{H}$ -enriched samples discovered in shield host rocks ( $d = 106$ ) which were reported by Gascoyne (2004) from porewater in granite at the Whiteshell Research Area (Figure 4.19).

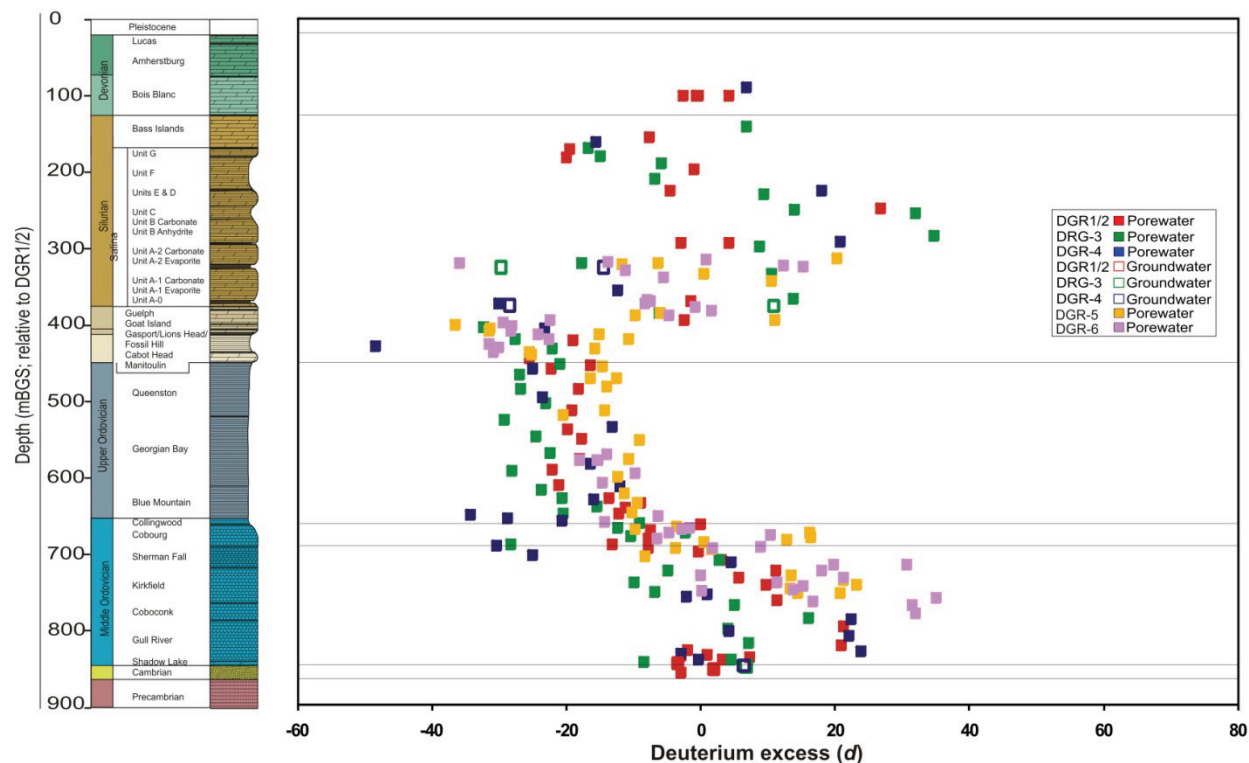


**Figure 4.20: Profile of Deuterium Excess ( $d$ ) Versus Depth for Porewater and Groundwater from DGR Boreholes**

#### 4.5 Illustrative Modelling of the Bruce Nuclear Site Geochemistry

The following section describes the conceptual model developed for the chemical evolution of the fluids at the Bruce nuclear site, followed by illustrative numerical modelling to simulate the trends in geochemical data collected from the DGR boreholes.

##### 4.5.1 Conceptual Model

Current understanding of the geologic history of the Michigan Basin indicates that the following conditions and/or events occurred. They are listed here for reference because they may have had an important influence on the fluid evolutionary history. Any conceptual model that is presented to explain the hydrogeochemical evolution at the eastern margin of the Michigan Basin should be consistent with the points below.

- During the Cambrian and Ordovician, the composition of groundwater and porewater in the Cambro-Ordovician stratigraphy was likely reflective of the seawater present in the basin at that time. The Cambrian is thought to have been a period of normal marine conditions, but based on analogy with the Siberian platform, evaporative conditions may have existed (Shouakar-Stash et al. 2007).
- One or more hydrothermal events related to Taconic orogenesis caused alteration of rocks at the Precambrian-Paleozoic unconformity. HTD that is observed in the Black River and Trenton groups may have formed during this time period.

- During the Silurian and Devonian, restricted marine conditions caused intermittent formation of marine evaporites, leading to the formation of dense hypersaline brines. The gravitational instability caused by accumulation of dense hypersaline brine above Ordovician porewaters of normal marine composition may have caused downward solute migration. Overturn by density-driven advection (Coniglio et al. 1994, Barnes et al. 2008) and diffusion are possible solute transport mechanisms under such conditions. Overturn results in the downward migration of hypersaline brine through localized structures that cross cut low-permeability formations, and then laterally through permeable stratigraphic units. The high salinity fluids then diffuse into the enclosing low-permeability formations. In the absence of advective transport pathways, the concentration gradient(s) between the overlying hypersaline brines and the underlying sedimentary porewaters would have resulted in diffusion. The presence of halite in the Middle and Upper Ordovician rocks (Herwegh and Mazurek 2008) is consistent with an ancient redistribution of brines in the basin by some solute transport mechanism.

The conceptual model adopted for the Bruce nuclear site must be able to account for the following primary features observed in the natural tracer profiles:

- A large decrease in concentration occurs for all tracers from the top of the Guelph Formation upward through the Silurian; and
- A less pronounced, but persistent, trend toward depleted  $\delta^{18}\text{O}$  values, reduced Cl and Br concentrations, and enriched  $\delta^2\text{H}$  values occurs in the Middle Ordovician limestone.

The conceptual model described below has been adopted because of its ability to explain the observed geochemical profiles for almost all of the data collected at the Bruce nuclear site.

#### 4.5.1.1 The Ordovician Tracer Profiles: Diffusion-from-above

Diffusion downward from the Silurian could provide an explanation for the salinity profile because the original porewater in the Ordovician would be expected to be close to normal seawater, and the high-salinity porewater in the overlying Silurian evaporites would create a strong downward gradient for diffusive transport. In support of this hypothesis, numerical modelling of diffusive transport downward from the Silurian suggests that the observed natural tracer profiles in the Ordovician could be generated over a period of approximately 300 Ma (see Section 4.5.2.3).

The presence of halite in the Middle Ordovician carbonates can be explained by asserting that localized halite occurrences formed by concentration mechanisms, such as hydration reactions (Drever et al. 1979) or hyperfiltration (Bredehoeft et al. 1963, Kharaka and Berry 1973). Carbonate would generally not be considered a suitable medium for concentration of salts by hyperfiltration, but Hart and Whitworth (2005) have demonstrated that, over a very short experimental time period, salinity can almost double by hyperfiltration across thin clay beds (0.00108 to 0.00250 m). Over a geologic time scale, it should be possible that the argillaceous component of the Ordovician carbonates can behave as a membrane in order to cause increases in salinity and form localized halite occurrences.

The “diffusion-from-above” conceptual model is summarized below.

- Deposition of the Cambro-Ordovician sequence under normal marine conditions, followed by deposition of evaporites during the Silurian and Devonian, created a condition with high-TDS

porewater overlying porewater of normal marine composition. This established a natural concentration gradient that promoted a downward mass flux of salts by diffusion.

- A very long period (~300 Ma) of diffusive transport followed, during which the high-salinity profile propagated downward into the Upper and Middle Ordovician by diffusion. During the same period, water-rock reactions in the underlying shield and siliciclastic Cambrian sediments caused the deep groundwater isotopic characteristics to evolve toward a shield signature with enriched  $\delta^2\text{H}$  and depleted  $\delta^{18}\text{O}$  values. Water-rock interactions yield the isotopic characteristics of the shield fluids that allow them to serve as a natural sink for  $^{18}\text{O}$ , resulting in a depletion profile for  $\delta^{18}\text{O}$  with depth in the overlying sedimentary units.

The very long period of diffusion-dominated transport and water-rock reaction required to justify the interpretations presented in the diffusion-from-above conceptual model is supported by multiple lines of hydrogeochemical evidence.

- The enriched  $\delta^{18}\text{O}$  signatures of most of the Ordovician fluids relative to the GMWL are indicative of an evaporated seawater origin and long time periods for water-rock interaction (i.e., long residence times).
- Separation between biogenic  $\text{CH}_4$  in the Upper Ordovician shales and thermogenic  $\text{CH}_4$  in the Middle Ordovician carbonates (Section 4.4.3.1), and between He with different  $^3\text{He}/^4\text{He}$  ratios in the Upper Ordovician shales and the Middle Ordovician carbonates (Section 4.4.3.2), suggests that advective mixing has not occurred and diffusive transport is extremely slow.
- The presence of radiogenic Sr in porewater from the Upper Ordovician shale and the Middle Ordovician carbonate suggests that the radiogenic Sr must have been derived either from in-growth from  $^{87}\text{Rb}$  decay, leaching from the siliciclastic sediments, or diffusion upward from a  $^{87}\text{Sr}$ -enriched end member in the shield (Section 4.4.4). All of these possibilities require extremely long time periods.

#### **4.5.1.2 The Devonian and Silurian Profiles: Glacial Melt Water and Meteoric Water Infiltration**

In addition to the diffusion-from-above model, glacial melt water infiltration is also proposed to explain the natural tracer profiles observed for the Devonian and Silurian porewaters and groundwaters at the Bruce nuclear site. The observed decrease in salinity and the depleted  $\delta^{18}\text{O}$  and  $\delta^2\text{H}$  values that are apparent from the top of the Guelph Formation to ground surface suggest that a combination of glacial melt water and recent meteoric water have contributed to evolution of the Silurian and Devonian tracer profiles. Based on the geologic history of the site, these signatures are best explained by infiltration of meteoric and/or glacial melt water during the Pleistocene.

### **4.5.2 Numerical Modelling**

#### **4.5.2.1 Model Justification**

The numerical simulations were conducted in one dimension (1D) and are intended to assess the feasibility of the conceptual model, and, if possible, to place time constraints on the development of the observed features in the natural tracer profiles in a diffusion-dominated system. The simulations are supported by stratigraphic and hydrostratigraphic information from DGR drilling, measured data for porewater  $\delta^{18}\text{O}$  values and Cl concentrations (Figures 4.7 and

4.8), an estimate of the Precambrian groundwater  $\delta^{18}\text{O}$  composition ( $-10 \pm 2\%$  based on Precambrian shield literature and trends in Figure 4.19), and the initial  $\delta^{18}\text{O}$  composition of the Michigan Basin brines ( $-2\%$ ) estimated from data reported by Graf et al. (1965), Dollar (1988), and Wilson and Long (1993a, b). The laboratory-determined diffusion coefficients (Figure 5.7; Table 5.4) were used to assign the diffusion properties throughout the domain. Numerous studies have shown that aqueous diffusion coefficients decrease under partially saturated conditions (Saripalli et al. 2002 and references therein). Based on the possibility that partially saturated conditions occur in the interval that straddles the top of the Ordovician limestone and the bottom of the Ordovician shale, and given the isotopic evidence for limited diffusion of  $\text{CH}_4$  and He gases across that interval (Sections 4.4.3.1 and 4.4.3.2), the diffusion-from-above simulation was conducted using diffusion coefficients for this interval that were reduced by an order of magnitude (Table 4.3). The diffusion parameters for the Precambrian listed in Table 4.3 are not constrained by measurements but are considered to be reasonable estimates.

#### 4.5.2.2 Computational Model

MIN3P is a general purpose flow and reactive transport code for variably saturated media (Mayer et al. 2002). The model is capable of simulating advective-diffusive transport in the water phase and diffusive transport in the gas phase. The equilibrium reactions considered are aqueous complexation, gas partitioning between phases, oxidation-reduction, ion exchange, dissolution and precipitation reactions, and surface complexation. The model reaction network is designed to handle kinetically controlled intra-aqueous and dissolution-precipitation reactions, and the dissolution of non-aqueous phase liquids (NAPLs). All reactions can be defined through a database, not requiring external code generation by the user. The MIN3P code is primarily used to aid in the quantitative assessment of laboratory experiments and field studies. In this case, reaction processes were not included and the model was used to simulate conservative solute transport by diffusion only.

#### 4.5.2.3 Diffusion-from-above: Tracer Profiles in the Ordovician

##### Initial and Boundary Conditions

Simulations of the downward diffusion of the natural tracers were conducted in a single stage lasting 300 Ma. Transport in all stratigraphic units was by diffusion only. For the salinity simulations, an initial concentration of 7 mol/kgw for Cl was assigned throughout the Silurian and Devonian (evaporated sea water brine), and an initial concentration of 0.6 mol/kgw for Cl was assigned in the Ordovician and below to represent normal marine sea water. Free exit boundary conditions were applied at the top and bottom of the domain. For the  $^{18}\text{O}$  simulations, an initial  $\delta^{18}\text{O}$  value of  $-2\%$  was assigned throughout the domain. The value of  $-2\%$  for  $\delta^{18}\text{O}$  is deemed appropriate for the Silurian and Devonian evaporated sea water brines because it represents the middle value in the ranges reported by Graf et al. (1965), Dollar (1988) and Wilson and Long (1993a, b) for Michigan Basin brines. The same  $\delta^{18}\text{O}$  value should also be appropriate for normal marine sea water in the Ordovician and Cambrian (Trotter et al. 2008). A free exit boundary condition was applied at the top of the domain, and a constant concentration ( $\delta^{18}\text{O} = -12\%$ ) boundary condition was assigned at the bottom of the domain to represent water-rock reactions operating in the crystalline bedrock (Pearson 1987; refer to Section 4.4.6). The bottom of the domain represents the modelled deep Precambrian, at a bottom depth of approximately 750 m below the Precambrian-Paleozoic unconformity (1610 mBGS). The model was run for two scenarios: 1) fully saturated conditions throughout the entire sedimentary sequence (blue dashed line in Figure 4.21), and 2) partially saturated conditions (modeled by a

decrease in total porosity by a factor of approximately ten; see Table 4.3) in the Upper Ordovician shale and Middle Ordovician limestone (yellow dashed line in Figure 4.21).

**Table 4.3: Distribution of Diffusion Parameters Used in Diffusion Simulations**

Depth (mBGS)	Stratigraphy	Porosity	Tortuosity <sup>1</sup>	D <sub>e</sub> (m <sup>2</sup> /s)
0 to 120	Devonian	0.1	0.188	5.0 x 10 <sup>-11</sup>
120 to 180	Silurian: Bass Islands	0.017	0.023	1.0 x 10 <sup>-12</sup>
180 to 220	Silurian: Salina Units F and G	0.11	0.038	1.1 x 10 <sup>-11</sup>
220 to 300	Silurian: Salina Units B to E	0.18	0.038	1.8 x 10 <sup>-11</sup>
300 to 450	Silurian: Manitoulin to Salina Unit A	0.059	0.0038	6.0 x 10 <sup>-13</sup>
450 to 610	Upper Ordovician Shale – Saturated	0.084	0.016	3.6 x 10 <sup>-12</sup>
610 to 660	Upper Ordovician Shale	0.084 (0.01) <sup>2</sup>	0.016	4.3 x 10 <sup>-13</sup>
660 to 700	Middle Ordovician Limestone	0.013 (0.002) <sup>2</sup>	0.02	1.1 x 10 <sup>-13</sup>
700 to 840	Middle Ordovician Limestone	0.013	0.02	6.9 x 10 <sup>-13</sup>
840 to 860	Cambrian Sandstone	0.14	0.2	7.4 x 10 <sup>-11</sup>
860 to 1160	Shallow Precambrian	0.005 <sup>3</sup>	0.2 <sup>3</sup>	2.7 x 10 <sup>-12</sup>
1160 to 1610	Deep Precambrian	0.0025 <sup>3</sup>	0.2 <sup>3</sup>	1.3 x 10 <sup>-12</sup>

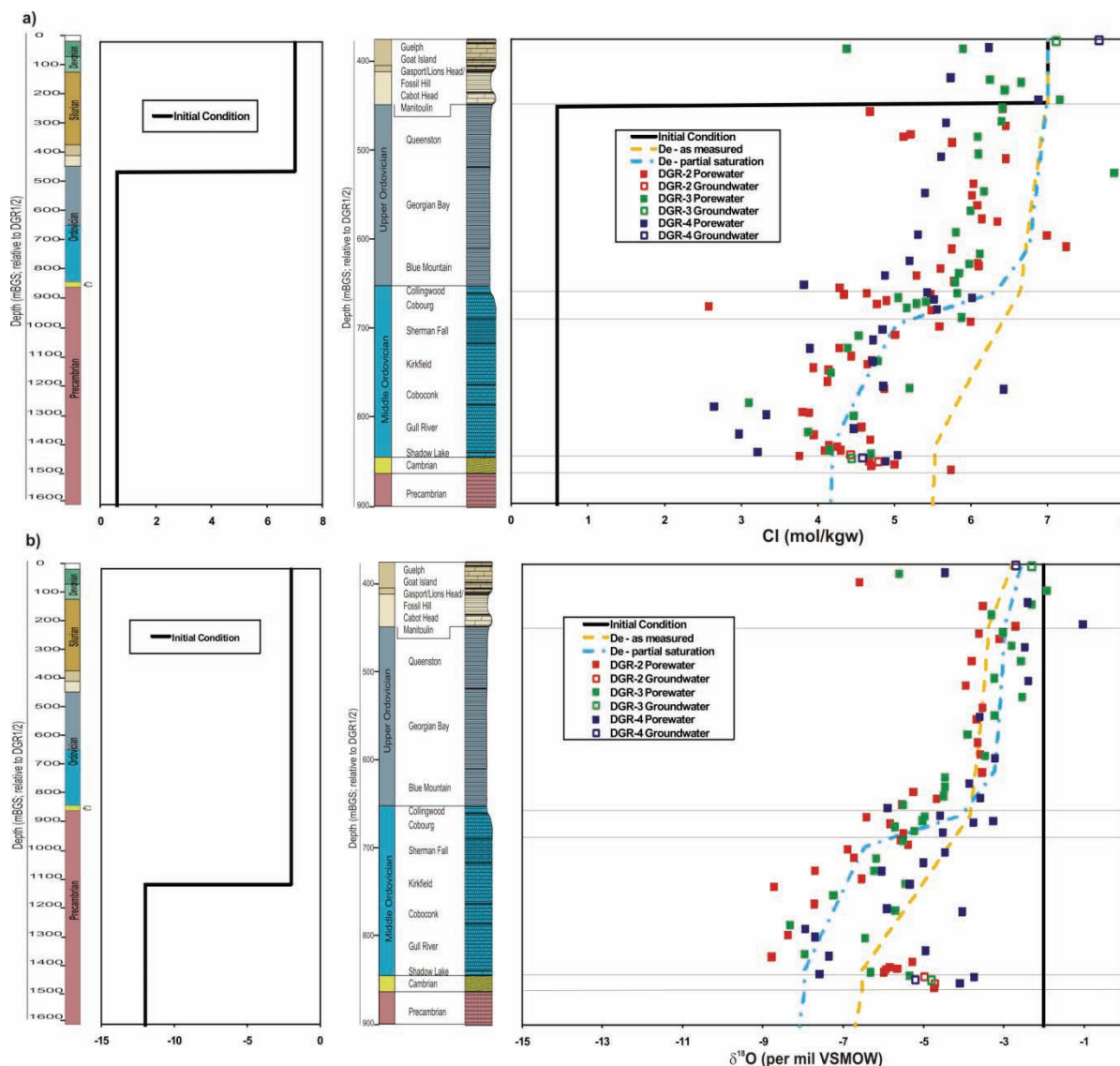
Notes: Data are from Al et al. (2010a, 2010b).

1. Calculated from D<sub>0</sub> and laboratory measurements of D<sub>e</sub> and porosity.
2. Reduction of porosity by a factor of approximately 10 for partially saturated conditions.
3. Assumed values.

## Model Results

The results for salinity and  $\delta^{18}\text{O}$  diffusion simulations over a period of 300 Ma provide a good fit to the measured porewater data (Figure 4.21a and 4.21b, respectively) which suggests that the “diffusion-from-above” conceptual model could be used to explain the natural tracer profiles. Figure 4.21a and 4.21b show the initial boundary conditions assigned to the entire domain, from the top of the Devonian to the bottom depth defined for the Precambrian at 1610 mBGS. The Cl and  $\delta^{18}\text{O}$  modelling results are shown only for the investigated interval, from the Guelph Formation downward to the base of the Cambrian. The principal controls on the shape of the simulated profiles are the boundary conditions, the contrast in D<sub>e</sub> between the Upper and Middle Ordovician, and the effect of partial saturation or secondary mineral precipitation in lowering the D<sub>e</sub> values at the boundary between the Upper and Middle Ordovician.

The results also suggest that a decrease in D<sub>e</sub> (due to partial saturation or occlusion of pores by secondary mineral precipitation) in the Blue Mountain and Cobourg formations may be necessary in order to adequately explain the salinity tracer profile, and, to a lesser extent, the  $\delta^{18}\text{O}$  profile in terms of the known geologic history of the basin.



Notes: The salinity (Cl) tracer profile develops as a result of salt diffusion downward from the Silurian and the  $\delta^{18}\text{O}$  profile results from diffusive mixing with shield brine at the base of the profile.

**Figure 4.21: Results of the Diffusion-from-above Modelling Scenario**

In addition to the diffusion-from-above model, consideration was given to the idea that glacial melt water infiltration along the Precambrian-Paleozoic unconformity could have been responsible for the observed natural tracer profiles within the deep Ordovician carbonates. Modelling of glacial infiltration was included in the paleoclimate simulations described in the hydrogeological modelling in Section 5.4.6.6. The modelling scenarios included the release of a unit amount of tracer across the entire RSA and the depth of penetration of the tracer was modeled for single and multiple glaciation scenarios. The results were similar for all scenarios modeled and the tracer never infiltrated to depth below the Salina B Unit across the entire RSA (see Figure 5.34). The hydrogeologic modelling, therefore, does not support any assertions that glacial melt water infiltration would reach the Precambrian-Paleozoic unconformity within the

RSA. Thus, the observed tracer profiles in the Ordovician do not appear to be related to infiltration of glacial melt water along the Precambrian-Paleozoic unconformity over the past 1 Ma.

#### 4.5.2.4 Glacial Melt Water and Meteoric Water Infiltration: Tracer Profiles in the Silurian and Devonian

The following simulation was conducted to assess the possibility that the observed decrease in salinity and  $\delta^{18}\text{O}$  values from the top of the Guelph Formation upward toward the surface can be explained by infiltration of meteoric and/or glacial melt water during the Pleistocene.

##### Initial and Boundary Conditions

The simulated diffusion profile for  $\delta^{18}\text{O}$  after 300 Ma, as described in Section 4.5.2.3 for the diffusion-from-above conceptual model and shown by the blue dashed line in Figure 4.21b, also represents the system conditions prior to glaciation in the glacial melt water and meteoric water infiltration conceptual model (indicated by the yellow dashed line on Figure 4.22). For the glacial infiltration scenario, the top boundary cannot be well defined in terms of the position (elevation) of the boundary because sufficient data are not available for the erosion rates through time. Therefore, the top boundary is assigned at the present-day ground surface. In order to simulate infiltration of glacial and meteoric water, a constant-concentration boundary condition ( $\delta^{18}\text{O} = -14\text{‰}$ ; mix of glacial and meteoric waters) is assigned in the shallow aquifer (0 to 180 mBGS) and in the thin aquifer in the Salina A1 carbonate (hydrostratigraphic unit 4a, as defined in Figure 5.8) for 2 Ma during the Pleistocene.

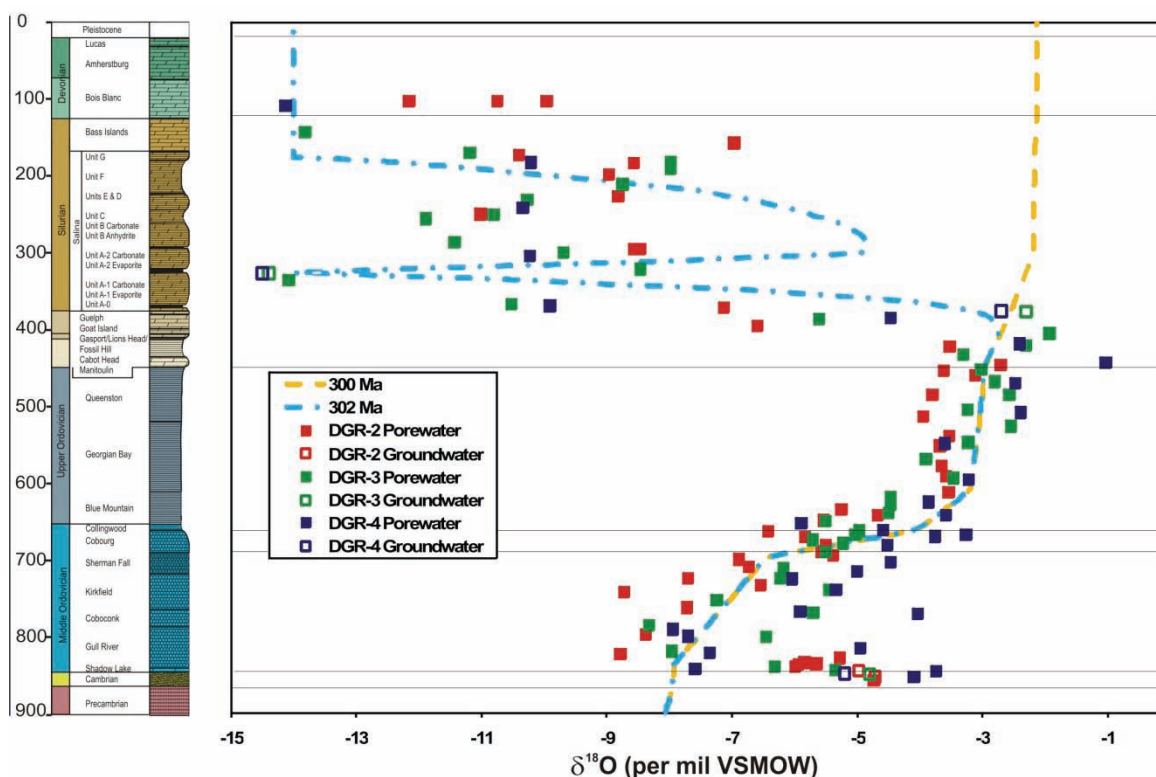


**Figure 4.22: Results of  $\delta^{18}\text{O}$  Diffusion Simulation (dashed lines) Compared to Measured Porewater  $\delta^{18}\text{O}$  Data**



## Model Results

There is considerable uncertainty in attempting to translate the conceptual model into a numerical model to describe advective and diffusive mixing between basin water and infiltrating glacial and/or meteoric water. The most important issues include: 1) when these units “opened up” to glacial and meteoric water infiltration; 2) if they opened up sequentially, or all at once; and 3) the volume and duration of glacial melt water infiltration. The fit to the data is generally good (Figure 4.22) in that it describes a general depletion in  $\delta^{18}\text{O}$  values upward through the Silurian and Devonian that is consistent with the data. The incomplete fit in the upper units of the Salina Group suggests that the hydrogeologic properties of these rocks, and perhaps the hydrologic history at the site, are more complex than has been represented in the model. The general correspondence between the model results and the data provide support for the conceptual model, suggesting that there is a glacial meltwater component in the shallow system fluids.

### **4.5.3 Modelling Summary**

The numerical modelling results presented are not intended to be unique, but rather are intended to provide a test, through reasoned illustrative modelling, of various elements of the conceptual model presented in Section 4.5.1. The key conclusions that can be drawn from the hydrogeochemical modelling are indicated below.

- The diffusion-from-above conceptual model is able to explain the observed natural tracer profiles of the Ordovician fluids. The numerical simulations are able to reproduce the measured Cl and  $\delta^{18}\text{O}$  profiles, and the data are particularly well matched under the partial saturation case, indicating that some form of diffusion barrier (partial saturation or secondary mineral precipitation) may exist near the boundary between the Ordovician shales and carbonates.
- The profiles are best matched for both Cl and  $\delta^{18}\text{O}$  under partially saturated conditions for a time period of 300 Ma, assuming diffusive transport only. The simulated profiles are consistent with the site-specific data, supporting the hypothesis that solute transport in the Ordovician sediments is diffusion dominated.
- The glacial melt water and meteoric water infiltration scenario provides a good fit to the observed tracer profiles in the Devonian and Silurian formations, consistent with the assertion in Section 4.4.1 that there is a glacial melt water and/or meteoric water component in the shallow groundwaters and porewaters.

There is one feature of the natural tracer profiles that is not represented by the simulated diffusion profiles – the current Cambrian fluid chemistry – indicating that the Cambrian fluid evolutionary history may be more complex than can be explained by a 1D diffusion model. The Cambrian fluid chemistry is discussed in more detail in Section 4.5.4.

### **4.5.4 Cambrian Fluid Chemistry**

The Cambrian chemistry displays a distinct rebound in the natural tracer profiles relative to the overlying Ordovician carbonates. The rebound in the profiles (Figures 4.7 and 4.8) is abrupt compared to the gradual decline in concentrations and isotope ratios observed with depth through the Ordovician carbonates. The composition of the Cambrian groundwater below the Bruce nuclear site is very similar to Cambrian groundwater samples from elsewhere in southern Ontario. For example,  $\delta^{18}\text{O}$  values from brines in the Cambrian sandstone in the Appalachian Basin of southwest Ontario range between -5‰ and -3‰ (Cambrian groundwater (UW) on

Figure 4.19). There are no known isotopic data from the Cambrian in the Michigan Basin, but Graf et al. (1965) report data for brine from the Lower Ordovician Oneota Dolomite in central Michigan ( $\delta^{18}\text{O} = -1.95\text{‰}$  and  $\delta^2\text{H} = -60\text{‰}$  VSMOW) and Dollar (1988) reports values of  $\delta^{18}\text{O} = -1.6\text{‰}$  and  $\delta^2\text{H} = -50\text{‰}$  for brine from the Lower Ordovician Prairie du Chien sandstone in central Michigan. The similarity between the present-day brine in the Cambrian below the Bruce nuclear site and the Cambrian and deep Ordovician brines elsewhere in the Appalachian and Michigan basins, respectively, suggests that the Cambrian fluid underlying the Bruce nuclear site originated at depth within the Michigan Basin.

The hydraulic conductivity of the Cambrian aquifer is approximately six orders of magnitude higher than that of the overlying Middle Ordovician limestones (see Figure 5.1). The groundwater in the Cambrian sandstone would thus be more susceptible than porewater in the Ordovician carbonates to advection-driven changes in composition through geologic time. Winter et al. (1995) report mineralogical and geochemical evidence for the occurrence of at least four different fluids in the Ordovician St. Peter Sandstone in central Michigan, but there is little evidence to document similar changes through time for the fluid composition in the Cambrian aquifer below the Bruce nuclear site.

Under the influence of diffusion, it is expected that an abrupt concentration gradient, such as is presently documented above the Cambrian aquifer, would be attenuated over time. Conventional hydrogeologic rationale would suggest that this feature of the profiles could represent a geologically recent movement of groundwater in the permeable Cambrian formation, thereby disrupting the diffusion-controlled mixing relationship that had developed previously between basin and shield end members. Assuming that the Cambrian fluid composition represents a recent change, the mechanism responsible for the re-supply of basin water is not known. Based on the evolutionary history of the Michigan Basin, the possible driver(s) for fluid migration from basin centre in the recent geologic past are rather limited. These drivers include 1) fluid migration in response to the anomalous pressures deep in the Michigan Basin (Bahr et al. 1994) and/or 2) fluid migration in response to differential uplift of the basin due to repeated isostatic adjustments related to glaciation and deglaciation.

Irrespective of the mechanism(s) responsible for the current Cambrian fluid chemistry beneath the Bruce nuclear site, the fundamental hypothesis that solute migration with the Ordovician sediments is diffusion dominated is well supported by the geochemical and hydrogeological data (presented in Chapter 5); the data also support the assertion that solute residence times in the Ordovician shales and carbonates are long.

#### 4.6 Summary

It was stated in the introduction to this chapter that hydrogeochemical studies can provide data that may be used to test the validity of two of the fundamental hypotheses.

- **Solute Transport is Diffusion Dominated:** deep groundwater regime is ancient showing no evidence of cross-formational flow or glacial perturbation.
- **Multiple Natural Barriers:** multiple low-permeability bedrock formations enclose and overlie the DGR.

The following points may be made in support of these hypotheses based on the interpretation of hydrogeochemical data presented in this chapter.

- The current understanding regarding the origin of brines from the Michigan Basin indicates that they were formed by evaporation of sea water that was subsequently modified by i) dilution of brines by lower salinity water; ii) dissolution of halite by lower salinity water, and iii) diagenetic water-rock reaction processes, particularly dolomitization. The data collected from the Bruce nuclear site are consistent with the regional data, which indicates that the brines at both the regional scale and the site scale are of the same origin.
- The widespread occurrence of ancient brines in the basin demonstrates that, under most conditions prevalent since the Paleozoic, it has not been possible for hydraulic heads generated in freshwater aquifers at the top boundary of the basin to drive infiltration events capable of displacing the brines. Glacial melt water infiltration has been identified to depths of 200-300 mBGS in northern Michigan within the RSA. The data from the Bruce nuclear site show that concentrations of Cl and Br increase with depth from the surface toward the top of the Guelph Formation, and stable O and H isotope compositions range from relatively depleted values near surface to more enriched values toward the top of the Guelph Formation. In the interval between the Salina F Unit and the A1 Unit carbonate, the stable isotope compositions are somewhat variable, representing varying degrees of dilution of the sedimentary brines, consistent with the assertion that these fluids are a mixture of saline brine and glacial and/or meteoric water. Consistent with data collected along the Michigan Basin margins, glacial melt water infiltration is identified to a maximum depth of 328.5 mBGS at the Bruce nuclear site within the A1 Unit carbonate aquifer.
- On a regional scale, evidence for cross-formational flow exists for ancient events such as dolomitization of Ordovician and Silurian formations, the emplacement of Mississippi-Valley-Type sulphide mineralization in Silurian formations, and emplacement of hydrocarbons within structural, stratigraphic or diagenetic traps in formations of Cambrian, Ordovician, Silurian and Devonian age. Although the timing of these cross-formational flow events is not known, the requirement for sufficient driving forces for movement of these fluids suggests that these events occurred in association with tectonic or orogenic events; the most recent event being the Alleghenian Orogeny, which ended approximately 250 MaBP.
- At the Bruce nuclear site, concentrated brines occur at all depths below the top of the Silurian Guelph Formation.
- $^{18}\text{O}$  enrichment with respect to the GMWL in the majority of the Ordovician porewaters suggests long periods of water rock interaction (i.e., long residence times in the sedimentary system).
- $\text{CH}_4$  within the Ordovician carbonates has a thermogenic signature – indicative of high temperature formation – which suggests that the methane within the Trenton and Black River groups is hundreds of millions of years old.
- Separation between biogenic  $\text{CH}_4$  in the Upper Ordovician shales and thermogenic  $\text{CH}_4$  in the Middle Ordovician carbonates indicates that advective mixing has not occurred since the gases have been resident in the system and that diffusive transport is extremely slow.
- In conjunction with the  $\text{CH}_4$  isotopic data, separation between He with different  $^3\text{He}/^4\text{He}$  ratios in the Upper Ordovician shales and the Middle Ordovician carbonates suggests that diffusion is extremely slow and that there is a barrier to vertical solute migration within the Cobourg Formation.
- Radiogenic  $^{87}\text{Sr}/^{86}\text{Sr}$  ratios in the Middle and Upper Ordovician porewater are interpreted to result from a combination of water-rock interaction, in situ  $^{87}\text{Rb}$  decay, and diffusion of  $^{87}\text{Sr}$  upward from an enriched end member in the shield. All of these mechanisms indicate a very long residence time, on the order of tens to hundreds of millions of years.

- The presence of sulphide minerals and organic carbon suggests that redox conditions in the Ordovician and Cambrian formations are strongly reducing, in the range of iron- and/or sulphate reduction and methanogenesis.
- The Middle Ordovician Trenton Group carbonates, and the Upper Ordovician Blue Mountain, Georgian Bay, and Queenston formation shales, represent more than 300 m of continuous low permeability limestone and shale which will act to isolate the proposed DGR. In addition, these formations are overlain by approximately 200 m of low permeability carbonate, shale, and anhydrite of the Silurian Salina Group.
- Illustrative modelling suggests that the timeframes required for the development of the salinity and  $\delta^{18}\text{O}$  profiles within the Ordovician sediments are on the order of 300 Ma; the results are consistent with the fundamental hypothesis that solute transport in the Ordovician is diffusion dominated.

## 5. HYDROGEOLOGY

### 5.1 Introduction

Hydrogeological studies seek to understand groundwater migration and mass transport of solutes through the subsurface. Field hydrogeological studies typically focus on estimation of the basic hydrologic parameters that control fluid movement through particular formations, such as hydraulic conductivity (permeability), specific storage, and hydraulic head (pressure). Laboratory studies are typically performed on core samples collected from the formations of interest, and may be used to determine: porosity; the phases (gas, water, oil) that may be present in the pores of the rock; horizontal and vertical permeabilities to water, oil, and gas; diffusive properties of the rock; and elastic properties related to storage. Numerical modelling analyses complement these studies through integration of field and laboratory information necessary to illustrate and bound understanding of groundwater system behaviour with respect to groundwater and solute migration at time and spatial scales relevant to repository safety.

In the context of the evaluation of the geologic suitability of the Bruce nuclear site to host the DGR, hydrogeological studies provide data pertinent to three of the fundamental hypotheses, as follows.

- **Multiple Natural Barriers:** multiple low-permeability bedrock formations enclose and overlie the DGR.
- **Solute Transport is Diffusion Dominated:** deep groundwater regime is ancient, showing no evidence of cross-formational flow or glacial perturbation.
- **Shallow Groundwater Resources are Isolated:** near-surface groundwater aquifers are isolated from the deep saline groundwater system.

This section summarizes the field, laboratory, and modelling studies performed to understand the hydrogeology of the Bruce nuclear site and predict how the hydrogeologic system will respond to the presence of a DGR over the next 1 Ma. It concludes with a discussion of how the information gained supports the three hypotheses listed above and contributes to confidence in the suitability of the Bruce nuclear site to host the DGR.

### 5.2 Field Studies

Field hydrogeologic studies performed at the Bruce nuclear site provide both basic information on hydrologic properties (e.g., hydraulic conductivity) and observations (e.g., hydraulic heads) that are both used to rationalize and justify conceptual and numerical models of the subsurface. Data on the shallow bedrock units come largely from investigations conducted prior to the DGR project. Additional hydrogeologic information was obtained through the installation of three multilevel Westbay MP38 monitoring systems in shallow bedrock US-series boreholes US-3, US-7, and US-8. Further field hydrogeologic studies for the DGR project consisted of straddle-packer hydraulic testing performed in each of the six deep DGR boreholes shortly after drilling. This was followed by installation of multilevel Westbay MP55 monitoring systems in boreholes DGR-1, DGR-2, DGR-3, and DGR-4. Information obtained from visual and geophysical core logging was used to define intervals for hydraulic testing and to interpret the test results.

#### 5.2.1 Shallow Bedrock Information

Data on formation horizontal hydraulic conductivity for the shallow bedrock (Lucas, Amherstburg, Bois Blanc and Bass Islands formations) are available from summaries of

geotechnical bedrock investigations; Bruce A and B cooling water intake tunnelling experience (GOLDER 2003); straddle-packer testing of US-1 to US-7 (106 tests – Lukajic 1988); slug testing of Westbay test intervals in US-5 and US-6 (14 tests – GOLDER 2003); and from drilling fluid loss observations made during drilling of US-8 (Briscoe 2009) and DGR boreholes (Sterling 2010b, Briscoe et al. 2010a, 2010b). Packer test flow rates and injection pressures and drilling fluid loss rates and heads were converted to equivalent hydraulic conductivities assuming conditions of confined steady radial flow. Table 5.1 summarizes representative estimates of horizontal hydraulic conductivities for the Lucas, Amherstburg, Bois Blanc and Bass Islands formations, the basis/rationale for the estimate, and the data source for their inclusion in this report (INTERA 2011). Of note are the very permeable sections ( $1 \times 10^{-4}$  m/s) of the upper 20 m of Bass Islands Formation that created significant drilling fluid losses during drilling of all DGR boreholes and US-8.

**Table 5.1: Summary of Horizontal Hydraulic Conductivities for Lucas, Amherstburg, Bois Blanc and Bass Islands Formations**

Formation	Hydraulic Conductivity (m/s)	Basis/Rationale	Source
Lucas and Amherstburg (< 30 m)	$6 \times 10^{-9}$ to $3 \times 10^{-5}$ ( $2 \times 10^{-6}$ )	Range (geometric mean) from packer tests in US boreholes	Analysis of Lukajic (1988) Data
Lucas and Amherstburg (< 30 m)	$4 \times 10^{-9}$ to $2 \times 10^{-4}$ ( $5 \times 10^{-7}$ )	Range (geometric mean) from Bruce A site investigations	GOLDER (2003)
Amherstburg (> 30 m)	$8 \times 10^{-10}$ to $8 \times 10^{-5}$ ( $8 \times 10^{-8}$ )	Range (geometric mean) from packer tests in US boreholes	Analysis of Lukajic (1988) Data
Amherstburg (> 30 m)	$1 \times 10^{-8}$ to $2 \times 10^{-5}$ ( $2 \times 10^{-7}$ )	Range (geometric mean) from Bruce A site investigations	GOLDER (2003)
Bois Blanc (to 100 m)	$6 \times 10^{-10}$ to $1 \times 10^{-5}$ ( $1 \times 10^{-7}$ )	Range (geometric mean) from packer tests in US boreholes	Analysis of Lukajic (1988) Data
Combined Amherstburg and Bois Blanc	$1 \times 10^{-6}$ to $1 \times 10^{-4}$ ( $1 \times 10^{-5}$ )	Range (geometric mean) from tunnel dewatering experience and slug testing of US-5 & US-6	GOLDER (2003)
Bass Islands (upper 20 m)	$1 \times 10^{-5}$ to $3 \times 10^{-4}$ ( $1 \times 10^{-4}$ )	Range (geometric mean) from analysis of drilling fluid losses in US-8 and DGR boreholes	Sterling (2010b), Briscoe (2009), Briscoe et al. (2010a, 2010b)
Bass Islands	$1 \times 10^{-5}$	Estimated average representative value	GOLDER (2003)

## 5.2.2 Straddle-packer Hydraulic Testing

Field measurements of deep bedrock formation horizontal hydraulic conductivity were made in all DGR boreholes using a custom-built straddle-packer hydraulic testing tool (Roberts et al. 2011), as well as during opportunistic groundwater sampling using a bottom-hole, production-injection packer (PIP) during drilling. Hydraulic test responses were obtained from 3 intervals (12 m test zone) in DGR-1, 15 intervals (30.5 m test zone) in DGR-2, 23 intervals (30.7 m test zone) in DGR-3, 24 intervals (30.7 m test zone) in DGR-4, 11 intervals (30.3 m test zone) in DGR-5, and 12 intervals (10.2 m test zone) in DGR-6. The hydraulic tests performed in DGR boreholes included pulse, slug, and drill-stem tests (DST).

The testing in DGR-1 targeted selected intervals from 199.76 to 447.75 mBGS based on the stratigraphy and information obtained during fluid electrical conductivity logging (Beauheim and Pedler 2009). The testing in DGR-2, DGR-3 and DGR-4 provided continuous coverage of the open sections of each borehole typically from near the bottom of the intermediate steel casing in the Salina F Unit to near the top of the PIP set in the Shadow Lake Formation, which was installed to control artesian flow from the Cambrian sandstone. The testing in DGR-5 provided continuous coverage of the Ordovician shale and limestone. DGR-6 testing targeted fractured/suspected permeable intervals and unfractured/tight intervals within the Ordovician shales and limestones with shorter test-interval lengths than were used in DGR-2, DGR-3, DGR-4 and DGR-5.

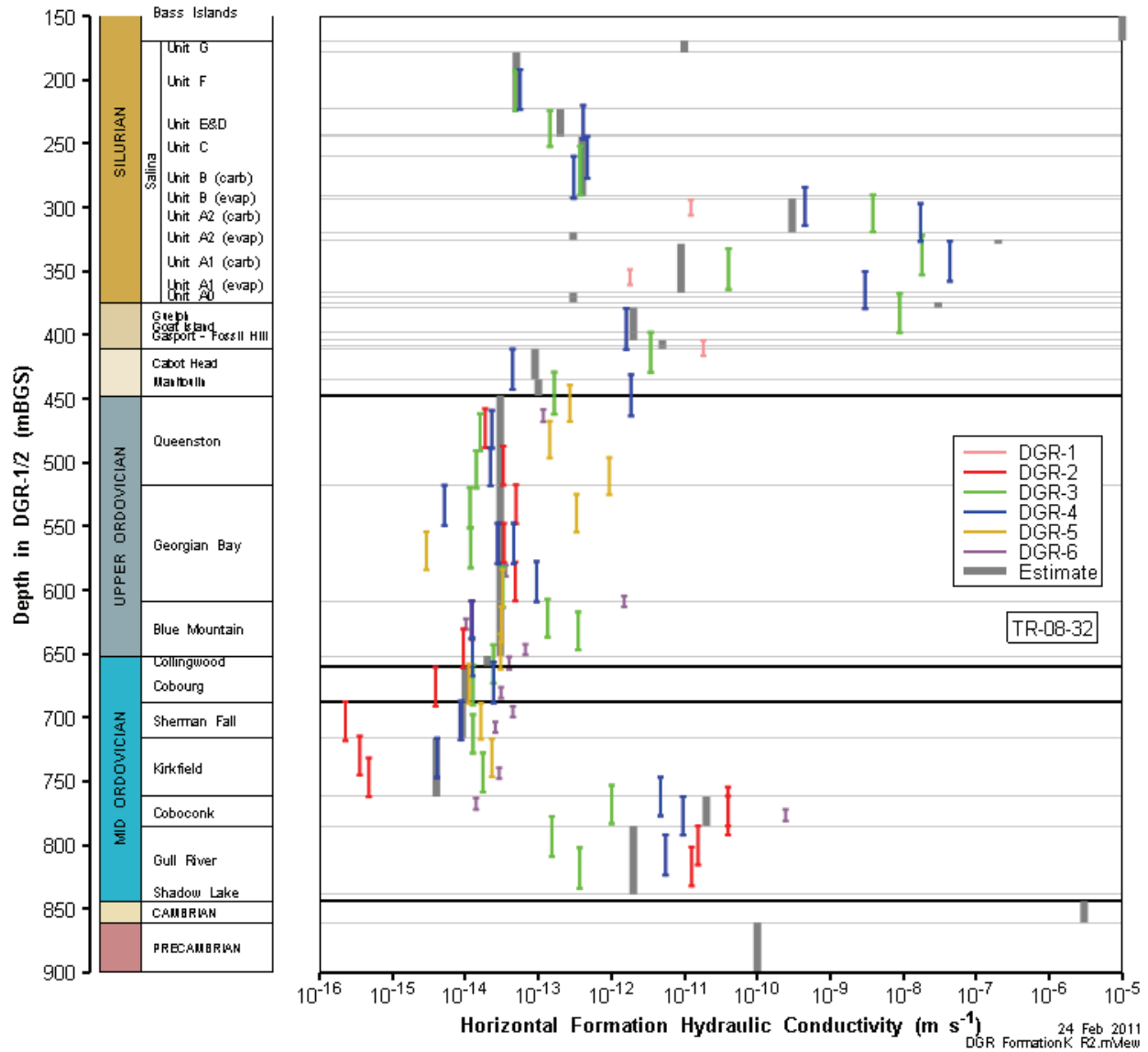
The DGR borehole hydraulic-test data were analysed by Roberts et al. (2011) using the nSIGHTS code developed by Sandia National Laboratories to determine best-fit, minimum, maximum and mean estimates of formation hydraulic conductivity and formation pressure, and other formation parameters including borehole skin thickness and hydraulic conductivity, and formation specific storage. Test analyses included consideration of test-interval pressure history based on drilling and drilling fluid density information and in-hole pressures recorded prior to packer isolation of the test interval. The test responses also provided data on the compressibility of the intervals tested. Test-interval compressibilities more than two to three times greater than the compressibility of water indicate unusual borehole conditions, such as deformable fractures, free gas in the test interval, or a soft (compressible) formation.

### 5.2.2.1 Hydraulic Conductivity

Interpretation of straddle-packer hydraulic tests with nSIGHTS (or any other analytical method) provides estimates of the overall transmissivity of the straddled interval. The average hydraulic conductivity ( $K$ ) of the interval is obtained by dividing the transmissivity by the interval length. In a (near) vertical borehole passing through strata dipping as slightly as those at the Bruce nuclear site, this  $K$  value is the average horizontal  $K_H$  of the interval—the testing provides no information on the vertical  $K_V$  of the strata. For the tests in the slanted boreholes, DGR-5 and DGR-6, compensations were made to the test-interval geometry as proposed by Beauheim et al. (1993) to allow interpretations as if the intervals were vertical.

Figure 5.1 shows the average horizontal  $K_H$  values inferred from the hydraulic testing in boreholes DGR-1/2, DGR-3, DGR-4, DGR-5, and DGR-6. The  $K_H$  estimates presented are all based on an assumption that the intervals tested are homogeneous—individual layers within the tested intervals may actually have  $K_H$  values greater or less than the average values. Because of the straddle lengths used during the hydraulic testing of the DGR boreholes (10.2 to 30.7 m), all test intervals contained multiple layers with differing degrees of heterogeneity and some intervals contained portions of different geological formations. Figure 5.1 also shows the

formation-specific  $K_H$  values (grey bars) inferred from the testing performed in all the holes while taking account of heterogeneity among formations (INTERA 2011). Test results from the 10.2 m intervals in DGR-6 provide an indication of the heterogeneity present among layers within individual formations. Figures 5.1 through 5.6 include references to the specific technical reports from which the presented data were compiled (e.g. TR-08-32 in Figure 5.1). Refer to Table 2.1 in INTERA (2011) for a complete list of these technical reports.



Notes: Formation estimates determined from all tests are shown by the thick grey bars. From Walsh (2011; their Figure 1).

**Figure 5.1: Best-fit Interval Horizontal Hydraulic Conductivities from Borehole Straddle-packer Tests and Estimated Formation Average Values**



Figure 5.1 shows that the estimated formation-average Silurian  $K_H$  values are typically less than  $10^{-12}$  m/s except in the following horizons: Salina A2 carbonate, Salina A1 carbonate and Guelph-Goat Island-Gasport-Lions Head (Niagaran). Based on the testing in DGR-1, DGR-3 and DGR-4, the estimated average horizontal formation  $K_H$  value for the Salina A2 carbonate is  $3 \times 10^{-10}$  m/s. INTERA (2011) divide the Salina A1 carbonate into a 3.7 m thick upper vuggy unit and a 38.5 m-thick lower unit. They assign a  $K_H$  value of  $2 \times 10^{-7}$  m/s to the upper A1 carbonate and a  $K_H$  value of  $9 \times 10^{-12}$  m/s to the lower A1 carbonate. Based on testing performed in DGR-3 and DGR-4, the estimated average horizontal formation  $K_H$  value for the Guelph is  $3 \times 10^{-8}$  m/s. Estimating individual formation  $K_H$  values for the Goat Island, Gasport, Lions Head and Fossil Hill units is difficult because all of the test intervals in DGR-1, DGR-3 and DGR-4 included several of these units rather than just one; INTERA (2011) estimates that the average formation  $K_H$  values of these units range from  $2 \times 10^{-12}$  to  $5 \times 10^{-12}$  m/s.

The estimated formation-average horizontal  $K_H$  values for the Ordovician units shown on Figure 5.1 are all less than  $10^{-13}$  m/s except in the Coboconk and Gull River formations. INTERA (2011) estimates the average Coboconk  $K_H$  value to be  $2 \times 10^{-11}$  m/s and that of the Gull River to be  $2 \times 10^{-12}$  m/s.

### 5.2.2.2 Formation Pore Pressure

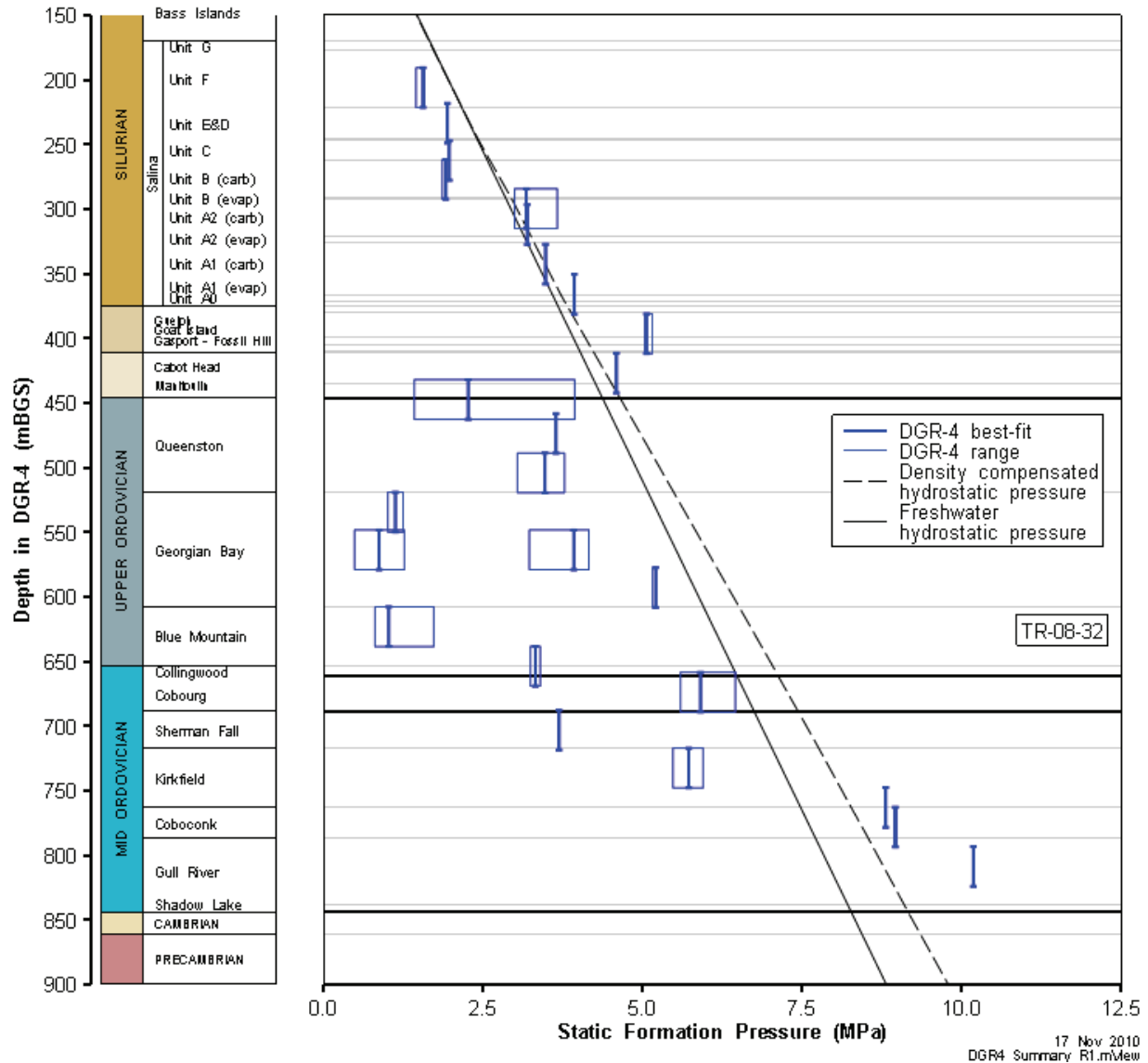
Figure 5.2 shows the formation pressure ( $P_f$ ) values inferred from the hydraulic testing in borehole DGR-4, along with the estimated uncertainty associated with each of the  $P_f$  estimates. Similar plots for the other tested boreholes can be found in Roberts et al. (2011), showing similar pressure profiles. Also shown are lines representing hydrostatic pressure profiles through the stratigraphy assuming fresh water (solid lines) and the water density profile shown in Figure 5.3 (dashed lines). The pressure profile shows that the Salina B carbonate through F units are slightly underpressured, while the remainder of the Silurian units apart from the Goat Island to Fossil Hill interval are essentially at hydrostatic conditions. The Goat Island to Fossil Hill interval appears to be slightly overpressured. The Upper Ordovician and Trenton Group are generally underpressured, although individual discrete intervals are near hydrostatic pressure. The Black River Group is generally overpressured as is the underlying permeable Cambrian.

### 5.2.2.3 Test-zone Compressibility

Test-zone compressibility ( $C_{tz}$ ) is calculated during pulse testing when a displacement of known volume in the test zone creates a measured pressure change. An estimate of  $C_{tz}$  is necessary to interpret hydraulic tests, but beyond that, its significance lies in what it reveals about the intervals being tested. In a completely brine-saturated system in unfractured, stiff rock,  $C_{tz}$  should be very close to the compressibility of brine ( $\sim 3.3 \times 10^{-10}$  Pa<sup>-1</sup>; Walsh 2011), with small deviations caused by the compressibility of the packers and other test tool components. Higher  $C_{tz}$  values may indicate the presence of deformable fractures, the presence of a free gas phase, a soft (compressive) formation, or other compressible features in immediate hydraulic communication with the test interval.

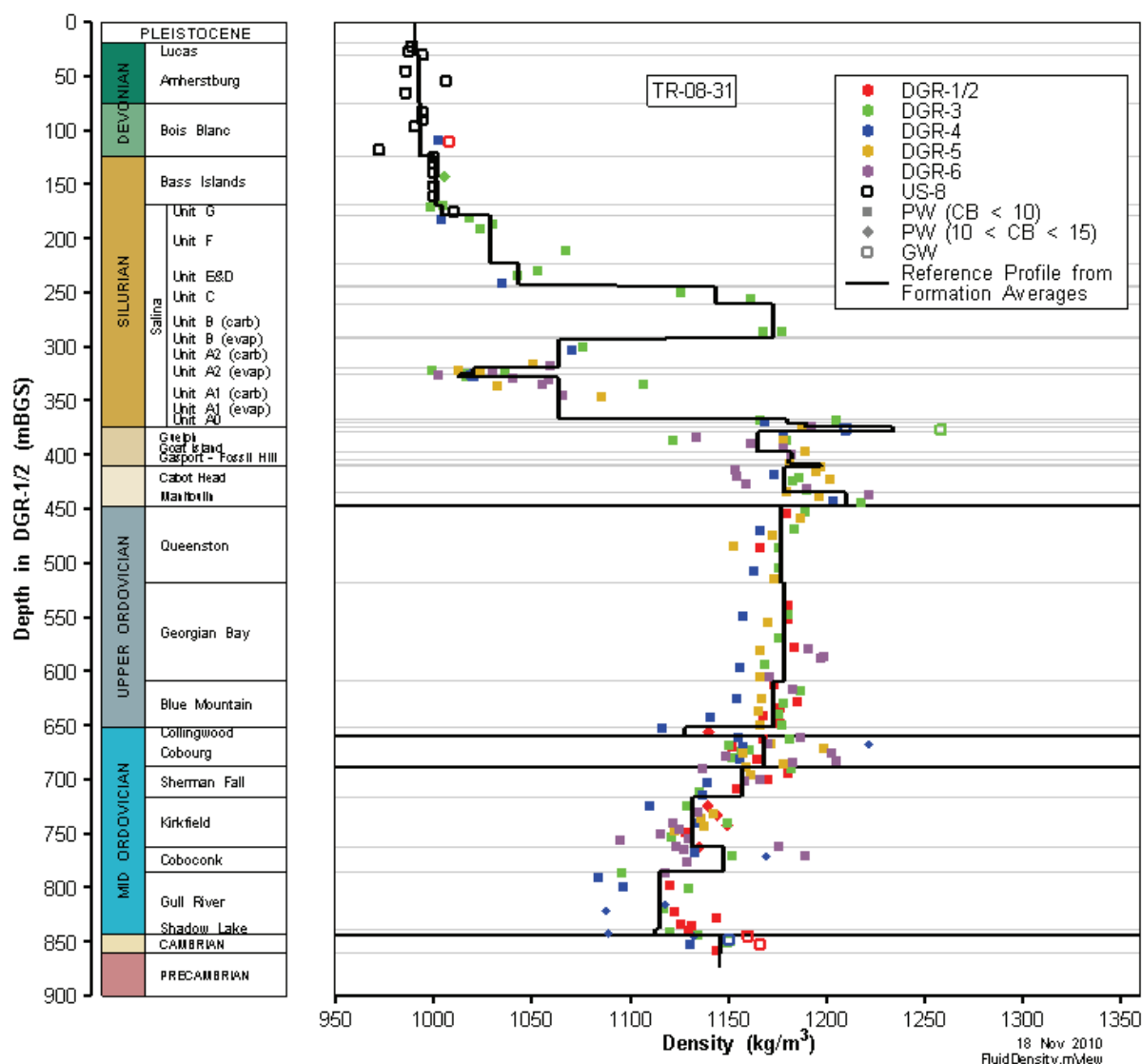
Figure 5.4 shows the  $C_{tz}$  estimates determined for each of the straddle-packer intervals in the DGR boreholes. Test-zone compressibility estimates for most of the high-permeability intervals, such as the Guelph, are not available because slug tests rather than pulse tests were performed. The majority of the  $C_{tz}$  estimates are less than  $10^{-9}$  Pa<sup>-1</sup>, as expected. The Middle Ordovician units, in particular, show  $C_{tz}$  values little different from the compressibility of brine. Other units, however, show higher  $C_{tz}$  values. Test-zone compressibilities of  $6.6 \times 10^{-9}$  Pa<sup>-1</sup>,  $1.0 \times 10^{-8}$  Pa<sup>-1</sup> and  $4.6 \times 10^{-9}$  Pa<sup>-1</sup> were observed in the Manitoulin-Queenston test intervals of

DGR-3, DGR-4, and DGR-5, respectively. Fractures were observed in the uppermost Queenston core from DGR-3 and in the lowermost Manitoulin core from DGR-4 (Briscoe et al. 2010a), and in both the lowermost Manitoulin and uppermost Queenston in DGR-5. High  $C_{tz}$  values were also observed in lower Georgian Bay intervals in all DGR boreholes, and in the Blue Mountain in DGR-3 and DGR-6, all in association with observed fractures. Test intervals that included the Gasport, Lions Head, and/or Fossil Hill formations typically had high  $C_{tz}$  values.



Notes: From Roberts et al. (2011; their Figure 4-77).

**Figure 5.2: Formation Pressure Estimates and Uncertainty Ranges from Straddle-packer Tests in DGR-4**

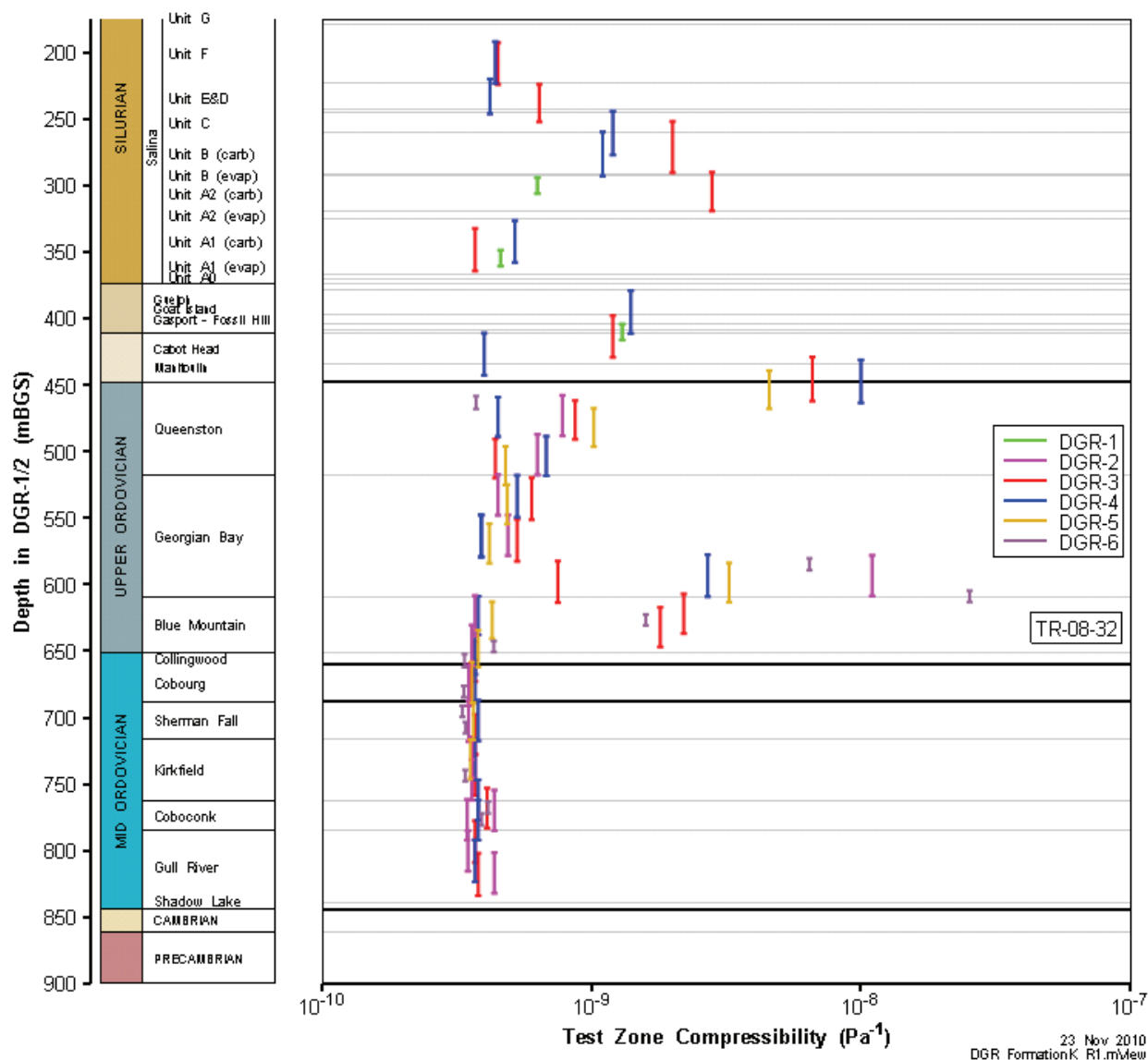


Notes: From INTERA (2011; their Figure 4.81).

**Figure 5.3: Reference Fluid Density Profile and Formation Averages Based on US-8 and DGR Borehole Groundwater and Porewater Data**

### 5.2.3 Westbay Pressure Measurements in the DGR Boreholes

Boreholes DGR-1, DGR-2, DGR-3 and DGR-4 were completed with Westbay stainless steel and PVC MP55 multi-level monitoring casings, primarily to provide access for formation pressure measurement, but also to allow for future groundwater sampling. Westbay casings were not installed in DGR-5 and DGR-6. The MP55 casing originally installed in DGR-2 in December 2007 was removed in June 2009, and replaced with an improved and upgraded MP55 casing system in December 2009. Information about the Westbay installations in the DGR boreholes is given in Table 5.2.



Notes: From INTERA (2011; their Figure 4.89).

**Figure 5.4: Test-zone Compressibility Estimates from Straddle-packer Tests in DGR Boreholes**

Pressure profiles have been completed in the Westbay casings at different times since installation to monitor pressure equilibration in the various stratigraphic intervals. Figure 5.5 shows the measured Westbay pressures and estimated environmental head profile for borehole DGR-4, along with the formation pressure estimates derived from the straddle-packer testing. Environmental head, as defined by Lusczynski (1961), accounts for changes in fluid density that occur with depth in a stratigraphic sequence, allowing for the determination of vertical, but not horizontal, hydraulic gradients. Similar profile figures for the Westbay installations in boreholes DGR-1/2 and DGR-3 are given in INTERA (2011). The Westbay intervals are generally shorter

than the straddle-packer intervals, and therefore provide more detail and involve less averaging of pressures.

**Table 5.2: Major Design Elements of MP55 Casing Systems Installed in DGR Boreholes**

MP55 Casing Element	DGR-1	DGR-2 (old)	DGR-2 (new)	DGR-3	DGR-4
Monitored Depth Range (mBGS)	190.7 to 462.9	460.4 to 848.0	460.7 to 846.7	218.3 to 869.2	194.3 to 852.5
Number of Packers	23	28	27	43	43
Number of Formation Pressure Monitoring Intervals	22	25	24	42	42
Average Monitoring Interval Length (m)	11.3	14.4	14.7	14.0	14.3
Range of Monitoring Interval Lengths (m)	3.4 to 24.0	3.0 to 23.0	5.2 to 24.2	4.7 to 28.7	3.2 to 24.2
Number of Pressure Profiles Completed to June 2010	13	6 + Continuous MOSDAX	2	3	4

Notes: From INTERA (2011; their Table 4.15).

The units with hydraulic conductivities greater than approximately  $10^{-13}$  m/s (most of the Silurian and the Black River Group) show pressures nearing equilibration after a few months, at values in reasonably good agreement with the estimates provided by the straddle-packer testing. Pressures in the lower permeability Ordovician units are equilibrating more slowly, but are generally trending toward the straddle-packer estimates.

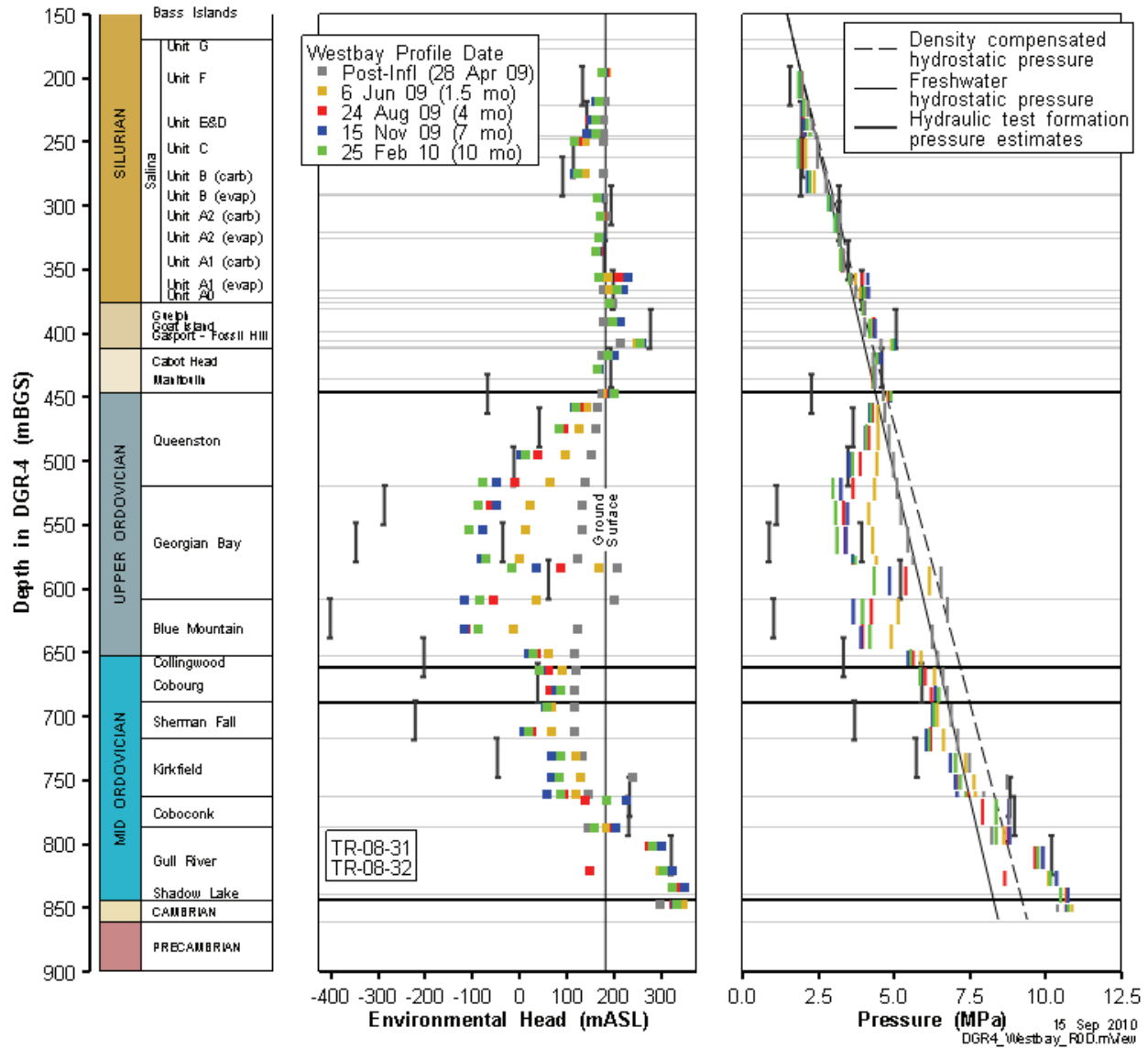
The primary features shown by the Westbay monitoring are:

- Underpressures in the Salina Group, with maximum underpressures occurring within the C and B units equal to environmental heads of 70 mBGS;
- Overpressures in the Salina A1 and A0 units, and Gasport to Fossil Hill formations, with maximum overpressures equal to environmental heads of 75 mAGS;
- Underpressures in the Ordovician shales and Trenton Group limestones, with maximum underpressures occurring within the Blue Mountain Formation equal to environmental heads of 300 mBGS; and
- Overpressures in the Black River Group limestones and siltstones and the Cambrian sandstone, with maximum overpressures equal to environmental heads of 165 mAGS.

### 5.3 Laboratory Studies

Laboratory studies have been performed on core and groundwater samples collected from the DGR boreholes to provide information on a variety of factors related to groundwater flow and transport. Analyses of the groundwater samples and porewaters extracted from core samples

are discussed in Chapter 4. Petrophysical measurements performed on core samples are discussed below.



Notes: From INTERA (2011; their Figure 4.102).

**Figure 5.5: Measured Westbay Pressures and Estimated Environmental Head Profile for Borehole DGR-4**

### 5.3.1 Porosity

Porosity represents the ratio of the volume of voids in a rock to the total volume of the rock. Three types of porosity are defined to differentiate 1) the type of fluid occupying the void space

and 2) the measurements made by different testing laboratories: total porosity, liquid porosity and water-loss porosity. Total porosity, also known as physical porosity, is the sample volume not occupied by mineral grains (i.e., total volume of voids) divided by the volume of the sample. Liquid porosity is the volume of the voids occupied by liquid (i.e., pure water plus dissolved solutes and oil) divided by the total volume of the sample. Water-loss porosity is the volume of the voids occupied by pure water divided by the total volume of the sample. Total porosity should equal liquid porosity plus porosity occupied by any gas (e.g., methane).

INTERA (2011) presents the porosity data derived from the three different types of measurements, and discusses differences in the data sets and their possible causes. Figure 5.6 shows the total porosities measured in the DGR borehole cores, along with the arithmetic formation average values.

### 5.3.2 Permeability

The permeability ( $k$ ) of DGR rock cores to gas and brine was measured using pulse-decay tests as described in Whitney and Lee (2010) and Jackson and Wigston (2010). Tests were performed on “as received” core that contained porewater, on “clean and dry” cores that had porewater and salts removed, and on brine-saturated cores. INTERA (2011) present and discuss the various laboratory permeability measurements, and conclude that “the lab  $k$  data are considered to be unrealistically high values due to irrecoverable damage of core during drilling, recovery and shipment to the lab for testing and handling, and sample preparation in the lab.” The data provided by in situ hydraulic tests are considered to be more reliable.

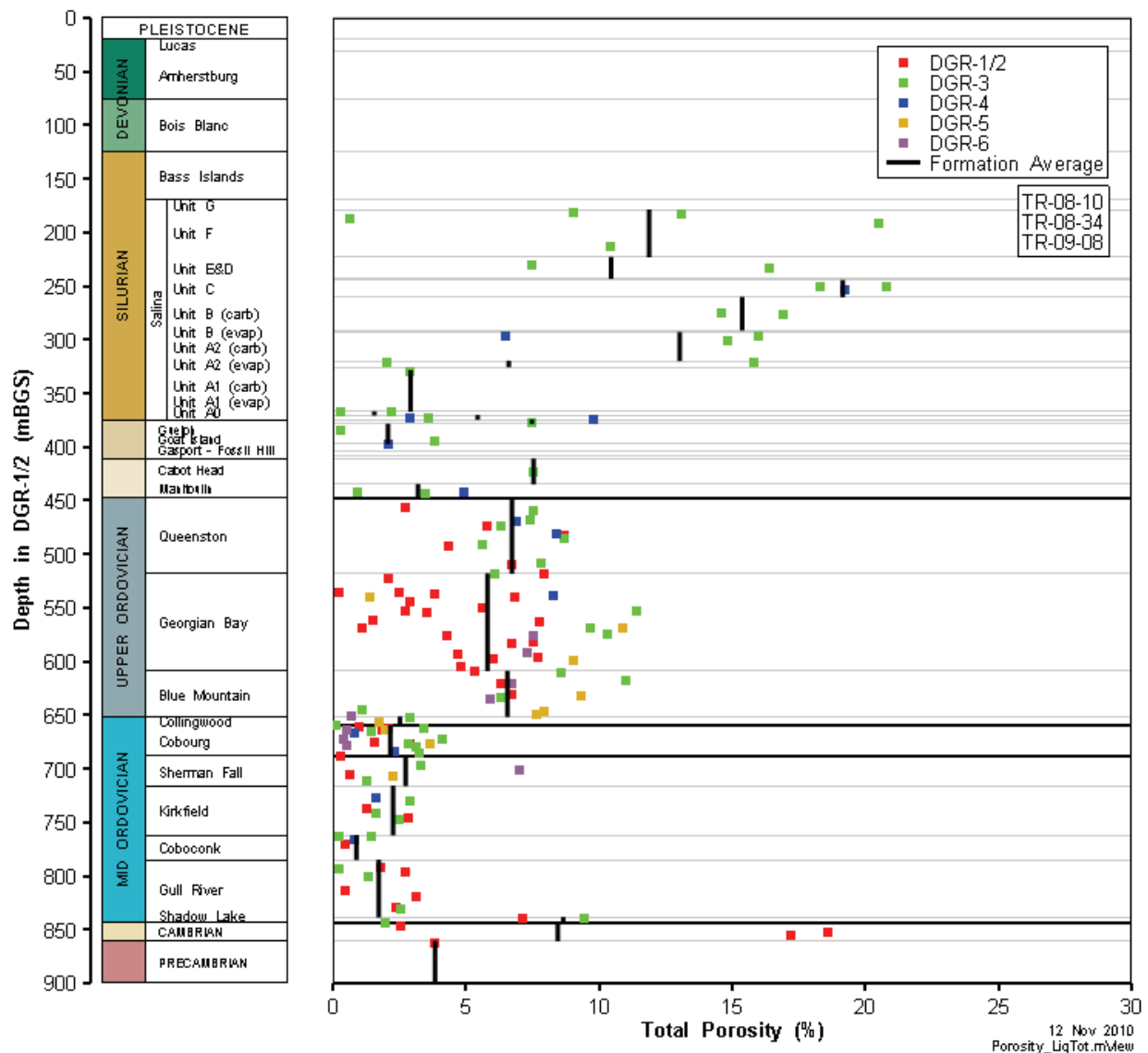
### 5.3.3 Fluid Saturations

The fraction (or percentage) of brine, oil and gas in the pore volume of a core plug drilled from a core sample is the “saturation”. Relative fluid saturations were estimated from testing on 106 samples using Dean-Stark or NMR/He methods (e.g., Raven and Jackson 2010). Confidence in the reported gas saturations is judged to be low, principally because of the concern that the generally small values reported (formation group means of 7-14%, formation means of 0-20%) may be artefacts due to sample drying and irrecoverable core relaxation effects during sample collection, handling and preparation for testing, and the difficulty of accurately measuring such properties in low porosity (< 2%) formations. Because gas saturations are determined as the difference between calculated total porosity and calculated brine and oil saturations in Dean-Stark testing, the estimate of gas saturation incorporates all of the errors accumulated in estimating total porosity and both water saturation and oil saturation.

As discussed in INTERA (2011), irrecoverable core damage cannot fully explain the resultant gas saturations, but sample drying and measurement error remain potential explanations for the reported gas saturations. Uncertainty in gas saturations due to measurement error associated with Dean-Stark testing is significant (+/- 50 to 100%) for formations with porosity of < 2%. Consequently, all of the reported gas saturations for the Ordovician limestones that have porosity of less than 2% may be the result of measurement error. For the higher porosity Ordovician shales, measurement error is not a reasonable explanation for the reported gas saturations. On balance, the available data indicate that gas is likely present as a discrete separate phase within the pore space of some of the Silurian and Ordovician formations, but confidence in the quantitative estimates presented in INTERA (2011) is low.

### 5.3.4 Constitutive Properties and Specific Storage

Stress-strain data collected during uniaxial compression testing of DGR borehole core samples were analyzed to determine undrained Young's moduli and Poisson's ratio, undrained and drained bulk moduli, and undrained and drained rock compressibility. Specific storage values were then calculated from formation-averaged liquid porosity and pore fluid density values and individual core rock drained compressibility data. The methods and results of these calculations are provided in Walsh (2011).



Notes: From INTERA (2011; their Figure 4.3).

**Figure 5.6: Total Porosity Profiles from the DGR Borehole Cores**



Table 5.3 shows the calculated ranges of geometric mean formation averages of specific storage by formation from testing of DGR core. The Devonian and most of the Silurian units have specific storage of  $3 \times 10^{-7}$  to  $2 \times 10^{-6}$   $m^{-1}$ . The Salina C Unit, Salina upper B Unit, Cabot Head shale and the Ordovician shales have higher values, with specific storage values ranging from  $1 \times 10^{-6}$  to  $3 \times 10^{-5}$   $m^{-1}$ . Specific storage tends to increase with depth within the Ordovician shales, with maximum values (specific storage =  $3 \times 10^{-5}$   $m^{-1}$ ) evident within the Blue Mountain Formation. The Sherman Fall and Kirkfield formations have poroelastic properties similar to those of the Devonian/Silurian units with specific storage of  $7 \times 10^{-7}$  to  $2 \times 10^{-6}$   $m^{-1}$ . The units with the lowest specific storage values, ranging from  $2 \times 10^{-7}$  to  $7 \times 10^{-7}$   $m^{-1}$ , include the Lucas Formation, the Salina D, B evaporite, A2 evaporite, A1 evaporite, and A0 units, and the Goat Island, Gasport, Lions Head, Fossil Hill, Coboconk and Gull River formations.

### 5.3.5 Diffusion Properties

Laboratory-scale diffusion measurements were undertaken using core samples from the DGR boreholes to determine effective diffusion coefficients ( $D_e$ ) for the Silurian and Ordovician sections of the stratigraphy. With the exception of just a few samples from the Upper Silurian, the  $D_e$  values measured from DGR drill cores are all less than  $10^{-12}$   $m^2/s$  (Figure 5.7, Table 5.4). The highest values occur in the Upper Silurian Salina B, C, E and F units, with values greater than  $10^{-11}$   $m^2/s$  in the silty shale of the Salina B. The lowest values, on the order of  $10^{-14}$   $m^2/s$ , are obtained in the gypsum-anhydrite layers of the Salina A0 to A2 units, in the carbonate "hardbeds" within the Georgian Bay Formation, and several limestone samples in the Gull River Formation. These extremely low values may be the lowest measured for sedimentary rocks anywhere. The majority of the data are in the range  $10^{-13} < D_e < 10^{-11}$   $m^2/s$ , with Lower Silurian and Upper Ordovician shale samples representing the higher end of this range because of their relatively high porosity (7 to 9%). The lower porosity of the Middle Ordovician limestones (< 2%) results in lower  $D_e$  values, which cluster in the range  $10^{-13} < D_e < 10^{-12}$   $m^2/s$ , with only a few samples displaying values greater than  $10^{-12}$   $m^2/s$ .

The data display systematic variability as a function of the tracer used to make the measurements, and  $D_e$  values obtained with HTO tracer are on average 1.9 times greater (range of 0.8 to 4.9) than  $D_e$  values obtained with iodide tracer. This difference is attributed to the influence of anion exclusion in lowering the tracer-accessible porosity for iodide. There is also a systematic difference in  $D_e$  values as a function of the orientation of the measurements with respect to the bedding direction. With only two exceptions in the Upper Silurian (Figure 5.7), the  $D_e$  values are greatest for diffusion in the orientation parallel to bedding. The anisotropy ratio ( $D_e$  parallel/ $D_e$  normal) ranges from 1 to 4 for measurements made with the iodide tracer, and from 1 to 7 for measurements made with HTO (Xiang et al. 2009). An investigation of diffusive anisotropy at the formation scale was conducted by Cavé et al. (2010). They used detailed lithologic logs and laboratory-scale diffusion measurements to calculate formation-scale  $D_e$  values for transport normal to bedding (harmonic average) and transport parallel to bedding (arithmetic average). The study was conducted on the Georgian Bay Formation, which contains over 700 cm-scale hardbed layers (limestone and siltstone; INTERA 2011) that increase diffusive anisotropy. A formation-scale anisotropy ratio of 7.2 was obtained from the ratio of the arithmetic to the harmonic mean.

**Table 5.3: Specific Storage Estimates Derived from Laboratory Measurements on DGR Core**

Formation	Range of $S_s$ Estimates ( $m^{-1}$ )	$S_s$ Used in Modelling ( $m^{-1}$ )
Lucas	5E-07 - 7E-07	1.4E-06
Amherstburg (upper 20 m)	7E-07 - 2E-06	1.4E-06
Amherstburg (lower 20 m)	7E-07 - 2E-06	1.4E-06
Bois Blanc	6E-07 - 1E-06	1.4E-06
Bass Islands (upper 20 m)	1E-06 - 2E-06	2.0E-06
Bass Islands (lower 25 m)	1E-06 - 2E-06	2.0E-06
Salina G Unit	1E-06 - 2E-06	1.1E-06
Salina F Unit	1E-06 - 7E-06	9.5E-07
Salina E Unit	1E-06 - 7E-06	6.5E-07
Salina D Unit	5E-07 - 7E-07	6.4E-07
Salina C Unit	2E-06 - 1E-05	9.5E-07
Salina B Unit - Carbonate	5E-06 - 2E-05	9.5E-07
Salina B Unit - Evaporite	5E-07 - 7E-07	6.9E-07
Salina A2 Unit - Carbonate	1E-06 - 2E-06	7.2E-07
Salina A2 Unit - Evaporite	5E-07 - 6E-07	5.8E-07
A1 Unit – Upper Carbonate	5E-07 - 1E-06	4.1E-07
A1 Unit – Lower Carbonate	5E-07 - 1E-06	4.1E-07
Salina A1 Unit - Evaporite	3E-07 - 4E-07	4.5E-07
Salina A0 Unit	3E-07 - 3E-07	4.5E-07
Guelph	9E-07 - 1E-06	2.7E-07
Goat Island	3E-07 - 5E-07	2.7E-07
Gasport	3E-07 - 5E-07	2.7E-07
Lions Head	5E-07 - 7E-07	2.7E-07
Fossil Hill	3E-07 - 4E-07	2.9E-07
Cabot Head	4E-06 - 3E-05	1.1E-06
Manitoulin	7E-07 - 1E-06	7.5E-07
Queenston	1E-06 - 5E-06	9.0E-07
Georgian Bay	2E-06 - 1E-05	1.2E-06
Blue Mountain	3E-06 - 3E-05	1.2E-06
Cobourg – Collingwood	5E-07 - 1E-06	1.2E-07
Cobourg - Lower	3E-07 - 6E-07	2.6E-07
Sherman Fall	8E-07 - 2E-06	4.9E-07
Kirkfield	7E-07 - 2E-06	4.9E-07
Coboconk	2E-07 - 4E-07	4.6E-07
Gull River	3E-07 - 6E-07	4.9E-07
Shadow Lake	8E-07 - 1E-06	7.4E-07
Cambrian	8E-07 - 1E-06	3.7E-07
Upper Precambrian	1E-06	2.6E-07

Notes: From Sykes et al. (2011; their Table 4.3).

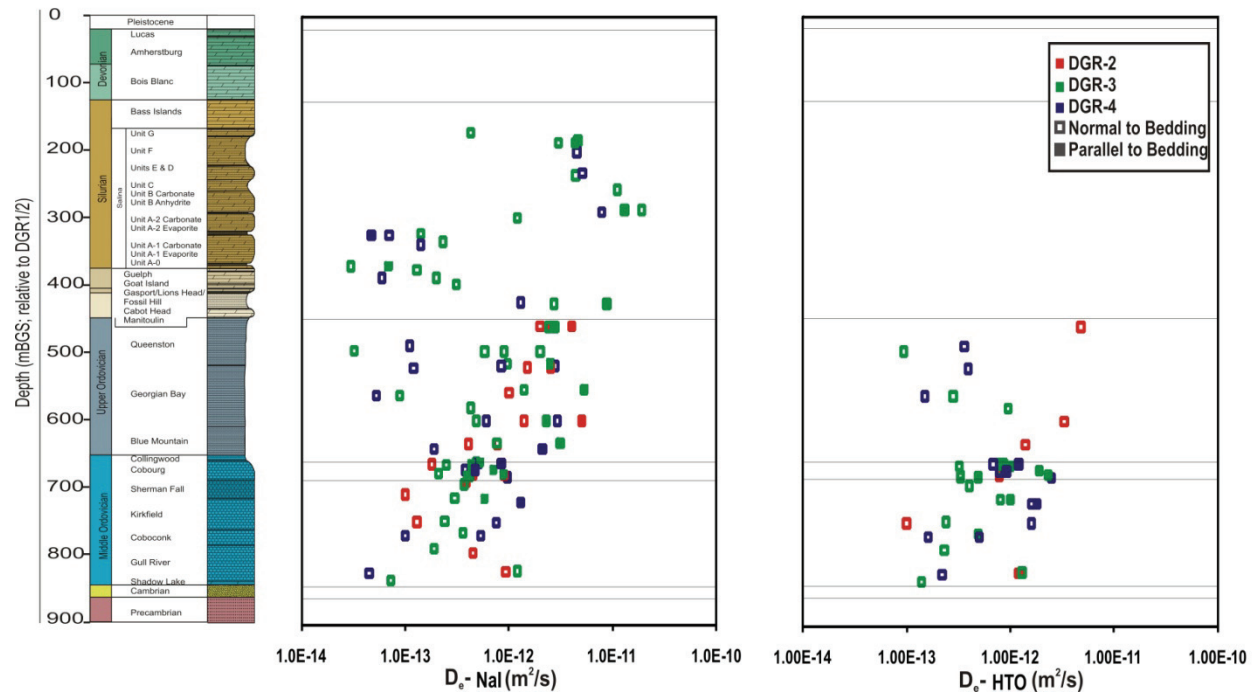


Figure 5.7: Effective Diffusion Coefficients ( $D_e$ ) versus Depth

Table 5.4: Iodide Effective Diffusion Coefficients

Model Layer	Vertical Iodide Diffusion Coefficient $D_{e-v}$ ( $m^2/s$ )	Anisotropy Ratio $D_{e-h}:D_{e-v}$ (-)
Clay till overburden	6.0E-10	1:1
Lucas	6.0E-12	1:1
Amherstburg (upper 20m)	6.0E-12	1:1
Amherstburg (lower 20m)	6.0E-12	1:1
Bois Blanc	6.0E-12	1:1
Bass Islands (upper 20m)	1.3E-11	1:1
Bass Islands (lower 25m)	1.3E-11	1:1
Salina G Unit	4.3E-13	2:1
Salina F Unit	4.1E-12	2:1
Salina E Unit	4.7E-12	2:1
Salina D Unit	4.7E-12	2:1
Salina C Unit	1.1E-11	2:1

Model Layer	Vertical Iodide Diffusion Coefficient $D_{e-v}$ ( $m^2/s$ )	Anisotropy Ratio $D_{e-h}:D_{e-v}$ (-)
Salina B Unit – Carbonate	1.2E-11	2:1
Salina B Unit – Evaporite	7.7E-14	2:1
Salina A2 Unit – Carbonate	1.2E-12	2:1
Salina A2 Unit – Evaporite	7.7E-14	2:1
A1 Unit – Upper Carbonate	4.9E-12	1:1
A1 Unit – Lower Carbonate	1.8E-13	2:1
Salina A1 Unit – Evaporite	3.0E-14	2:1
Salina A0 Unit	3.0E-14	2:1
Guelph	3.2E-12	1:1
Goat Island	1.5E-13	2:1
Gasport	1.5E-13	2:1
Lions Head	6.2E-12	2:1
Fossil Hill	1.6E-11	2:1
Cabot Head	3.1E-12	2:1
Manitoulin	1.5E-13	2:1
Queenston	1.0E-12	2:1
Georgian Bay	4.3E-13	7:1
Blue Mountain	8.2E-13	2:1
Cobourg – Collingwood Member	4.9E-13	2:1
Cobourg – Lower	3.7E-13	2:1
Sherman Fall	2.2E-13	2:1
Kirkfield	4.2E-13	2:1
Coboconk	2.7E-13	2:1
Gull River	2.6E-13	2:1
Shadow Lake	6.1E-12	2:1
Cambrian	7.7E-12	1:1
Upper Precambrian	3.0E-13	1:1

Notes: Data are from INTERA (2011).

#### 5.4 Hydrogeological Modelling

The objective of hydrogeological modelling is to assist in developing the safety case for the proposed DGR at the Bruce nuclear site. This assistance is provided by characterizing and

analyzing the groundwater system in the deep geologic formations by creating robust numerical groundwater models (e.g., Sykes et al. 2011). In order to develop an understanding of groundwater migration and mass transport in the deep geological units, it is especially pertinent to ensure that the basis for the numerical models is developed from sound geologic interpretations and conceptual models (i.e., INTERA 2011). This will contribute to a more accurate distribution of unit properties such as permeability for a given numerical model and an appropriate realization of the domain geometry. The distribution of permeability is of importance due to the requirements of sufficient thickness, lateral continuity, and predictability of the geologic units contributing to the performance of the proposed repository.

The analyses of the modelling study were designed to gain insight on regional-scale and site-scale groundwater system hydrodynamics and evolution relevant to understanding groundwater pathways and solute migration from the location of the proposed DGR in the Cobourg Formation. A primary focus of the numerical modelling study is the investigation of the hypothesis that solute transport in the Ordovician sediments is diffusion dominant.

This section summarizes the hydrogeological modelling performed for the DGR project at the Bruce nuclear site. It is a summary of the work that is described in detail in the Hydrogeologic Modelling report (Sykes et al. 2011).

#### **5.4.1 Conceptual Models**

From a hydrogeological viewpoint, the Michigan Basin can be conceptualized as a closed system, closed in the sense that groundwater flows neither in nor out from outside the basin. Recharge occurs where formations crop out (or subcrop) and discharge occurs into lakes and streams at topographical low points. Thus, gravitational driving forces are strongly controlled by the topographic relief of the basin.

The salinity (or density) distribution within the stratigraphic column exerts a strong influence on flow. All concentrations increase significantly below the shallow groundwater system. Without significant driving forces, dense brines at depth cannot be displaced by fresh waters entering the system at the surface, so the deep brines in the Michigan Basin are likely to be effectively stagnant (i.e., mass transport is diffusion dominant).

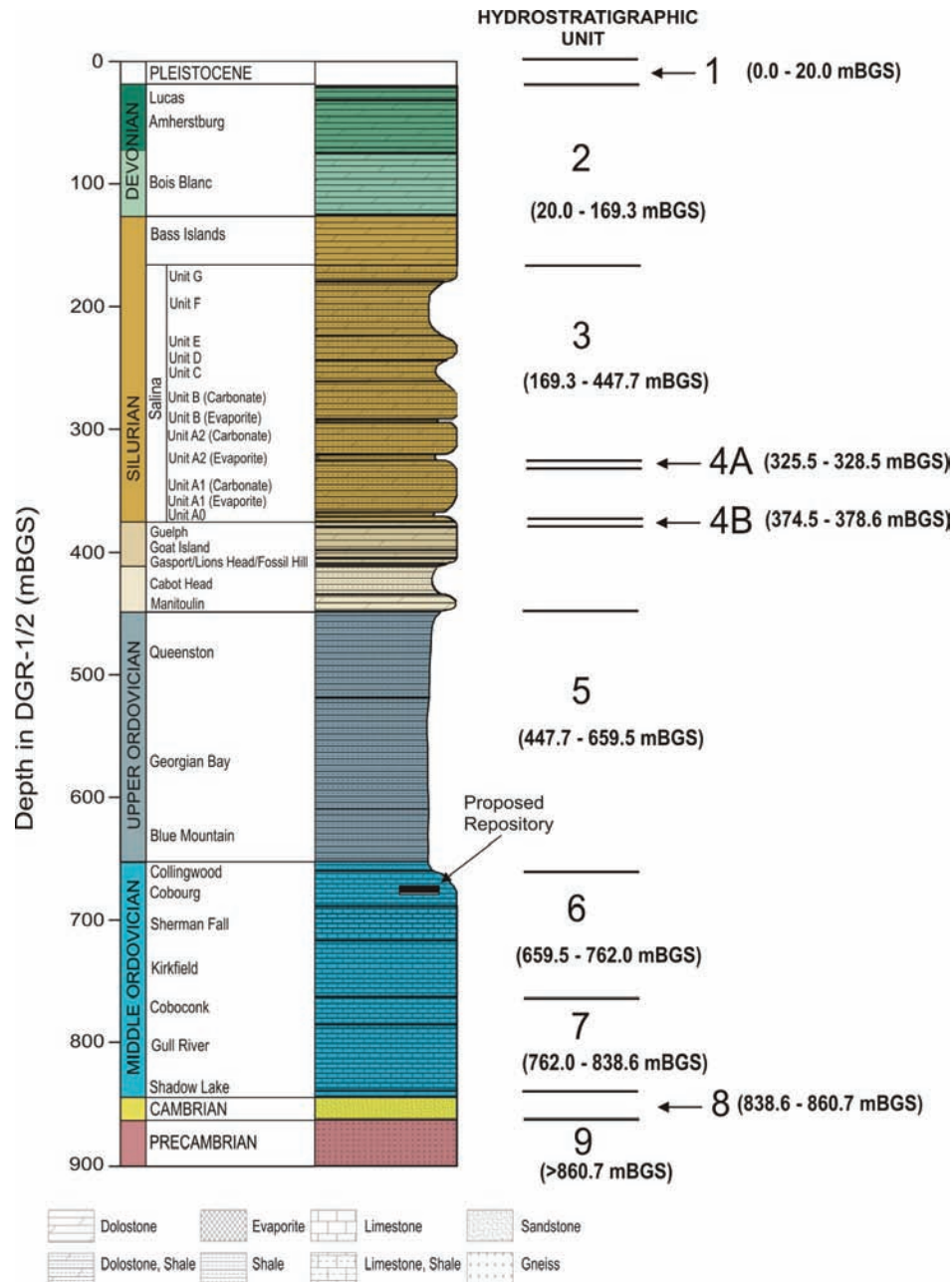
The regional-scale modelling integrated aspects of the Geosynthesis studies in one framework through the development and analysis of a regional and site-scale geosphere conceptual model. The conceptual model for the DGR site was defined by both the field and laboratory investigations of the site characterization study (INTERA 2011). The work product of the Regional Geology Study together with the data from the DGR boreholes defines the geologic framework of the conceptual model. Hydraulic parameters for the model hydrostratigraphic units were defined using data from the DGR site boreholes and from lab analyses of cores. Borehole data included hydraulic conductivities from straddle-packer hydraulic tests and pressure measurements from the Westbay MP38 and MP55 multi-level groundwater monitoring systems.

The regional-scale and site-scale porewater chemistry are defined in Chapter 4. Rock cores and opportunistic water samples were used to define the spatial distribution of the TDS concentration and fluid density. Core analyses yielded estimates of porosity, elastic modulus, Poisson's ratio, water saturations and gas saturations. Layer-dependent specific storage coefficients and one-dimensional loading efficiencies were calculated using appropriate field and laboratory data. The Long-Term Climate Change study defined the glacial loading and the

evolution of the formation properties for paleohydrogeologic analyses (Peltier 2011). The numerical model of the Bruce nuclear site requires the development of constitutive models that relate the fluid density to the fluid TDS concentration. The linking of the field program to the development of the parameters of the numerical models adds to the confidence and robustness of conclusions developed from the modelling.

The stratigraphic units observed at the Bruce nuclear site are grouped into three groundwater regimes (listed below) associated with different high-permeability units that behave independently of one another because they are separated by low-permeability strata (INTERA 2011).

- **Shallow Regime:** The shallow hydrogeological regime includes surficial Pleistocene deposits, Devonian strata, and the Silurian Bass Islands Formation. It extends to the top of the Salina G Unit which is encountered at a reference depth of 169.3 mBGS in DGR-1/2 (see Figure 5.8). Groundwater within the permeable bedrock regime flows from recharge areas toward Lake Huron, where it discharges. Groundwaters and porewaters are transitional from fresh Ca:Mg-HCO<sub>3</sub> water (TDS ~0.5 g/L) near the top of the bedrock to brackish Ca-SO<sub>4</sub> water (TDS ~5.0 g/L) at the bottom of the shallow regime. Representative horizontal hydraulic conductivities ( $K_H$ ) range from  $8 \times 10^{-8}$  to  $1 \times 10^{-4}$  m/s (see Figure 5.1). Solute migration within this permeable shallow groundwater regime is driven principally by advection.
- **Intermediate Regime:** The intermediate hydrogeological regime extends from the top of the Salina G Unit to the top of the Queenston, and occurs between reference depths of 169.3 to 447.6 mBGS in DGR-1/2 (see Figure 5.8). This is a predominantly low-permeability regime ( $K_H = 5 \times 10^{-14}$  to  $3 \times 10^{-10}$  m/s) with groundwater flow likely restricted to the two permeable aquifer zones ( $K_H = 5 \times 10^{-9}$  to  $2 \times 10^{-8}$  m/s) present at DGR-1 reference depths of 325.5 to 328.5 mBGS in the top of the Salina A1 Unit and at 374.5 to 378.6 mBGS in the Guelph Formation. These aquifers appear to be recharged east of the Bruce nuclear site where they outcrop (or subcrop) along the Niagara Escarpment, and discharge into Lake Huron in different locations tens of kilometres from the Bruce nuclear site. Groundwaters and porewaters in this intermediate regime are transitional from saline Ca-SO<sub>4</sub> water (TDS ~10 g/L) near the top to Na-Cl brine (TDS ~370 g/L) in the Guelph Formation (refer to Figure 4.6).
- **Deep Regime:** The deep hydrogeological regime extends from the top of the Queenston to the top of the Precambrian. It occurs at reference depths of 447.6 to 860.7 mBGS in DGR-2 (see Figure 5.8). This deep regime consists of the Upper Ordovician shales, the Trenton and Black River group limestones, and the Cambrian sandstone. The rocks of the Upper Ordovician and Trenton Group are of exceptionally low horizontal hydraulic conductivity ( $K_H = 4 \times 10^{-15}$  to  $1 \times 10^{-13}$  m/s), and are significantly underpressured. Porewaters in these units are Na-Cl brine with TDS of 220 to 300 g/L that decrease in concentration with depth (refer to Figure 4.6). These hydrogeological properties indicate a regime with no advection of brine, and a regime in which gas flow would also be diffusion controlled. The deeper Black River Group and Cambrian are overpressured and exhibit increased horizontal permeability relative to the overlying units. The formation horizontal hydraulic conductivities decrease upwards from the Cambrian sandstone ( $K_H = 3 \times 10^{-6}$  m/s) through the Shadow Lake Formation ( $K_H = 1 \times 10^{-9}$  m/s) to the Gull River and Coboconk ( $K_H = 2 \times 10^{-12}$  and  $2 \times 10^{-11}$  m/s, respectively). Groundwaters and porewaters in this group are Na:Ca-Cl to Na-Cl brine with TDS of about 200 to 235 g/L (refer to Figure 4.6).



Notes: From INTERA (2011; their Figure 4.106).

**Figure 5.8: Reference Stratigraphic Column Showing Hydrostratigraphic Units at the Bruce Nuclear Site**

A further subdivision of these three bedrock groundwater regimes beneath the Bruce nuclear site was proposed in the DGSM (INTERA 2011). As depicted in Figure 5.8, nine hydrostratigraphic units, including the Precambrian were identified. A detailed description and justification for this subdivision is provided in the DGSM (INTERA 2011).

The shallow groundwater regime comprises HS Units 1 and 2, the intermediate groundwater regime comprises HS Units 3 and 4, and the deep regime comprises HS Units 5 through 8.

Within this report, units are described as aquifers, aquitards and aquicludes. Aquifers are defined as formations or units that are sufficiently porous and permeable to store, transmit and yield significant quantities of groundwater. For the DGR project, aquifers are practically defined as formations or units that yield sufficient water to allow for groundwater sampling. Use of the word aquifer in this report in no way implies that the formation or unit contains potable water. All units below HS Unit 2 contain only non-potable water (brines) and the designation as “aquifer” is based solely on the physical characteristics of the host rock. Aquitards are formations or units that retard but do not prevent flow of water to or from adjacent aquifers. Aquitards do not readily yield water, but over long periods of time may exhibit evidence of advection. Aquicludes are formations or units with very low permeability such that they are almost impermeable and do not exhibit evidence of advection even over very long periods of time.

For the regional-scale model, a groundwater divide (no-flow boundary) may be assumed to exist below the center of Lake Huron. The Cambrian is absent over the Algonquin Arch to the southeast of the DGR site. The OGSR data (e.g., OGSR 2004) and the 3DGF model (ITASCA CANADA and AECOM 2011) discussed in Section 2.2.5.2 indicate that the Cambrian is also absent northeast of the Bruce nuclear site, as shown in the cross-section. To the south, units such as the Cambrian are discontinuous as a result of compartments and traps, with these being more prevalent in the Niagara Megablock region defined in Figure 2.5 (Armstrong and Carter 2006, Carter et al. 1996, Sanford et al. 1985).

Physical hydrogeological attributes of the conceptual model, which are explored and illustrated through systematic numerical simulation at basin-, regional- and site-specific scales, include:

- Only the shallow system receives recharge from present-day precipitation at the Bruce nuclear site and surrounding region;
- The shallow system is isolated from the intermediate system by the low permeabilities of the Salina Group;
- The intermediate system aquifers may be recharged where they crop out (or subcrop) near the Niagara Escarpment east of the Bruce nuclear site, however, the very high density of the water in aquifers such as the Guelph impedes the flow of the recharge water to the location of the proposed DGR at the Bruce nuclear site;
- Vertical advection through the system at the Bruce nuclear site is effectively non-existent because of the presence of hundreds of metres of lateral continuous, near-horizontally layered, low-permeability sediments;
- Diffusion is the dominant transport mechanism in all the low-permeability units such as the Ordovician sediments and also the dominant vertical transport mechanism within the intermediate and deep groundwater regimes;
- Hydraulic gradients are upwards from the permeable Cambrian, which is over-pressured relative to density-compensated hydrostatic conditions, through the Black River Group to the Trenton Group; and
- The Upper Ordovician shales and Trenton Group limestones are significantly underpressured and, at least at the present, act as a hydraulic sink from both below and above.



Data from the DGR field program, for example the dataset from borehole DGR-4 shown in Figure 5.24, support the assertion that these Ordovician strata are underpressured; fluid saturations indicate the possible presence of a discontinuous immiscible gas phase, as discussed in Section 4.3.3 of the DGSM (INTERA 2011). Qualitative indications of the presence of gas come from several different sources (hydraulic testing, core logging, laboratory testing). Gas saturations were calculated for seven Silurian formations or units and nine Ordovician formations, as discussed in Section 4.3.3 of the DGSM (INTERA 2011).

#### 5.4.2 Modelling Strategy

It is standard practice in radioactive waste programs around the world to perform an analysis of the features, events, and processes (FEPs) that affect the suitability and safety of a potential repository site. A catalogue of FEPs specifically for argillaceous formations proposed as host rocks for repositories has been developed (Mazurek et al. 2003). Numerical modelling, whether as part of site-characterization, Geosynthesis, performance assessment or safety assessment, provides an important tool in the evaluation of the FEPs that may be relevant to the long-term safety of a repository. With regard to the hydrogeological setting and performance of the proposed DGR at the Bruce nuclear site, the geology (in a broad sense including both hydrogeology and hydrogeochemistry) provides the primary features to be evaluated. Events of concern include glaciation, and the primary processes of interest are the transport processes of advection, mechanical dispersion and diffusion, two-phase flow, glacial loading and unloading, and recharge induced by glaciation. The numerical models that are the basis for the investigation of FEPs honour the data from the DGR site characterization program with spatial and temporal up-scaling being minimized. The most important FEP considered in the hydrogeologic study is solute transport in the Ordovician sediments.

The hydrogeological modelling strategy adopted for the proposed DGR at the Bruce nuclear site was to explore the FEPs relevant to the performance of the geologic barrier hosting and isolating the DGR. The strategy was not one of trying to create a single calibrated model that could reasonably reproduce all the observed characteristics of the system, but rather to understand what FEPs were truly relevant and place bounds on the performance of different elements of the overall system. This strategy was developed because it is not feasible to fully characterize the strata of the Michigan Basin beyond the site scale over an area of thousands of square kilometres, nor is such a characterization necessary to demonstrate the safety of the proposed DGR. Thus, the modelling strategy entailed the identification of FEPs that might be relevant to DGR performance, and then performing the modelling necessary to determine if they were in fact relevant, and if so, what their ranges of possible behaviours implied with respect to DGR performance.

The features of the hydrogeologic environment that were considered necessary to consider in the modelling include:

- The geologic framework (stratigraphy, unit thicknesses, lateral extent and geometrical relationships);
- Hydrogeological and hydromechanical properties of the strata (hydraulic conductivity, specific storage, porosity and one-dimensional loading efficiencies);
- Hydraulic head distribution;
- Solute distributions, including environmental isotopes;
- Relative fluid saturations;

- Diffusion properties of the strata; and
- Hypothetical undetected faults.

The only event that was identified as potentially affecting the performance of the DGR was glaciation. The influence of glaciation on mass transport mechanisms was examined through numerical modelling.

The processes that were considered to be potentially operative and relevant to DGR safety include:

- Advection;
- Mechanical dispersion;
- Diffusion;
- Two-phase flow;
- Physical (matrix diffusion) and chemical (sorption) retardation processes;
- Glacial loading and unloading; and
- Recharge induced by glaciation.

Physical and chemical retardation processes were purposely omitted from the modelling performed because they act only to increase the safety of the DGR. If the repository is otherwise safe, these processes simply increase the margin of safety. Retardation processes are included in the safety assessment analysis for the DGR that is separate from the Geosynthesis work program.

From a modelling perspective, consideration of these FEPs led to the following broad modelling strategy.

- Model what the system would look like at equilibrium (base-case), using parameter values that honour the site characterization program as described in the DGSM (INTERA 2011), geologically reasonable boundary conditions, and assuming full water (or brine) saturation. Compare equilibrium solution to current observations (e.g., head, solute distributions), and estimate performance measures for the equilibrium system.
- Model alternatives to the base-case, varying boundary and/or initial conditions, parameter values, loading conditions, etc., and incorporating alternative processes such as two-phase flow. Compare alternative solutions to current observations (e.g., head, solute distributions), and estimate performance measures for the alternative systems.
- Model at different scales, or using different codes, as appropriate to the issue/process to be addressed.
- Identify aspects of the performance of the system that are robust (invariant through all alternative models) and those that are sensitive to the modelling assumptions/ parameters.
- Identify factors, if any, which may lead to concerns about the ability of a DGR in the Cobourg Formation to safely contain and isolate the L&ILW.

The parameter perturbation and scenario analyses of the hydrogeological modelling study involve a large number of simulations using four different numerical models. This

comprehensive design provides confidence in the study conclusions through the development of multiple lines of model evidence linked to field observation. The final step of the numerical modelling study is to determine what has been learned about the system and its performance in relation to the fundamental hypotheses of site suitability introduced in Chapter 1.

### 5.4.3 Computational Models

This study uses four different numerical models and two different computational models to evaluate groundwater flow and solute transport. These models consider:

- Regional-scale saturated density-dependent flow for a domain with an area of approximately 18,000 km<sup>2</sup> centred on the DGR (see Section 5.4.5);
- Site-scale saturated density-dependent flow for a domain with an area of approximately 400 km<sup>2</sup> centred on the DGR (see Section 5.4.7);
- Density-dependent flow for an approximately 677 km east-west cross-section of the Michigan Basin (see Section 5.4.8); and
- One-dimensional two-phase gas and water flow analyses of a stratigraphic column at the DGR (see Section 5.4.9).

The regional-scale, site-scale, and cross-section modelling was accomplished using FRAC3DVS-OPG (FRACtured 3D Variably Saturated-OPG) as described in the Hydrogeologic Modelling report (Sykes et al. 2011). To investigate the hypothesis that the underpressures in the Ordovician sediments may indicate the presence of a gas phase, the two-phase air and water model TOUGH2-MP (Pruess et al. 1999) was used.

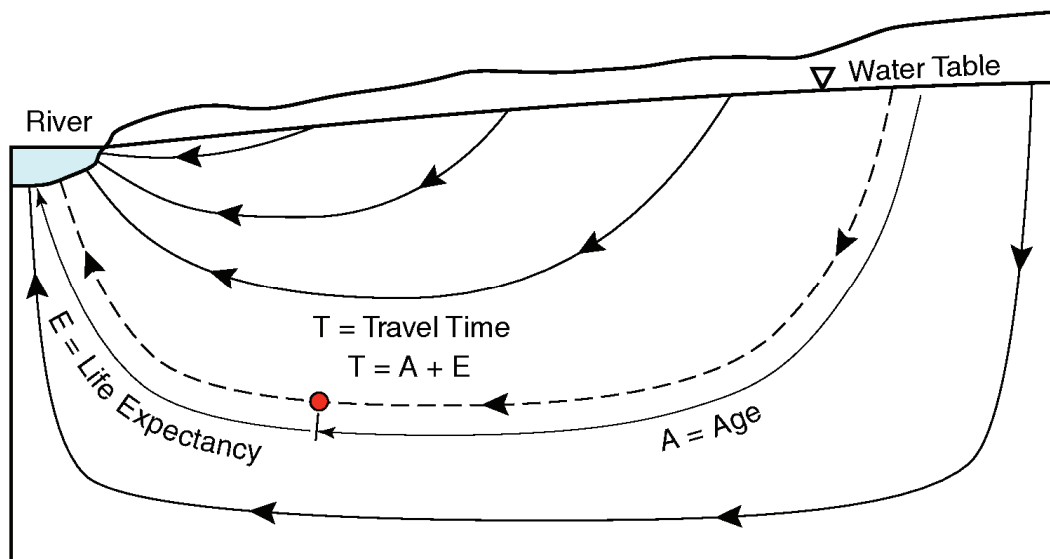
### 5.4.4 System Performance Measures

Common measures of the performance of a groundwater system include equivalent freshwater head or environmental head and the derived porewater velocity, the solute concentration for a conservative tracer, average water particle paths and travel time, the Péclet number of molecular diffusion (Bear 1988; Huysmans and Dassargues 2005), and, as developed in Normani et al. (2007), mean lifetime expectancy. Mean lifetime expectancy (MLE) represents the average time it would take conservative, nonsorbing particles to travel from given points to a potential outflow point in the environment, such as Lake Huron, under the influence of advection, dispersion, and diffusion. Figure 5.9 illustrates the MLE concept.

The Péclet number defining the ratio between the rate of solute transport by advection and the rate of solute transport by molecular diffusion (Bear 1988; Huysmans and Dassargues 2005) is:

$$Pe = \frac{VL}{D_e} \quad (5.1)$$

in which  $V$  is the porewater velocity,  $L$  is a characteristic length, and  $D_e$  is the effective diffusion coefficient calculated as the product of the tortuosity ( $\tau$ ) of the porous medium [-] and the molecular diffusion coefficient ( $D_m$ ) [L<sup>2</sup>/T]. Bear (1988) states that a Péclet number < 0.4 is indicative of solute transport that is dominated by molecular diffusion. Bear (1988) indicates that the scale length is that of the mean grain or pore size or any other characteristic medium length. A value of  $L = 1$  m was used in this study to provide conservatively high estimates of the Péclet number.



Notes: From Sykes et al. (2011).

**Figure 5.9: Illustration of Life Expectancy Concept for an Idealized Cross-section**

#### 5.4.5 Regional-scale Model

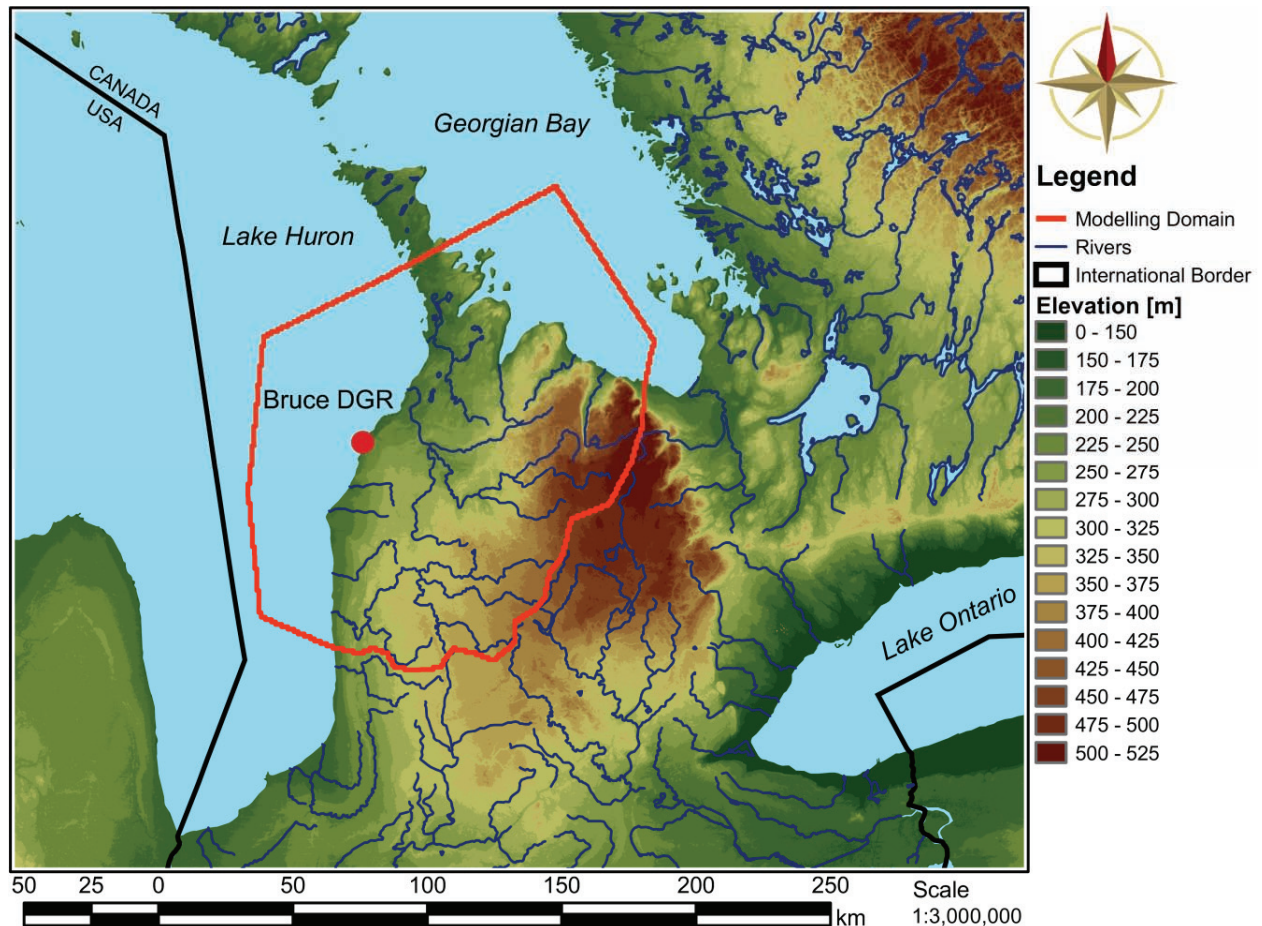
The purpose of the regional-scale model was to examine aspects of the hydrogeology of the Bruce nuclear site in three dimensions at a scale large enough to include natural hydrogeologic boundary conditions for the surface. The simulations are designed to illustrate that processes affecting groundwater flow and transport can be evaluated without assumed boundary conditions for the shallow domain exerting an undue influence on predicted outcomes. The primary focus of the regional-scale model is the assessment of solute transport in the Ordovician sediments; specifically, whether or not transport is diffusion dominant in the present state, and whether or not it will remain diffusion dominant during glacial episodes.

##### 5.4.5.1 Model Domain and Spatial Discretization

The spatial scale required to assess solute transport in the Ordovician shale and limestone is on the order of kilometres or less. For paleoclimate analyses and to fully characterize flow in the more permeable units such as the Guelph dolostone and the Cambrian sandstone, a considerably larger spatial domain is required. Ideally, the spatial domain should include the outcrop and subcrop for the permeable units, such as the Guelph, that are potential pathways for solute migrating from the Ordovician at the location of the proposed DGR. The regional-scale spatial domain meets this criterion for all of the units above the Ordovician. While it does not strictly meet this criterion for the Cambrian, potential pathways in the Cambrian can be investigated through scenario analyses.

The regional-scale modelling domain boundary (Figure 5.10) was chosen from within the 3DGF domain (Section 2.2.5.2) by Sykes (2007). The southeastern portion of the boundary follows the regional surface water divides surrounding the Bruce nuclear site; these divides were determined by using a digital elevation model (DEM) from the Shuttle Radar Topography Mission (SRTM) and a river network in ArcGIS. Based on the assumption that the water table is

a subdued reflection of surface topography, the topographic divides are a reasonable choice for the shallow regime and for the higher permeability A1 and Guelph aquifers within the intermediate regime, which outcrop/subcrop within the model domain.



Notes: From Sykes et al. (2011).

**Figure 5.10: Location of Proposed DGR Site, Regional-scale Modelling Domain, Land Surface Elevations and River Courses**

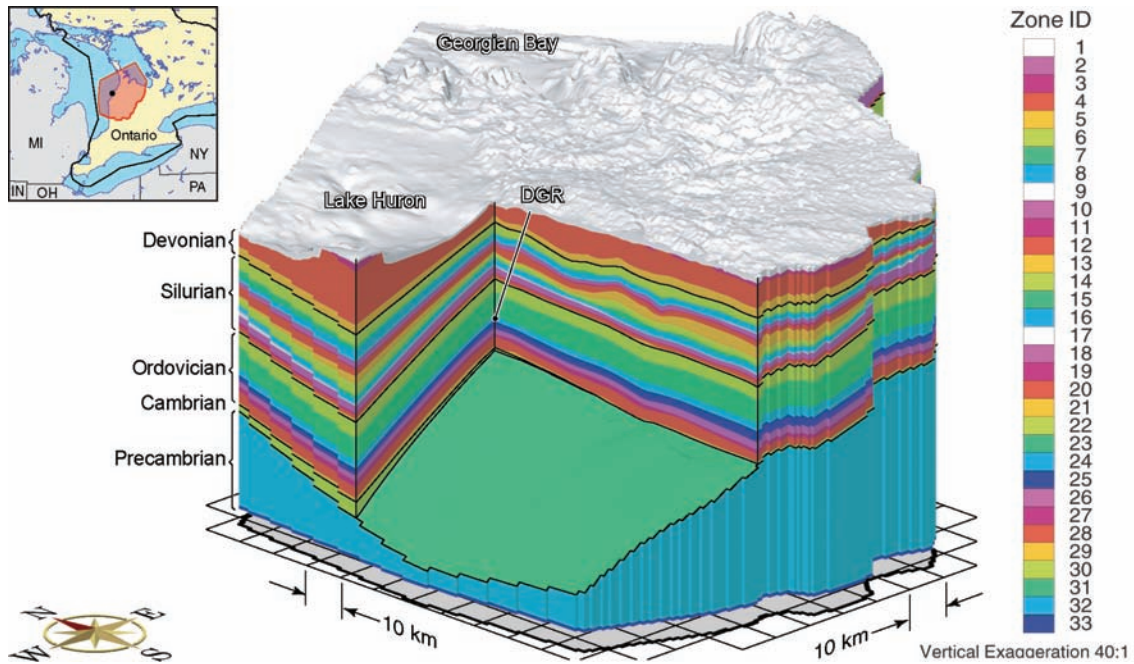
The modelling domain includes the local topographic high in southern Ontario, and the domain extends to the deepest portions of both Lake Huron and Georgian Bay. The conceptual model hypothesizes that at a point in all units/formations beneath Lake Huron, either a divide for groundwater flow occurs or horizontal flow is negligible. The bathymetric data of both water bodies, provided by National Oceanic and Atmospheric Administration (NOAA), was combined with the DEM to provide a continuous surface for the top of the Earth's solid surface. The eastern boundary of the modelling domain is west of the Algonquin Arch (Sykes et al. 2011).

The potential energy gradients that occur at depth in the Michigan Basin will be reduced due to the presence of dense saline groundwater found within the formations of the lower regime.

Where these formations outcrop at recharge areas, there will be a potential for fresh water to infiltrate the geologic units and displace higher density water until there is a balance between the elevation gradient and the density gradient. At this equilibrium point, the energy gradient will approach zero. With the dense brine, there will be associated higher viscosities, which will act to further impede flow. The combination of 1) negligible horizontal energy gradients in dense brine and 2) low permeabilities in the deep groundwater regime leads to a system that is dominated by diffusion. Thus, the groundwater in the deep formations of the Michigan Basin is expected to be effectively stagnant.

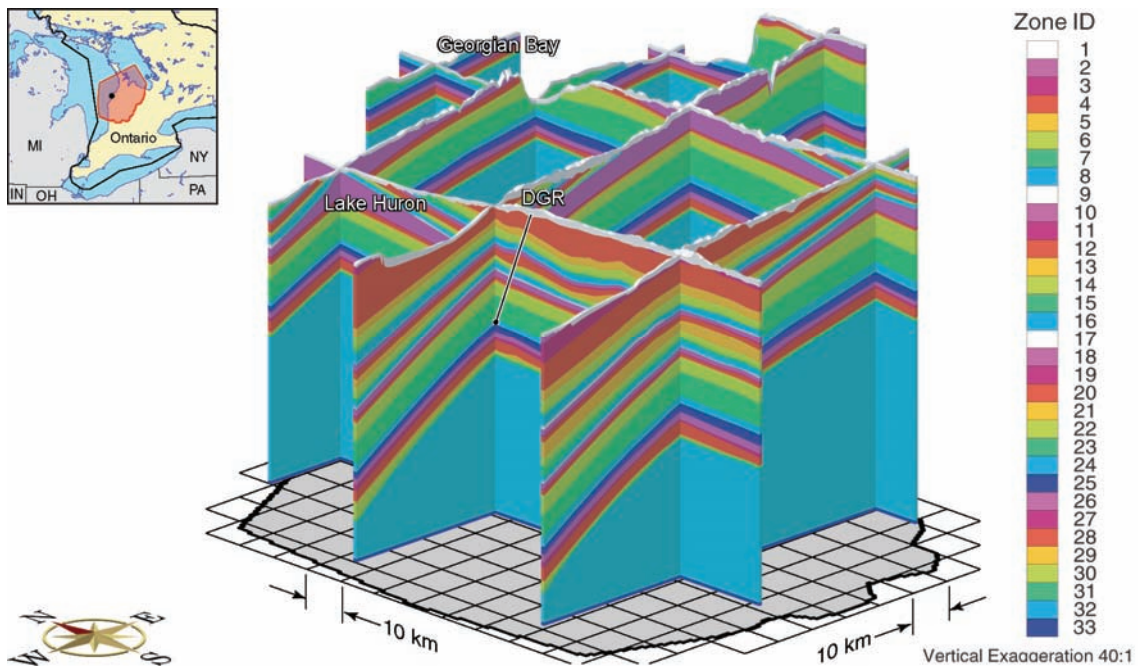
A two-dimensional grid was developed to fit within the regional-scale modelling boundary. Each quadrilateral element measures  $\Delta x = 762.8$  m by  $\Delta y = 900.9$  m. The grid has an east-west extent of 151.8 km, a north-south extent of 179.3 km, 27,322 elements, 27,728 nodes, and covers an area of 18,775 km<sup>2</sup>. The two-dimensional grid forms a horizontal template to develop the three-dimensional grid by interpolating the vertical position of each node from the 32 interfaces provided in the 3DGF model (ITASCA CANADA and AECOM 2011). Each interface was provided as a triangulated irregular network (TIN).

The base-case data set for the regional-scale model consists of 39 model layers, with each of the 31 top layers corresponding to a unit in the stratigraphic section provided by the geologic framework model (refer to Section 2.2.5.2). The bottom 8 layers are associated with the Precambrian (7 layers) and the upper Precambrian (1 layer). These layers provide a finer discretization of the system for modelling purposes than the nine hydrostratigraphic units described in Section 5.4.1. Block-cut and fence views of the assigned geologic layer zone identifiers are shown in Figure 5.11 and Figure 5.12. Each zone identifier is associated with a specific geologic layer or geologic grouping. The layers and their constituent geologic units are listed in Table 5.5, along with the measured layer thicknesses at DGR-1/2. Due to lack of differentiation of some units in the regional database (ITASCA CANADA and AECOM 2011, AECOM and ITASCA CANADA 2011), the Guelph Formation, the Goat Island and Gasport members of the Lockport Formation, and the Lions Head Member of the Amabel Formation were lumped into a single layer referred to by Sykes et al. (2011) as the Niagaran Group for the modelling discussed in this report (Figure 2.8). Similarly, Sykes et al. (2011) followed ITASCA CANADA and AECOM (2011) in lumping the Georgian Bay Formation, Blue Mountain Formation, and Collingwood Member (the bottom three stratigraphic units in HS Unit 5) into a single model layer.



Notes: From Sykes et al. (2011).

**Figure 5.11: Block-cut View of FRAC3DVS-OPG Zone Identifiers for 33 Layers in Regional-scale Model**



Notes: From Sykes et al. (2011).

**Figure 5.12: Fence View of FRAC3DVS-OPG Zone Identifiers for 33 Layers in Regional-scale Model**

**Table 5.5: FRAC3DVS-OPG Model Layers and Corresponding Geologic Units**

Period	Stratigraphic Unit	Model Layer	Model Layer Number	Layer Thickness at DGR-1/2 (m)
Quaternary	Drift	Drift	1	--
Devonian	Kettle Point	Kettle Point	2	--
	Hamilton Group	Hamilton Group	3	--
	Dundee	Dundee	4	--
	Lucas	Detroit River Group	5	55.0
	Amherstburg (top 20 m)			
	Amherstburg (lower 25 m)			
	Bois Blanc	Bois Blanc	6	49.0
Silurian	Bass Islands (upper 20(m))	Bass Islands	7	45.3
	Bass Islands (lower 25 m)			
	Salina G	Salina G	8	9.3
	Salina F	Salina F	9	44.4
	Salina E	Salina E	10	20.0
	Salina D	Salina D	11	1.6
	Salina C	Salina C and B	12	46.6
	Salina B carbonate			
	Salina B evaporite	Salina B evaporite	13	1.9
	Salina A2 carbonate	Salina A2 carbonate	14	26.6
	Salina A2 evaporite	Salina A2 evaporite	15	5.8
	Salina A1 upper carbonate	Salina A1 carbonate	16	41.5
	Salina A1 carbonate			
	Salina A1 evaporite	Salina A1 evaporite and A0	17	7.5
	Salina A0			
	Guelph	Niagaran	18	34.3
	Goat Island			
	Gasport			
	Lions Head			
	Fossil Hill	Fossil Hill	19	2.3
	Cabot Head	Cabot Head	20	23.8
Manitoulin	Manitoulin	21	12.9	
Ordovician	Queenston	Queenston	22	70.3
	Georgian Bay	Georgian Bay/Blue	23	133.6



Period	Stratigraphic Unit	Model Layer	Model Layer Number	Layer Thickness at DGR-1/2 (m)
	Blue Mountain	Mountain		
	Collingwood			
	Cobourg	Cobourg	24	28.6
	Sherman Fall	Sherman Fall	25	28.0
	Kirkfield	Kirkfield	26	45.9
	Coboconk	Coboconk	27	23.0
	Gull River	Gull River	28	53.6
	Shadow Lake	Shadow Lake	29	5.2
Cambrian	Cambrian	Cambrian	30	16.9
Precambrian	Upper Precambrian	Upper Precambrian	31	--
	Precambrian	Precambrian	32-39	--

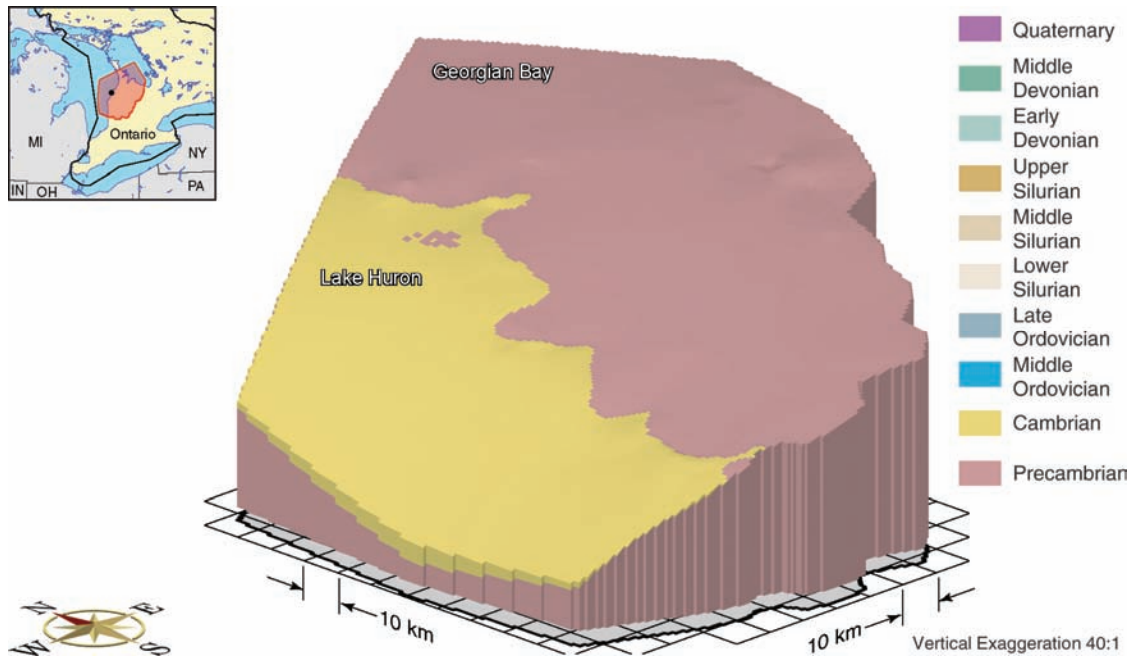
Notes: Data are from Sykes et al. (2011).

The geologic reconstruction also makes use of the outcrop limits or extent of the various geologic units, coloured by geologic period, as shown in Figure 2.3. Note that the vertical exaggeration is 40:1 in this figure, and others, describing the regional-scale spatial domain. The Cambrian Formation pinches out against the Precambrian flanking the Algonquin Arch (Carter et al. 1996). A three-dimensional view of the Cambrian Formation as represented in the modelling grid is shown in Figure 5.13. An important attribute of this permeable unit is that it is present only over the more westerly part of the domain.

A view of the Middle Silurian geologic units (top of the Niagaran Group) is shown in Figure 5.14; the portion of the surface appearing rougher represents outcrops or subcrops, and has been defined using OGS Digital Bedrock topography and overburden thickness mapping. The zone with a smooth surface corresponds to the portion of the Niagaran that is overlain by the Upper Silurian. Pinnacle reef structures are visible as protuberances in the Middle Silurian surface to the right of the DGR location on the figure. A view of the subcrop of all geologic units below the Quaternary drift deposits is shown in Figure 5.15.

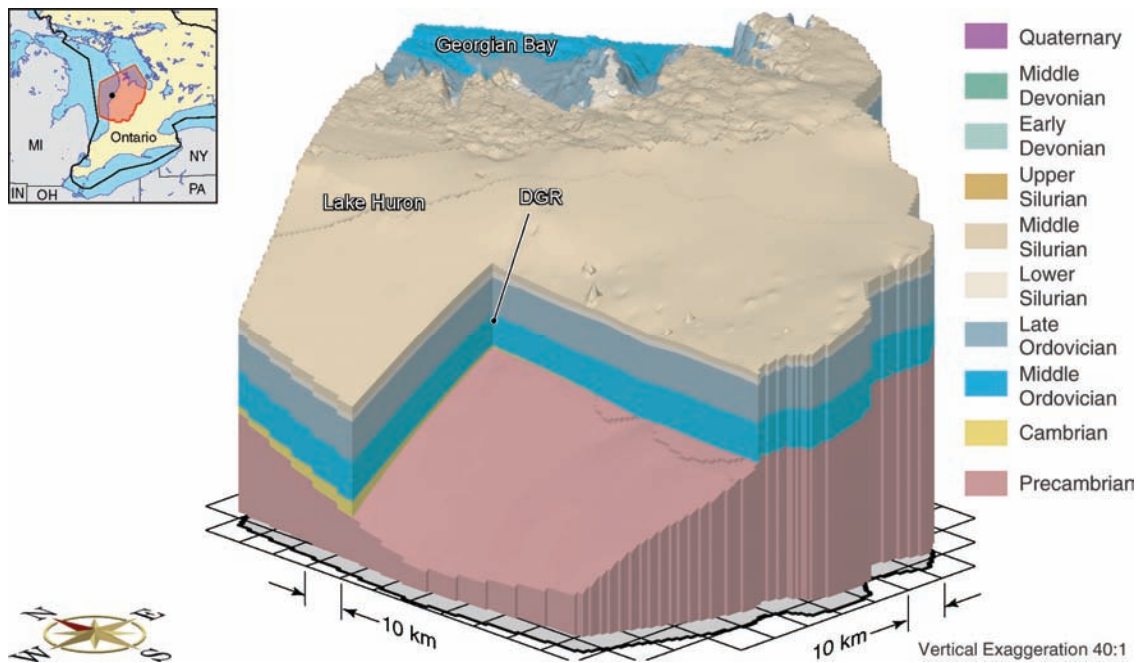
#### 5.4.5.2 Model Parameters

The hydrogeologic parameters defined in this section are based on the DGR borehole investigations and are applied to the regional-scale and site-scale numerical models. The 3DGF model (Section 2.2.5.2; ITASCA CANADA and AECOM 2011) defines a lithology, which aggregates various layers identified at the site-scale. The relationship between the site-scale lithology and the lithology applied to the numerical models is shown in Table 5.5. Model layer thicknesses vary over the modelling domain; the thicknesses of the layers as measured at the DGR-1/2 location are also given in Table 5.5.



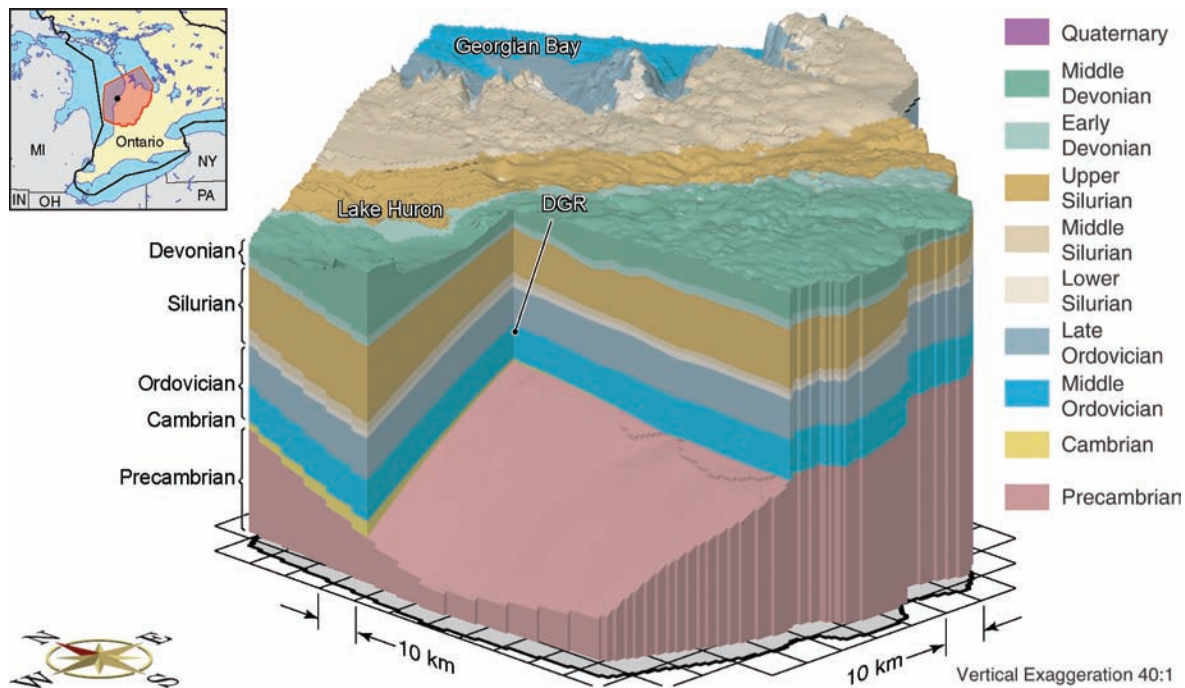
Notes: From Sykes et al. (2011).

**Figure 5.13: Block-cut View Showing Spatial Extent of the Cambrian (Yellow), Underlain by the Precambrian Basement (Pink), for the Regional Modelling Domain**



Notes: From Sykes et al. (2011).

**Figure 5.14: Block-cut View Showing Spatial Extent of the Middle Silurian (Top of the Niagaran Group) for the Regional Modelling Domain**



Notes: From Sykes et al. (2011).

**Figure 5.15: Block-cut View Showing Subcrop of the Bedrock Units Beneath Quaternary Drift Deposits for the Regional Modelling Domain**

### ***Flow and Transport Parameters***

The base-case parameter values used for the regional-scale and site-scale groundwater modelling are listed in Table 5.6. Horizontal hydraulic conductivity ( $K_H$ ) values were derived from the field studies described in Section 5.2.2. Vertical hydraulic conductivity ( $K_V$ ) values were estimated for most units by assuming an anisotropy ratio ( $K_H/K_V$ ) of 10:1. Higher anisotropy ratios were assumed for units in which both high- $K_H$  and low- $K_H$  layers were aggregated, particularly the Salina Unit A1 carbonate, the Niagaran Group, and the Black River Group, because  $K_V$  is dominated by the lowest  $K_V$  in a succession of strata. Little to no anisotropy was assumed for the high- $K_H$  drift and Cambrian aquifers, and for the Precambrian.

**Table 5.6: Base-case Hydrogeological Parameter Values for Regional-scale and Site-scale Modelling**

Period	Formation	$K_H$ [m/s]	$K_V$ [m/s]	$K_H:K_V$	$\theta$	$\rho$ [kg/m <sup>3</sup> ]	TDS [g/L]	$S_s$ [m <sup>-1</sup> ]	$\zeta$	$\tau$
Quaternary	Drift	1.00E-08	5.00E-09	2:1	0.2	1000	0	9.90E-05	0.99	4.00E-01
	Kettle Point	3.00E-09	3.00E-10	10:1	0.1	1006	9	1.50E-06	0.8	1.20E-01
Devonian	Hamilton Group	2.20E-11	2.20E-12	10:1	0.1	1008	12	1.50E-06	0.8	1.20E-01
	Dundee	8.40E-08	8.40E-09	10:1	0.1	1005	8	1.50E-06	0.8	1.20E-01
	Detroit River Group	5.90E-07	2.00E-08	30:1	0.077	1001	1.4	1.40E-06	0.84	9.40E-02
	Bois Blanc	1.00E-07	1.00E-08	10:1	0.077	1002	3.2	1.40E-06	0.84	9.40E-02
	Bass Islands	5.00E-05	1.70E-06	30:1	0.056	1004	6	2.00E-06	0.92	2.80E-01
	Unit G	1.00E-11	1.00E-12	10:1	0.172	1010	14.8	1.10E-06	0.55	3.00E-03
Silurian	Unit F	5.00E-14	5.00E-15	10:1	0.1	1040	59.6	9.50E-07	0.68	4.90E-02
	Unit F Salt	5.00E-14	5.00E-15	10:1	0.1	1040	59.6	9.50E-07	0.68	4.90E-02
	Unit E	2.00E-13	2.00E-14	10:1	0.1	1083	124	6.50E-07	0.51	5.70E-02
	Unit D	2.00E-13	2.00E-14	10:1	0.089	1133	200	6.40E-07	0.53	6.40E-02
	Units B and C	4.00E-13	4.00E-14	10:1	0.165	1198	296.7	9.50E-07	0.38	8.40E-02
	Unit B Anhydrite	3.00E-13	3.00E-14	10:1	0.089	1214	321	6.90E-07	0.53	1.00E-03
	Unit A-2 Carbonate	3.00E-10	3.00E-11	10:1	0.12	1091	136	7.20E-07	0.46	1.20E-02
	Unit A-2 Evaporite	3.00E-13	3.00E-14	10:1	0.089	1030	45.6	5.80E-07	0.53	1.00E-03
	Unit A-1 Carbonate	1.40E-08	9.70E-13	14912:1	0.023	1120	180.2	4.10E-07	0.82	1.20E-02
	Unit A-1 Evaporite	3.00E-13	3.00E-14	10:1	0.02	1229	343.7	4.50E-07	0.83	1.80E-03
	Niagara Group	3.60E-09	2.50E-13	14431:1	0.026	1206	308.4	2.70E-07	0.66	1.20E-02
	Reynales/Fossil Hill	5.00E-12	5.00E-13	10:1	0.031	1200	300	2.90E-07	0.62	6.20E-01
	Cabot Head	9.00E-14	9.00E-15	10:1	0.116	1204	306	1.10E-06	0.6	3.20E-02
	Manitoulin	9.00E-14	9.00E-15	10:1	0.028	1233	350	7.50E-07	0.86	6.40E-03

Period	Formation	$K_H$ [m/s]	$K_V$ [m/s]	$K_H:K_V$	$\theta$	$\rho$ [kg/m <sup>3</sup> ]	TDS [g/L]	$S_s$ [m <sup>-1</sup> ]	$\zeta$	$\tau$
Ordovician	Queenston	2.00E-14	2.00E-15	10:1	0.073	1207	310	9.00E-07	0.71	1.60E-02
	Georgian Bay/Blue Mtn.	3.50E-14	3.30E-15	11:1	0.07	1200	299.4	1.20E-06	0.79	8.80E-03
	Cobourg	2.00E-14	2.00E-15	10:1	0.015	1181	272	2.60E-07	0.8	3.00E-02
	Sherman Fall	1.00E-14	1.00E-15	10:1	0.016	1180	270	4.90E-07	0.88	1.70E-02
	Kirkfield	8.00E-15	8.00E-16	10:1	0.021	1156	234	4.90E-07	0.85	2.40E-02
	Coboconk	4.00E-12	4.00E-15	1000:1	0.009	1170	255	4.60E-07	0.93	3.60E-02
	Gull River	7.00E-13	7.00E-16	1000:1	0.022	1135	203	4.90E-07	0.85	1.40E-02
Cambrian	Shadow Lake	1.00E-09	1.00E-12	1000:1	0.097	1133	200	7.40E-07	0.56	7.60E-02
	Cambrian	3.00E-06	3.00E-06	1:1	0.071	1157	235	3.70E-07	0.34	1.30E-01
Precambrian	Upper Precambrian	1.00E-10	1.00E-10	1:1	0.038	1200	300	2.60E-07	0.49	9.50E-03
	Precambrian	1.00E-12	1.00E-12	1:1	0.005	1200	300	1.50E-07	0.88	7.20E-02

Notes: Refer to text for explanation of listed parameters. From Sykes et al. (2011).

The specific storage  $S_s$  and one-dimensional loading efficiency  $\zeta$  were calculated based on preliminary data on the Young's modulus  $E$ , Poisson's ratio  $\nu$ , and mineral grain modulus  $K_s$  for the rock formations, the coefficient of vertical compressibility  $\beta'$  for the drift, porosity  $\theta$ , and the fluid density  $\rho$ . The resulting  $S_s$  estimates are compared to the final laboratory determinations of  $S_s$  (INTERA 2011) in Table 5.3. The majority of the  $S_s$  estimates used for modelling fall within the final lab-derived ranges, and all but four values are within a factor of two of the laboratory values. The remaining four values range from 19 to 40% of the lower laboratory estimate of  $S_s$ .

The fluid density values given in Table 5.6 are determined from the TDS concentrations as detailed in Sykes et al. (2011). The tortuosity  $\tau$  varies by layer and is calculated from the iodide effective diffusion coefficient  $D_e$  (Section 5.3.5), the porosity  $\theta$  (Section 5.3.1), the free solution diffusion coefficient for iodide of  $1.66 \times 10^{-9} \text{ m}^2/\text{s}$  (CRC 1983), and assuming that only 50% of the porosity is accessible to iodide diffusion. In the case of the Niagaran Group (including the Guelph, Goat Island, Gasport, and Lions Head) and other combined-formation model layers, their parameters are calculated using parameter-appropriate averaging of the site formation parameters. Further details on how the hydrogeological parameters were developed from the site-specific parameters and their use in the regional-scale and site-scale numerical models are discussed in Sykes et al. (2011).

Table 5.7 summarizes various transport parameters, which are used for brine movement for the variably dense pore fluids, for tracer movement to determine the depth of recharge water penetration, and for MLE calculations. Smaller dispersivity values were attempted in the preliminary modelling phase of this study, however, severe numerical instabilities resulted due to the large grid spacing in proportion to smaller longitudinal dispersivity values. Dispersivities for MLE calculations are double the values listed in Table 5.7. The site-scale modelling uses the same brine diffusion coefficient as shown in Table 5.7 but differs in that an iodide tracer diffusion coefficient of  $1.66 \times 10^{-9} \text{ m}^2/\text{s}$  is used instead of the tritiated water tracer value. Also, the site-scale dispersivities are one-tenth of those used in the regional numerical model (see also Table 4.9 of Sykes et al. 2011).

Different parameter values were used to investigate specific scenarios. The values used and their justification are discussed in the sections detailing the individual scenarios.

**Table 5.7: Groundwater Transport Parameters for Regional-scale Modelling**

Parameter	Value
Brine Diffusion Coefficient (NaCl at 1 mol/L)	$1.484 \times 10^{-9} \text{ m}^2/\text{s}$
Tracer Diffusion Coefficient ( $\text{H}_2^{18}\text{O}$ )	$2.66 \times 10^{-9} \text{ m}^2/\text{s}$
Longitudinal Dispersivity	500 m
Horizontal Transverse Dispersivity	50 m
Vertical Transverse Dispersivity	5 m

Notes: From Sykes et al. (2011; their Table 4.8).

### **Shallow Weathered Zone**

The OGSR borehole data define a thin drift at the surface; in many logs it is less than a metre thick. No shallow weathered zone is identified for the most shallow rock horizons. Where the units of the Silurian and Ordovician outcrop, their low permeabilities would occur at the surface of the regional-scale domain. To simulate the impact that a weathered zone will have on shallow flow, the entire upper 20 m of the spatial domain was assumed to be characterized by more permeable rock; the horizontal hydraulic conductivity for the zone was assumed to be  $1.0 \times 10^{-8}$  m/s. The anisotropy ratio given in Table 5.6 was assumed to be applicable.

### **Precambrian Properties**

The Precambrian underlies the sedimentary deposits of the Michigan Basin. Due to limited site-specific data for the Precambrian, both the hydraulic conductivity and TDS concentrations below the Cambrian or Shadow Lake formations are based on characteristics derived from studies of the Canadian Shield. Relationships between horizontal permeability and the depth below ground surface of the Precambrian were applied to the Precambrian depth data acquired from the 3DGF model (ITASCA CANADA and AECOM 2011) to provide Precambrian permeability data to be used in the modelling (e.g., Normani 2009).

The salinity of groundwater generally increases with increasing depth in plutonic rock on the Canadian Shield. The highly saline pore fluids can have TDS concentrations up to 300 g/L (Bottomley et al. 2003; Frappe and Fritz 1987). The Hydrogeologic Modelling report (Sykes et al. 2011) developed an initial TDS distribution for the Precambrian rock required for the pseudo steady-state model based on Figure 2b in Frappe and Fritz (1987). The Hydrogeologic Modelling report also developed a general expression relating TDS concentration to density for use in modelling groundwater flow in the Michigan Basin on a variety of scales (Sykes et al. 2011).

#### **5.4.5.3 Flow Boundary Conditions**

Various boundary conditions are applied to the regional modelling domain. A Dirichlet (prescribed head) hydraulic boundary condition is applied to the top nodes of the domain to set the water table 3 m below ground surface, regardless of streams or other inland water bodies such as lakes or wetlands. The water table was never set lower than the elevation of Georgian Bay or Lake Huron which were set to a mean water elevation of 176 m. For the regional-scale grid used in this study, the elevation of the water table is estimated at grid block nodes.

Both the sides and bottom of the modelling domain are specified as a zero-flux boundary condition. Zero-flux boundary conditions are appropriate for the shallow groundwater system and the Salina A1 Unit upper carbonate aquifer because both their recharge areas and their presumed discharge areas in Lake Huron are included in the model domain. The high-permeability Niagaran Group and Cambrian Formation, however, might be thought to have the potential to allow influx and efflux across the model boundary (Sanford et al. 1985). The use of the no-flux boundary condition for the Niagaran beneath Lake Huron is consistent with the hypothesis that at a point in units/formations beneath Lake Huron, either a divide for groundwater flow occurs or horizontal flow is negligible. As described previously, the Cambrian is known to pinch out east of the Bruce nuclear site toward the Algonquin Arch; thus, no-flow boundaries are considered reasonable for that unit. Potential pathways that may exist in the Cambrian to the west and northwest are investigated through scenario analyses.

#### 5.4.5.4 Initial Conditions and Solution of Density-dependent Flow

Salinity plays an important role with regard to fluid flow at the proposed DGR. The higher density of the deep fluids inhibits active flow at depth (Park et al. 2009). The methodology for developing a solution for regional-scale density-dependent flow is described in Sykes et al. (2011); the methodology is described in the following paragraphs.

In the absence of a source term for salinity, a transient analysis is required to determine an equilibrium solution at a time ( $t$ ) for density-dependent flow. The analysis requires the specification of an initial distribution throughout the regional-scale spatial domain for both freshwater heads and TDS concentration. In a transient analysis, the initial prescribed salinity distribution is allowed to equilibrate to a new state that reflects the boundary conditions, hydraulic properties and transport properties of the regional-scale domain. For the coupled density-dependent flow and transport system, fresh water can recharge at the surface, reducing the TDS concentration in the shallow zone. However, the time to flush the dissolved solids from a unit is a function of the permeability of the unit and the energy potential of the displacing fluid as compared to the energy potential of the fluid being displaced. Fluids with lower TDS, such as recharging water, will have a lower energy potential as compared to higher TDS water with the same elevation and pressure. Therefore, for low-permeability units with a relatively high TDS concentration, the time to flush the unit or displace the fluids can be very long (millions of years). Complete flushing may only occur as a result of diffusion because energy gradients and/or low permeabilities may yield low fluid fluxes that may not be sufficient for advective displacement to occur. In using this method to synthesize a spatial salinity distribution, the total mass of dissolved solids and its distribution in the model domain is assumed to be known and will be a maximum initially as there are no sources to generate dissolved solids. With this approach, as time progresses, the dissolved solids will gradually reduce as the groundwater discharges from the system. However, as an alternate model, TDS can be introduced using a Dirichlet boundary condition at, for example, the bottom of the domain.

The initial condition for TDS must specify concentrations for all lithologies at all locations in the regional-scale domain. Field data are not completely available for the spatial distribution of TDS in the low-permeability units of the deep regime. The values from Table 5.6 for a given lithology were assigned to all areas of the spatial domain assigned to that zone. For the model zones representing the Precambrian, a depth-dependent initial TDS distribution was determined using the method defined by Sykes et al. (2011). The rationale for this model is the hypothesis that transport of TDS would have occurred, through long-term diffusion, to the upper crystalline rock from either the overlying higher TDS sediments or the deeper Precambrian rock. The initial TDS distribution developed for this study is shown in a block-cut view in Figure 5.16 and in a fence view in Figure 5.17.

The final freshwater head distribution for the base-case analysis was calculated as follows.

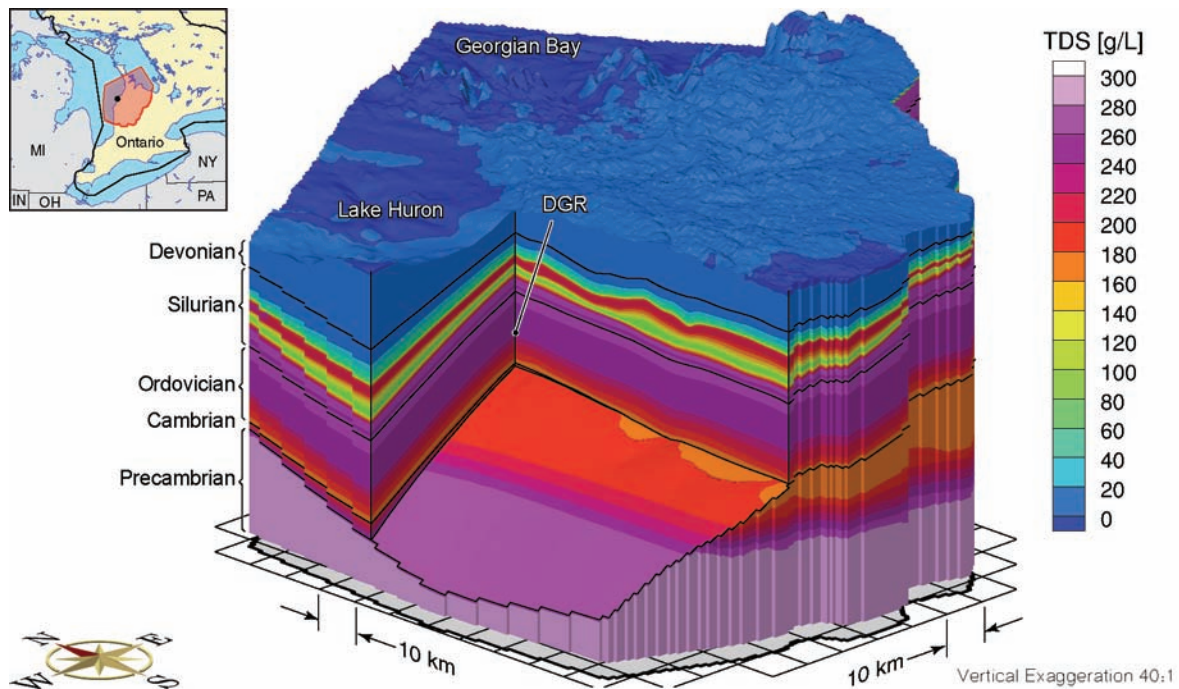
- An initial distribution of freshwater heads was calculated by running the model to steady state under the boundary conditions described in Section 5.4.5.3 assuming that only freshwater was present in the system. The results are shown in fence view in Figure 5.18.
- A TDS concentration distribution was assigned throughout the domain as an initial condition using the procedure described in the preceding paragraph. The density-independent freshwater heads were allowed to equilibrate to the assigned TDS distribution in a transient analysis, while not allowing the TDS distribution to evolve. This step allowed the freshwater heads to reflect the variation of fluid density, as specified by the initial TDS distribution. The



converged, time-invariant results for freshwater heads from this step are shown in fence view in Figure 5.19.

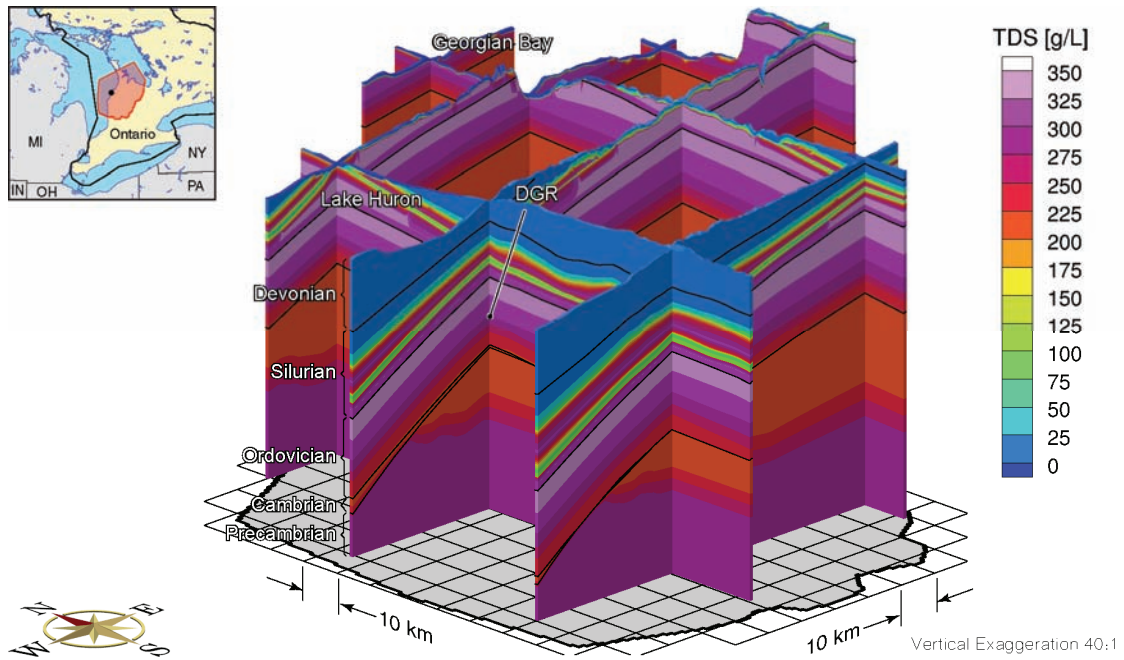
- The TDS distribution was allowed to vary with the freshwater heads in a 1 Ma transient analysis. The results at 1 Ma for freshwater heads are shown in fence view in Figure 5.20. The final TDS distribution is shown in fence view in Figure 5.21. The flushing of TDS from the shallow units is revealed with a comparison of this figure to the initially assigned distribution shown in Figure 5.17.

After reaching pseudo-equilibrium at 1 Ma, the model produces salinity profiles that are compatible with the geological framework, boundary conditions and hence the flow domain. In the northeastern part of the model domain, the brine will be flushed because of a combination of the absence of a source term for brine and the effect of meteoric recharge near Georgian Bay where the Ordovician formations outcrop. This is contrasted to the deeper Ordovician shale and limestones units in the western portion of the domain which, because of the absence of a velocity to transport the brine from the system, will maintain a high salinity concentration. The proposed DGR repository is located within this area. At such a location, stagnation of the groundwater is expected due to both the low permeability of the Ordovician units and the effect that density will have on reducing energy gradients.



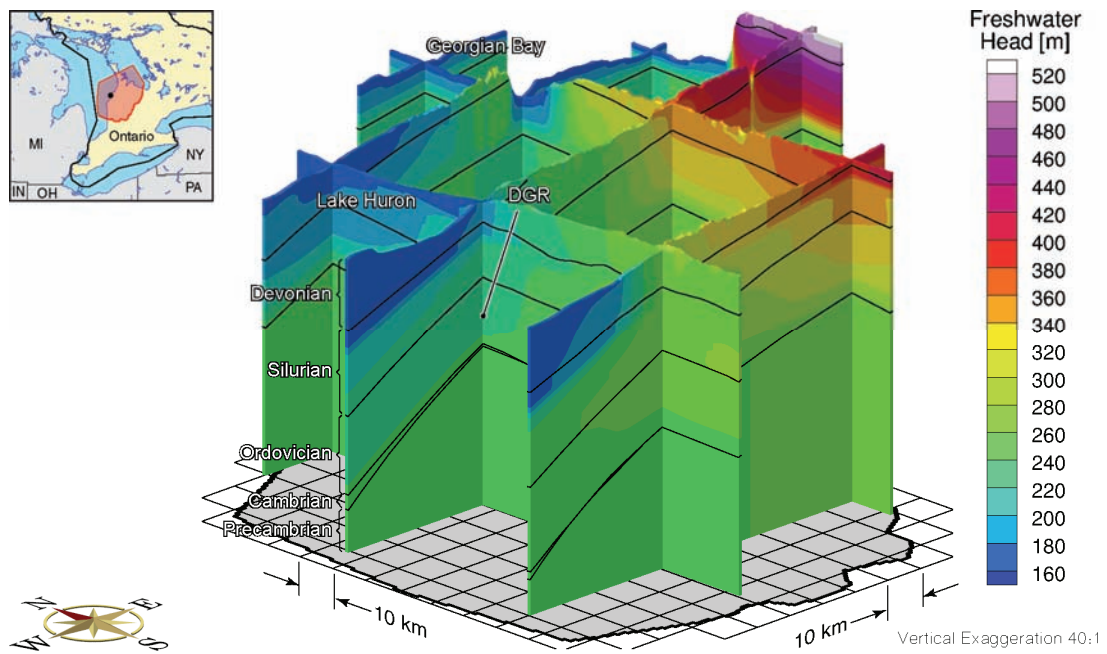
Notes: From Sykes et al. (2011).

**Figure 5.16: Block-cut View of Initial TDS Concentration Distribution**



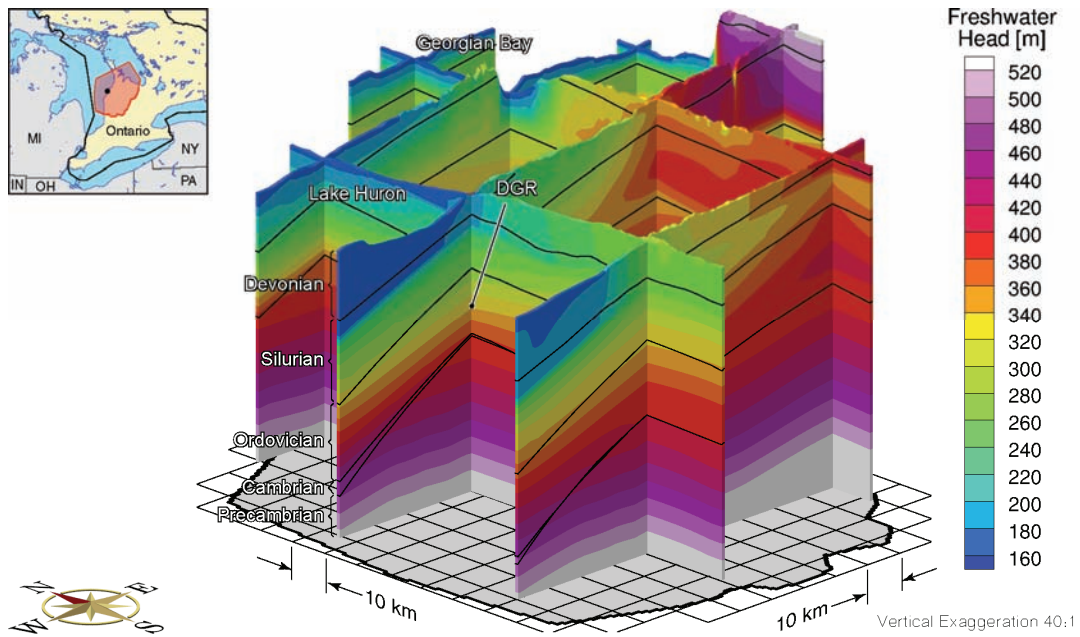
Notes: From Sykes et al. (2011).

**Figure 5.17: Fence View of Initial TDS Concentration Distribution**



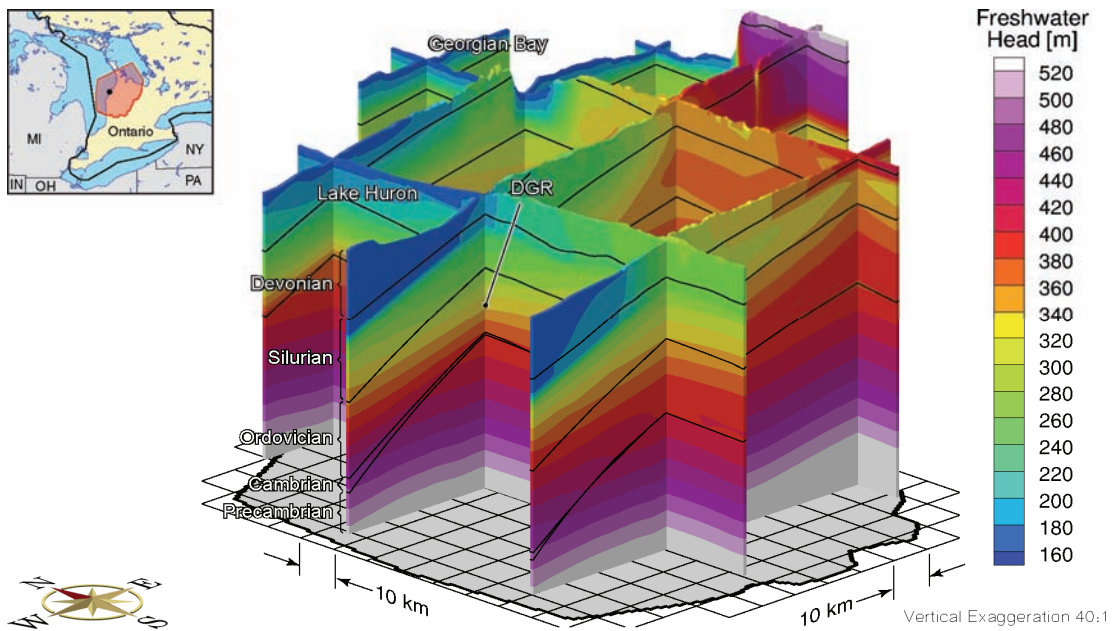
Notes: From Sykes et al. (2011).

**Figure 5.18: Fence View of Steady-state Density-independent Freshwater Heads**



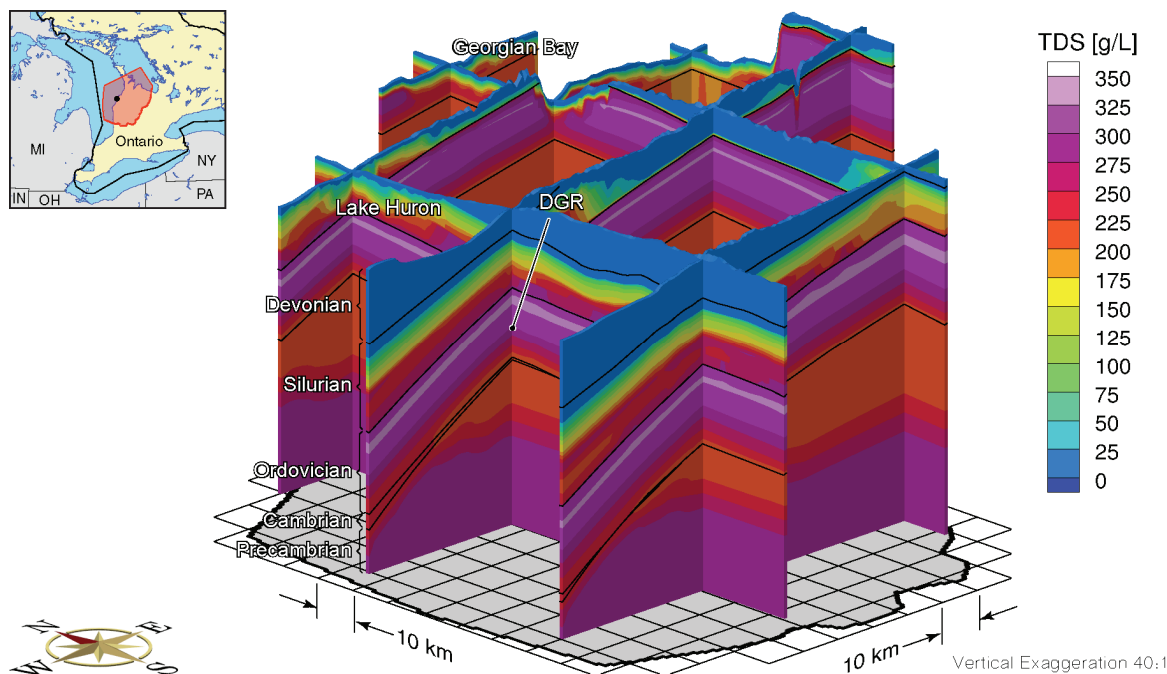
Notes: From Sykes et al. (2011).

**Figure 5.19: Fence View of Freshwater Heads that have Equilibrated to the Static TDS Distribution**



Notes: From Sykes et al. (2011).

**Figure 5.20: Fence View of Freshwater Heads that have Equilibrated at 1 Ma to the Temporally Varying TDS Distribution**



Notes: From Sykes et al. (2011).

**Figure 5.21: Fence View of TDS Concentration Distribution that has Equilibrated at 1 Ma to the Freshwater Heads**

#### 5.4.5.5 Base-case Simulations

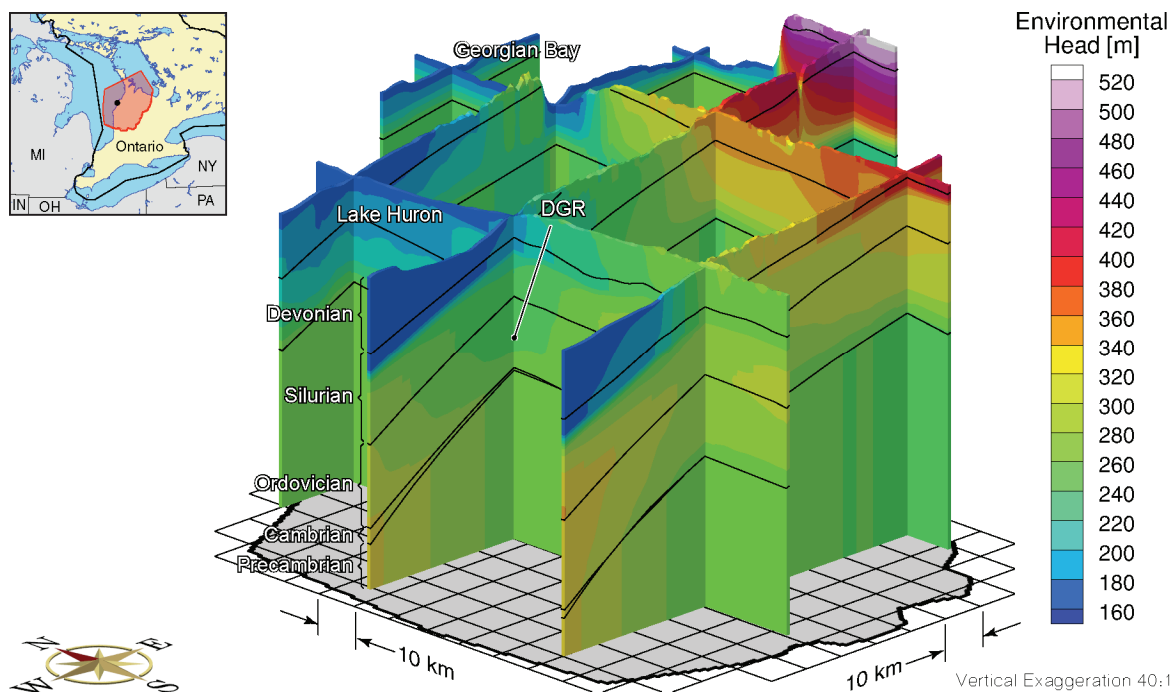
The conceptual model described in Section 5.4.1 describes the present-day state of the groundwater system. The base-case regional-scale model attempts to replicate the observed present-day conditions using the geological framework model, hydraulic parameters, transport parameters, porewater solute concentrations, and boundary conditions based on observations, analyses, and interpretations of this state. Importantly, the model also assumes that the system is completely water (or brine) saturated. The initial conditions of TDS concentration and equivalent freshwater heads assumed for the model evolve to a pseudo-equilibrium solution for this state. The objective of the analysis, in part, is to reveal system behaviour and to identify observed attributes that may be the signature of a different state.

Given the boundary conditions applied to the base-case model, the surface water level for Lake Huron of 176 metres above sea level (mASL) represents the minimum head possible in the model; the observed fluid underpressures in the Ordovician and Lower Silurian units at the DGR boreholes (refer to Figure 5.5) are clearly a consequence of a different state than that described by the base-case conceptual model. The pressures may be the result of rock dilation, from either glacial unloading or significant removal of mass through erosion that was at a rate that is greater than that of water influx to these low-permeability units from the over and underlying units with higher pressure; the pressure distribution is still evolving. Alternatively, the low pore fluid pressures may indicate the presence of a trapped non-wetting gas phase, the impact of osmosis, or the result of crustal flexure (Sykes et al. 2011). In any case, the base-case model, as formulated, cannot be expected to simulate the Ordovician underpressures.

Modelling of the pressure profile at the DGR boreholes can be approached from two perspectives: an assessment of the cause of the underpressures of the Ordovician and Lower Silurian and the overpressures of the Cambrian, or an assessment of the evolution of the pressures from their current state. The former analysis would require either realizations of the previous state of the regional-scale system or the simulation of immiscible, two-phase flow of gas and water. Realizations of the previous state of the system during the most recent episodes of glaciation are described in Section 5.4.6.6. An analysis of two-phase water and gas flow using the model TOUGH2-MP is developed in Section 5.4.9 for a one-dimensional column. An assessment of the future evolution of the pressures cannot be undertaken at the regional-scale due to a lack of data on the pressures at other locations in the domain; however, an analysis can be developed at the site-scale (refer to Section 5.4.7).

The following discussion considers the conclusions that can be drawn from the base-case model despite its inability to replicate the observed Ordovician underpressures. The equivalent freshwater head distribution for the base-case simulation after 1 Ma (pseudo-equilibrium time) is shown in a fence view in Figure 5.20. The environmental head distribution for the base-case parameters and boundary conditions is shown in Figure 5.22. Plots of equivalent freshwater heads can be used to interpret horizontal flow gradients but not vertical gradients; conversely, the plots of environmental heads can be used to interpret vertical gradients but not horizontal gradients. At the location of the proposed DGR, the model-calculated equivalent freshwater head in the Niagaran from the regional-scale base-case analysis is 263.1 m compared to the August 24, 2009 measured equivalent freshwater head at the DGR-4 borehole of 210.4 m for the Guelph, the highest permeability unit in the Niagaran. The model-calculated environmental head in the Niagaran from the regional-scale base-case analysis is 238.9 m compared to the August 24, 2009 estimated environmental heads in the DGR-4 borehole of 186.3 m for the Guelph. Higher heads were measured in the Lions Head Formation, which forms part of the Niagaran Group. For the Cambrian, the base-case model-estimated equivalent freshwater head is 380.6 m compared to a measured value of 422.1 m, while the base-case model environmental head is 268.3 m compared to an estimated value in the DGR-4 borehole of 317.6 m. Thus, the base-case regional-scale model overpredicts the head measured in the Guelph in DGR-4, while underpredicting the head measured in the Cambrian. The model does, however, correctly predict that the gradient between the Cambrian and the Niagaran is upward, as observed in DGR-4.

The shallow groundwater regime above the Salina is dominated by flow that mimics topography. Beneath the shallow groundwater zone, the heads are not controlled to the same extent by the local elevation of the surface. The main control for the horizontal component of the density-dependent energy gradient at depth is the elevation difference between Lake Huron and the topographic high at the Niagara Escarpment. The head signature will be transmitted from the outcrop area and will be dissipated, depending on the energy gradient, across the domain (refer to Figure 5.20). At a given location, the vertical component of the energy gradient is controlled by the difference in the environmental heads between the more permeable units that are separated by low-permeability units (refer to Figure 5.22). For the regional domain, the higher permeability Cambrian (where present) and Niagaran Group formations are separated by the low-permeability units of the Ordovician and Lower Silurian. The Niagaran is confined in the southwestern part of the domain by the overlying low-permeability units of the Salina. Flow in the Niagaran, where it is unconfined, is controlled by surface topography.



Notes: From Sykes et al. (2011).

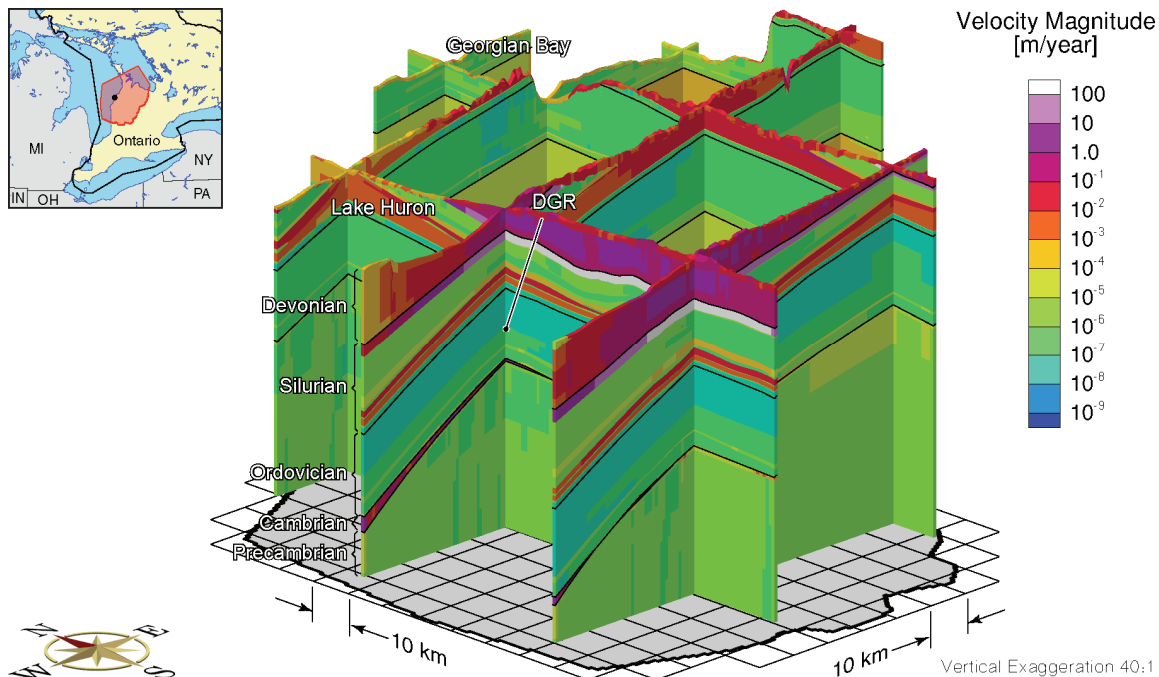
**Figure 5.22: Fence View of the Base-case Environmental Heads that have Equilibrated at 1 Ma to the Temporally Varying TDS Distribution**

The overpressured environmental heads observed in the Cambrian at the DGR-4 borehole (Figure 5.5) are underpredicted in the pseudo-steady-state analysis with the base-case parameters, initial conditions and boundary conditions. Several causes can be postulated for why the observed Cambrian pressures are higher than those modelled. Because the Cambrian pinches out east of the Bruce nuclear site, it does not outcrop or subcrop within the modelling domain and, therefore, is not connected to any recharge area in the model. Within the model, the Cambrian head is generated by the fluid density distribution and depth of the Cambrian. In actuality, the Cambrian may derive its head from a higher elevation recharge area outside the model domain and/or from connection to the centre of the Michigan Basin where it is several kilometres deep with a significant column of higher density saline fluids above. Either of these possibilities would require continuity of the Cambrian's permeability over much of the basin. The heads may also reflect a pressure distribution from a state of thermal, hydraulic and geomechanical conditions that were significantly different from that simulated by the base-case analysis; this would imply that the pressures are evolving to a distribution that is compatible with the current state and boundary conditions of the groundwater system. The pressures also may be the result of the presence of a gas phase that provides pressure support for the unit. The overpressurization of the Cambrian is further investigated in Section 5.4.8.

In addition to the elevation component of the gravitational gradient imposed by the topographic high at the Niagara Escarpment, the density of the brine in the deep groundwater zone will have an impact on the energy gradients. The salinity profile for the base-case at a pseudo-equilibrium time of 1 Ma (Figure 5.21) consists of relatively fresh groundwater for the shallow groundwater zone and an area with much higher TDS concentrations for the

intermediate and deep groundwater zone (below the Salina, where present). The shallow groundwater zone will remain devoid of salinity because the continual inflow of meteoric water through recharge to the zone will dilute any salinity that diffuses upward through the Silurian or Ordovician. The brine concentrations in the low-permeability Ordovician units at the Niagara Escarpment, where the Silurian is absent, will also experience some flushing as well; however, the higher density groundwater found in the deeper zone, that has a higher energy than water with low TDS, will prevent any significant penetration of freshwater. The TDS transition zone occurs across the Salina.

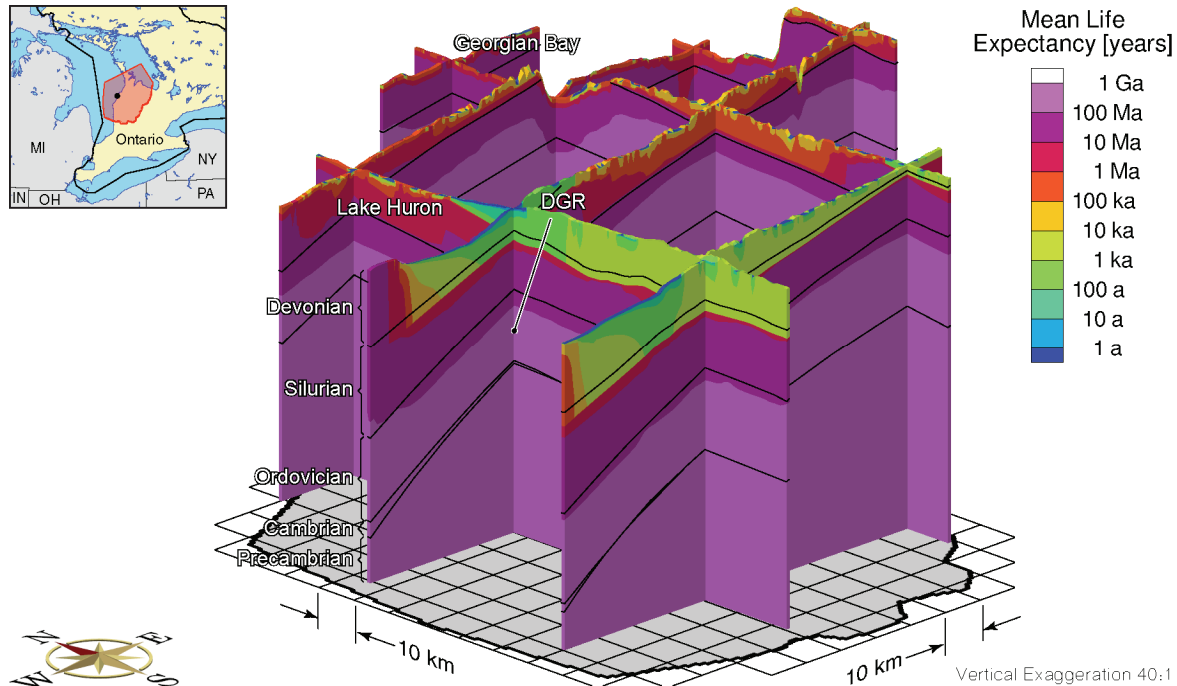
The base-case porewater velocity magnitudes are presented in Figure 5.23. The highest velocities occur in the more permeable shallow groundwater zone. The lower velocities beneath Lake Huron and Georgian Bay are the result of the absence of a horizontal gradient. The reduction of the velocities in the Salina Group is shown as the greenish band below the upper reddish-purple band at the proposed DGR location, while the higher velocities of the Niagaran in the Silurian appear as the first orange/red band above the indicated DGR position. Above the Niagaran, higher velocities are also evident in the Salina A1 Unit carbonate. Within the Ordovician in the vicinity of the proposed DGR, the groundwater pore velocities are less than  $1 \times 10^{-6}$  m/year; the porewater velocity estimated for the Cobourg is  $2.3 \times 10^{-7}$  m/year. The estimated Péclet number for the Cobourg for the base-case analysis is  $2.9 \times 10^{-4}$  assuming a characteristic length of one metre, indicating that solute transport in the Ordovician will be diffusion dominated.



Notes: Diffusion is the dominant transport mechanism wherever velocity is  $< 10^{-4}$  m/year. From Sykes et al. (2011).

**Figure 5.23: Fence View of Base-case Porewater Velocity Magnitude**

The performance measure selected for the evaluation of the groundwater system is the MLE (Figure 5.24). The general trend for the MLE is similar to that found in the head and velocity distributions. The shallow groundwater zone has significantly shorter MLEs compared to the deep groundwater zone. The areas of recharge versus discharge can be noted in the figure as the recharge areas have a high MLE while the discharge areas have low MLEs. The groundwater area surrounding the proposed DGR is calculated to have an MLE of 164 Ma for the base-case regional-scale conceptual model.



Notes: From Sykes et al. (2011).

**Figure 5.24: Fence View of Base-case Mean Life Expectancy**

#### 5.4.5.6 Alternative Simulations

To evaluate the potential effects of alternative conceptualizations of various features of the base-case model, different boundary conditions, and different parameter values, a variety of alternative simulations were performed with the regional-scale model. Two sets of simulations involved variations in the hydraulic conductivity of the Precambrian and of the Cambrian. Another set examined the effects of varying the surface boundary conditions. One simulation evaluated the effect of changing the lateral boundary condition on the model. An extensive suite of simulations focused on the effects of past glacial cycles is described in Section 5.4.6. The alternative simulations were designed to reveal the attributes of the flow system that are important in the development of a safety case for a deep geologic repository and to investigate the sensitivity of predicted numerical outcomes to selected parameters. The performance measure for the analyses is MLE.



Table 5.8 provides a matrix of the alternative simulations performed, showing how different conditions and assumptions were combined. Details about all the simulations performed are given in Sykes et al. (2011). The scenario names in Table 5.8 correspond to the prefix of the file names for the computer runs. The "f" designates the FRAC3DVS-OPG computational model, the "r" designates the regional-scale model, the middle descriptor of "base" designates that the analysis is a perturbation of the base-case regional-scale model, while the third and fourth descriptors designate the scenario. The third descriptor "paleo" indicates that the analysis is one of the paleoclimate scenarios described in Section 5.4.6.

Table 5.9 lists the MLE estimates at the location of the proposed DGR for each of the non-paleo scenarios modeled.

The permeability or hydraulic conductivity versus depth model for the Precambrian rock developed by Normani (2009) and used for the base-case model reflects a weathered zone for rock near the ground surface. Two alternative conceptualizations of the Precambrian hydraulic conductivity were modelled: one in which a 20-m-thick weathered layer with a minimum hydraulic conductivity of  $1 \times 10^{-8}$  m/s was present at the top of the Precambrian throughout the modelling domain (scenario fr-base-hkp), and one in which the entire Precambrian was assigned a uniform hydraulic conductivity of  $1 \times 10^{-12}$  m/s (scenario fr-base-up). For the first of these scenarios, hydraulic conductivities greater than  $1 \times 10^{-8}$  m/s were assigned to the weathered upper Precambrian zone wherever the model of Normani (2009) indicated a higher value was appropriate. Note that the hydraulic conductivity of the assumed weathered zone is still approximately two orders of magnitude lower than the base-case hydraulic conductivity for the Cambrian. However, the assumed hydraulic conductivity for the weathered zone is approximately four orders of magnitude higher than the minimum value assigned to the Precambrian at the location of the DGR boreholes in the base-case analysis. As shown in Table 5.9, the MLE at the repository location is insensitive to the variations in Precambrian hydraulic conductivity that were modeled.

The upper surface of the base-case regional-scale model was defined by a Dirichlet (prescribed head) boundary condition representing either the regional water table or the elevation of Lake Huron. The influx and efflux of water across the surface was controlled, in part, by the hydraulic conductivity of the top layer of the model, as well as by topographic gradients. It was assumed that, on average, the water table was located 3 m below the ground surface and that, to reflect weathering, the upper 20 m had a higher hydraulic conductivity than the underlying units. The overall conclusion from the scenarios examining different surface boundary conditions is that they are unimportant to the performance of a DGR in the Cobourg. Table 5.9 shows that the MLEs calculated for these scenarios are very similar to the MLE for the base-case scenario.

The regional-scale spatial domain is a subset of the Michigan Basin. For the more permeable units of the intermediate and deep groundwater zones such as the Niagaran and the Cambrian, the use of a no-flow boundary condition for the lateral edges of the domain could have an impact on the flow in the units and on the estimate of MLE at the location of the proposed DGR. A scenario was modeled (fr-base-hbc) in which the constraint on lateral flow imposed by the no-flow boundary condition was relaxed. This was achieved by assigning a vertical hydraulic conductivity of  $1 \times 10^{-5}$  m/s from the surface to the Precambrian at the perimeter of the domain. The upper boundary condition was identical to that of the base-case analysis. The described zone at the boundary allows communication at the domain edges between all of the deeper units and the surface where the equivalent freshwater heads were assigned based on either surface topography or the water elevation of Lake Huron and Georgian Bay. The hydraulic parameters for the analysis were the same as those of the base-case analysis.

**Table 5.8: Matrix of Regional-scale Simulations Performed**

Factor Varied	Condition	fr-base	fr-base-up	fr-base-hkp	fr-base-hbc	fr-base-rech	fr-base-paleo <sup>1</sup>	fr-base-paleo-biot	fr-base-paleo-gas	fr-base-paleo-head80	fr-base-paleo-head30	fr-base-paleo-zero-head	fr-base-paleo-le-zero	fr-base-paleo-nn921	fr-base-paleo-openbd
Precambrian Conductivity	Uniform		x												
	Vary with depth	x		x	x	x	x	x	x	x	x	x	x	x	x
	At least 1E-10 m/s	x	x		x	x	x	x	x	x	x	x	x	x	
	At least 1E-8 m/s			x											x
Lateral Boundary Conditions	Neumann Zero Flux	x	x	x		x	x	x	x	x	x	x	x	x	
	Dirichlet heads for A1 Carb., Niagaran, and Cambrian														x
	High K open to surface				x										
Surface Boundary Conditions	Dirichlet	x	x	x	x										
	Neumann					x									
	Dirichlet 100% ice thickness						x	x	x				x	x	x
Paleo Surface Boundary Conditions	Dirichlet 80% ice thickness									x					
	Dirichlet 30% ice thickness										x				
	Dirichlet 0% ice thickness											x			
Paleo Simulation	nn9930								x	x	x	x	x		x
	nn9921													x	
Hydromechanical	Biot coefficient = 1.0						x		x	x	x	x	x	x	x

Factor Varied	Condition	fr-base	fr-base-up	fr-base-hkp	fr-base-hbc	fr-base-rech	fr-base-paleo <sup>1</sup>	fr-base-paleo-biot	fr-base-paleo-gas	fr-base-paleo-head80	fr-base-paleo-head30	fr-base-paleo-zero-head	fr-base-paleo-le-zero	fr-base-paleo-mn921	fr-base-paleo-openhd
Coupling	Biot coefficient = 0.5						x	x							
Presence of Gas Phase	No gas phase						x	x		x	x	x	x	x	x
	Partial gas phase								x						
Loading Efficiency	Actual						x	x	x	x	x	x		x	x
	Zero												x		
Paleo Cycles	1 – 120 ka						x	x	x	x	x	x	x	x	x
	2 – 240 ka						x								

Notes: <sup>1</sup> includes fr-base-paleo-2 simulation. From Sykes et al. (2011; their Table 4.10).

Even in this extremely unrealistic scenario in which the isolation properties of all units are short-circuited at the model boundary, the MLE at the location of the proposed DGR was estimated to be 44 Ma (Table 5.9). Changes in the lateral boundary condition do not alter the condition of diffusion-dominant transport in the Ordovician.

**Table 5.9: Mean Life Expectancy at the Location of the Proposed DGR for Alternative Modelling Scenarios**

Simulation	Cobourg MLE (Ma)
fr-base (no density)	155
fr-base	164
fr-base-hkp	164
fr-base-up	161
fr-base-rech	172
fr-base-hbc	44

Notes: From Sykes et al. (2011).

#### 5.4.5.7 Conclusions from Regional-scale Modelling

As formulated, the regional-scale model does not accurately represent the present-day state of the system because it cannot account for Ordovician underpressures; it represents an equilibrium state condition toward which the present-day system may be evolving. In order to reach this equilibrium state, flow must occur from the Cambrian and/or Niagaran into the Ordovician to restore a normal pressure profile. Modelling of a variety of different scenarios has shown that the head conditions and resultant energy gradients between the Niagaran and Cambrian have no significant effect on transport through the Ordovician because that transport is so strongly dominated by diffusion.

Alternative scenarios that were simulated with the regional-scale model included:

- A conceptualization of the Precambrian that included an upper weathered zone with a higher hydraulic conductivity than in the base-case model;
- A conceptualization using a recharge rather than fixed-head surface boundary condition; and
- A conceptualization in which the lateral model boundaries were open to the surface.

The performance measure used to evaluate the consequences of the various scenarios with respect to DGR performance was the MLE, which is the time required for a conservative tracer at the DGR location in the groundwater system to reach a potential outflow point. With the exception of the scenario with lateral boundaries open to the surface, the MLEs ranged only from 148 to 172 Ma (see Table 4.12 in Sykes et al. 2011). Opening the lateral boundaries to the surface reduced the MLE only to 44 Ma (Table 5.9). None of the changes modelled altered the condition of an upward gradient from the Cambrian to the Niagaran, except for scenario fr-base-hbc.

Table 5.10 presents a summary of the Péclet numbers for the Cobourg calculated using Equation (5.1) with a characteristic length of 1 m for each of the scenarios modelled. The

Péclet numbers are all less than  $10^{-3}$ , clearly supporting the hypothesis that solute transport in the Ordovician sediments is diffusion dominant. Vertical pore velocities would have to be three orders of magnitude greater than the modelled scenarios indicate before advection would constitute a significant transport mechanism. No plausible parameter variation could cause such an increase in velocity.

**Table 5.10: Péclet Numbers for the Cobourg from Regional-scale Analyses**

Simulation	Péclet Number [ $l = 1 \text{ m}$ ]
fr-base (no density)	2.17E-04
fr-base	2.91E-04
fr-base-hkp	3.13E-04
fr-base-up	3.04E-04
fr-base-rech	2.72E-04
fr-base-hbc	7.59E-04

Notes: From Sykes et al. (2011).

#### 5.4.6 Regional-scale Paleoclimate Modelling

In this section, the regional-scale model (Sykes et al. 2011) is adapted to a study of how it would respond to changes in paleoclimate associated with glaciation. This assessment includes:

- Evaluating the expected flow system perturbation by glacial events (boreal, peri-glacial or ice sheet);
- Assessing the depth of penetration by glacial meltwaters into Paleozoic formations;
- Illustrating numerically the transient influence of glacial event(s) on the DGR site flow system;
- Estimating pore fluid residence times during Quaternary glacial events;
- Determining the impact of glaciation on the spatial distribution and temporal evolution of water pressure in the Ordovician sediments;
- Determining the influence on water pressure evolution of a residual gas phase in the Ordovician sediments; and
- Assessing the impact, if any, of glaciation on solute transport in the Ordovician sediments.

##### 5.4.6.1 Climate Change and Glaciation

As described in Section 2.2.7.1, the North American continent has experienced nine glacial cycles over the past 1 Ma. Peltier (2002) and Marshall et al. (2000) have developed glaciological reconstructions of the Laurentide ice sheet over the North American continent using numerical models. According to Peltier (2002), these reconstructions of the Pleistocene ice-sheet history are based on three areas of study:

- Geological and paleogeological records;

- The isostatic record of crustal deformation; and
- The behaviour of modern-day glaciers and ice sheets.

During ice-sheet advance, the Bruce nuclear site would evolve from periglacial to subglacial conditions and eventually be overlain by up to 3 km of ice. Permafrost develops below ground surface in advance of the ice sheet. The thermal conditions at the base of the ice could be above or below the pressure melting point of the ice; a temperature above this point could result in subglacial flow of water or the development of streams, while colder temperatures could freeze the ice sheet to bedrock (Hooke 2005). The ice sheet provides a thermal break between the atmosphere and the bedrock; allowing the geothermal heat flux radiating towards the ground surface to reduce the depth of permafrost (Peltier 2002).

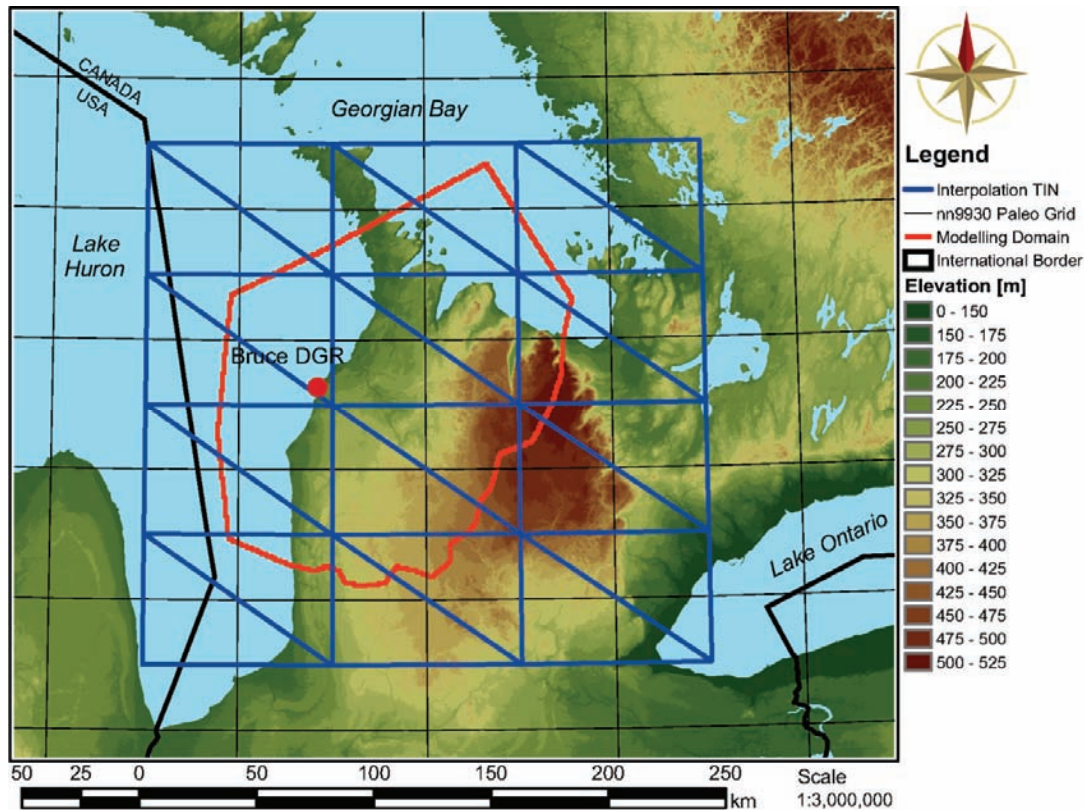
The physical model used for these simulations is the UofT GSM (Peltier 2011). The UofT GSM is used for modelling ice-sheet evolution in a transient manner over a period of 120 ka. The model performs its calculations on a geographic grid measuring 1.0° in longitude by 0.5° in latitude. Various model outputs include normal stress on the ground surface due to an ice sheet, permafrost depth, basal temperature relative to the pressure melting point of ice, surface lake depth, basal meltwater production, basal surface elevation subject to isostatic adjustment, surface elevation of ice sheet, and ice sheet thickness.

#### 5.4.6.2 Glacial Meltwater

The water pressure at the base of a glacier is an important factor in assessing the impact of glaciation on a groundwater system. Beneath warm-based glaciers, free water can exist at the ice-bed contact and interstitially in subglacial sediment. Water at the contact can include porewater that has exfiltrated as a result of mechanical loading, basal meltwater, and surface meltwater that has penetrated or flowed englacially to the base through ice-walled conduits that include fractures, fissures, crevices and moulins when they occur (Clarke 2005; Zwally et al. 2002; Fountain and Walder 1998). Surface melting is typically one to four orders of magnitude larger than basal melting and when it reaches the bed, it can supply sufficient water to require drainage at the ice-bed interface even when there are underlying aquifers (Arnold and Sharp 2002; Boulton et al. 1995). The presence of water at the ice-bed contact contributes to increased water pressure at the boundary, with a corresponding reduction of the effective pressure given as  $P_e = P_i - P_w$  (Clarke 2005) where  $P_w$  is the pressure of the subglacial water, and  $P_i = \rho_i g h_i$  is the overburden ice pressure in which  $\rho_i$  is the ice density,  $g$  is the gravitational acceleration and  $h_i$  is the ice thickness. The subglacial water also can penetrate into the subsurface. In sedimentary basins, subglacial water can migrate from the basin margins to depth through the more permeable layers (McIntosh and Walter 2006).

#### 5.4.6.3 Linking to the UofT GSM

The modelling domain is restricted to southwestern Ontario, and the UofT GSM covers most of North America (Peltier 2011); vertical stress due to ice, and permafrost depth, were spatially interpolated as shown in Figure 5.25. A TIN was created, whose nodes lie at the midpoint of each paleo grid block; the value of vertical stress or permafrost depth is taken at the midpoint of each paleo grid block, and linearly interpolated across each triangular facet of the TIN. Hydraulic boundary condition values for vertical stress corresponding to the FRAC3DVS-OPG grid are interpolated from the TIN for each 500-year time step in the 120 ka UofT GSM simulation.

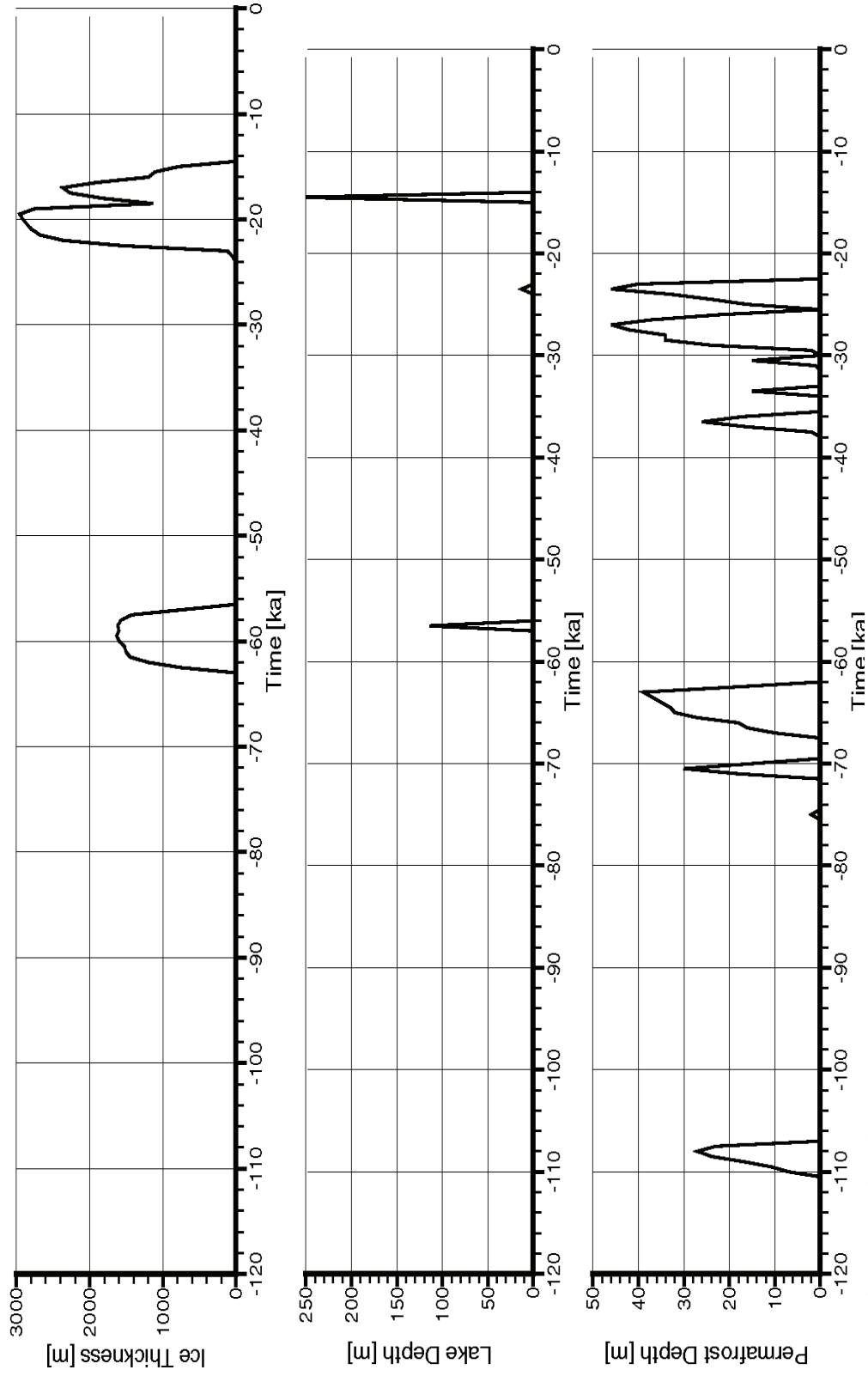


Notes: Grid block from the UofT GSM (Peltier 2011; models nn9930 and nn9921).

**Figure 5.25: TIN Used to Interpolate Properties for the Regional-scale Spatial Domain**

Peltier (2011) describes eight models that “span the apparent range of model characteristics that provide acceptable fits to the totality of the observational constraints.” Of these eight models, nn9921 and nn9930 are two of the best models based on aggregate misfit, and both include high-resolution permafrost development. Less permafrost leads to deeper recharge meltwater penetration into the subsurface (see Normani et al. 2007); of the two models selected for the paleoclimate simulations presented herein, nn9921 and nn9930, model nn9930 had less permafrost than nn9921. Plots of the nn9930 and nn9921 UofT GSM model outputs for ice thickness, lake depth, and permafrost depth at the grid cell at the Bruce nuclear site (Peltier 2011) are shown in Figure 5.26 and Figure 5.27, respectively.

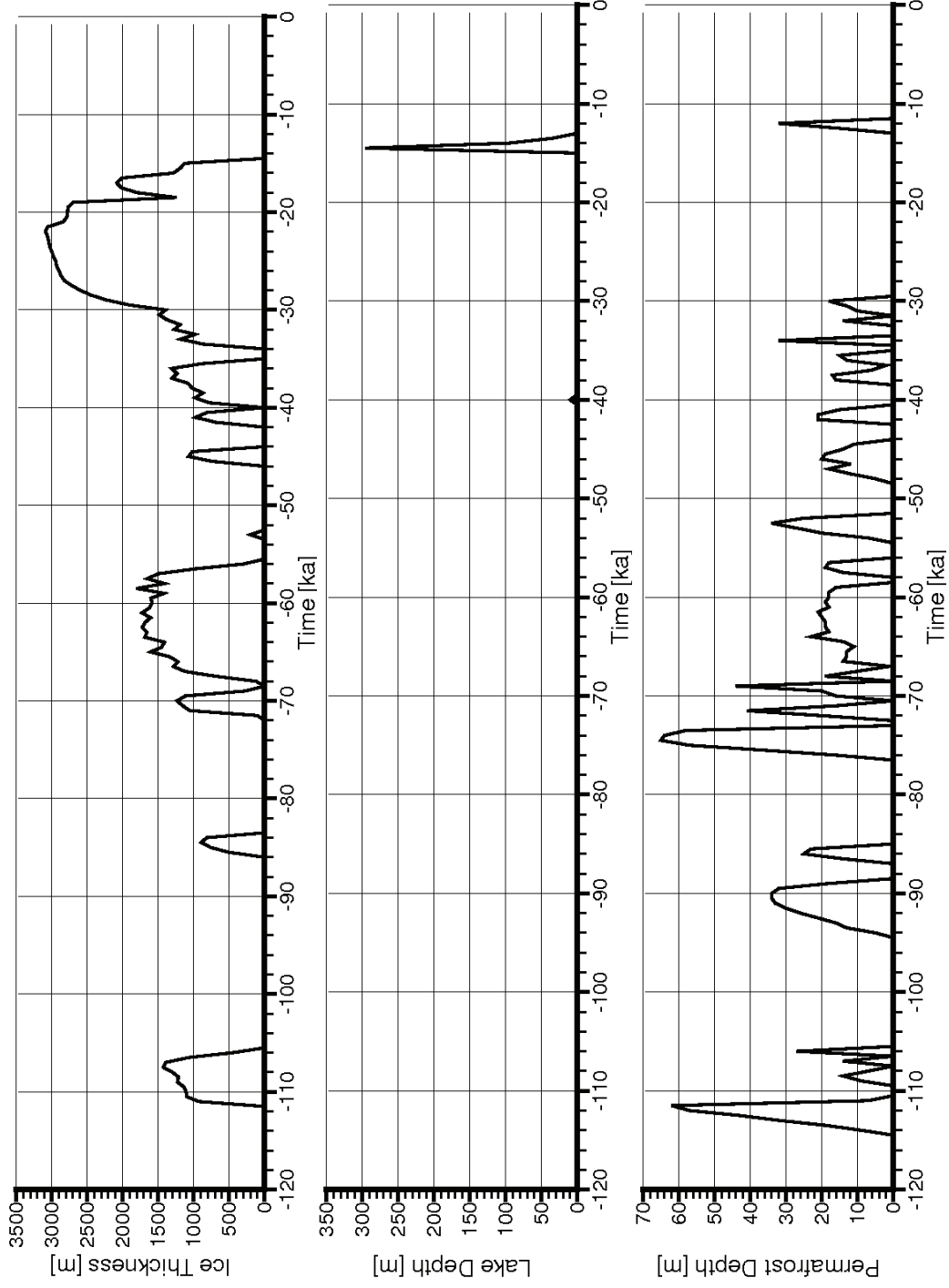
The isostatic movement of the ground surface due to ice loading is not considered. Applied hydraulic boundary conditions are stated in terms of elevation, assuming the grid does not move vertically. The application of lake depth is also a relative term independent of isostatic movement, although isostatic depression is required for a proglacial lake to form. Although lake depth could be interpolated across the TIN in a similar manner to permafrost depth and vertical stress due to ice, large gradients could be created across the site which would not exist in the presence of a large proglacial body of water because isostatic movement is not considered. As a result, lake depth is added to the existing lake elevation and hydraulic boundary conditions are adjusted accordingly. Changes in surface topography due to glacial stripping of sediments are not considered.



Notes: From Sykes et al. (2011).

**Figure 5.26: Plots of Ice Thickness, Lake Depth, and Permafrost Depth versus Time for the nn9930 GSM Grid Block at the Bruce Nuclear Site**





Notes: From Sykes et al. (2011).

**Figure 5.27: Plots of Ice Thickness, Lake Depth, and Permafrost Depth versus Time for the nn9921 GSM Grid Block at the Bruce Nuclear Site**

#### 5.4.6.4 Paleoclimate Boundary Conditions

Glaciogeomorphological evidence and numerical simulations (Tarasov and Peltier 2004; Bense and Person 2008) indicate that it is likely that thawed bed conditions persisted during the last glacial maximum across the Michigan Basin. Under such conditions, the mechanical loading upon ground surface due to the presence of an ice sheet can be implemented as a hydraulic boundary condition in a groundwater flow model assuming the height of the ice sheet can be replaced with an equivalent height of freshwater resulting in the same pressure or stress at its base. This approach has been applied by Boulton et al. (1995), Person et al. (2003, 2007), and Bense and Person (2008) for two-dimensional cross-sectional groundwater flow models.

#### 5.4.6.5 Paleoclimate Simulations

The base-case paleoclimate simulation uses the parameters listed in Table 5.6 and Table 5.7 with the nn9930 paleoclimate model. The remaining paleoclimate analyses represent variations on the base-case to investigate the influence of changes to the base-case parameters or climate model on the modelling results. Table 5.8 provides a matrix of the paleoclimate simulations performed. The initial conditions for all paleoclimate simulations were as described in Section 5.4.5.4 for the base-case regional-scale model.

##### **Base-case**

Freshwater heads at the end of the base-case paleoclimate simulation (fr-base-paleo), representing the present time, are shown in Figure 5.28; environmental heads are shown in Figure 5.29. The paleoclimate boundary conditions of nn9930 represent the most recent 120-ka glacial episode over the Canadian landscape. In comparing Figure 5.29 to the base-case paleoclimate initial conditions shown in Figure 5.22, the environmental heads are higher throughout most of the Silurian and at the top of the Ordovician, namely the Queenston Formation. This elevated head is also shown in Figure 5.30, where the vertical profiles of freshwater head and environmental head are plotted versus depth at the DGR location. In Figure 5.30, the black line represents the end of the base-case paleoclimate simulation at 0 ka. (The other lines represent results of other simulations, as discussed in the following paragraphs.) The residual elevated heads persist even 14 ka after deglaciation. The high heads associated with the paleoclimate surface boundary condition propagate into the Salina Group and the Queenston Formation, and are slow to dissipate. According to Table 5.6, the Salina is characterized by slightly higher specific storage values and lower one-dimensional loading efficiencies than the Ordovician, leading to a greater storage capacity, and higher gradients due to reduced in situ pore pressures resulting from hydromechanical coupling.

In comparing the modelled freshwater and environmental heads to measured heads in DGR-4 (Figure 5.30), a clear mismatch exists for both the underpressured Ordovician and overpressured Cambrian relative to ground surface. The glacial loading and unloading cycles simulated have not resulted in present-day Ordovician underpressures. The use of FRAC3DVS-OPG assumes that the entire modelling domain is fully saturated, while a possible cause for the underpressurization in the Ordovician units is the presence of a gas phase, resulting in a partially saturated porous medium. The overpressure in the Cambrian may be related to higher density fluids in the central portion of the Michigan Basin, coupled with the high hydraulic conductivity of the Cambrian.

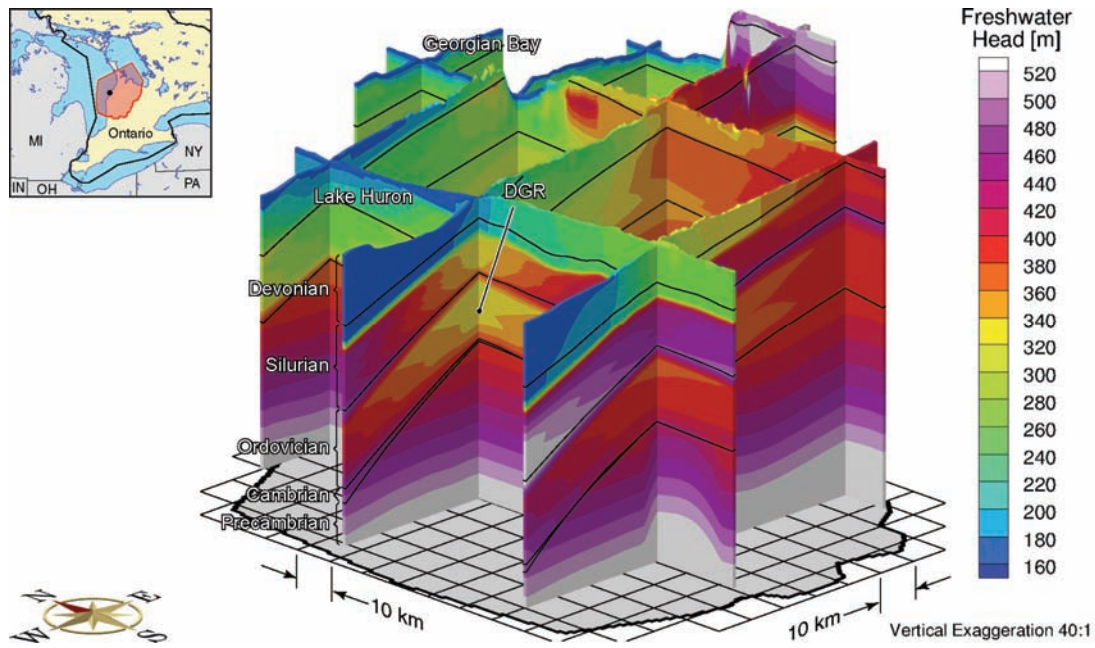


**Figure 5.28: Fence View of Freshwater Heads at Present for the Base-case Paleoclimate Scenario**

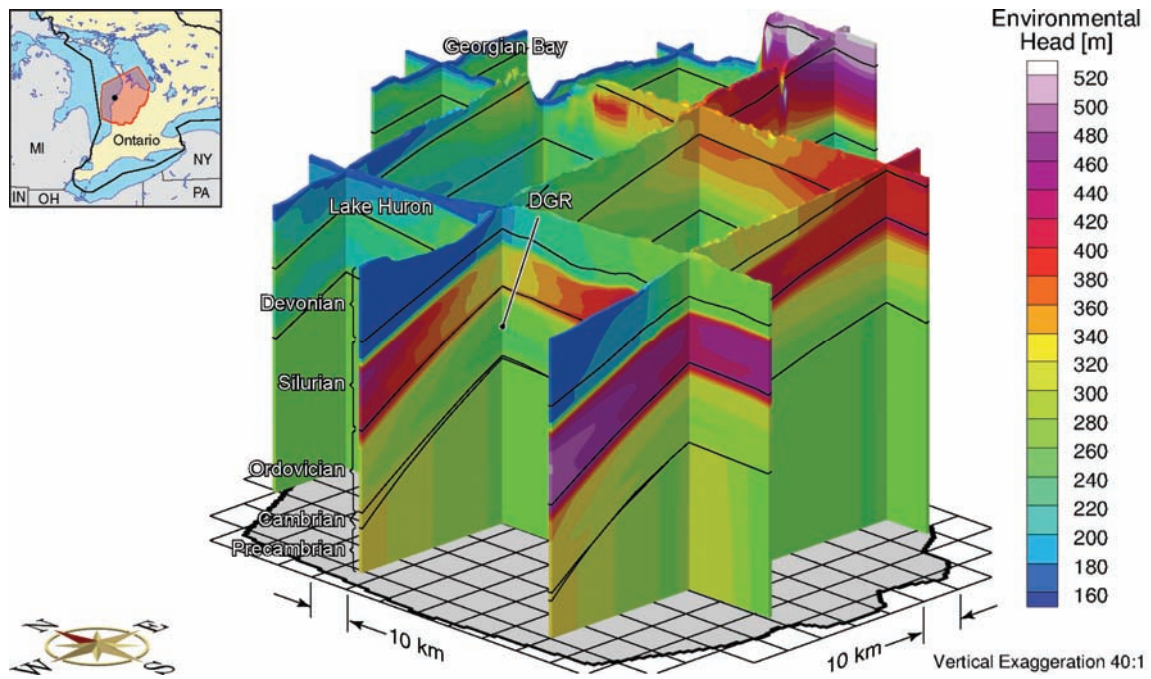
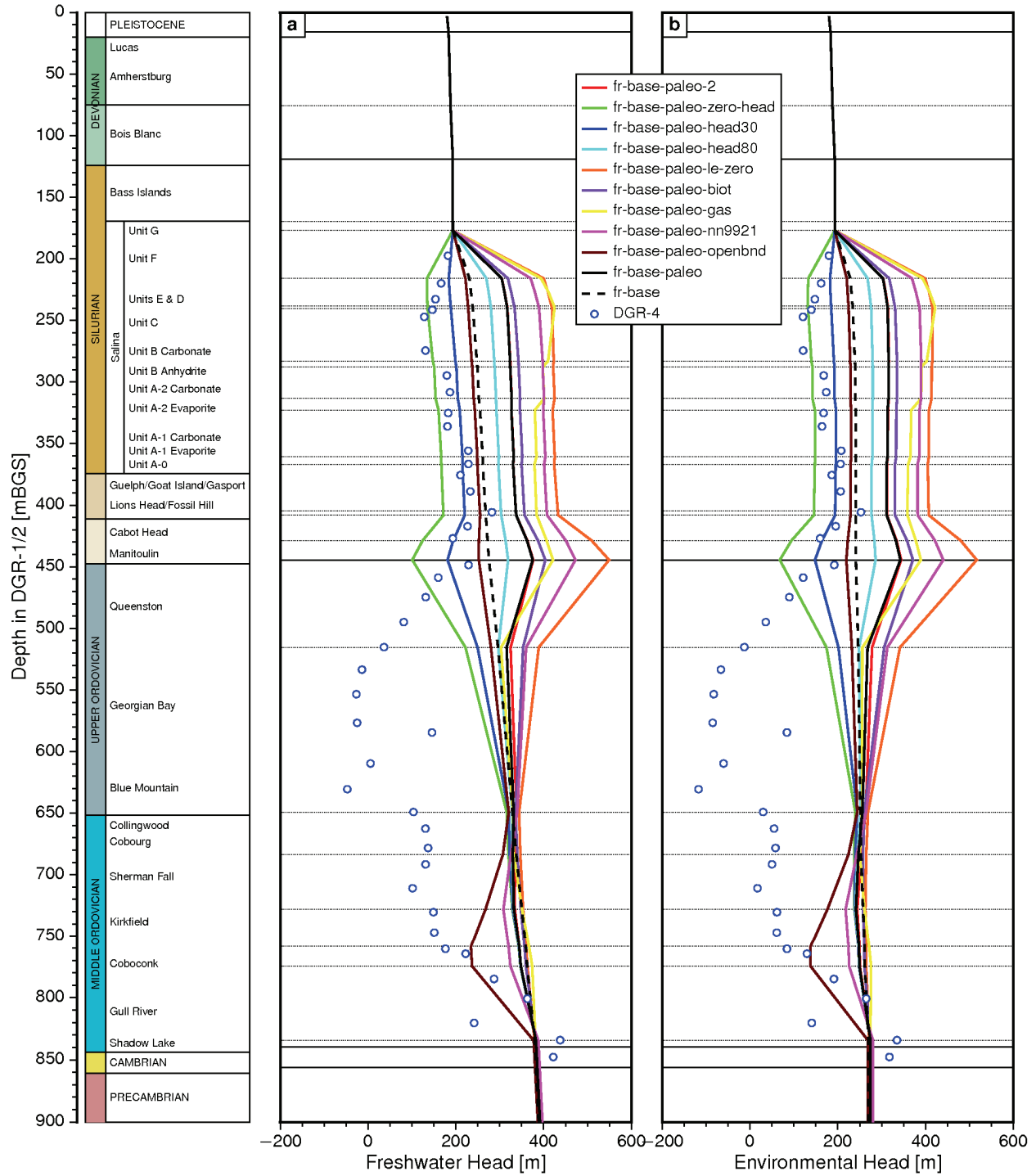


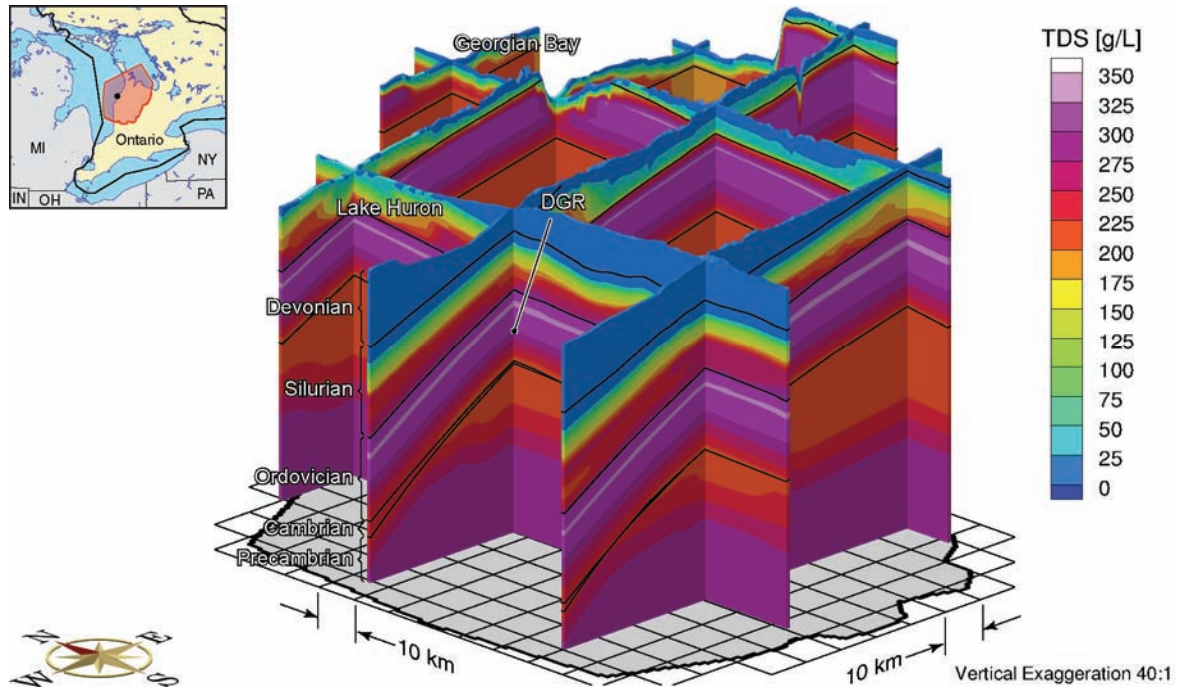
**Figure 5.29: Fence View of Environmental Heads at Present for the Base-case Paleoclimate Scenario**



Notes: Freshwater and environmental heads for DGR-4 are shown as measured on August 24, 2009. From Sykes et al. (2011).

**Figure 5.30: Plot of Freshwater Head and Environmental Head Results from Paleoclimate Simulations**

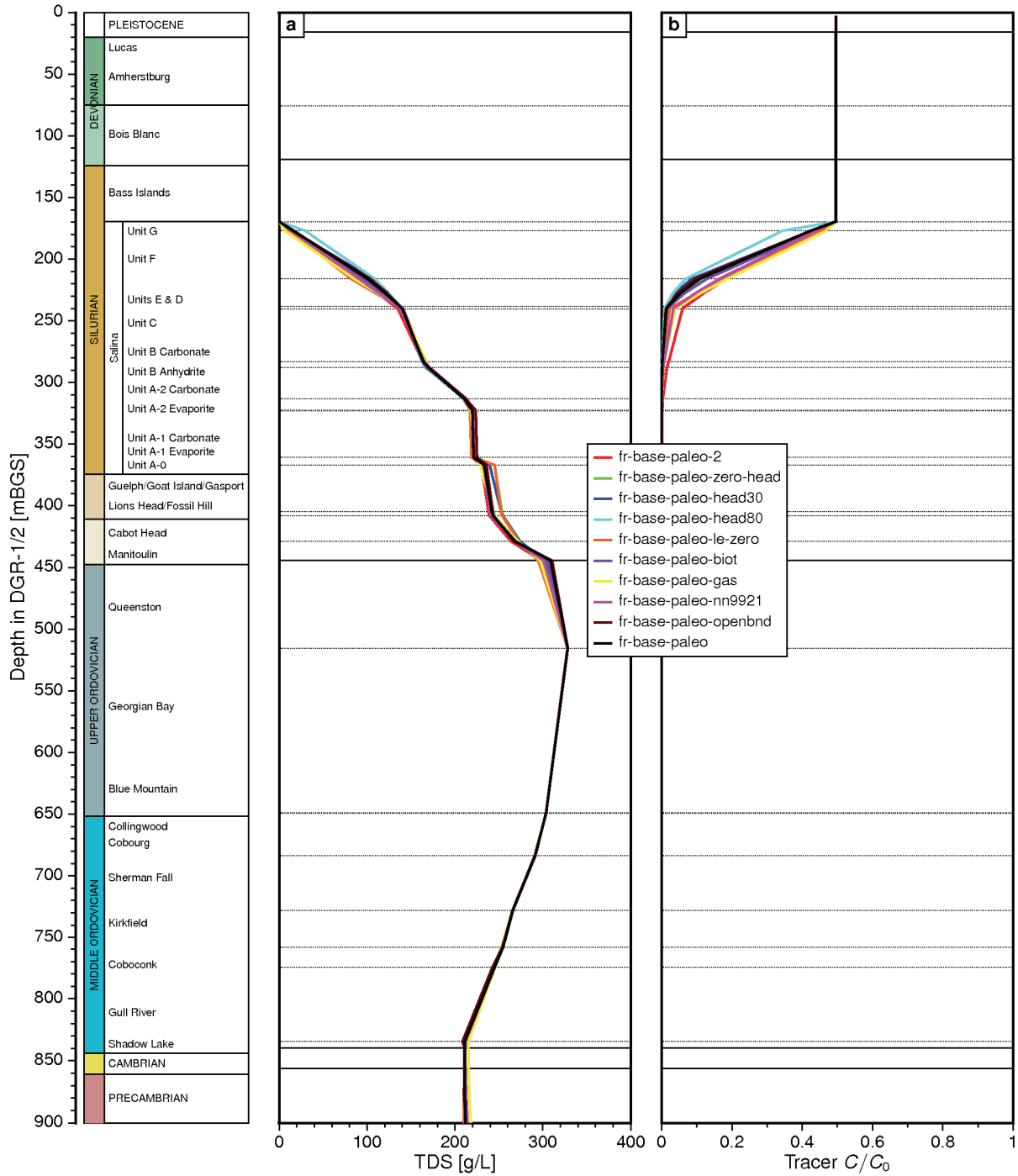
TDS concentrations at the end of the paleoclimate simulation period are presented in Figure 5.31, while the initial conditions for the simulation are shown in Figure 5.21. The TDS concentration profile at the DGR in Figure 5.32a changed only slightly over the simulation, as some of the steeper gradients imposed by the initial conditions dissipated, with most of the changes occurring near the top of the Salina and in the vicinity of the Niagaran Group.



Notes: From Sykes et al. (2011).

**Figure 5.31: Fence View of TDS at Present for the Base-case Paleoclimate Scenario**

Porewater velocity magnitudes at the end of the paleoclimate simulation are shown in Figure 5.33. The plot clearly shows the higher velocity zones associated with higher hydraulic conductivity, namely, the zones above the Salina, the A1 Carbonate, the Niagaran Group, and the Cambrian. Due to the transient nature of the paleoclimate simulation, flow is predominantly vertically downward through the Ordovician. This downward migration at the end of the paleoclimate simulation can be seen in the environmental head plot of Figure 5.30b. As more time passes since the paleoclimate forcing is applied, these downward velocities will reverse.

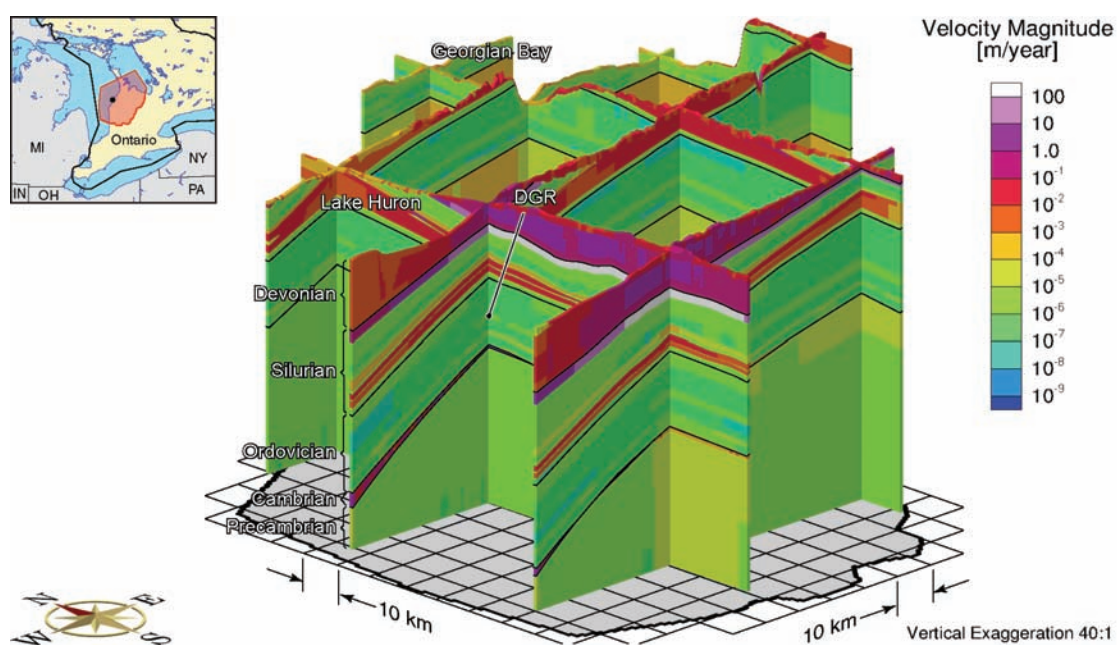


Notes: From Sykes et al. (2011).

**Figure 5.32: Plot of TDS and Tracer Concentration versus Depth from Paleoclimate Simulations**

A tracer of unit concentration is applied as a Cauchy boundary condition to all surface nodes at the beginning of the paleoclimate simulation. This tracer is used to characterize the migration,

from the surface, of recharge water that occurs during the paleoclimate simulation; the recharge water includes glacial meltwater, the importance of which was discussed in Section 5.4.6.2. Tracer concentrations for the modelling domain at the end of the base-case paleoclimate simulation are presented in Figure 5.34. The 5% isochlor migrates approximately a third of the way into the Silurian sediments and is nearly in the same location as the top of the environmental head transition in Figure 5.29. Figure 5.32b shows the tracer concentration with depth at the DGR location. Lithologic units from ground surface to the Bass Islands Formation are characterized by higher hydraulic conductivities, while the units in the Salina are of comparatively lower conductivity. The downward migration of the tracer in Figure 5.32b is retarded by the Salina and demonstrates diffusion as the dominant transport mechanism below the top of the Salina.



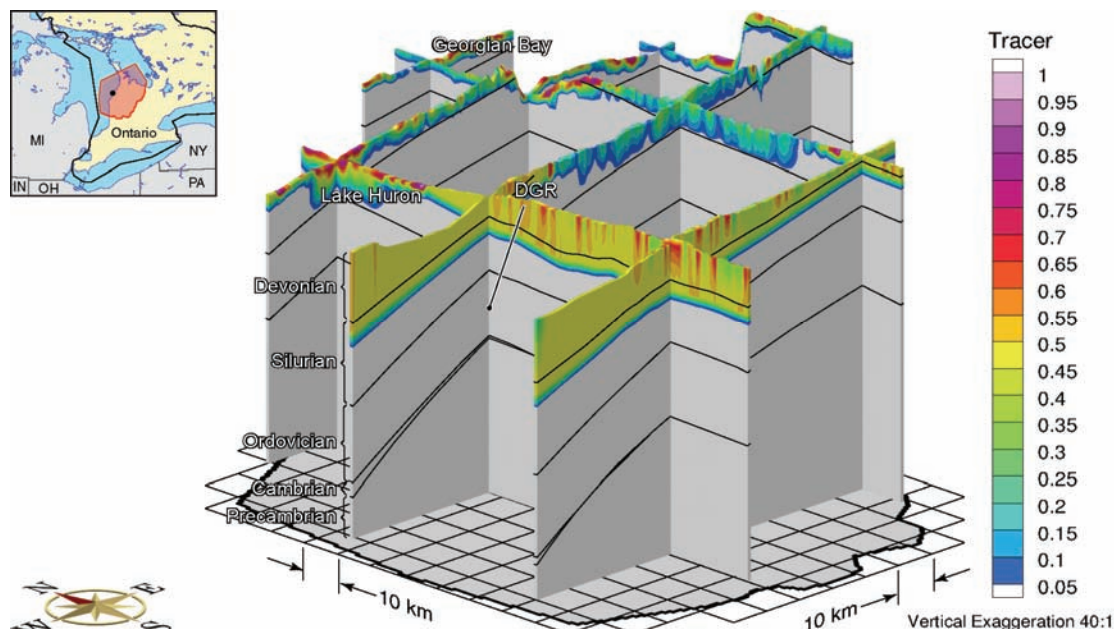
Notes: From Sykes et al. (2011).

**Figure 5.33: Fence View of Pore Velocity Magnitude at Present for the Base-case Paleoclimate Scenario**

### **Surface Boundary Condition Based on 80% and 30% of Ice Thickness**

Alternative scenarios were simulated in which the hydraulic boundary condition applied to the surface of the modelling domain was 80% and 30% of the ice thickness to allow for some reduction in heads beneath the ice sheet. For the 80% of ice thickness case (fr-base-paleo-head80), present-day (0 ka) head profiles (shown in aqua) are qualitatively similar to those of the base-case shown in Figure 5.30, but display slightly less deviation from the initial conditions. For the 30% of ice thickness case (fr-base-paleo-head30), present-day Silurian and upper Ordovician heads (shown in dark blue) are lower than the initial conditions, as shown in Figure 5.30. The measured pattern of underpressures in the Salina is approximately matched by the simulated results, while the greater underpressures in the

Ordovician are not matched at all, indicating that the underpressures in this portion of the system are not a result of the imposed pattern of glacial loading and unloading.



Notes: From Sykes et al. (2011).

**Figure 5.34: Fence View of Tracer Concentrations at Present for the Base-case Paleoclimate Scenario**

The TDS profiles in Figure 5.32a show slight changes between the beginning and end of the paleoclimate simulation, with the changes occurring mainly at the top of the Salina and at the top of the Ordovician where the gradients imposed by the initial conditions were steepest. Otherwise, the TDS profile was essentially unchanged through the course of the simulation, as observed in the base-case paleoclimate simulation.

The pattern of tracer migration into the subsurface was similar to the base-case for both reduced ice thickness scenarios, but with shallower penetration into the Silurian due to the reduced vertical gradients (Figure 5.32b).

### **Free-draining Surface Boundary Condition**

An alternative scenario (fr-base-paleo-zero-head) was simulated in which a zero pressure hydraulic surface boundary condition was used; this choice of boundary condition creates a free-draining surface boundary condition where water can enter or exit the boundary as needed. During the glacial loading stage, the excess fluid pressure that develops due to hydromechanical coupling can be dissipated at the ground surface. The exiting water effectively “disappears” and is not accumulated or routed in a subglacial hydrology sense. During subsequent unloading, negative pressures can result as the rock dilates, and water may be drawn back in to the rock. In Section 5.4.6.2, subglacial hydraulic conditions were discussed



and field evidence was presented to show that subglacial water pressures are not zero, and that the subglacial flow system is not free draining everywhere. Nevertheless, this scenario examines the implications of this type of surface boundary condition.

Vertical profiles of freshwater and environmental heads at the DGR location are shown in green in Figure 5.30. Present-day heads in the Silurian and Upper Ordovician are underpressured due to water lost during glacial loading that has not yet been replenished. The pressure depletion does not extend to the bottom of the Ordovician, however, nor does it match the magnitude of the underpressures observed in the Ordovician. The overpressures in the Cambrian Formation are also not matched. Although the units above the Silurian are quite permeable, the presence of permafrost acts to significantly reduce the near-surface hydraulic conductivity, thereby reducing vertical drainage fluxes that would occur during glacial loading.

The TDS concentration profile in Figure 5.32a shows the same characteristics as the profiles from other scenarios, with the only changes being dissipation of some of the steeper gradients.

Figure 5.32b shows the migration of the tracer into the subsurface, and appears very similar to the base-case. Instead of surface waters entering the system during a glacial loading event, as in the base-case, the waters enter the system upon glacial unloading due to water being pulled back into the domain. The cumulative effect over the course of a paleoclimate simulation is that glacial waters do enter the system regardless of how the geosphere hydraulic surface boundary condition is applied.

This scenario results in present-day upward flow through the Ordovician and Silurian in contrast to the base-case result of downward flow in the Ordovician. This is due to the free-draining surface boundary condition.

### **Zero Loading Efficiency ( $\zeta = 0$ )**

The role of hydromechanical coupling was investigated in a scenario in which the one-dimensional loading efficiency ( $\zeta$ ) was set to zero (fr-base-paleo-le-zero). In the absence of hydromechanical coupling, the rock carries the full mechanical load and does not impact the water pressure as it either compresses or dilates.

Vertical profiles of freshwater and environmental heads at the DGR location are shown in orange in Figure 5.30. The vertical gradients for this simulation are greater than for the base-case, resulting in the differences in the profiles shown in Figure 5.30. The lack of hydromechanical coupling results in larger vertical gradients since the hydromechanical term, described in Section 5.4.4 and behaving as a fluid source/sink term, does not allow for an increase in pore pressure throughout the domain due to glacially induced mechanical loading. For a non-zero loading efficiency, the increase in pore pressure thereby reduces the vertical fluid energy gradient. Both freshwater heads and environmental heads are higher at depth at the end of the paleoclimate simulation as compared to the base-case. The increased gradients in this simulation lead to higher residual heads at the end of the simulation, but with a similar pattern to the base-case, controlled by the diffusivities of the various layers. For this scenario, higher pore pressures have propagated into the Georgian Bay and Blue Mountain formations. The pattern of underpressures throughout the Silurian and Ordovician is not represented in the simulation results; in fact, the entire profile is significantly overpressured.

The TDS distribution and tracer profiles shown in Figure 5.32 are similar to those of all the other scenarios.

### **Biot Coefficient of 0.5**

Sensitivity of the paleoclimate modelling results to the value used for the Biot coefficient was investigated in a scenario assuming a compressible grain modulus with a Biot coefficient of 0.5 (fr-base-paleo-biot); resulting in a grain modulus which is twice the bulk modulus. This change lowered the calculated specific storage values and loading efficiencies of the modelled layers by less than a factor of two (Sykes et al. 2011).

Figure 5.30 presents the freshwater and environmental heads at the end of the paleoclimate simulation in purple. The present-day heads are slightly higher in the Silurian and Upper Ordovician when compared to the base-case. These simulation results do not mimic the underpressures in either the Silurian or Ordovician. The overpressure propagates deeper into the domain to the top of the Cobourg Formation. Lower storage coefficients will tend to allow pressure pulses to propagate deeper into the system, while diminishing the ability to store changes in pore pressure. The TDS distribution and tracer profiles shown in Figure 5.32 are similar to those of all the other scenarios.

### **Analysis of the Effect of a Gas Phase**

Partial gas saturation is noted in some layers by INTERA (2011). The presence of gas will affect fluid compressibility, and thereby specific storage, loading efficiency, and pore compressibility. The fluid compressibility is the saturation-weighted average of the brine compressibility of  $3.0 \times 10^{-10} \text{ Pa}^{-1}$  and an average air compressibility of  $8.0 \times 10^{-8} \text{ Pa}^{-1}$  corresponding to an in situ average gas phase pressure of 12.5 MPa, based on TOUGH2-MP modelling. The changes to specific storage and loading efficiency resulting from the gas saturations given in INTERA (2011) are shown in Table 5.11. These changes probably overestimate the effects of gas, as INTERA (2011) reports that confidence in the gas saturation values is low.

A paleoclimate simulation (fr-base-paleo-gas) was performed to investigate the effect of partial saturation from the perspective of mechanical and storage effects and not to investigate two-phase flow. Inclusion of a gas phase increases specific storage, while decreasing the loading efficiency. Figure 5.30 shows that the heads (in yellow) in the Silurian and Queenston Formation at the DGR-4 location are generally higher at the end of this simulation compared to the base-case, and are also higher than for the paleoclimate simulation with a Biot coefficient of 0.5 through the Silurian. The higher storage coefficients through most of the Silurian lead to an enhanced ability to retain elevated pore pressures arising from the paleoclimate surface boundary conditions. These simulated overpressures, which are on the order of 200 m, are not representative of the measured underpressures in both the Silurian and Ordovician. Below the Queenston, very little difference is noted between the initial heads and the heads at the end of the simulation. The TDS distribution and tracer profiles shown in Figure 5.32 are similar to those of all the other scenarios.

### **Analysis of Two Paleoclimate Cycles of 120 ka Each**

Whereas the paleoclimate scenarios modeled in the preceding sections considered only a single 120 ka paleoclimate cycle, the effects of two consecutive cycles are also of interest. Two consecutive paleoclimate cycles were simulated using the nn9930 paleoclimate model with all the base-case parameters (fr-base-paleo-2). The initial conditions for the second paleoclimate cycle were the final freshwater heads, brine and tracer concentrations from the first paleoclimate cycle.

**Table 5.11: Summary of Formation Parameters for Regional- and Site-scale Models Including the Presence of a Gas Phase**

Period	Formation	$K_H$ [m/s]	$K_V$ [m/s]	$K_H:K_V$	$\theta$	$\rho$ [kg/m <sup>3</sup> ]	TDS [g/L]	$S_s$ [m <sup>-1</sup> ]	$\zeta$	$\tau$
Quaternary	Drift	1.00E-08	5.00E-09	2:1	0.2	1000	0	9.90E-05	0.99	4.00E-01
	Kettle Point	3.00E-09	3.00E-10	10:1	0.1	1006	9	1.50E-06	0.8	1.20E-01
Devonian	Hamilton Group	2.20E-11	2.20E-12	10:1	0.1	1008	12	1.50E-06	0.8	1.20E-01
	Dundee	8.40E-08	8.40E-09	10:1	0.1	1005	8	1.50E-06	0.8	1.20E-01
	Detroit River Group	5.90E-07	2.00E-08	30:1	0.077	1001	1.4	1.40E-06	0.84	9.40E-02
	Bois Blanc	1.00E-07	1.00E-08	10:1	0.077	1002	3.2	1.40E-06	0.84	9.40E-02
	Bass Islands	5.00E-05	1.70E-06	30:1	0.056	1004	6	2.00E-06	0.92	2.80E-01
	Unit G	1.00E-11	1.00E-12	10:1	0.172	1010	14.8	1.10E-06	0.55	3.00E-03
	Unit F	5.00E-14	5.00E-15	10:1	0.1	1040	59.6	1.40E-05	0.05	4.90E-02
	Unit F Salt	5.00E-14	5.00E-15	10:1	0.1	1040	59.6	1.40E-05	0.05	4.90E-02
	Unit E	2.00E-13	2.00E-14	10:1	0.1	1083	124	1.90E-05	0.02	5.70E-02
	Unit D	2.00E-13	2.00E-14	10:1	0.089	1133	200	6.40E-07	0.53	6.40E-02
Silurian	Units B and C	4.00E-13	4.00E-14	10:1	0.165	1198	296.7	1.20E-05	0.03	8.40E-02
	Unit B Anhydrite	3.00E-13	3.00E-14	10:1	0.089	1214	321	6.90E-07	0.53	1.00E-03
	Unit A-2 Carbonate	3.00E-10	3.00E-11	10:1	0.12	1091	136	1.00E-06	0.32	1.20E-02
	Unit A-2 Evaporite	3.00E-13	3.00E-14	10:1	0.089	1030	45.6	1.10E-05	0.03	1.00E-03
	Unit A-1 Carbonate	1.40E-08	9.70E-13	14912:1	0.023	1120	180.2	4.10E-07	0.82	1.20E-02
	Unit A-1 Evaporite	3.00E-13	3.00E-14	10:1	0.02	1229	343.7	3.20E-06	0.12	1.80E-03
	Niagaran Group	3.60E-09	2.50E-13	14431:1	0.026	1206	308.4	2.70E-07	0.66	1.20E-02
	Reynales/Fossil Hill	5.00E-12	5.00E-13	10:1	0.031	1200	300	2.90E-07	0.62	6.20E-01
	Cabot Head	9.00E-14	9.00E-15	10:1	0.116	1204	306	1.10E-06	0.6	3.20E-02
	Manitoulin	9.00E-14	9.00E-15	10:1	0.028	1233	350	7.50E-07	0.86	6.40E-03
Ordovician	Queenston	2.00E-14	2.00E-15	10:1	0.073	1207	310	5.40E-06	0.12	1.60E-02
	Georgian Bay/Blue Mtn.	3.50E-14	3.30E-15	11:1	0.07	1200	299.4	7.70E-06	0.12	8.80E-03
	Cobourg	2.00E-14	2.00E-15	10:1	0.015	1181	272	1.90E-06	0.11	3.00E-02
	Sherman Fall	1.00E-14	1.00E-15	10:1	0.016	1180	270	2.70E-06	0.16	1.70E-02

Period	Formation	$K_H$ [m/s]	$K_V$ [m/s]	$K_H:K_V$	$\theta$	$\rho$ [kg/m <sup>3</sup> ]	TDS [g/L]	$S_s$ [m <sup>-1</sup> ]	$\zeta$	$\tau$
	Kirkfield	8.00E-15	8.00E-16	10:1	0.021	1156	234	4.30E-06	0.1	2.40E-02
	Coboconk	4.00E-12	4.00E-15	1000:1	0.009	1170	255	7.60E-07	0.56	3.60E-02
	Gull River	7.00E-13	7.00E-16	1000:1	0.022	1135	203	4.60E-06	0.09	1.40E-02
	Shadow Lake	1.00E-09	1.00E-12	1000:1	0.097	1133	200	7.40E-07	0.56	7.60E-02
Cambrian	Cambrian	3.00E-06	3.00E-06	1:1	0.071	1157	235	2.60E-06	0.05	1.30E-01
Precambrian	Upper Precambrian	1.00E-10	1.00E-10	1:1	0.038	1200	300	2.60E-07	0.49	9.50E-03
	Precambrian	1.00E-12	1.00E-12	1:1	0.005	1200	300	1.50E-07	0.88	7.20E-02

Notes: From Sykes et al. (2011).

Figure 5.30 presents the freshwater and environmental heads at the end of the 240 ka paleoclimate simulation in red with a comparison to the heads at the end of the first paleoclimate cycle at 0 ka in black. The head profiles at the DGR-4 location are nearly the same at the end of each paleoclimate cycle (the black line largely overlays the red line), although heads are very slightly higher through the Upper Ordovician after the second cycle. Such little change can be attributed to the long period of time prior to the first glacial advance and retreat, which allows sufficient time to equilibrate heads to a state close to the initial conditions for the base-case. In either case, both the freshwater heads and the environmental heads are higher relative to the initial state throughout the Silurian and the Upper Ordovician, and do not represent the underpressures measured in the Silurian and Ordovician.

The TDS concentration profile in Figure 5.32a shows minor continued dissipation of the initial steep gradients between the ends of the first and second paleoclimate cycles. Figure 5.32b shows the migration of the tracer into the subsurface after a second paleoclimate cycle. This migration is deeper than what occurred at the end of the first paleoclimate cycle, but is still contained within the middle Salina.

#### **Analysis of Paleoclimate Model nn9921**

To evaluate the effects of the particular paleoclimate model selected on simulated heads, flow patterns, TDS distribution, and tracer migration, a simulation was performed using paleoclimate model nn9921 (fr-base-paleo-nn9921) along with the parameters used for the base-case nn9930 modelling (Section 5.4.6.6.1). In comparing Figure 5.27 to Figure 5.26, nn9921 exhibits more glaciation episodes, with the major episodes centred at approximately -60 ka and -25 ka, of nearly double the temporal duration over the DGR site. The duration over which permafrost is present is also greater in nn9921. Lake depth at approximately -14 ka is also greater in nn9921 than in nn9930.

Both freshwater and environmental heads are greater at the end of this simulation compared to the nn9930 base-case. The environmental heads are also higher at 90 ka before present due to the first glaciation episode beginning at approximately -112 ka in nn9921, and at -63 ka in nn9930. Figure 5.30 presents the freshwater and environmental heads at the DGR site at the end of the paleoclimate simulation in magenta. Both the freshwater and environmental heads are overpressured relative to the initial condition, and are significantly different than the measured underpressures in the Silurian and Ordovician. An underpressure relative to initial conditions is generated in the Middle Ordovician from the Sherman Fall to the Gull River.

The TDS concentration profile and the tracer migration profile in Figure 5.32 are similar to those produced using the nn9930 paleoclimate model.

#### **Analysis of Open Boundary Paleoclimate Model**

The effects that open lateral boundaries for high-conductivity units such as the Salina A1 carbonate, the Niagaran Group, and the Cambrian Formation would have on the paleoclimate modelling results were investigated in scenario fr-base-paleo-openbnd. In this scenario, a specified-head boundary condition equal to the initial condition was applied for the entire 120 ka to nodes which met all of the following conditions.

- Node is located on the lateral outer boundary of the modelling domain.
- Node is located on the top of each of the following lithologic units: Salina A1 Carbonate, Niagaran Group, and Cambrian. Only nodes along the top of a layer were used to prevent

short circuiting between node pairs that would define both the top and bottom of a unit as the TDS changes.

- Node is at or below an elevation of zero metres. This is important to prevent short circuiting of flow, and generating high velocities, with the high heads that are applied to the surface of the modelling domain during a paleoclimate cycle.

In addition, a high hydraulic conductivity of  $1 \times 10^{-8}$  m/s was applied to the Upper Precambrian. The goal of this simulation was to provide a high-conductivity pathway through the Cambrian and Upper Precambrian, to apply the highest possible heads during a paleoclimate cycle, and to create the highest possible gradients through the high-conductivity units by maintaining the boundary heads for these units at their pre-glaciation levels throughout the paleoclimate cycle. It is unrealistic to expect that these units would be free draining. The Cambrian is connected to the centre of the Michigan Basin, which would provide a pathway for migration as well as providing pressure support during a glacial event. A tracer was applied to all recharge waters to determine if the tracer could migrate through the high-gradient, high-conductivity layers from their recharge points to the DGR site during the course of a paleoclimate simulation.

The heads at the end of the paleoclimate simulation are quite different than in the base-case. Figure 5.30 presents the freshwater and environmental heads at the DGR-4 location at the end of the paleoclimate simulation in brown. At this location, the heads are slightly underpressured relative to the initial condition from the Salina through to the Cobourg. Below the Cobourg Formation, the heads drop to create an underpressure and match a few of the measured DGR-4 data from the Coboconk to the Cambrian. Most of the underpressures measured for the Silurian and Ordovician are not matched by the heads resulting from this paleoclimate simulation. At the end of the paleoclimate simulation, the tracer had migrated into the subsurface in a pattern very similar to that shown in Figure 5.34 for the base-case. Lateral migration from the Salina A1 carbonate and Niagaran recharge areas was not notably greater than in the base-case. Figure 5.32b shows that the migration of the tracer into the subsurface at the DGR-4 location was nearly identical to what occurred at the end of the base-case paleoclimate simulation.

### **Conclusions from Paleoclimate Modelling**

Paleoclimate modelling was performed by using information produced by the University of Toronto Glacial Systems Model (GSM) in the regional-scale model. Ice thicknesses, permafrost depths, and lake depths from a 120-ka GSM simulation were applied as boundary conditions to the regional-scale model to evaluate the groundwater system response to glaciation. In addition to a base-case scenario, alternative scenarios were modeled in which:

- Ice thickness was reduced to 80% and 30% of the predicted amount;
- Free-draining conditions were allowed at the base of the glacier;
- The loading efficiency of the rock units was reduced to zero;
- The Biot coefficient of the rock units was reduced to 0.5;
- A gas phase was present in the pores of most rock units;
- Two 120 ka paleoclimate cycles occurred in succession;
- Different GSM results were used; and
- High-permeability units were given open lateral boundaries.

The base-case paleoclimate model shows slight Silurian and Queenston overpressures at the end of the paleoclimate cycle, and no underpressures at all. Decreasing the hydraulic boundary condition at surface causes Silurian and Upper Ordovician pressures to decrease, with slight

underpressures appearing for a surface hydraulic boundary condition set to 30% ice thickness. A free-draining boundary condition at the base of the glacier causes more underpressure in the Silurian and Upper Ordovician.

The base-case used a loading efficiency calculated from layer-specific geomechanical properties. Decreasing the loading efficiency, whether directly (fr-base-paleo-le-zero), by introducing gas (fr-base-paleo-gas), or by lowering the Biot coefficient (fr-base-paleo-biot), causes overpressures in the Silurian and Upper Ordovician to increase from the base-case results. Placing open boundaries on the high-permeability units holds Silurian heads largely unchanged and produces Middle Ordovician underpressures, with essentially hydrostatic conditions everywhere else.

The alternate paleoclimate model nn9921 produced more overpressures than the base-case nn9930 model in the Silurian and Upper Ordovician; the overpressures were intermediate between those from the zero loading efficiency case and those from the lowered Biot coefficient case. Slight underpressures developed from the Sherman Fall to the Gull River.

Most of the paleoclimate scenarios affected heads only in the Silurian and Upper Ordovician. None of the paleoclimate scenarios produced Upper and Middle Ordovician underpressures like those observed at DGR-4, and the underpressures could not be reproduced using any plausible parameter variations in the base-case values for the paleoclimate scenarios. Increasing hydraulic diffusivity, whether by increasing hydraulic conductivity or decreasing specific storage, would allow the system to respond more rapidly to glacially induced perturbations and return to equilibrium conditions more rapidly. Decreasing the diffusivity would decrease the depth to which the glacially induced perturbations were felt, decreasing the possibility of Ordovician underpressures. None of the alternative scenarios showed recharge water penetrating below the middle Salina, or a different distribution of TDS in the system from the base-case scenario. Diffusion remained the dominant transport mechanism in the Ordovician in all scenarios.

In short, none of the paleoclimate scenarios modelled was able to produce a head profile similar to that observed in the DGR boreholes. The Ordovician underpressures that are observed do not appear to be the result of glacial loading and unloading.

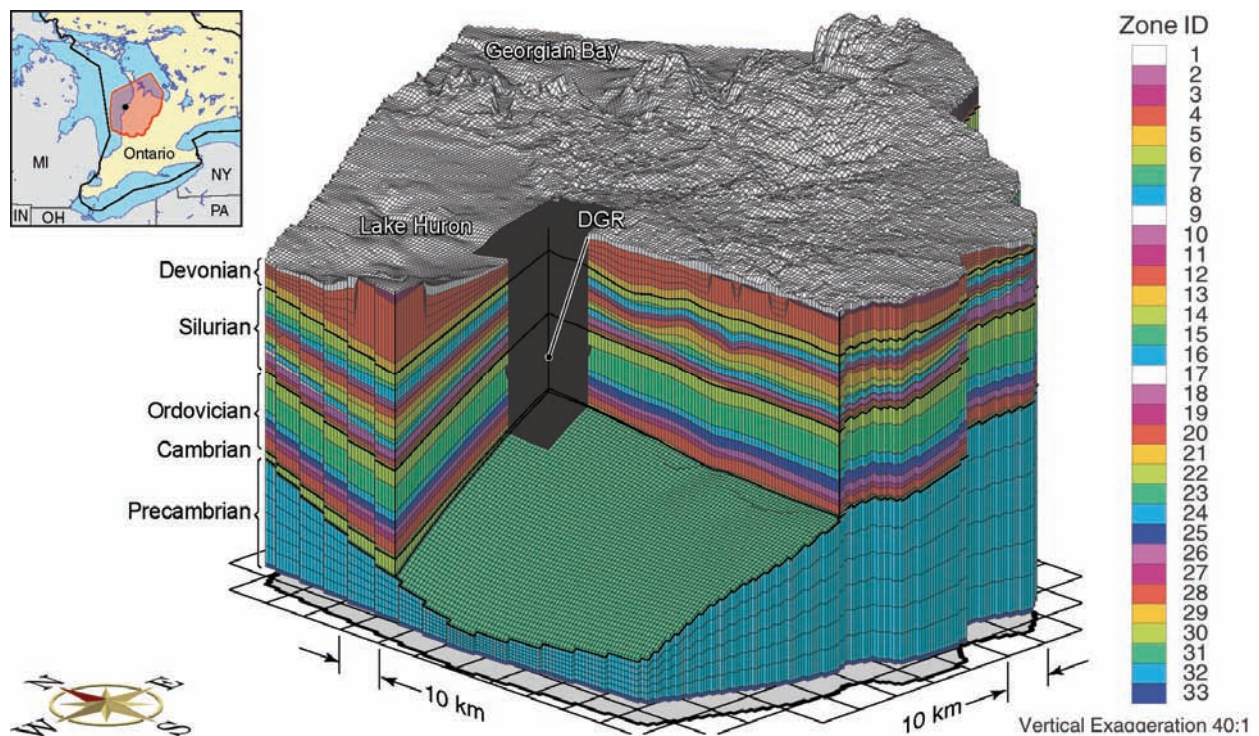
#### **5.4.7 Site-scale Model**

The objective of the site-scale hydrogeologic modelling of the proposed DGR was to provide a refined spatial discretization that would allow the simulation of features, events and processes that could not be appropriately investigated with the regional-scale model. For this study, the direct-embedment approach was developed to provide initial and boundary conditions for site-scale analyses. Each node in the site-scale model had a counterpart with exactly the same coordinates in the regional-scale model with the direct-embedment approach. No interpolation was needed to extract the initial and boundary conditions from the regional-scale model. The site-scale model was used to investigate the evolution of the tracer plume originating from the proposed DGR site (the base-case model), the measured pressure profile in the DGR boreholes, and the impact of hypothetical discrete fracture zones connecting the Cambrian and Niagaran.

##### **5.4.7.1 Model Geometry and Boundary Conditions**

The site-scale spatial domain relative to that of the regional-scale domain is depicted in Figure 5.35. The domain has a spatial extent of 19.078 km in the west-to-east direction and

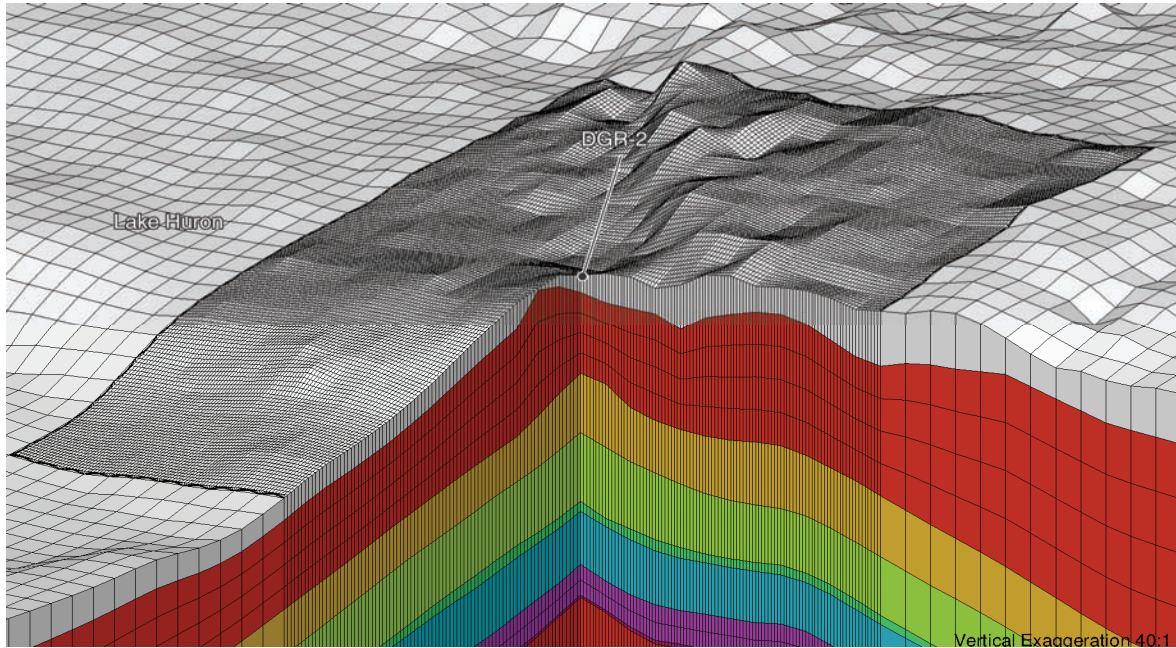
18.918 km in the south-to-north direction centred on borehole DGR-2. The site-scale domain was discretized by using 6 columns (west-to-east sub-gridding) for each regional-scale column and 8 rows (south-to-north sub-gridding) for each regional-scale row. The resulting site-scale domain has 150 columns and 168 rows with each grid block being 127 m in the west-to-east direction and 112.6 m in the south-to-north direction. The areal discretization is shown in Figure 5.36. Sub-gridding was also used to refine the discretization of the Cobourg Formation, with three layers being used in the site-scale model to represent the single regional-scale layer. As shown in Figure 5.37, the overlying Collingwood/Blue Mountain/Georgian Bay, Queenston and Niagaran layers were subdivided into 8, 4 and 3 layers, respectively. The underlying Gull River, Kirkfield and Sherman Fall formations were further subdivided into 4, 2 and 3 layers in the site-scale model. Also evident in Figure 5.37 are the transition elements between the larger regional-scale elements and the site-scale mesh.



Notes: From Sykes et al. (2011).

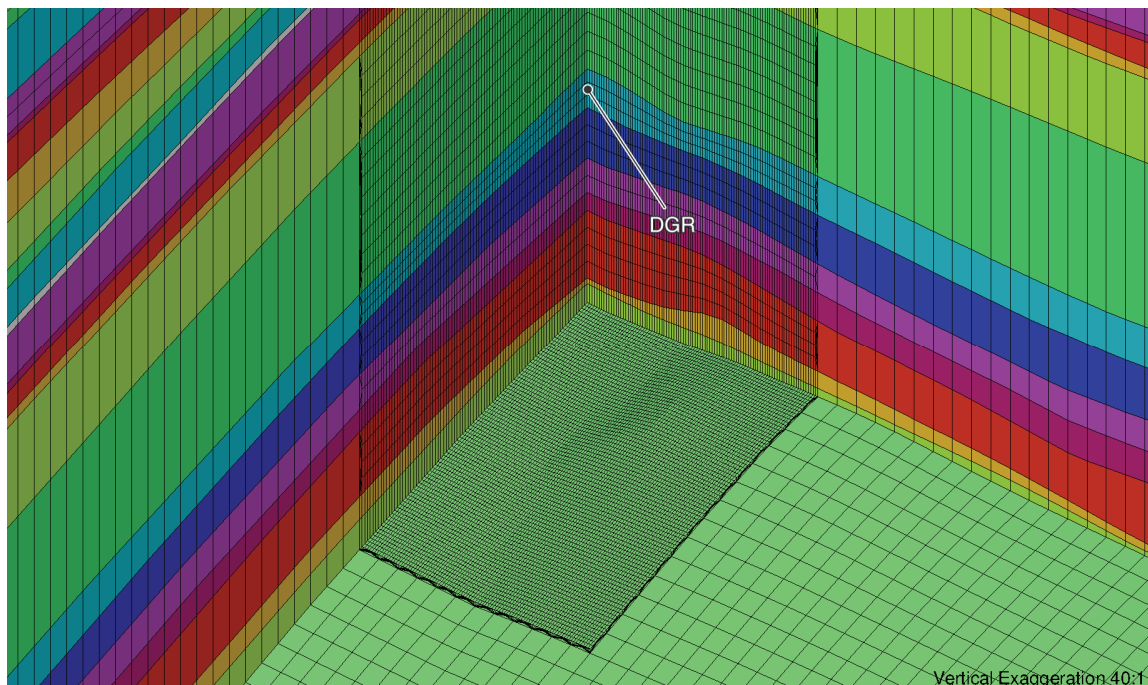
**Figure 5.35: Regional-scale Discretization Showing Location of Site-scale Spatial Domain**





Notes: From Sykes et al. (2011).

**Figure 5.36: Regional-scale Discretization Showing Site-scale Discretized Spatial Domain**



Notes: From Sykes et al. (2011).

**Figure 5.37: Regional-scale Discretization Showing Vertical Details of Site-scale Discretized Spatial Domain**

### 5.4.7.2 Model Parameters

The hydraulic properties used for the site-scale analyses are the values developed in the site investigation (INTERA 2011) as presented in Section 5.4.5.2. The hydraulic and transport parameter values for each formation, unit or group are listed in Table 5.6. Each model layer was assigned unique but homogeneous properties. Using a grid Péclet number constraint, the longitudinal dispersivity coefficient was selected as approximately one half of the maximum length of the side of a site-scale grid block. As a consequence, the contribution to solute migration of mechanical dispersion may be overestimated. The boundary conditions for the embedment approach are those imposed on the regional-scale domain; the solution methodology is the same as that followed in the regional-scale analyses.

### 5.4.7.3 Base-case Simulations

The purpose of the base-case site-scale simulations was to evaluate the transport of a conservative solute from the DGR to the edge of the modelling domain under equilibrium, fully water-saturated conditions.

A three-part methodology was used to determine solutions for the site-scale model.

- A converged, temporally invariant, density-dependent solution for the regional-scale numerical model with the site-scale discretization embedded in it was obtained following the procedure described in Section 5.4.5.4.
- For the transient analyses with solely the site-scale numerical model, the initial conditions were the results for the equilibrated solution (pseudo-equilibrium at 1 Ma) for freshwater heads and TDS obtained in the preceding step. Dirichlet (prescribed head) boundary conditions for the site-scale domain sides and bottom were based on the initial state (i.e., the solution from the preceding step). A Dirichlet boundary condition related to surface topography was used to represent the water table at the top of the site-scale domain. The zones for properties were identical to those used for the regional-scale analysis; this requirement is a constraint of the use of the embedment approach in FRAC3DVS-OPG.
- Transient site-scale analyses were obtained for freshwater head with brine transport disabled. This maintained a time-invariant TDS concentration distribution equal to the initial condition. The freshwater heads were dependent on the TDS distribution. The transient analyses assumed saturated flow with the base-case parameters outlined in Table 5.6.

The base-case site-scale solution for freshwater heads is depicted in a fence view in Figure 5.38. To clearly display the solution for freshwater heads at a pseudo-equilibrium time of 1 Ma, the results are presented in cross-section form in Figure 5.39. The upper figure is the north-to-south cross-section through the location of the DGR. The lower figure is the west-to-east cross-section through the DGR. The base-case site-scale pseudo-equilibrium solution for environmental heads is presented in a fence view in Figure 5.40 and in cross-section view in Figure 5.41. Environmental heads can be used to estimate vertical gradients while the freshwater heads can be used to estimate horizontal gradients.

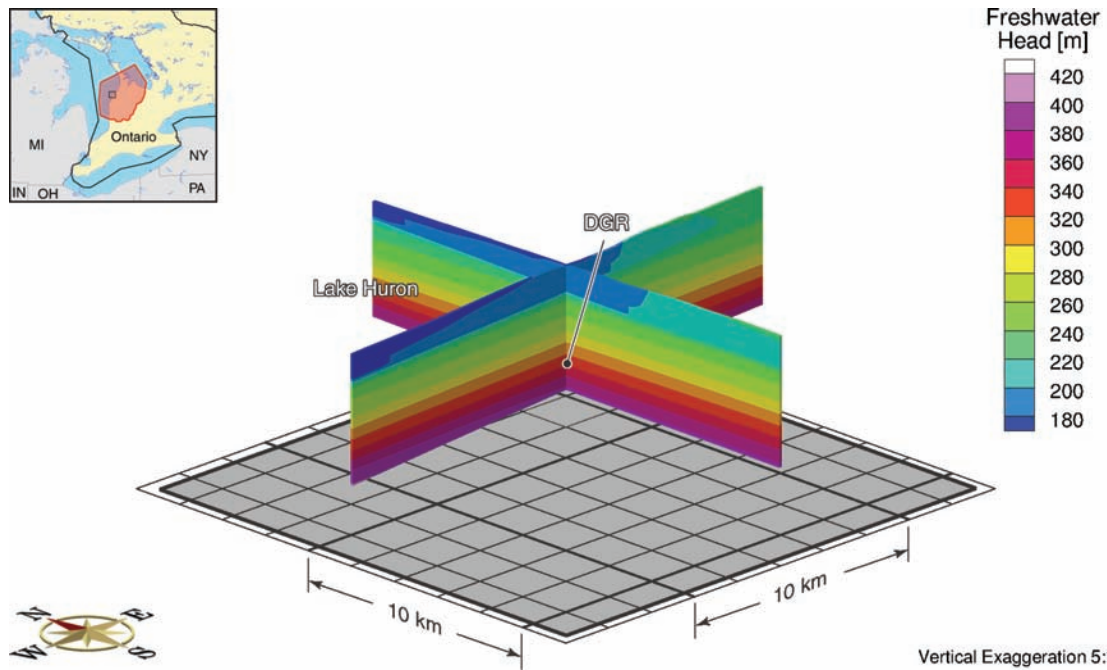
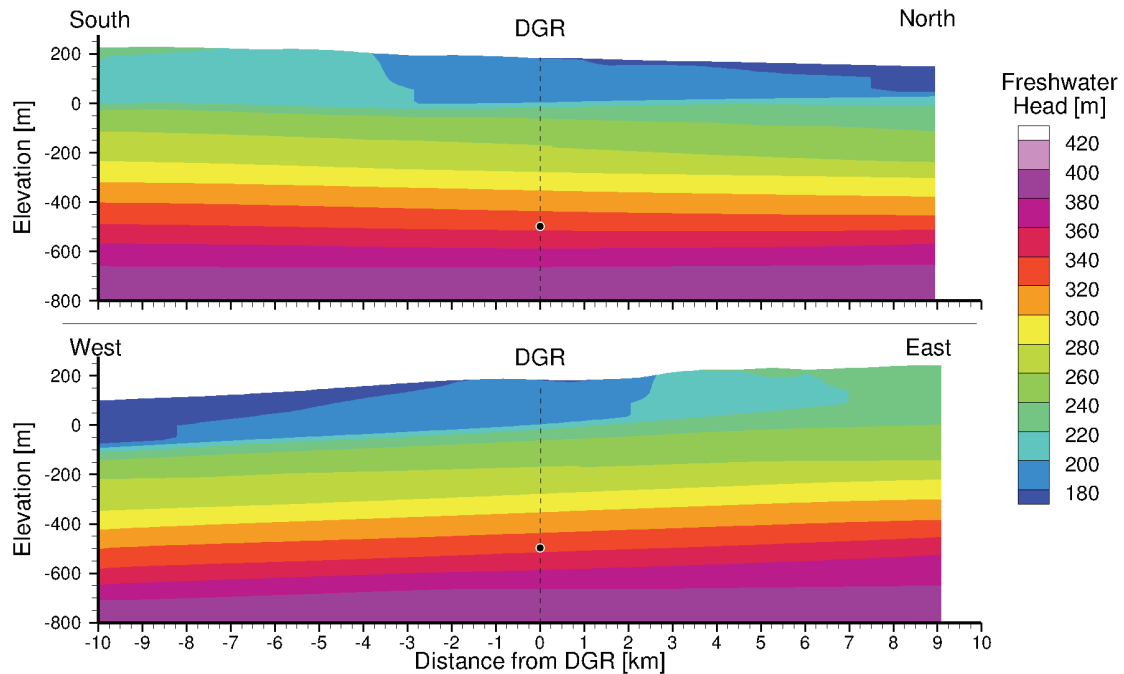


**Figure 5.38: Fence View of Freshwater Heads for the Base-case Site-scale Analysis Shown in Figure 5.39**



Notes: From Sykes et al. (2011).

**Figure 5.39: Cross-sections of Freshwater Heads for the Base-case Site-scale Analysis with Equilibrated Regional-scale Heads as the Initial Condition**

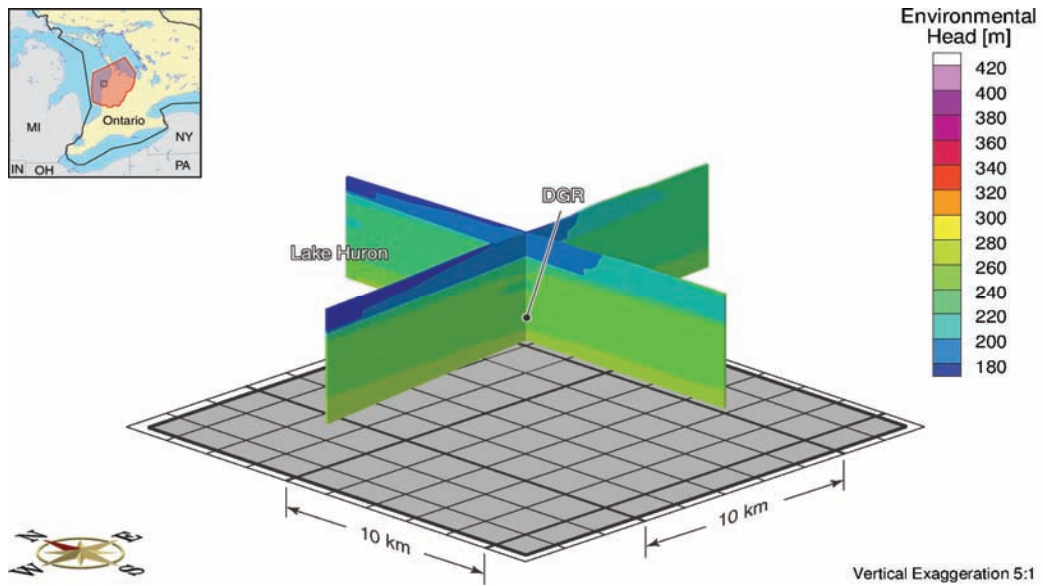
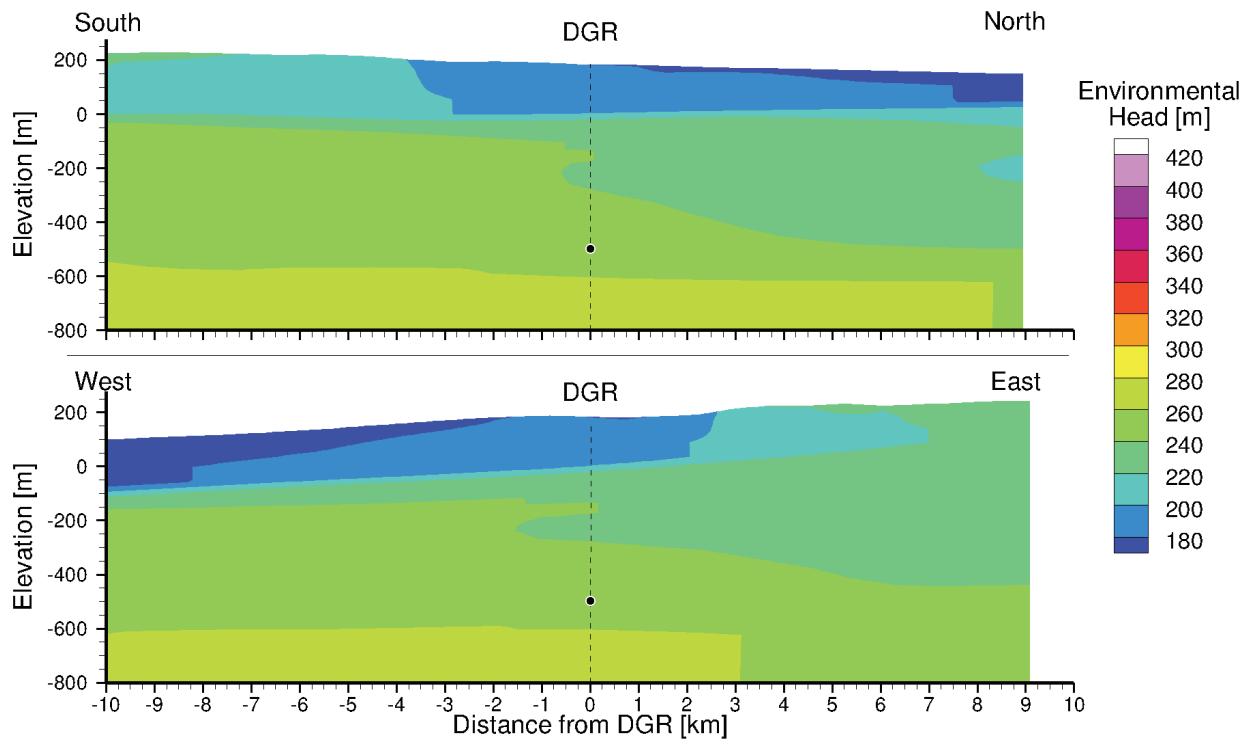


**Figure 5.40: Fence View of Environmental Heads for the Base-case Site-scale Analysis Shown in Figure 5.41**

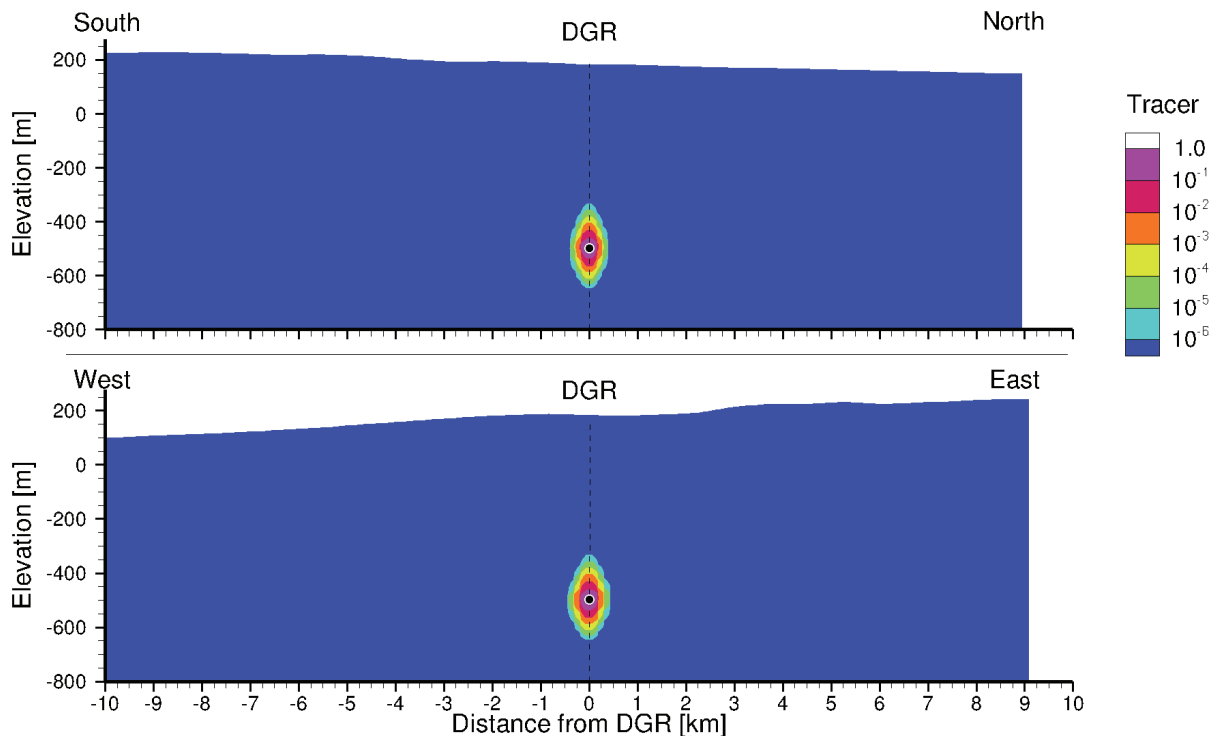


Notes: From Sykes et al. (2011).

**Figure 5.41: Cross-sections of Environmental Heads for the Base-case Site-scale Analysis with Equilibrated Regional-scale Heads as the Initial Condition**

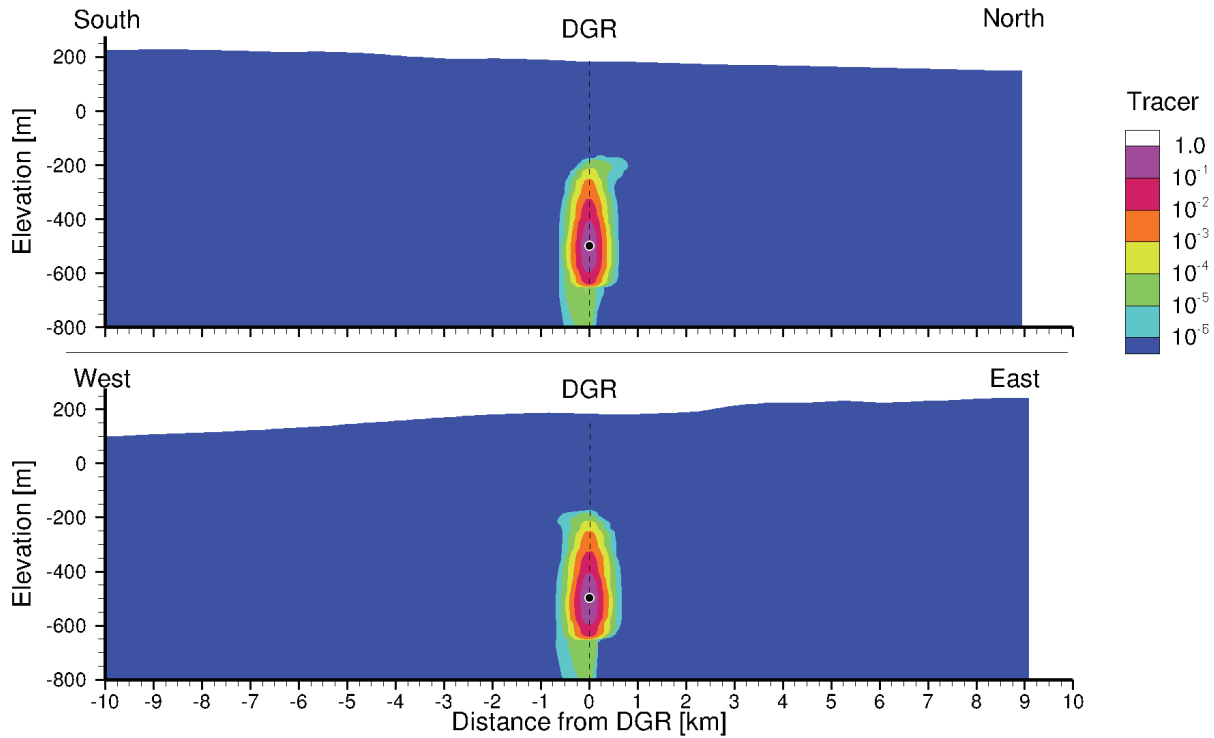
The migration of a conservative tracer released to the Cobourg limestone at the proposed DGR site was investigated for the saturated base-case site-scale flow case. The source term for the conservative tracer was defined using prescribed concentrations of unity for the eight nodes of a grid block at the horizontal direction centre of the site-scale grid in the middle layer of the three layers used to discretize the Cobourg. The analysis assumes that there is no decay of the source and that the solute neither decays nor adsorbs as it migrates, both highly conservative assumptions. The transport parameters used for the analysis are given in Section 5.4.5.2. Unless otherwise specified, these settings apply to all the subsequent site-scale analyses.

Cross-section views of the tracer distribution at 100 ka and 1 Ma are shown in Figure 5.42 and Figure 5.43, respectively. At 100 ka, no tracer at a relative concentration exceeding  $10^{-6}$  has reached either the Niagaran or Cambrian. By 1 Ma, the tracer has reached both the Niagaran and Cambrian.



Notes: From Sykes et al. (2011).

**Figure 5.42: Cross-section View of the Spatial Distribution of a Tracer at 100 ka with Equilibrated Regional-scale Heads as the Initial Condition**

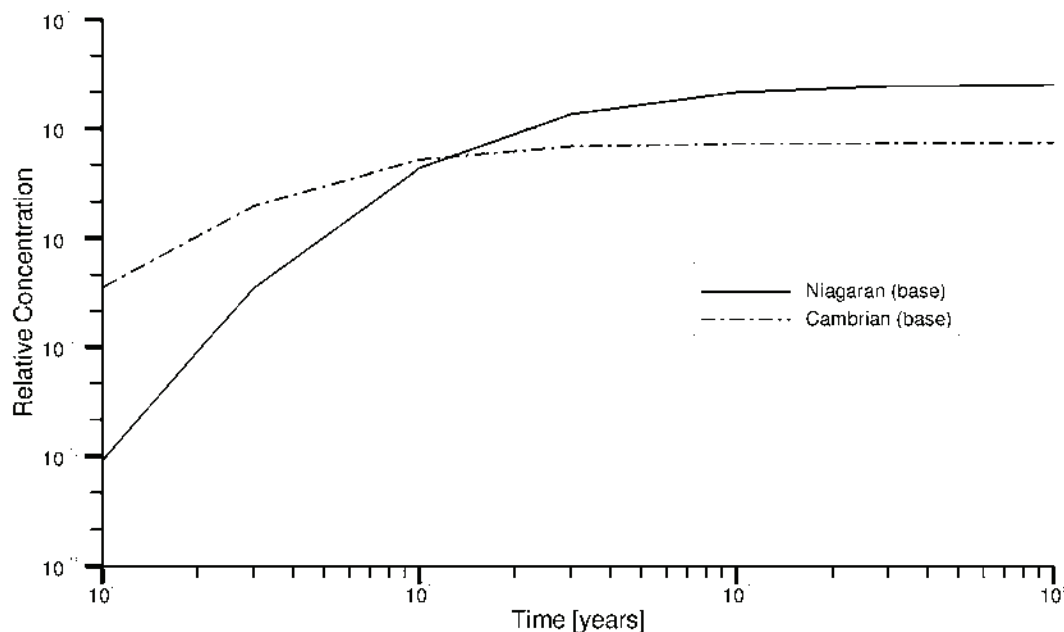


Notes: From Sykes et al. (2011).

**Figure 5.43: Cross-section View of the Spatial Distribution of a Tracer at 1 Ma with Equilibrated Regional-scale Heads as the Initial Condition**

Figure 5.44 presents a log-log plot of the simulated breakthrough curve in the Niagaran Group and the Cambrian at the horizontal centre of the site-scale grid for the base-case analysis. The plot shows that the relative concentration of tracer reaching the Cambrian in 100 ka was less than  $10^{-7}$ , while that reaching the Niagaran was approximately  $10^{-12}$ . Breakthrough to the Cambrian occurs sooner than breakthrough to the Niagaran because the Cambrian is closer to the tracer source at the centre of the Cobourg limestone. The relative tracer concentration in the Cambrian remained below  $10^{-3}$  for the 100 Ma duration of the simulation, while that in the Niagaran slightly exceeded  $10^{-2}$  after approximately 10 Ma. Tracer is more diluted by advection and dispersion in the Cambrian than in the Niagaran.

One variation on the base-case was modelled, in which a weathered zone was incorporated in the upper Precambrian as described in Section 5.4.5.6. Inclusion of the weathered zone resulted in no obvious differences in the spatial distribution of the tracer at 100 ka and 1 Ma, because the permeable Cambrian unit tends to diminish the impact of the weathered zone on the migration of the tracer plume.



Notes: From Sykes et al. (2011).

**Figure 5.44: Tracer-breakthrough Curves at the Niagaran Group and Cambrian for the Base-case Site-scale Model**

#### 5.4.7.4 Alternative Simulations

In addition to the base-case analysis of solute migration from the DGR, the site-scale model was also used to investigate two questions related to:

- The effect of different hydraulic anisotropies in the Black River Group on Ordovician underpressures; and
- The effect of a fracture zone connecting the Cambrian and Niagaran on pressure profiles.

The suite of base-case and alternative simulations performed using the site-scale model are listed in Table 5.12.

#### **Ordovician Underpressures and Black River Group Anisotropy**

The environmental head distribution versus depth for the DGR-4 borehole is plotted in Figure 5.5. The data in the figure are based on the pressure measurements in DGR-4 on June 6, 2008, August 24, 2009 and November 15, 2009 (INTERA 2011). Relative to the ground surface elevation at DGR-4 of 181.6 mASL, the profile indicates that the Cambrian is overpressured while units in the Upper Ordovician are significantly underpressured, thus reflecting a water deficit relative to the amount of water that would be in the pores for pressures that are hydrostatic relative to the elevation of the ground surface. This section does not address whether the water deficit is related to either the presence of a separate gas phase in the pores or is a result of a stress effect and the dilation of the pores. The evolution of these pressures as they equilibrate to the present-day boundary conditions was investigated using the site-scale model assuming fully saturated (single phase) conditions. Instead of using the

equilibrated regional-scale heads as the initial condition, as was done for the base-case modelling, this modelling used the August 24, 2009 measured environmental head profile at DGR-4 as the initial condition.

**Table 5.12: Parameters and Initial Conditions for Site-scale Analyses**

Parameters						Underpressure in the Ordovician			
		Base-case	Weathered Zone	1 km Fracture	5 km Fracture	Base-case	10 Kv	100 Kv	1 km Fracture
Scenario		1	2	3	4	5	6	7	8
Initial Heads	Steady State	•	•	•	•				
	Underpressured					•	•	•	•
Hydraulic Conductivity of the Upper Precambrian	$1 \times 10^{-8}$ m/s		•						
	$1 \times 10^{-10}$ m/s	•		•	•	•	•	•	•
Fracture Zone Distance from DGR site	1 km			•					•
	5 km				•				
Anisotropy in the Black River Group ( $K_H:K_V$ )	10:1						•		
	100:1							•	
	1000:1	•	•	•	•	•			•

Notes: From Sykes et al. (2011; their Table 4.14).

The environmental head profile of Figure 5.5 indicates an upward gradient from the Cambrian to the Ordovician and a downward gradient from the Niagaran to the Ordovician. To simulate the evolution of the measured pressure gradient using the site-scale model, the initial heads for each site-scale layer were calculated from the pseudo-equilibrium heads from the sub-gridded regional-scale model by subtracting the difference between the pseudo-equilibrium and measured heads at the DGR-4 borehole for a given layer. The procedure ensured that the gradients in each model layer of the adjusted model were the same as those calculated for the base-case site-scale model.

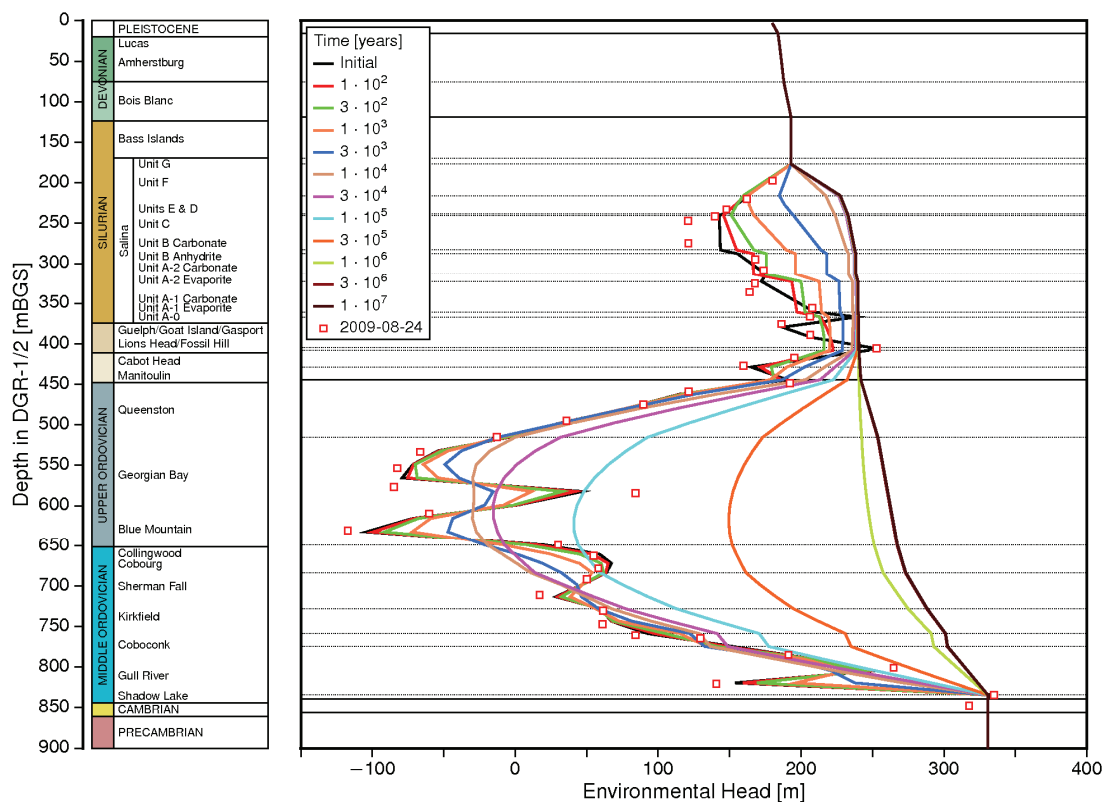
Instead of the Dirichlet (prescribed head) boundary condition that was used for the base-case site-scale analysis, the lower Silurian (except the Niagaran), Ordovician and Cambrian units were assigned a zero-flux Neumann boundary condition. Pressure support for the Niagaran was provided by the Dirichlet boundary condition retained on that unit, while pressure support for the Cambrian was provided by using a Dirichlet boundary condition for all layers of the Precambrian with the freshwater head level being determined by the measured head for the Cambrian in the DGR-4 borehole. It is noted that the Cambrian sandstone is not continuous



across the site-scale model domain. The gradient across the Precambrian was maintained to be that of the base-case site-scale analysis.

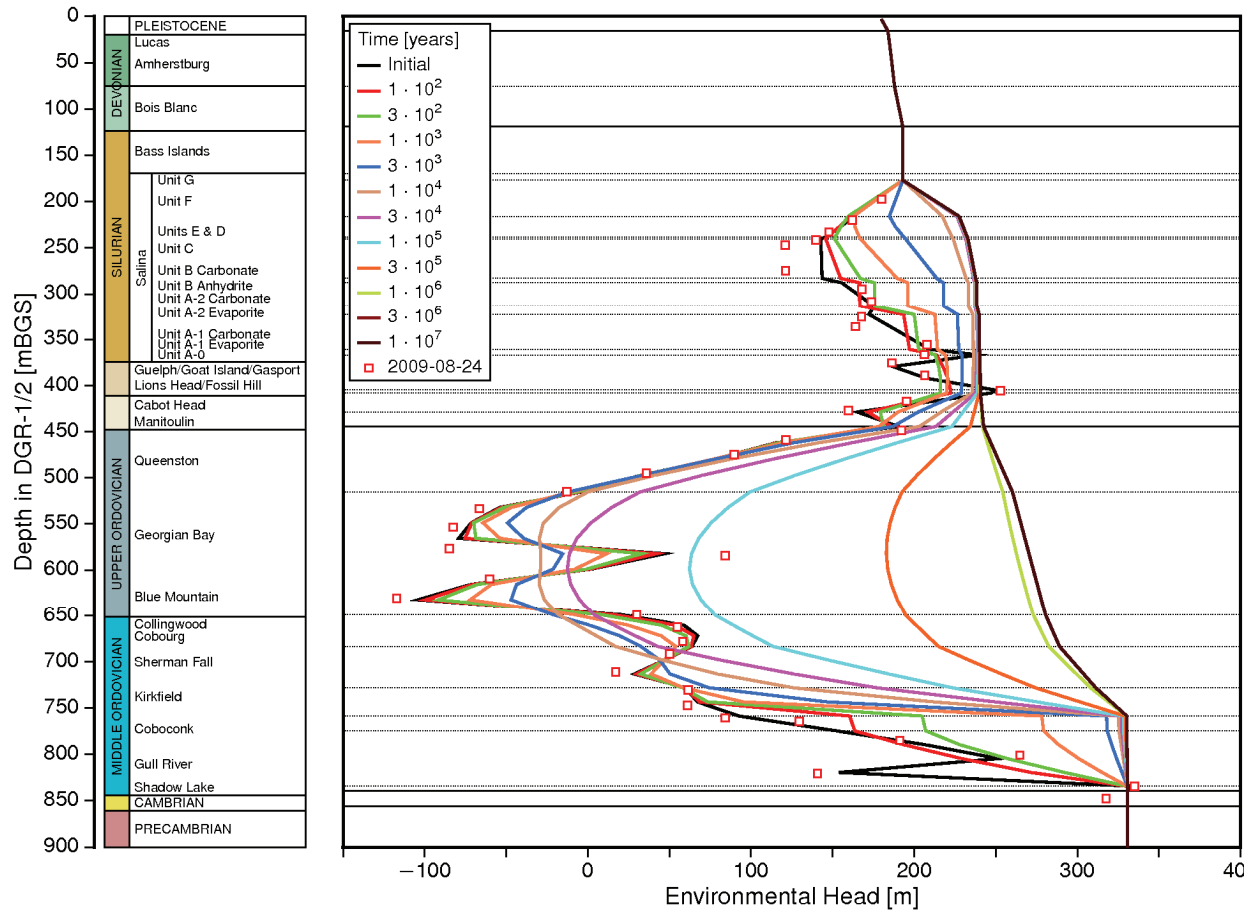
The issue investigated in this section is the effect of the vertical hydraulic conductivities for the units of the Black River Group, the Shadow Lake, Gull River and Coboconk formations on the evolution of the Trenton Group and Upper Ordovician underpressures. In addition to the base-case vertical-to-horizontal hydraulic conductivity anisotropy ratio of 0.001 for the Black River Group, ratios of 0.1 and 0.01 were used to assess the sensitivity of the head profile to the anisotropy ratio. The horizontal hydraulic conductivities for the Ordovician units were constant for all analyses, while the vertical hydraulic conductivities were determined from the horizontal values using the given factors.

The results for the three cases are plotted in Figure 5.45, Figure 5.46 and Figure 5.47. For all three cases, the results show that a downward gradient from the Niagaran to the Ordovician persisted for over 300 ka. The pressure and related water deficit in the Ordovician was met by approximately 1 Ma. Steady-state pressures were reached by 3 Ma with an upward gradient developing from the Cambrian to the surface. With an anisotropy ratio of 0.1, the environmental head profiles of Figure 5.46 indicate that the overpressurization of the Cambrian propagates quickly through the Black River Group such that the hydrostatic state with minimal vertical hydraulic gradient through these units was reached by 10 ka. For all three cases, the water deficit in the Ordovician was met by very slow influx from the Cambrian and/or the Niagaran Group.



Notes: Includes pressure support in both the Niagaran Group and Cambrian. From Sykes et al. (2011).

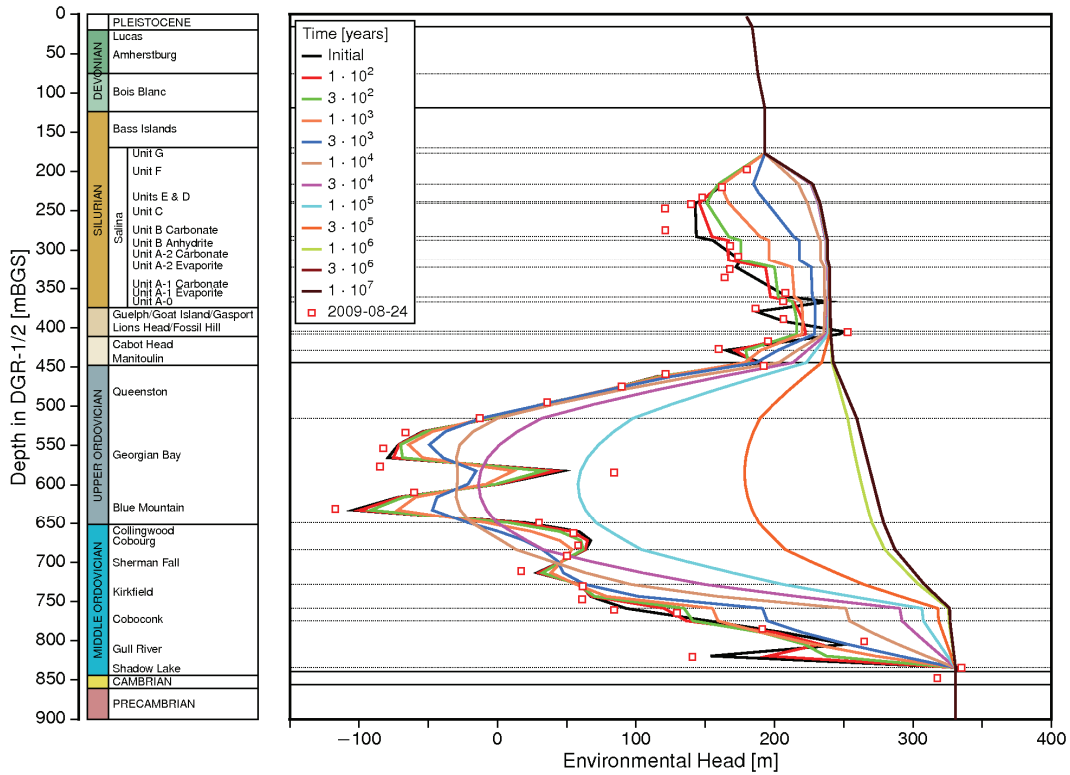
**Figure 5.45: Predicted Evolution of Environmental Heads with Base-case Black River Group Anisotropy of 0.001**



Notes: Includes pressure support in both the Niagaran Group and Cambrian. From Sykes et al. (2011).

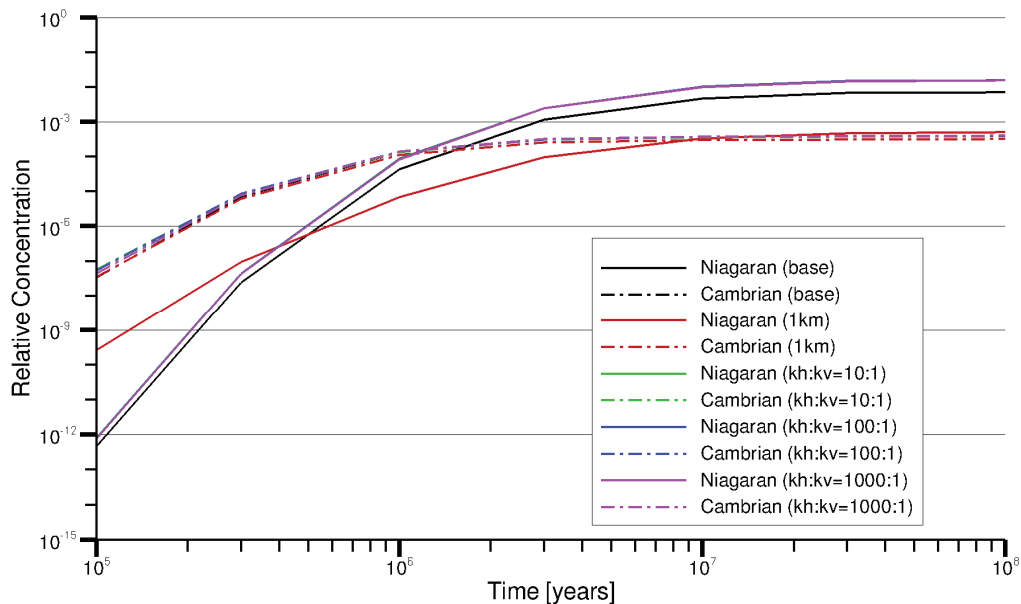
**Figure 5.46: Predicted Evolution of Environmental Heads with Black River Group Anisotropy of 0.1**

The tracer-breakthrough curves at the Niagaran and the Cambrian for the three alternative anisotropy cases for the Black River Group are plotted in Figure 5.48. Also shown are the base-case breakthrough curves from Figure 5.44. Not all curves are visible because they largely overlap. The similarity of the breakthrough curves despite the different head conditions and anisotropies confirms the conclusion that solute transport in the Ordovician is dominated by diffusion and that the impact of pore velocity on solute transport in the deep Ordovician limestone is negligible.



Notes: Includes pressure support in both the Niagaran Group and Cambrian. From Sykes et al. (2011).

**Figure 5.47: Predicted Evolution of Environmental Heads with Black River Group Anisotropy of 0.01**



Notes: Measured environmental head profile represents the initial condition. From Sykes et al. (2011).

**Figure 5.48: Tracer-breakthrough Curves at the Niagaran Group and Cambrian for Site-scale Simulations**

### **Effects of Faults**

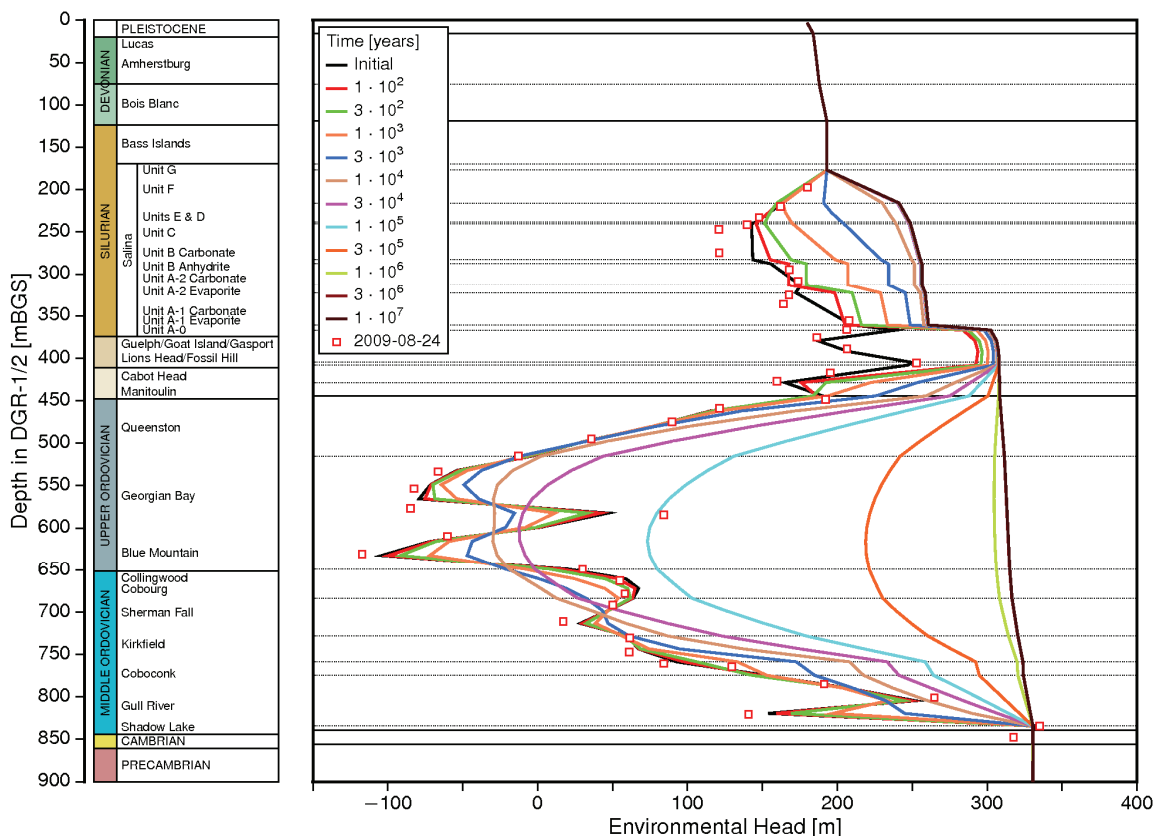
The possible presence of faults at the Bruce nuclear site was investigated using 2D seismic reflection surveys as described in Section 2.3.6.2. Inclined boreholes DGR-5 and DGR-6 were drilled/cored through two inferred fault structures (Figure 2.24). Continuous core retrieved from both inclined boreholes showed no indication of the existence of either one of these potential faults. Consequently, there is no evidence that faults or fault zones exist within or proximal to the DGR footprint which could potentially influence the deep groundwater regime or DGR performance. Nevertheless, the impact on both the pressure evolution in the Ordovician limestone and shale and the migration of a tracer from the Cobourg limestone was investigated for cases in which a hypothetical undetected fault connecting the Cambrian sandstone and the Niagaran Group is located at an arbitrary distance from the tracer source grid block. The fault was conceptualized as a vertical discrete fracture zone oriented in the north-south direction at a distance west of the tracer grid block. This provides a conservative analysis, as the impact of a fracture zone east of the site would be lessened by the possible absence of the Cambrian. An equivalent porous medium approach was used to characterize the 2-km-long fracture zone, which was assigned a hydraulic conductivity of  $3.0 \times 10^{-6}$  m/s and a width of 1 m. The configurations investigated include a hypothetical discrete fracture zone 1 km west of the tracer source zone grid block and a fracture zone 5 km west. Simulations were performed using both the equilibrium-state pressure distribution and the observed environmental head profile at DGR-4 as initial conditions.

The first analyses use the flow boundary conditions, initial equilibrium-state pressure distribution, parameters, and solution methodology of the base-case site-scale analysis. The spatial distribution of the tracer concentration for the simulations of a fracture zone at 1 km at 100 ka was identical to the base-case results shown in Figure 5.42, with tracer not yet having reached either the Cambrian or Niagaran at a relative concentration above  $10^{-6}$ . At 1 Ma, the upward hydraulic gradient from the Cambrian to the Niagaran forces an upward groundwater flow via the fracture zone, reducing the heads in the Cambrian at the fracture, creating a small sink, and raising the heads in the Niagaran at the fracture, creating a mound. The result is a reduced vertical gradient at the fracture compared to that estimated for the Ordovician without a fracture. The pathway for the tracer is still migration by diffusion upward to the Niagaran Group and downward to the Cambrian.

For the case with a fracture zone 5 km west of the DGR, the plume at 100 ka is identical to the base-case plume shown in Figure 5.42, and the plume at 1 Ma is very similar to that of the base-case without a fracture shown in Figure 5.43, indicating that a fracture 5 km west of the proposed DGR site is too far from the DGR to have a significant impact on the evolution of the tracer plume in the Cambrian. There is no component of the tracer drawn toward the fracture and no upward migration of the tracer through the fracture from the Cambrian to the Niagaran Group for the 5-km fracture case.

The impact of a fracture zone 1 km from the tracer source on the pressure distribution observed in the DGR-4 borehole was also investigated. The parameters, boundary conditions and initial conditions were the same as those used for the analyses in Section 5.4.7.4.1, including pressure support in both the Niagaran Group and Cambrian. The evolution of the environmental heads observed in the DGR-4 borehole for the case with a discrete fracture zone 1 km west of the tracer source grid block is shown in Figure 5.49. A comparison of the analyses with the base-case results without a discrete fracture zone (Figure 5.45) reveals that the fracture zone significantly perturbs the pressure in the Niagaran Group by propagating the overpressure

of the Cambrian to the Niagaran Group through the hypothetical discrete fracture. It still takes 3 Ma for the pressures in the Ordovician limestone and shale to reach steady state.



Notes: Includes pressure support in both the Niagaran Group and Cambrian. From Sykes et al. (2011).

**Figure 5.49: Predicted Evolution of Environmental Heads with Fracture Zone 1 km from DGR**

The tracer-breakthrough curves at the Niagaran and the Cambrian for the case with a fracture zone at 1 km and the DGR-4 environmental head profile are plotted in Figure 5.48. The effect of the fracture zone is to increase the very low ( $10^{-12}$  to  $10^{-7}$ ) relative concentrations in the Niagaran before approximately 40 ka, but reduce the later peak concentration to less than  $10^{-3}$ , while tracer breakthrough to the Cambrian is almost unchanged from the other cases considered. As for all other cases, solute transport in the Ordovician is dominated by diffusion.

### 5.4.7.5 Conclusions from Site-scale Modelling

The site-scale model was used to investigate the evolution of a conservative tracer plume originating from the proposed DGR site assuming fully saturated conditions. Two different sets of initial pressure conditions were modeled: one set was the pseudo-equilibrium heads from the regional-scale model (the base-case model), and the other set was based on the environmental head profile measured at the DGR-4 borehole showing Ordovician underpressures combined

with three different values of hydraulic anisotropy in the Black River Group. The choice of initial head conditions or anisotropy was found to make no difference in the transport of the tracer - transport in the Ordovician was dominated by diffusion. No tracer at a relative concentration above  $10^{-7}$  reached either the Cambrian or Niagaran in 100 ka. The maximum relative concentration reached in the Cambrian over 100 Ma was less than  $10^{-3}$ , while that in the Niagaran was slightly above  $10^{-2}$ . The effects on tracer transport of permeable faults connecting the Cambrian and Ordovician were also evaluated for both initial pressure conditions. A fault at 5 km from the tracer source had no effect whatsoever on tracer transport, while a fault at 1 km led to tracer migrating from the Cambrian to the Niagaran. The maximum relative concentration reaching the Niagaran, however, was lower than in the other cases, remaining below  $10^{-3}$ .

For all simulations using the DGR-4 environmental head profile to define initial conditions, the results showed that a downward gradient from the Niagaran to the Ordovician persisted for over 300 ka. The pressure and related water deficit in the Ordovician was met by approximately 1 Ma. Steady-state pressures were reached by 3 Ma with an upward gradient developing from the Cambrian to the surface.

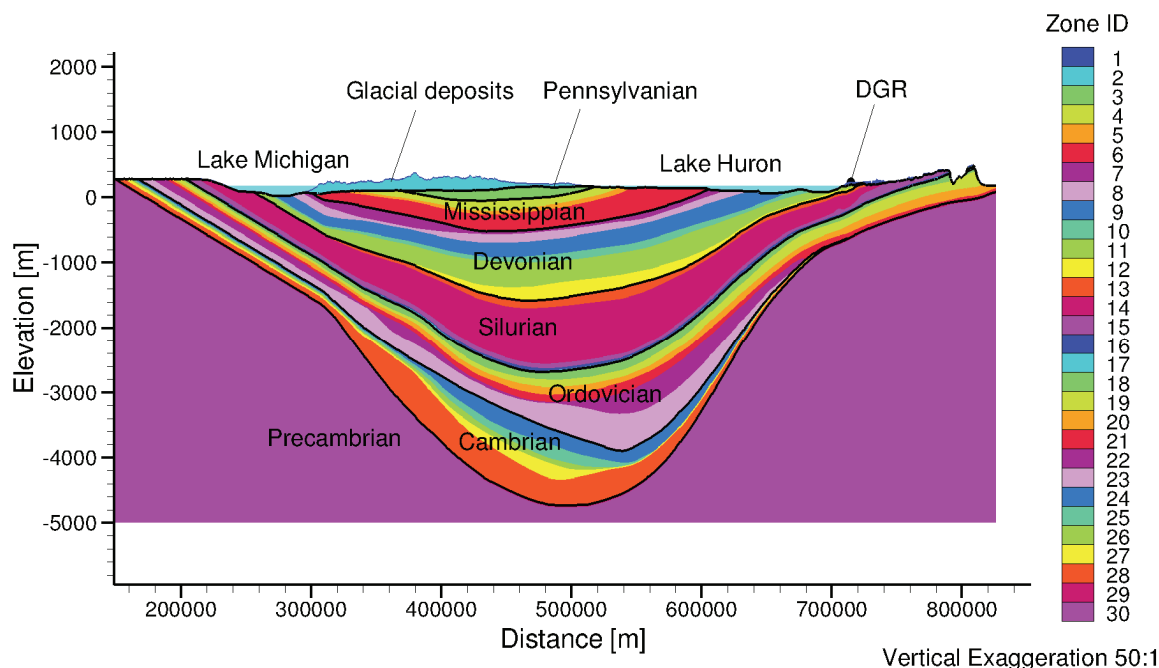
Under fully water saturated conditions, the head profile through the Ordovician is irrelevant to DGR performance – transport is diffusion dominated. If the assumption of full water saturation is invalid (i.e., if a gas phase occupies some portion of the Ordovician pore space), diffusion of solutes through the Ordovician will be even slower than shown by the site-scale model because of the phase-dependence of diffusion coefficients.

#### **5.4.8 Michigan Basin Cross-section Model**

A cross-section of the Michigan Basin was modelled to investigate the overpressures measured in the Cambrian at the DGR site (Figure 5.50). The objective was to assess how the geometry of the basin and the salinity distribution could contribute to overpressures in the high-permeability Cambrian at the Bruce nuclear site, sandwiched as it is between the low-permeability Precambrian and low-permeability Ordovician units. No attempt was made to calibrate the model to conditions in the Cambrian or in any other unit; the intent was simply to illustrate how Cambrian overpressures might arise.

##### **5.4.8.1 Model Domain and Mesh Generation**

The Michigan Basin cross-section modelling domain extends laterally from southwestern Ontario to Wisconsin across Lake Huron, the State of Michigan, and Lake Michigan, a distance of approximately 677 km (Figure 2.4; note that the westernmost ~100 km of the domain is not shown). The vertical elevations range from approximately -5,000 m at the lowest point in the Precambrian to 509 m at the highest point on the Niagara Escarpment. The Cambrian sandstone outcrops in Wisconsin and is absent at the Algonquin Arch. The Cambrian also outcrops in the upper peninsula of Michigan and north of Sault Sainte Marie, Ontario. The Michigan Basin cross-section figures shown in this report have vertical exaggeration of 50:1.



Notes: From Sykes et al. (2011).

**Figure 5.50: Stratigraphic Zones for the Michigan Basin Cross-section Model**

The domain under zero metres above sea level (mASL), where a density-dependent flow simulation was necessary due to the high salinity in the Michigan Basin groundwater system, was finely discretized into a planar hexahedral mesh with 1,355 columns, 600 rows, and 1 block in thickness to create a vertical two-dimensional mesh. These hexahedral elements have sides of 500 m in the horizontal direction by 10 m in the vertical direction by 1 m in thickness. The non-orthogonal mesh above sea level has 100 evenly distributed layers with 1,355 nodes each. The elevation of the nodes for each layer were determined from the 3DGF model (ITASCA CANADA and AECOM 2011). Given the fact that the continuity of each geologic unit was strictly maintained, 30 stratigraphic units for the Michigan Basin cross-section were mapped to the mesh.

#### 5.4.8.2 Flow Boundary and Initial Conditions

The eastern boundary of the domain is the water divide for the surface water system, and conceptualized as a Neumann (no-flow) boundary condition. The western boundary roughly corresponds to the surface water divide between Lake Michigan and the Mississippi River in Wisconsin, and can also be conceptualized as a Neumann no-flow boundary condition. The bottom of the Michigan Basin cross-section is in Precambrian granitic gneiss with very sparse fractures (INTERA 2011). Therefore, a Neumann no-flow boundary condition was assumed for the bottom of the model. The elevations of the nodes at the top of the model domain are defined by either the DEM or the lake bathymetry. For surface nodes, including those occupied by Lake Huron and Lake Michigan, the assigned prescribed head was set as the elevation minus 3 m, but not less than the 176 m Lake Huron and Lake Michigan water elevation. The imposed surface boundary condition permits recharge and discharge to occur as determined by

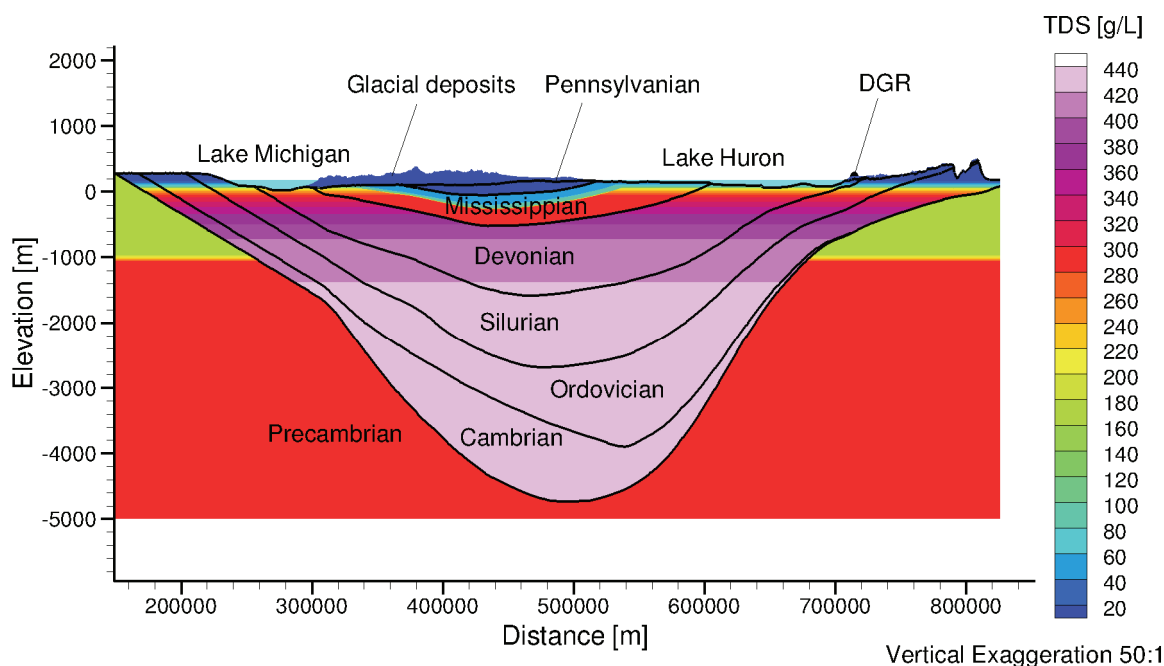
the surface topography and the hydraulic conductivity of the top model layer. The assigned head represents a water table occurring at an assumed depth of 3 m below ground surface. Because of the resolution of the DEM (grid blocks that are 500 m), stream channels are conceptualized to have a depth to water that is 3 m less than defined by the DEM.

### 5.4.8.3 Hydraulic and Transport Parameters

The base-case data set for the conceptual model consists of 30 model layers, with each layer corresponding to a unit in a stratigraphic section. Sykes et al. (2011) shows the layers and their associated hydraulic conductivities, anisotropy ratios, porosities, and specific storage values. For those geologic units existing at the Bruce nuclear site, the hydraulic parameter values were inherited from the regional-scale model (refer to Section 5.4.5.2). The variation of hydraulic conductivity in the Precambrian with depth was calculated using the relationship of Normani (2009). Some other Michigan Basin geologic units, such as the Saginaw, Marshall, the Ancell Group, and the Prairie du Chien, pinch out to the west of the proposed DGR and are therefore absent in the 3DGF. Their values were either derived from the literature or estimated by appropriate assumptions as described in Sykes et al. (2011).

### 5.4.8.4 TDS

Salinity plays an important role with regard to a density-dependent groundwater system. For the base-case scenario, the initial prescribed TDS distribution was developed from data presented in Frappe and Fritz (1987), Hanor (1979), and Lampe (2009), as described in Sykes et al. (2011). The resulting base-case TDS concentration distribution is shown in Figure 5.51. As can be noted in the figure, the described TDS concentration distribution model results in a discontinuity in the concentration at the top of the Precambrian.



Notes: From Sykes et al. (2011).

**Figure 5.51: Initial TDS Distribution**



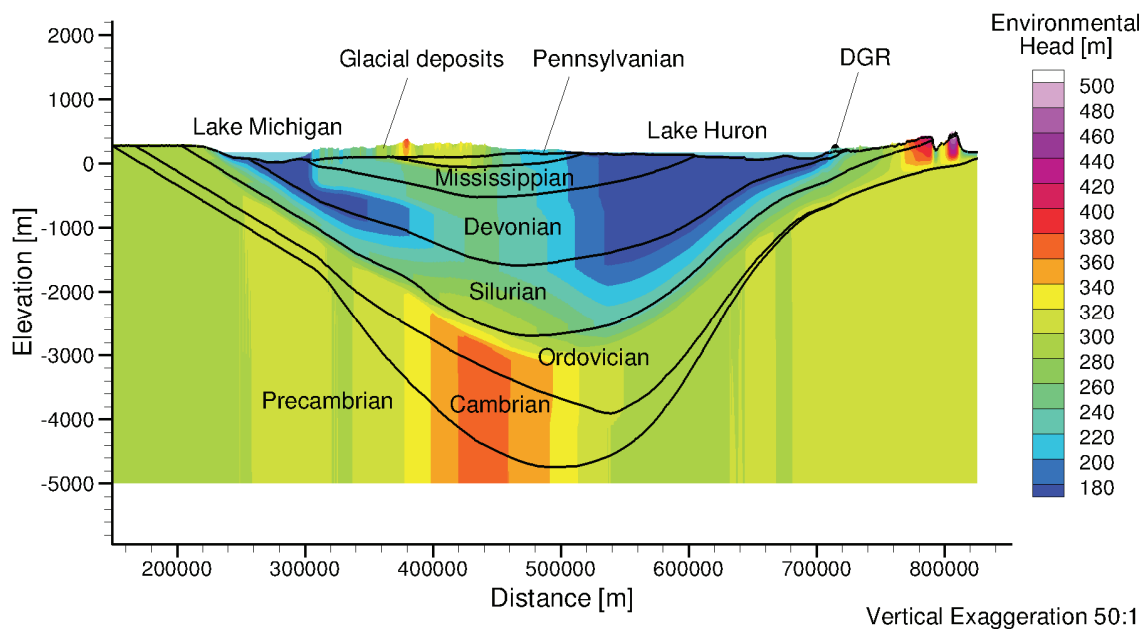
The conceptual model for TDS used in the Michigan Basin cross-section analysis is the same as that of the regional-scale analysis: no TDS sources were considered in the groundwater domain. As a consequence, the dissolved solids will gradually reduce in a temporal analysis as groundwater discharges from the system. To resolve this, the calculation procedure for the analysis of density-dependent flow is as follows:

1. Determine the distribution of freshwater heads for the steady-state density-independent system;
2. Assign a temporally invariant distribution for the TDS concentration in the cross-section based on literature data; and
3. With the TDS transport module in FRAC3DVS-OPG turned off, and the freshwater head distribution of the first step as an initial condition, determine a solution for the freshwater heads that has equilibrated to the defined TDS concentration distribution.

The equilibrium solution for the described transient analysis was reached at 10 Ma; no change was observed in the equivalent freshwater head distribution after this time.

#### 5.4.8.5 Results from Michigan Basin Cross-section Model

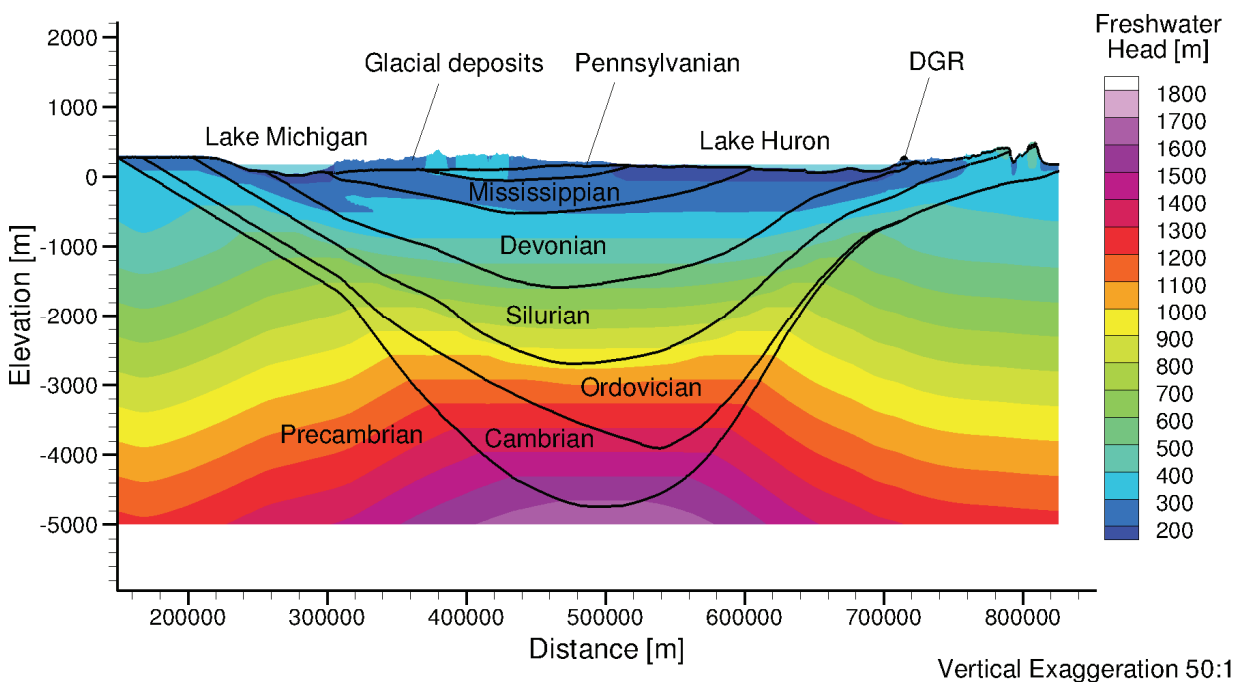
The environmental head and equivalent freshwater head distributions for the density-dependent case and TDS concentration distribution of Figure 5.51 are shown in Figure 5.52 and Figure 5.53, respectively. Figure 5.52 shows that the environmental head gradient that controls vertical flow is effectively nonexistent in the Cambrian and high-permeability Lower Ordovician units in the central portion of the basin, and is upward through the lower permeability Ordovician units. Figure 5.53 shows that the freshwater head gradient controlling horizontal flow is also effectively nonexistent in the Cambrian.



Notes: From Sykes et al. (2011).

**Figure 5.52: Equilibrium Environmental Heads for Defined TDS Distribution**

The density-dependent simulation resulted in a calculated equivalent freshwater head in the Cambrian at the location of the DGR of 472.6 m and a calculated environmental head of 305.3 m. The August 24, 2009 measured freshwater head and estimated environmental head in the Cambrian at the DGR-4 borehole are 422.1 m and 317.6 m, respectively. An upward environmental head gradient is predicted in the analysis. Relative to the ground surface at 181.6 mASL, the measured overpressures in the Cambrian are reconstructed by the Michigan Basin cross-section model.



Notes: From Sykes et al. (2011).

**Figure 5.53: Equilibrium Freshwater Heads for Defined TDS Distribution**

#### 5.4.8.6 Conclusions from the Michigan Basin Cross-section Analyses

The analyses developed in this section indicate that Cambrian overpressures at the Bruce nuclear site result from a combination of the topographic elevation of the Cambrian outcrop areas and the fluid density distribution in the basin. An upward gradient between the Cambrian and the Niagaran is predicted and the difference between the measured and model calculated heads is less than the difference obtained with the regional-scale model (refer to the analyses of Section 5.4.5). This study investigated only a single TDS concentration versus depth model for the sedimentary rock. An alternate TDS versus depth model for the sedimentary rock may result in an improved fit. Regardless, based on the results, the overpressures in the Cambrian can be attributed to the spatial distribution of fluid density and the geometry of the various stratigraphic layers in the Michigan Basin.

### 5.4.9 1D Two-phase Model

The discretization that is required for a 3D regional-scale model of the geosphere surrounding the Bruce DGR is too coarse for the modelling of two-phase gas and water flow. In addition, while there is evidence that a gas phase may exist in the Ordovician sediments, the spatial extent of a gas phase is unknown and the degree of saturation for the gas phase is uncertain. Two-phase gas and water flow is thus investigated in this study using a one-dimensional vertical column. It is assumed that both horizontal pressure gradients and horizontal solute concentration gradients are negligible in the Ordovician.

A 1D two-phase air-water analysis was performed using TOUGH2-MP (Pruess et al. 1999) to determine whether or not the presence of a free gas phase could lead to a non-hydrostatic pressure profile between the Guelph and Cambrian formations. This study was motivated by the pressure profiles defined by straddle-packer testing and Westbay monitoring, as shown in Figure 5.5. The primary feature of interest shown by these profiles is underpressures in the Upper Ordovician and Trenton Group strata. A secondary feature of interest is apparent discontinuities in the pressure profiles, as isolated intervals of normal pressure or overpressure are sandwiched between underpressured intervals.

One such discontinuity in the pressure profile occurs in the lower Georgian Bay interval of DGR-2 at a depth of approximately 585 mBGS. Both the formation pressure inferred from the hydraulic testing of the interval from 578.1 to 608.6 mBGS and the pressures subsequently observed in the Westbay interval from 580.9 to 587.1 mBGS were considerably higher than the pressures in the adjacent intervals (INTERA 2011). A strong odour of hydrocarbons was noted in this section of core (Sterling 2010b). The calculated test-zone compressibility of the straddle-packer interval that contained this core interval was approximately  $1 \times 10^{-8} \text{ Pa}^{-1}$ , the highest encountered in any of the DGR boreholes (Figure 5.4) and suggestive of the presence of gas. Similar seemingly anomalous high-pressure and high test-zone compressibility intervals are observed in other DGR boreholes, such as at approximately 602 mBGS in DGR-4. Thus, the two-phase modelling included an attempt to determine whether or not localized overpressures could be related to the presence of gas-containing features having different two-phase flow properties from the surrounding rock.

The scope of the two-phase air-water analysis was limited to demonstrating the effects that the presence of a gas phase in the Ordovician sediments (and a facies change) could have on water-phase pressures. A detailed sensitivity analysis was not performed.

The base-case scenario for the TOUGH2-MP modelling assumed that a uniform gas saturation was present in all strata from the Gasport to the Coboconk (inclusive) as an initial condition. The evolution of the saturation profile and associated gas and water pressure profiles was modelled for 4 Ma while gas saturations in the Cambrian and Guelph were held at zero. An alternative scenario was modelled in which the initial gas saturation in all units was zero. Gas was introduced uniformly for 200 ka from the Coboconk to the Queenston inclusive, and the system evolved for another 800 ka. A variant on both scenarios included a thin zone at a depth of 585 mBGS in the Georgian Bay Formation having a different capillary pressure versus saturation curve than the rest of the formation. For all simulations, the measured Westbay pressure and estimated head profiles from August 2009 for the DGR-4 borehole (INTERA 2011), shown in Figure 5.5, provided a qualitative comparison to the model results - no attempt was made to calibrate the model to the DGR-4 data.

### 5.4.9.1 Model Description

The TOUGH2-MP computational model was selected for this study based on its capabilities, multi-phase flow attributes, the validation and verification reports for the model, and its broad use throughout the world. Details of the capillary pressure and relative permeability versus saturation relationships used in the model are given in Sykes et al. (2011).

The modelling domain was one-dimensional, composed of 982 blocks approximately 0.5 m in height. The TOUGH2-MP model required boundary conditions to be set for the top and bottom blocks in the modelling domain representing the Guelph Formation and the Cambrian Formation, respectively. Both blocks were set to specified gas pressure and gas saturation, the state variables solved for by TOUGH2-MP. A gas saturation of zero was assumed for both formations yielding a corresponding capillary pressure of zero.

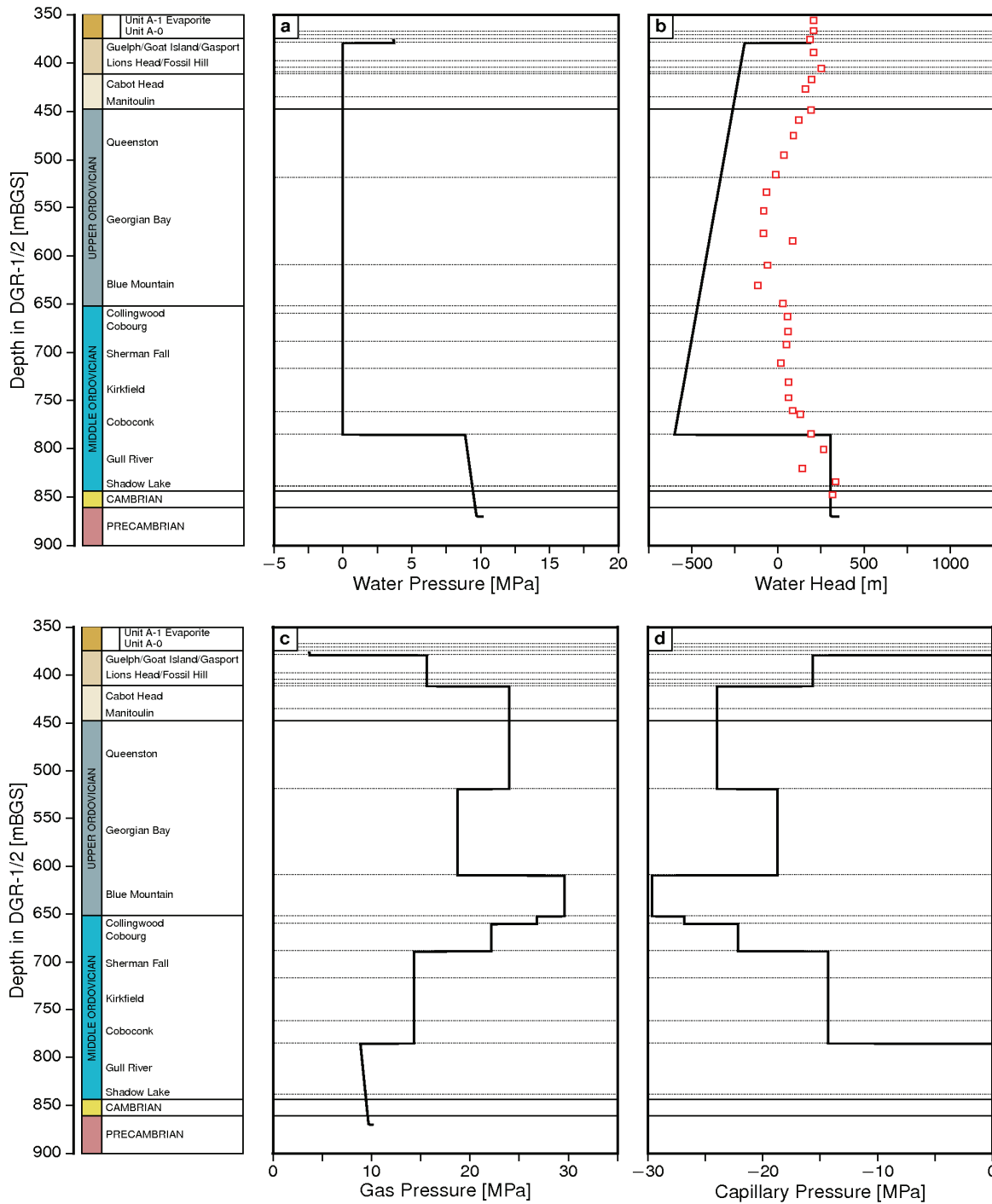
For the base-case simulations, the initial gas saturation for the units between the Coboconk and the Gasport was set to 0.17, resulting in an initial water saturation of 0.83. The Gull River and Shadow Lake were assumed to have an initial gas saturation of zero. The initial conditions for pressures are shown in Figure 5.54a. The equivalent freshwater heads, gas pressure and capillary pressure are also shown in Figure 5.54. The initial saturations were used to determine the capillary pressure within a formation. The initial water pressure was specified to account for hydrostatic conditions in the Guelph Formation, and hydrostatic conditions with 120 m overpressure in the Gull River, Shadow Lake and Cambrian formations. Initial water pressures were set to zero between the Guelph Formation and the Gull River Formation. The initial gas pressure was calculated from the water pressure minus the capillary pressure.

For the alternative scenario, the initial gas saturation was set to zero for all units, resulting in an initial water saturation of 1.0. The initial water pressure and water head distribution for the alternative scenario are shown in Figure 5.55. The boundary conditions, properties and parameters for the analyses were identical to those used for the base-case simulations.

To determine whether or not localized overpressures could be related to conductive layers having different two-phase flow properties from the surrounding rock, separate TOUGH2-MP simulations were performed for both the base-case and alternative scenarios that included a thin zone (termed a “fracture” by INTERA 2011 and Sykes et al. 2011) with different two-phase properties in the Georgian Bay Formation at a depth of 585 m, represented using a single block with a height of 0.5 m. The initial saturations and initial water pressures were identical to those assumed for the cases lacking this feature.

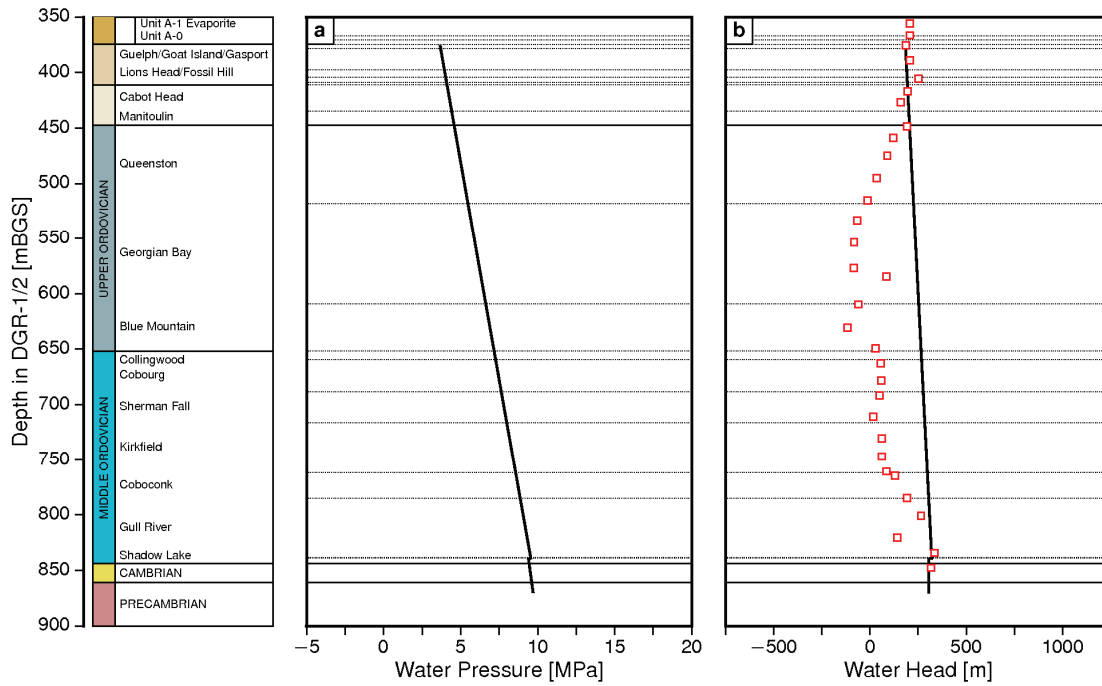
### 5.4.9.2 Model Parameters

The hydrogeologic parameters for the domain are shown in Table 5.13. The formation permeability is calculated from the formation hydraulic conductivity, formation fluid density and fluid viscosity of  $2.0 \times 10^{-3}$  Pa-s. The van Genuchten (1980) parameters for the non-hysteretic capillary pressure and relative permeability curves for use in TOUGH2-MP are shown in Table 5.13. The capillary pressure versus water saturation curves for the formations listed in Table 5.13 are shown in Figure 5.56. The “fracture” feature is modelled using the capillary pressure curve shown in Figure 5.56. It should be noted that different capillary pressure versus water saturation curves will yield different pressures and saturations within the fracture feature. The full investigation of this aspect of two-phase flow was beyond the scope of this study.



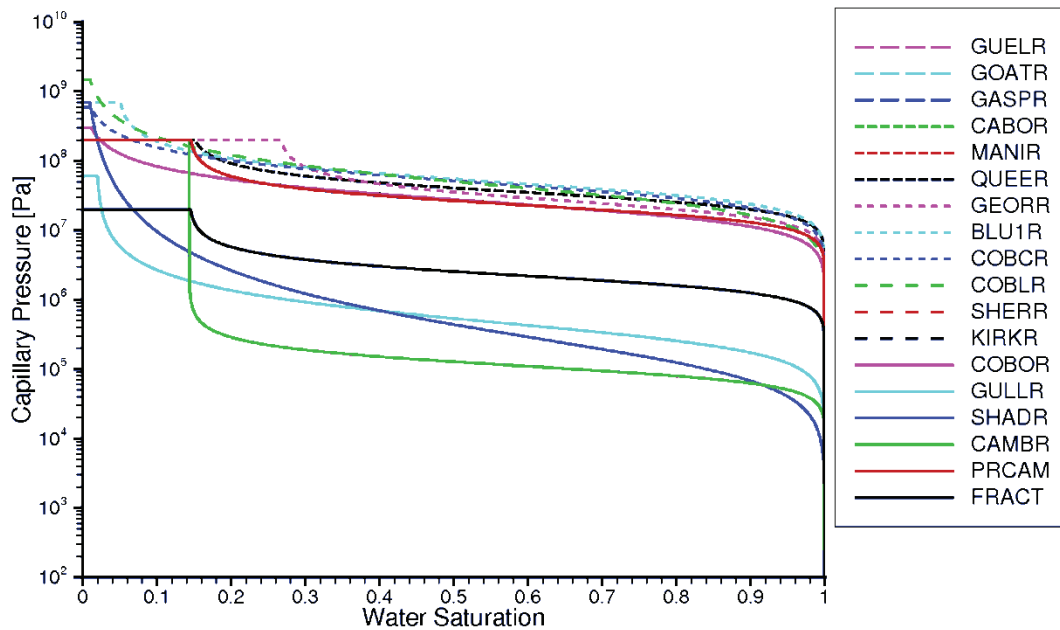
Notes: From Sykes et al. (2011).

**Figure 5.54: Initial Conditions Base-case Two-phase Gas-water Flow Analysis: (a) Water Pressure, (b) Freshwater Head, (c) Gas Pressure, (d) Capillary Pressure**



Notes: From Sykes et al. (2011)

**Figure 5.55: Initial Conditions Two-phase Gas-water Flow Analysis with Air Generation: (a) Water Pressure, (b) Freshwater Head**



Notes: Unit identifiers in legend correspond to formations as indicated in first column of Table 5.13 below. From Sykes et al. (2011).

**Figure 5.56: Capillary Pressure versus Saturation Relationships for the Two-phase Flow Analysis**

Table 5.13: Hydrogeologic and Two-phase Flow Properties for TOUGH2-MP Simulations

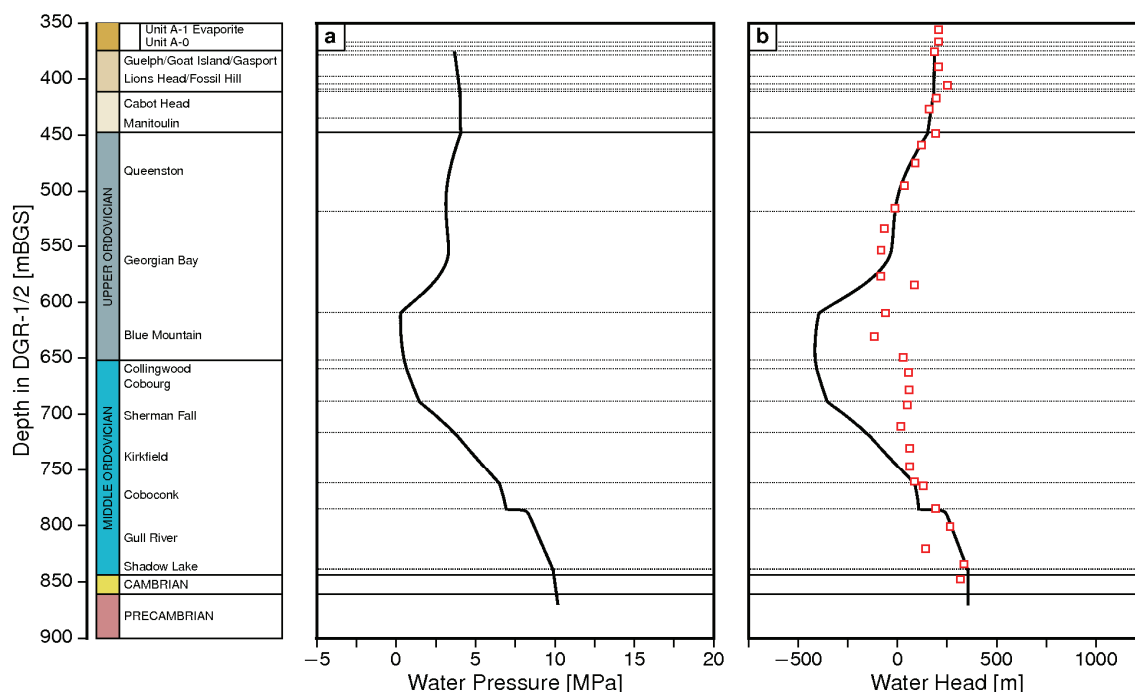
Formation	ID	Density [kg/m <sup>3</sup> ]	Porosity [-]	Permeability			Relative Permeability Curves				Capillary Pressure Curves				
				k <sub>x</sub> [m <sup>2</sup> ]	k <sub>y</sub> [m <sup>2</sup> ]	k <sub>z</sub> [m <sup>2</sup> ]	λ	S <sub>ir</sub> [-]	S <sub>is</sub> [-]	S <sub>or</sub> [-]	λ	S <sub>ir</sub> [-]	1/α [MPa]	P <sub>max</sub> [MPa]	S <sub>is</sub> [-]
Guelph	GUELR	2810	0.057	4.91E-15	4.91E-15	4.91E-15	0.718	0.14	1	0.08	0.718	0.14	1.00E5	2.00E8	1
Goat Island	GOATR	2730	0.02	3.40E-19	3.40E-19	3.40E-20	0.718	0.14	1	0.08	0.718	0.14	2.10E7	2.00E8	1
Gasport	GASPR	2730	0.02	3.40E-19	3.40E-19	3.40E-20	0.718	0.14	1	0.08	0.718	0.14	2.10E7	2.00E8	1
Cabot Head	CABOR	2790	0.116	1.52E-20	1.52E-20	1.52E-21	0.718	0.14	1	0.08	0.718	0.14	3.20E7	2.00E8	1
Manitoulin	MANIR	2720	0.028	1.49E-20	1.49E-20	1.49E-21	0.718	0.14	1	0.08	0.718	0.14	3.20E7	2.00E8	1
Queenston	QUEER	2770	0.073	3.38E-21	3.38E-21	3.38E-22	0.718	0.14	1	0.08	0.718	0.14	3.20E7	2.00E8	1
Georgian Bay	GEORR	2760	0.071	5.08E-21	5.08E-21	5.08E-22	0.706	0.26	1	0.12	0.706	0.26	2.40E7	2.00E8	1
Blue Mountain	BLU1R	2770	0.078	8.52E-21	8.52E-21	8.52E-22	0.656	0.05	1	0	0.656	0.05	4.30E7	7.00E8	1
Cobourg – Collingwood	COBCR	2700	0.012	3.55E-21	3.55E-21	3.55E-22	0.626	0	1	0.13	0.626	0	4.00E7	6.00E8	1
Cobourg - Lower	COBLR	2710	0.015	3.45E-21	3.45E-21	3.45E-22	0.549	0	1	0	0.549	0	3.30E7	1.50E9	1
Sherman Fall	SHERR	2720	0.016	1.73E-21	1.73E-21	1.73E-22	0.626	0	1	0.14	0.626	0	2.10E7	3.00E8	1
Kirkfield	KIRKR	2710	0.021	1.41E-21	1.41E-21	1.41E-22	0.626	0	1	0.14	0.626	0	2.10E7	3.00E8	1
Cobocokk	COBOR	2690	0.009	6.97E-19	6.97E-19	6.97E-22	0.626	0	1	0.14	0.626	0	2.10E7	3.00E8	1
Gull River	GULLR	2730	0.022	1.26E-19	1.26E-19	1.26E-22	0.547	0.02	1	0	0.547	0.02	3.40E5	6.00E7	1
Shadow Lake	SHADR	2760	0.097	1.80E-16	1.80E-16	1.80E-19	0.35	0	1	0	0.35	0	1.30E5	7.00E8	1
Cambrian	CAMBR	2700	0.071	5.29E-13	5.29E-13	5.29E-13	0.718	0.14	1	0.08	0.718	0.14	1.00E5	2.00E8	1
Precambrian	PRCAM	2590	0.038	1.70E-17	1.70E-17	1.70E-17	0.718	0.14	1	0.08	0.718	0.14	2.10E7	2.00E8	1
Fracture - P <sub>c</sub>	FRACT	2760	0.071	5.08E-21	5.08E-21	5.08E-22	0.718	0.14	1	0.08	0.718	0.14	2.00E6	2.00E7	1

Notes: From Sykes et al. (2011; their Table 6.10).

### 5.4.9.3 Base-case Simulations

For the base-case scenario, the water pressure and water head at 400 ka are shown in Figure 5.57. Saturations at 400 ka are shown in Figure 5.58. As is shown, pressures are continuous from one formation to the next, but saturations are discontinuous. The pressure profiles are still evolving at this stage in the simulation. In Figure 5.57a, the water head is negative within the middle formations and remains overpressured in the Gull River and Shadow Lake formations. The water pressure and water head at 1.25 Ma are shown in Figure 5.59 while the corresponding saturations at 1.25 Ma are shown in Figure 5.60. A comparison of the plots at 1.25 Ma with those presented at 400 ka reveals that the gas phase is dissipating with a corresponding increase in the water pressure (head) occurring. The dissipation of the gas phase occurs as a result of both gas transport as a separate phase from the domain as well as partitioning of the water vapour and air phases from the gas to the water phase and then diffusion in the solution phase to the bounding layers (Guelph and Cambrian).

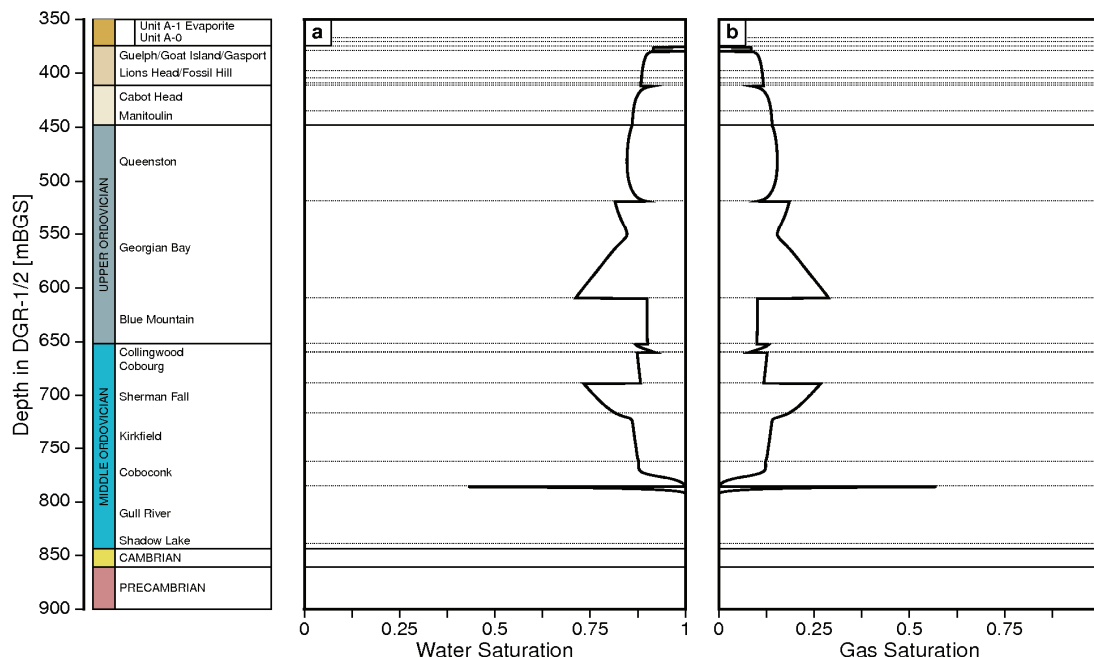
Migration of the gas phase is sensitive to the relative permeability versus saturation curves for both the water phase and the gas phase, while diffusion of air in the water phase is sensitive to the diffusion model used in the analysis. With the diffusion model used, the gas phase has completely dissipated by 3 to 4 Ma; alternative diffusion models might allow more rapid dissipation. Regardless, the results for the water head at 1.25 Ma as shown in Figure 5.59 indicate that underpressures in the Ordovician sediments could be related to the presence of a gas phase.



Notes: Freshwater head represents August 24, 2009 measurements in DGR-4. From Sykes et al. (2011).

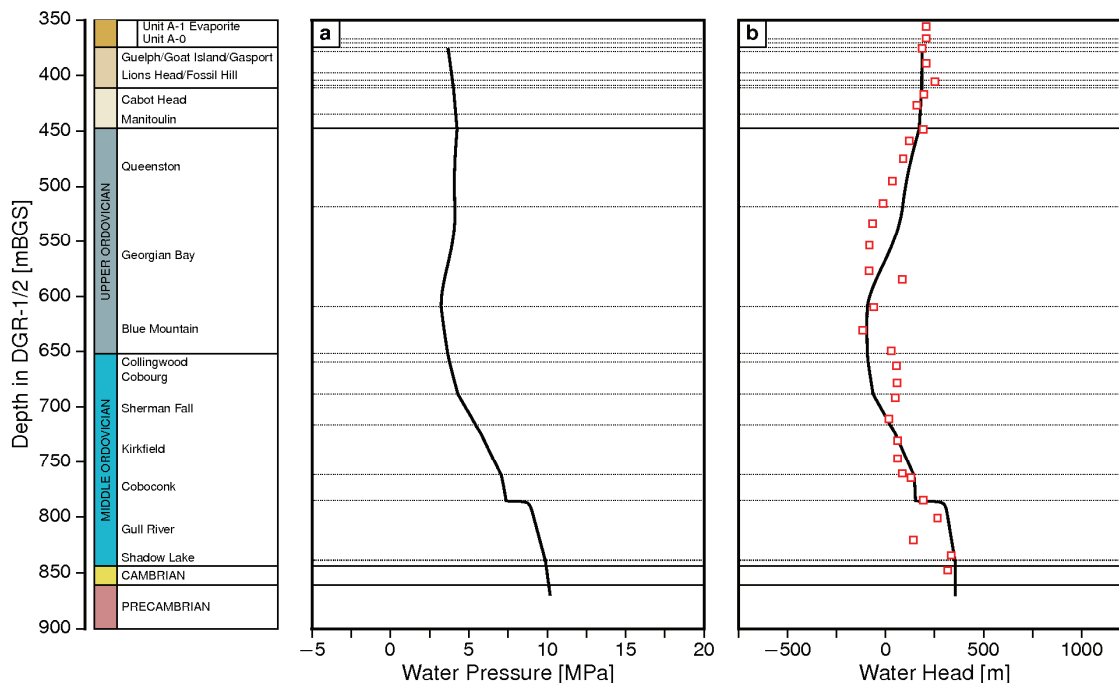
**Figure 5.57: Two-Phase Flow Analysis at 400 ka for Base-case Scenario: (a) Water Pressure, (b) Freshwater Head**





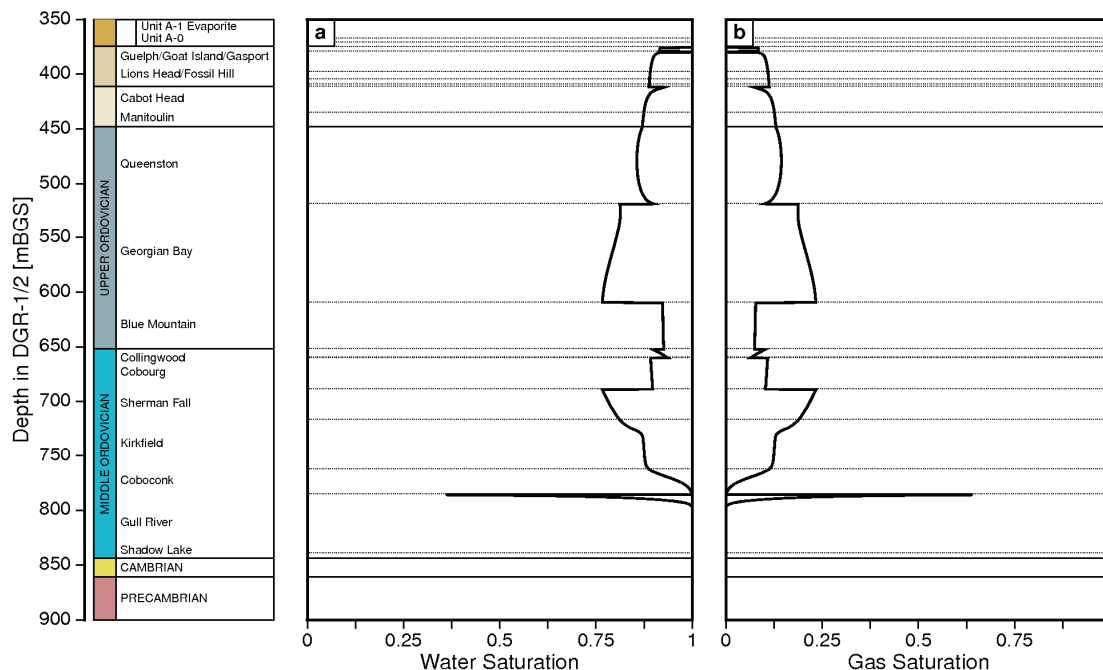
Notes: From Sykes et al. (2011).

**Figure 5.58: Saturations for the Two-phase Flow Analysis at 400 ka for Base-case Scenario: (a) Gas Saturation Profile, (b) Water Saturation Profile**



Notes: Freshwater head represents August 24, 2009 measurements in DGR-4. From Sykes et al. (2011).

**Figure 5.59: Two-phase Flow Analysis at 1.25 Ma for Base-case Scenario: (a) Water Pressure, (b) Freshwater Head**



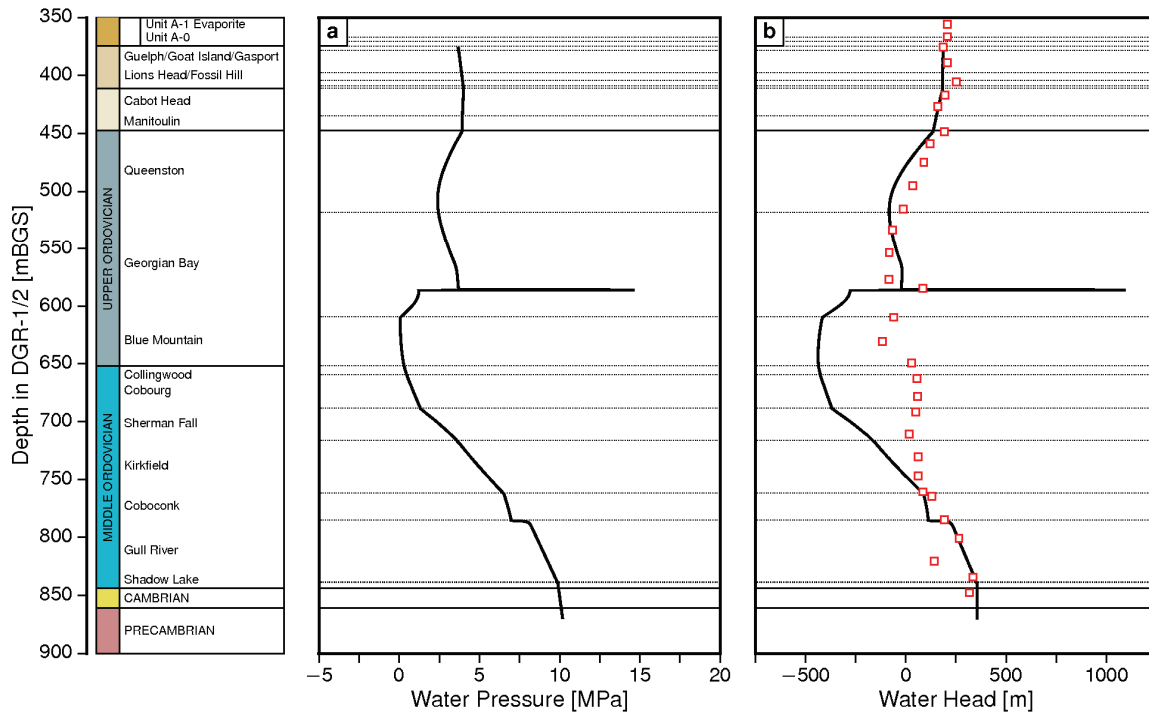
Notes: From Sykes et al. (2011).

**Figure 5.60: Saturations for the Two-phase Flow Analysis at 1.25 Ma for Base-case Scenario: (a) Gas Saturation Profile, (b) Water Saturation Profile**

Including a fracture in the base-case simulations at 585 mBGS altered the pressure and saturation profiles. At 300 ka, the effects of the fracture are seen in Figure 5.61 for pressures and in Figure 5.62 for saturations. The discontinuity created by the fracture is evident in Figure 5.61. The water pressure in the fracture feature could be adjusted by choosing a different capillary pressure versus saturation curve for the fracture, but no attempt was made to adjust either the capillary pressure versus saturation curves or the relative permeability versus saturation curves in order to yield a better comparison between the modelled results and the measured pressures in DGR-4. Gas pressures, but not saturations, are continuous throughout the formation. The fracture feature exhibits a high gas saturation and high water pressure relative to the adjacent Georgian Bay Formation. The profiles changed only slightly as the modelling period was extended from 300 to 500 ka (Sykes et al. 2011).

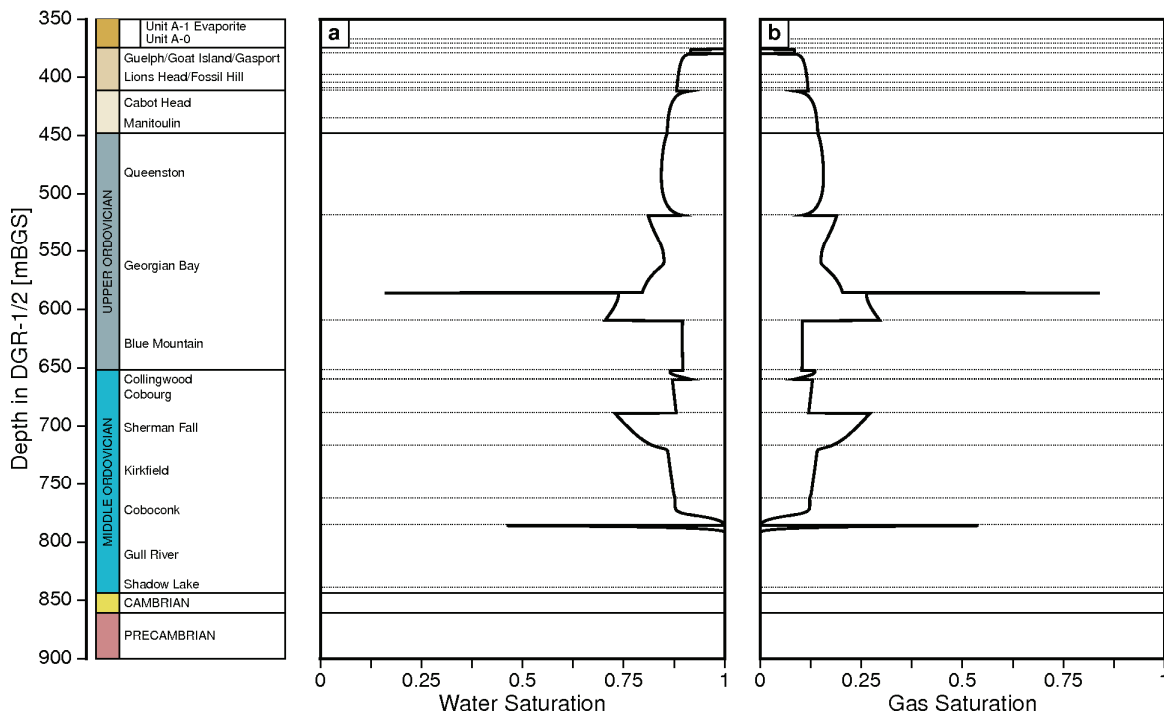
#### 5.4.9.4 Alternative Scenario

For the alternative scenario, air was introduced uniformly for 200 ka from the Coboconk to the Queenston inclusive to provide a temporary gas source. The total amount of air introduced per unit length of rock was assumed to be 98% of the air that would be contained in a volume of rock with a water saturation of 95% and a gas saturation of 5%. Alternate gas generation rates were not investigated in this study.



Notes: Freshwater head represents August 24, 2009 measurements in DGR-4. From Sykes et al. (2011).

**Figure 5.61: Two-Phase Flow Analysis at 300 ka with a Fracture Zone at 585 mBGS: (a) Water Pressure, (b) Freshwater Head**

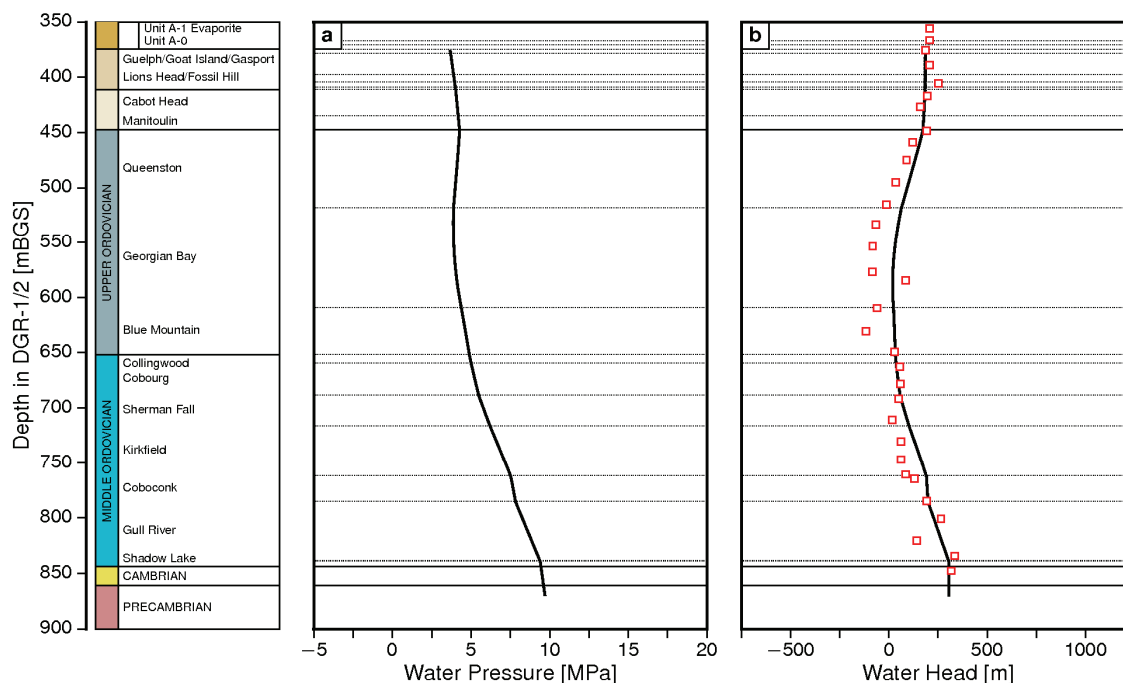


Notes: From Sykes et al. (2011).

**Figure 5.62: Saturations for the Two-phase Flow Analysis at 300 ka with a Fracture Zone at 585 mBGS: (a) Gas Saturation Profile, (b) Water Saturation Profile**

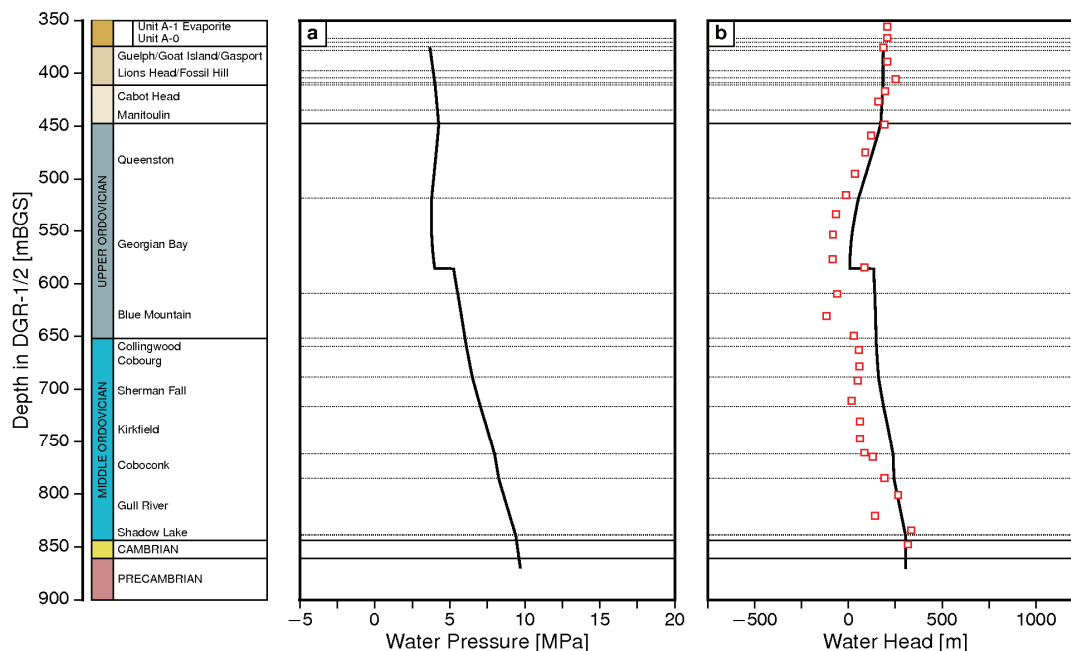
After time zero, air generation, greater than the amount that can be accommodated by the pore compressibility, results in increased water pressures in the Ordovician. The water that is being displaced by the gas phase migrates from the domain under the resulting efflux water gradients. The air in the gas phase partitions into the water phase and migrates from the domain through diffusion in the solution phase. The air also migrates from the domain as a separate phase. After gas generation ceases, the dissipation of both the displaced water phase and the air phase results in a decrease in the water pressure, eventually resulting in underpressures. The water pressure is sensitive to the pore compressibility, while the pore volume is sensitive to the high air entry gas pressure for the capillary pressure versus saturation curves for the Ordovician rock. The underpressures that develop at 1.0 Ma are shown in Figure 5.63. The water pressures compare favourably with the measured pressures in DGR-4. Continued diffusion of air in the solution phase results in the gradual dissipation of the air phase and a return of the water pressures to a hydrostatic state. The rate of return is sensitive to the diffusion coefficient. Thus, generation of a gas phase can result in the development of underpressures in the water phase that may persist for hundreds of thousands of years.

Including a fracture at 585 mBGS in the model with air generation described above results in the pressure distributions shown in Figure 5.64 at 1.0 Ma. Compared to the pressure distributions without the fracture (Figure 5.63), the primary difference is an offset toward higher water pressures at the elevation of the fracture. Notably, this offset is maintained below the fracture.



Notes: Freshwater head represents August 24, 2009 measurements in DGR-4. From Sykes et al. (2011).

**Figure 5.63: Two-phase Flow Analysis at 1 Ma with Air Generation: (a) Water Pressure, (b) Freshwater Head**



Notes: Freshwater head represents August 24, 2009 measurements in DGR-4. From Sykes et al. (2011).

**Figure 5.64: Two-phase Flow Analysis at 1 Ma with a Fracture Zone at 585 mBGS and Air Generation: (a) Water Pressure, (b) Freshwater Head**

#### 5.4.9.5 Conclusions from 1D Two-phase Modelling

The 1D two-phase modelling shows that water-phase underpressures, such as those observed in the Ordovician rock in the DGR boreholes, can be caused by the presence of a gas phase. The modelling shows that water pressure is sensitive to the rock-dependent capillary pressure versus saturation relationships. The results demonstrate that gas saturations should not be expected to be continuous but may vary significantly throughout the rock column. The modelling also shows that significant discontinuities in the phase saturations can occur at the boundaries between formations having different two-phase properties, as well as at heterogeneities in the rock mass such as fractures. Fractures may also have a much higher water pressure than the surrounding rock.

From a solute-transport perspective, higher gas-phase saturation and lower water-phase saturation in a fracture compared to the adjacent rock will result in a reduction of the water-phase diffusion in the fracture through its dependence on the water-phase saturation. This implies that water-phase diffusion can be significantly reduced as a result of the presence of zones in the rock with higher gas saturation.

#### 5.4.10 Conclusions from Hydrogeological Modelling Studies

The hydrogeological modelling studies for the proposed DGR followed the strategy described in Section 5.4.2 (see below).

- Model what the system would look like at equilibrium (base-case), using best-estimate parameter values, geologically reasonable boundary conditions, and assuming full water

(or brine) saturation. Compare equilibrium solution to current observations (e.g., head, solute distributions), and estimate performance measures for the equilibrium system.

- Model alternatives to the base-case, varying boundary and/or initial conditions, parameter values, loading conditions, etc., and incorporating alternative processes such as two-phase flow. Compare alternative solutions to current observations (e.g., head, solute distributions), and estimate performance measures for the alternative systems.
- Model at different scales, or using different codes, as appropriate to the issue/process to be addressed.
- Identify aspects of the performance of the system that are robust (invariant through all alternative models) and those that are sensitive to the modelling assumptions/ parameters.
- Identify factors, if any, which may lead to concerns about the ability of a DGR in the Cobourg to safely store L&ILW for 1 Ma.

The regional-scale base-case model represents an equilibrium state condition toward which the present-day system may be evolving. In order to reach this equilibrium state from the conditions currently observed, flow must occur from the Cambrian and/or Niagaran into the Ordovician to restore a normal pressure profile. Modelling indicates it may take 1 Ma for the system to reach this equilibrium state. In any case, modelling of a variety of different scenarios has shown that the head conditions in the Niagaran and Cambrian that drive advective flow through the Ordovician have no significant effect on transport through the Ordovician because that transport is so strongly dominated by diffusion. Vertical advection through the Ordovician would have to be 1000 times greater than the equilibrium-state model predicts before advection became a significant transport mechanism. No plausible parameter variations could increase vertical advection to such a degree. In all cases, the MLE for solutes originating at the proposed DGR location is greater than 10 Ma, providing a robust demonstration that a DGR in the Cobourg can effectively isolate radionuclides for any reasonable period of concern.

The site-scale model confirmed that the choice of initial head conditions or anisotropy makes no difference in the transport of a conservative tracer through the Ordovician – that transport is dominated by diffusion. Assuming that diffusion occurs under fully water (or brine) saturated conditions, no tracer from the DGR at a relative concentration above  $10^{-7}$  reaches either the Cambrian or Niagaran in 100 ka. The maximum relative concentration reached in the Cambrian over 100 Ma is less than  $10^{-3}$ , while that in the Niagaran is slightly above  $10^{-2}$ . The presence of nearby permeable faults would not alter these conclusions. If the assumption of full water saturation is invalid, that is, if a gas phase occupies some portion of the Ordovician pore space, diffusion of solutes through the Ordovician will be even slower than shown by the site-scale model because of the phase-dependence of diffusion coefficients.

For all simulations using the DGR-4 environmental head profile to define initial conditions, the site-scale model showed that a downward gradient from the Niagaran to the Ordovician persisted for over 300 ka. The pressure and related water deficit in the Ordovician was met by approximately 1 Ma. Steady-state pressures were reached by 3 Ma with an upward gradient developing from the Cambrian to the surface, consistent with the results of the regional-scale base-case model.

The paleoclimate scenarios showed that glaciation would affect heads only in the Silurian and Upper Ordovician. None of the paleoclimate scenarios produced Upper and Middle Ordovician underpressures like those observed at DGR-4, nor could any reasonable parameter variations. Thus, the Ordovician underpressures that are observed do not appear to be the result of glacial loading and unloading. None of the alternative scenarios showed recharge water penetrating below the Upper Salina, or a different distribution of TDS in the system from the base-case

scenario. Diffusion remained the dominant transport mechanism in the Ordovician in all scenarios.

The Michigan Basin cross-section model showed that Cambrian overpressures result from the spatial distribution of fluid density and the geometry of the various stratigraphic layers in the Michigan Basin.

The 1D two-phase modelling shows that water-phase underpressures, such as those observed in the Ordovician rock in the DGR boreholes, can be caused by the presence of a gas phase. The modelling shows that water pressure is sensitive to the rock-dependent capillary pressure versus saturation relationships, and that gas saturations should not be expected to be continuous but may vary significantly throughout the rock column. The most significant effect of a separate gas phase is to reduce the rate of diffusion through the Ordovician, further contributing to the safety of the DGR.

## 5.5 Summary

The hydrogeologic studies described in this chapter have provided evidence to support the three hypotheses related to the suitability of the Bruce nuclear site to host a DGR described in Section 5.1.

- **Multiple Natural Barriers:** multiple low permeability bedrock formations enclose and overlie the DGR.
- **Solute Transport is Diffusion-dominated:** deep groundwater regime is ancient showing no evidence of glacial perturbation or cross-formational flow.
- **Shallow Groundwater Resources Are Isolated:** near surface groundwater aquifers are isolated from the deep saline groundwater system.

Lines of evidence supporting each of the hypotheses are summarized below.

Evidence that multiple low-permeability bedrock formations enclose and overlie the DGR comes from both direct measurements and inferences from modelling.

- The Cobourg host formation has very low hydraulic conductivity ( $\sim 10^{-15}$  to  $10^{-14}$  m/s) and is the primary barrier to the migration of radionuclides from the repository.
- There are 200 m of low hydraulic conductivity ( $10^{-14}$  m/s) Ordovician shale above the repository. These rocks are demonstrated cap rocks to long-lived hydrocarbon traps in both the Michigan and Appalachian basins.
- There are ten low hydraulic conductivity ( $< 10^{-12}$  m/s) layers within the Silurian sequence above the Ordovician shales.
- There are 150 m of low hydraulic conductivity ( $10^{-14}$  to  $10^{-11}$  m/s) limestones and dolostones below the repository horizon.
- Cambrian environmental heads 165 m above ground surface can only persist if the Cambrian is overlain by low-permeability strata.
- Underpressures observed in the Ordovician strata could not have developed, and would not persist, if permeabilities were not low.
- Environmental isotope and other solute profiles observed in the Ordovician are inconsistent with a system in which significant advective vertical transport is occurring. For the profiles to exist today, diffusion must be the dominant transport mechanism.

Evidence that the deep groundwater regime is ancient, showing no evidence of cross-formational flow or glacial perturbation, is listed below.

- Hydraulic testing of the Cobourg Formation (DGR host rock), the overlying Ordovician shales (Georgian Bay, Blue Mountain and Queenston formations), and underlying Ordovician limestones and dolostones (Sherman Fall, Kirkfield, Coboconk, and Gull River formations) shows that hydraulic conductivities are sufficiently low that transport would be dominated by diffusion.
- Péclet numbers from all model simulations indicate that diffusion is the dominant transport mechanism. Vertical advection would have to increase by three orders of magnitude to become a significant transport mechanism; the increase in vertical hydraulic conductivity that this would require is inconsistent with measured values and with the observed present-day heads.
- Model simulations show that changes to Cambrian and Niagaran boundary conditions, or the presence of high-conductivity fracture zones connecting those units, do not alter the dominance of diffusion as the principal transport mechanism in the Ordovician.
- Low heads in the Ordovician can only be supported by low-permeability bounding rocks.
- Under large hydraulic gradients in the Ordovician shales and limestones, hydrochemical evidence does not suggest advective transport; transport processes are dominated by diffusion.
- No geochemical evidence has been found of glacial meltwater or recent meteoric water infiltration to depth below the Salina A1 upper carbonate.
- Dense brines at depth cannot be displaced by freshwater under physically possible gradients, leading to virtually stagnant flow conditions.

Evidence that near-surface groundwater aquifers are isolated from the deep saline groundwater system is listed below.

- Regionally, the hydrogeochemistry of the Michigan Basin defines two distinct groundwater regimes: i) a shallow bedrock system at depths above 200 m; and ii) an intermediate to deep saline system characterized by elevated TDS (> 200 g/L), with distinctly different isotopic signatures.
- The shallow groundwater system is underlain by a Silurian sequence containing ten low hydraulic conductivity ( $< 10^{-12}$  m/s) layers.
- Observed abnormal hydraulic heads and vertical gradients in the Ordovician and Silurian sediments at the Bruce nuclear site strongly suggest that significant vertical connectivity across bedrock aquitards/aquicludes does not exist.
- The persistence of low hydraulic heads in the Ordovician and high heads in the Cambrian indicates that they are not interconnected by conductive vertical features.
- Hydraulic testing of sub-vertical fractures in angled boreholes demonstrates low permeabilities similar to those observed in vertical boreholes.
- Groundwater and porewater isotopic and chemical signatures (e.g., salinity) indicate that glacial meltwater did not infiltrate to depth below the Salina A1 upper carbonate (Silurian) during the latter half of the Pleistocene.



## 6. FUTURE EVOLUTION OF THE BRUCE NUCLEAR SITE

### 6.1 Introduction

This section examines the future evolution of the DGR at timeframes relevant to demonstrating DGR performance and safety. For the purposes of this assessment a focus has been placed on time scales out to 1 Ma, although some information can be extrapolated beyond this period. The operational life of the DGR is nominally 100 a, and over this period of time, access (shafts) and below-ground facilities have to remain stable to allow for facility operations and closure procedures. Repository evolution following closure is evaluated as part of the DGR safety case. Two broad categories of disturbance to the DGR might influence its long-term performance (Figure 6.1):

- Long-term natural processes such as climate change, erosion, and seismicity; and
- Repository-induced disturbances to existing natural systems, which include geomechanical responses to shaft and repository construction, as well as, generation of gas within the repository.

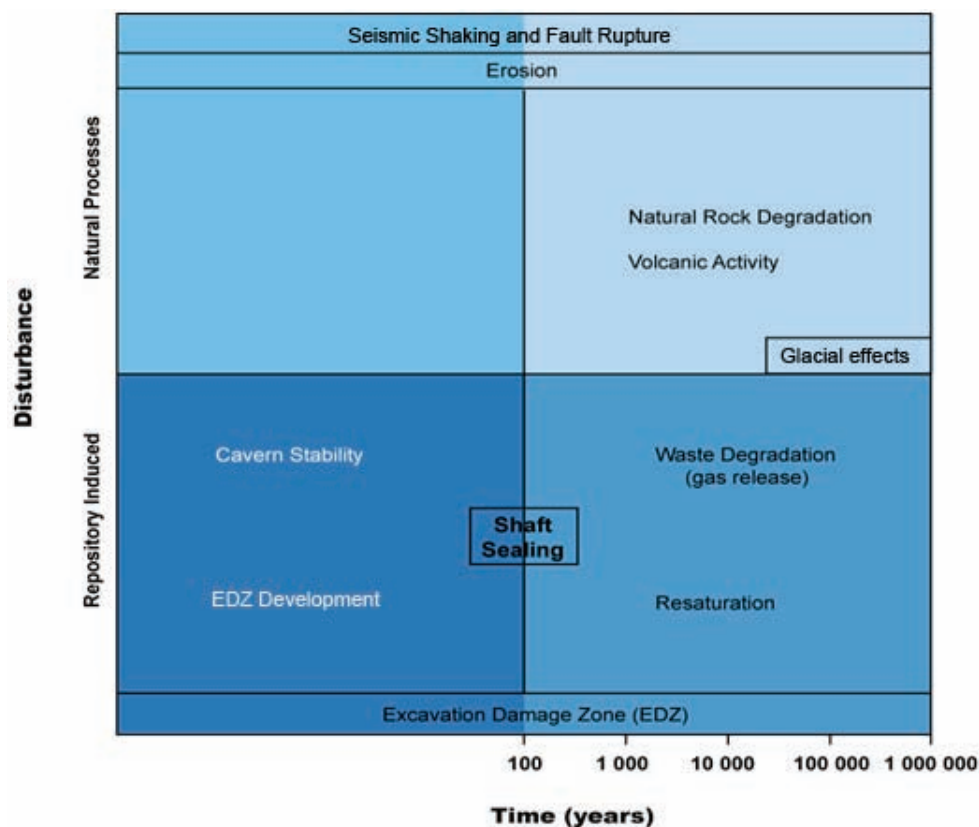


Figure 6.1: Factors Influencing the Future Evolution of the DGR

The various processes that might affect the evolution of the site are discussed below, followed by a description of the modelling studies undertaken to evaluate the effects of these processes on the performance of the DGR.

## **6.2 Long-term Natural Evolution**

Natural processes that might affect the performance of the DGR were they to occur at the Bruce nuclear site include climate change (specifically glaciation) and geologic processes such as glacial erosion, seismicity, fault rupture/reactivation and volcanism. The probability and likely effects of each of these processes are discussed below.

### **6.2.1 Climate Change (Glaciation)**

Over a 1 Ma period, climate change can have a profound effect on the environment hosting the DGR. Climate change is a natural phenomenon that has been shown to occur over geologic time (Peltier 2011). More recently, accelerated climate change has been shown to be forced by anthropogenic effects, specifically increase in carbon dioxide levels in the atmosphere from combustion of fossil fuels. For the next century of Earth history, as described most recently in the Fourth Assessment Report of the Intergovernmental Panel on Climate Change (IPCC 2007), the Earth system is committed to considerable warming of its mean surface temperature as a consequence of increasing greenhouse gas concentrations. Steps taken today to reduce greenhouse gas emissions will not see meaningful results for decades to come. If the CO<sub>2</sub> levels are not reduced, then the onset of the next glacial cycle could be delayed.

Over the past million years of Earth history, climate variability has been dominated by the cyclic expansion of northern hemisphere land ice cover. Southern Ontario is located near what was the southern edge of the Laurentide ice sheet during its sequence of Late Quaternary expansions (e.g., Peltier 2011). Nine glacial cycles occurred over the past million years. The recurrent sequence of glaciation events during the Late Quaternary period is now widely understood to be caused by the so-called "Milankovitch effect". Small changes in effective solar insolation caused by the changing geometry of Earth's orbit around the Sun are highly significant and have been such as to induce continental-scale glaciation events to recur on a timescale of approximately 100 ka. In each such glacial cycle, the glaciation phase has lasted approximately 90 ka and the deglaciation phase approximately 10 ka.

If a reglaciation of the Canadian land mass should occur again in the future, such an event is most likely to begin approximately 60 ka from present (Peltier 2011). If at that time the concentration of carbon dioxide and other greenhouse gases in the atmosphere were similar to the present concentration, it is unlikely that a renewed episode of glaciation could occur. Since our ability to predict the CO<sub>2</sub> level that will exist at a time so far into the future is negligible, we cannot discount the possibility of a renewed glacial event and must therefore take it into account when developing the safety case for a L&ILW repository.

The numerous characteristics of the glaciation process that are relevant to the understanding of repository performance include erosion related to ice-sheet movement across the land surface and mechanical properties such as the time dependence of the thickness of glacial ice that could develop over the site and the normal stress regime associated with the weight of this load. Similarly relevant is the evolution of the temperature at the base of the ice sheet, a characteristic of the glaciation process that turns out to be somewhat counterintuitive, as times of thickest ice cover are associated with the warmest basal temperatures, a consequence of the degree of thermal insulation provided by thick ice and the continuing flow of heat from the

Earth's interior into the ice-sheet base. The subsurface thermal regime is also important to repository performance, in particular the depth to which frozen ground (permafrost) may extend when the surface temperature is below freezing. This issue is important not only in the regions that are episodically ice-covered but also in exterior regions where the influence of permafrost may be even more extreme. In regions within which the base of the ice sheet is temperate, i.e., having temperatures above the freezing point, meltwater is continually generated by the outflow of geothermal heat and the rate of such generation is crucial to understanding the extent to which such meltwater may be forced to infiltrate into the subsurface and thus impact subsurface hydrology. The final process considered in Peltier's analysis (Peltier 2011) is the time dependence of the depression and uplift of the crust at the location of the Bruce nuclear site. Such vertical motions are due to the process of glacial isostatic adjustment (GIA) that involves the viscoelastic response of the Earth to the time-dependent surface mass load associated with the glaciation and deglaciation process.

These phenomena associated with glaciation that have the potential to affect the DGR and/or the geologic setting at the Bruce nuclear site can be grouped into three broad categories: glacial erosion, glacial loading and permafrost formation. These are discussed under the headings below.

#### **6.2.1.1 Glacial Erosion**

Glacial activity will be the primary process over the next million years leading to erosion of the existing geologic sequence. Glacially induced erosion can occur by abrasion, quarrying, and mechanical erosion by meltwater. Regardless of the erosion mechanism, the rate of erosion can be limited by the ability of meltwater to evacuate debris. Such evacuation is possible until water and sediment can no longer be removed due either to an insufficient hydraulic head gradient or the lack of adequate subglacial pathways for water.

To evaluate the glacial erosion that might occur in the future, Hallet (2011) combined information on past erosion rates with predictions of future glaciations made using the University of Toronto Glacial Systems Model (Peltier 2011). The model defines the expected duration of ice cover and temperate basal conditions, and the rate of basal melting, which is expected to control erosion rates (Section 2.2.7.2). Taking into account diverse geologic evidence, the present topography and bathymetry that reflect only modest preferential erosion, the spatial distribution of glacial sediments, and results of two independent computer models, Hallet (2011) estimated that a future glacial advance similar in characteristics to the Laurentide Ice Sheet (LIS) at the Last Glacial Maximum (LGM) would likely result in less than 30 m of erosion over the Bruce Peninsula. On a 1 Ma time scale with multiple glacial advances, estimates of erosion range from a few metres to ~200 m, although no erosion and net deposition of sediments is also possible. Hallet (2011) concludes that "In view of the absence of topographic features or other known factors that would tend to localize erosion by ice or water over the Bruce nuclear site, and the absence of evidence of preferential past erosion over the site, a more realistic but still quite conservative site-specific estimate is 100 m for 1 Ma."

Thus, glacial erosion is not expected to affect the DGR at a depth of 680 m. More details on erosion are provided in Section 2.2.7.2 and in Hallet (2011).

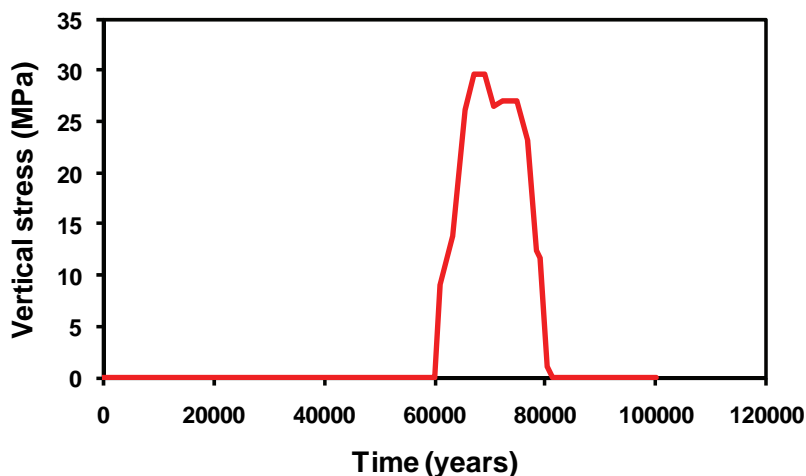
#### **6.2.1.2 Glacial Loading**

As indicated above, the onset of the next glacial event will likely be 60 ka into the future assuming atmospheric CO<sub>2</sub> levels are reduced to about 280 ppmv (Peltier 2011). Climate

modelling of the late Quaternary ice advances and retreats has predicted ice thicknesses of up to 4 km over northern Canada and approaching 2.5 km in southern Ontario. This mass of ice significantly increased the normal stress as it moved across the proposed DGR site. Such movement resulted in loading and unloading cycles on the underlying rock with every major glacial advance and retreat.

Peltier (2011) has shown that the maximum crustal depressions from the equilibrium level occur at LGM and reach values in excess of 500 m. After the ice retreated, the earth's surface has rebounded. This process is known as isostasy and is still occurring today. In the Great Lakes area, the continental isostasy contour represents zero with increasing uplift to the north of about 1.5 mm/a and subsidence to the south at about the same rate, thus indicating that the continent is tilting slightly upward in the north (Peltier 2011).

The UofT GSM, which is a model of continental-scale glaciation events, was used by Peltier (2011) to develop a description of glaciation of the Canadian Shield as a means of assessing the impact that such an event would have on performance of the DGR. A maximum glacial event time profile for ice loading was developed based on Peltier (2011) as shown in Figure 6.2 and shows that the vertical stress reached a maximum value of approximately 30 MPa.



Notes: Time from present is for first event.

**Figure 6.2: Simulated Evolution of Ice Sheet Load**

In addition to changing the vertical stress at depth, glaciation can also cause the horizontal stress to increase due to both Poisson's effect and plate bending. The horizontal stress increase due to Poisson's effect is:

$$\Delta\sigma_h = \frac{\nu}{1-\nu} \Delta\sigma_v \quad (6.1)$$

The increase in the horizontal stress due to plate bending is also proportional to the increase in vertical stress, with the maximum increase assumed to be 2 MPa. Glacially induced shear

stresses, which typically occur close to the ground surface along the glacial margins, were not considered in the analyses because detailed numerical analyses carried out by Lund et al. (2009) showed that these shear stresses are relatively minor compared to the vertical and horizontal normal stresses.

Modelling of the effects of the stress changes associated with glacial advance and retreat described above on the DGR is described in Section 6.4.

### **6.2.1.3 Permafrost Formation (Changes in Groundwater Recharge)**

Permafrost formation during a cycle of glacial advance and retreat is a determinant of the extent to which water generated by the melting of a continental-scale ice sheet may infiltrate the subsurface. The present-day depth and distribution of permafrost across polar regions is a reflection of the history, as well as, the present characteristics of surface thermodynamic forcing (Peltier 2011). Model-based analyses that employ 3D thermo-mechanically coupled ice-sheet models and constrained climate chronologies offer a means of analyzing and predicting past and present subsurface temperature fields and, thus, permafrost depth. Modelling has shown that permafrost at the Bruce nuclear site seldom reached more than 60 m depth (Peltier 2011). Most notable was the absence of permafrost at the last glacial maximum (25 ka) due to the fact that the thick ice sheet trapped the warmth generated by the solid Earth.

Glacial meltwater beneath continental ice sheets can be pressurized to achieve freshwater hydraulic heads far in excess of ambient heads during interglacial periods. These conditions have been effective in causing recharge of glacial meltwater to depths of several hundred metres in Paleozoic aquifers around the periphery of the Illinois and Michigan basins (McIntosh and Walter 2005, 2006, Person et al. 2007).

Isotopic evidence indicates that glacial meltwater has entered only the Devonian and Upper Silurian formations above the Salina F Unit shale (~180 mBGS) at the Bruce nuclear site (Section 4.4.1.3). The meltwater may have penetrated these shallow units by local infiltration, but the low permeability of the Salina F and deeper Salina units provides a barrier to further infiltration of glacial meltwater. The deeper (~327 mBGS) Salina Upper A1 Unit aquifer also shows isotopic evidence of glacial meltwater penetration, but this is more likely related to recharge occurring where the A1 Unit outcrops (or subcrops under glacial drift) than to vertical percolation from the land surface at the Bruce nuclear site.

Hydrogeological modelling was completed for the Laurentide glacial episode (120 to 10 ka) to assess the depth of penetration of glacial waters into the underlying formations (Section 5.4.6). The two most important factors to be considered are permafrost depth and stress changes developed from the ice load. Simply put, when permafrost exists, it inhibits flow to depth created by the high environmental head imposed by the ice sheet, whereas if the glacier is warm-bottomed, i.e., no permafrost, then enhanced recharge can occur.

Results presented in Section 5.4.6 suggest that neither the presence nor the lack of permafrost below a glacier overlying the study area would impact or alter the intermediate to deep hydrogeologic system. These results combined with other evidence support the conclusion that the DGR is unlikely to be affected by changes in groundwater recharge during a glacial event.

## 6.2.2 Geologic Disturbances

Natural geologic evolution of landmasses takes place over many millions or even billions of years. The last major orogeny to occur with effects in southern Ontario was the Alleghenian Orogeny some 250 Ma ago. Since that time, southern Ontario has been tectonically stable with only mass wasting and glacial processes taking place. This section deals with the following three natural processes that may affect the DGR over the next million years: seismicity, fault rupture/reactivation, and volcanism.

### 6.2.2.1 Seismicity and Seismic Hazard Assessment

Southwestern Ontario and the Bruce region lie within the tectonically stable interior of the North American continent; a region characterized by low rates of seismicity. Most recorded seismic events have magnitudes less than 5. A detailed description of the regional seismicity is presented in Section 2.2.6.5. In general, earthquakes in stable interior regions, such as the Bruce region, occur at depths of 5 to 20 km, on faults formed hundreds of millions of years ago during previous active tectonic episodes. For 76 events in eastern Ontario and western Quebec (Ma and Atkinson 2006) with known focal depth, the average depth is 7 km. The depth distribution is as follows:

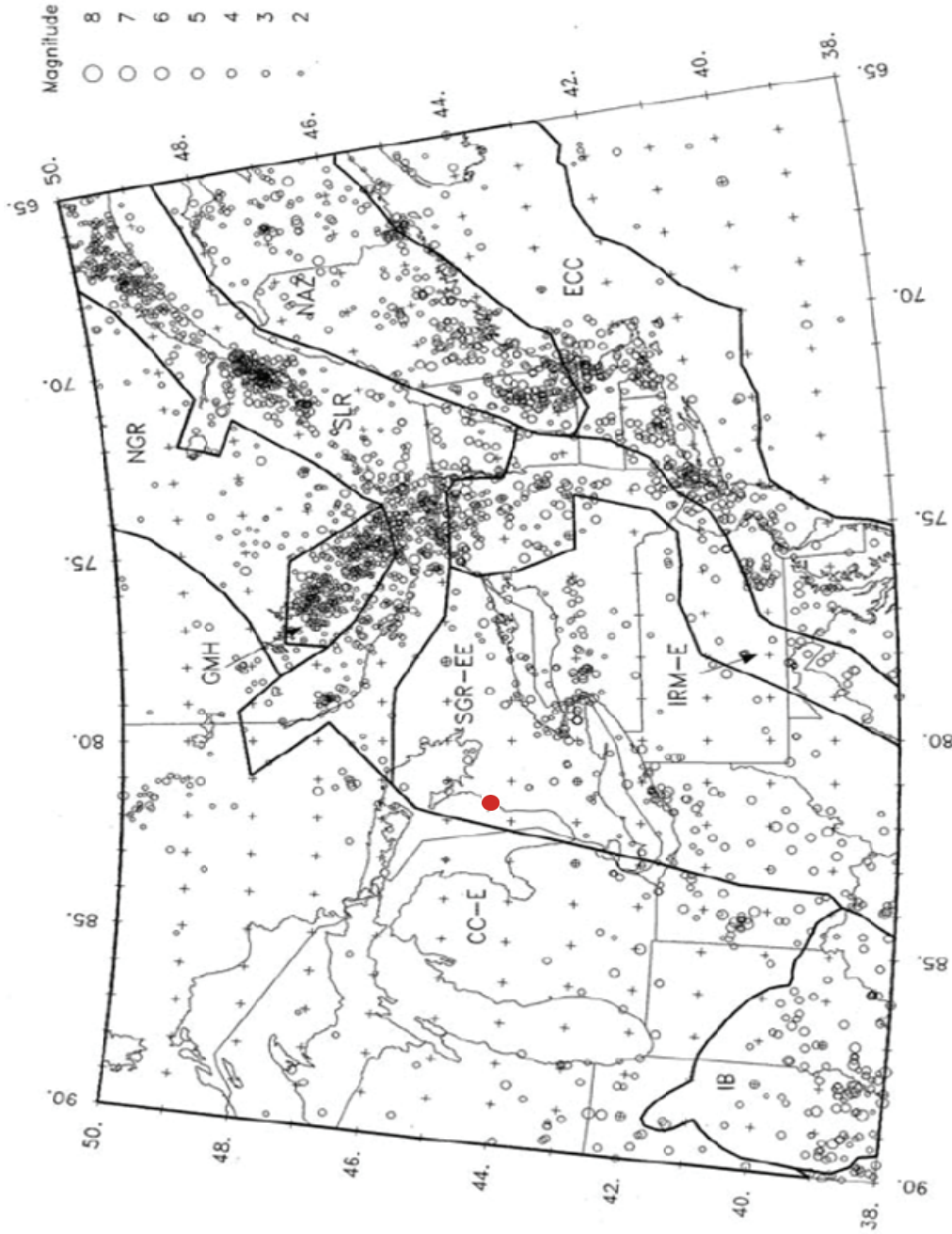
- 38% of the events occurred at depths less than 5 km;
- 43% occurred in the depth range from 5 to 10 km;
- 16% were at depths of 10 to 15 km; and
- 2% were at depths of 15 to 20 km.

Based on the lack of seismic activity in the Bruce region and no appreciable concentrations of activity that might indicate regional seismogenic features or active faults (INTERA 2011), an assessment of earthquake ground shaking hazards, in which an evaluation is made of the earthquake ground motions that could occur during the design/service life of the repository, was conducted (AMEC GEOMATRIX 2011). The proposed repository would be designed to withstand the effects of very rare events to provide adequate protection for the public and the environment, including the occurrence of strong earthquake ground shaking at the site. A probabilistic seismic hazard assessment (PSHA) approach was selected incorporating uncertainties in the models and parameters that affect seismic hazard. A landmark report by the Senior Seismic Hazard Advisory Committee (SSHAC 1997) provides guidance on conducting a PSHA with the goal of capturing the knowledge of the informed scientific community regarding the inputs to the analysis. In the PSHA for the repository, the interpretations of the larger scientific community were incorporated through a review of the available literature, combined with correspondence with researchers to obtain unpublished data and observations (a SSHAC Level 2 process). The study for the Bruce nuclear site builds on the 1997 PSHA sponsored by the Atomic Energy Control Board to characterize seismic hazards in southern Ontario (Geomatrix 1997) and on a recent PSHA conducted for the region surrounding the Darlington nuclear site for OPG (Youngs 2009).

In the present PSHA (AMEC GEOMATRIX 2011), seismic sources are used to model the occurrence of future earthquakes that may affect a site. Seismic source characterization provides a probabilistic model for the rate of occurrence, spatial distribution, and size distribution of earthquakes within the region surrounding the site. A primary data set that is used to develop this probabilistic model is the catalogue of regional earthquakes. The

catalogue is limited by the duration of the sample (a few hundred years), and imperfect recording of past events, particularly in the period before the development of modern seismic monitoring networks. Thus, interpretations of other data guided by scientific knowledge of the earthquake process is used to extend the earthquake catalogue data to model the occurrence of potentially damaging earthquakes in the site region. To do so, alternative models for the spatial distribution of future earthquakes are constructed based on interpretations of regions of the earth's crust that have homogeneous properties. These regions represent seismic sources in a PSHA.

A seismic source characterization model was developed that characterises all seismic sources that could be of significance to the hazard at the Bruce nuclear site. Three alternative approaches were used to define the models for the spatial distribution of future seismicity: (1) seismic source zones based primarily on geologic and tectonic bases; (2) seismic source zones that enclose zones of elevated seismicity; and (3) a zoneless approach based on smoothing the observed seismicity without imposed source zone boundaries. Figure 6.3 presents one of the twenty-six alternative regional seismic source zone models used to assess seismic hazard in the repository PSHA. Alternative source zone boundaries were used in the hazard model to examine the influence of different zone boundary configurations on the hazard calculation. In addition to the regional source zones, a number of local geologic features near the site, such as the Grenville Front Tectonic Zone and the Georgian Bay Linear Zone, were considered as potential seismic sources. A key uncertainty in the assessment of local seismic sources is whether or not they are seismogenic, defined as active and capable of generating moderate-to-large earthquakes. A list of the local source zones considered and the weights assigned to the criteria used to evaluate the probability of activity of each source is provided in Table 6.1 below. A detailed description of each of the seismic sources used in the PSHA is documented in AMEC GEOMATRIX (2011).



Notes: Bruce nuclear site location is indicated by red dot. Seismic zone abbreviations include: CC – Central Craton, ECC – Extended Continental Crust, GMH – Great Meteor Hotspot, IRMa – Irapetian Rifted Margin, NAZ – Northern Appalachians, NGR – Northern Grenville, OG – Ottawa Graben, SG – Saguway Graben, SGRa – Southern Grenville. Figure is from AMEC GEOMATRIX (2011).

**Figure 6.3: Regional Source Zone Boundaries and Seismic Events used for the Probabilistic Seismic Hazard Assessment**



**Table 6.1: Seismic Zones and Their Seismogenic Probability**

Seismic Source Zone	Association with $M_N \geq 5$ Seismicity	Association with $2 \leq M_N < 5$ Seismicity	Evidence of Reactivation	Slip Favourable W/ Present Stress Regime	Seismogenic Crustal Extent	Probability of being Seismogenic
Grenville Front Tectonic Zone (GFTZ)	0	0	0.2	0.1	1.0	--
Georgian Bay Linear Zone (GBLZ) <sup>1</sup>	0	0.1	0.1	0.1	0.1	--
Georgian Bay Linear Zone (GBLZ) <sup>2</sup>	0.1	0.1	0.1	0.1	0.1	<b>0.12</b>
Niagara-Pickering Linear Zone <sup>3</sup>	0	0.1	0.5	0.2	1.0	<b>0.08</b>
Niagara-Pickering Linear Zone <sup>4</sup>	0.2	0.25	0.5	0.2	1.0	<b>0.30</b>
Wilson-Port Hope magnetic Lineament	0	0.1	0.4	0.1	0.2	<b>0.06</b>
Hamilton-Presqu'ile Lineament	0	0.15	0.2	0.1	0.5	<b>0.08</b>
Clarendon-Linden Fault System	0.1	0.25	1.0	0.1	0.6	<b>0.25</b>
Mississauga Magnetic Domain Seismic Zone	0	0.3	0.4	0.1	0.9	<b>0.16</b>

Notes: 1 - Assuming truncation at the Niagara-Pickering Lineament, 2 - Assuming extension into New York State, 3 - Assuming no association with the Akron magnetic lineament and 4 - Assuming an association with the Akron magnetic lineament. Data are from AMEC GEOMATRIX (2011).

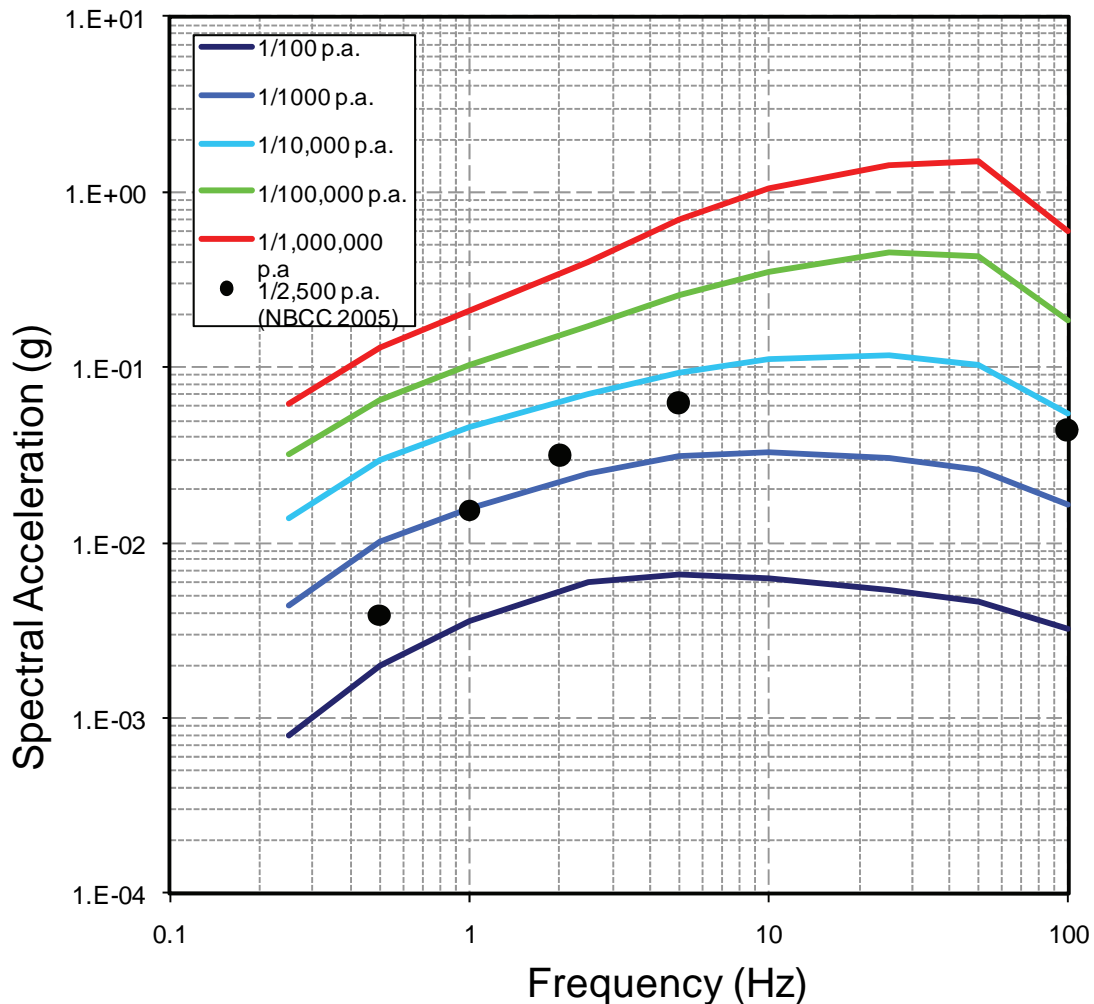
Figure 6.4 shows the uniform hazard response spectra for horizontal ground motions at the Bruce nuclear site with 5% damping coefficient. These curves express annual probability of exceedance as a function of spectral acceleration on a hard rock surface, derived from the mean hazard curve from the weighted average result for all of the alternative models used in the PSHA calculation.

Based on the results of the PSHA performed for the Bruce nuclear site, the estimated surface bedrock peak ground accelerations (PGA) inferred from Figure 6.4 are expected to be less than 70 %g for probabilities of  $10^{-5}$  per annum (1/100,000 p.a.) for the reference case and  $10^{-6}$  per annum for an extreme scenario (AMEC GEOMATRIX 2011). The PGAs for events of different probabilities of exceedance obtained from the PSHA are summarized in Table 6.2.

Table 6.2 also presents the PGA of a  $4 \times 10^{-3}$  (1/2500) per annum probability of exceedance from the study and that defined in the 2005 National Building Code of Canada (NBCC 2005).

The PSHA results reveal typical seismic hazard estimates in central and eastern North America (CENA) where a wide confidence band reflects the large uncertainties in most input parameters. Similar to that of other CENA regions, the results also show skewed frequency of exceedance distribution where skewness increases with increasing seismic intensity. The assessment reveals the regional sources are the dominant contributors to the hazard for both high and low

frequencies at ground level. The contribution of individual assessments to the uncertainty for various components in the seismic hazard computation was also examined. The results indicated that uncertainty in the ground motion attenuation models is the largest contributor to the PSHA uncertainty. Other significant sources of uncertainty are: the regional seismotectonic source spatial distribution models, the maximum magnitude assessments, and the estimation of the b-value of the Gutenberg-Richter magnitude-frequency relationship.



Notes: Curves are colour coded for probabilities ranging from 1/100 to 1/1,000,000 per annum (p.a.). Black dots show National Building Code of Canada (NBCC 2005) model results at 1/2500 p.a. Figure is from AMEC GEOMATRIX (2011).

**Figure 6.4: Uniform Seismic Spectra for Surface Ground Motions on Hard Rock at the Bruce Nuclear Site**

To develop the seismic response spectra for the Bruce nuclear site, a two part approach was employed. The first part involved performing a PSHA using regional seismic sources identified

in Table 6.1 and alternative ground motion models that represent the ground motions for a reference hard rock site condition (results briefly described above). The second part utilized the dynamic properties obtained from the site characterization investigation to develop site hazard responses specifically for the repository horizon. According to the Electric Power Research Institute (EPRI) ground motion intensity at depth is less severe than that at the ground surface, due to surface ground motion amplification (EPRI 1994). Also, case histories of tunnels subjected to earthquakes have shown that underground structures are less susceptible to damage (Power et al. 1998; Backblöm and Munier 2002). Recent seismic monitoring at different mine levels to 2 km depth at the Sudbury Neutrino Observatory reveals that the relationship between underground and surface motions is complex, with the ratio of surface/underground motions a frequency-dependent function that depends on the type of earthquake and the depth of the underground emplacement room. Measurements for near-field shallow earthquakes also indicate strong surface wave peak at about 2 Hz with an amplification factor between surface motion and those underground exceeding 2 (Atkinson and Kraeva 2010).

**Table 6.2: Summary of Seismic Hazard Analysis Results**

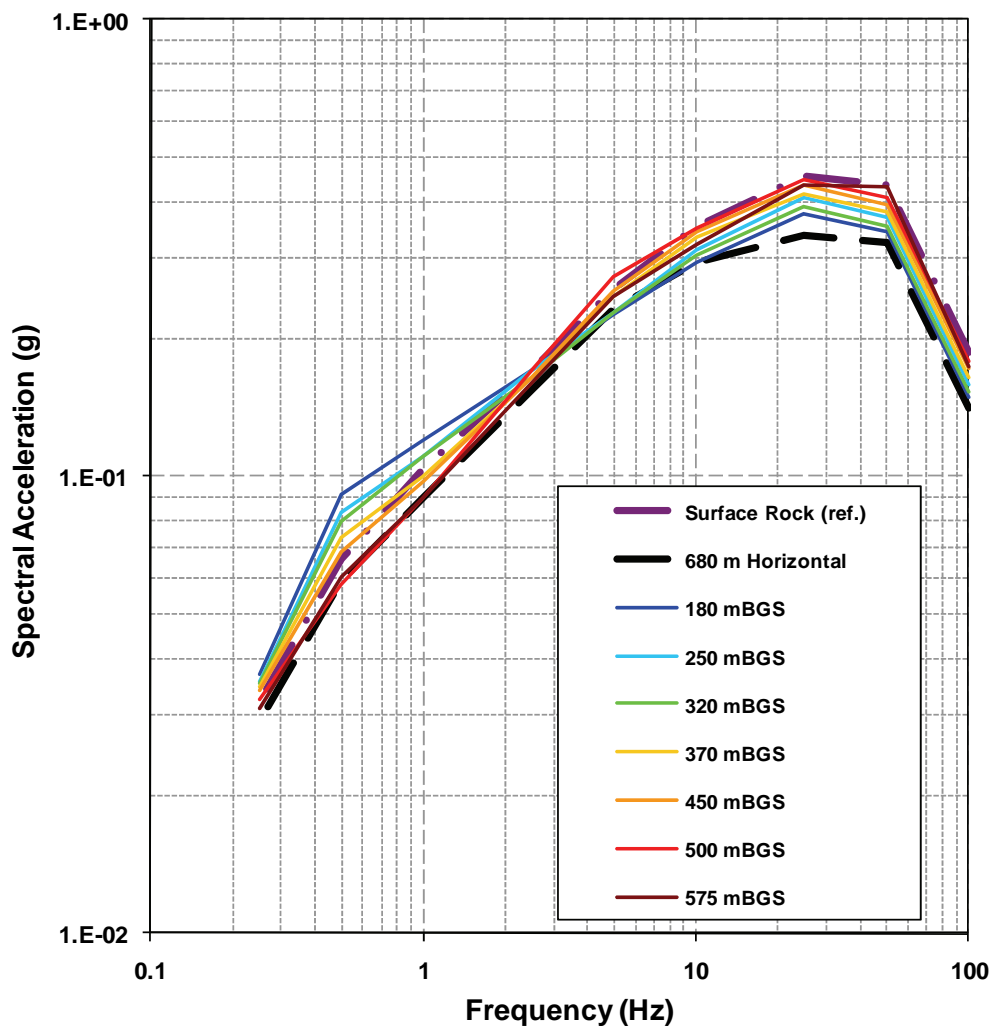
<b>Event (Prob. of exceed. p.a)</b>	<b>Peak Ground Accel. (%g)</b>
1/1000	1.7
1/2500 (NBCC 2005)	4.4
1/100,000	18.7
1/1,000,000	60.1

Notes: Data are from National Building Code of Canada (NBCC 2005) and AMEC GEOMATRIX (2011).

In the current analysis, the ground response at the repository horizon and at various depths of interest were computed by integrating the surface hazard curve with the probability distribution of the transfer function defining the ground motion at depth to that at ground surface. Figure 6.5 and Figure 6.6 show the mean seismic response spectra of horizontal and vertical ground motion components with probabilities of exceedance of  $10^{-5}$  and  $10^{-6}$  Pa at various horizons down to the repository invert at 680 mBGS. These spectra show response reduction due to surface effect. Orthogonal time series of the ground motion were generated to simulate high-, medium-, and low-frequency scenario events for the repository level and selected horizons along the access shafts. The high-frequency scenario event represents small close earthquakes. The low-frequency scenario represents large distant earthquakes and the intermediate-frequency scenario represents earthquakes of intermediate magnitude and distance. All three scenario events are required to cover the entire frequency range for the long-term stability analysis described in Sections 6.4.2 and 6.4.3.

In the long-term, renewed glaciations could impose significant environmental change during the DGR life span period. An ice sheet advancing over the DGR would have a modulation of the seismicity. During this period, seismicity would be initially suppressed due to surcharge loading from the ice sheet, and later enhanced while unloading during the retreat of the ice sheet. The seismicity rate could temporarily increase due to changes in ground stress (Adams 1989, Hora and Jensen 2005). Based on the lack of neotectonic deformation or evidence for faulting

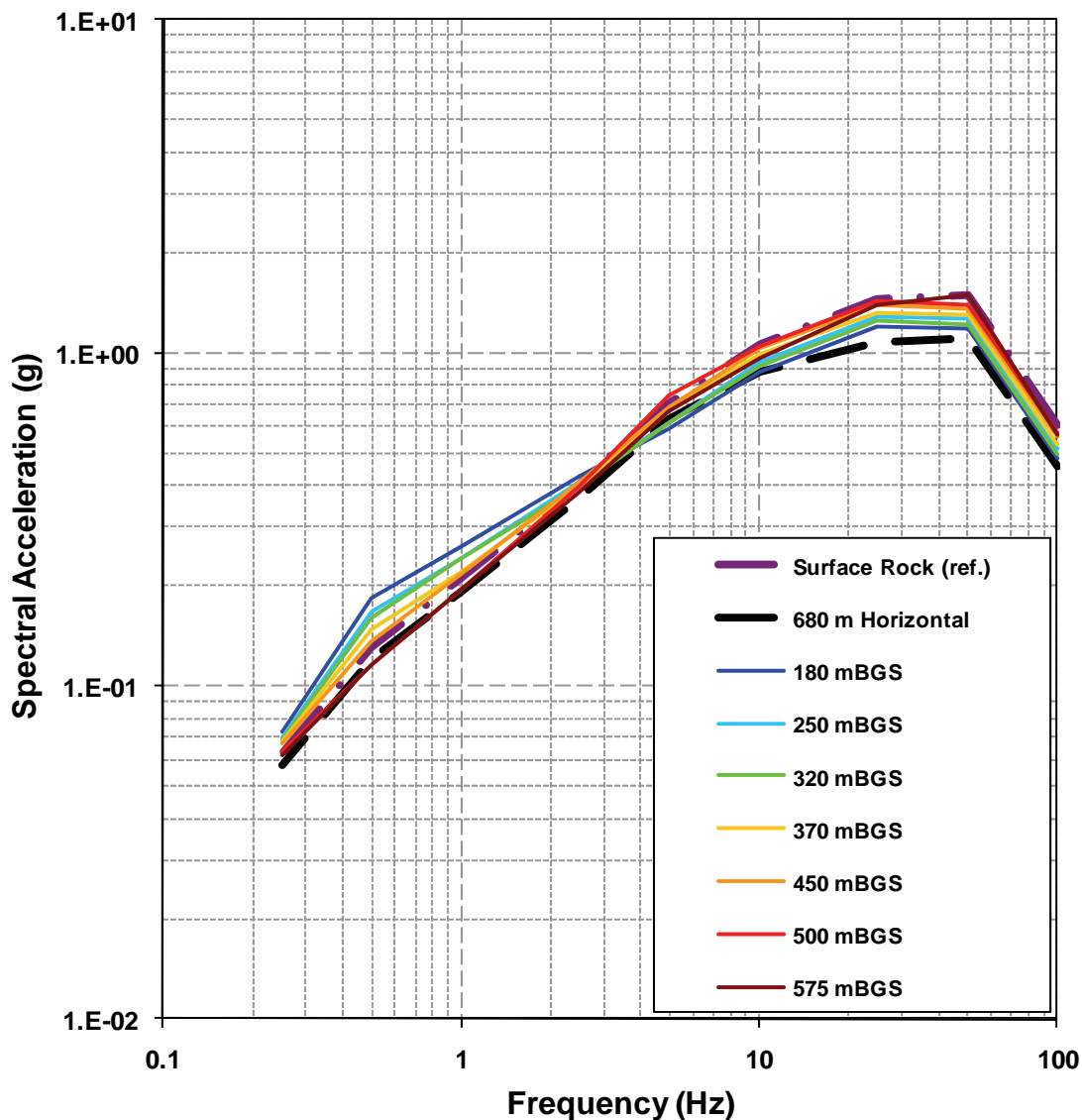
proximal to the site (Cruden 2011, INTERA 2011, Slattery 2011), and the lack of evidence for cross formational mixing of groundwater beneath the site, the seismic events induced by past glacial activities are not considered to have been significant.



Notes: Represents probability of exceedance at horizons between ground surface and repository nominal invert at 680 mBGS. Figure modified from AMEC GEOMATRIX (2011).

**Figure 6.5: Total Mean Seismic Response Spectra of Horizontal Ground Motion Components with Probabilities of Exceedance of  $10^{-5}$  per annum**

There are two potential effects of seismic activity on deep repositories, namely, emplacement room instability as results of seismic shaking and reactivation of a nearby fault. Modelling of the effects of seismic shaking on the DGR is described in Section 6.4. The treatment of rupture due to fault reactivation is discussed in Section 6.2.2.1.



Notes: Represents probabilities of exceedance at horizons between ground surface and repository nominal invert at 680 mBGS. Figure modified from AMEC GEOMATRIX (2011).

**Figure 6.6: Total Mean Seismic Response Spectra of Horizontal Ground Motion Components with Probabilities of Exceedance of  $10^{-6}$  per annum**

### 6.2.2.1 Fault Rupture and Reactivation

Fault rupture or reactivation is a concern as it may compromise the isolation potential of the repository for the migration of radioactive waste degradation products. Findings from existing seismic information, a neotectonic investigation of Quaternary sediments, structural surface bedrock mapping, micro-seismic monitoring, and the impact of glaciation were reviewed and assessed to provide an understanding of the likelihood of fault rupture and reactivation at the

Bruce nuclear site. The following evidence argues against any significant effect on DGR performance due to fault rupture or reactivation.

Based on existing seismic information, the likelihood of fault rupture is extremely low, as it would require a moderate-to-large event to occur right at the repository site, with rupture to shallow depths. Furthermore, since the repository is sited in an area where no faults have been observed, it would require earthquake faulting to propagate into previously unfaulted rock. Most earthquakes in the region are deep and occur on pre-existing basement faults and are very rare in this area. There are no known seismic events in the region with a focal depth in the Paleozoic sequence.

An investigation undertaken to characterize deformation features within Quaternary landforms and soil exposures surrounding the Bruce nuclear site, concluded that none of the features observed (e.g. soft sediment disturbance and paleoliquefaction) resulted from post-glacial neotectonic activity (Slattery 2011).

No significant faults or shear zones were observed in outcrop (Cruden 2011). Consequently, in the absence of any evidence suggesting that faulting or other neotectonic deformation has occurred at or in the vicinity of the Bruce nuclear site, the likelihood of the occurrence of a fault rupture event would be very low.

A micro-seismic monitoring network was installed and commissioned in August 2007. Thus far, the results show a lack of low level seismicity (> M1.0) within the vicinity of the Bruce nuclear site, implying the absence of seismogenic structures or faults within or in close proximity to the DGR footprint.

Renewed glacial ice-sheet cycles of advance and retreat, over the DGR, may result in periods of enhanced seismic activity (6.2.2.1). Based on the lack of evidence for surface faulting (Cruden 2011), neotectonic deformation (Slattery 2011) or cross formational groundwater mixing at the site (see section 4.5), any seismic event that may have been induced by such glacial activity in the past must have occurred either deep in the Precambrian basement or was too small to disrupt the intact rock mass proximal to the Bruce nuclear site. The impact of subsequent glaciations, therefore, is unlikely to result in fault rupture within the Paleozoic rock sequence.

#### **6.2.2.2 Volcanism**

The only recognized evidence of volcanic activity at the Bruce nuclear site is ancient and in the form of a 8-10 cm thick bentonite seam interpreted as altered volcanic ash. This bentonite seam is observed at the same stratigraphic horizon, approximately 7 m below the Coboconk Formation top, in boreholes DGR-2 to DGR-4 and DGR-6 (DGR-5 drilling terminated above this ash horizon). Based on a regional correlation, this particular bentonite is one of several distinct ash layers deposited throughout the Appalachian and Michigan basins during episodic volcanic activity associated with the onset of the Taconic Orogeny on the southeastern margin of Laurentia, approximately 454 Ma (e.g. Huff et al. 1992, Kolata et al. 1998).

The majority of recognized Mesozoic magmatic activity is localized around pre-existing faults, which are presently at a considerable distance away (> 150 km) from the RSA, and the Bruce nuclear site, in particular. This includes kimberlites and other mafic intrusions within the Canadian Shield (Heaman and Kjarsgaard 2000) and the ca. 130 – 110 Ma Monteregian Hills alkaline intrusions near Montreal, Quebec (McHone and Butler 1984), which are related to

passage of an interpreted hotspot through this region (e.g., Crough 1981). Other recognized activity includes a suite of 173 Ma Middle Jurassic ultramafic dykes, which intrude Middle Ordovician strata in the Picton Quarry, Ontario (Barnett et al. 1984). A lack of active orogenic activity in southern Ontario under the currently stable tectonic regime suggests strongly that volcanic activity is not expected to influence the DGR.

### **6.3 Repository-induced Disturbances**

This section describes the repository-induced phenomena that may disturb the natural system and potentially affect the long-term stability and performance of the DGR over a 1 Ma period. It focuses on disturbances to the geological systems by the Excavation Damaged Zone (EDZ) around the two shafts and by generation of gas within the DGR after the facility is closed and sealed. Modelling of the effects of these disturbances is described in Section 6.4. The disturbances caused by site and near-surface facilities construction (e.g., drainage, dewatering) are not covered here but will be assessed as part of the Environmental Impact Statement (OPG 2011b).

#### **6.3.1 EDZ**

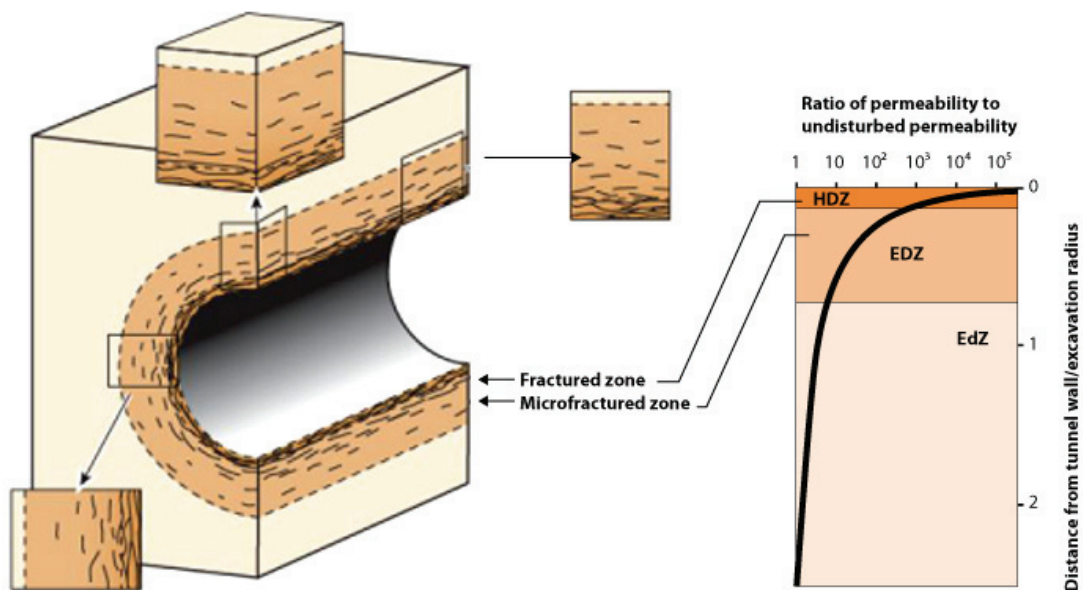
##### **6.3.1.1 Definitions and Mechanisms**

Various terminologies have been used to describe the excavation-induced damaged or disturbed zone. FRACTURE SYSTEMS (2011) expanded the excavation induced damage/disturbed definitions by Tsang and Bernier (2004) and Tsang et al. (2005) to incorporate a highly fractured zone around excavated openings. FRACTURE SYSTEMS (2011) suggested dividing the damaged/disturbed zone into three categories (Figure 6.7):

- The Highly Damaged Zone (HDZ) is a zone where macro-scale fracturing or spalling may occur. The effective permeability of this zone is determined by the interconnected fracture system and may be several orders of magnitude greater than that of the undisturbed rock mass;
- The Excavation Damaged Zone (EDZ) is a zone with hydromechanical and geochemical modifications inducing significant changes in flow and transport properties. These changes can, for example, include one or more orders of magnitude increase in permeability; and
- The Excavation Disturbed Zone (EdZ) with possible hydromechanical and geochemical modifications but without material changes in flow and transport properties.

The shape of each zone can vary significantly from that shown in Figure 6.7, depending on factors such as the shape and size of the opening, the stiffness and strength of the rock mass, and the in situ stresses (Blümling et al. 2007).

FRACTURE SYSTEMS (2011) found that regardless of the damage mechanism, the extent of the EDZ measured around underground openings is typically less than 1.5 times the radius of the openings (measured from the centre of the opening). Table 6.3 summarizes the measurements compiled by FRACTURE SYSTEMS (2011). Also tabulated in the table are the corresponding ranges of EDZ hydraulic conductivities from point measurements at each URL. These estimated hydraulic conductivities range from  $10^{-12}$  m/s to  $10^{-4}$  m/s. The EDZ geometry for the purpose of hydraulic and transport analyses is typically treated as one or more concentric zones around the excavations as illustrated in Figure 6.7.



Notes: Figure modified after ANDRA (2005).

**Figure 6.7: Schematic Illustration Defining EdZ, EDZ, and HDZ for an Unjointed Rock**

The properties within these zones strongly depend on the effective axial transmissivity of the whole system, which is controlled by factors such as the interconnectivity of individual fractures. This was illustrated using a discrete fracture network realization of the EDZ which yielded a relationship between groundwater flux and the effective axial permeability which is controlled by several factors including fracture interconnectivity (Bock et al. 2010). Blümling et al. (2007) report that although effective axial permeability measurements within the EDZ at length scales in excess of several metres have not been successful, in situ evidence indicates that such permeabilities are much lower than estimates obtained from point scale measurements.

Tsang et al. (2005) showed that the key factors that influence excavated damage zone are:

- Stress magnitude (relative to the strength of the rock);
- Stress orientation and ratio (for anisotropic stresses);
- Excavation shape;
- Excavation method; and
- Type of rock response (brittle or plastic).

Rocks that exhibit a more plastic response typically have a continuous and gradational EDZ that can be identified in modelling by the identification of yield stresses. For these plastic rocks, a well-defined HDZ is not often apparent even at very high levels of yielding. However, for rocks that display a brittle/strain-weakening response changes in volumetric strain is a good indicator of the development of the damage zone.

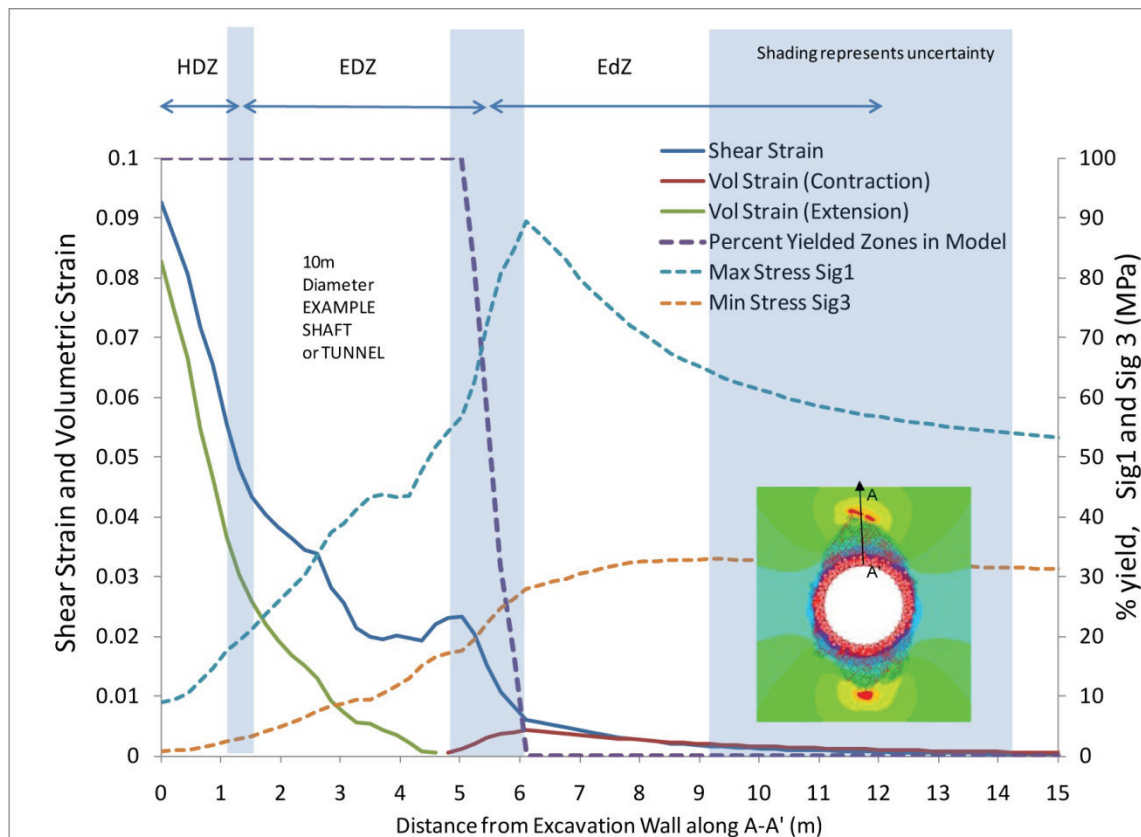


**Table 6.3: EDZ Extent and Properties Observed from Underground Excavations**

	Excavation	Method	EDZ	Host Rock Undisturbed Hydraulic Conductivity (m/s)	EDZ Hydraulic Conductivity Range (m/s)	Effective EDZ Hydraulic Conductivity (m/s)	Reference
<b>Mont Terri UCS=12 MPa</b>	HG-A	Auger		0.8-2x10 <sup>-13</sup>		Outer EDZ: K=5x10 <sup>-13</sup> m/s (K <sub>factor</sub> =5)	Lanyon et al. (2009)
	ED-B	Roadheader	2r		6x10 <sup>-12</sup> - 9x10 <sup>-9</sup>	Inner EDZ: k=10 <sup>-12</sup> m/s (K <sub>factor</sub> =10)	Martin and Lanyon (2003)
<b>Bure</b>	Shaft	Drill & blast	1.5r		10 <sup>-12</sup> - 3x10 <sup>-11</sup>		Bauer et al. (2003)
	445m level	Drill & blast	1.2r	10 <sup>-14</sup> -10 <sup>-12</sup>			Delay et al. (2010)
<b>Bure UCS=21 MPa</b>	490m level	Pneumatic hammer	1.2- 1.5r	10 <sup>-14</sup> -10 <sup>-12</sup>	10 <sup>-11</sup> - 10 <sup>-8</sup>	Micro-fracture Zone: K= 5x10 <sup>-11</sup> m/s (K <sub>factor</sub> =100)	Delay et al. (2007,2010)
	GMR Drift	Pneumatic hammer	1.2- 1.5r		10 <sup>-11</sup> - 10 <sup>-8</sup>	Fracture Zone: K=5x10 <sup>-9</sup> m/s (K <sub>factor</sub> =10000)	Delay et al. (2010)
	GK-E Drift	Pneumatic hammer	1.2- 1.5r		10 <sup>-11</sup> - 10 <sup>-4</sup>		Shao et al. (2008)
<b>Tournemire UCS=20 MPa</b>	1881 Tunnel	Manual		10 <sup>-13</sup>	10 <sup>-12</sup> - 10 <sup>-4</sup>		Matray et al. (2007)
	1996 & 2003 Galleries	Roadheader	1.2r		10 <sup>-12</sup> - 10 <sup>-4</sup>		Matray et al. (2007)
<b>Tono UCS=6.6 MPa</b>	Test Drift 2	Boomheader	1.1r	<10 <sup>-11</sup> - 5x10 <sup>-8</sup>	No increase		Sato et al. (2000)
	Test Drift 2M	Drill & Blast	1.6r		10 <sup>-9</sup> - 2x10 <sup>-4</sup>		Sato et al. (2000)
<b>Maximum</b>			2r				

Notes: K factor represents the increase in hydraulic conductivity relative to undisturbed host rock.

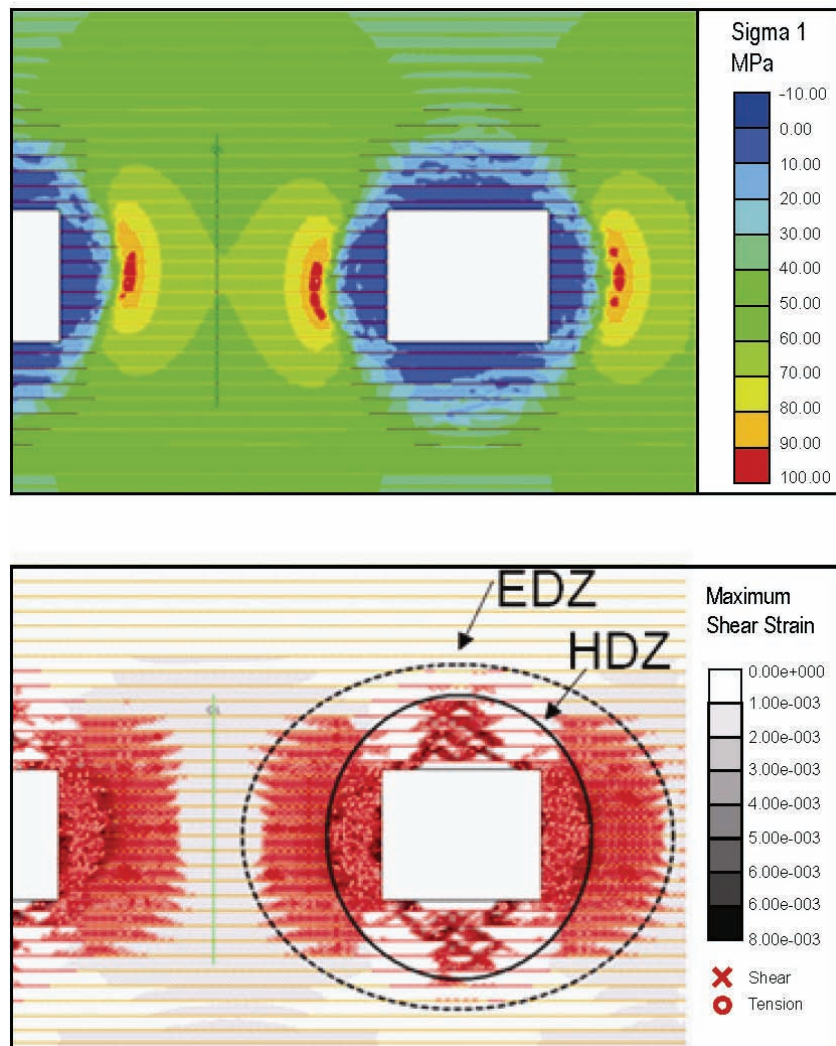
Volumetric strain can be empirically related to permeability increase and this can be used as a delineator between EDZ and HDZ based on operational specifications for allowable damage. Another approach is to consider a level of total volumetric expansion, beyond the theoretical volume change due to the elastic relaxation of in situ stresses, to be indicative of crack opening and dominant fracture flow – key characteristics of the HDZ. When the stress ratio is not equal to one and anisotropic stresses are present, plastic shear strain as a modelling output becomes a reliable indicator of EDZ. Used in combination with volumetric strain it can indicate zone boundaries as shown in Figure 6.8.



Notes: Various indicators for EDZ and HDZ using a strain-weakening model (strength reduces after yield) with a stress ratio of 1.7:1 (horizontal stress: vertical stress). Results are for the vertical line A-A' above the roof. Tunnel diameter is 10 m.

**Figure 6.8: Example of Typical EDZ Model Output Using Arbitrary Material Parameters**

Similar logic can be used to determine EDZ and HDZ boundaries using Diederichs' brittle model (Diederichs 2007). For this material, yield (red indicators in Figure 6.9) is indicative of the EDZ while excessive shear strain is the primary indicator of HDZ. Note that no single indicator should be used and that all of the indicators described should be examined to robustly and holistically establish the damage zone boundaries. Further discussion of modelling is given in Sections 6.4.2 and 6.4.3.



Notes: Upper image depicts drop in compressive stress within HDZ. Lower image depicts distribution of EDZ (red shade) and HDZ (grey shade) yield indicators. Results shown are those at the 1<sup>st</sup> interglacial period.

**Figure 6.9: EDZ and HDZ Defined by Pseudo-continuum (Finite Element) Model**

### 6.3.1.2 Long-term EDZ Behaviour: Self-sealing

Fractured argillaceous rocks tend to become less permeable with time through the natural process of self-sealing. Self-sealing can also be an effective process in reducing the permeability of the EDZ. Bock et al. (2010) showed that self-sealing is a common phenomenon in a wide variety of argillaceous formations with clay content of more than 40% and with low to moderate (< 50 MPa) strength. Bock et al. (2010) compiled field data from underground openings in such formations and concluded that EDZ self-sealing leading to a reduced permeability was a measured phenomenon. Bock et al. (2010) proposed that the fractures are sealed by one of the following seven mechanisms. These are evaluated in Table 6.4 for the cap rocks at the Bruce nuclear site.

**Table 6.4: Overview of Self Sealing Potential of EDZ in Barrier Rocks**

Requirements for Self Sealing	Potential Effect at DGR
1. Additional compaction of the rock matrix	Possible
2. Increase in the effective normal stress across the fracture plane	Likely when subjected to glacial loading
3. Contraction of fractures when subjected to shear	Likely when subjected to shear loads
4. Creep of fractured wall material	Unlikely except in anhydrite units
5. Swelling of fractured wall material	Likely when fresh water encountered
6. Body and surface slaking	Possible where subjected to wet and dry cycles near the excavated face
7. Mineral precipitation	Very likely due to high TDS

Notes: Requirements are from Bock et al. (2010).

The Ordovician shales at the Bruce nuclear site contain between 15% to 70% clay and are considered to have a moderate degree of induration, having undergone an estimated maximum burial depth in excess of 1500 m. In regard to these shales, the first four self-sealing mechanisms listed above involve the change of stress field around the excavation openings. Swelling would require the presence of both fresh water in EDZ fractures, and sufficient smectite and other swelling clay in the host rock. Free swell tests on the Ordovician shales indicate a horizontal swelling potential of about 1% per log cycle of time in fresh water. Bock et al. (2010) further suggest that a threshold of 15% smectite is generally required to activate the swelling mechanism should all conditions be met. Slaking of the rock and rock surface is limited because of the constant temperature and humidity inside the DGR.

The following evidence of self-sealing in the geologic past has been observed in the Ordovician shales that form the cap rock at the proposed DGR at the Bruce nuclear site.

- Completely sealed fractures are present in the form of veins throughout the Paleozoic sequence. These are filled with calcite, gypsum/anhydrite, and/or halite and probably representing different periods of mineral formation.
- Large portions of the brecciated Salina (Units B to F) Formation have been sealed by a clay matrix deposited in between the shale and/or dolostone breccia fragments, during and after the dissolution of major salt beds. This was followed by the formation of numerous sub-horizontal fibrous gypsum veins.
- Engelder (2011) demonstrates the long-term integrity of the Ordovician shale sequence by studying suitable analogues and their attendant self-healing abilities in sealing local fractures.

Mineral precipitation accompanies changes in chemical composition, pressure, temperature and other factors that may induce self-sealing. Some minerals that are found as common fracture-fill materials in the rock cores in the DGR series of boreholes and could act as self-sealing materials in the EDZ include calcite, gypsum, anhydrite and halite. Because the groundwater chemistry of the Ordovician shales at the Bruce nuclear site contains a large amount of TDS

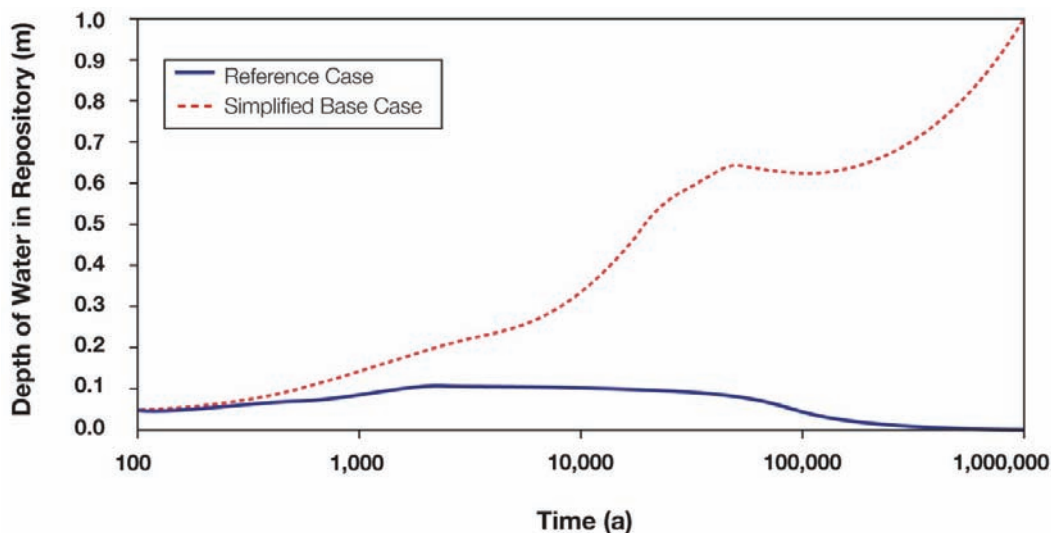
(about 300 g/L) classifying it as brine (INTERA 2011), the likelihood of such precipitation in the EDZ is high during the operation period, depending on the availability of groundwater.

### 6.3.2 Gas Generation

The waste emplaced in a repository may change with time, as components of the waste and waste packages interact with one another, as well as with any water that may enter the repository. Hydrogen may be generated by corrosion of metals, while methane and carbon dioxide may be generated by microbial degradation of organic materials in the waste. If generated in sufficient quantities, these gases may cause the pressure in the repository to rise, affecting the rate of fluid and gas migration into (or out of) the repository. If gas is generated faster than it can leave the repository through the rock, the potential for gas fracturing of the rock arises. Gas pressure within the repository may also affect the geomechanical stability of the excavations. Hence, gas-generation processes must be modelled to evaluate their effects on the repository (Section 6.4.1).

### 6.3.3 Repository Resaturation

Another post-closure behaviour of the repository is the slow ingress of groundwater from the Ordovician host rock. The potential risk of releasing radionuclides into the groundwater increases depending on the degree to which the waste contacts the groundwater. Figure 6.10 shows the calculated level of water in the DGR emplacement room for the Reference and Simplified base-cases of post-closure safety assessment (GEOFIRMA and QUINTESSA 2011). The results show that the DGR remains unsaturated with the water level of the Reference Cases never exceeding 0.1 m within the first 1 Ma and only approaching 1 m in the simplified base-case. The low saturation is attributed in part to the low permeability of the enclosing host rock, and in part due to the anaerobic generation of gases within the repository, which further reduces water entry (GEOFIRMA and QUINTESSA 2011). Because the effect of repository resaturation to the long-term DGR stability is minimal, this scenario is not considered in the long-term stability analysis.



Notes: Emplacement room height is 7.1 m. Figure is from GEOFIRMA and QUINTESSA (2011).

**Figure 6.10: Depth of Water in the Repository**

## 6.4 Modelling of Repository Evolution

Excavation of shafts and emplacement rooms causes stress changes in the surrounding rock mass. How the rock mass responds to those changes and to loads applied internally and externally is dependent on the geomechanical properties of the rock. Seismic and glacial events may provide external loads that affect repository stability, while gas generation in the repository may create an internal load that could potentially cause fracturing. Thus, geomechanical modelling of all of these processes is needed to evaluate the stability of the DGR over 1 Ma.

Modelling of repository evolution was primarily focused on the emplacement panels and rooms, as well as on the shafts. The effects of different loading conditions expected during a timeframe of 1 Ma on repository performance, including the overall stability of the emplacement rooms and the shaft, damage and deformation of the surrounding rock mass, and evolution of the EDZ, were analyzed. The loads and conditions relevant for stability and performance of the repository that were modelled are listed below.

- **In situ stresses:** The Cobourg Formation (repository host rock) is under significant in situ stress at the repository depth. Excavation of the repository will cause perturbation to the in situ stress state and stress concentrations around the excavations that will cause deformation and, potentially, damage and failure of the rock mass.
- **Time-dependent strength degradation of the stressed rock mass:** Strength of the rocks subjected to certain stress levels and exposed to atmosphere gradually degrades with time. Time-dependent strength degradation of the rock mass can cause time-dependent evolution of damage and failure of the rock mass.
- **Water and gas pore pressure and pressure inside the emplacement rooms:** During repository evolution, gases will be generated inside the emplacement rooms as a result of waste degradation. These gases will impose pressure on the emplacement room wall which, if sufficiently large, can cause hydraulic fracturing of the rock and escape of gas from the repository.
- **Glacial loading:** During previous glacial episodes, an ice sheet developed over southern Ontario. The repository is expected to be subjected to multiple glacial events during the next 1 Ma. Glacial loading, future ice sheets have been assumed to be up to 2.5 km thick, and will impose additional loading on the repository, causing additional deformation, damage and potential failure of the emplacement rooms and pillars.
- **Seismic shaking:** Over the period of 1 Ma, the repository will be subjected to multiple seismic events, some of which will have very small probability of recurrence and relatively strong intensity.

The repository layout, shown in Figure 6.11, indicates that there are two distinct scales that affect the stability of the emplacement rooms and the pillars between them. The scale of the pillars (17.2 m width) and emplacement rooms (8.6 m span) is much smaller than the scale of the panels (approximately 200 m span). The repository or panel scale is important for pillar stability because stress arching above the panel will result in reduction of the loads on the pillars. Furthermore, the effect of panel deformation on deformation and damage of the capping shales can only be investigated at this larger scale.

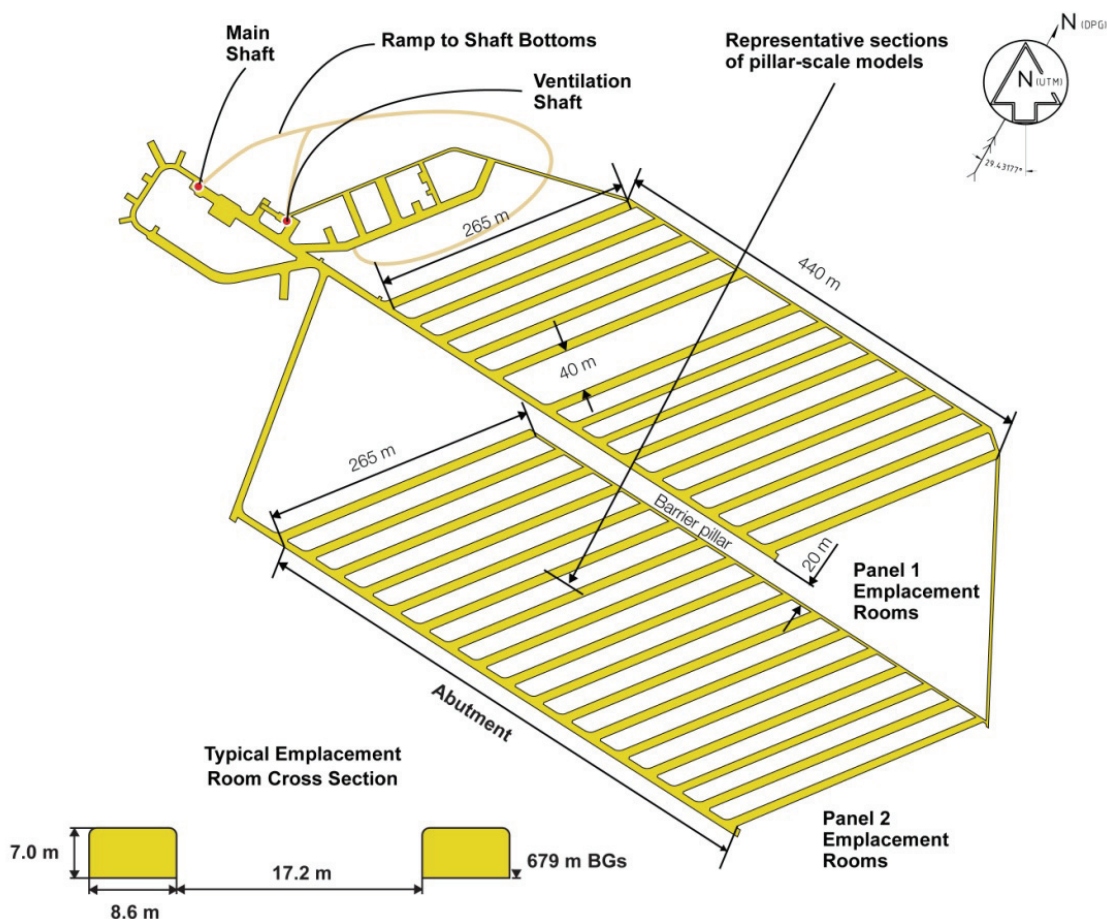


**Figure 6.11: Repository Layout and Typical Emplacement Room Cross-section**

A variety of numerical modelling studies were performed to evaluate the effects of the various processes described above on the behaviour and long-term performance of the DGR shafts and disposal emplacement rooms. Modelling related to gas generation is described first, as the results of that modelling were used in the geomechanical modelling of the other processes listed above. Results of the geomechanical modelling of the shafts and shaft seals are presented next, followed by the results of repository modelling at the room-pillar scale and then at the panel scale.

#### 6.4.1 Selection of Short-term and Long-term Strengths

As described in Chapter 3, the uniaxial compression tests were carried out on cylindrical core samples (75 mm in diameter) taken from different depths in boreholes, DGR-1 to DGR-6. The properties of different units obtained by averaging the representative test results are listed in Table 3.14. Because the Cobourg is the proposed host rock, the largest number of UCS tests were carried out in this formation. An average UCS of 113 MPa was obtained from the testing. In the massive Cobourg, the bedding planes are poorly defined and appear to form the only

known possible planes of discontinuity. Because there are no large-scale joint sets, the mechanical properties for the Cobourg do not need to be reduced to account for the effect of rock mass jointing. This assumption also applies to the Cobourg and Sherman Fall interface, or the weak Sherman Fall unit as described in later sections on modelling analysis. However, because of their importance for emplacement room stability, the strengths of these two units were reduced relative to the averages by approximately one standard deviation, to account for uncertainty in the data resulting from sample disturbance and local variability in material properties. Thus, the UCS values in the analyses were 90 MPa and 30 MPa for the Cobourg and the weak Sherman Fall limestones, respectively. Details on developing rock mass properties of various rock units used in the shaft and repository analyses are described in ITASCA (2011).

The long-term strength testing of the Cobourg was carried out on the samples taken from DGR-2 (Gorski et al. 2009b), DGR-3 and DGR-4 (Gorski et al. 2010b). The results of long-term strength testing on all samples indicate that there is no obvious trend in data suggesting any decrease in strength with time. In the literature, long-term strength of cylindrical laboratory samples of rock is associated with uniaxial or unconfined CD (Brace et al. 1966, Schmidtke and Lajtai 1985, Martin 1997) and the associated confined yield envelope. The mean CD for the Cobourg is 97 MPa with a measured range of 45 to 162 MPa. Actual excavation wall strength (under low confining stress) in excavations over construction and service life is observed to vary between CI and CD (Martin et al. 1999, Diederichs 2007). The conservative theoretical stress minimum limit (Diederichs 2003, Damjanac and Fairhurst 2010) for any time dependant degradation within a brittle rock over geological time is the CI stress (below CI there can be no new damage initiation and therefore no propagation and degradation). Mean CI for the Cobourg is 45 MPa. Given that the stress–strain response for the Cobourg is similar to other brittle rocks, the long-term strength of the Cobourg was assessed using the methodology developed by Damjanac et al. (2007), whereby the CI stress is used to represent the lowest bound of the long-term rock strength. The long-term minimum strength degradation threshold for the Cobourg in the emplacement room stability analysis is set to 45 MPa corresponding to the mean CI threshold from test data (approximately 40% of the mean UCS). The use of CI for long-term strength is already a very conservative assumption and thus the mean CI is used as a bounding value.

#### **6.4.2 Gas Generation and Its Effects**

Corrosion and microbial degradation of the wastes and packages inside the DGR will result in the generation of gases. Because of the low permeability of the host rock, a significant amount of gas will remain inside the repository, which could result in a gradual build-up of gas pressure. To estimate this gas pressure, detailed gas flow and transport modelling was employed using T2GGM. T2GGM comprises a TOUGH2/EOS3 2-phase gas and water transport model (Pruess et al. 1999), coupled to a custom gas-generation model (GGM).

The gas generation model (GGM) has been developed to simulate various microbial and corrosion processes, the gas evolution of the repository, and its interaction with the geosphere. GGM tracks the production and consumption of the key chemical species (e.g., metals, organic wastes, gases, water) and tracks the fluxes of the water and gases into and out of the repository. GGM includes four key mechanisms for the generation of gas and consumption of water:

- Microbial degradation of organic wastes;



- Methanogenesis via the microbial hydrogen mechanism;
- Corrosion of metallic wastes;
- CO<sub>2</sub>-enhanced corrosion of metallic wastes and formation of siderite (FeCO<sub>3</sub>); and
- These processes may occur in either the saturated (water submerged) or vapour phases.

The rates of generation or consumption of water and gas within the repository are interpreted as sources for water and gas within TOUGH2's 2-phase flow model of the repository. TOUGH2 simulates the transport of gas and water through the repository and geosphere. TOUGH2 is able to calculate the flux of bulk gas leaving the repository and GGM provides the composition and generation rate of that gas.

The GGM model of the repository and the TOUGH2 model of the geosphere are coupled via the total gas pressure, repository gas/water saturation, relative humidity, and repository void volume. These couplings determine the flows of water and of gas into and out of the repository.

The principal results of the modelling as they relate to gas generation and water processes within the repository (ITASCA 2011) are summarized below.

- Oxygen within the repository is consumed quickly and conditions become anaerobic shortly after repository closure.
- Moisture initially present in the wastes, plus water that seeps into the repository from the surrounding rock and the shaft, support the anaerobic corrosion of metals and the degradation of organic wastes, resulting in generation of hydrogen, CO<sub>2</sub> and CH<sub>4</sub> gases. The gas pressure in the repository rises.
- There is a pressure balance between the water seepage into the repository and the gas generation within the repository. For most calculation cases, the very low permeability of the rock precludes significant water saturation of the repository for the 1 Ma simulation period. In some sensitivity cases, the repository is virtually dry (or completely unsaturated) after 100 ka.
- For most calculation cases considered, the peak repository gas pressure is approximately 7 to 8 MPa, which is comparable to the environmental head at the repository horizon of around 7.2 MPa, and much less than the lithostatic pressure of about 17 MPa at the repository horizon.
- Methane is generally the dominant gas throughout the evolution of the repository, due to degradation of organic wastes and the consumption of hydrogen and carbon dioxide via the microbial methanogenic reaction. The balance of the initial inventories of metallic and organic wastes results in the repository atmosphere containing small levels of either hydrogen or carbon dioxide.

For the DGR geomechanical stability analysis, two simplified cases of gas pressure histories were developed representing a base-case condition with gas pressure plateau at about 7 MPa at about 100 ka and an extreme case scenario with 15 MPa peak gas pressures approaching lithostatic pressure (ITASCA 2011). Figure 6.12 shows these gas pressure profiles bounding various gas generation scenarios for normal repository evolution (GEOFIRMA and QUINTESSA 2011). The base and extreme case gas pressure histories will be used to provide insight on the mechanical effects on the DGR emplacement room stability in Section 6.4.4.

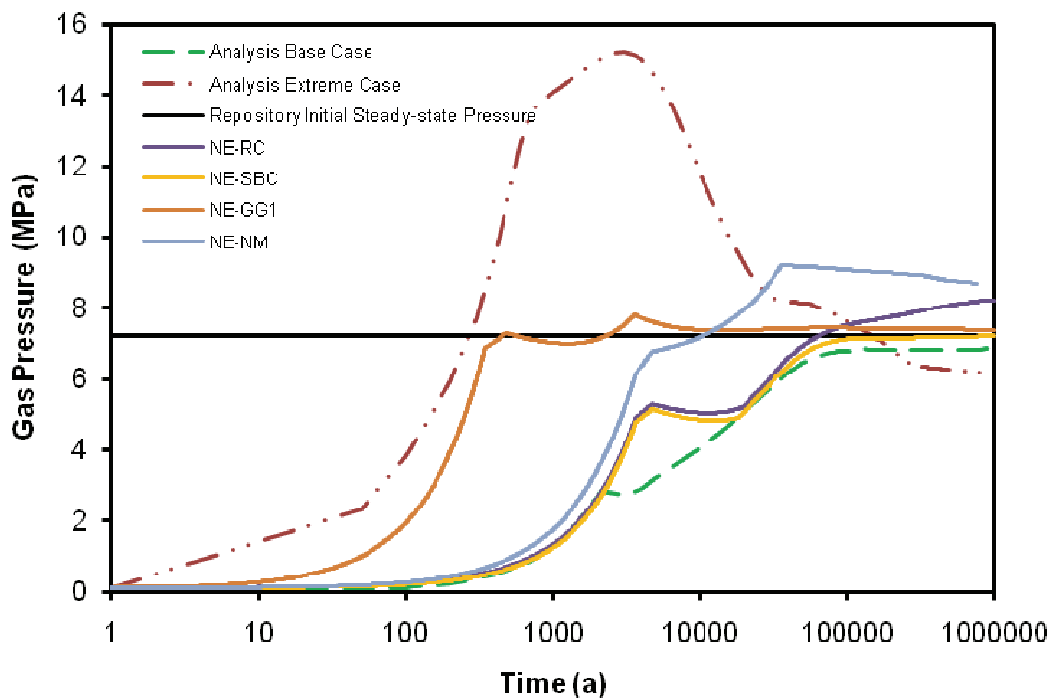


**Figure 6.12: Repository Gas Pressure Histories Used in Geomechanical Stability Analyses**

### 6.4.3 Shaft Seals and Long-term Performance

This section summarizes the results of geomechanical numerical simulations performed and reported by Itasca Consulting Group, Inc. (ITASCA 2011) to evaluate the effect of long-term processes on the evolution of the EDZ around the access shaft and backfill-seal systems for the DGR. It is known that the EDZ could be the primary pathway for the migration of radionuclides from the repository. The planned shaft seal system consists of a series of sections with engineered backfill/seal material comprised of compacted engineered fill, compacted bentonite/sand backfill, concrete bulkheads, and asphalt waterstop seals. The purpose of this backfill/seal system is to inhibit gas/fluid migration along the shaft. The geomechanical simulations capture the dominant mode of behaviour and understanding on the evolution of the EDZ with respect to specific sealing elements, in situ stress environments, rock conditions, and pore pressure response in the rock mass due to the presence of water and gas during long-term repository development.

The geomechanical simulation results are based on the analysis of the seal system for the access shaft as presented in the Preliminary Safety Report (OPG 2011a). A total of six types of seals, including a waterstop seal, an asphalt column, and four concrete bulkheads with different surrounding host rocks, were studied. The study in the following section covers the rock mass response in varied rock formations, specific seal behaviour (i.e., waterstop, asphalt, concrete bulkhead), in situ stress environment, and pore pressure response around excavated openings.

### 6.4.3.1 EDZ Prediction

Stability analyses of the DGR shaft seal system explored the following key scenarios during the evolution of the repository:

- Time-dependent strength degradation (base-case);
- Strength degradation with additional effects of gas pressure build-up;
- Strength degradation with additional effects of seismic ground shaking;
- Strength degradation with additional effects of glacial loading; and
- Combinations of all of the above loading scenarios.

The analyses of the shaft seal elements were carried out using the three-dimensional finite-difference continuum code FLAC3D (Fast Lagrangian Analysis of Continua in Three Dimensions; ITASCA 2005 and 2009). These model simulations explored short-term mechanical behaviour, long-term strength degradation, glacial loading, generated gas pressure, and seismic ground motion over a period of 1 Ma. Two-dimensional finite-element calculations (using Phase<sup>2</sup>-v7, Rocscience 2009) were carried out to compare to the 3D base-case analyses.

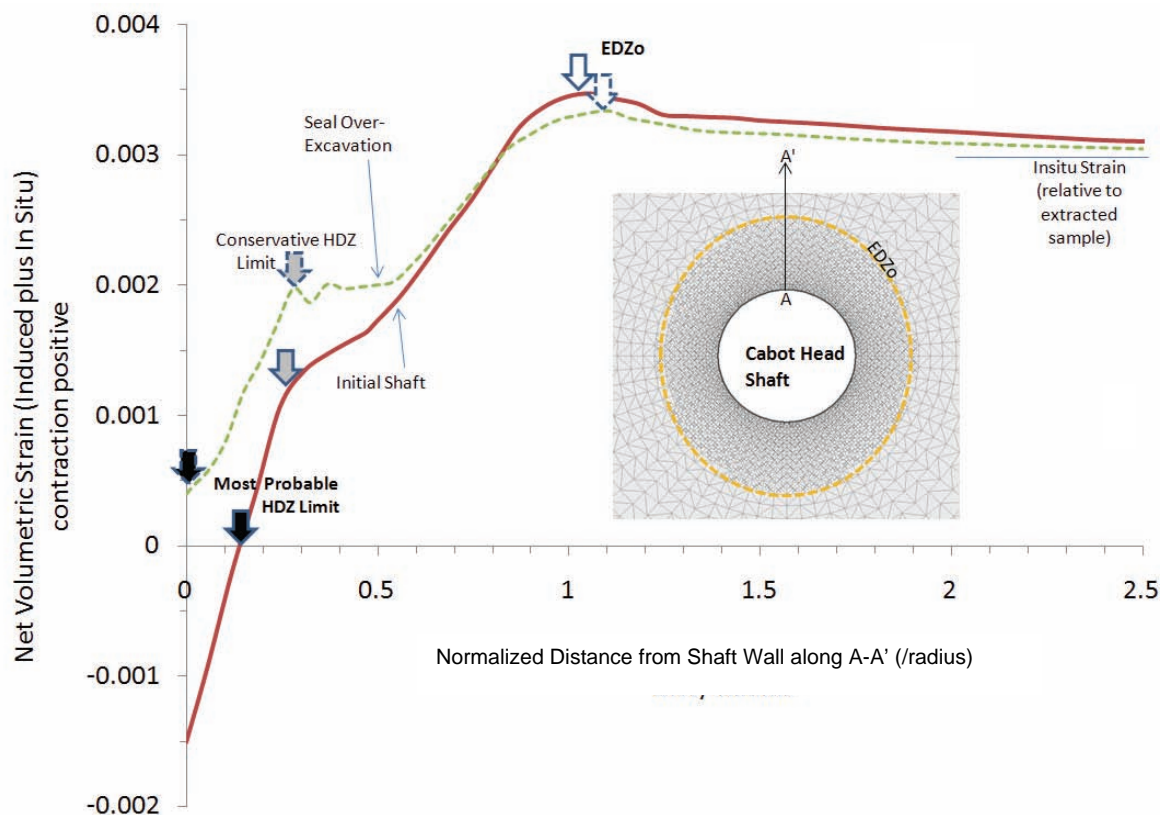
Figure 3.1 shows the layout of the shaft seal arrangement. The shaft seal system consists of one asphalt column (S1), three concrete bulkheads (B1, B2, and B3) and four bentonite/sand backfill columns (OPG 2011a). The three key concrete bulkheads are planned at horizons in the upper 4 m of the Salina A1 Unit and in the Guelph Formation, which have higher permeabilities within the sedimentary sequence, and in the upper Salina F Unit, below the shallow groundwater system. The over-excavation during repository closure includes the removal of the HDZ.

The extent of excavation damage can be predicted using a number of constitutive models within the continuum analyses presented here. Using Hoek and Brown (1980) parameters, the damage zones can be estimated using various failure criteria as indicators simulating perfectly plastic, strain weakening, and brittle conditions. The EDZ boundary, delineated by the plastic yield indicator, encompasses a zone where stress exceeds material strength and damage occurs in the form of small cracks distributed throughout the material. From the outer boundary to the inner boundary of the EDZ, the level of damage accumulation and crack propagation and interaction increases. There is, by definition, no induced CD outside of the outer EDZ boundary.

An accurate prediction of the HDZ is more difficult. This zone lies inside the inner EDZ boundary and is the innermost damage zone containing open and likely connected fractures. Conventional continuum codes are not well suited to accurately assess the mechanics of this zone. They can, however, be used to approximate the potential for a significant HDZ. Figure 6.13 illustrates a subjective approach to HDZ delineation in continuum models. In this approach, the HDZ will be conservatively overestimated.

Alternatively, plotting the net volumetric strain (relative to an elastically destressed rockmass) can be used to delineate the most probable EDZ based on the concept that negative (extensile) volumetric strain corresponds to an opening up of the rock and the creation of open fractures. This is illustrated in Figure 6.13 for the 2D analysis of the shaft in the Cabot Head Formation. It is difficult to simulate fracture development in the continuum model. Utilizing a strain-weakening approach, which suggests that strength reduction occurs at the onset of crack interaction, it is

possible to identify zones with reduced strength once the yield threshold has been exceeded using Hoek and Brown (H-B) post peak parameters (Hoek et al. 2002). This is indicated by the negative net volumetric strain shown in Figure 6.13, which represents true dilatancy, i.e., opening of fractures in the HDZ.



Notes: Net volumetric strain is plotted (equal to the induced strain plus the in situ strain relative to an unstressed extracted sample). EDZ is clearly defined (open arrows) by yield indicators and by a maximum (compressive) strain with extensile strain increasing towards the excavation. Maximum (conservative) HDZ estimate corresponds to increase in extensile volumetric strain (shaded arrows). More probable HDZ is indicated by negative net volumetric strain (true dilatancy representing opening of fractures) represented by the solid arrows. For the shaft seal over-excavation, there is no HDZ according to this more probable indicator. The EDZ scales with radius of opening.

**Figure 6.13: Simplified 2D Analysis of Shaft and Potential Over-excavation (Seal) for the Cabot Head Formation**

#### 6.4.3.2 Shaft Seal Geometry

A quarter-symmetrical 3D model of an 80 m length shaft section was created using FLAC3D with 60 x 60 m dimensions in plan. The model included the Main Shaft excavation, the over-excavation boundary, and the seal arrangement built into the grid using actual design dimensions. A refined mesh region was included around the shaft to improve plasticity calculations near the shaft.

Figure 6.14 illustrates the currently proposed shaft seal geometries. Figure 6.15 shows an example of the model geometry (grid) for seal B1 along with the seal/backfill sections and geological units.

A uniform stress field was used within each geological unit in the individual models, with principal stresses based on the FLAC3D-determined in situ stresses for the Bruce nuclear site, described in Section 3. Because the models of the individual shaft seal sections included only a relatively short vertical distance (80 m), an average stress relevant to each zone was included in the models. Vertical stresses ( $\sigma_v$ ) were calculated based on an average density of 2600 kg/m<sup>3</sup>.

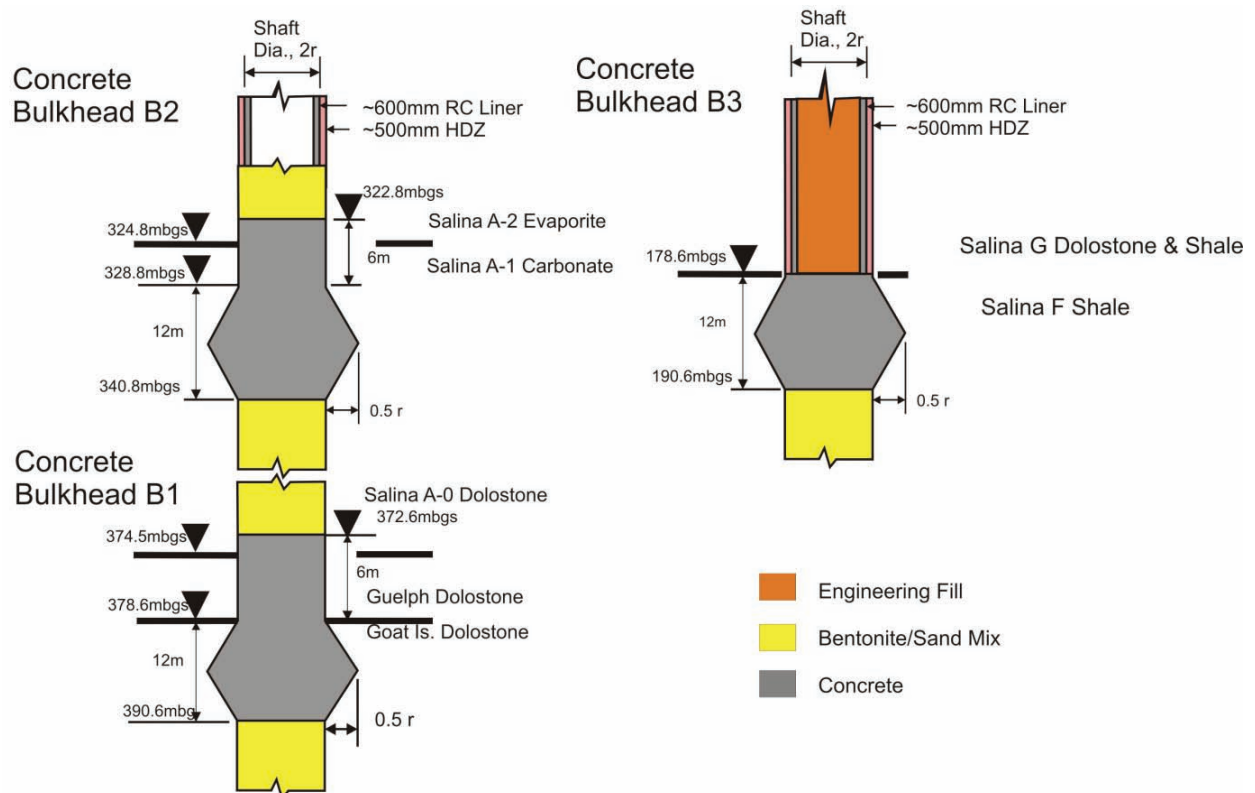
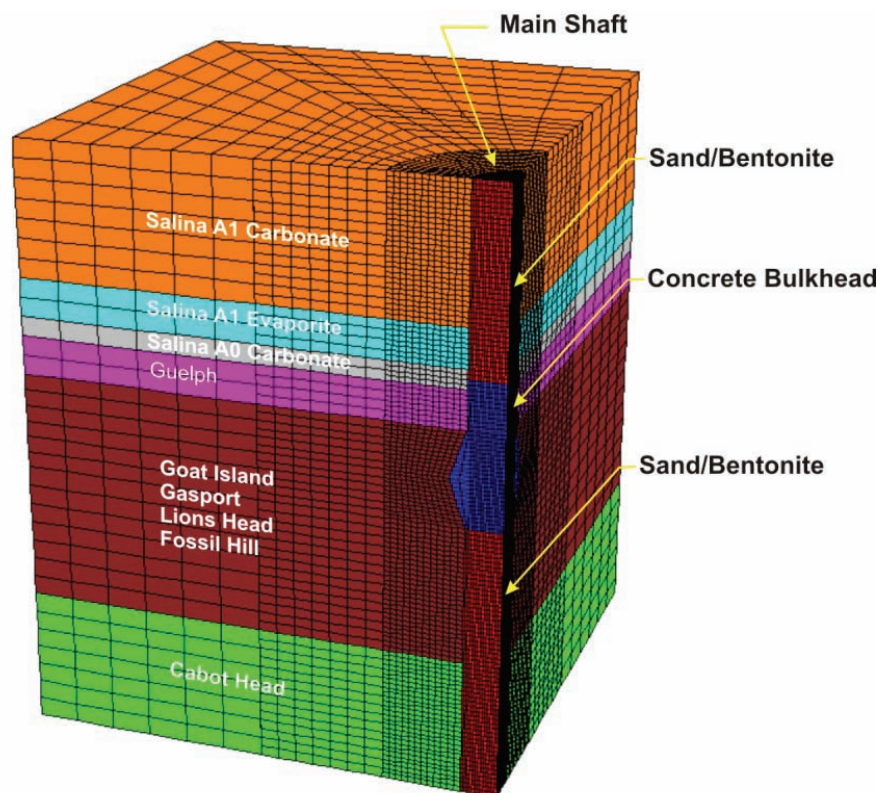


Figure 6.14: Details of the Three Concrete Bulkhead Geometries



**Figure 6.15: Layout of Quarter-symmetrical FLAC3D Model of Over-excavated and Backfilled Access Shaft for B1 Seal**

Rock mass properties used are based on the laboratory test results conducted on rock cores retrieved from DGR-2 to -6 (ITASCA 2011) from the relevant seal locations. In order to obtain the best results, these layer-specific values were used rather than the averaged 'recommended estimates' provided by INTERA (2011), as the latter values represent averages across each MS unit that may not be as representative for these purposes. The shaft geometry, rock support, content, rock mass behaviour, and in situ stress condition assumed for these initial analyses were as follows:

- The shaft is considered to be 7.85 m in diameter and unsupported;
- Long-term strength test data from Lac du Bonnet granite and Cobourg limestone were utilized for the long-term strength degradation analysis;
- Horizontal bedding planes were not modeled explicitly, but were accounted for using the Geological Strength Index (GSI) approach (Hoek et al. 2002);
- Early deterioration of the concrete bulkhead within the first few hundred years was assumed; and
- Maximum and minimum horizontal in situ stresses were assumed to be factors of 2 and 1.5 greater than the vertical stress, respectively.

### 6.4.3.3 Shaft Sequencing

The initial shaft excavation, installation of ground support, and post-closure over-excavation and shaft backfill/seal placement were modelled based on the excavation and backfilling sequence described in Chapters 9 and 13 of the Preliminary Safety Report (OPG 2011a). The modelling sequence of the shaft excavation was constructed based on the stages listed below.

- Initial excavation of shaft and placement of concrete liner. To be conservative, the initial rock support was not considered. The final concrete liner was accounted for using the linear-elastic structural element logic in FLAC3D (ITASCA 2011).
- Time-dependent degradation of the rock mass over the repository pre-closure period which is expected to be approximately 100 years.
- Sequential over-excavation of the HDZ damaged zone and backfilling with bentonite/sand mix from the repository horizon up to the Salina F unit at closure. A 0.5 m thick HDZ is estimated based on 2D modelling using the Brittle Spalling Model proposed by Diederichs (2007).
- Excavation of concrete bulkhead and asphalt sections using controlled excavation techniques is assumed.
- Time-dependent degradation of rock mass and concrete bulkhead properties for a continuous period from repository closure to 1 Ma. Combinations of model-specific long-term loading, such as seismic shaking, glacial loading, and gas and water pore pressure build up were considered in this stage.

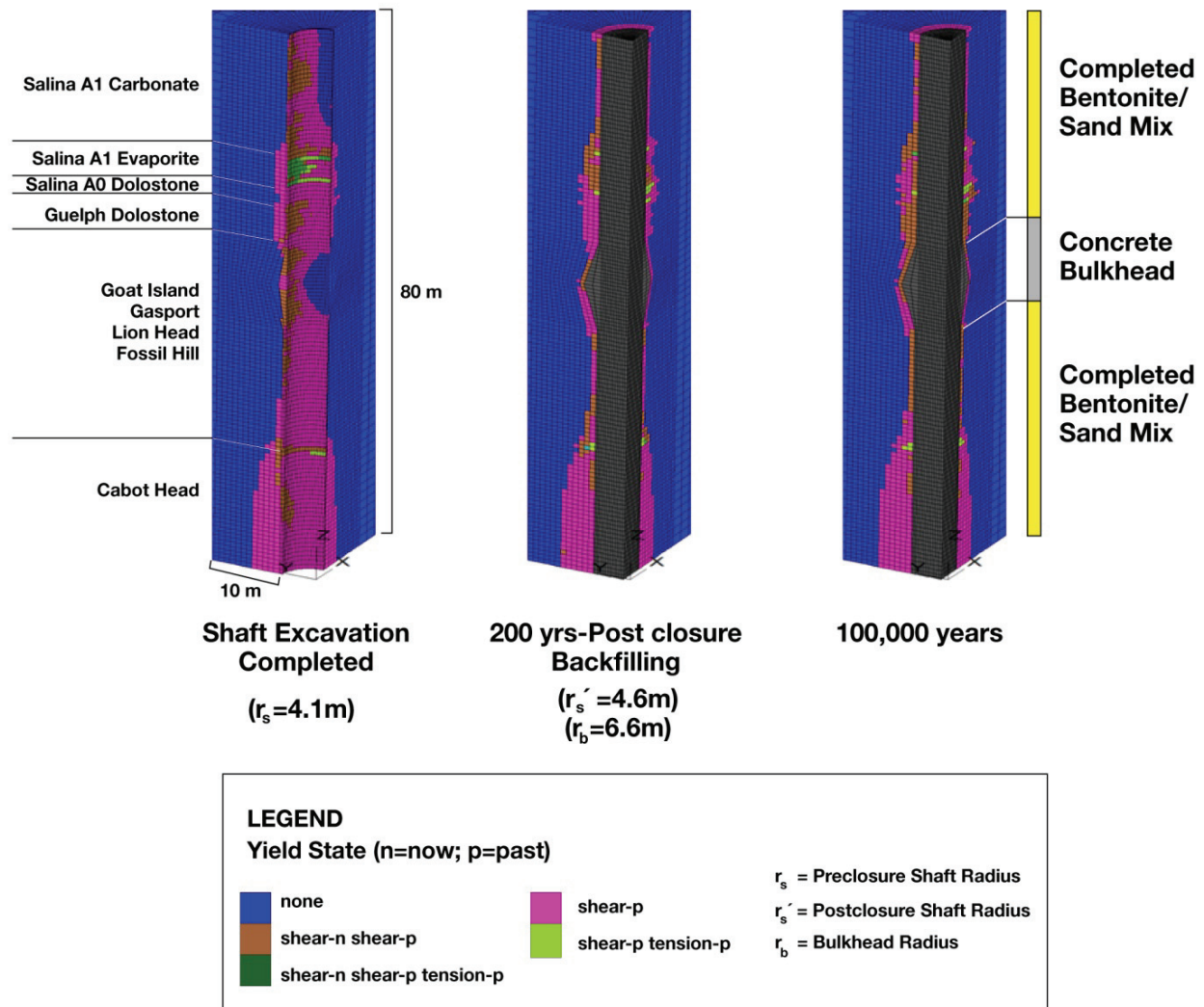
In the bottom and top portions of the models, away from the seals, the over-excavation and backfilling was done with relatively large vertical lengths to increase modelling efficiency; in the vicinity of the seal, near the middle of the model, the over-excavation and backfilling was carried out in 3 m long rounds. The over-excavation for each seal component location was excavated in one stage per seal component and then backfilled in the following stage.

### 6.4.3.4 Modelling Results

For selected seals, several other long-term loading conditions were considered in parallel with the time-dependent strength degradation: glacial loading, pore pressure evolution, and seismic ground motions. Each specific loading condition was simulated in the model that would result in worst-case increases in the extent of damage. These additional loading conditions are summarized in Table 6.5 and described in greater detail in the following section.

#### CASE 1 Time-dependent Strength Degradation

Time-dependent strength degradation is a measure of how the rock will perform over a period of time under existing stress conditions after an opening has been excavated. The models generally showed that most of the EDZ developed soon after the completion of the initial shaft excavation phase (Figure 6.16). For most of the seals analyzed, the time-dependent strength degradation resulted in less than 20% to 50% increase in the extent of damage depending on rock material. The additional time-dependent loading conditions had limited effect on evolution of the damaged zone around the shaft/seals because of the confining effect provided by the backfill-seal materials. The swelling pressure due to geological units and bentonite backfill are conservatively not accounted for in the modelling as they provide additional confinement to the rock. Specific observations from the shaft analysis are summarized below.



Notes: All colours other than blue represent yield and presence of EDZ.

**Figure 6.16: Yield State – Concrete Bulkhead B1: Time-dependent Strength Degradation – FLAC Yield States Coloured**

The relaxation of the rock mass around an opening, which mostly occurs during and shortly after excavation, and time-dependent strength degradation effects directly account for the majority of the EDZ formation and may persist on a diminutive scale for a period of 1 Ma, which was represented as a loss in cohesion in the model. A series of analyses (listed in Table 6.5) were carried out to determine the normalized extent of the EDZ (scaling with excavated radius). The results for the base-case (strength degradation only) are summarized in Figure 6.17.

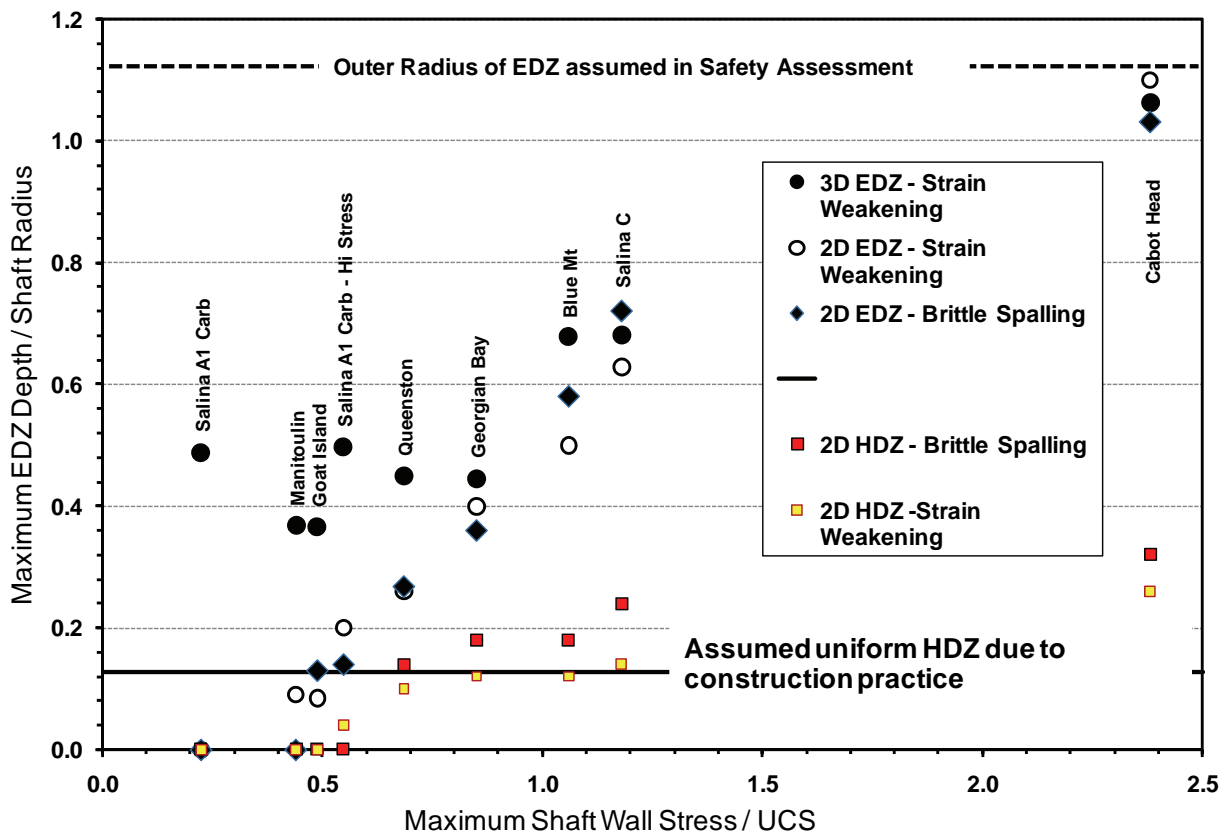


**Table 6.5: Summary of Properties Used and EDZ Estimates Obtained from 3D Models**

Formation/ Unit	Seal	Thick (m)	$\sigma_{xx}$ (MPa)	$\sigma_{yy}$ (MPa)	$\sigma_{max}^1$ (MPa)	UCS (MPa)	$a^2$ (m)	$d_f$ (m)	$\frac{\sigma_{max}}{UCS}$	$\frac{d_f}{a}$	Loads Modelled
Salina A1 (Carbonate)	B1	41	20	16	44	116.7	4.58	2.43	0.38	0.53	TD_Cd
			30	26	64		4.58	3.28	0.55	0.72	TD_Cd_GL
			30	26	64		4.58	3.28	0.55	0.72	TD_Cd_GL_PP
			30	26	64		4.57	2.45	0.55	0.54	TD_Cd_GL_DY
Salina A1 (Evaporite)	B1	4	20.1	16.1	44.2	20	4.58	3.27	2.21	0.71	TD_Cd
			30.1	26.1	64.2		4.58	3.27	3.21	0.71	TD_Cd_GL
			30.1	26.1	64.2		4.58	3.23	3.21	0.71	TD_Cd_GL_PP
			30.1	26.1	64.2		4.55	3.32	3.21	0.73	TD_Cd_GL_DY
Salina A0	B1	4	20.2	16.2	44.4	197.6	4.58	3.27	0.22	0.71	TD_Cd
			30.2	26.2	64.4		4.58	3.27	0.33	0.71	TD_Cd_GL
			30.2	26.2	64.4		4.58	4.04	0.33	0.88	TD_Cd_GL_PP
			30.2	26.2	64.4		4.59	3.25	0.33	0.71	TD_Cd_GL_DY
Guelph	B1	5	32.7	26.5	71.6	60.4	4.58	2.44	1.19	0.53	TD_Cd
			42.7	36.5	91.6		4.58	2.5	1.52	0.55	TD_Cd_GL
			42.7	36.5	91.6		4.58	2.46	1.52	0.54	TD_Cd_GL_PP
			42.7	36.5	91.6		4.59	2.42	1.52	0.53	TD_Cd_GL_DY
Goat Island Gasport Lions Head Fossil Hill	B1	31	33	26.5	72.5	148.3	4.58	1.68	0.49	0.37	TD_Cd
			43	36.5	92.5		4.58	1.62	0.62	0.35	TD_Cd_GL
			43	36.5	92.5		4.58	1.63	0.62	0.36	TD_Cd_GL_PP
			43	36.5	92.5		4.57	3.26	0.62	0.71	TD_Cd_GL_DY
Cabot Head	B1	24	14	12	30	12.6	4.58	4.87	2.38	1.06	TD_Cd
			24	22	50		4.58	4.87	3.97	1.06	TD_Cd_GL
			24	22	50		4.58	5.72	3.97	1.25	TD_Cd_GL_PP
			24	22	50		4.47	4.95	3.97	1.11	TD_Cd_GL_DY
Queenston	S1	73	15.2	12.7	32.9	48	6.13	2.03	0.69	0.33	TD_Cd
			25.2	22.7	52.9		6.12	2.04	1.10	0.33	TD_Cd_GL
			25.2	22.7	52.9		6.11	3.42	1.10	0.56	TD_Cd_GL_PP
Georgian Bay	S1	89	16.1	13.6	34.7	40.8	6.12	2.72	0.85	0.44	TD_Cd
			26.1	23.6	54.7		6.11	2.74	1.34	0.45	TD_Cd_GL
			26.1	23.6	54.7		6.12	2.73	1.34	0.45	TD_Cd_GL_PP

Notes: Maximum depth of yielding/EDZ ( $d_f$ ) in each unit is reported. This is not always typical of plane strain depth of yielding for given unit properties.

1.  $\sigma_{max}$  is elastically calculated maximum tangential stress around a circular opening.
2.  $a$  is the radius of the excavation at the location of the estimated depth of the EDZ ( $d_f$ ), not the initial shaft radius.
3. Loading abbreviations: time dependent strength degradation (TD), concrete degradation (Cd), glacial loading (GL), pore pressure (PP), seismic (DY).



Notes: Assumed geometries of the EDZ made for the safety assessment are shown as horizontal lines.

Figure 6.17: EDZ and HDZ Estimates for Base-case

Results of the FLAC3D analyses (including excavation sequence and layer geometry) were compared with 2D results from finite-element analyses using Phase<sup>2</sup> (Rocscience 2009). In both cases, the rock strength was estimated using the GSI system (Hoek et al. 2002) for peak strength without considering excavation damage. Residual (post yield) strengths were estimated using the same system but with excavation damage considered (damage parameter set to unity instead of 0.5, as in FLAC3D analysis). Additionally, the 2D analyses were carried out using the brittle spalling approach of Diederichs (2007). The GSI approach assumes plastic shearing as the failure mechanism while the brittle spalling approach assumes extensile fracturing. Many of the rock masses could experience one or the other behaviour depending on the thickness of the rock unit being analyzed and so these two analyses bracket the expected response. The EDZ is defined by the presence of yield in the model and represents a maximum estimate. The HDZ estimates are based on increased rates of strain as illustrated in Figure 6.13 and Figure 6.9 and negative net volumetric strain (Figure 6.13) and as such, represent conservative estimates of fracture damage.

**CASE 2 Effects of Gas Pressure Build-up**

A detailed 2D representation of the repository, shaft seal system and the surrounding Ordovician- and Silurian-age formations was modeled using two-phase flow and transport

modelling for a base-case and an extreme case. The shaft, shaft seals, and shaft EDZ were explicitly included in the model. Gas-generation processes within the repository were modeled and the pressure and flow response simulated for a 1 Ma period using T2GGM, a modified version of the TOUGH2/EOS3 model (Pruess et al. 1999). Pore pressure histories from the base-case model for seal B1 until 1 ka are shown in Figure 6.18. Although the pore pressures are shown until 1 ka only, they remain basically constant after 1 ka until 1 Ma. Over the long-term, the pore pressure gradually increased to a steady-state value of approximately 3.9 MPa, as the shaft materials responded to pressure changes transmitted from the repository, and equilibrated to pressures in the surrounding intact rock.

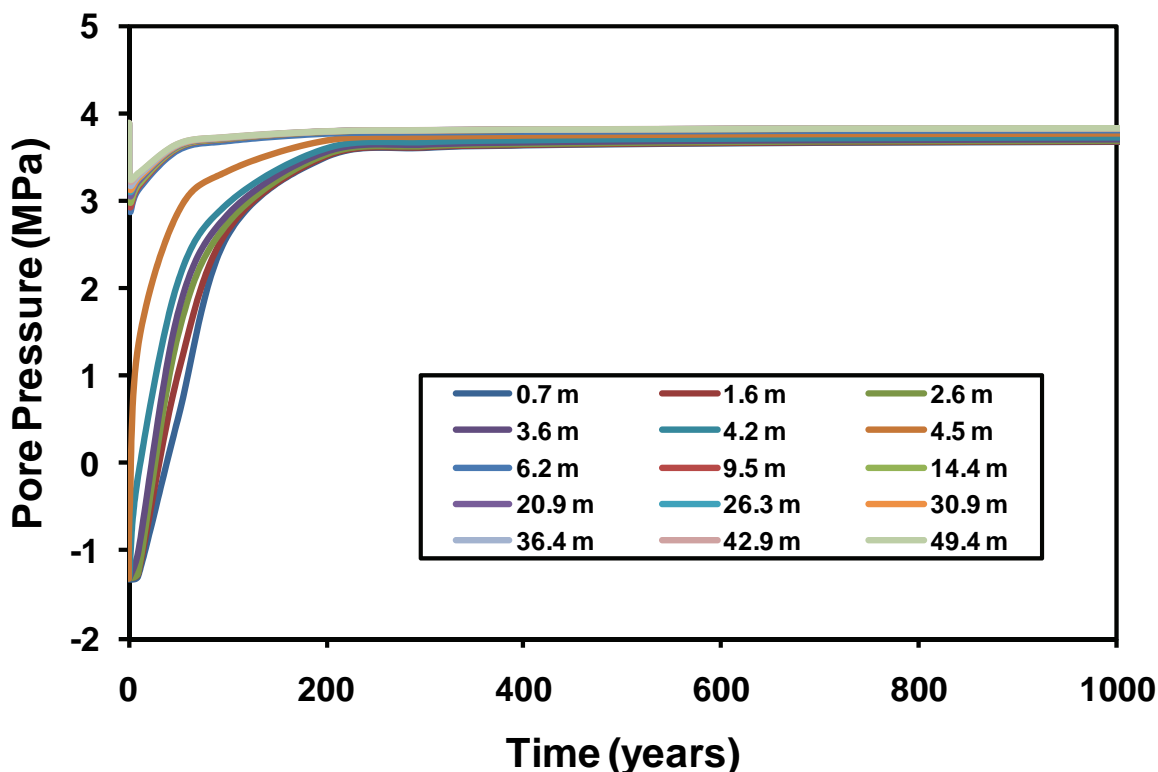


**Figure 6.18: Pore Pressure Data (Base-case) at Various Distances from the Shaft Centre for Seal B1**

For the effective stress analyses, seal B1 was modelled as it is the deepest and will be subject to the greatest water and gas pressures. For comparison, seal S1 was also modelled. For seal B1, the pore pressure had little short-term (initial excavation) effect on the extent of yielding, while the long-term pore pressure evolution resulted in some increased yielding around the shaft seal/backfill. The long-term pore pressure evolution combined with strength degradation and glacial loading could increase the extent of model-predicted damage locally by at most 1.4 m for seal S1.

### **CASE 3      Effects of Glacial Loads**

During the next advance of continental-scale glaciation, predicted to occur between 60 and 80 ka, it is anticipated that each seal will be subjected to glacial loading with a maximum vertical pressure of about 30 MPa (approximate ice thickness of 3 km; Peltier 2011). An assumed horizontal stress increase of 2 MPa due to bending of the strata was also imposed in the simulation in addition to the in situ stress profile described in Chapter 3.

The addition of glacial loading combined with strength degradation had only minimal effect on the extent of damaged rock due to the confinement provided by the shaft backfill. The effect of a single glacial event on the shaft EDZ is almost negligible, thus multiple events were not analyzed (Figure 6.19 and Figure 6.20).

### **CASE 4      Effects of Seismic Ground Shaking**

The effect of seismic ground shaking was evaluated by incorporating ground motions developed as part of the PSHA (AMEC GEOMATRIX 2011) directly into the simulation. Although time histories for a number of horizons were generated from the PSHA based on the P- and S-wave velocity profiles, only Seal B1 was analyzed to provide insight on the seal behaviour under seismic conditions.

A FLAC3D dynamic analysis was carried out for seal B1 with a full-scale model (i.e., no lateral symmetry). The model was run with time-dependent strength degradation and glacial loading until 67.2 ka — a point at which the maximum glacial cycle had been reached. At this state, the model was subjected to three  $10^{-6}$  Pa event ground motions. As shown in Figure 6.21, seismic loading had no effect on the extent of failure for seal B1. Because the effect of seismic loading on the shaft is negligible, no additional seismic analyses were carried out for other seals.

#### **6.4.3.5    Modelling Results**

A comparison of all of the 3D analyses described above is presented in Figure 6.22. Due to the vertical geometry of the shaft, glacial loading has only a minor effect on differential ground stresses in the horizontal plane. Consequently, the effect of EDZ increase during glaciations is minor for the shaft. Similarly, pore pressure and seismic loading will not significantly increase the predicted EDZ around the shaft. The extent of the damage zone, HDZ and EDZ, is generally in the range of 0.6 to 0.7 times or less of the shaft radius. If HDZ generation is linked to the EDZ, similarly minor influences of glaciations and pore pressure can be assumed with respect to the HDZ. The estimated thickness of the HDZ (from the shaft wall to the outer limit of the HDZ) is approximately 0.5 m, or 0.11 times the radius of the access shaft. Figure 6.22 also shows the distribution of the EDZ with depth, showing representative EDZ extent and maximum EDZ extents in formations under study. Because of the low rock strength, the Cabot Head shale reveals a much more significant EDZ (1.25 times the shaft radius) than the remaining sedimentary sequence. The extent of the EDZ varies with lithology and intersection with geological features and excavation methods. Because the EDZ behaves like a serial system, local increase in EDZ will not increase the effective axial permeability along the vertical shaft. The predictions of maximum EDZ from the shaft seal analysis summarized in Table 6.5 are consistent with observations from international waste management laboratories.

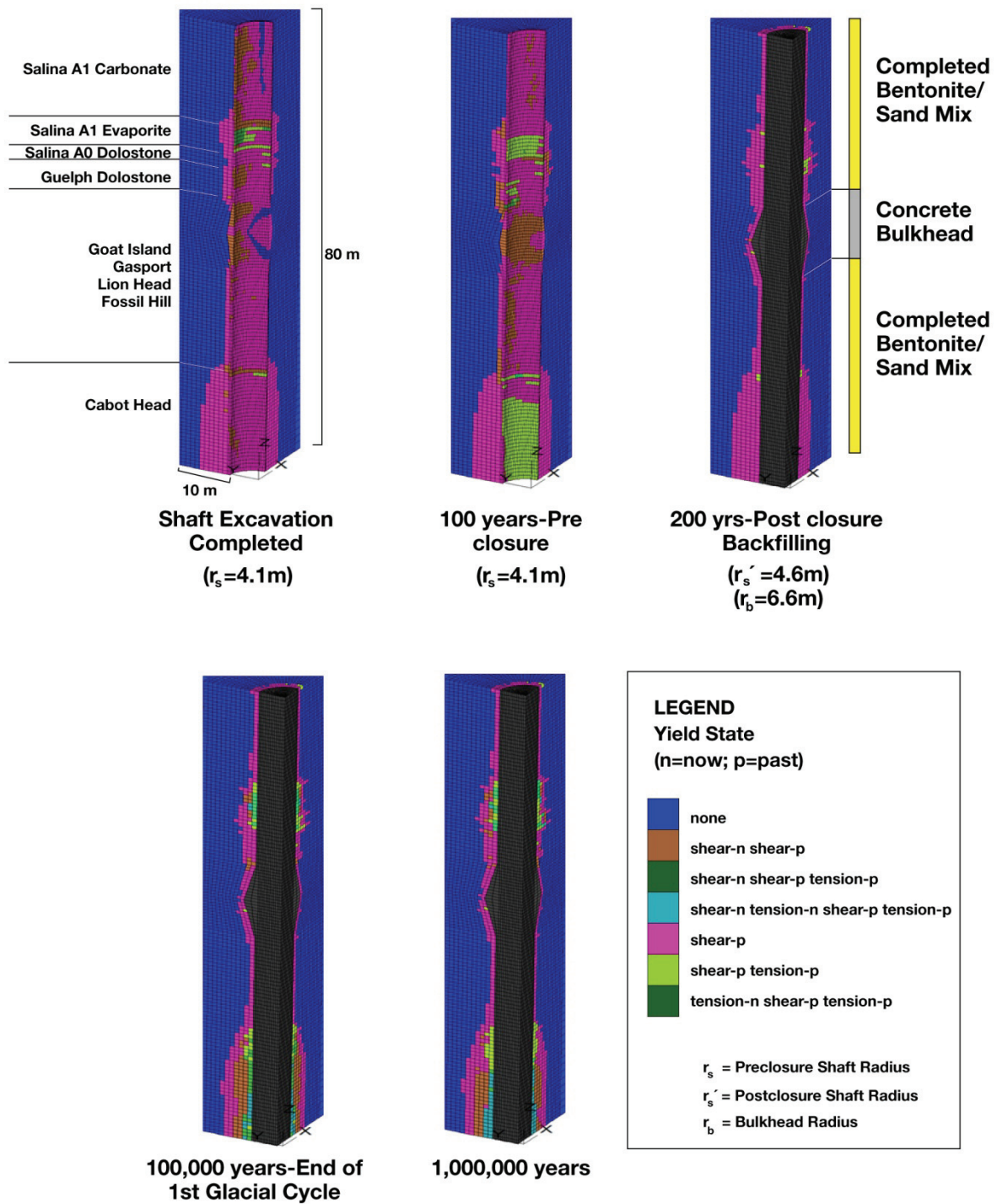


Figure 6.19: Yield State – Concrete Bulkhead B1: Time-dependent Strength Degradation + Glacial Load + Pore Pressure

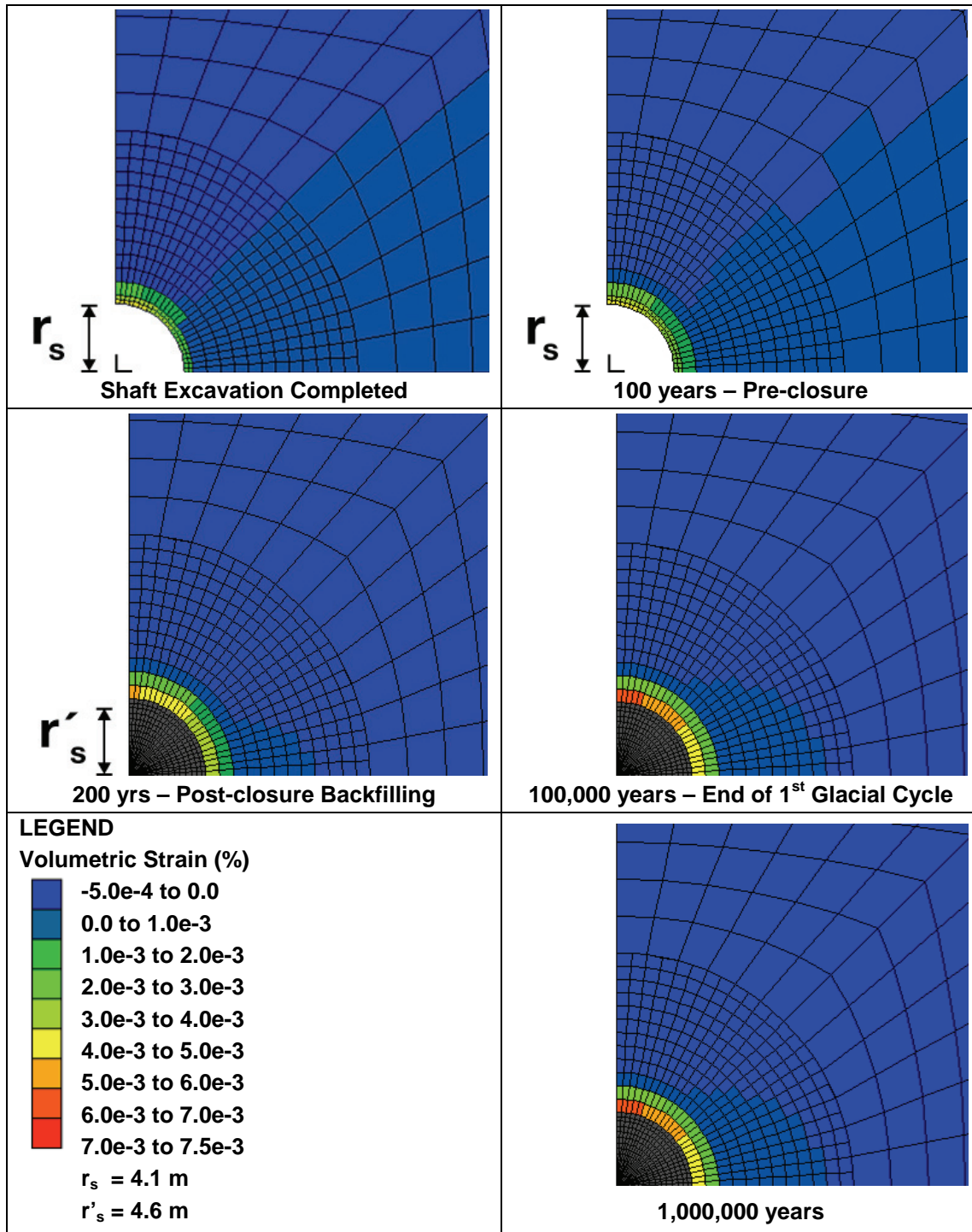
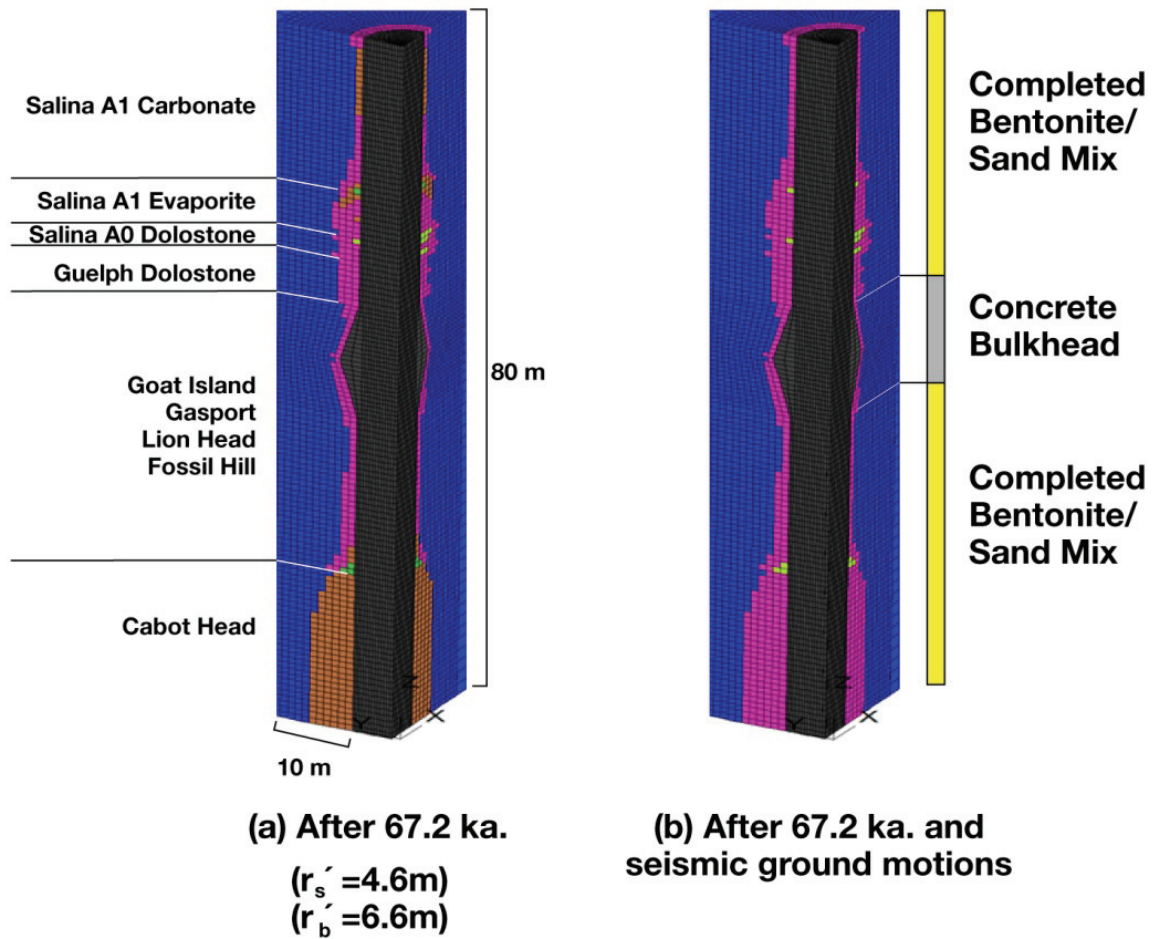


Figure 6.20: Volumetric Strain – Concrete Bulkhead B1 (Lions Head Formation): Time-dependent Strength Degradation + Glacial Load + Pore Pressure



**LEGEND**  
 Yield State (n=now; p=past)



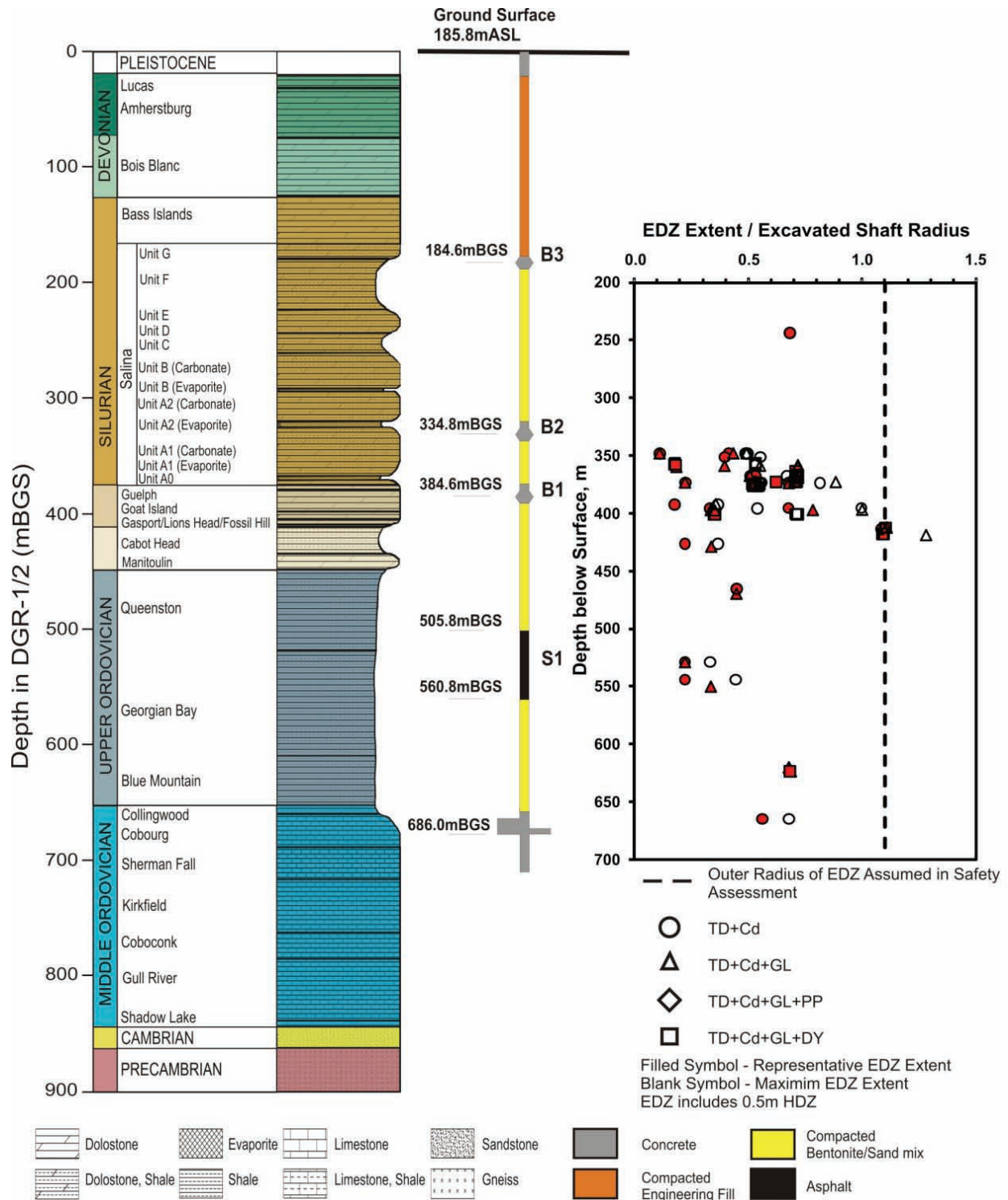
 none	 shear-p	$r_s$ = Preclosure Shaft Radius
 shear-n shear-p	 shear-p tension-p	$r'_s$ = Postclosure Shaft Radius
 shear-n shear-p tension-p		$r_b$ = Bulkhead Radius

Figure 6.21: Yielded Zones around the Shaft (Concrete Bulkhead B1) before and after 3 Seismic Events of  $10^{-6}$  Annual Exceedance Frequency Were Applied



Notes: EDZ extents include 0.5 m HDZ. Refer to Table 6.5 for loading abbreviations.

**Figure 6.22: Distribution of Representative EDZ Extents in Specific Formations and Maximum Local EDZ Extents**



The DGR will have an 8 m diameter access shaft and a 6 m diameter vent shaft. The distance between these shafts is approximately 80 m. The maximum radius of the shafts considering over-excavation for concrete seals and removal of the HDZ is less than 5 m. Based on the shaft seal analyses, the maximum depth of the yielded zone along the entire shafts, including both the HDZ and EDZ, is slightly above one shaft radius. It is known that if the distance between two excavations is three diameters or greater, the elastic interaction of rock mass due to the excavation is negligible. In the case of the DGR shafts, the overall relaxation zone including the yielded zone is less than 20 m. Considering the 80 m distance between the shafts, there will be no interaction between the shafts.

#### **6.4.4 Emplacement Room Stability: 2D Analyses**

The results of analyses of long-term stability of the DGR emplacement rooms are documented by Itasca Consulting Group, Inc. (ITASCA 2011). A preliminary analysis was based on test results obtained on rock samples taken from deep boreholes DGR-1 and DGR-2 (Gorski et al. 2009a). The 2011 analysis incorporated additional data on the mechanical behaviour of different rock units at the site obtained by testing samples from deep boreholes DGR-3 and DGR-4 (Gorski et al. 2010a, 2010c). The new data also included test results on the long-term strength of the Cobourg limestone (Gorski et al. 2009b, 2010b).

The performance of the emplacement room with time was broken up into a number of time intervals:

- End of operation (100 a);
- After long-term strength degradation (pre-glacial) (50-60 ka);
- After one glacial period (~100 ka); and
- After many glacial periods, multiple seismic events (to 1 Ma).

Analyses for emplacement room stability over the first 100 ka were based on reasonable extrapolation of measured material parameters and consideration of long-term material properties. Stability of the emplacement room over the first three time intervals resulted in a limited degree of overbreak with no influence extending to the overlying shales or the underlying limestones.

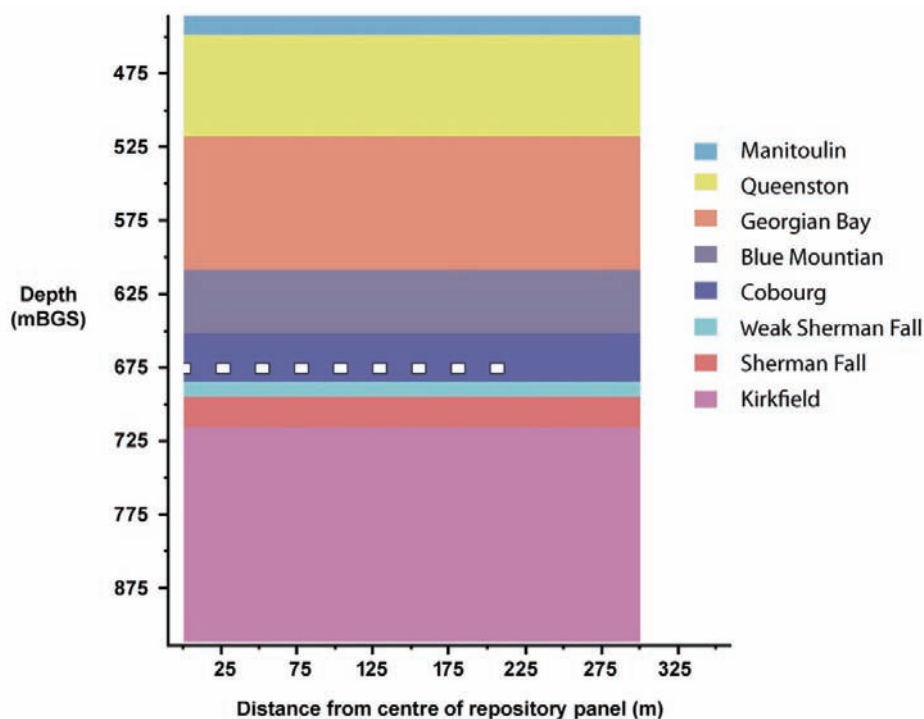
Due to the increasing uncertainties inherent in predicting of material behaviour and changes in the geological environment in the long-term, the stability of the repository beyond a few hundred thousand years must be defined as a self-arresting deterioration of each individual emplacement room and pillar. The long-term stability thereafter relies on material bulking (observed in mining and in natural caves). This is verified by complex simulations involving the unravelling and build-up of rock blocks within the emplacement room opening. Such material will expand in volume after failure from the roof and walls and will eventually fill up the void space in the emplacement room and stabilize the rock mass by preventing further collapse.

For laminated rocks at depth, where roof arching limits failure, it is not possible to calculate the height of failure and the effects of bulking using simple arithmetic. Numerical analysis is required to understand the geometry of failed rock that is generated in order to predict the influence of this bulking and associated settlement. The generally accepted values for the bulking factor (ratio of broken rock volume to intact rock mass volume) are 20-30%.

Stability in this extreme case is defined as a self-stabilization of the collapsing repository horizon with the terminal settlements within the damage tolerances of the overlying strata, preserving the integrity of the natural barrier system. Model results indicate this to be the case.

#### 6.4.4.1 Long-term Strength Selection

Any stability analysis of an underground opening requires an estimate of rock strength. The most widely used measure of intact rock strength is the laboratory UCS, hence all rock strengths used in this section are expressed in terms of the UCS. It was shown in Chapter 3 that the long-term in situ strength is an unknown parameter bounded by the laboratory peak strength (100% UCS) and CI stress (45% UCS). To evaluate the impact of the assumption of the long-term strength on the repository emplacement room performance, a parametric analysis was carried out for six values of the Cobourg (which, for modelling purposes in section 6.4, also includes the Collingwood Member) long-term strength using the geometry shown in Figure 6.23.



Notes: Cobourg includes the Collingwood member.

**Figure 6.23: Geometry of the Model for Panel-scale Parametric Analysis**

The sensitivity of the emplacement room stability to the assumption of the long-term strength was investigated using six long-term strength values for the Cobourg Formation (including the Collingwood Member):

- 90 MPa (81% UCS);
- 81 MPa (73% UCS);

- 72 MPa (65% UCS);
- 63 MPa (57% UCS);
- 54 MPa (49% UCS); and
- 45 MPa (40% UCS).

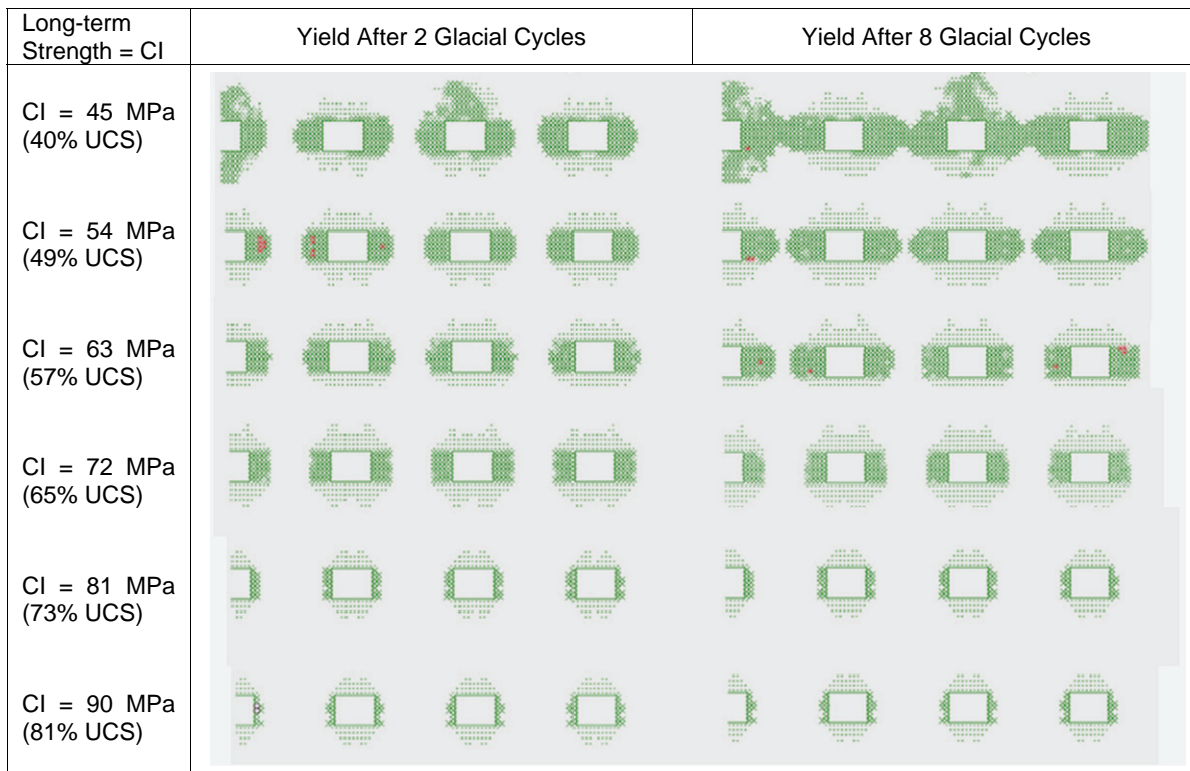
Ten glacial cycles were simulated for each long-term strength case. Because the time-dependent strength degradation was not explicitly simulated (i.e., from the beginning of the simulation it was assumed that the strength is equal to the long-term-strength), the glacial load cycles were applied quasi-statically, irrespective of time. In each cycle, the vertical stress on the top of the model in addition to the vertical stress due to overburden weight was gradually increased from zero to the maximum glacial load of 30 MPa and subsequently decreased again to zero. Figure 6.24 shows the evolution of plasticity around 7 emplacement rooms in the middle of the repository (only half are shown because of symmetry) after 2 and 8 glacial cycles for the 6 values of long-term strength investigated. Each figure shows regions of plastic deformation, where rock yields because stresses reach the yield strength. It is clear from Figure 6.24 that as the long-term strength decreases the damage to the emplacement room and pillar increases. The results also show that it is only at the lowest long-term strength (40% UCS) and only after 8 cycles of glaciation that the yield zone (EDZ) of the emplacement rooms and pillars starts to form a continuous yield zone. These are extreme assumptions, which are not supported by any field observations. Nonetheless this long-term strength is used to examine the potential effect of such yielding on the long-term stability of a single emplacement room. To simulate such effect a discrete element code is utilized to ensure that the outcome is not biased by numerical limitations.

#### 6.4.4.2 Numerical Analyses

Continuum analyses suffer from the limitation that the material cannot physically integrate into discrete blocks after yield and fracture. To include this effect in the analysis and to include full consideration of gas and water pressure, as well as seismic and glacial loading, a more complex analysis is necessary. Itasca Consulting Group, Inc. (ITASCA 2011) carried out the analysis using the hybrid discrete-element / finite-difference code UDEC (Universal Distinct Element Code; ITASCA 2006). The model and the methodology of the analysis were similar to those used in the 2008 analysis (Damjanac 2008), with slightly different emplacement room geometry. The emplacement room height used was 7 m, and the width used was 8.6 m. The width of the pillars between emplacement rooms was 17.2 m. A region extending below and above the emplacement rooms, where the greatest potential damage and unravelling are expected to occur, was discretized in 0.3 m Voronoi blocks, which allowed the simulation of initiation and propagation of stress-induced fractures in the rock mass and formation of loose blocks.

The material properties for different units used in the analysis and the derivation of micro-mechanical properties for the Voronoi complex were based on test data and calibration as documented by Itasca Consulting Group, Inc. (ITASCA 2011). The bedding planes, which were explicitly represented in the Cobourg and weak Sherman Fall limestones, were assumed to be at a 0.75 m spacing and have shear strength and stiffness properties consistent with test data. The analyses were carried out for thicknesses of the competent Cobourg limestone in the emplacement room floor between 2 m (very conservative) and 6 m (specified minimum floor cover). In all analyses, the vertical stress at the repository level was 18 MPa, while the

horizontal stress was 36 MPa (i.e.,  $K$  (stress anisotropy) = 2 as a conservative case although the emplacement rooms will be oriented in the direction of the major principal stress).



Notes: Top is the base-case for this analysis. Bottom represents response using CI=90 MPa or no strength degradation. Yield indicators (dots around rectangular openings) represent EDZ development.

**Figure 6.24: Evolution of Plasticity Around Emplacement Rooms After 2 and 8 Glacial Cycles for Different Long-term Strengths**

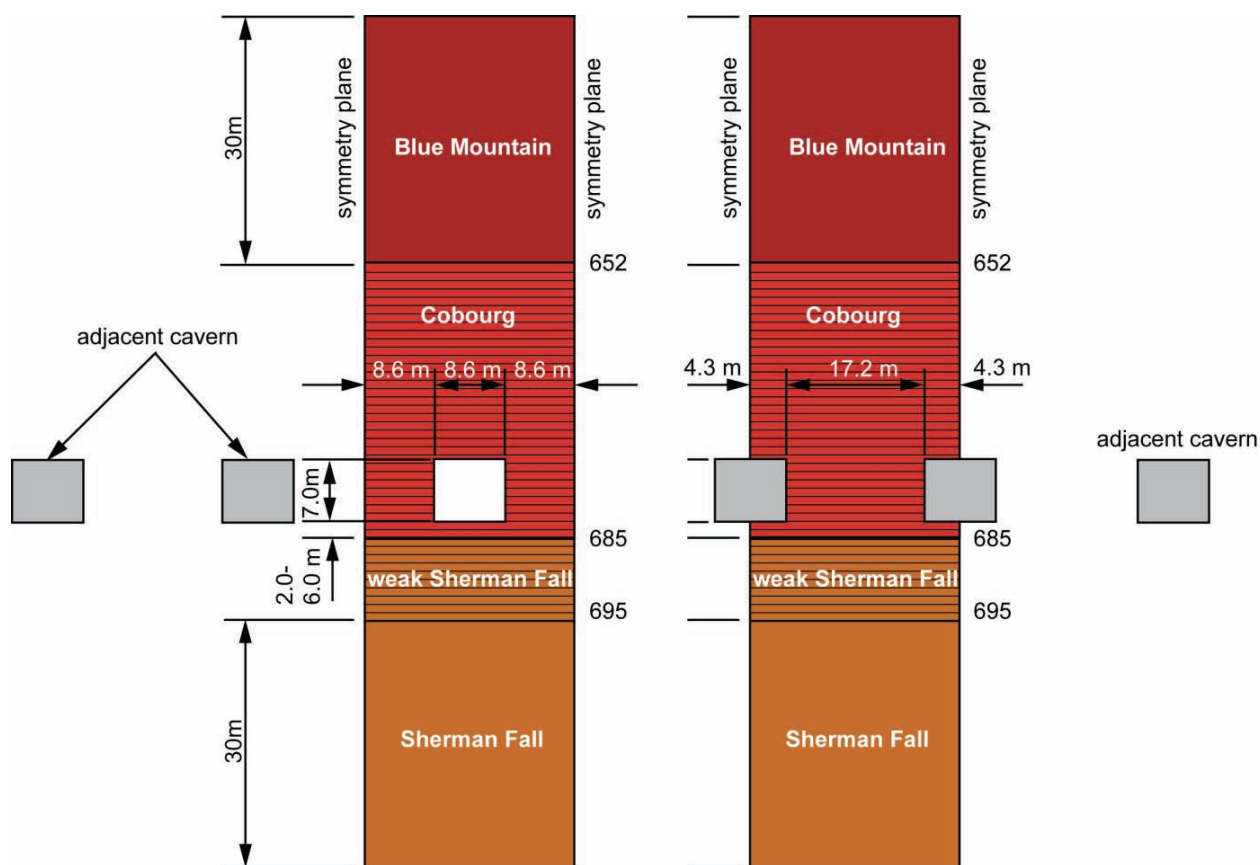
Similar to the shaft seal analyses described in Section 6.4.2, numerical analyses on DGR emplacement room stability were carried out to study the following possible cases:

- Time-dependent strength degradation;
- Strength degradation with additional effects of gas pressure build-up;
- Strength degradation with additional effects of seismic ground shaking;
- Strength degradation with additional effects of glacial loading; and
- Combinations of all of the above scenarios.

Corroborating analyses of emplacement room stability were undertaken using a finite-element code (Phase<sup>2</sup> v7; Rocscience 2009) that also incorporates discontinuity elements.

The emplacement room and pillar-scale analyses were carried out by Itasca Consulting Group, Inc. (ITASCA 2011) using the numerical code UDEC V4.01.203 (ITASCA 2006). The typical

geometries of the analyzed models for static calculations are shown in Figure 6.25 (elevations in the figures are shown as depths and, therefore, are positive values). Two 2D geometries were considered, one representative of the emplacement rooms and the other representative of the pillars, to ensure that the symmetry conditions applied along the vertical model boundaries do not affect the failure modes. The emplacement room lengths (265 m), compared to characteristic dimensions in the cross section, justify the use of a 2D approximation for the analysis. Although only one emplacement room or pillar is included explicitly, the models, with symmetry boundary conditions, approximate typical conditions in the middle of the panels. In fact, the models overestimate the vertical loads because stress arching above the panels is neglected.



Notes: Cobourg includes the Collingwood Member. Figure is modified from ITASCA (2011).

**Figure 6.25: Geometries for the Emplacement Room Models (DGR Inverts at 683 mBGS and 679 mBGS)**

Rock mass properties used were from the laboratory test results conducted on rock cores retrieved from DGR-2 to DGR-4. The emplacement room geometry, rock support, waste storage content, rock mass behaviour, and in situ stress conditions assumed for these analyses were as described below.

- The modelled DGR emplacement rooms have a height of 7 m, width of 8.6 m, and a pillar width of 17.2 m between emplacement rooms, and are unsupported with no backfill.
- All waste packages are excluded, the rooms are empty, or degraded waste is reduced to a frictional pile 1.4 m high on the floor at an early stage of the repository service life.
- The floor clearance to the top of the Sherman Fall Formation is 6 m for the optimum design case.
- Static fatigue test data from Lac du Bonnet granite were adopted to give an approximate rate of strength loss for the long-term strength degradation analysis (according to which the strength is reduced to the lower bound values prior to the first glacial event).
- For the rock material between the bedding planes, initial (upper bound) rock mass UCS is taken as 90 MPa (mean – 1 standard deviation). This is a comparable and conservative alternative to CD strength as a representative short-term wall strength.
- The long-term minimum strength degradation threshold for the Cobourg is set to 45 MPa corresponding to the mean CI threshold from test data (approximately 40% of the mean UCS). The use of CI for long-term strength is already a very conservative assumption and so the mean value CI is used for this purpose.
- A bedding-plane spacing of 0.75 m was assumed.
- The horizontal in situ stress in the analysis is conservatively assumed to be a factor of 2 times the vertical stress (NWMO and AECOM 2011).
- The rock mass between the bedding planes is allowed to break into discrete blocks less than 0.3 m in size (in UDEC simulations).
- The micromechanical properties are used as input into the UDEC discrete-element model. The calibration (based on bulk properties summarized above) and verification of this input are discussed in the long-term case (ITASCA 2011).

Selected bedding-plane strength data are listed in Table 6.6 based on interpretation of available test data. These parameters represent one possible fit for the strength data. As shown in the next section, this interpretation (higher cohesion but lower friction) is conservative compared to the alternative (low cohesion, higher friction).

**Table 6.6: Bedding-plane Strength Data**

Peak Cohesion (MPa)	Peak Friction Angle (°)	Residual Cohesion (MPa)	Residual Friction Angle (°)	Tensile Strength (MPa)	Joint Normal Kn GPa/m	Joint Shear Ks GPa/m
3.31	38.3	0	38.3	0.66	219	14.6

Notes: Data are from ITASCA (2011).

#### 6.4.4.3 Lower Bound Long-term Strength

Simulations of emplacement room and pillar evolution were also performed using lower bound strength conditions. Figure 6.26 shows the results of modelling two scenarios using the pillar-centred model (pillars and emplacement rooms are assumed to be infinitely repeated in both

directions). In both cases,  $CI = 45$  MPa was used as the long-term lower bound strength in the Cobourg. This represents a conservative approach. The floor thickness (to the weak Sherman Fall unit) was increased to the recommended 6 m and 1.4 m of frictional material was included in the emplacement room to represent degraded waste. In the upper case shown, dry conditions were maintained while two glacial loading cycles were simulated. In the lower case shown, formation pore pressures and repository gas pressures were included while one glacial loading cycle was simulated. Using a lower bound long-term strength, the dry condition (no pore or gas pressure) is the conservative case, as it shows more fracture and bedding separation into the roof (larger EDZ and HDZ) at 100 ka than the case including pore and gas pressures. Both cases show some upward stoping at both 100 ka and 1 Ma.

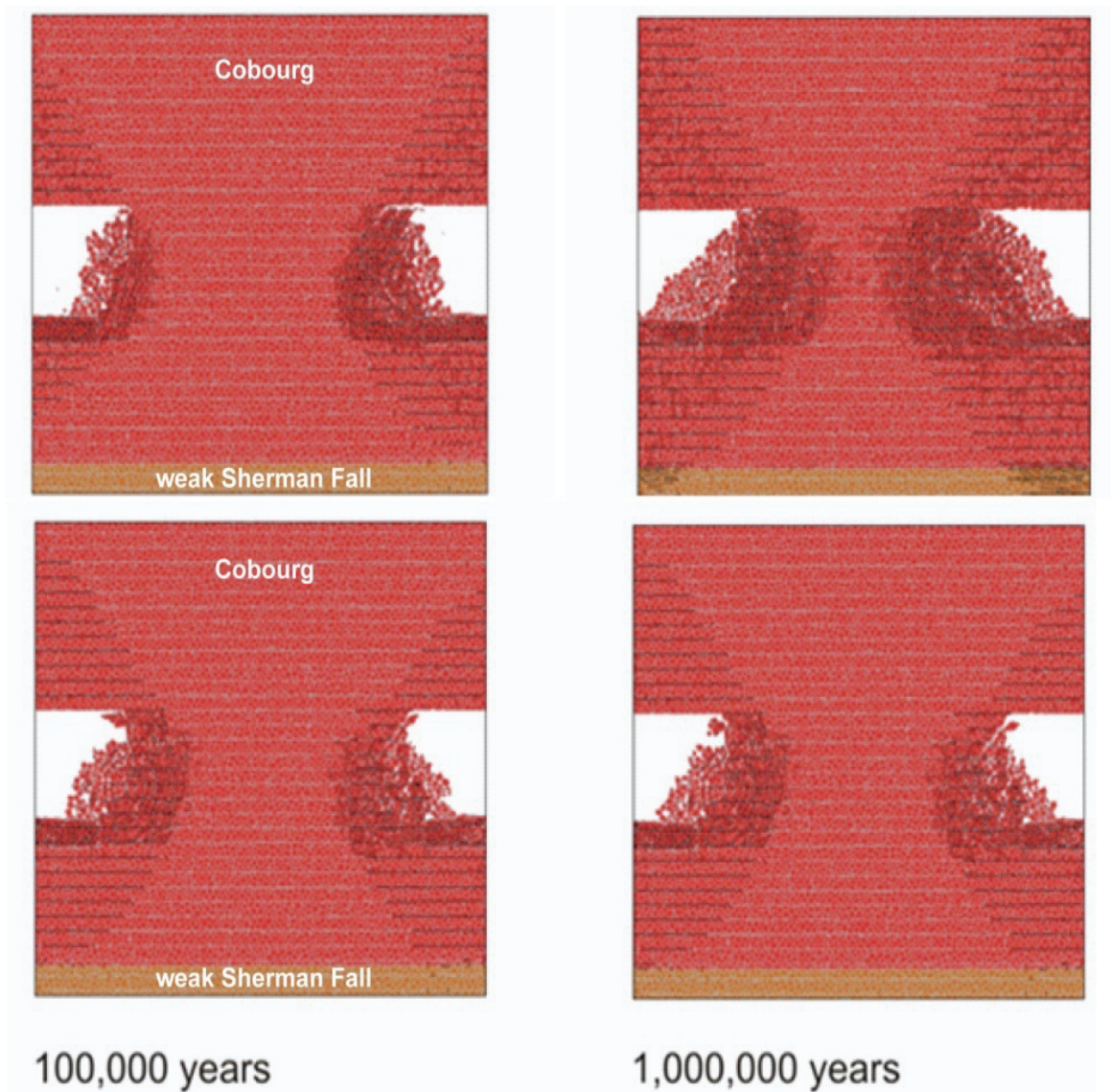
The emplacement room is located in the high-strength Cobourg Formation, which provides a competent roof for the emplacement room. The overlying Collingwood Member is a high-strength shale and limestone unit with mechanical properties that are only slightly lower than those of the Cobourg. The interval from 685 to 695 m BGS, comprising the lower 3 m of the Cobourg and the upper 7 m of the Sherman Fall Formation, has lower strength than the overlying and underlying rocks, and is here named the "weak Sherman Fall". In this study, two floor horizons at 683 mBGS and at 679 mBGS, 2 and 6 m above the top of the weak Sherman Fall unit, were examined, with 6 m providing the optimum balance between floor and roof cover within the Cobourg host rock.

A region extending below and above the emplacement rooms, where greatest potential damage and unravelling are expected to occur, was discretized in 0.3 m Voronoi blocks, which allowed simulation of initiation and propagation of stress-induced fractures in the rock mass and formation of loose blocks. The bedding planes, which were explicitly represented in the Cobourg and weak Sherman Fall formations (Figure 6.26), were assumed to be at 0.75 m spacing.

#### 6.4.4.4 Multiple Glaciations

Timeframes extending beyond 100 ka are not within the conventional scope of engineering geomechanics. It is not possible to predict the exact cycle or extent of glaciations in this timeframe. Therefore, maximum glacial events (3 km of ice) were applied in the model at 60, 100, 200, and 300 ka, peaking 7 ka later in each case. Each glacial event, predictably, induced additional damage to the emplacement rooms. This damaged material fails into the emplacement room with an increase in volume (typically 20-30%). Eventually, the failed and expanded material from the roof, floor, and walls chokes the emplacement room and provides a natural backfill. In old mining stopes and in natural caverns, this material will remain and prevent further collapse. Using the model parameters defined previously (short-term strength=mean UCS - 1 x std = 90 MPa, Long-term strength=CI=45 MPa), the results for the 2<sup>nd</sup>, 3<sup>rd</sup>, and 4<sup>th</sup> glacial periods are shown in Figure 6.27. By the fourth glacial cycle, this discontinuum model shows that the emplacement room is effectively choked and further collapse is prevented indefinitely.

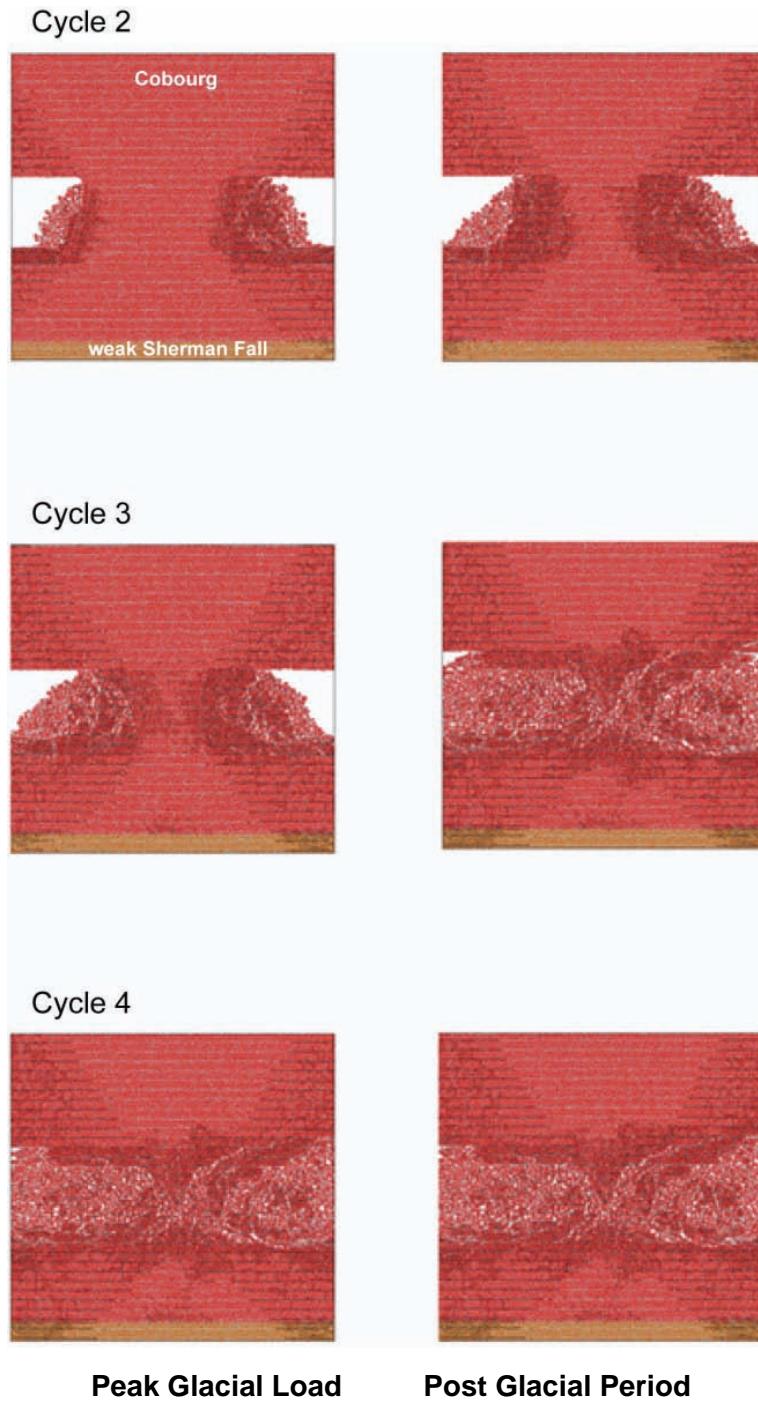
The choking of the excavation due to bulking is consistent with observations of collapses in large natural caverns where groundwater flow has been rediverted and the material is not dissolved but allowed to bulk. Typically, reported bulking factors of 25% are consistent with the results of the UDEC analyses. Typical bulked material in a collapsed limestone cavern is shown in Figure 6.28. This cavern is essentially stabilized by the bulking of material from the roof and walls.



Notes: Top row loading conditions: time-dependent strength degradation; dry conditions (no pore or gas pressure); 1st glacial cycle started at 60 ka and reached its peak at 67.2 ka; 2nd cycle started at 100 ka and peak at 107 ka; no seismic loading. Bottom row loading conditions: same as above but with pore and gas pressure; 1 glacial cycle started at 60 ka and reached its peak at 67.2 ka with ice removal by 80 ka. 6-m floor with 1.4 m degraded waste. Rubble is allowed to accumulate. The Cobourg Formation includes the Collingwood Member.

**Figure 6.26: Evolution of Emplacement Room Outline and Pillar Damage with Lower Bound Strength, Gas and Pore Pressures**





Notes: Time-dependent strength degradation and dry conditions; 1st glacial cycle started at 60 ka and peaked at 67.2 ka; 2nd cycle started at 100 ka and peaked at 107 ka; 3rd cycle started at 200 ka and peaked at 207 ka; 4th cycle started at 300 ka and peaked at 307 ka; no seismic load. DGR invert at 679 mBGS. The Cobourg Formation includes the Collingwood Member.

**Figure 6.27: Evolution of Emplacement Room Outline and Pillar Damage, Representative Case for Four Glacial Cycles**



Notes: The collapse shown on the left has evolved over 100,000 years. Photographs are from Waltham (1981).

**Figure 6.28: Bulking Examples of Collapsed Limestone Cavern Roofs**

The effect of pore and gas pressure evolution on the structural performance of the repository was investigated using the UDEC model. The rock formations at the DGR are saturated under in situ conditions. Corrosion of the waste inside the emplacement rooms will result in the generation of gases. During the post-closure phase of the repository, gases generated as a result of waste degradation will cause pressure changes inside the emplacement room, as well as in the surrounding damaged zones due to diffusion of the gas into the available porosity. Because of the low permeability and high gas entry pressure of the intact Cobourg limestone, a significant amount of the gas will remain inside the emplacement rooms, resulting in a gradual build-up of gas pressure.

Effective stress analyses that account for pore-pressure effects on the failure of rock (around the shaft seals and emplacement rooms) have been carried out in order to evaluate the long-term effect of gas and pore pressure evolution inside and around the emplacement rooms. The analyses were carried out using one-way coupling (as opposed to fully coupled), meaning that pore-pressure evolution with time was used as input into the model and these pore pressures were used by the material constitutive models.

A modelling study of the evolution of pressures in the emplacement rooms and rock for a number of different scenarios using the two-phase flow numerical code T2GGM, described in Section 6.4.2. Itasca Consulting Group, Inc. (ITASCA 2011) used these results to evaluate the effects of gas and pore pressures on emplacement room and pillar stability. The base-case represented the most unfavourable conditions for damage of rock as it predicted the largest pressures and pressure gradients.

In general, fluid flow around the emplacement rooms involves two phases: 1) gas generated inside the emplacement rooms and 2) in situ water. However, the two-phase flow analysis showed that the rock mass in the base-case remained almost completely saturated with water throughout 1 Ma, while the gas generated inside the emplacement rooms did not migrate far

into the rock. Thus, in order to resolve detailed pore pressures around the emplacement rooms, the analysis of water pressure evolution on the room scale was conducted in a single-phase continuum model using the numerical code FLAC (ITASCA 2008). In this model, the gas pressures inside the emplacement room, as calculated in T2GGM, were used as evolving boundary conditions for water flow inside the rock mass. The FLAC flow model also accounted for the effect of the glacial loads on the pore pressures. The changes in pore pressures due to stress change and water pressure dissipation during a glacial cycle were also simulated in FLAC.

The pore-pressure contours in the vicinity of the emplacement rooms and in the pillars as imported from FLAC into the UDEC model are shown in Figure 6.29. The pressure contours indicate that within the first 100 years, the horizontal pressure gradients become negligible. Even during the glacial cycle when pore pressures are generally increased by the weight of the overlying ice, the pressures throughout the pillar are in equilibrium with the pressure inside the emplacement room. That implies that pore pressures will not have a negative effect on the pillar stability. Although non-negligible pressure gradients in the vertical direction persist for a longer time, after 1000 years they become relatively small compared to the initial and early-time conditions.

The pressure contours shown in Figure 6.29 do not show the effect of fracturing on water pressures. Observations and in situ measurements indicate that predicting pore pressure using conventional poroelasticity concepts may not be correct for intact, low-porosity rocks because the formation extension and volumetric expansion of micro-cracks in the pre-peak stress range can result in a significant drop in formation pore pressure prior to the material reaching its effective stress yield limit. This has been demonstrated around a mine-by test tunnel in the Opalinus Clay formation in Switzerland (Souley et al. 2007). Because the porosity of most of the units in the geological profile is small (e.g., porosity of the Cobourg is ~2%), a small dilation due to rock micro-cracking would cause a pressure drop to zero. An approach is implemented in the models used for long-term stability analysis of the emplacement rooms and the shafts in which the pore pressure at the fracture location is conservatively set to the gas pressure inside the emplacement room at the instant the fracture is formed. Although fracturing would cause instantaneous pressure drop to zero, gas dissipation throughout the damaged zone (with increased permeability) will equilibrate over some time the pressures throughout the damaged zone with the emplacement room pressure.

#### **6.4.4.5 Potential for Hydraulic Fracturing**

The decaying waste will produce gas and the build-up of this gas pressure in the emplacement rooms has the potential to open any fracture planes that are normal to the minimum principal stress. At the repository depth, the vertical stress of 17 MPa is the minimum principal stress and, therefore, the potential for hydraulically induced fracturing is greatest along the sub-horizontal bedding planes, if the gas pressure should exceed the vertical stress of approximately 17 MPa. The gas pressure, using normal gas generation rates, is not expected to exceed 8 MPa (Figure 6.12). The results of the geomechanical analyses for the normal pressure evolution scenario, that include the effects of gas pressures in the repository, do not indicate any localized fracture development typical of hydraulic fracturing. No horizontal fractures can be observed propagating from the emplacement room to distances greater than a few metres.

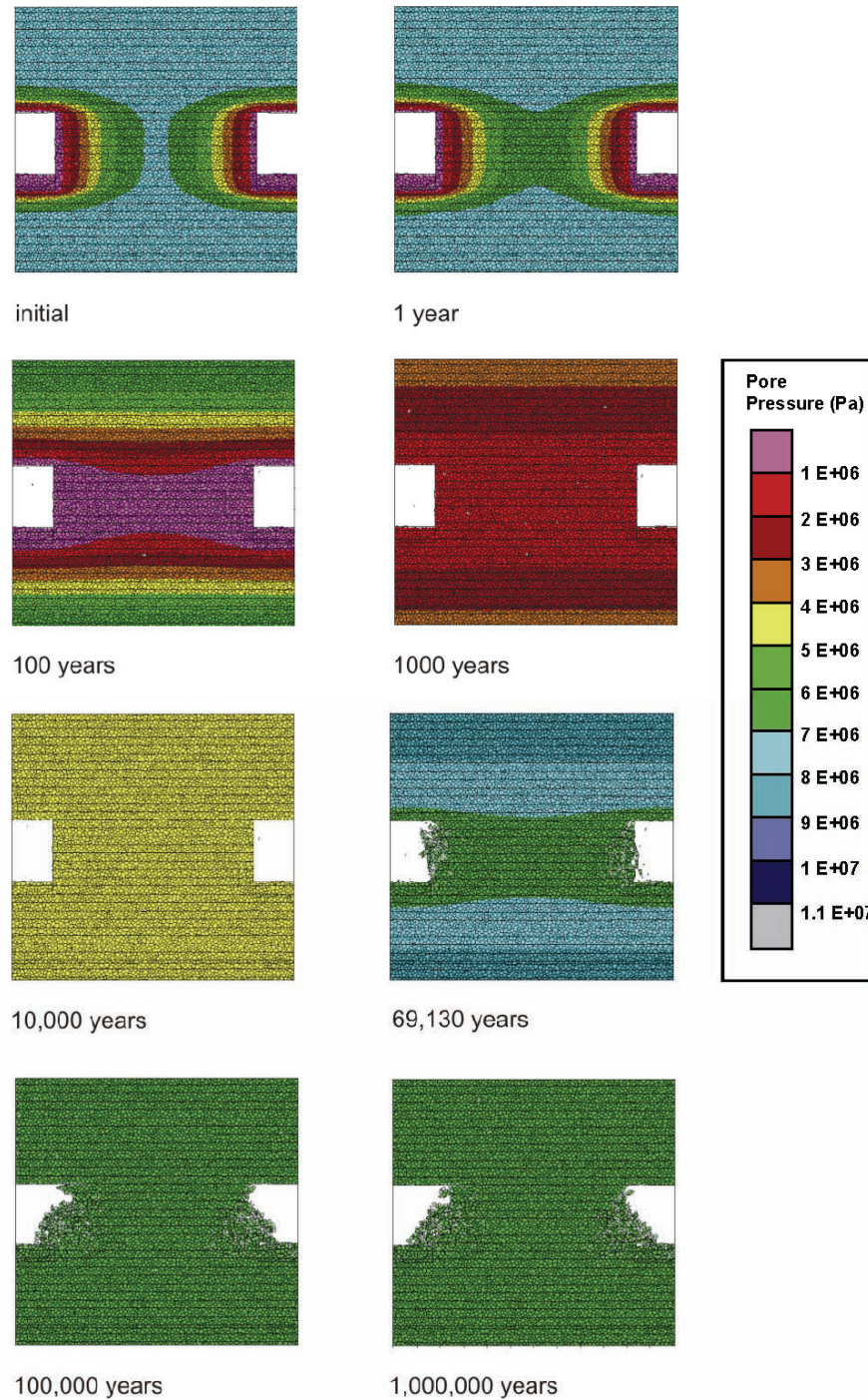
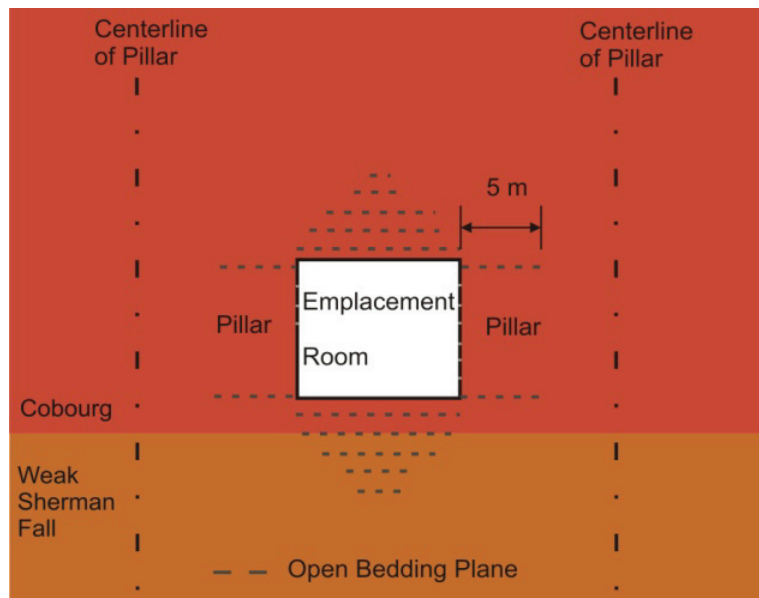


**Figure 6.29: Evolution of Pore Pressure (Pa) Around the Emplacement Room for 1 Ma Assuming One Glacial Cycle Starting at 60 ka**

The potential for fracturing of bedding planes due to extreme gas pressure was investigated assuming that there is no time-dependent rock strength degradation. The full gas pressure history, which reached a maximum of 15 MPa, was simulated. The results of this calculation at

100 ka are shown in Figure 6.30. In this case, the 5-m-long shear (not tensile) fractures localize along the bedding planes in the floor and in the crown of the emplacement room.



Notes: DGR invert is at 683 mBGS. The Cobourg Formation includes the Collingwood Member.

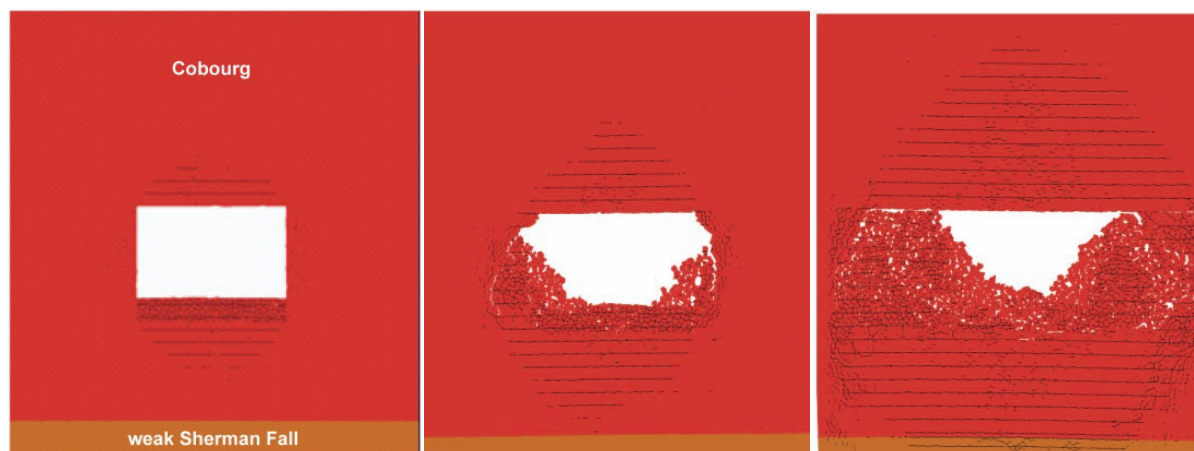
**Figure 6.30: Opening of Bedding Planes (Horizontal Dashed Lines) Around an Emplacement Room at 100 ka Due to Extreme Gas Pressure History (15 MPa)**

#### 6.4.4.6 Seismic Analysis

Itasca Consulting Group, Inc. (ITASCA 2011) carried out dynamic analyses of the effect of seismic ground shaking on stability of the emplacement rooms for 6 ground motion time periods, 3 each at  $10^{-5}$  and  $10^{-6}$  probabilities of annual exceedance. The time histories at the repository level were used in the emplacement room stability analyses. The dynamic analyses considered in situ stresses, time-dependent strength degradation and glacial loading. Because the gas and pore pressure do not have significant effect on the emplacement room stability, they were not included in the load combinations with dynamic analysis. Three different times of the occurrence of each seismic event are analyzed: 1) before the first glacial cycle; 2) at the peak of the first glacial cycle; and 3) at the peak of the second glacial cycle. A total of 18 dynamic simulations were completed.

The results of the dynamic analyses for a M7.4 event at 200 km are shown in Figure 6.31, for cases of the seismic events occurring before the glacial loading, at the peak of the first glacial cycle and at the peak of the second glacial cycle, respectively. The seismic shaking of the considered magnitudes does not cause any additional damage or fracturing of the rock mass. That is particularly the case for the events occurring early, before glacial events, when the rock mass is relatively unfractured. The seismic shaking does promote unravelling of already fractured and loose rock mass. That unravelling can result in additional fracturing of the rock

mass as a result of reduction in confinement, but not as a result of seismically induced stress change or inertial forces. Consequently, the effect of seismic shaking appears to have more effect as the area of the damaged rock mass increases as the rock mass is subject to more glacial events. Also, it seems that the events with larger peak ground velocity (PGV) (i.e., stronger events at greater distance) have more effect than the events with larger peak ground acceleration (PGA) (i.e., weaker events at shorter distance).



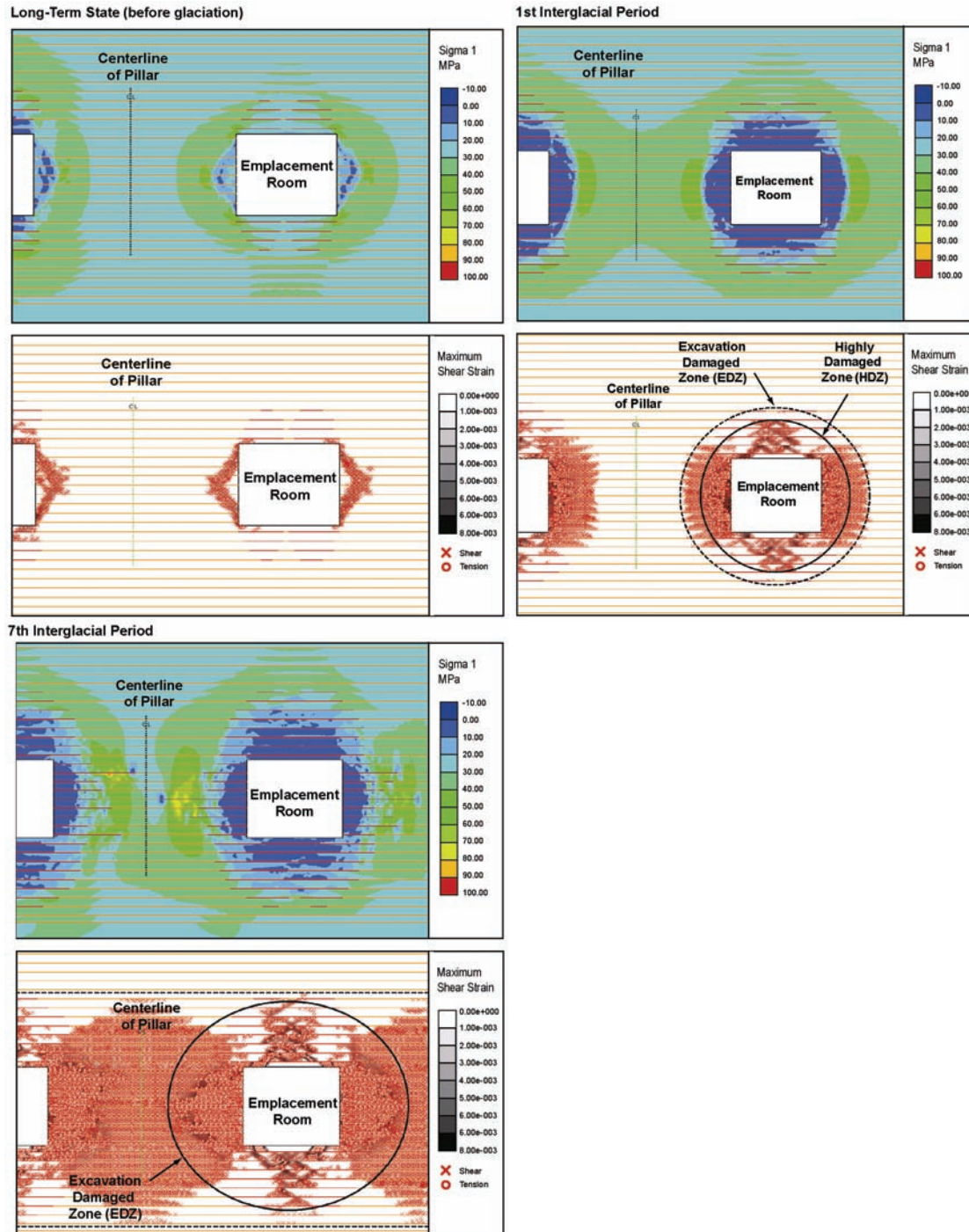
Notes: Shaking by an M7.4 earthquake at 200 km distance at 60 ka (left), 67.2 ka and one glaciation (middle), and 107 ka and 2 glaciations (right). Shaking occurs at glacial maximum. DGR invert is at 679 mBGS. The Cobourg Formation includes the Collingwood Member.

**Figure 6.31: Emplacement Room Models Subjected to Shaking**

#### 6.4.4.7 Alternate Numerical Approach

In order to further assess modelling assumptions made in the UDEC runs, a companion analysis in a finite-element code, Phase<sup>2</sup> (Rocscience 2009), was performed. The model includes joint elements that can be used to simulate the fracture development process similar to UDEC (albeit without the ability to physically separate and collect as rubble).

In this analysis, the brittle spalling model of Diederichs (2007) is used. The minimum strength envelope in the model is assumed to correspond to the mean CI value of 45 MPa as measured in laboratory tests. It is accepted that stress levels below this threshold result in no damage and therefore no long-term change in rock properties. At higher confining stresses, rock which exceeds this threshold may experience non-propagating damage and minor increase in permeability. At lower confining stress, the behaviour is brittle when CI is exceeded. To increase the degree of damage so that failure modes may be investigated, the CI and long-term strength are taken as 40 MPa (in terms of total stress). The results of a simplified model (continuum plus discrete bedding) using Phase<sup>2</sup> are shown in Figure 6.32. The stratigraphy above and below the emplacement room is modelled but not shown in Figure 6.32.



Notes: Inner solid ellipse is outer boundary of HDZ (highly damaged zone), outer dashed ellipse bounds the EDZ. Left = Max Stress (Contours from blue=-10 MPa to Red=100 MPa); Right=Shear Strain (darker shading indicates more strain and Red bedding = slip). Stress ratio = 1.5 in this example. CI is 40 MPa (conservative), tensile strength of intact rock is taken as 6.6 MPa and generalized Hoek-Brown parameters (with  $a=0.25$  and  $a_{res}=0.75$ ) calculated as per Diederichs (2007).

**Figure 6.32: EDZ and HDZ Determination from Finite-Element Results (Continuum with Bedding)**

The emplacement room shows limited bedding slip and wall damage (“hourglassing”), as well as, variable roof damage ranging from negligible failure to 3 m of fractured ground. After the first glaciation, the damage zone EDZ will extend halfway to the centre of the pillar. The highly fractured zone (failure of unsupported roof and wall material) will extend approximately 30% into the pillar. This increases steadily through each successive glaciation. At the end of the 7<sup>th</sup> glaciation (interglacial), the EDZ involves the entire pillar and 6-7 m of roof and floor in this analysis. The HDZ extends towards the centre of the pillar (75% in this analysis). As shown in Figure 6.33, the central core of the pillar continues to carry substantial load through 7 glacial peaks.

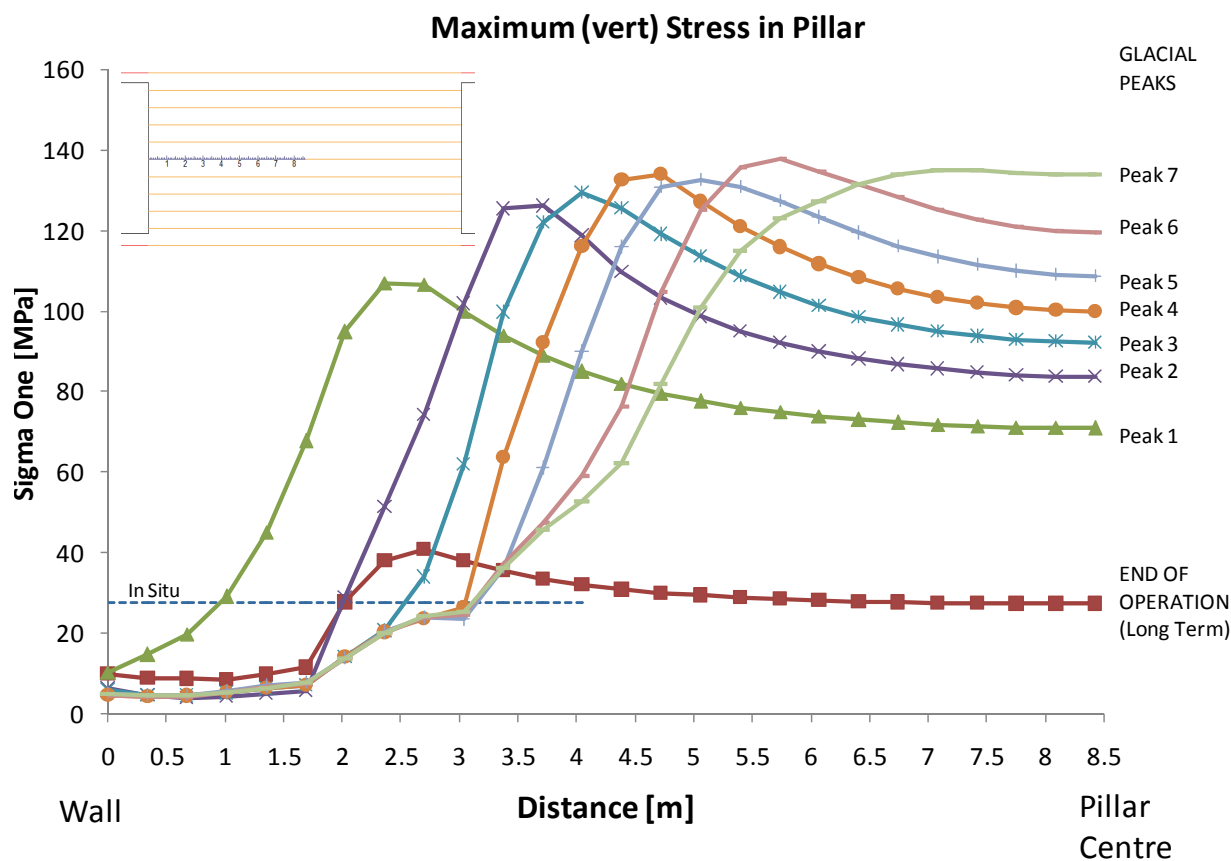


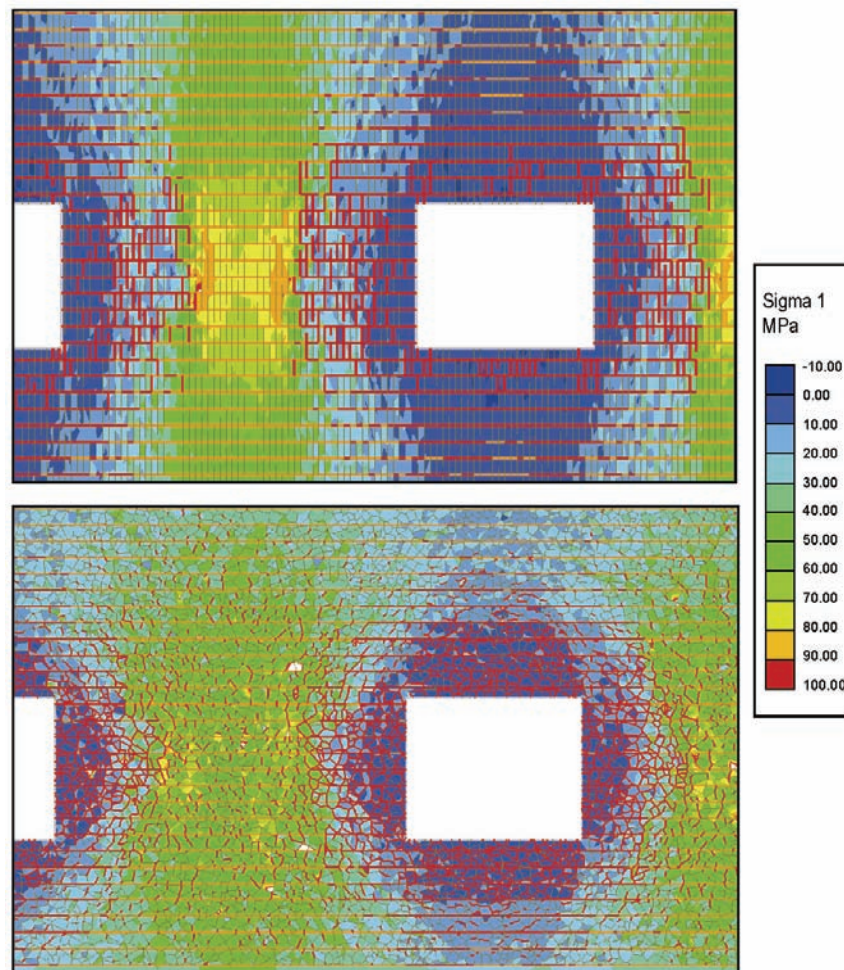
**Figure 6.33: Stresses Carried at the Spring-line Through the Pillar**

Eventually, after additional glaciations beyond glacial cycle 7 and probably within 1 Ma, the pillar will be fully damaged and possibly failed. At this point, it is important to consider the effect of the failed rock expanding in volume and providing backfill pressure to the remaining emplacement room boundaries. Estimates of the bulking factor (relative increase in volume for failed rock) in limestone obtained from numerous studies of large natural caves are approximately 25% (Waltham 1981). The volume of rock within the HDZ after the 7<sup>th</sup> glacial period would require a bulking factor of 25% to completely fill and choke the empty excavation at this point. If 1.4 m of disintegrated waste is assumed to sit on the floor of the excavation, the



required bulking factor for complete arrest of further disintegration drops to 20%. According to this finite-element continuum analysis, full choking of the emplacement room and indefinite self arrest of failure is inevitable after the 7<sup>th</sup> glaciation. In contrast, the discontinuum modelling showed that choking of the emplacement room would occur after the 4<sup>th</sup> glaciation.

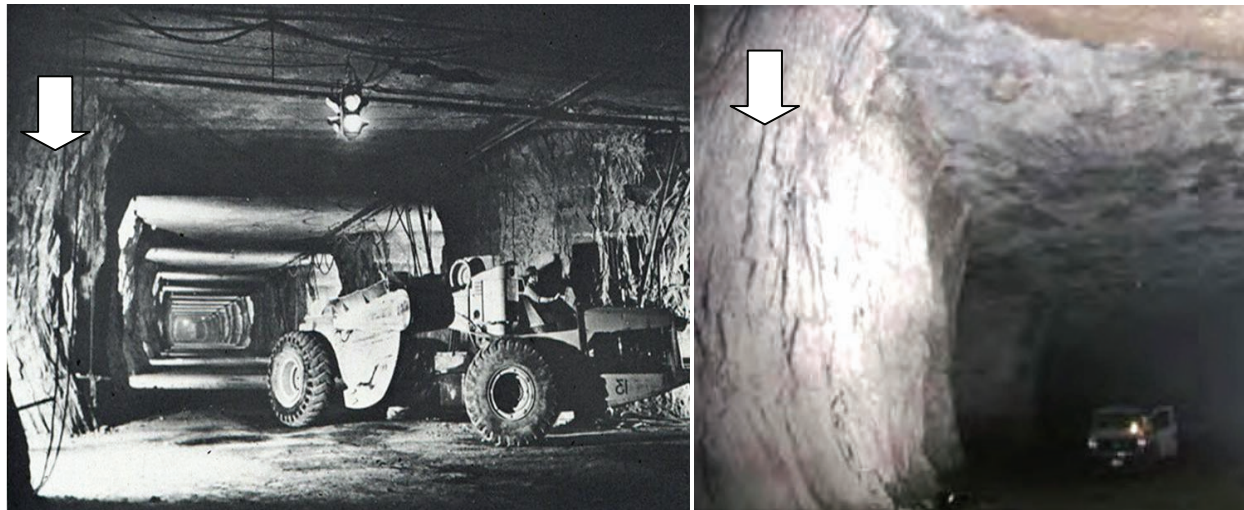
Two other configurations were tested to incorporate the influence of discrete fractures within the continuum model. Bedding is already modelled as discontinuity elements with shear strength properties obtained through testing as described in Section 3.2.1. Additional joint elements were incorporated, each having the same equivalent strength as the intact rock. This provides for a softer and discontinuous response after yield. In the first model, the fractures are assumed to propagate vertically as is observed in naturally fractured limestone formations (Figure 6.34). The second involves a Voronoi fracture network (randomly oriented joint elements). The selected Voronoi discretization in the current analysis represents a conservative approach to fracture generation (compared to oriented fractures).



Notes: Top = addition of vertical fractures with intact rock strength properties (material yield or EDZ is not shown but occupies full pillar at this point, red indicates macro-fracture generation or slip). Bottom = Voronoi fractures with intact rock strength properties. Vertical stress shown at 6<sup>th</sup> glacial peak.

**Figure 6.34: Sensitivity Analysis of Discrete Fractures in Modelling HDZ Formation**

The photos in Figure 6.35 indicate that the fractures in the pillar will more closely resemble the vertical model joints. It is not clear what form the roof fractures will take. Actual behaviour is likely between these two model results (Figure 6.34). In both cases, the pillar core after many glaciations is damaged (EDZ) but is not yet within the highly damaged zone (HDZ) and carries significant load.



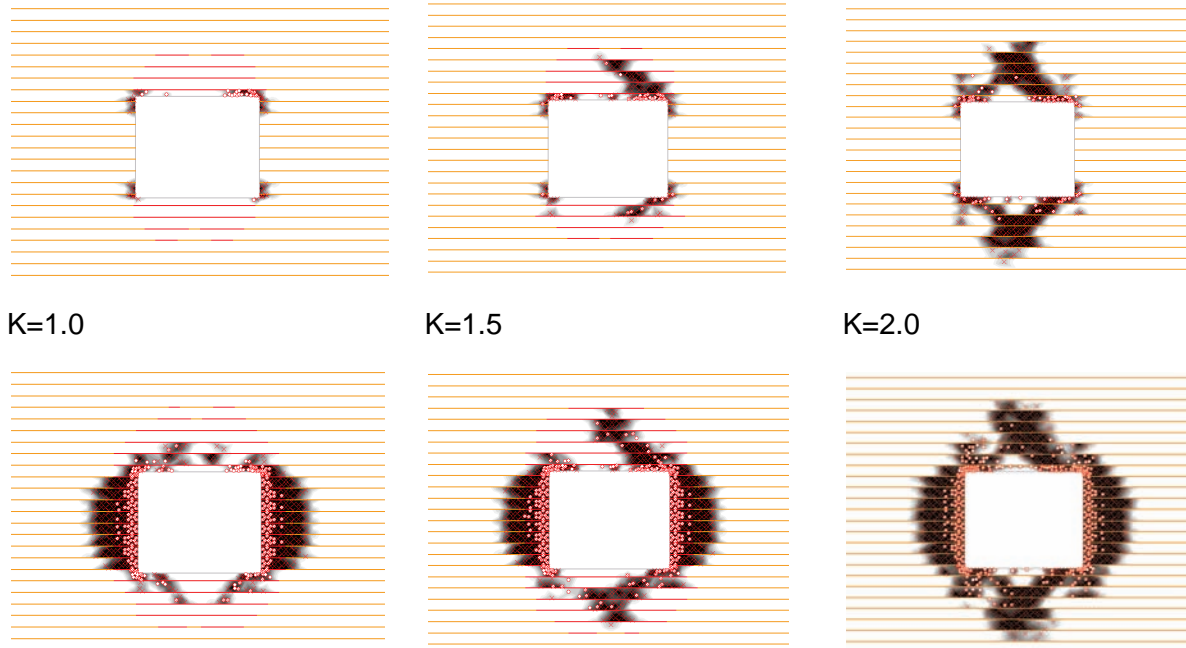
Notes: Photos from Esterhuizen et al. (2008). Left – approx. 670 m deep in Barberton (Norton) Mine, Ohio; right – mine pillar. Arrows point to cracks on excavation walls.

**Figure 6.35: Wall/Pillar Fractures in Underground Limestone Mines**

Model results are sensitive to floor cover above the Sherman Fall Formation. The minimum recommended floor cover is 6 m according to these analyses to account for uncertainty. This leaves 12 to 16 m of roof cover to the top of the Cobourg Formation given the currently proposed access inclinations.

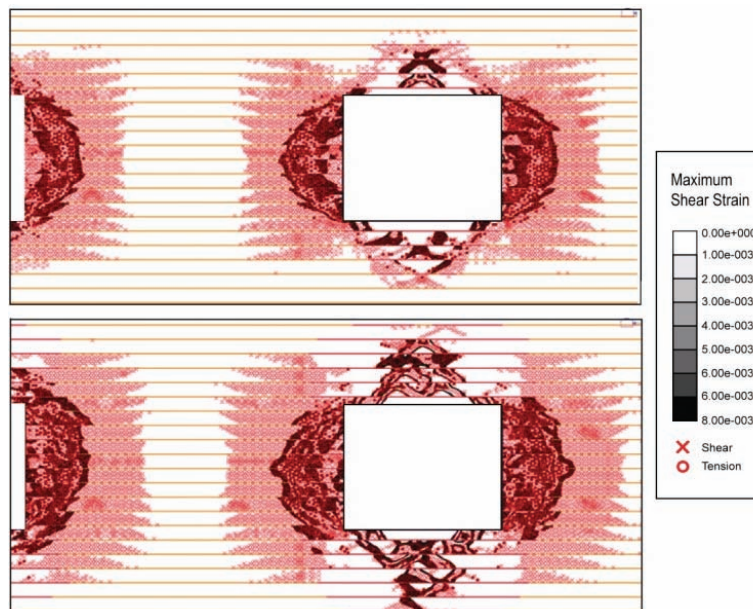
Sensitivity to in situ stress ratio is significant. Proper orientation of the repository with respect to in situ stress (most emplacement rooms collinear with maximum horizontal stress) will reduce initial damage, particularly in the roof, thereby increasing construction and operational safety and prolonging the integrity of the emplacement room through successive glacial cycles (Figure 6.36).

Sensitivity to bedding-plane shear strength is not so critical. In the Cobourg, the bedding is highly undulating at the core scale. Shearing becomes difficult under high confinement. The bedding planes in this model are primarily used to represent the strong tensile strength anisotropy (weaker perpendicular to bedding). Given the data available at the time of this reporting, two interpretations for shear strength are possible -- a high-cohesion, low-friction bedding plane or a low-cohesion, high-friction plane. Both results are shown in Figure 6.37. The more conservative model (top model in figure) is used for this reporting.



Notes: Upper: Long-term pre-glacial EDZ. Lower: first interglacial state of EDZ. EDZ damage [black] and bedding slip [red].

**Figure 6.36: Influence of In-plane Horizontal Stress Ratio, K**

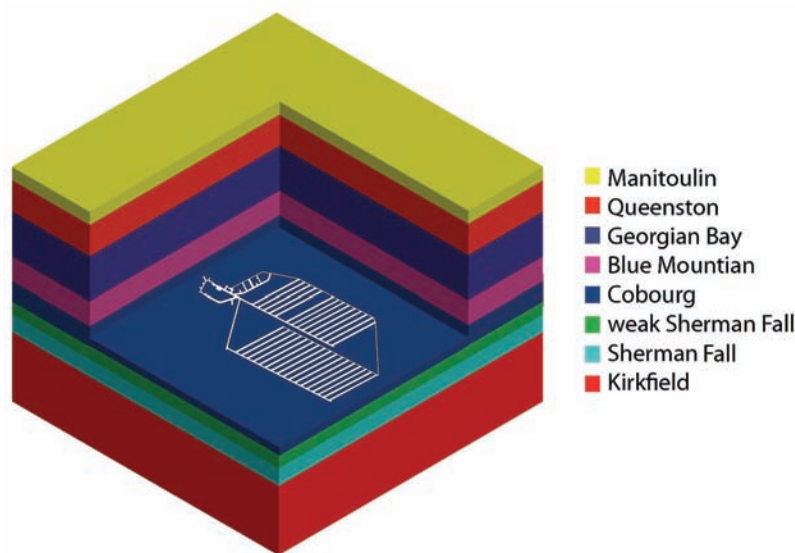


Notes: Bottom: Cohesion=3 MPa, Friction Angle = 35°; Top: Cohesion=0.1 MPa, Friction Angle = 60°. Red= damage, Black= failure.

**Figure 6.37: Influence of Strength Model for Bedding**

### 6.4.5 Emplacement Panel: 3D Analyses

Itasca Consulting Group, Inc. (ITASCA 2011) evaluated panel deformation through multiple glacial cycles using FLAC3D Version 4.00.35 (64 bit). An isometric model geometry including geological units is illustrated in Figure 6.38. The base of the model is at 861 m depth, while the top is at 435 m (including the Manitoulin dolostone).



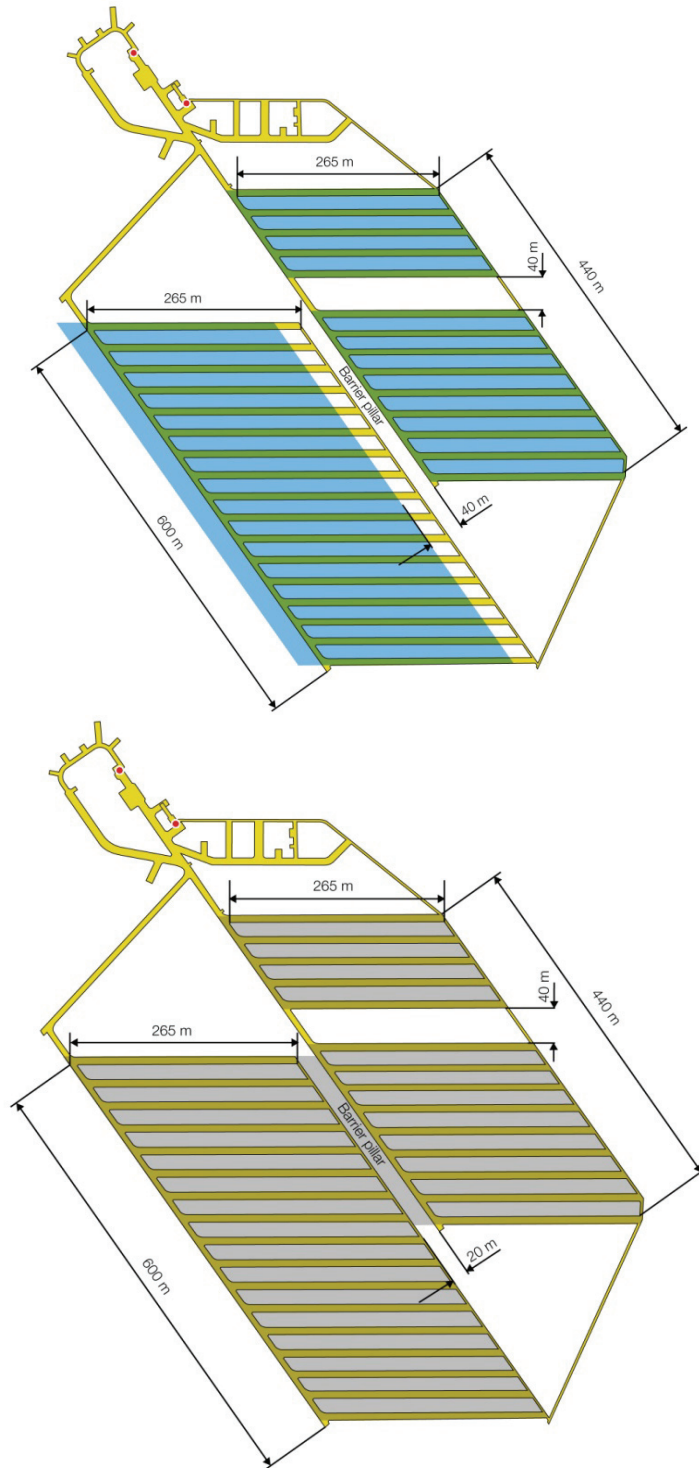
Notes: Cobourg includes the Collingwood Member.

**Figure 6.38: Geometry of the Panel-scale Model**

As shown in Figure 6.39, only the panels in the repository layout are represented in the model. Because the model simulates deformation of the rock mass above the panels and the repository, the rooms and the pillars are not explicitly represented. The effect of individual rooms and pillars on stresses and displacements extends above the top of the repository to a distance which is comparable to the emplacement room span. At greater distances, only average, smeared effects of multiple emplacement rooms and pillars can be seen.

After collapse of the pillars (e.g., Cycle 4), there is no significant distinction between the pillars and the emplacement rooms, because the entire repository is filled with rubble. Thus, in the panel-scale analysis, the rock within the panel layout is represented as an elastic material with stiffness determined based on deformation observed in the pillar-scale model during the steady-state glacial cycle after the pillars collapse as described in Section 6.4.4.

A Mohr-Coulomb strain softening constitutive model is used for all units except the Cobourg, which is represented as a perfectly plastic Mohr-Coulomb model with horizontal ubiquitous joints (representing bedding planes). The mechanical properties of the other geological units as used in the analysis are listed in Table 6.7.



Notes: Top panel geometry model (blue shade) incorporates double-width barrier pillars between all three panels while the bottom panel geometry model (grey shade) conservatively assumes a failed barrier pillar between the main panels. Red dots indicate shaft locations.

**Figure 6.39: Model Panel Geometry Overlain with Repository Layout**

The stiffness of the equivalent material,  $E_e$ , is calculated using the following relation:

$$E_e = \frac{H}{d_{\max}} \Delta\sigma \quad (6.2)$$

where  $H$  is the height of the equivalent material, in this case equal to 7 m repository height,  $d_{\max}$  is the maximum displacement (0.85 m), and  $\Delta\sigma$  is the vertical stress increase. The vertical stress increase includes the additional stress due to glacial load (30 MPa) and increase in the pillar stress due to excavation of the emplacement rooms under in situ stress conditions:

$$\Delta\sigma_{ini} = \frac{l_{span}}{l_{spacing}} \sigma_v = 0.33 \times 18 \text{ MPa} = 6 \text{ MPa} \quad (6.3)$$

where  $l_{span}$  is the emplacement room span (8.6 m) and  $l_{spacing}$  is the emplacement room spacing (25.8 m). The calculated equivalent stiffness is:

$$E_e = \frac{7.0 \text{ m}}{0.85 \text{ m}} 36 \text{ MPa} = 296 \text{ MPa} \quad (6.4)$$

Displacement boundary conditions are applied along the vertical and bottom model boundaries. The stress, equal to overburden weight, is applied on the top. The vertical in situ stresses are in equilibrium with overburden weight assuming a rock mass density of 2,700 kg/m<sup>3</sup>. The horizontal in situ stresses in the units above the Blue Mountain shale are assumed to be isotropic with magnitude equal to the minimum horizontal stress as indicated in Table 6.8. The stress ratio for the other units are taken as estimated based on regional stress modelling as described in Itasca Consulting Group, Inc. (ITASCA 2011). A horizontal stress ratio of 2 is assumed in the Cobourg Formation and the units below it.

**Table 6.7: Material Parameters for the Panel-scale Models**

Unit	Intact Rock		Rock Mass Properties							
	UCS (MPa)	E (GPa)	GSI	mi	E (GPa)	c (MPa)	$\phi$ (°)	T (MPa)	C <sub>r</sub> (MPa)	$\phi_r$ (°)
Sherman Fall	(55.6)*	(26.6)	(65)	(12)	(16.8)	(4.27)	(34.7)	(0.33)	(3.45)	(31.4)
Blue Mountain	21.7	5.2	75 (70)	8	4.2 (3.8)	1.62 (2.61)	36.3 (26.3)	0.41 (0.28)	1.12 (2.13)	34.8 (23.8)
Georgian Bay	40.8	11.8	75	8	9.6	2.75 (3.78)	38.1 (32.8)	0.77	1.80 (2.83)	36.6 (30.9)
Queenston	48.0	15.4	75	8	12.6	2.97 (3.82)	39.7 (35.2)	0.91	1.83 (2.71)	38.4 (33.5)
Manitoulin	70.7	23.9	75	8	19.5	3.77 (4.51)	42.8 (39.2)	1.34	2.02 (2.84)	42.2 (37.7)
Cabot Head	12.6	4.5	75	8	3.7	1.37	30.3	0.24	1.07	28.4
Goat Island/ Gasport/ Lions Head/ Fossil Hill	148.3	37.0	75	8	30.2	8.15	42.2	2.81	4.5	41.2

Unit	Intact Rock		Rock Mass Properties							
	UCS (MPa)	E (GPa)	GSI	mi	E (GPa)	c (MPa)	$\phi$ (°)	T (MPa)	C <sub>r</sub> (MPa)	$\phi_r$ (°)
Sherman Fall	(55.6)*	(26.6)	(65)	(12)	(16.8)	(4.27)	(34.7)	(0.33)	(3.45)	(31.4)
Blue Mountain	21.7	5.2	75 (70)	8	4.2 (3.8)	1.62 (2.61)	36.3 (26.3)	0.41 (0.28)	1.12 (2.13)	34.8 (23.8)
Georgian Bay	40.8	11.8	75	8	9.6	2.75 (3.78)	38.1 (32.8)	0.77	1.80 (2.83)	36.6 (30.9)
Queenston	48.0	15.4	75	8	12.6	2.97 (3.82)	39.7 (35.2)	0.91	1.83 (2.71)	38.4 (33.5)
Guelph	60.4	27.8	75	8	22.7	4.65	35.8	1.15	3.26	34.1
Salina A0 Dolostone	197.6	63.4	75	8	51.8	8.98	47.0	3.75	3.58	47.4
Salina A1 Evaporite	20.0	11.7	75	8	9.6	2.07	31.1	0.38	1.60	29.2
Salina A1 Carbonate	116.7	39.7	75	8	32.4	5.95	43.9	2.21	2.98	43.3
Salina C	35.0	8.0	75	8	6.5	2.68	35.9	0.66	1.87	34.2

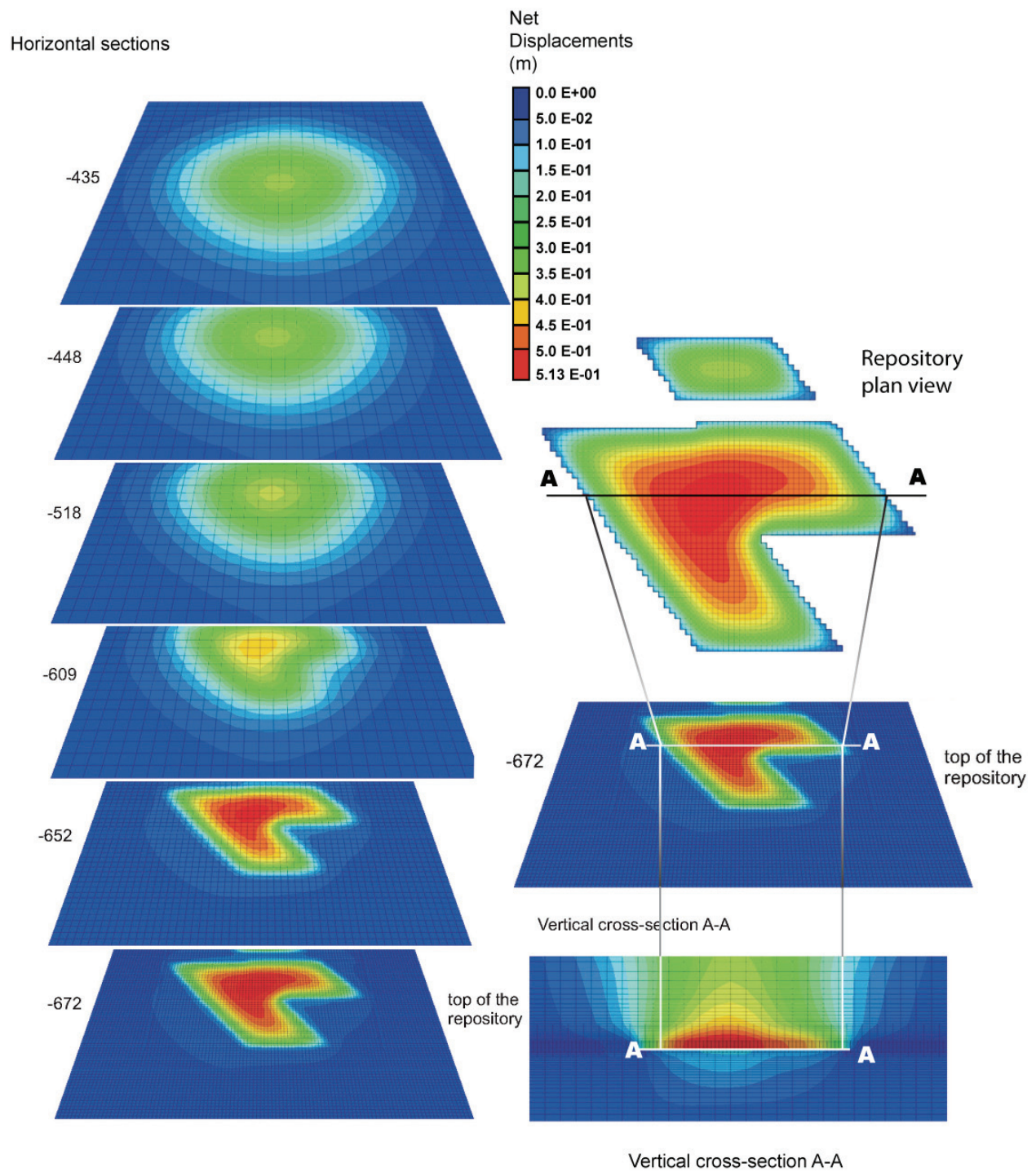
Notes: Values in parentheses were used in the repository panel-scale analysis; the difference in the peak and residual cohesion and friction angle is because in the panel-scale analysis the maximum stress in the calculation of Mohr-Coulomb fit to the Hoek-Brown failure envelope was assumed to be horizontal stress calculated using horizontal stress coefficient equal to 2.

No time-dependent strength degradation is considered in this analysis. Instead, the Cobourg is assumed to have long-term strength (i.e., 40% UCS or 45 MPa) from the beginning of the simulation.

The horizontal in situ stress and Poisson's ratio are two parameters that can have significant effect on prediction of yielding and damage in the cap rock, and particularly in the Blue Mountain shale. Two bounding assumptions are made in Table 6.8. The results are shown in Figure 6.40 to Figure 6.42.

**Table 6.8: Material and Stress Assumptions in the Blue Mountain Formation**

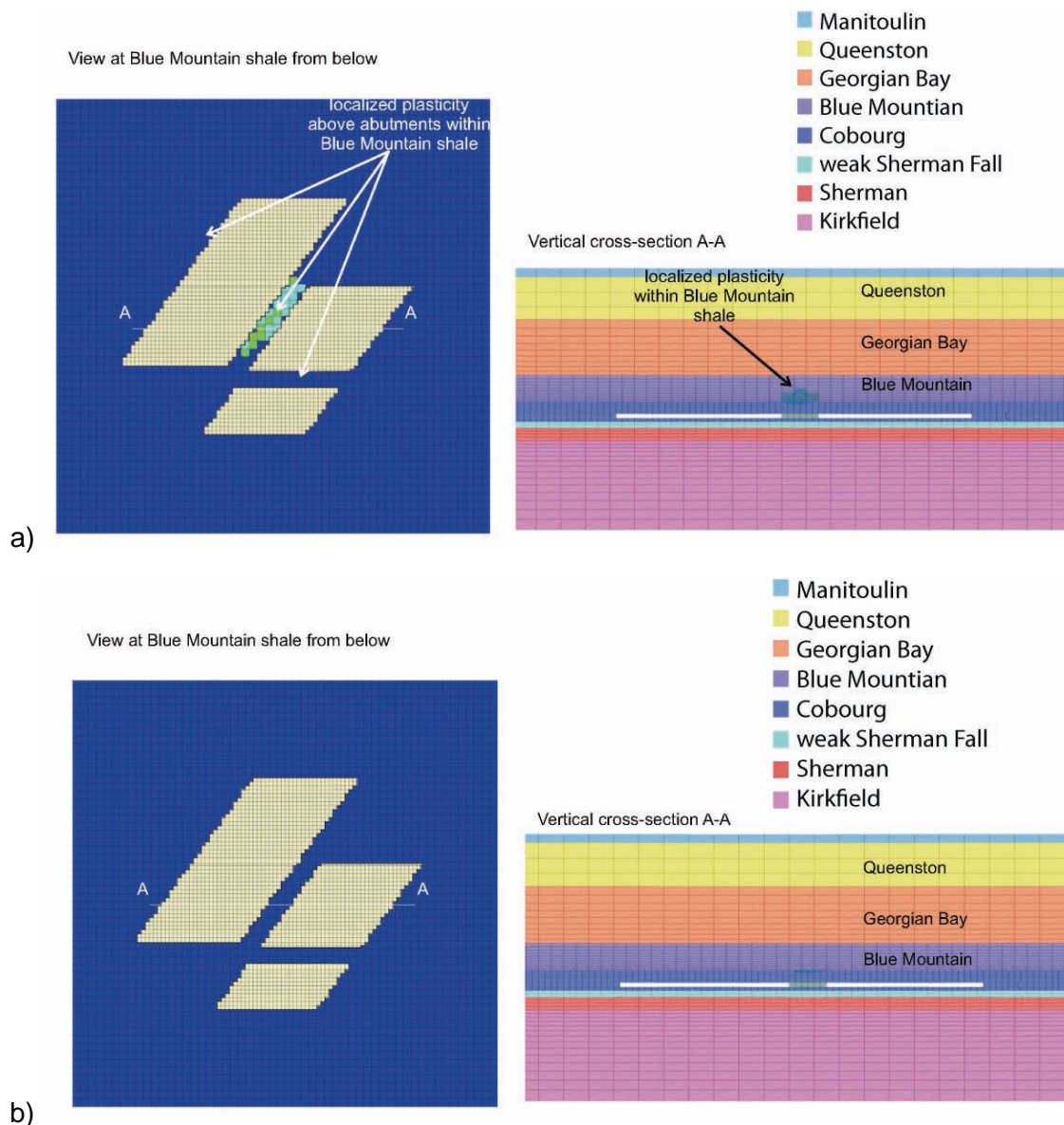
Case	Poisson's Ratio	Horizontal Stress Ratio
1	0.25	0.83
2	0.3	1.0



Notes: Regional displacements due to glaciations are not included. DGR invert at 679 mBGS.

**Figure 6.40: Net Displacements (m) Induced by the Repository at the Peak of the Glacial Load: Case 1 with No Central Pillar**

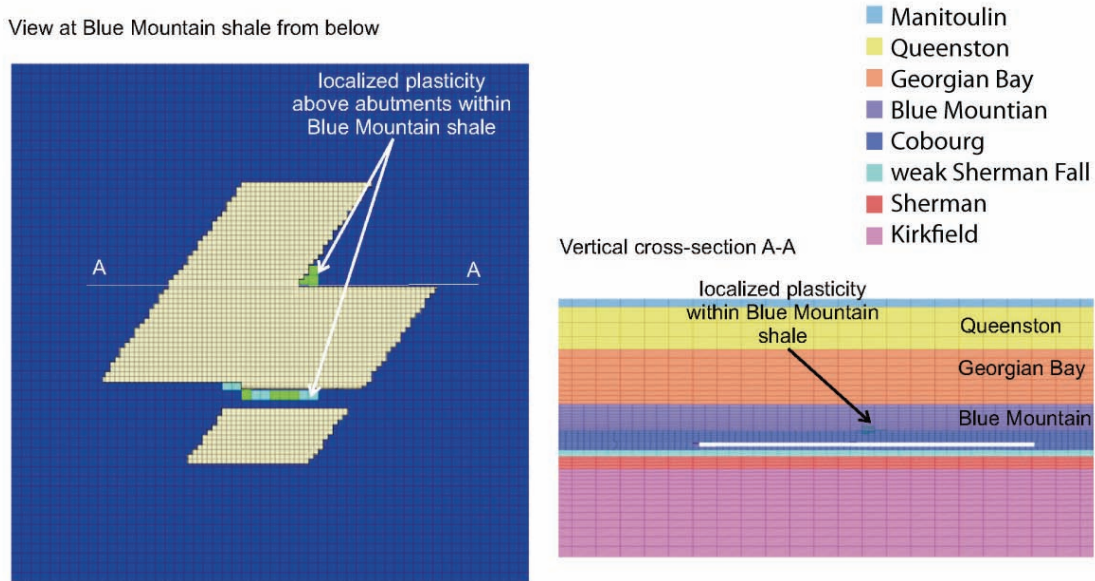




Notes: DGR invert at 679 mBGS. The Cobourg Formation includes the Collingwood Member.

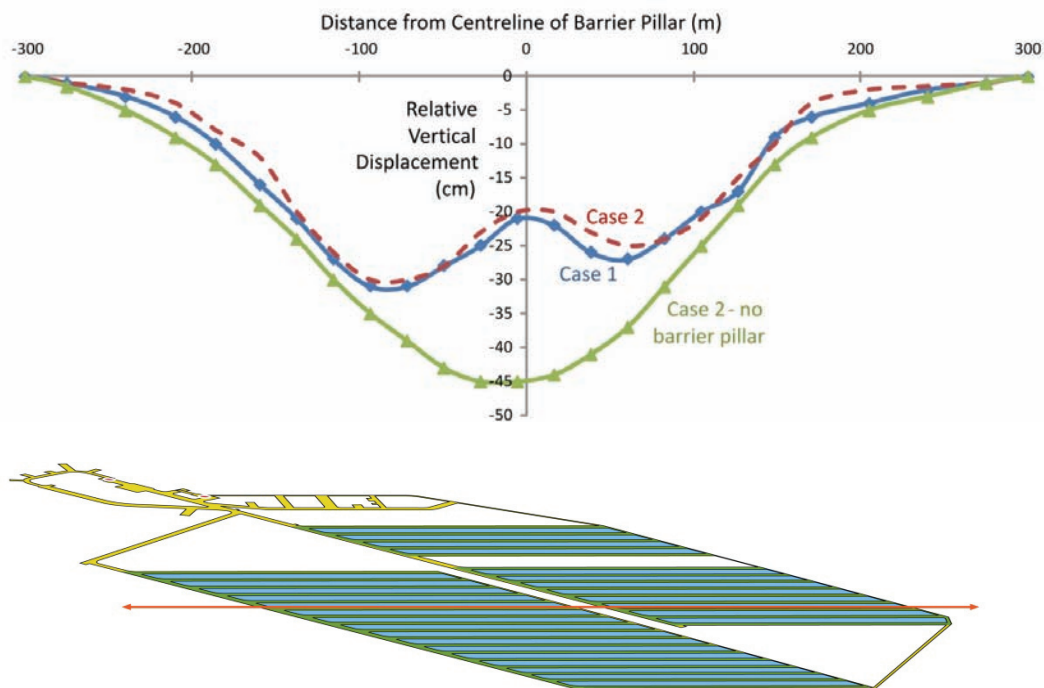
**Figure 6.41: Yielding in the Blue Mountain Shale above the Repository for a) Case 1 and b) Case 2 with a Central Pillar in Place**

For the case with a wide central pillar (double the width of the inter-emplacment room pillars) for material Case 1, a small amount of plastic yielding is apparent over the barrier pillars. The barrier pillar itself does not yield. However, kinematically, this indicates that the yielding in the Blue Mountain shale cannot propagate and will be in the form of minor local degradation only and not extensive shear (large strain). There is no such yield indicated in Case 2. For the cases with no central pillar (single width pillar assumed to fail along with the other inter-emplacment room pillars), there is a slight increase in the degree of perimeter yielding in the Blue Mountain shale. None of the cases indicates any damage or undue influence on the Georgian Bay or Queenston shale barrier rocks.



Notes: DGR invert at 679 mBGS. The Cobourg includes the Collingwood Member.

**Figure 6.42: Plastic Deformation at Peak of Glacial Load: Case 1 with No Central Pillar**



Notes: For the two cases on Table 6.8 of material properties and stress assumptions as well as for the option of an enlarged and intact central pillar versus a small and ultimately failed barrier pillar.

**Figure 6.43: Differential Displacements (cm) at the Lower Contact of the Georgian Bay Formation**

A large amount of uniform vertical displacement occurs during glaciations due to elastic compression of the layers. This would occur with or without the repository present. The key to instability is differential settlement over the repository compared to the lateral far field. The analysis of differential closure above the repository at the base of the Georgian Bay shale is summarized in Figure 6.43. For the case with a wide and intact central pillar, the Blue Mountain - Georgian Bay contact interface has a maximum differential deflection of 30 cm over 200 m or 0.15%.

#### **6.4.6 Geomechanical Modelling Results and Discussion**

A comprehensive suite of analyses have been performed to test the repository design and the Cobourg limestone against the challenges imposed by stress, material strength degradation, fracture generation, seismic loading, pore pressure effects, and multiple glacial cycles over a period of 1 Ma.

The long-term strength of the Cobourg is based on a lower bound consistent with the CI threshold for the limestone. A large number of tests were carried out to establish this critical limit. The resultant representative value (45 MPa) has been used in these analyses. Previous experience has shown that the mean CI represents the lower bound conservative assumption for long-term strength. Properties for other lithologies and for bedding planes are assigned as per the data in Chapter 3.

The emplacement rooms will be stable during construction and operation, requiring standard support. They will suffer increasing degradation over 60 ka as the long-term strength is reached.

Each period of glacial loading will create an additional increment of damage and pillar degradation. Reasonable assumptions indicate full pillar load capacity for 3 to 5 glacial periods.

Seismic loading creates insignificant damage of the pillar and roof. Under no circumstances does failure migrate into the Blue Mountain shale directly above the repository, except for minor damage associated with relatively small strains that may occur in this unit in the case of complete panel collapse. Rock mass, if allowed to break up and move into the excavation with a reasonable bulking factor, will completely choke off the emplacement room and prevent further roof collapse. The frictional properties of the pillar material and the presence of this "backfill" will stabilize the emplacement room in time, with resultant displacements within the tolerance of the overlying strata of key barrier rock units - Georgian Bay and Queenston shales.

The normal distance from the ventilation shaft, which is closer to the emplacement rooms, to the axis of the closest emplacement room is approximately 110 m. The analyses show that plasticity and damage is fairly localized in the emplacement room walls for most of the loading conditions. Only in the case of the multiple glacial events and significant time-dependent degradation of rock strength, the damage in the walls might extend enough to cause pillars collapse. The extent of damage in the abutments in the case if the pillar collapse occurs would stabilize within 20 m distance from the emplacement room wall. Thus, damage or yielding around the emplacement rooms and the repository will not extend to the closer, ventilation shaft. The repository will cause some elastic deformation and stress change along the shafts. Those changes will have insignificant effect on the shaft performance. Considering the design of the shaft seals, which includes bentonite/sand fix, asphalt and relatively short concrete bulkheads, they will not be affected by repository-induced elastic deformation even if the entire repository collapses. The main stress change along the shaft caused by the repository will be increase in

the vertical stress. The analyses have shown that the shafts are insensitive to stress change along their axes (The glacial load does not have significant effect on deformation and damage around the shafts).

Figure 6.44 schematically shows the evolution of emplacement room roof stability over the 1 Ma time horizon.

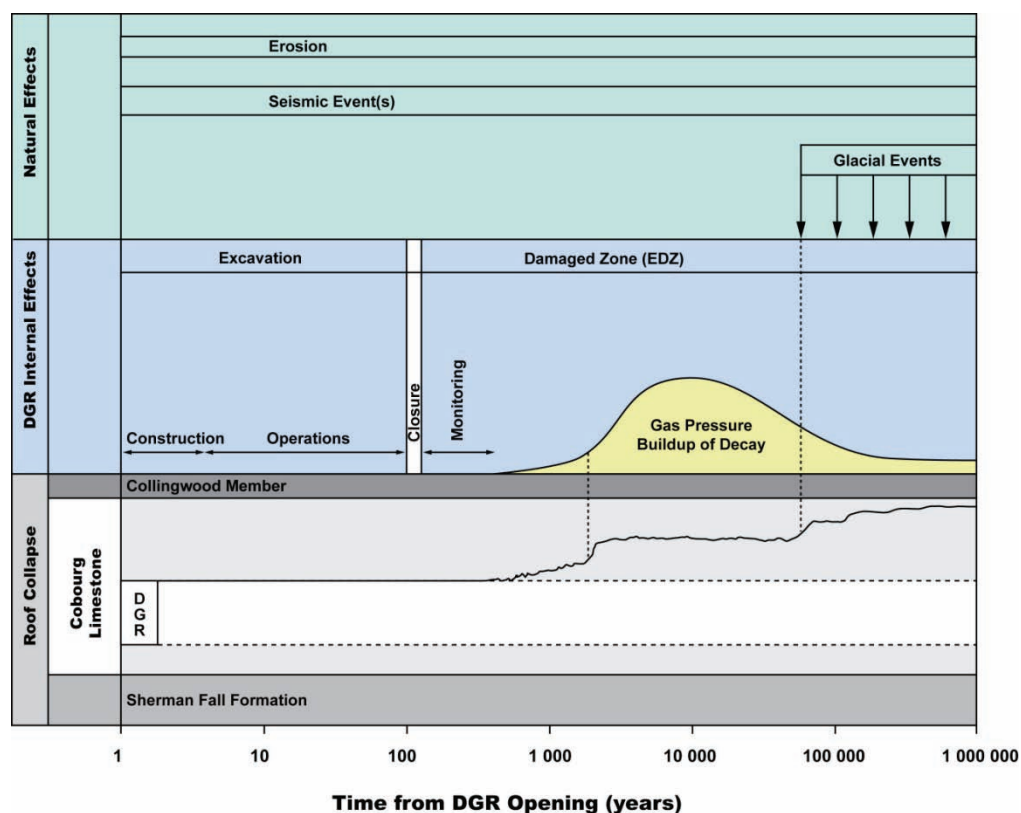


**Figure 6.44: Evolution of Emplacement Room Roof Stability**

The EDZ evolution within the emplacement rooms can be summarized as follows:

- **Construction to 100 a:** Minor wall spalling and possible minor slabbing in the roof.
- **100 a to 10 ka:** Strength decay and expansion of EDZ into pillar and into roof/floor including rock fracture and possible bedding delamination.
- **10 ka to 100 ka:** At least one glaciation serves to significantly enlarge HDZ and extend EDZ into pillar and several metres into roof and floor.
- **500 ka:** Multiple glaciations and seismic events cause complete damage through the pillar system and damage into the roof extending 4 to 8 m. The damage zone may reach the base of the Cobourg limestone. Expansion of failed rock (bulking) within the emplacement room void; however, will serve to choke off further failure by this time. The final damage profile may extend into the Collingwood Member with potential for isolated zones of minor

damage within the Blue Mountain shale. The Georgian Bay and Queenston shales are undisturbed.

- **1 Ma:** No change from 500 ka.

## 6.5 Summary

This chapter has discussed the potential processes and events that could compromise the operation and long-term performance of the DGR. Both repository-induced and natural processes have been considered in this analysis. The findings are summarized below.

The primary significance of long-term climate change on the DGR is related to future deglaciation of the Canadian landmass. The present prediction is that the onset of the next glacial event will be in 60 ka. Assuming that the next glacial event has the same dimensions in time and space as the Laurentide Ice Sheet, then:

- The erosion expected due to glacial activity is likely to total only about 100 m over the next 1 Ma.
- The normal stress generated by multiple glacial advances and retreats will cause the emplacement rooms to collapse; however, the top of the host rock will not be breached and the cap rocks will remain intact.
- Permafrost depths are not expected to exceed 60 m at the Bruce nuclear site.
- Groundwater recharge beneath the glacier at the Bruce nuclear site will not penetrate further than the Silurian Salina A1 Unit shale based on hydrogeological and hydrochemical evidence.

Three natural geologically induced processes that could potentially affect the DGR, were they to occur over the next million years, include: seismicity, fault rupture or reactivation, and volcanism. Existing knowledge of these processes leads to several conclusions.

- The Bruce nuclear site lies within the stable interior of the North American craton, an area characterized by low rates of seismicity.
- Seismic events recorded in the region are  $M < 5$ .
- A Probabilistic Seismic Hazard Assessment (PSHA) based on SSHAC Level 2 process was conducted for the Bruce nuclear site. The PSHA conducted for the DGR explicitly incorporated uncertainties in the probabilistic models and model parameters that affect seismic hazard at the site. The results of the PSHA are generally consistent with values published in the 2005 National Building Code of Canada when corrected to a common site condition and accounting for the differences in the selected ground motion models used in the two studies.
- The results of the PSHA indicate that the estimated ground motions at the surface on hard rock are expected to be less than 70 %g for annual exceedance frequencies of  $10^{-5}$ , the reference case, and  $10^{-6}$ , the extreme case.
- Geomechanical modelling has demonstrated that the emplacement rooms and pillars will remain stable for seismic shaking for events of  $M \leq 5.0$  at 15 km and of  $M \leq 6.5$  at 50 km from the site (details in emplacement room stability summary).
- The potential for fault rupture or reactivation is extremely low given the location, seismic history and neotectonic evidence of the Bruce region.

Gas generation in the repository was modelled under a variety of Normal Evolution and Disturbed scenarios. The principal findings are listed below.

- For most cases considered, the peak repository gas pressure is in the range of 7 to 10 MPa, which is comparable to the environmental head at the repository horizon of around 7.2 MPa, and much less than the lithostatic pressure of 17 MPa.
- For most cases, the very low permeability of the rock precludes significant water saturation of the repository for the 1 Ma simulation period. Resaturation will only result in, at maximum, 1 m depth of water inside the DGR and will not compromise the integrity of the DGR. In some sensitivity cases, the repository is virtually dry (or completely unsaturated) after 100 ka.

Shaft stability was assessed through a series of geomechanical modelling scenarios and concluded. The principal findings are listed below.

- Most rock damage is caused during the excavation phase of the project.
- The shafts will be backfilled at the end of the operational period. Consequently, the long-term shaft stability will not be an issue. As the seals provide stability to the shafts over the long-term, the focus of the shaft analysis is the evolution of the EDZ around the shafts. The depth of damage, for all load combinations after 1Ma, exceeds the shaft radius (by a maximum of 28%) only in the case of the very weak Cabot Head Formation. Otherwise, the maximum depth of damage is typically in the range of 60% to 70% of the shaft radius or less.
- Time-dependent strength degradation typically causes an increase of 25% to 50% in the damage zone around the shaft seals.
- Effective stress analyses indicated that long-term pore pressure evolution (combined with strength degradation and glacial loading) could increase the extent of yielding by at most 1.4 m.
- Seismic shaking and glacial loading are practically inconsequential for the EDZ and performance of the shafts.

A comprehensive suite of analyses have been performed to date to test the repository design in the host rock against the challenges imposed by stress, material strength degradation, fracture generation, seismic loading, pore pressure effects, and multiple glacial cycles over a period of 1 Ma. The principal findings are listed below.

- The emplacement rooms will be stable during construction and operation, requiring only standard support. They will suffer increasing degradation over 60 ka as the long-term strength is reached.
- With time-dependent strength degradation under in situ stress conditions and assuming a long-term strength of 45 MPa (40% UCS), no breakouts are predicted with yielding along the bedding planes in the roof and the floor limited to a depth of approximately 2 m.
- Gas and pore pressure variations within the emplacement rooms do not have significant effect on damage around the emplacement rooms or the breakout depth. The preferential direction for potential hydraulic fracturing is horizontal, along the bedding planes, perpendicular to the vertical minor principal stress. Under the assumption of a high gas generating rate (resulting in maximum gas pressure of 15 MPa), bedding-parallel fractures may propagate up to 5 m beyond the emplacement room walls. However, the gas

pressures, in all analyzed cases, will not generate hydraulic fractures that can result in gas release into the biosphere.

- Multiple glacial events and associated loading/unloading cycles are expected to cause failure of the pillars between the emplacement rooms and eventual emplacement room collapse. The number of glacial cycles that will cause pillar collapse and the timing of the pillar collapse depend on the long-term strength of the Cobourg. Even using a conservative assessment for the Cobourg long-term strength of 45 MPa, the emplacement rooms will stay open for at least 100 ka. For a realistic assumption of the long-term strength of the Cobourg using 72 MPa (65% UCS), the pillars and the emplacement rooms are expected to remain stable even after 1Ma.
- In the event of a total collapse under the assumption of 45 MPa (40% UCS), rubble that accumulates inside the emplacement rooms as a result of collapses during multiple loading/unloading cycles will eventually arrest further propagation of the caved region due to volume increase. A steady state is reached when glacial cycles cause no further expansion of the damaged or caved regions. Reasonable assumptions indicate full pillar load capacity for 7 to 8 glacial cycles. Importantly, the models predict that the steady state is reached prior to propagation of the caving related damage into the Blue Mountain shale, the lowest unit of the shale cap rock. Therefore, all damage remains contained within the host rock under all loading conditions.
- The 3D panel-scale analysis shows that deformation of the cap rock due to potential complete pillar collapse, when assuming a lower-bound long-term strength of 45 MPa (40% UCS) for the Cobourg, will cause no or insignificant damage in the cap shales including the Blue Mountain shale. Thus, the repository-induced damage remains contained within the host rock under all loading conditions.
- The analyses show that the effect of the six seismic scenarios on emplacement room stability, three for each the  $10^{-6}$  and  $10^{-5}$  probabilities of annual exceedance, is relatively small. The seismic ground shaking causes some additional unravelling of already fractured rock mass, but no new damage is predicted irrespective of the probability level of the seismic events.

## **7. ORDOVICIAN HOST AND BARRIER ROCK ATTRIBUTES**

### **7.1 Introduction**

An important element of the DGR Safety Case concerns demonstrating that the Ordovician rock mass beneath the Bruce nuclear site will provide long-term containment and isolation of the L&ILW enclosed within the repository. This chapter presents quantitatively some of the important physical attributes of the DGR-hosting Cobourg Formation, and bounding Ordovician sedimentary rocks, as primary evidence that these rocks represent a suitable host and barrier system (Table 7.1). Firstly in Section 7.2, favourable attributes of the entire Ordovician interval are discussed in brief, followed by a more detailed analysis of, 1) the Cobourg Formation which is the proposed host formation for the DGR, 2) the Upper Ordovician shales which are the primary cap rock to the proposed repository horizon, and 3) the Ordovician carbonaceous rocks which underlie the Cobourg Formation. As in previous sections of this report, all unqualified references to the Cobourg Formation refer to the Lower Member of Armstrong and Carter (2006, 2010) only. This discussion draws on key data determined during the individual studies which comprise the Geosynthesis work program, as well as key data and analysis presented in the DGSM (INTERA 2011).

International programs for the disposal of radioactive waste provide important benchmarks of host rock physical attributes against which those of the Bruce nuclear site can be evaluated. In Section 7.3 of this chapter key attributes of the site dataset, described in Section 7.2, are compared with those of several international research sites (Table 7.1). This comparison with such international experience offers insight and context into both the sufficiency of the sedimentary sequence beneath the Bruce nuclear site to safely host the DGR and the role of the geosphere as a long-term contaminant transport barrier in the Safety Case.

### **7.2 Favourable Geological Attributes of the Ordovician Interval**

The Bruce nuclear site is situated along the northeastern flank of the Michigan Basin in a region characterized by very low seismogenic activity (Section 2.2.6.4). A high degree of site-scale predictability, with respect to geometry, stratigraphic relationships, lithofacies variability and physical properties for the Ordovician interval, is indicated by the high degree of uniformity between datasets from the individual DGR boreholes (e.g., Figure 7.1). In accordance with the geometry interpreted from the 2D seismic analysis (Watts et al. 2009), the Ordovician strata beneath the site dip uniformly at  $0.59^\circ \pm 0.08^\circ$  (~10 m/km) southwestward toward the basin depocentre in central Michigan. This observation is in accordance with the  $0.23^\circ$  to  $1^\circ$  (4 to 17 m/km) dip of the entire Paleozoic succession at the regional-scale (e.g., Liberty and Bolton 1971, Wigston and Heagle 2009).

Total Ordovician thickness varies by only metres within the almost 400 m thick interval (Table 2.14). Formation-scale thicknesses vary by less than 5% and bedding dips vary by less than  $0.1^\circ$ , averaging  $0.60^\circ$  to the SW (Sterling and Melaney 2010). Intraformational centimetre- to decimetre-scale marker beds within the Queenston, Georgian Bay, and Cobourg formations (Section 2.3.4, Figure 2.31) occur at predicted intervals in all boreholes and their structural attitude is consistent with that of the bounding formation tops (Tables 2.14 and 2.15), as described by Wigston and Heagle (2009) and Sterling and Melaney (2010). Intraformational marker bed analysis and borehole triangulation supports this assessment by exhibiting an average dip of  $0.59^\circ$ . The consistency of data between DGR boreholes suggest that a vertical offset in the stratigraphy between the boreholes related to faulting would be constrained to approximately 1.7 m or less.



**Table 7.1: Comparison of Bruce Nuclear Site Dataset for Host and Cap Rock Units with Those from International DGR Programs**

Property/parameter	Ordovician shales (OPG DGR cap rock)	Ordovician Cobourg Formation limestone (OPG DGR host rock)	Callovo-Oxfordian (Bure)	Opalinus Clay (Zurcher Weinland) <sup>a,t</sup>	Opalinus Clay (Mont Terri)
Age (Ma)	>443 <sup>b</sup>	<454 <sup>b</sup>	ca. 163-158	ca. 174	ca. 174
Maximum temperature reached during diagenesis (°C)	ca. 65-70 <sup>c</sup>	ca. 70 <sup>c</sup>	33-38	85	85
Present burial depth (centre of unit (m))	550 <sup>d</sup>	675 <sup>d</sup>	488	596	275
Maximum burial depth (centre (m))	ca. 1550 <sup>e</sup>	ca. 1675 <sup>e</sup>	850	1650	1350
Thickness (m)	211.9 <sup>d</sup>	28.6 <sup>d</sup>	138	113	160
Sheet silicate minerals (weight %)	40-50 <sup>f</sup>	<10 <sup>f</sup>	25-55	54	66
Sheet silicate minerals (in order of decreasing abundance)	Illite & mica, chlorite, illite/smectite, trace kaolinite <sup>g</sup>	Illite & mica, chlorite, illite/smectite, trace kaolinite <sup>g</sup>	Illite/smectite mixed layers, illite, chlorite, kaolinite	Illite, kaolinite, illite/smectite mixed layers, chlorite	Illite, kaolinite, illite/smectite mixed layers, chlorite
TOC (weight %)	0.01-2.5 <sup>h</sup>	0.225-1.387 <sup>h</sup>	0.0-1.0	0.6	0.8
Pore-water type	Na-Cl <sup>i</sup>	Na-Cl <sup>i</sup>	Na-Cl-SO <sub>4</sub>	Na-Cl-SO <sub>4</sub>	Na-Cl-SO <sub>4</sub>
Mineralization/TDS (mg/L)	300,000 <sup>o</sup>	286,000 <sup>o</sup>	ca. 6500	ca.13000	ca.18000
Eh (mV)	-150 <sup>j</sup>	-150 <sup>j</sup>	<-150	-170	-227
Physical (Total) porosity (-)	0.072 <sup>j</sup>	0.019 <sup>j</sup>	0.14 <sup>k</sup> -0.18	0.12	0.16
Eff. diffusion coeff. D <sub>e</sub> (HTO) normal to bedding (m <sup>2</sup> /s) <sup>s</sup> ,	9.3E-14 to 4.8E-12 <sup>m</sup> , 1.2 to 4.9	3.2E-13 to 2.3E-12 <sup>m</sup> , 1 to 4.2	2.6E-11, <2 <sup>n</sup>	6.1E-12, 5	1.5E-11, 5

Property/parameter	Ordovician shales (OPG DGR cap rock)	Ordovician Cobourg Formation limestone (OPG DGR host rock)	Callovo-Oxfordian (Bure)	Opalinus Clay (Zurcher Weinland) <sup>a,t</sup>	Opalinus Clay (Mont Terri)
anisotropy factor <sup>r</sup>					
Hydraulic conductivity, K, parallel to bedding (m/s), anisotropy factor <sup>r</sup>	2.0E-14 to 3.0E-14 <sup>o</sup> , 10	1.0E-14 <sup>o</sup> , 10	1E-13 to 1E-12, 2-10	2.4E-13, 1-10	2.0E-13, ca. 5
UCS, normal to bedding (MPa)	22-48 <sup>p</sup>	113 <sup>p</sup>	21 <sup>q</sup>	30	16 <sup>f</sup>

Notes: Table is modified from Mazurek et al. (2008) which is the source for the international data sets indicated above.

a - Includes Murchisonae Beds in Opalinus Clay facies.

b - Minimum age of shales is from Gradstein et al. (2004); maximum age of limestone is estimated from ca. 454 Ma ash layer in the underlying Coboconk Formation.

c - See discussion in Section 2.2.5.3 herein.

d - From Table 3.17 of INTERA (2011) (shale thickness includes Collingwood Member).

e - Based on estimate of ca. 1000 m of erosion, see discussion in Section 2.2.5.3 herein.

f - From Figure 3.6 of INTERA (2011) based on values from Jackson (2009).

g - From Figure 3.8 of INTERA (2011).

h - From Figure 3.15 of INTERA (2011) and range of values from Wigston and Jackson (2010a, 2010b).

i - From Table 4.17 of INTERA (2011).

j - From Table 4.18 of INTERA (2011) (shale value excludes Collingwood Member porosity of 0.023).

k - Value for the most carbonate-rich beds (upper part of formation).

l - Anisotropy factor - value parallel/value normal to bedding.

m - From range of values in Table 9 of Al et al. (2010a) and Table A.2 of Al et al. (2010b) (DGR-2 to DGR-4 data only).

n - From Pocachard et al. (1997) in Mazurek et al. (2008).

o - From Table 4.19 of INTERA (2011) (TDS for cap rock excludes Collingwood Member TDS of 225,000 mg/L).

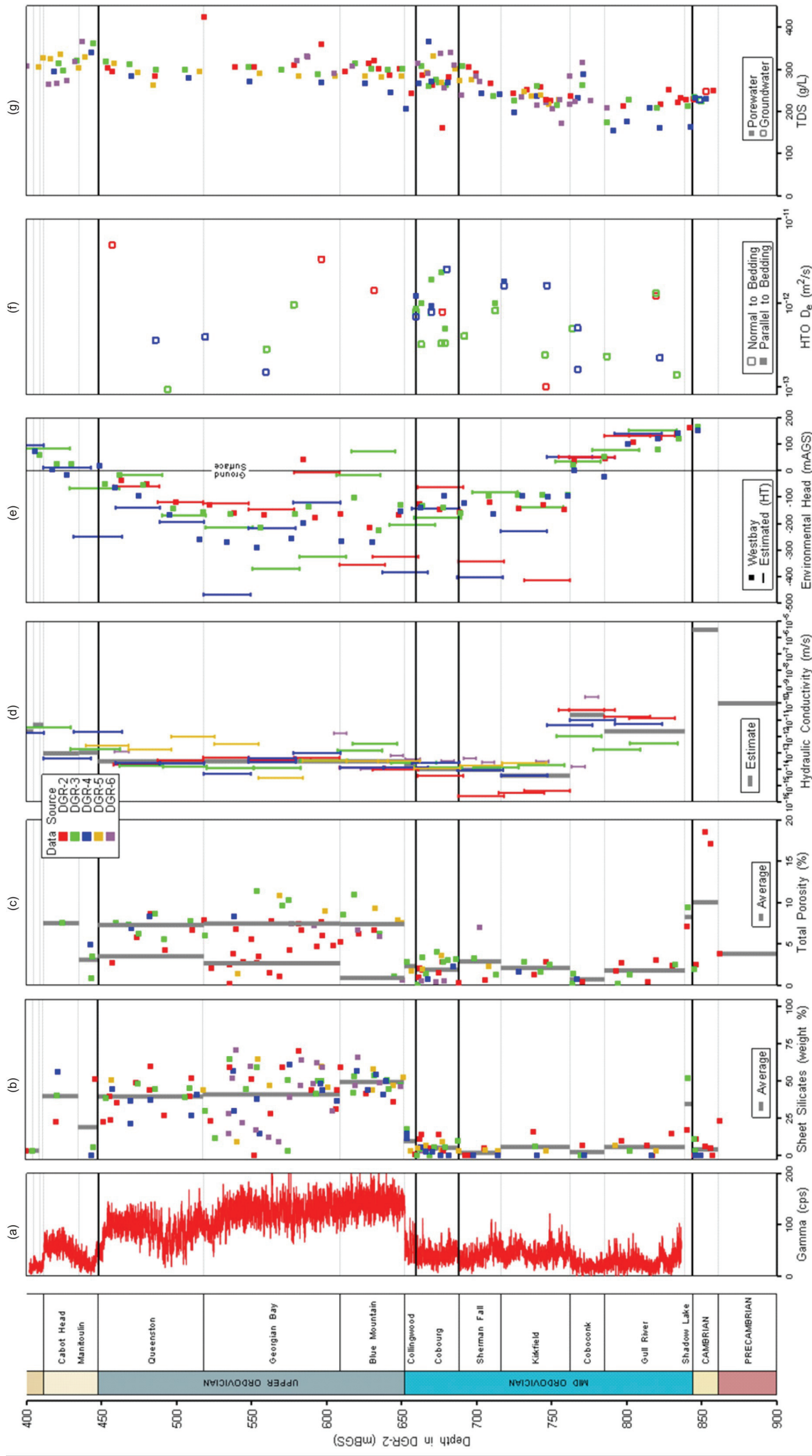
p - From Table 5.22 of INTERA (2011) (shale range excludes Collingwood Member UCS of 107 MPa).

q - Value at the level of the underground research laboratory.

r - Recommended value according to Bock (2001).

s - Diffusion coefficients (D<sub>e</sub>) were measured at ambient laboratory temperature (~22°C).

t - Benken borehole only.



Notes: Data are plotted against reference stratigraphy from DGR-2. Average values are indicated by thick grey vertical bars where appropriate. Measured test intervals in (d) and (e) are indicated by length of vertical bar. (a) Gamma profile (for DGR-2 only) in counts per second (cps). (b) Sheet silicate content is measured in weight percent (wt%). (c) Total porosity is measured in percent (%). (d) Hydraulic conductivity is measured in metres per second (m/s). (e) Environmental head is measured in metres above ground surface (mAGS). (f) Diffusion coefficient is measured in metres squared per second (m<sup>2</sup>/s) and is based on HTO tracer analyses. (g) TDS is measured in grams per litre (g/l). Data are from INTERA (2011).

Figure 7.1: Summary Plot Indicating Key Physical Properties of the Ordovician Sedimentary Rock Interval Beneath the Bruce Nuclear Site

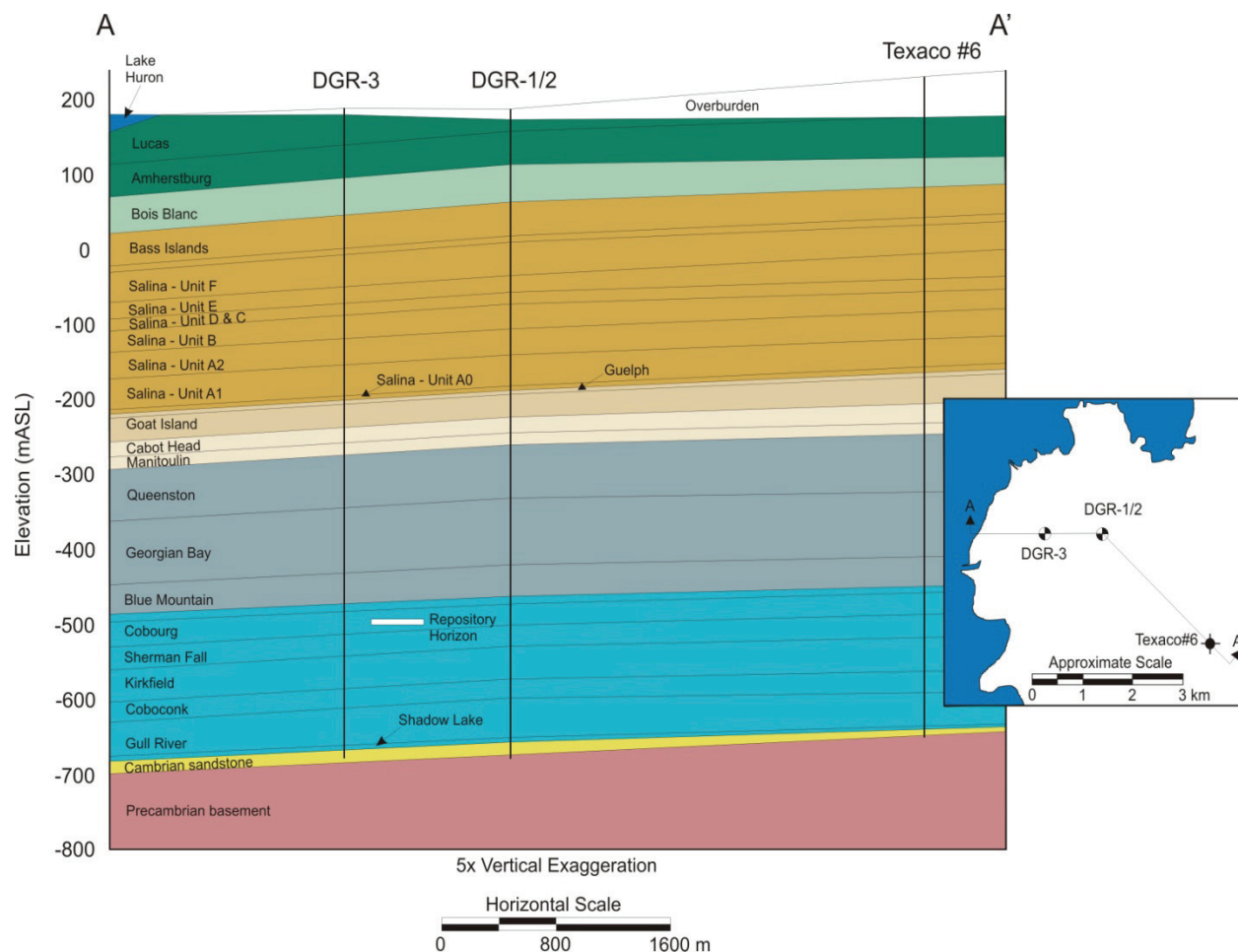
**THIS PAGE HAS BEEN LEFT BLANK INTENTIONALLY**

The Ordovician gamma profiles from the vertical DGR boreholes (DGR-2, DGR-3 and DGR-4) highlight this consistency at the greater than formation scale as shown in Figure 2.30 (Section 2.3.4.1 herein). One representative gamma profile shown in Figure 7.1a (profile is from DGR-2), highlights the bimodal nature of the Ordovician interval. A high relative CPS (see Section 2.3.4.1 for further discussion of CPS) for the upper shaley Queenston Formation to Blue Mountain Formation interval transitions sharply to a lower CPS value through the carbonaceous Middle Ordovician Collingwood Member to Shadow Lake Formation interval (Figure 7.1a). The distribution of the major mineralogical components between these shale or carbonate dominant intervals is also generally consistent between boreholes (Figure 2.30). For example, the weight percent distribution of sheet silicates (Figure 7.1b) is consistent with the change from a shale-rich upper to carbonate-rich lower Ordovician succession. This mineralogical transition also appears to correlate with the vertical porosity distribution (Figure 7.1c). Variability within the mineralogical and porosity datasets, especially within the shaley interval, is a function of the cm and smaller-scale lithological variation observed within the DGR cores (e.g., Figure 2.31 in Section 2.3.4.1 herein).

Extrapolation of the DGR stratigraphy beyond the Bruce nuclear site highlights the broader consistency of the Ordovician interval at the greater than km scale. Figure 7.2 shows a cross-section which links the subsurface stratigraphy encountered at the Bruce nuclear site with that encountered in the wildcat Texaco #6 borehole. The match in formation thicknesses, especially within the Ordovician interval, is evident in the simple geometry of the cross-section. This result is not surprising given that the Ordovician paleo-depositional environments evolved at a scale much larger than that of the DGR footprint (e.g., Figure 2.9 and discussion in Section 2.2.5.1). However, it is important because it provides greater confidence in our interpretation of predictability within the DGR footprint.

Based on analysis of the 2D seismic data of Watts et al. (2009), the DGR-5 and DGR-6 inclined boreholes were drilled at orientations specifically chosen in order to intersect two features (faults) that were most confidently identified within and proximal to the DGR footprint. Results from this drilling showed no evidence of faulting, as described in Section 3.11.4 of INTERA (2011). The detailed fracture mapping exercise found no evidence for major fault or shear zones in bedrock exposures along the Lake Huron shoreline, and further was able to prescribe a probable late Paleozoic timing to development of the observed systematic joint and vein sets (Cruden 2011).

Predictability is also evident in the consistency between hydrogeologically relevant physical properties of the DGR boreholes, for example hydraulic conductivity shown in Figure 7.1d, environmental head distribution shown in Figure 7.1e, diffusion coefficient (HTO) shown in Figure 7.1f and TDS salinity profile in Figure 7.1g. Westbay monitoring systems have been installed in the deep vertical DGR boreholes to allow for long-term monitoring of hydraulic formation pressures, and where possible, sampling of groundwater for water quality analysis. Formation pressure monitoring results demonstrate significant underpressures in the cap rocks and Cobourg Formation (Figure 7.1e and Section 4.12 in INTERA 2011). There are also strong downward gradients from the Manitoulin Formation to the cap rock shales and strong upward gradients from the Cambrian to the Ordovician shale (Figure 7.1e) and within the lower bounding carbonaceous interval (Coboconk Formation to Kirkfield Formation). The hydraulic testing results and the maintenance of large hydraulic gradients created by strong overpressures in the Cambrian and underpressures in the Ordovician indicate that if any faults do exist proximal to the DGR, they do not act as permeable pathways for fluid migration.



Notes: The section also includes location and formation top data from the Texaco #6 borehole. Locations of all boreholes used in the section are shown on the inset map (INTERA 2011).

**Figure 7.2: Cross-section Through the Paleozoic Succession Beneath the Bruce Nuclear Site**

Taken together with the observations of stratigraphic consistency and predictability at the site scale and greater, these results argue against the likelihood of major undetected faults of concern being located proximal to the Bruce nuclear site.

Numerical simulations of the groundwater system, which provided a systematic framework to explore uncertainty in long-term behaviour, yield estimates of mean life expectancies for a non-retarded, non-decaying solute released at DGR horizon on the order of many millions of years. These simulations combined with knowledge of formation properties, past external perturbations (i.e., glaciation) and existing distribution of environmental tracers provide strong evidence that solute transport has remained diffusion dominant at timeframes relevant to DGR safety.

### 7.2.1 Host Cobourg Formation

The host formation for the proposed DGR is the ca. 28 m thick Middle Ordovician Cobourg Formation. Important physical attributes of the Cobourg Formation are listed in Table 7.1. This formation is an argillaceous limestone that exhibits a low average porosity of 1.9% and extremely low average horizontal hydraulic conductivity ( $K_H$ ,  $1.0 \times 10^{-14}$  m/s) throughout (Figures 7.1c and 7.1d). This formation is sandwiched between more than 200 m of shale-dominated sedimentary rock above and more than 150 m of argillaceous limestone below (Figures 7.1 and 7.2). The centre of the Cobourg Formation is encountered at approximately 675 mBGS in the reference DGR-2 borehole (Table 3.1 in INTERA 2011). The Cobourg Formation will completely enclose the excavated DGR with the repository floor 6 m above its basal contact with the underlying Sherman Fall Formation.

Major mineralogical components are consistent with the lithological description of the Cobourg Formation as a fossiliferous argillaceous limestone – packstone/wackestone with abundant calcareous fossil fragments contained in a fine-grained calcareous, Fe-stained matrix (INTERA 2011). Calcite predominates with minor amounts of dolomite, interstitial clays, pyrite, accessory quartz and trace chlorite also identified (Section 2.3.5). Sheet silicates comprise up to approximately 10% of the formation (Figure 7.1b), and include, in order of decreasing abundance, illite, mica (chlorite), and smectite (Section 2.3.5).

A maximum burial depth of approximately 1675 m for the top of the Cobourg Formation, situated in the middle of the Ordovician succession, occurred during the late Paleozoic or early Mesozoic era (Figure 2.12). This burial depth maximum is based on the interpretation that approximately 1000 m of sediment has been eroded from the Paleozoic succession at the Bruce nuclear site. Based on estimates of paleo-geothermal gradient, discussed in Section 2.2.5.3, a peak temperature of approximately 70°C was reached within a similar timeframe as peak burial (Table 7.1). Therefore these sedimentary rocks only barely reached the oil window in terms of thermal maturity. Along with a low total organic content (TOC), ranging from 0.225 to 1.387 wt%, this precludes the likelihood of encountering commercial hydrocarbon resources in the host Cobourg Formation.

The Cobourg Formation comprises MS Unit 4 discussed in detail in Section 3.3.1 herein and Section 5.1.1 in INTERA (2011). Based on core logging, the formation is unfractured to very sparsely fractured with excellent core quality and core recovery. An average RQD of 99% and a mean fracture frequency of  $0.1 \text{ m}^{-1}$  are consistent with this interpretation (Section 3.6 of INTERA 2011). The Cobourg Formation has a peak (mean) UCS of ca. 113 MPa (Table 7.1). Based primarily on regional studies, the approximate range of stress ratios likely to be encountered at the repository horizon are as follows:  $\sigma_H/\sigma_V$  will likely vary from 1.7 to 2.5;  $\sigma_h/\sigma_V$  from 1.0 to 1.2; and  $\sigma_H/\sigma_h$  from 1.5 to 2.1, where:  $\sigma_H$  is the maximum horizontal stress,  $\sigma_h$  is the minimum horizontal stress and  $\sigma_V$  is the vertical stress (NWMO and AECOM 2011; see also Chapter 3 herein).

Due to the Cobourg Formation's extremely low permeability, no groundwater samples could be collected from this formation during site characterization activities (INTERA 2011). Instead, core samples were submitted to laboratories for porewater extraction. The collected porewaters were then analysed for a suite of major chemistry parameters as well as a number of stable environmental isotopes (Section 4.6.6 in INTERA 2011). The porewater chemistry from samples collected from the Cobourg Formation confirms the water is of a Na-Cl type with a TDS concentration averaging 285,000 mg/L (Figure 7.1g). Master variables of pH and Eh are approximately 5.5 +/- 1 (computed from measured  $\text{pCO}_2$ ) and -150 mV, respectively, reflecting iron and/or sulphur-reducing conditions (Section 4.13.6 in INTERA 2011).

Diffusion coefficients in the Cobourg Formation, measured normal to bedding and with HTO tracer, range between  $3.2 \times 10^{-13}$  and  $2.3 \times 10^{-12}$  m<sup>2</sup>/s, with anisotropy factor ranging from 1 to 4.2 (Table 7.1; Al et al. 2010a, 2010b), as shown in Figure 7.1f. Modelling results conclude that about 275 Ma is required to obtain a good fit to the measured porewater  $\delta^{18}\text{O}$  profile that is observed in the Ordovician stratigraphic sequence (Chapter 4). This points to the waters in the Cobourg Formation specifically, and its bounding formations in general, as being extremely old and most likely connate.

## 7.2.2 Cap Rock Upper Ordovician Shales

The ca. 212 m thick Upper Ordovician cap rock succession at the Bruce nuclear site includes the shale-dominated Queenston, Georgian Bay and Blue Mountain formations, as well as the underlying calcareous shale and argillaceous limestone of the Collingwood Member (Figure 7.1 and Table 7.1). The middle of this package occurs at a depth of approximately 550 mBGS in the reference DGR-2 borehole (Table 3.1 in INTERA 2011).

The Queenston, Georgian Bay and Blue Mountain formations, which comprise the majority of the cap rock thickness, have shale-dominant compositions but they also exhibit, in varying amounts, mm- to cm-thick hardbeds of limestone, siltstone and sandstone within m-scale horizons evident, for example, in the gamma profile (Figure 7.1a) and sheet silicate wt% distribution (Figure 7.1b). This small-scale lithological variation is important because it is encountered within the same stratigraphic interval in all of the DGR boreholes and thus provides further evidence that the stratigraphy is laterally consistent and predictable (see also Section 2.3.4). The ranges in major mineralogical compositions identified for the shale cap rock (Section 2.3.5) also reflect the vertically variable but laterally traceable lithology of the Upper Ordovician formations observed in the DGR boreholes (Figures 7.1 and 7.2, see also Section 2.3.4). Sheet silicates comprise 40-50 wt% on average of the cap rock interval (Figure 7.1b), including, in order of decreasing abundance, illite, mica (chlorite), and smectite (Section 3.7.1 in INTERA 2011).

This vertical variation appears to control very favourably the petrophysical properties of the cap rock, including yielding some extremely low diffusion coefficients ranging from  $9.3 \times 10^{-14}$  in a limestone hardbed to  $4.8 \times 10^{-12}$  m<sup>2</sup>/s in red shale (Figure 7.1f), and with an anisotropy factor ranging from 1.2 to 4.9 (Table 7.1). These values are based on measurements made normal to bedding with HTO tracer (Al et al. 2010a, 2010b). An estimate of average porosity for the Upper Ordovician cap rock is 7.2% and this value does not include a porosity estimate of 2.3% for the Collingwood Member (Figure 7.1c herein; Table 4.18 of INTERA 2011).

Based on core logging, the Upper Ordovician shale cap rock is unfractured to sparsely fractured with excellent core quality (Section 3.6 of INTERA 2011). Local fracture sets observed during core logging, comprising two or more parallel en echelon joints, are broadly separated between intervals of intact core several metres in length. Core logging identified the sporadic occurrence of smooth natural fractures throughout the Queenston interval, most of which were sealed and infilled with halite, calcite and/or gypsum. The fractures not infilled with cements are interpreted to have remained sealed at depth based on the very low hydraulic conductivity values obtained during borehole testing of those intervals. Measured averages for RQD and fracture frequency were 94% and  $0.3 \text{ m}^{-1}$ , respectively. This sparse number of measured fractures is consistent with an estimated peak burial temperature of 70°C (see discussion in Section 2.2.5.3), which would have been too low to stimulate the development of pervasive natural hydraulic fractures (e.g., Engelder 2011). The few observed natural fractures are clustered, predictably, at the



base of the Blue Mountain Formation where the highest levels of TOC and methane have been measured (Figures 3.15 and 4.6, respectively, in INTERA 2011).

The peak temperature range indicated above is based on the peak burial depth of approximately 1550 m for the middle of the cap rock interval, as discussed in Section 2.2.5.3. Interestingly, this temperature range straddles the boundary between thermal immaturity for the Type III kerogen found in shales of the Queenston Formation, and marginal maturity for the Type II to Type III kerogen in shales of the Georgian Bay Formation, in terms of hydrocarbon potential (Figure 3.17 in INTERA 2011). Low TOC, which averages < 1.0 wt% and ranges between 0.01 and 2.5 wt% for the entire cap rock interval, as shown in Figure 7.2, is consistent with the low degree of thermal maturity and observed lack of commercial quantity of hydrocarbons encountered during drilling of the DGR boreholes (INTERA 2011).

The geomechanical properties under uniaxial compression have been grouped together into a single cap rock unit without distinction with respect to stratigraphy, although there is a slight trend for the strength, stiffness and Poisson's Ratio values to decline somewhat in the lower part of the unit (Georgian Bay, Blue Mountain, Collingwood units) compared to the Queenston Formation (Table 5.22 in INTERA 2011). It is noted that the single test conducted on core from the Blue Mountain Formation indicated a very weak material, with a UCS of 22 MPa as compared to 48 MPa for the Queenston Formation (Table 7.1). Two tests in the immediately underlying calcareous Collingwood shale indicated a higher strength material with an average UCS of 107 MPa.

Direct shear tests were conducted on one sample taken from within the Georgian Bay Formation, and two samples from the Blue Mountain Formation. Residual shear strength parameters appear to be relatively consistent for the samples from both formations. The proposed best estimate values are apparent cohesion 0.25 MPa and residual friction angle of 27 degrees. Slake durability testing values indicate a mean slake durability index (SDI) of 80%, with higher values in the Queenston Formation. In formation water, the swelling potential for the shales is essentially zero, as expected. No swelling was observed during testing. Swelling potential in fresh water was minor or zero in all cases, likely a result of the pervasive calcite cements and absence of swelling sheet silicates such as smectite. As mentioned above, the dominant sheet silicate is illite.

Porewater in shale cap rocks consist of Na-Cl brine and exhibit remarkably uniform chemistry, for example a very uniform TDS of approximately 300,000 mg/L (Figure 7.1g; Table 4.19 of INTERA 2011). Chemical uniformity is also evidenced by major ion ( $\delta^{18}\text{O}$  and  $\delta\text{D}$ ) and fluid density profiles (Section 4.6 in INTERA 2011). Master variables of pH and Eh are approximately 5.5 +/- 1 (computed from measured  $\text{pCO}_2$ ) and -150 mV, respectively, reflecting iron and/or sulphur-reducing conditions (Section 4.13.5 in INTERA 2011).

Hydrostratigraphically, the Ordovician shales and Collingwood Member are considered as aquicludes. Interpretation of borehole straddle-packer results provides estimated average horizontal hydraulic conductivities ( $K_H$ ) for the cap rock in the range of  $2 \times 10^{-14}$  to  $3 \times 10^{-14}$  m/s (Table 7.1 and Figure 7.1d), with a horizontal:vertical K anisotropy of 10:1 (Table 4.19 in INTERA 2011). Based on environmental heads, a strongly downward (~1.2 m/m) vertical hydraulic gradient is indicated for the cap rocks, at least to the Blue Mountain Formation (Figure 7.1e). Although the genesis of the Ordovician underpressures is ambiguous, their occurrence and persistence are clearly indicative of very low formation permeability (Section 4.11 in INTERA 2011). A single zone within the lower part of the Georgian Bay Formation in boreholes DGR-2, 3 and 4 has a formation pressure approaching hydrostatic. This

condition may be attributed to an interval of increased fracture frequency or a discrete lithofacies change, both associated with possible gas occurrence despite extremely low permeabilities (INTERA 2011). The gas pressure in this isolated shale bed is interpreted to push the interval formation pressures toward hydrostatic. The persistent formation underpressures and the uniform porewater chemistry profiles indicate that no significant fluid flow has occurred within the Ordovician shale units, supporting its designation as an aquiclude and natural cap rock seal.

The interpretation that contaminant transport in the shales is dominated by diffusion is strongly supported by low hydraulic conductivity values, maintenance of large hydraulic gradients, porewater salinity, and stable isotope values (e.g.,  $\delta^{18}\text{O}$  and  $\delta\text{D}$ ). These results are consistent with the observation that at the basin-scale, these Ordovician shales have sufficient seal quality (low permeability) to trap gas for millions of years (Engelder 2011).

### 7.2.3 Lower Bounding Ordovician Carbonates

The lower bounding rocks include the low-permeability Middle Ordovician limestone formations beneath the Cobourg Formation. These include the Sherman Fall and Kirkfield formations of the Trenton Group, and the Coboconk and Gull River formations of the Black River Group (Figures 7.1 and 7.2). Together this lower bounding interval has a thickness of 150.5 m (Table 3.17 in INTERA 2011). The top of this interval, the Sherman Fall Formation, is encountered at depths ranging from 688.1 to 700.1 mBGS in the vertical DGR boreholes (Table 3.1 in INTERA 2011).

Based on core logging, all of the lower bounding rocks are unfractured to sparsely fractured with excellent core quality. Measured averages for RQD and fracture frequency were 100% and  $0.1\text{ m}^{-1}$ , respectively. However, it is noted that minor local zones of lower quality may occur in the Sherman Fall Formation (Section 3.6 in INTERA 2011). From a geotechnical perspective the principal unit of interest within these lower carbonates is the 28-m-thick Sherman Fall Formation which is located directly beneath the repository horizon. The Sherman Fall and Kirkfield formations have a peak (mean) UCS of approximately 45 MPa, and are therefore significantly weaker than the overlying rocks of the Cobourg Formation, which hosts the DGR. The elevation of the DGR within the Cobourg Formation is, as stated above, 6 m above the top of the Sherman Fall Formation. This elevation was selected to assure greater geomechanical stability of the lateral development. In the Sherman Fall Formation, the SDI value was approximately 85%, whereas in the lower units beneath the Sherman Fall, the SDI was close to 100%. Swelling Potential for the Sherman Fall Formation in both fresh and brine water was observed to be zero.

The lower bounding limestones exhibit carbonate-dominant compositions with a relatively consistent sheet silicate (wt%) composition (Figure 7.1b) in the form of mm- to cm-scale argillite/shale interbeds which are observed vertically through the section (Figure 7.2). The lower half of the Coboconk Formation is petroliferous with minor out-gassing and hydrocarbon bubbling from stylolites and some thin vuggy zones. Petrographic analysis of core collected from the middle sections of the Coboconk Formation shows the sample to be partly dolomitized bioclastic limestone with traces of pyrite. Selected thin vuggy and stylolitic sections of the Gull River Formation are slightly petroliferous showing out-gassing and traces of liquid hydrocarbons (Section 3.7.4.2 in INTERA 2011).

Porewater chemistries in the lower limestone units are consistent with a Na-Cl brine. There is a definite transitional trend with depth from the chemistry of the Cobourg Formation to that of the

Cambrian formation. TDS varies between a high of 269,000 mg/L in the Sherman Fall to 204,000 mg/L in the Gull River Formation as shown in Figure 7.1g herein and Table 4.19 in INTERA 2011). An average porosity value is estimated at 2.1% for these lower bounding carbonates (Figure 7.1c). Laboratory diffusion testing undertaken on core samples showed effective diffusion coefficients ranging from  $1.0 \times 10^{-13}$  to  $1.3 \times 10^{-12}$  m<sup>2</sup>/s (Figure 7.1f) and with an anisotropy factor estimated at 1.3 (Table 7.1). These values are based on measurements made normal to bedding with HTO tracer (Al et al. 2010a, 2010b). Variables of pH and Eh approximate 5.5 (computed from measured pCO<sub>2</sub>) and -100 mV respectively, reflecting iron and/or sulphur-reducing conditions.

Borehole straddle-packer testing shows that the average horizontal hydraulic conductivity for the lower bounding Middle Ordovician limestone ranges from  $10^{-15}$  to  $10^{-14}$  m/s in the Sherman Fall and Kirkfield formations to  $10^{-12}$  to  $10^{-11}$  m/s in the Coboconk and Gull River formations (Figure 7.1d). The horizontal:vertical K anisotropy is assumed to be 10:1 within the near horizontally bedded limestones (Table 7.1). A possible exception is the Black River Group in which low but relative elevated permeabilities are attributed to discrete, thin near horizontal dolomitized horizons (INTERA 2011). In this situation horizontal:vertical K anisotropy may be on the order on 1000:1.

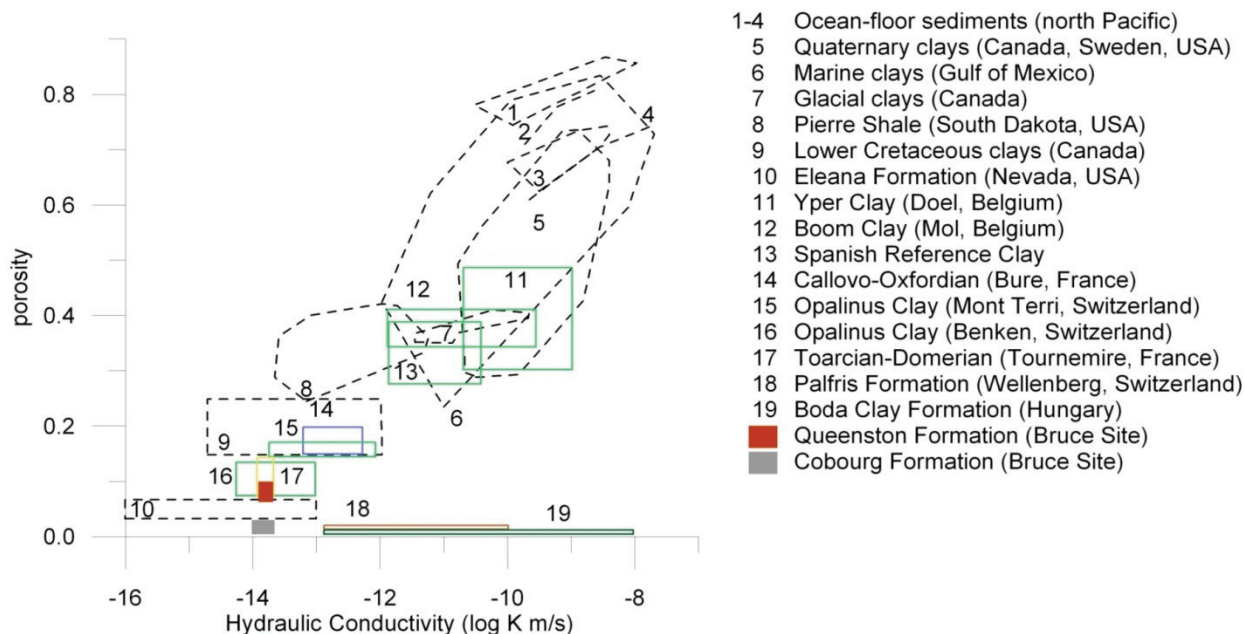
Formation pressures and calculated fresh water and environmental heads in the Middle Ordovician are below hydrostatic equilibrium values and very slow to achieve stable conditions for the Sherman Fall and Kirkfield formations, but are stable and normally pressured to overpressured in the deeper Coboconk and Gull River formations (Figure 7.1e). These different transient formation pressure responses support the interpretation that the Sherman Fall and Kirkfield formations are less permeable than the deeper Coboconk and Gull River formations. Based on environmental head data, the vertical hydraulic gradients are generally strongly upward (~1.2 m/m) to the Blue Mountain Formation, reflecting overpressuring from the deeper Cambrian formation. Very low measured permeabilities combined with diffusion and site-scale hydrogeological modelling support the interpretation of diffusion-dominated contaminant transport in the Middle Ordovician limestones (Sections 4.3 and 4.4 of INTERA 2011).

### 7.3 Comparison with International Programs

Several international groups are studying the potential for the deep geological disposal of radioactive waste in argillaceous formations (Mazurek et al. 2008). A broad spectrum of research programs including both field and laboratory analyses, in various stages of progress, are benefitting from a collaborative relationship between these groups. In particular, the investigations have recognized and compiled a set of important physical parameters which together may be used to characterize a host rock for its potential to contain waste for the requisite long-term (Mazurek et al. 2008 and references therein). In order to provide context for the DGR concept and its' Safety Case, it is useful to compare the understanding of site properties with those of advanced international programs. A comparison of key attributes is provided in Table 7.1 and Figures 7.3 and 7.4.

A comparison of the results from site characterization activities described in this report and those of international programs highlights several consistently reported observations. These include: conditions of generally low seismogenic activity, a laterally extensive and predictable lithostratigraphy, a lack of hydraulically significant fractures, a reducing environment, and diffusion-dominated transport. In particular, the proposed DGR for the Bruce nuclear site compares favourably with other international programs in terms of its hydraulic conductivity,

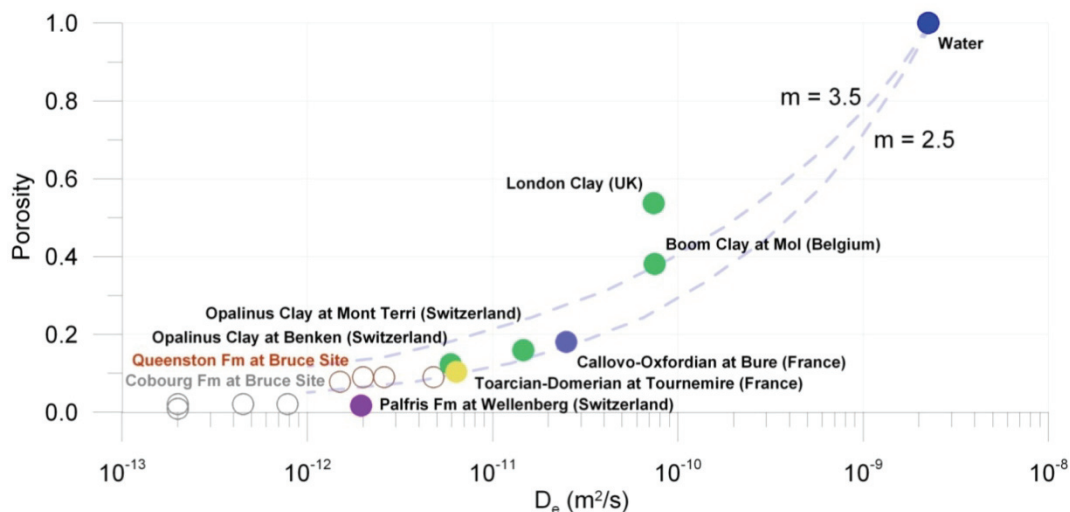
porosity and effective diffusion coefficients, with measured values consistently in the lowest range of those determined elsewhere (Figures 7.3 and 7.4).



Notes: Adapted from Mazurek et al. (2008).

**Figure 7.3: Relationship Between Porosity and Hydraulic Conductivity in Clays**

In some cases, the geological conditions experienced by the rock mass at the Bruce nuclear site vary markedly from the international examples. For example, the Cobourg Formation experienced maximum burial conditions of up to 800 m more than the Callovo-Oxfordian clay unit being considered by the French radioactive waste disposal program. However, effects such as over-consolidation and fracturing due to compaction appear to have not significantly affected the conditions of extremely low hydraulic conductivity at the Bruce nuclear site. It further emphasizes that the physical conditions the Bruce nuclear site experienced during its past geological evolution were below a threshold at which fractures would have become hydraulically important. In contrast, the Boda Clay Formation in Hungary and the Palfris Formation in Switzerland (Figure 7.3), which have undergone a much deeper burial than the other clay rocks discussed in Figure 7.3, are examples of media where fracture flow dominates under conditions of extremely low porosity. The observation of low hydraulic conductivity at the Bruce nuclear site also indirectly supports the notion that the overlying shale cap rocks possess the capacity for self-sealing (see also Engelder 2011).



Notes: This dataset provides a direct comparison between European argillaceous formations (filled circles) and the Cobourg (unfilled grey circles) and Queenston (unfilled red circles) Formations at the Bruce nuclear site (adapted from Mazurek et al. 2008).

**Figure 7.4: Relationship Between Porosity and Effective Diffusion Coefficient for HTO (Normal to Bedding) in Low Permeability Rocks**

These results confirm that the physical properties of the host and bounding formations at the Bruce nuclear site are comparable with those encountered in international site characterization programs (e.g., Mazurek et al. 2008). Confidence in the safety case for the development of a DGR in the Cobourg Formation beneath the Bruce nuclear site, and for the long-term isolation of the disposed materials and protection from radionuclide migration to the biosphere, is regarded as high.

## 8. SUMMARY AND CONCLUSIONS

This document provides an assessment of the Bruce nuclear site with respect to its geologic suitability for implementation of OPG's proposed DGR concept. This assessment is supported by a number of specific geoscience reports commissioned by the NWMO as part of the overall Geosynthesis program described above. In addition to these studies, the Geosynthesis integrates the results of the Bruce nuclear site geoscientific site characterization activities that comprise detailed site investigations including drilling programs, field testing, laboratory analyses and geophysical surveys. The geoscientific information generated from these programs is summarized in the DGSM (INTERA 2011) and this report.

Chapter 1 outlined seven key hypotheses regarding site attributes and characteristics that, if satisfied, will provide confidence that the geologic setting of the Bruce nuclear site is suitable to host the DGR. Each subsequent chapter has provided in part, by way of detailed descriptions and analysis, evidence used to support these hypotheses. The seven hypotheses are generally adopted, in some fashion, by radioactive waste programs internationally. The scientific support that can be developed for the hypotheses provides regulators, the scientific community and other stakeholders with multiple lines of evidence to allow them to judge site suitability. The seven hypotheses and the supporting evidence are presented below.

- **Site Predictability: near-horizontally layered, undeformed sedimentary shale and limestone formations of large lateral extent**
  - The occurrences of individual bedrock formations, facies assemblages, marker horizons, and major minerals, and the distribution of hydrocarbons and karst, are predictable and traceable at the site-scale (Section 2.3). Comparing the Paleozoic bedrock stratigraphy encountered in the DGR boreholes to that derived from an assessment of historic oil and gas well records demonstrates traceability at the local scale (e.g., Texaco #6 well) and indicates a high degree of consistency with the regional stratigraphic framework of Armstrong and Carter (2006) as described in Sections 2.2.5 and 7.2 herein and in Section 3.13 of the DGSM (INTERA 2011).
  - The thickness and orientation of bedrock formations encountered beneath the Bruce nuclear site are highly consistent as indicated by the dataset shown in Tables 3.1 and 3.2 of the DGSM (INTERA 2011). Within an area of approximately 1.5 km<sup>2</sup> enclosing the DGR footprint, information derived from the deep drilling and coring program confirms that Ordovician formation thickness variations are on the order of meters (Table 2.14). Formation dips within the same chronostratigraphic sequence are uniformly 0.59° +/- 0.08° (≈10 m/km) to the southwest towards the Michigan Basin.
  - The results of the 2D seismic reflection survey (19.7 km of data collected) provide evidence for the traceable nature of the bedrock stratigraphy beneath the site as discussed in Section 2.3.9.2 (Watts et al. 2009). The inclined drilling and coring of DGR-5 and DGR-6 targeted potential subvertical faults or fault zone structures in proximity to the DGR footprint. Continuous core retrieved from both boreholes showed no evidence of faulting or stratigraphic offset through the target interval as discussed in Section 2.3.9.1 herein and in Section 3.11.4 of the DGSM (INTERA 2011).
  - Evidence supporting vertical fault displacement or the occurrence of steeply oriented linear and elongate HTD reservoirs within the Ordovician carbonate rocks is absent.

No proximal deep-seated fault system was identified during the 2D seismic survey as discussed in Section 2.3.9.2.

- As shown in Figure 2.5 and discussed in Section 2.2.6, mapped faults are not known to penetrate Paleozoic sedimentary rocks younger than Ordovician age within the RSA (Armstrong and Carter 2010). This conclusion is consistent with the results of the detailed fracture mapping study, which found no evidence for complex fault structures or shear zones in the exposed bedrock proximal to the Bruce nuclear site (Cruden 2011), and it is also consistent with the results of the 2D seismic survey (Watts et al. 2009).
- **Multiple Natural Barriers: multiple low-permeability bedrock formations enclose and overlie the DGR**
  - The sedimentary sequence underlying the Bruce nuclear site comprises 34 near horizontally layered, laterally continuous bedrock formations (Section 2.3.3). Within the Ordovician sediments that host and enclose the proposed DGR there are numerous units characterized as aquicludes that possess extremely low rock mass permeabilities (Section 5.4.1). The host Cobourg Formation has a very low horizontal hydraulic conductivity ( $K_H$ )  $\approx 10^{-14}$  m/s. The overlying > 200 m of Ordovician shales (3 formations) have rock mass horizontal hydraulic conductivities  $<10^{-13}$  m/s. The underlying 150 m of Ordovician carbonates (5 formations) have  $K_H$  values ranging from  $\approx 10^{-15}$  to  $10^{-10}$  m/s. Above the Ordovician sediments, the Silurian sediments have  $K_H$  values, which are on the order of  $<10^{-11}$  m/s. These values are presented in Table 5.1 and Section 5.2.2 herein and in Section 4.9 of the DGSM (INTERA 2011).
  - The Appalachian Basin has gas traps below the Marcellus black shale that reach more than 70% of the overburden stress. The Marcellus black shale is also overpressured throughout the northern Appalachian Basin, leaving no doubt about its effectiveness as a regional seal. In a similar manner, the underpressured nature of the Ordovician shales beneath the Bruce nuclear site, as described in Section 5.2.3, indicates that this sedimentary package represents a long-lived and stratigraphically controlled cap rock seal as discussed in Section 2.2.8.2 (Engelder 2011).
  - Other site-scale observations which provide further evidence for the long-term barrier integrity of the Ordovician shale cap rock include: sealed fractures filled with calcite, gypsum/anhydrite, and/or halite (e.g., Figure 2.33 and Sections 2.3.5 and 2.3.7), low formation hydraulic conductivities (Table 5.1 and Section 5.2.2.1), a low degree of thermal maturation (Section 2.2.5.3), which inhibited the pervasive development of natural hydraulic fractures and commercial hydrocarbon accumulations (Section 2.2.8.2), and compartmentalization of the minor hydrocarbon phases present (Section 2.3.6).
  - No seismically imaged faults are interpreted to have breached the top of the Upper Ordovician shale-dominated sedimentary package as discussed in Section 2.3.9.2 (Watts et al. 2009).
  - No geochemical evidence has been found for the infiltration of glacial or recent meteoric recharge water into the host or bounding formations. The stable water isotopes ( $^{18}\text{O}$  and  $^2\text{H}$ ) indicate that the maximum depth of glacial meltwater penetration

- is 328.5 mBGS (reference depth in DGR-1/2) within the Salina A1 carbonate aquifer (Section 4.4.1). Further, the results of numerical simulations – paleohydrogeology – provide insight into long-term groundwater system performance, and indicate: 1) that glacial perturbations do not alter the governing solute transport mechanisms within the deep groundwater system; and 2) that single and multiple glaciation scenarios, when modelled using regional and site specific parameters, do not result in the infiltration of glacial meltwater into the deep groundwater system (Sections 5.4.6.5 and 5.4.7.4).
- The Paleozoic succession beneath the Bruce nuclear site compares favourably with respect to the key physical parameters and geological attributes recognized internationally as necessary for a rock mass to successfully contain and isolate L&ILW for the long-term (Chapter 7 and Table 7.1 therein; Mazurek et al. 2008).
- **Contaminant Transport is Diffusion Dominated: deep groundwater regime is ancient showing no evidence of glacial perturbation or cross-formational flow**
    - Horizontal hydraulic conductivities ( $K_H$ ) within the Cobourg Formation (DGR host rock), the overlying Ordovician shales (Georgian Bay, Blue Mountain and Queenston formations, and the Collingwood Member of the Cobourg Formation), and underlying Ordovician limestones and dolostones (Sherman Fall, Kirkfield, Coboconk, Gull River, and Shadow Lake formations) are extremely low ( $\approx 10^{-15}$  to  $10^{-10}$  m/s). Vertical hydraulic conductivities ( $K_V$ ) within the same formations are lower. Such conditions are consistent with a diffusion dominated regime (Sections 5.2 and 5.4.1 and Figure 5.1).
    - The effective diffusion coefficient ( $D_e$ ) for HTO in the Ordovician shales is on the order of  $10^{-12}$  m<sup>2</sup>/s, and in the carbonates  $10^{-13}$  to  $10^{-12}$  m<sup>2</sup>/s (Table 4.3 and Figure 5.7).  $D_e$  values obtained with HTO are on average 1.9 times greater than  $D_e$  values obtained with an iodide tracer. This difference is attributed to the influence of anion exclusion in lowering the tracer-accessible porosity for iodide (Section 5.3.5). The low  $D_e$  values, coupled with the low hydraulic conductivities of the Ordovician sediments, indicate that solute migration is diffusion dominated in the deep groundwater system.
    - The occurrence of isotopically distinct types of methane and helium in separate zones (one zone in the Upper Ordovician shale and another zone in the Middle Ordovician carbonates) demonstrates that there has been little to no cross-formational mixing (advective or diffusive) while these gases were resident in the porewater (Section 4.4.3). The occurrence of radiogenic  $^{87}\text{Sr}/^{86}\text{Sr}$  ratios in the Middle and Upper Ordovician porewater are interpreted to result from a combination of water-rock interaction, in situ  $^{87}\text{Rb}$  decay, and diffusive transport upward from the shield (section 4.4.4). These mechanisms indicate extremely long residence times.
    - The chemistries of the deep brines indicate that they were formed by evaporation of seawater, which was subsequently modified by fluid-rock interaction processes (Section 4.3.3). The Cl/Br and Na/Cl ratios, as well as the stable water isotope data, suggest that the deep groundwater system contains evolved ancient sedimentary brines at, or near, halite saturation. The nature of the brines, in particular the high salinities and the enriched  $^{18}\text{O}$  values (enriched in  $^{18}\text{O}$  with respect to the GMWL) in the porewaters, indicate that the deep system is isolated from the shallow groundwater system and that the porewaters have resided in the system for a very long time.



- **Seismically Quiet: comparable to stable Canadian Shield setting**
  - The Bruce nuclear site is located within the tectonically stable interior of the North American continent, which is characterized by low rates of seismicity. No earthquake exceeding magnitude 5 has been observed in the regional monitoring area in 180 years of record. The maximum earthquake within the 150 km radius study area is an M4.3 event at 99 km from the site (15 km north of Meaford, Ontario) with a focal depth of about 11 km (Section 2.2.6.5). This is consistent with the seismic hazard information provided in the 2005 National Building Code of Canada (NBCC05) as discussed in Section 6.2.2.1.
  - A neotectonic remote-sensing and field-based study that analysed Quaternary landforms for the presence of seismically induced soft-sediment deformation concluded that the Bruce nuclear site has not likely experienced any post-glacial tectonic activity as discussed in Section 6.2.2.2 (Slattery 2011). No evidence has been found from detailed fracture mapping (Cruden 2011) or deep drilling (INTERA 2011) for the presence of structural features that would indicate a higher seismic hazard near the Bruce nuclear site than that estimated from the regional rate of earthquake occurrence.
  - The micro-seismic monitoring network installed and commissioned in August 2007 confirms the lack of low level seismicity ( $> M1.0$ ) within the vicinity of the Bruce nuclear site implying no seismogenic structures or faults within or in close proximity to the DGR footprint (Section 6.2.2.2).
  - Based on the results of a probabilistic seismic hazard assessment performed for the Bruce nuclear site, the far field/regional seismic sources are the dominant contributors to the hazard for the site at ground level. The estimated surface bedrock peak ground motions are 18.7 and 60.1%g for events of annual probabilities of  $10^{-5}$  and  $10^{-6}$ , respectively as discussed in Section 6.2.2.1 (AMEC GEOMATRIX 2011).
  - Seismic analysis of a DGR emplacement room using ground motions of  $10^{-5}$  and  $10^{-6}$  annual probability events reveals that seismic shaking would not induce damage to the host rock other than dislodging already fractured rock mass around the opening (Section 6.4.4.6).
- **Geomechanically Stable: selected DGR limestone formation will provide stable, virtually dry openings**
  - Precedent construction experience with the excavation of underground openings in the Ordovician sediments indicates that excavated openings in either the Ordovician shale or Ordovician limestone are likely to be dry and stable (Section 3.2.1.3).
  - The laboratory testing of the Cobourg Formation core rock samples reveals a high strength argillaceous limestone with an average UCS value of 113 MPa (Section 3.2.1.1). These rock strength conditions compare favourably with other sedimentary formations considered internationally for long-term radioactive waste management purposes (Table 7.1).

- No borehole breakouts were observed in the deep DGR boreholes (Section 3.3.2), which provides a constraint on the possible range of the in situ stress magnitudes. At the repository horizon, the range of stress ratios is estimated to be:  $\sigma_H/\sigma_V$  from 1.5 to 2.0;  $\sigma_h/\sigma_v$  from 1.0 to 1.2 (Table 3.12). Observed borehole deformation over timeframes up to 16 months strongly suggests that the orientation of maximum horizontal stress is similar to that of the Michigan Basin, a NE to ENE direction (Section 3.3.1).
- Numerical simulation of the lateral development considering varied long-term rock mass properties and loading scenarios (i.e., glacial ice sheet, seismic ground motions and repository gas pressure) illustrate that the barrier integrity of the enclosing Ordovician bedrock formations is unaffected (Section 6.4).
- A 3D numerical simulation that explored DGR shaft stability for a range of observed geomechanical formation properties under similar loading scenarios described above was undertaken. Due to the vertical geometry of the shaft, glacial loading has only a minor effect on differential ground stress in horizontal plane. Contrary to the repository, the effect of damage zone (HDZ and EDZ) along the shaft is minor. Similarly, pore pressure and seismic shaking will not significantly increase the predicted damage zone around the shaft. The maximum extent of the damage zone is generally, less than 1.1 times the shaft radius (Section 6.4).
- **Natural Resource Potential is Low: commercially viable oil and gas reserves are not present**
  - No commercial oil hydrocarbon accumulations were encountered during site characterization activities as discussed in Section 2.3.6 and in INTERA (2011). No structural, lithological, chemical or hydrological evidence suggests that the Bruce nuclear site is proximal to an ancient HTD system as discussed in Sections 2.2.8.2 and 2.3.9.2 and in INTERA (2011).
  - An average TOC content for the Upper Ordovician shales of less than 1.0% (Section 2.2.8.1; INTERA 2011), the recognition of low thermal maturity throughout the RSA which indicates that these sedimentary rocks only reached the lower threshold of the oil window as discussed in Section 2.2.5.3, and the absence of natural gas shows during drilling of the DGR boreholes (INTERA 2011) argues against the likelihood of commercial accumulations of either thermogenic or biogenic shale gas beneath the Bruce nuclear site (see also Engelder 2011).
  - Lateral traceability between the Bruce nuclear site boreholes and other proximal dry wells (e.g., Union Gas #1 and Texaco #6) as discussed in Section 2.3.9 and in Chapter 7, demonstrates that locally around the Bruce nuclear site (~7 km radius), no pockets of oil or gas hydrocarbon are likely to exist (INTERA 2011).
  - A transition from fresh to saline groundwater is recorded through the shallow and intermediate hydrogeological systems with saline groundwater dominating from ca. 180 m depth within the Silurian Salina F Unit (Section 4.4; INTERA 2011). A transition into more permeable rock occurs in the lower Ordovician and the underlying Cambrian sandstone (ca. 830 mBGS). The porewater at the repository depth (680 mBGS) is not potable (TDS > 200 g/L) and this extremely low permeability bedrock formation

(hydraulic conductivities  $<10^{-13}$  m/s) cannot yield groundwater. This combination of extremely high salinities and low hydraulic conductivities in the rock surrounding the proposed repository depth would discourage deep drilling for groundwater resources.

- Sphalerite (Lucas and Georgian Bay Formations), marcasite (Kirkfield Formation and Cambrian), and pyrite (entire Paleozoic interval) are present in trace amounts within the host rock and secondary vein infillings. These occurrences are not associated with any commercially exploitable base metal accumulation and are best described as minor gangue mineral occurrences (INTERA 2011). No commercial MVT base metal deposits have been found within the Huron domain, therefore the likelihood that the Bruce nuclear site, or its immediate surroundings, hosts an undiscovered base metal deposit is negligible (Section 2.2.8.3).
- The Salina salt has been removed beneath the Bruce nuclear site and does not represent a commercial resource as found occurring further to the south at Goderich.
- **Shallow Groundwater Resources are Isolated: near surface groundwater aquifers are isolated from the deep saline groundwater system**
  - Regionally, the hydrogeochemistry of the Michigan Basin defines two distinct groundwater regimes: i) a shallow bedrock system containing potable groundwater at depths above 200 m; and ii) an intermediate to deep saline system characterized by elevated TDS ( $> 200$  g/L) and distinct isotopic signatures.
  - Groundwater resources in the vicinity of the Bruce nuclear site are obtained from shallow overburden or bedrock wells extending to depths of ca. 100 m into the permeable Devonian carbonates. At increasing depth groundwater becomes brackish then saline and yields decrease which provides a passive marker that would prevent or discourage deep drilling for potable water.
  - Evidence of modern karst is observed to a depth of approximately 180 mBGS. Conditions necessary to generate karst connections to the shallow groundwater system do not exist within the intermediate to deep groundwater system (Section 2.3.8).
  - Groundwater modelling illustrates that the Guelph Formation is the upper boundary for vertical radionuclide transport from the repository, whether by advection or diffusion; water borne radionuclides would not reach the shallow groundwater system at the Bruce nuclear site even after millions of years (Section 5.4).
  - Observed abnormal hydraulic heads in the Ordovician and Cambrian rocks and high vertical hydraulic gradients strongly suggest that vertical connectivity across bedrock aquitards/aquicludes does not exist (Section 5.2).

Thus, given all the information summarized above that supports the key hypotheses, the geological setting at the Bruce nuclear site is suitable to support the development of a DGR for L&ILW in the Cobourg Formation.

## 9. REFERENCES

- Acres Bechtel Canada. 1993. Definition Engineering Phase 2, Geotechnical Investigations and Evaluation, Volume 1 – Investigation Report. OPG NAW130-P40-10120-0005-00.
- Adams, J. 1989. Postglacial faulting in eastern Canada: nature, origin and seismic hazard implications. *Tectonophysics* **163**, 323-331.
- Adams, J. and P.W. Basham. 1991. The seismicity and seismotectonics of eastern Canada. In: Slemmons, D.B. et al. (Eds.), *Neotectonics of North America*. Geological Society of America, Decade Map vol. 1, 261-275.
- AECOM and ITASCA CANADA. 2011. Regional Geology – Southern Ontario. AECOM Canada Ltd. and Itasca Consulting Canada, Inc. report for the Nuclear Waste Management Organization NWMO DGR-TR-2011-15 R000. Toronto, Canada.
- Al, T., Y. Xiang and L. Cavé. 2010a. Measurement of Diffusion Properties by X-Ray Radiography and by Through-Diffusion Techniques Using Iodide and Tritium Tracers: Core Samples from OS-1 and DGR-2. Intera Engineering Ltd. Report TR-07-17 Rev.3. University of New Brunswick, Fredericton, Canada.
- Al, T., Y. Xiang, D. Loomer and L. Cavé. 2010b. Measurement of Diffusion Properties by X-Ray Radiography and by Through-Diffusion Techniques Using Iodide and Tritium Tracers: Core Samples from DGR-3 and DGR-4. Intera Engineering Ltd. Report TR-08-27 Rev.0. University of New Brunswick, Fredericton, Canada.
- AMEC GEOMATRIX. 2011. Seismic Hazard Assessment. AMEC Geomatrix, Inc. report for the Nuclear Waste Management Organization NWMO DGR-TR-2011-20 R000. Toronto, Canada.
- Andersson, J., H. Ahokas, J.A. Hudson, L. Koskinen, A. Luukkonen, J. Löfman, V. Keto, P. Pitkänen, J. Mattila, A. Ikonen and M. Ylä-Mella. 2007. Olkiluoto Site Description 2006. POSIVA 2007-03. Posiva Oy, Finland.
- Andjelkovic, D., A.R. Cruden and D.K. Armstrong. 1996. Structural geology of Southcentral Ontario. Preliminary results of joint mapping studies. In: *Summary of Field Work and Other Activities 1996*, Ontario Geological Survey, Misc. Paper 166.
- Andjelkovic, D., A.R. Cruden and D.K. Armstrong. 1997. Joint orientation trajectories in South-Central Ontario. In: *Summary of Field Work and Other Activities 1997*, Ontario Geological Survey, Misc. Paper 168.
- Andjelkovic, D. and A.R. Cruden. 1998. Relationships between fractures in Paleozoic cover rocks and structures in the Pre-Cambrian basement, south central Ontario. In: *Summary of Field Work and Other Activities 1998*, Ontario Geological Survey, Misc. Paper 169.
- ANDRA. 2005. Dossier 2005 Argile. Synthesis: Evaluation of the Feasibility of a Geological Repository in an Argillaceous Formation, Meuse/Haute Marne Site. Paris, France.
- Armstrong, D.K. 1993. Paleozoic Geology of the Central Bruce Peninsula. Ontario Geological Survey, Open File Report 5856.

- Armstrong, D.K. and T.R. Carter. 2006. An Updated Guide to the Subsurface Paleozoic Stratigraphy of Southern Ontario. Ontario Geological Survey, Open File Report 6191.
- Armstrong, D.K. and T.R. Carter. 2010. The Subsurface Paleozoic Stratigraphy of Southern Ontario. Ontario Geological Survey, Special Volume 7.
- Armstrong, D.K. and J.E.P. Dodge. 2007. Paleozoic geology of southern Ontario. Ontario Geological Survey, Miscellaneous Release-Data 219.
- Armstrong, D.K. and W.R. Goodman. 1990. Stratigraphy and depositional environments of Niagaran carbonates, Bruce Peninsula, Ontario. Field Trip No. 4 Guidebook. American Association of Petroleum Geologists, 1990 Eastern Section Meeting, hosted by the Ontario Petroleum Institute. London, Ontario.
- Armstrong, D.K. and J.K. Meadows. 1998. Stratigraphy and resource potential of the Eramosa Member (Amabel Formation), Bruce Peninsula, Ontario, Ministry of Northern Development and Mines. Toronto, Ontario.
- Arnold, N. and M. Sharp. 2002. Flow variability in the Scandinavian ice sheet: modelling the coupling between ice sheet flow and hydrology. *Quaternary Science Reviews* 21, 485-502.
- Atkinson, G.M. and N. Kraeva. 2010. Ground motions underground compared to those on the surface: a case study from Sudbury, Ontario. *Bulletin of the Seismological Society of America* 100(3), 1293-1305.
- Atwater, B.F. 1986. Pleistocene glacial-lake deposits of the Sanpoil River valley, northeastern Washington. *U.S. Geological Survey Bulletin* 1661.
- Backblöm, G. and R. Munier. 2002. Effects of Earthquakes on the Deep Repository for Spent Fuel in Sweden Based on Case Studies and Preliminary Model Results. SKB Technical Report TR-02-24. SKB Stockholm.
- Bahr, J.M., G.R. Moline and G.C. Nadon. 1994. Anomalous pressures in the deep Michigan Basin. In: P. Ortoleva (Ed.), *Basin Compartments and Seals*. AAPG Memoir 61, 153-165.
- Bailey Geological Services Ltd. and R.O. Cochrane. 1984a. Evaluation of the conventional and potential oil and gas reserves of the Cambrian of Ontario. Ontario Geological Survey, Open File Report 5499.
- Bailey Geological Services Ltd. and R.O. Cochrane. 1984b. Evaluation of the conventional and potential oil and gas reserves of the Ordovician of Ontario. Ontario Geological Survey, Open File Report 5498.
- Bailey, S.M.B. 2005. A Comparison of Cambrian Reservoir Rocks Onlapping the S.E. and N.W. Sides of the Algonquin Arch in SW Ontario: A Regional Correlation Project. Proceedings 44<sup>th</sup> Annual Ontario Petroleum Institute Conference, Technical Paper 5. London, Canada.
- Baird, A. and S.D. McKinnon. 2007. Linking stress field deflection to basement structures in southern Ontario: results from numerical modelling. *Tectonophysics* 432, 89-100.

- Baker, V.R. 1973. Paleohydrology and sedimentology of Lake Missoula flooding in Eastern Washington. Geological Society of America Special Paper 144.
- Barker, J.F. and S.J. Pollock. 1984. The Geochemistry and Origin of Natural Gases in Southern Ontario. Bulletin of Canadian Petroleum Geology 32, 313-326.
- Barnes, D.A., T.M. Parris and G.M. Grammer. 2008. Hydrothermal Dolomitization of Fluid Reservoirs in the Michigan Basin, USA. AAPG Search and Discovery Article #50087. AAPG Annual Convention, April 20-23. San Antonio, Texas, USA.
- Barnett, R.L., M. Arima, J.D. Blackwell, C.G. Winder, H.C. Palmer and A. Hayatsu. 1984. The Picton and Varty Lake ultramafic dikes: Jurassic magmatism in the St. Lawrence Platform near Belleville, Ontario. Canadian Journal of Earth Sciences 21, 1460-1472.
- Barnett, P.J. 1992. Quaternary geology of Ontario. In: Geology of Ontario, Ontario Geological Survey, Special Volume 4, Part 2, 1008-1088.
- Bauer, C., J.P. Piguet and Y. Wileveau. 2003. Disturbance Assessment at the Wall of a Vertical Blasted Shaft in Marls. ISRM 2003 – Technology Roadmap for Rock Mechanics, South African Institute of Mining and Metallurgy.
- Bauer, S.J., D.E. Munson, M.P. Hardy, J. Barrix and B. McGunegle. 2005. In Situ Stress Measurements and Their Implications in a Deep Ohio Mine. ARMA/USRMS 05.
- Bear, J. 1988. Dynamics of Fluids in Porous Media. Dover Publications Inc., New York, USA.
- Beauheim, R.L. and W.H. Pedler. 2009. Fluid Electrical Conductivity Logging in Borehole DGR-1. Intera Engineering Ltd. Report TR-07-14 Rev.2. Ottawa, Canada.
- Beauheim, R.L., R.M. Roberts, T.F. Dale, M.D. Fort and W.A. Stensrud. 1993. Hydraulic Testing of Salado Formation Evaporites at the Waste Isolation Pilot Plant Site: Second Interpretive Report. Sandia National Laboratories Technical Report SAND92-0533. Albuquerque, New Mexico, USA.
- Beaumont, C., G. Quinlan and J. Hamilton. 1988. Orogeny and stratigraphy: numerical models of the Paleozoic in the Eastern Interior of North America. Tectonics 7, 389-416.
- Beland-Otis, C. 2010. Shale Gas Assessment in Southern Ontario. GeoCanada 2010, Calgary, Alberta, Abstract with Programs.
- Bell, M. and E. Laine. 1985. Erosion of the Laurentide Region of North America by Glacial and Glacio-fluvial Processes. Quaternary Research 23, 154-174.
- Bense, V. and M. Person. 2008. Transient hydrodynamics within intercratonic sedimentary basins during glacial cycles. Journal of Geophysical Research 113, 1-17.
- Bethke, C.M. and S. Marshak. 1990. Brine migrations across North America: the plate tectonics of groundwater. Annual Review of Earth and Planetary Sciences 18, 287-315.
- Bieniawski, Z.T. 1976. Rock mass classification in rock engineering. In: Exploration for Rock Engineering, A.A. Balkema, Cape Town, 97-106.

- Blümling, P., F. Bernier, P. Lebon and C.D. Martin. 2007. The excavation damaged zone in clay formations time-dependent behaviour and influence on performance assessment. *Physics and Chemistry of the Earth* 32(8-14), 588-599.
- Bock, H. 2001. RA experiment, Rock mechanics analyses and synthesis: data report on rock mechanics. Mont Terri Technical Report TR 2000-02.
- Bock, H., B. Dehandschutter, C.D. Martin, M. Mazurek, A. de Haller, F. Skoczylas and C. Davy. 2010. Self-sealing of fractures in argillaceous formations in context with the geological disposal of radioactive waste review and synthesis. OECD, NEA No. 6184, OECD Nuclear Energy Agency, Paris, France.
- Bottomley, D.J. and I.D. Clark. 2004. Potassium and boron co-depletion in Canadian Shield brines: evidence for diagenetic interactions between marine brines and basin sediments. *Chemical Geology* 203, 225–236.
- Bottomley, D.J., I.D. Clark, N. Battye and T. Kotzer. 2005. Geochemical and isotopic evidence for a genetic link between Canadian Shield brines, dolomitization in the Western Canada Sedimentary Basin, and Devonian calcium-chloridic seawater. *Canadian Journal of Earth Sciences* 42, 2059–2071.
- Bottomley, D.J., L.H. Chan, A. Katz, A. Starinsky and I.D. Clark. 2003. Lithium Isotope Geochemistry and Origin of Canadian Shield Brines. *Ground Water* 41(6), 847-856.
- Bottomley, D.J., A. Katz, L.H. Chan, A. Starinsky, M. Douglas, I.D. Clark and K.G. Raven. 1999. The origin and evolution of Canadian Shield brines: evaporation or freezing of seawater? New lithium isotope and geochemical evidence from the Slave craton. *Chemical Geology* 155, 295–320.
- Boulton, G.S., P.E. Caban, and K. van Gijssel. 1995. Groundwater flow beneath ice sheets: Part I – Large scale patterns. *Quaternary Science Reviews* 14(6), 545–562.
- Boyce, J.J. and W.A. Morris. 2002. Basement-controlled faulting of Paleozoic strata in southern Ontario, Canada. New evidence from geophysical lineament mapping. *Tectonophysics* 353, 151-171.
- Brace, W.F., B.W. Paulding Jr. and C. Scholz. 1966. Dilatancy in the Fracture of Crystalline Rocks, *Journal of Geophysical Research* 71(16), 3939–3953.
- Bredehoeft, J.D., C.R. Blyth, W.A. White and G.B. Maxey. 1963. Possible mechanism for concentration of brines in subsurface formations. *Bulletin of the American Association of Petroleum Geologists* 47, 257-269.
- Brett, C.E., D.H. Tepper, W.M. Goodman, S.T. LoDuca and B.-Y. Eckert. 1995. Revised Stratigraphy and Correlations of the Niagaran Provincial Series (Medina, Clinton, and Lockport Groups) in the Type Area of Western New York. United States Geological Survey, Bulletin 2086.
- Brigham, R.J. 1971. Structural geology of southwestern Ontario and southeastern Michigan. Ontario Department of Mines and Northern Affairs Paper 71-2.

- Briscoe, G. 2009. Drilling and Logging of US-8. Intera Engineering Ltd. Report TR-07-19 Rev.0. Ottawa, Canada.
- Briscoe, G., A. Wigston and M. Melaney. 2010a. Drilling, Logging and Sampling of DGR-3 and DGR-4. Intera Engineering Report TR-08-13 Rev.1. Ottawa, Canada.
- Briscoe, G., S. Gaines and M. Melaney. 2010b. Drilling, Logging and Sampling of DGR-5 and DGR-6. Intera Engineering Report TR-09-01 Rev.1. Ottawa, Canada.
- Brogly, P.J. 1990. The Depositional Environments of the Queenston Formation (Upper Ordovician) in Southern Ontario. M.Sc. Thesis, University of Guelph. Guelph, Ontario.
- Brogly, P.J., I.P. Martini and G.V. Middleton. 1998. The Queenston Formation: shale-dominated, mixed terrigenous carbonate deposits of Upper Ordovician, semiarid, muddy shores in Ontario, Canada. *Canadian Journal of Earth Sciences* 35, 702-719.
- Brookfield, M.E. and C.E. Brett. 1988. Paleoenvironments of the Mid-Ordovician (Upper Caradocian) Trenton limestones of southern Ontario, Canada: storm sedimentation on a shoal-basin shelf model. *Sedimentary Geology* 57, 75-105.
- Brunton, F.R. and J.E.P. Dodge. 2008. Karst of southern Ontario and Manitoulin Island. Ontario Geological Survey, Groundwater Resources Study 5.
- BSC. 2004. Development of Earthquake Ground Motion Input for Preclosure Seismic Design and Postclosure Performance Assessment of a Geologic Repository at Yucca Mountain, NV, Yucca Mountain Project Report MDL-MGR-GS-000003 REV 01. Bechtel SAIC Company, Las Vegas, Nevada.
- Budai, J.M. and J.L. Wilson. 1991. Diagenetic history of the Trenton and Black River Formations in the Michigan Basin. *Geological Society of America Special Paper* 256, 73-88.
- Carr, S.D., R.M. Easton, R.A. Jamieson and N.G. Culshaw. 2000. Geologic transect across the Grenville orogen of Ontario and New York. *Canadian Journal of Earth Sciences* 37(2-3), 193-216.
- Carter T.R., R.A. Treveil and R.M. Easton. 1996. Basement controls on some hydrocarbon traps in southern Ontario, Canada. In: B.A. van der Pluijm and P.A. Catacosinos (eds.), *Basement and Basins of Eastern North America*. Geological Society of America Special Paper 308, 95-107.
- Carter, T.R. (Ed.). 1990. *Subsurface Geology of Southwestern Ontario; a Core Workshop*, America Association of Petroleum Geologists, 1990 Eastern Section Meeting. Ontario Petroleum Institute, London, Ontario.
- Carter, T.R. and R.M. Easton. 1990. Extension of Grenville basement beneath southwestern Ontario: lithology and tectonic subdivisions. In: Carter, T.R. (ed.), *Subsurface Geology of Southwestern, a Core Workshop*, America Association of Petroleum Geologists, 1990 Eastern Section Meeting. Ontario Petroleum Institute, London, Ontario.
- Cartwright, J. 2007. The impact of 3D seismic data on the understanding of compaction, fluid flow and diagenesis in sedimentary basins. *Journal of the Geological Society of London* 164(5), 881-893.



- Cavé, L., T. Al, Y. Xiang and D. Loomer. 2010. Investigations of Diffusive Transport Processes in Sedimentary Rock. Nuclear Waste Management Organization Report NWMO TR-2010-04. Toronto, Canada.
- Cercone, K.R. 1984. Thermal history of Michigan basin; American Association of Petroleum Geologists Bulletin 68, 130-136.
- Cercone, K.R. and H.N. Pollack. 1991. Thermal maturity of the Michigan Basin. Geological Society of America, Special Paper 256, 1-11.
- Chacko, T. and P. Deines. 2008. Theoretical calculation of oxygen isotope fractionation factors in carbonate systems. *Geochimica et Cosmochimica Acta* 72, 3642–3660.
- Chapman, L.J. and D.F. Putnam. 1984. The Physiography of Southern Ontario. Ontario Geological Survey, Special Volume 2.
- Chemical Rubber Company (CRC). 1983. CRC Handbook of Chemistry and Physics. Weast, R.C. (Ed.). Eighteenth Edition. CRC Press, Inc., Boca Raton, Florida, USA.
- Choi, J.W. and D.W. Oscarson. 1996. Diffusive transport through compacted Na- and Ca-bentonite. *Journal of Contaminant Hydrology* 22, 189-202.
- Clark, I.D. and P. Fritz. 1997. Environmental Isotopes in Hydrogeology. Lewis Publishers, Boca Raton, Florida, USA.
- Clark, I., R. Mohapatra, H. Mohammadzadeh and T. Kotzer. 2010a. Pore Water and Gas Analyses in DGR-1 and DGR-2 Core. Intera Engineering Ltd. Report TR-07-21 Rev.1. Ottawa, Canada.
- Clark, I., I. Liu, H. Mohammadzadeh, P. Zhang, R. Mohapatra and M. Wilk. 2010b. Pore Water and Gas Analyses in DGR-3 and DGR-4 Core. Intera Engineering Ltd. Report TR-08-19 Rev.0. Ottawa, Canada.
- Clark, I., R. Jackson, I. Liu and D. Heagle. 2010c. Vacuum Distillation Experiments on DGR Core. Intera Engineering Ltd. Report TR-08-37 Rev.0. Ottawa, Canada.
- Clark, I., and M. Herod. 2011. Radioisotopes in DGR Groundwater and Porewater. Intera Engineering Ltd. Report TR-08-38 Rev.0. Ottawa, Canada.
- Clark, I., V. Scharf, J. Zuliani and M. Herod. 2011. Technical Report: Pore Water Analysis in DGR-5 and DGR-6 Core, TR-09-04, Revision 0, University of Ottawa, Ottawa, Canada.
- Clarke, G.K. 2005. Subglacial processes. *Annual Review of Earth and Planetary Sciences* 33, 247–276.
- Coakley, B. and M. Gurnis. 1995. Far field tilting of Laurentia during the Ordovician and constraints on the evolution of a slab under an ancient continent, *Journal of Geophysical Research* 100, 6313-6327.
- Coakley, B.J., G.C. Nadon, and H.F. Wang. 1994. Spatial variations in tectonic subsidence during Tippecanoe I in the Michigan Basin. *Basin Research* 6, 131-140.
- Colgan, P.M., P.R. Bierman, D.M. Mickelson and M. Caffee. 2002. Variation in glacial erosion near the southern margin of the Laurentide Ice Sheet, south-central Wisconsin, USA.

- Implications for cosmogenic dating of glacial terrains. *Bulletin of the Geological Society of America* 114, 1581-1591.
- Colquhoun, I. 2004. Middle Ordovician Trenton-Black River Group carbonate play, Ontario Oil & Gas Journal, 15-19.
- Colquhoun, I. and H.P. Johnston. 2004. A Comprehensive Evaluation of the Dover 7-5-VE Trenton-Black River Field, Ontario Petroleum Institute 43, Technical Paper. London, Canada.
- Coniglio, M., M.J. Melchin and M.E. Brookfield. 1990. Stratigraphy, sedimentology and biostratigraphy of Ordovician rocks of the Peterborough–Lake Simcoe area of southern Ontario; American Association of Petroleum Geologists, 1990 Eastern Section Meeting, hosted by Ontario Petroleum Institute, Field Trip Guidebook no.3. London, Canada.
- Coniglio M. and A.E. William-Jones. 1992. Diagenesis of Ordovician carbonates from the north-east Michigan Basin, Manitoulin Island area, Ontario: Evidence from petrography, stable isotopes and fluid inclusions. *Sedimentology* 39, 813-836.
- Coniglio, M., R. Sherlock, A.E. Williams-Jones, K. Middleton and S.K. Frape. 1994. Burial and hydrothermal diagenesis of Ordovician carbonates from the Michigan Basin, Ontario, Canada. In: Purser, B., M. Tucker and D. Zenger (Eds.), *Dolomites – A volume in honour of Dolomieu*, International Association of Sedimentologists, Special Publication 21, 231-254.
- Coniglio M., Q. Zheng and T.R. Carter. 2003. Dolomitization and recrystallization of middle Silurian reefs and platformal carbonates of the Guelph Formation, Michigan Basin, southwestern Ontario. *Bulletin of Canadian Petroleum Geology* 51, 177-199.
- Coordinating Committee on Great Lakes Basic Hydraulic and Hydrologic Data (CCGLBHHD). 1977. Coordinated Great Lakes physical data Physical Data Subcommittee, Coordinating committee on Great Lakes Basic Hydraulic and Hydrologic Data, U.S. Army Corps of Engineers. Detroit District, Detroit, Michigan.
- Crough, S. 1981. Mesozoic hotspot epeirogeny in eastern North America, *Geology* 9, 2-6.
- Cruden, A. 2011. Outcrop Fracture Mapping. Nuclear Waste Management Organization Report NWMO DGR-TR-2011-43 R000. Toronto, Canada.
- Csontos, L., G. Tari, F. Bergerat and L. Fodor. 1991. Evolution of the stress-fields in the Carpatho-Pannonian area during the Neogene. *Tectonophysics* 199, 73-91.
- Culotta, R.C., T. Pratt and J. Oliver. 1990. A tale of 2 sutures- COCORPS deep seismic surveys of the Grenville Province in the eastern United States mid-continent. *Geology* 18, 646-649.
- Curtis, J.B., D.G. Hill and P.G. Lillis. 2009. Shale Gas from onerous stepchild to premier resource. Research partnership to secure energy for America (RPSEA), Mid-continent gas shale forum. RPSEA Mid-Continent Gas Shales Forum, June 4, 2009. Chicago, Illinois, USA.
- Damjanac, B., M. Board, M. Lin, D. Kicker and J. Leem. 2007. Mechanical degradation of emplacement drifts at Yucca Mountain — A Modelling Case Study: Part II.

- Lithophysical Rock, *International Journal of Rock Mechanics and Mining Sciences* 44, 368-399.
- Damjanac, B. 2008. *Analyses of Long-Term Cavern Stability*, Itasca Consulting Group, Inc. Report for Ontario Power Generation OPG 00216-REP-01300-00005-R00. Toronto, Canada.
- Damjanac, B. and C. Fairhurst. 2010. Evidence for a long-term strength threshold in crystalline rock. *Rock Mechanics and Rock Engineering* 43(5), 513-531.
- Davies, G.R. and L.B. Smith Jr. 2006. Structurally controlled hydrothermal dolomite reservoir facies: An overview. *AAPG Bulletin* 90(11), 1641–1690.
- Deere, D.U., A.J. Hendron Jr., F.D. Patton and E.J. Cording. 1967. Design of Surface and Near Surface Construction in Rock. In *Failure and Breakage of Rock*. C. Fairhurst, (Ed.) Society of Mining Engineers of AIME, New York, 237-302.
- Delay, J., A. Vinsot, J.M. Krieguer, H. Rebours and G. Armand. 2007. Making of the underground scientific experimental programme at the Meuse/Haute-Marne underground research laboratory, North Eastern France. *Physics and Chemistry of the Earth* 32(1-7), 2-18.
- Delay, J., P. Lebon and H. Rebours. 2010. Meuse/Haute-Marne centre: next steps towards a deep disposal facility. *Journal of Rock Mechanics and Geotechnical Engineering* 2(1), 52–70.
- Derry Michener Booth and Wahl and Ontario Geological Survey. 1989. *Limestone Industries of Ontario, Volume III – Limestone Industries and Resources of Central and Southwestern Ontario*; Ontario Ministry of Natural Resources, Land Management Branch.
- Desayi, P. and C.S. Viswanatha. 1967. True ultimate strength of plain concrete. *Bulletin Rilem* 36, 163-173.
- Dineva, S., D. Eaton and R. Mereu. 2004. Seismicity of the southern Great Lakes: revised earthquake hypocenters and possible tectonic controls. *Bulletin of the Seismological Society of America* 94, 1902-1918.
- Di Prisco, G. and J.S Springer. 1991. The Precambrian-Paleozoic unconformity and related mineralization in southeastern Ontario. Ontario Geological Survey, Open File Report 5751.
- Dickinson, W.R., G.E. Gehrels and J.E. Marzolf. 2010. Detrital zircons from fluvial Jurassic strata of the Michigan basin: Implications for the transcontinental Jurassic paleoriver hypothesis. *Geology* 38, 499-502.
- Diederichs, M.S. 2003. Rock fracture and collapse under low confinement conditions. *Rock Mechanics and Rock Engineering* 36(5), 339-381.
- Diederichs, M.S. 2007. The 2003 Canadian Geotechnical Colloquium. Mechanistic Interpretation and Practical Application of Damage and Spalling Prediction Criteria for Deep Tunneling. *Canadian Geotechnical Journal* 44, 1082-1116.

- Diraison, M., P.R. Cobbold, D. Gapais and E.A. Rossello. 1997. Magellan Strait: part of a Neogene rift system. *Geology* 25, 703–706.
- Dollar P.S., S.K. Frappe and R.H. McNutt. 1991. Geochemistry of Formation Waters, Southwestern Ontario, Canada and Southern Michigan U.S.A.: Implications for Origin and Evolution. Ontario Geoscience Research Grant Program, Grant No. 249. Ontario Geological Survey, Open File Report 5743.
- Dollar, P.S. 1988. Geochemistry of Formation Waters, Southwestern Ontario, Canada and Southern Michigan, U.S.A.: Implications for origin and evolution. M.Sc. Thesis. University of Waterloo. Waterloo, Canada.
- Douglas, M., I. D. Clark, K. Raven and D. Bottomley. 2000. Groundwater mixing dynamics at a Canadian Shield mine. *Journal of Hydrology* 235, 88–103.
- Drever, J.I., J.R. Lawrence and R.C. Antweiler. 1979. Gypsum and halite from the Mid-Atlantic Ridge, DSDP Site 395. *Earth and Planetary Science Letters* 42, 98-102.
- Duan, Z. and S. Mao. 2006. A thermodynamic model for calculating methane solubility, density and gas phase composition of methane-bearing aqueous fluids from 273 to 523 K and from 1 to 2000 bar. *Geochimica et Cosmochimica Acta* 70, 3369–3386.
- Dyke, A.S., A. Moore and L. Robertson. 2003. Deglaciation of North America. Geological Survey of Canada, Calgary, Canada.
- Easton, R.M. 1992. The Grenville Province and the Proterozoic history of central and southern Ontario. In: *The Geology of Ontario*, Ontario Geological Survey, Special Volume 4, Part 2, 714-904.
- Easton, R.M. and T.R. Carter. 1995. Geology of the Precambrian basement beneath the Paleozoic of southwestern Ontario. In: Ojakangas, R.W., A.B. Dickas and J.C. Green (Eds.), *Basement Tectonics* 10, Kluwer Academic Publishers, The Netherlands, 221-264.
- Easton, R.M. 2008. E-mail to B. Semec, 2008 OPG Core workshop, DGR-01330-P.
- Electric Power Research Institute (EPRI). 1994. Identification of Seismic Hazards and Considerations for Determining Seismic Design Parameters for a High-level Nuclear Waste Repository, EPRI TR-104233.
- Elverhøi, A., E.S. Andersen, T. Dokken, D. Hebbeln, R. Spielhagen, J.-I. Svendsen, M. Sørflaten, A. Rørnes, M. Hald and C.F. Forsberg. 1995. The growth and decay of the Late Weichselian ice sheet in western Svalbard and adjacent areas based on provenance studies of marine sediments. *Quaternary Research* 44, 303-316.
- Engelder, T. 1990. Smoluchowski's dilemma revisited: A note on the fluid-pressure history of the Central Appalachian Fold-Thrust Belt. In Norton, D. and J.D. Bredehoeft (Eds.), *Studies in Geophysics; The Role of Fluids in Crustal Processes*. National Academy of Science, Washington, D.C., p.140-147.
- Engelder, T. 2011. Analogue Study of Shale Cap Rock Barrier Integrity. Nuclear Waste Management Organization Report NWMO DGR-TR-2011-23 R000. Toronto, Canada.

- Engelder, T. 1982. Is There a Genetic Relationship Between Selected Regional Joints and Contemporary Stress Within the Lithosphere of North America? *Tectonics* 1(2), 161-177.
- Engelder, T. and A. Whitaker. 2006. Early jointing in coal and black shale; evidence for an Appalachian-wide stress field as a prelude to the Alleghanian Orogeny. *Geology* 34, 581-584.
- Engelder, T. and P. Geiser. 1980. On the use of regional joint sets as trajectories of paleostress fields during the development of the Appalachian plateau, New York. *Journal of Geophysical Research* 85(B11), 6319-6341.
- Esterhuizen, G.S., D.R. Dolinar and J.L. Ellenberger. 2008. Assessment of Stable and Failed Pillars in Underground Limestone Mines. *Minerals Engineering* 61(11), 43-48.
- Evans, K. and T. Engelder. 1989. Some problems in estimating horizontal stress magnitudes in "thrust" regimes. *International Journal of Rock Mechanics and Mining Sciences* 26(6), 647-660.
- Fakundiny, R.H. and J.T. Myers. 1978. Structural instability features in the vicinity of the Clarendon-Linden fault system western New York and Lake Ontario. In: *Advances in Analysis of Geotechnical Instabilities*. University Of Waterloo Press, SM Study No. 13, Paper 4, 121-171.
- Farquhar, R.M., S.J. Haynes, M.A. Mostaghel, A.G. Tworo, R.W. MacQueen and I.R. Fletcher. 1987. Lead isotope ratios in Niagara Escarpment rocks and galena: implications for primary and secondary sulphide deposition. *Canadian Journal of Earth Sciences* 24, 1625-1633.
- Fountain, A.G. and J.S. Walder. 1998. Water flow through temperate glaciers. *Reviews of Geophysics* 36(3), 299-328.
- FRACTURE SYSTEMS. 2011. Excavation Damaged Zones Assessment. Fracture Systems Ltd. report for the Nuclear Waste Management Organization NWMO DGR-TR-2011-21 R000. Toronto, Canada.
- Frape S.K., P. Fritz and R.H. McNutt. 1984. The role of water-rock interaction in the chemical evolution of groundwaters from the Canadian Shield. *Geochimica et Cosmochimica Acta* 48, 1617-1627.
- Frape, S.K. and P. Fritz. 1987. Geochemical trends for groundwaters from the Canadian Shield. In: Fritz, P. and S.K. Frape (Eds.). *Saline Water and Gases in Crystalline Rocks*. Geological Association of Canada Special Paper 33, 211-233.
- Fritz, P. and S.K. Frape. 1982. Saline groundwaters in the Canadian Shield – A first overview. *Chemical Geology* 36, 179-190.
- Gaines, S. and S. Sterling. 2009a. Bedrock Field Geomechanical Testing of DGR-1 and DGR-2 Core. Intera Engineering Ltd. Report TR-07-07 Rev.1. Ottawa, Canada.
- Gaines, S. and S. Sterling. 2009b. Field Geomechanical Testing of DGR-3 and DGR-4 Core. Intera Engineering Ltd. Report TR-08-14 Rev.0. Ottawa, Canada.

- Gaines, S. and S. Sterling. 2010. Bedrock Formations in DGR-1 to DGR-6. Intera Engineering Ltd. Report TR-09-11 Rev.1. Ottawa, Canada.
- Gaines, S., K.G. Raven and M. Melaney. 2011. Oriented Core Logging of DGR-5 and DGR-6 Core. Intera Engineering Ltd. Report TR-09-09 Rev.0. Ottawa, Canada.
- Gao, C., J. Shirota, R.I. Kelly, F.R. Brunton and S. van Haaften. 2006. Project Unit 05-013; bedrock topography and overburden thickness mapping, southern Ontario. Open File Report, Ontario Geological Survey Report 6192, 1-34.
- Gartner Lee Limited. 1996. Regional Geologic Model: Smithville Phase IV. Prepared for Smithville Phase IV Bedrock Remediation Program. GLL 95-160.
- Gascoyne, M. 2004. Hydrogeochemistry, groundwater ages and sources of salts in a granitic batholith on the Canadian Shield, southeastern Manitoba. Applied Geochemistry 19, 519–560.
- Geomatrix Consultants, Inc. 1997. Seismic Hazard in Southern Ontario, Final Report, Part 1 & 2. Prepared for the Atomic Energy Control Board of Canada.
- GEOFIRMA and QUINTESSA. 2011. Postclosure Safety Assessment: Gas Modelling. Geofirma Engineering Ltd. and Quintessa Ltd. report for the Nuclear Waste Management Organization NWMO DGR-TR-2011-31 R000. Toronto, Canada.
- GOLDER. 2003. LLW Geotechnical Feasibility Study, Western Waste Management Facility, Bruce Site, Tiverton, Ontario. Report to Municipality of Kincardine and Ontario Power Generation. Golder Associates Ltd, Technical Report 021-1570.
- GOLDER. 2005. Hydrocarbon Resource Assessment of the Trenton-Black River Hydrothermal Dolomite Play in Ontario; Ontario Oil, Gas and Salt Resources Library. Mississauga, Canada.
- Goldthwait, J.W. 1907. Abandoned shorelines of eastern Wisconsin. Wisconsin Geological and Natural History Survey, Bulletin 17.
- Goldthwait, R.P. and H.B. Willman. 1973. The Wisconsinan Stage: Geological Society of America Memoir 136, 71-106.
- Gordon, R.G., and D.M. Jurdy. 1986. Cenozoic Global Plate Motions, Journal of Geophysical Research 91, 12,389–12,406.
- Gorski, B., T. Anderson and B. Conlon. 2009a. Laboratory Geomechanical Strength Testing of DGR-1 & DGR-2 Core. Intera Engineering Ltd. Document TM-07-03 Rev.1. CANMET Mining and Mineral Sciences Laboratories, Natural Resources Canada. Ottawa, Canada.
- Gorski, B., T. Anderson and B. Conlon. 2009b. DGR-2 Long-Term Strength Degradation Tests, Bruce DGR Project - Task GM5. Intera Engineering Ltd. Document TM-08-11R01. CANMET Mining and Mineral Sciences Laboratories, Natural Resources Canada. Ottawa, Canada.

- Gorski, B., T. Anderson and B. Conlon. 2010a. Long-Term Strength Degredation Testing of DGR-3 & DGR-4 Core. Intera Engineering Ltd. Report TR-08-36 Rev.1. CANMET Mining and Mineral Sciences Laboratories, Ottawa, Canada.
- Gorski, B., T. Anderson and B. Conlon. 2010b. Laboratory Geomechanical Strength Testing of DGR-2 to DGR-6 Core. Intera Engineering Ltd. Report TR-09-07 Rev.0. CANMET Mining and Mineral Sciences Laboratories, Ottawa, Canada.
- Gorski, B., T. Anderson and B. Conlon. 2010c. Supplementary Uniaxial Compressive Strength Testing of DGR-3 and DGR-4 Core. Intera Engineering Ltd. Report TR-08-39 Rev.1. Ottawa, Canada.
- Gradstein, F.M., J.G. Ogg and A.G. Smith (Eds.). 2004. A Geologic Time Scale. Cambridge University Press, p.188-201.
- Graf, D.L., I. Friedman and W. Meents. 1965. The origin of saline formation waters, II: isotopic fractionation by shale micropore systems. Illinois State Geological Survey. Circular 393.
- Greene, S., N. Battye, I. Clark, T. Kotzer and D. Bottomley. 2008. Canadian Shield brine from the Con Mine, Yellowknife, NT, Canada: Noble gas evidence for an evaporated Palaeozoic seawater origin mixed with glacial meltwater and Holocene recharge. *Geochimica et Cosmochimica Acta* 72, 4008–4019.
- Gross, M.R. and T. Engelder. 1991. A case for Neotectonic joints along the Niagara escarpment. *Tectonics* 10(3), 631-641.
- Gross, M.R., T. Engelder and S.R. Poulson. 1992. Veins in the Lockport dolostone: evidence for an Acadian fluid circulation system. *Geology* 20, 971-974.
- Hallet, B. 2011. Glacial Erosion Assessment. Nuclear Waste Management Organization Report NWMO DGR-TR-2011-18 R000. Toronto, Canada.
- Hamblin, A. 1999. Upper Ordovician strata of southwestern Ontario: Synthesis of literature and concepts. Geological Survey of Canada, Open File 3729.
- Hamblin, A. 2003. Detailed outcrop and core measured sections of the Upper Ordovician/Lower Silurian succession of southern Ontario. Geological Survey of Canada, Open File 1525.
- Hamblin, A. 2006. The “Shale Gas” concept in Canada. a preliminary inventory of possibilities. Geological Survey of Canada, Open File 5384.
- Hamblin, A. 2008. Hydrocarbon potential of the Paleozoic succession of southwestern Ontario. Preliminary conceptual synthesis of background data. Geological Survey of Canada, Open File 5730.
- Hamilton, G.D. 1991. Styles of reservoir development in Middle Devonian Carbonates of Southwestern Ontario. In: Coniglio, M. and Frape, S. K. (Eds.), 1992. Ontario Geological Survey, Open File Report 5822.
- Hancock, P.L. 1985. Brittle microtectonics. Principles and practice. *Journal of Structural Geology* 7, 437-457.

- Hancock, P.L. and T. Engelder. 1989. Neotectonic joints. *Geological Society of America Bulletin* 101, 1197-1208.
- Hanmer, S. and S.J. McEachern. 1992. Kinematical and rheological evolution of a crustal-scale ductile thrust zone, Central Metasedimentary Belt, Grenville Orogen, Ontario. *Canadian Journal of Earth Sciences* 29, 1779-1790.
- Hanor, J.S. 1979. *Geochemistry of Hydrothermal Ore Deposits*. John Wiley & Sons, New York, USA.
- Harper, D.A., F.J. Longstaffe, M.A. Wadleigh and R.H. McNutt. 1995. Secondary K-feldspar at the Precambrian-Paleozoic unconformity, southwestern Ontario. *Canadian Journal of Earth Sciences* 32, 1432-1450.
- Harrison, J.E. 1972. Quaternary geology of the North Bay-Mattawa region. Geological Survey of Canada Paper 71-26. Ottawa, Canada.
- Hart, M. and T.M. Whitworth. 2005. Hyperfiltration of potassium nitrate through clay membranes under relatively low-head conditions. *Geochimica et Cosmochimica Acta* 69, 4817-4823.
- Hawlder, B.C., N.Y. Lee and K.Y. Lo. 2002. Modelling of three-dimensional stress effects on swelling behaviour of Queenston shale. *Ground and Water. Theory to Practice. Proceedings of the 55<sup>th</sup> Canadian Geotechnical and 3<sup>rd</sup> Joint IAH-CNC and CGS Groundwater Specialty Conferences*. D. Stolle, A.R. Piggott, and J.J. Crowder (Eds.). Niagara Falls Ontario. Southern Ontario Section of the Canadian Geotechnical Society, 623-631.
- Hayek, S.J., J.A. Drysdale, J. Adams, V. Peci, S. Halchuk and P. Street. 2008. Seismic Monitoring Annual Report 2007. Ontario Power Generation Report, OPG 00216-REP-01300-00011-R00. Toronto, Canada.
- Hayek, S.J., J.A. Drysdale, J. Adams, V. Peci, S. Halchuk, C. Woodgold and P. Street. 2009. Seismic Monitoring Annual Report 2008. Nuclear Waste Management Organization Report DGR-TR-2009-10. Toronto, Canada.
- Hayek, S.J., J.A. Drysdale, J. Adams, V. Peci, S. Halchuk and P. Street. 2010. Seismic Monitoring near the DGR - Annual Report 2009. Nuclear Waste Management Organization Report DGR-TR-2010-03. Toronto, Canada.
- Heagle, D. and L. Pinder. 2010. Opportunistic Groundwater Sampling in DGR-3 and DGR-4. Intera Engineering Ltd. Report TR-08-18 Rev.0. Ottawa, Canada.
- Heaman, L.M. and B.A. Kjarsgaard. 2000. Timing of eastern North American kimberlite magmatism. Continental extension of the Great Meteor Hotspot Track? *Earth and Planetary Science Letters Journal* 178, 253-268.
- Heidbach, O., J. Reinecker, M. Tingay, B. Müller, B. Sperner, K. Fuchs and F. Wenzel. 2007. Plate boundary forces are not enough. Second- and third-order stress patterns highlighted in the World Stress Map database. *Tectonics* 26, TC6014.
- Herwegh, M. and M. Mazurek. 2008. Feasibility SEM Study. Primary and Secondary Salts and Sulfates in the Paleozoic of the DGR-2 Borehole, Bruce, Southwestern Ontario.



- Progress Report PR 08-03. Institute of Geological Sciences, University of Bern, Switzerland.
- Hildes, D.H.D., G.K.C. Clarke, G.E. Flowers, and S.J. Marshall. 2004. Subglacial erosion and englacial sediment transport modelled for North American ice sheets. *Quaternary Science Reviews* 23, 409–430.
- Hobbs, M.Y., S.K. Frape, O. Shouakar-Stash and L.R. Kennell. 2011a. Regional Hydrogeochemistry – Southern Ontario. Nuclear Waste Management Organization Report NWMO DGR-TR-2011-12 R000. Toronto, Canada.
- Hobbs, M.Y., A. deHaller, M. Koroleva, M. Mazurek, J. Spangenberg, U. Mäder and D. Meier. 2011b. Borehole DGR-3 and DGR-4 Porewater Investigations. Intera Engineering Ltd. Report TR-08-40 Rev.0. Ottawa, Canada.
- Hoek, E. and E.T Brown. 1980. Underground excavations in rock. Institution of Mining and Metallurgy, London, England.
- Hoek, E., C. Carranza-Torres and B. Corkum. 2002. Hoek-Brown Failure Criterion — 2002 Edition, in NARMS-TAC 2002. Mining and Tunnelling Innovation and Opportunity, 1. 267-273. R. Hammah et al. (Eds.). University of Toronto Press, Toronto, Canada.
- Hogarth, C.G. and D.F Sibley. 1985. Thermal history of the Michigan Basin: evidence from conodont coloration index. In: K.R. Cercone and J.M. Budai (Eds.) Ordovician and Silurian Rocks of the Michigan Basin. Michigan Basin Geological Society Symposium, Special Paper 4, 45-58.
- Holst, T.M. 1982. Regional jointing in the Michigan Basin. *Geology* 10, 273-277.
- Hooke, R.L. 2005. Principles of Glacier Mechanics. Second edition. Cambridge University Press, Cambridge, UK.
- Hora, S. and M. Jensen. 2005 Expert Panel Elicitation of Seismicity Following Glaciation in Sweden, SSI Report No. 2005:20.
- Hough, J.L. 1958. Geology of the Great Lakes. University of Illinois Press.
- Howell, P.D. and B.A. van der Pluijm. 1990. Early history of the Michigan Basin: subsidence and Appalachian tectonics. *Geology* 18, 1195-1198.
- Howell, P.D. and B.A. van der Pluijm. 1999. Structural sequences and styles of subsidence in the Michigan basin. *Geological Society of America Bulletin* 111, 974-991.
- Huff, W.D., S.M. Bergstrom and D.R. Kolata. 1992. Gigantic Ordovician volcanic ash fall in North America and Europe: biological, tectonomagmatic, and event-stratigraphic significance. *Geology* 20, 875-878.
- Hunt, J.M. 1996. Petroleum geochemistry and geology. W.H. Freeman & Co., New York, New York, USA.
- Hurley, N.F. and R. Budros. 1990. Albion-Scipio and Stoney Points Fields – USA. Michigan Basin. In: E.A. Beaumont and N.H. Foster (Eds.), Stratigraphic Traps I: Treatise of

- Petroleum Geology, Atlas of Oil and Gas Fields. American Association of Petroleum Geologists, 1-32.
- Huysmans, M. and A. Dassargues. 2005. Review of the use of Péclet numbers to determine the relative importance of advection and diffusion in low permeability environments. *Hydrogeology Journal* 13, 895–904.
- INTERA. 2006. Geoscientific Site Characterization Plan, OPG's Deep Geologic Repository for Low and Intermediate Level Waste Report INTERA 05-220-1, OPG 00216-REP-03902-00002-R00. Ottawa, Canada.
- INTERA. 2008. Phase 2 Geoscientific Site Characterization Plan, OPG's Deep Geologic Repository for Low and Intermediate Level Waste, Report INTERA 06-219-50-Phase 2 GSCP-R0, OPG 00216-PLAN-03902-00002-R00. Ottawa, Canada.
- INTERA. 2011. Descriptive Geosphere Site Model. Intera Engineering Ltd. report for the Nuclear Waste Management Organization NWMO DGR-TR-2011-24 R000. Toronto, Canada.
- IPCC. 2007. IPCC Fourth Assessment Report (AR4). Pachauri, R.K. and A. Reisinger (Eds.) *Climate Change 2007: Synthesis Report. Contribution of Working Groups I, II and III to the Fourth Assessment Report of the Intergovernmental Panel on Climate Change.* IPCC, Geneva, Switzerland.
- ITASCA CANADA and AECOM. 2011. Three-Dimensional Geological Framework Model. Itasca Consulting Canada, Inc. and AECOM Canada Ltd. report for the Nuclear Waste Management Organization NWMO DGR-TR-2011-42 R000. Toronto, Canada.
- ITASCA. 2005. FLAC3D (Fast Lagrangian Analysis of Continua in 3 Dimensions), Version 3.1. Minneapolis, Minnesota, USA.
- ITASCA. 2006. Universal Distinct Element Code (UDEC), Version 4.00. Minneapolis, Minnesota, USA.
- ITASCA. 2008. FLAC (Fast Lagrangian Analysis of Continua), Version 6.0. Minneapolis, Minnesota, USA.
- ITASCA. 2009. FLAC3D (Fast Lagrangian Analysis of Continua in 3 Dimensions) Version 4.0. Itasca Consulting Group Inc., Minneapolis, USA.
- ITASCA. 2011. Long-Term Geomechanical Stability Analysis. Itasca Consulting Group, Inc. report for the Nuclear Waste Management Organization NWMO DGR-TR-2011-17 R000. Toronto, Canada.
- Jackson, R. 2009. Organic Geochemistry and Clay Mineralogy of DGR-3 and DGR-4 Core. Intera Engineering Ltd. Report TR-08-29 Rev.0. Ottawa, Canada.
- Jackson, R. and D. Heagle. 2010. Opportunistic Groundwater Sampling in DGR-1 and DGR-2. Intera Engineering Ltd. Report TR-07-11 Rev.0. Ottawa, Canada.
- Jackson, R.E and A. Wigston. 2010. Laboratory Petrophysical Testing of DGR-3 and DGR-4 Core. Intera Engineering Ltd. Report TR-08-28 Rev.0. Ottawa, Canada.

- Jacobi, R. and J. Fountain. 1993. The Southern Extension and Reactivations of the Clarendon-Linden Fault System. *Géographie Physique et Quaternaire* 47, 285-302.
- Jamieson, S.S.R., N.R.J. Hulton, D.E. Sugden, A.J. Payne and J. Taylor. 2005. Landscape evolution of the Lambert basin, East Antarctica: the relative role of rivers and ice sheets. *Global and Planetary Change* 45, 35-49.
- Johnson, M.D., D.K. Armstrong, B.V. Sanford, P.G. Telford and M.A. Rutka. 1992. Paleozoic and Mesozoic geology of Ontario. In: *The Geology of Ontario*, Ontario Geological Survey, Special Volume 4, Part 2, 907-1008.
- Karrow, P.F. and O.L. White. 2002. A history of neotectonic studies in Ontario. *Neotectonics and seismicity in the eastern Great Lakes Basin*. *Tectonophysics* 353, 3-15.
- Kesler, S.E. and C.W. Carrigan. 2002. Discussion on "Mississippi Valley-type lead-zinc deposits through geological time: implications from recent age-dating research" by D.L. Leach, D. Bradley, M.T. Lewchuk, D.T.A. Symons, G. de Marsily, and J. Brannon (2001). *Mineralium Deposita* 36, 711-740.
- Ketchum, J. and A. Davidson. 2000. Crustal architecture and tectonic assembly of the Central Gneiss Belt, southwestern Grenville Province, Canada: a new interpretation. *Canadian Journal of Earth Sciences* 37, 217-234.
- Kharaka Y.K. and F.A.F. Berry. 1973. Simultaneous flow of water and solutes through geological membranes I: Experimental investigation. *Geochimica et Cosmochimica Acta* 37, 2577-2603.
- Kharaka, Y. K. and D.J. Specht. 1988. The solubility of noble gases in crude oil at 25-100°C. *Applied Geochemistry* 3, 137-144.
- Kolata, D.R., W.D. Huff and S.M. Bergström. 1998. Nature and regional significance of unconformities associated with the Middle Ordovician Hagan K-bentonite complex in the North American midcontinent. *Geological Society of America Bulletin* 110, 723-739.
- Koppes, M. and B. Hallet. 2006. Erosion rates during rapid deglaciation in Icy Bay, Alaska. *Journal of Geophysical Research* 111, F02023.
- Kor, P.S. and D.W. Cowell. 1998. Evidence for catastrophic subglacial meltwater sheetflood events on the Bruce Peninsula, Ontario. *Canadian Journal of Earth Sciences* 35, 1180-1202.
- Kor, P.S., J. Shaw and D.R. Sharpe. 1991. Erosion of bedrock by subglacial meltwater, Georgian Bay, Ontario: a regional view. *Canadian Journal of Earth Sciences* 28, 623-642.
- Koroleva, M., A. de Haller, U. Mader, H.N. Waber and M. Mazurek. 2009. Technical Report. Borehole DGR-2. Pore-Water Investigations, TR-08-06, Revision 0, August 4, Rock Water Interaction (RWI), Institute of Geological Sciences, University of Bern, Bern, Switzerland.
- Kumarapeli, P.S. 1976. The St. Lawrence rift system, related metallogeny, and plate tectonic models of Appalachian evolution, 301 -320. In D.F. Strong (Ed.), *Metallogeny and Plate Tectonics*. Geological Association of Canada, Special Paper 14.

- Kumarapeli, P.S. 1985. Vestiges of lapetan Rifting in the Craton West of the Northern Appalachians Geoscience Canada, 12, Number 2.
- Kumarapeli, P.S. and V.A. Saul. 1966. The St. Lawrence Rift Valley System. A North American Equivalent of the East African Rift Valley System. Canadian Journal of Earth Sciences 3, 639-658.
- Kyser, K. and E.E. Hiatt. 2003. Fluids in sedimentary basins: an introduction. Journal of Geochemical Exploration 80, 139-149.
- Lam, T.M., C.D. Martin and D. McCreath. 2007. Characterizing the Geomechanics. Properties of the Sedimentary Rocks for the DGR Excavations, Canadian Geotechnical Conference. Ottawa, Canada.
- Lampe, D.C. 2009. Hydrogeologic framework of bedrock units and initial salinity distribution for a simulation of groundwater flow for the Lake Michigan Basin. U.S. Geological Survey, Scientific Investigations Report 2009-5060. Reston, Virginia.
- Lanyon, G.W., P. Marschall, T. Trick, R. de la Vaissière, H. Shao and H. Leung. 2009. Hydromechanical evolution and self-sealing of damage zones around a microtunnel in a claystone formation of the Swiss Jura mountains, 43<sup>rd</sup> U.S. Rock Mechanics Symposium & 4<sup>th</sup> U.S. – Canada Rock Mechanics Symposium, Paper 09-152, June/July 2009, Asheville, USA.
- Larson, G. and R. Schaetzl. 2001. Origin and evolution of the Great Lakes. Journal of Great Lakes Research 27, 518–546.
- Lau, J.S.O., B. Gorski, B. Conlon and T. Anderson. 2000. Long-term Loading Tests on Saturated Granite and Granodiorite. Ontario Power Generation Report 06819-REP-01300-10016 R00. Toronto, Canada.
- Lazorek, M. and T. Carter. 2008. The Oil and Gas Plays of Ontario. Ontario Oil and Gas 2008 Edition. Ontario Petroleum Institute. London, Canada.
- Legall, F.D., C.R. Barnes and R.W. Macqueen. 1981. Thermal maturation, burial history and hotspot development, Paleozoic strata of southern Ontario-Quebec, from conodont acritarch colour alteration studies. Bulletin of Canadian Petroleum Geology 29, 492-539.
- Lehmann, D., C.E. Brett, R. Cole and G. Baird. 1995. Distal sedimentation in a peripheral foreland basin. Ordovician black shales and associated flysch of the western Taconic foreland, New York State and Ontario. Geological Society of America Bulletin 107, 708-724.
- Leighton, M.W. 1996. Interior cratonic basins: a record of regional tectonic influences. In: van der Pluijm, B.A. & Catacosinos, P.A. (Eds.), Basement and Basins of North America, Geological Society of America Special Paper 308, 77-93.
- Letouzey, J. 1986. Cenozoic paleo-stress pattern in the Alpine foreland and structural interpretation in a platform basin. Tectonophysics 132, 215-231.
- Leverett, F. and F.B. Taylor. 1915. The Pleistocene of Indiana and Michigan and the history of the Great Lakes. U.S. Geological Survey Monograph 53.

- Lewis, C.F.M. and T.W. Anderson. 1989. Oscillations of levels and cool phases of the Laurentian Great Lakes caused by inflows from glacial lakes Agassiz and Barlow-Ojibway. *Journal of Paleolimnology* 2, 99-146.
- Liberty, B.A. 1960. Belleville and Wellington map areas, Ontario. Geological Survey of Canada, Paper 60-61.
- Liberty, B.A. and T.E. Bolton. 1971. Paleozoic geology of the Bruce Peninsula area, Ontario. Geological Survey of Canada, Memoir 360.
- Lidmar-Bergström, K. 1997. A long-term perspective on glacial erosion. *Earth Surface Processes and Landforms* 22, 297-306.
- Lindholm, R.C. 1978. Triassic-Jurassic faulting in eastern North America – A model based on pre-Triassic structures. *Geology* 6, 365-368.
- Lo, K.Y. 1989. Recent advances in design and evaluation of performance of underground structures on rocks. *Tunnelling and Underground Space Technology* 4(2), 171-183.
- Lo, K.Y., R.S.C. Wai, J.H.L. Palmer and R.M. Quigley. 1978. Time-dependent deformation of shaly rocks in Southern Ontario. *Canadian Geotechnical Journal* 15, 537-547.
- Lo, K.Y. and M. Hori. 1979. Deformation and strength properties of some rocks in southern Ontario. *Canadian Geotechnical Journal* 16(1), 108-120.
- Lo, K.Y., M. Devata and C.M.K. Yuen. 1979. Performance of a shallow tunnel in a shaly rock with high horizontal stresses. In: *Tunnelling '79'*. Proceedings of the 2<sup>nd</sup> International Symposium on Tunnelling. Edited by M.J. Jones. Institution of Mining and Metallurgy, London, United Kingdom, p.1-12.
- Lo, K.Y. and B. Lukajic. 1984. Predicted and measured stresses and displacement around Darlington Intake Tunnel. *Canadian Geotechnical Journal* 21(1), 147-165.
- Lukajic, B.J. 1988. Preliminary Results of the 1986-87 Geological Investigations, BNPD Proposed Underground Irradiated Fuel Storage Facility. Ontario Hydro Report GHED-DR-8801, Toronto, Canada.
- Lumbers, S.B., L.M. Heaman, V.M. Vertolli and T.W. Wu. 1990. Nature and timing of middle Proterozoic magmatism in the Central Metasedimentary Belt, Grenville Province, Ontario. Special Paper- Geological Association of Canada 38, 243-276.
- Lund, B., P. Schmidt and C. Hieronymus. 2009. Stress evolution and fault stability during the Weichselian glacial cycle. SKB Technical Report TR-09-15, Svensk Kärnbränslehantering AB, Stockholm, Sweden.
- Luszczynski, N.J. 1961. Head and flow of ground water of variable density. *Journal of Geophysical Research* 66(12), 4247-4256.
- Ma, S. and G. Atkinson. 2006. Focal depth distribution for earthquakes with  $M_N \geq 2.8$  in western Quebec, southern Ontario and northern New York. *Bulletin of the Seismological Society of America* 96, 609-623.

- Mainville, A. and M.R. Craymer. 2005. Present-day tilting of the Great Lakes region based on water level gauges. *Geological Society of America Bulletin* 117, 1070-1080.
- Maloney, S. 2010. Technical Report. CERCHAR Abrasivity Testing of Argillaceous Limestone of the Cobourg Formation, TR-07-04, Revision 2, May 18, MIRARCO/Geomechanics Research Centre, Laurentian University, Sudbury, Canada.
- Maloney, S. and N. Bahrani. 2009. Technical Report. CERCHAR Abrasivity Testing of Argillaceous Limestone of the Cobourg Formation from DGR-3 and DGR-4, TR-08-25, Revision 0, October 30, MIRARCO/Geomechanics Research Centre, Laurentian University, Sudbury, Canada.
- Marshak, S. and J.R. Tabor. 1989. Structure of the Kingston Orocline in the Appalachian fold-thrust belt, New York, *Geological Society of America Bulletin* 101, 683-701.
- Marshak, S. and T. Paulsen. 1996. Mid-continent U.S. fault and fold zones: A legacy of Proterozoic intracratonic extensional tectonism? *Geology* 24, 151-154.
- Marshall, S.J., L. Tarasov, G.K.C. Clarke and W.R. Peltier. 2000. Glaciological reconstruction of the Laurentide ice sheet: Physical processes and modelling challenges. *Canadian Journal of Earth Sciences* 37(5), 769-793.
- Martin, C.D. 1997. Seventeenth Canadian Geotechnical Colloquium: The effect of cohesion loss and stress path on brittle rock strength. *Canadian Geotechnical Journal* 34(5), 698-725.
- Martin, C.D. and G.W. Lanyon. 2003. EDZ in clay shale: Mont Terri. Mont Terri Technical Report 2001, 1. With contributions from P. Bossart and P. Blümling. Falmouth, United Kingdom.
- Martin, C.D. and N.A. Chandler. 1994. The progressive fracture of Lac du Bonnet Granite. *International Journal of Rock Mechanics and Mining Sciences* 31, 643-659.
- Martin, C.D., P.K. Kaiser and D.R. McCreath. 1999. Hoek-Brown Parameters for Predicting the Depth of Brittle Failure Around Tunnels. *Canadian Geotechnical Journal* 36, 136-151.
- Martin, R.J., J.S. Noel, P.J. Boyd, and R.H. Price. 1997. Creep and static fatigue of welded tuff from Yucca Mountain, Nevada. *International Journal of Rock Mechanics and Mining Sciences* 34(3-4), Paper 190.
- Matray, J., S. Savoye and J. Cabrera. 2007. Desaturation and structures relationships around drifts excavated in the well-compacted Tournemire's argillite and their impact on the hydraulic head profiles. *Engineering Geology* 90, 1-16.
- Mayer, K.U., E.O. Frind and D.W. Blowes. 2002. Multicomponent reactive transport modelling in variably saturated porous media using a generalized formulation for kinetically controlled reactions. *Water Resources Research* 38(9), 1174.
- Mazurek, M., F.J. Pearson, G. Volckaert, and H. Bock. 2003. FEPCAT project: Features, events and processes evaluation catalogue for argillaceous media. OECD/NEA Technical Report.

- Mazurek, M. 2004. Long-term Used Nuclear Fuel Waste Management - Geoscientific Review of the Sedimentary Sequence in Southern Ontario. Institute of Geological Sciences University of Bern Technical Report TR 04-01, Switzerland.
- Mazurek, M., A. Gautschi, P. Marschall, G. Vigneron, P. Lebon, and J. Delay. 2008. Transferability of geoscientific information from various sources (study sites, underground rock laboratories, natural analogues) to support safety cases for radioactive waste repositories in argillaceous formations. *Physics and Chemistry of the Earth* 33, S95-S105.
- McCaffrey M.A., B. Lazar and H.D. Holland. 1987. The evaporation path of seawater and the coprecipitation of Br<sup>-</sup> and K<sup>+</sup> with halite. *Journal of Sedimentary Petrology* 57, 928-937.
- McFall, G.H. 1990. Faulting of a Middle Jurassic, ultramafic dyke in the Picton Quarry, Picton, southern Ontario. *Canadian Journal of Earth Sciences* 27, 1536-1540.
- McFall, G.H. and A. Allam. 1989. Neotectonic Investigations in Southern Ontario. Prince Edward County, Phase I. Atomic Energy Control Board Report 89-02. Ottawa, Ontario.
- McHone, J.G. 1996. Broad-terranic Jurassic flood basalts across northeastern North America. *Geology* 24, 319-322.
- McHone, J.G. and J.R. Butler. 1984. Mesozoic igneous provinces of New England and the opening of the North Atlantic Ocean. *Geological Society of America Bulletin* 95, 757-765.
- McIntosh, J.C. and L.M. Walter. 2005. Volumetrically significant recharge of Pleistocene glacial meltwaters into epicratonic basins: Constraints imposed by solute mass balances. *Chemical Geology* 222, 292-309.
- McIntosh, J.C. and L.M. Walter. 2006. Paleowaters in the Silurian-Devonian carbonate aquifers: Geochemical evolution of groundwater in the Great Lakes region since the late Pleistocene. *Geochimica et Cosmochimica Acta* 70, 2454-2479.
- McKay, D.A. 1989. DGR Bruce NGS, "B" Stress Measurements, Co-operative Pilot Project – Ontario Hydro Research Report 89-156-K. Toronto, Canada.
- McKenna, C.M., R.H. McNutt and S.K. Frape. 1992. Lead and strontium isotopic data on brines from the Michigan Basin, Ontario and Michigan. In: Kharaka, Y.K. and A.S. Maest (Eds.). *Proceedings 7<sup>th</sup> International Water-Rock Interaction Conference*. Park City, Utah, USA.
- McNutt, R.H., S.K. Frape and P. Dollar. 1987. A strontium, oxygen and hydrogen isotopic composition of brines, Michigan and Appalachian Basins, Ontario and Michigan. *Applied Geochemistry* 2, 495-505.
- McWilliams, C.K., R.P. Wintsch and M.J. Kunk. 2007. Scales of equilibrium and disequilibrium during cleavage formation in chlorite and biotite-grade phyllites, SE Vermont. *Journal of Metamorphic Geology* 25, 895-913.
- Melaney, M. 2009. Borehole Geophysical Logging of US-3 and US-7. Intera Engineering Ltd. Report TR-08-03 Rev.1. Ottawa, Canada.

- Melchin, M.J., M.E. Brookfield, D.K. Armstrong and M. Coniglio. 1994. Stratigraphy, sedimentology and biostratigraphy of the Ordovician rocks of the Lake Simcoe area, south-central Ontario; Geological Association of Canada–Mineralogical Association of Canada, Joint Annual Meeting, Waterloo, Ontario, Guidebook for Field Trip A4.
- Michigan State Geological Survey. 2007. Michigan State Geological Survey, Department of Environmental Quality. Mapping and Petroleum Well Database Downloads, <http://www.michigan.gov/deq>.
- Micic, S. and K.Y. Lo. 2009. Laboratory Free Swell Testing of DGR-3 and DGR-4 Core. Intera Engineering Ltd. Report TR-08-26 Rev.0. K.Y. Lo Inc., London, Canada.
- Micic, S. and K.Y. Lo. 2010. Laboratory Swell Testing of DGR-2 Core. Intera Engineering Ltd. Report TR-07-16 Rev.2. K.Y. Lo Inc., London, Canada.
- Middleton K., M. Coniglio, R. Sherlock and S.K. Frape. 1993. Dolomitization of Middle Ordovician carbonate reservoirs, southwestern Ontario. *Bulletin of Canadian Petroleum Geology* 41, 150-163.
- Milkereit B., D.A. Forsyth, A.G. Green, A. Davidson, S. Hanmer, D.R. Hutchinson, W. Hinze and R.F. Mereu. 1992. Seismic images of a Grenvillian terrane boundary. *Geology* 20, 1027-1030.
- Minster, J. and T. Jordan. 1978. Present Day Plate Motions. *Journal of Geophysical Research* 83, 5331-5354.
- Morel, P. and E. Irving. 1978. Tentative paleocontinental maps for the early Phanerozoic and Proterozoic, *Journal of Geology* 86, 535–561.
- Morgan, P. 1983. Constraints on rift thermal processes from heat flow and uplift. *Tectonophysics* 94, 277-298.
- Morrow, D.W. 1990. Dolomite- Part 2. Dolomitization Models and Ancient Dolostones. In: McIlreath, I.A. and D.W. Morrow (Eds.). *Diagenesis Geoscience Canada Reprint Series Number 4*, 125-139.
- Morton, J.D., K.Y. Lo and D.J. Belshaw. 1975. Rock Performance considerations for shallow tunnels in bedded shales with high lateral stresses. *Proceedings of the 12<sup>th</sup> Canadian Rock Mechanics Symposium*, Kingston, Ontario, 339-379.
- Murphy, S. and D. Heagle. 2010. Phase 2 Groundwater Monitoring. US-3, US-7 and US-8. Intera Engineering Ltd. Report TR-08-30 Rev.0. Ottawa, Canada.
- Nadon G.C., J.A. Simo, R.H. Dott and C.W. Byers. 2000. High-resolution sequence stratigraphic analysis of the St. Peter Sandstone and Glenwood Formation (Middle Ordovician), Michigan Basin, U.S.A. *AAPG Bulletin* 84, 975-996.
- National Building Code of Canada (NBCC). 2005.
- National Oceanic and Atmospheric Administration (NOAA). 2007. Great Lakes Bathymetry Gridding Project. <http://www.ngdc.noaa.gov/mgg/greatlakes/greatlakes.html>



- Nicholson, R.P. and V.N.H. Hough. 1967. Jointing in the Appalachian Plateau of Pennsylvania. *Geological Society of America Bulletin* 78, 609-630.
- Normani, S.D. 2009. Paleoevolution of pore fluids in glaciated geologic settings. Ph.D. thesis, University of Waterloo, Waterloo, Canada.
- Normani, S.D., Y.J. Park, J.F. Sykes, and E.A. Sudicky. 2007. Sub-regional modelling case study 2005-2006 status report. Nuclear Waste Management Organization, Technical Report NWMO TR-2007-07. Toronto, Canada.
- NWMO. 2011. Geoscientific Verification Plan. Nuclear Waste Management Organization Document NWMO DGR-TR-2011-38 R000. Toronto, Canada.
- NWMO and AECOM. 2011. Regional Geomechanics – Southern Ontario. AECOM Canada Ltd. and Nuclear Waste Management Organization Report NWMO DGR-TR-2011-13 R000. Toronto, Canada.
- Obermajer, M., M.G. Fowler, F. Goodarzi and L.R. Snowdon. 1996. Assessing thermal maturity of Palaeozoic rocks from reflectance of chitinozoa as constrained by geothermal indicators: an example from southern Ontario, Canada. *Marine and Petroleum Geology* 13, 907-919.
- Obermajer, M., M.G. Fowler, L.R. Snowdon and R.W. Macqueen. 2000. Are the Silurian Reef-hosted oils locally sourced in Ontario? *AAPG Bulletin* 84(9), 1390-1391.
- Obert, L. 1962. In Situ Determination of Stress in Rock. *Mining Engineering* 14, 51-58.
- OECD. 2010. Geoscientific Information in the Radioactive Waste Management Safety Case: Main Messages from the AMIGO Project. Organisation for Economic Co-operation and Development – Nuclear Energy Agency, OECD/NEA No. 6395.
- Ontario Geological Survey. 1991. Bedrock geology of Ontario, southern sheet; Ontario Geological Survey, Map 2544, scale 1:1 000 000.
- Ontario Geological Survey. 2004. Aggregate resources inventory of Huron County; Ontario Geological Survey, Aggregate Resources Inventory Paper 177.
- Ontario Oil, Gas and Salt Resources (OGSR) Library. 2004. Cumulative oil and gas production in Ontario to the end of 2004. Excel format data. In. Members Package Dataset. Petroleum Resources Centre, Ministry of Natural Resources Oil, Gas & Salt Resources Library.
- Ontario Oil, Gas and Salt Resources (OGSR) Library. 2006. Oil and Gas Pools and Pipelines of Southern Ontario, revised October 2006. Petroleum Resources Centre, Ministry of Natural Resources Oil, Gas & Salt Resources Library UTM NAD83. Ontario Digital Base Data.
- Ontario Hydro. 1991. Niagara River Hydroelectric Development. Definition Phase Geotechnical Investigations and Evaluation. Ontario Hydro Report 91150, Volumes 1 to 5. Toronto, Canada.

- OPG. 2011a. OPG's Deep Geologic Repository for Low and Intermediate Level Waste - Preliminary Safety Report. Ontario Power Generation Report 00216-SR-01320-00001 R000. Toronto, Canada.
- OPG. 2011b. Deep Geologic Repository for Low and Intermediate Level Waste – Environmental Impact Statement. Ontario Power Generation Report 00216-REP-07701-00001 R000. Toronto, Canada.
- Park, R.G. and W. Jaroszewski. 1994. Craton tectonics, stress and seismicity. *Continental Deformation*, 200-222.
- Park, Y-J., E.A. Sudicky and J.F. Sykes. 2009. Effects of shield brine on the safe disposal of waste in deep geologic environments. *Advances in Water Resources* 32, 1352–1358.
- Parker, J.M. 1942. Regional systematic jointing in slightly deformed sedimentary rocks. *Bulletin of the Geological Society of America* 53, 381-408.
- Pearson, F.J., Jr. 1987. Models of mineral controls on the composition of saline groundwaters in the Canadian Shield. In: Fritz, P. and S.K. Frappe (Eds.). *Saline waters and gases in crystalline rocks*. Geological Association of Canada Special Paper 33, 39–51.
- Pehme, P. and M. Melaney. 2010a. Borehole Geophysical Logging in DGR-1 and DGR-2. Intera Engineering Ltd. Report TR-07-08 Rev.3. Ottawa, Canada.
- Pehme, P. and M. Melaney. 2010b. Borehole Geophysical Logging in DGR-3 and DGR-4. Intera Engineering Ltd. Report TR-08-15 Rev.1. Ottawa, Canada.
- Pehme, P. and M. Melaney. 2011. Technical Report: Borehole Geophysical Logging of DGR-5 and DGR-6. Intera Engineering Ltd. Report TR-09-03 Rev.3. Ottawa, Canada.
- Peltier, W.R. 2002. A design basis glacier scenario. Ontario Power Generation Report 06819-REP-01200-10069-R00. Toronto, Canada.
- Peltier, W.R. 2011. Long-Term Climate Change. Nuclear Waste Management Organization Report NWMO DGR-TR-2011-14 R000. Toronto, Canada.
- Peltier, W.R. and R.G. Fairbanks. 2006. Global glacial ice volume and Last Glacial Maximum duration from an extended Barbados sea level record. *Quaternary Science Reviews* 25, 3322-3337.
- Percival, J.A. and R.M. Easton. 2007. Geology of the Canadian Shield in Ontario. An Update. OPG Report No. 06819-REP-01200-10158-R00, OGS Open File Report 6196, GSC Open File Report 5511.
- Person, M., B. Dugan, J.B. Swenson, L. Urbano, C. Stott, J. Taylor, and M. Willett. 2003. Pleistocene hydrogeology of the Atlantic continental shelf, New England. *Geological Society of America Bulletin* 115(11), 1324–1343.
- Person, M., J. McIntosh, V. Bense and V.H. Remenda. 2007. Pleistocene hydrology of North America: The role of ice sheets in reorganizing groundwater flow systems. *Reviews of Geophysics* 45, RG3007.

- Pocachard, J., B. Duding, G. Beaudoin, M. Launay, D. Thoby, and D. Mourzagah. 1997. Coefficients de diffusion et de permeation d'eau à travers 8 échantillons du site Meuse – Forage EST 104. Andra Report D.RP.3CEA.97.004, Andra, Châtenay-Malabry, France.
- Potyondy, D.O., 2007. Simulating stress corrosion with a bonded-particle model for rock. *International Journal of Rock Mechanics and Minerals Sciences* 44, 677-691.
- Powell, T.G., R.W. MacQueen, J.F. Barker and D.G. Bree. 1984. Geochemical Character and Origin of Ontario Oils. *Bulletin of Canadian Petroleum Geology* 32, 289-312.
- Power, M.S., D. Rosidi and J.Y. Kaneshiro. 1998. Seismic Vulnerability of Tunnels and Underground Structures Revisited, Newport Beach, CA, Balkema, Rotterdam, The Netherlands, 243-250.
- Price, G.D. 1999. The evidence and implications of polar ice during the Mesozoic. *Earth-Science Reviews* 48, 183–210.
- Prouty, C.E. 1988. Trenton exploration and wrench tectonics; Michigan Basin and environs. In: B.D. Keith (Ed.), *The Trenton Group (Upper Ordovician series) of eastern North America*, American Society of Petroleum Geologists Studies in Geology 29, 207-236.
- Pruess, K., C. Oldenburg and G. Moridis. 1999. TOUGH2 users guide, version 2.0. Lawrence Berkeley National Laboratory Technical Report LBNL43134.
- Quinlan, G. and C. Beaumont. 1984. Appalachian thrusting, lithospheric flexure and the Paleozoic stratigraphy of the Eastern Interior of North America. *Canadian Journal of Earth Sciences* 21, 973-996.
- Ramsey D.W. and C.M. Onasch. 1999. Fluid migration in a cratonic setting. the fluid histories of two fault zones in the eastern midcontinent. *Tectonophysics* 305, 307-323.
- Roberts, R., D. Chace, R. Beauheim and J. Avis. 2011. Analysis of Borehole Straddle-packer Tests in DGR Boreholes. Intera Engineering Ltd. Report TR-08-32 Rev.0. Ottawa, Canada.
- Rocscience. 2009. Rocscience Phase<sup>2</sup> Version 7.011. <http://www.rocscience.com/products/3/Phase2>.
- Roest, W. 1995. Interpretation of aeromagnetic and gravity anomalies in the Precambrian shield of southern Ontario. Program, List of Participants and Abstracts from the Atomic Energy Control Board Workshop on seismic hazard assessment in southern Ontario, Ottawa, Ontario, June 19-21, INFO-0604-1.
- Rona, P.A. and E.S. Richardson. 1978. Early Cenozoic global plate reorganization. *Earth and Planetary Science Letters* 40, 1-11.
- Rutty, A. L. and A.R. Cruden. 1993. Pop-up structures and the fracture pattern in the Balsam Lake area, southern Ontario. In *Neotectonics of the Great Lakes area*. J.L. Wallach and J.A. Heginbottom (Ed.), *Géographie physique et Quaternaire* 47, 379–388.
- Sage, R.P. 1991. Paleozoic and Mesozoic geology of Ontario. In: *Geology of Ontario*, Ontario Geological Survey, Special Volume 4, Part 1, 683-709.

- Sanford, B.V. 1961. Subsurface stratigraphy of Ordovician rocks in southwestern Ontario. Geological Survey of Canada. Paper 60-26.
- Sanford, B.V. 1968. Devonian of Ontario and Michigan. In: D. H. Oswald, ed., International symposium on the Devonian System, 1967, Calgary, Alberta. Proceedings, Alberta Society Of Petroleum Geologists 1, 973-999.
- Sanford, B.V. 1969. Silurian of southwestern Ontario; in Proceedings, Ontario Petroleum Institute, 8th Annual Conference, Technical Paper 5, 1-44.
- Sanford, B.V., F.J. Thompson and G.H. McFall. 1985. Plate tectonics – A possible controlling mechanism in the development of hydrocarbon traps in southwestern Ontario. Bulletin of Canadian Petroleum Geology 33, 52-71.
- Sanford, B.V. 1993. St. Lawrence Platform: economic geology. In: Stott, D.F. and J.D. Aitken (Eds.), Sedimentary Cover of the Craton in Canada, Geological Survey of Canada, Geology of Canada Series, no.5, 787-798.
- Sangster, D.F. and B.A. Liberty. 1971. Sphalerite concretions from Bruce Peninsula, Southern Ontario, Canada. Economic Geology 66, 1145-1152.
- Saripalli, K.P., R.J. Serne, P.D. Meyer and B.P. McGrail. 2002. Prediction of Diffusion Coefficients in Porous Media Using Tortuosity Factors Based on Interfacial Areas. Ground Water 40, 346-352.
- Sato, T., T Kikuchi and T. Sugihara. 2000. Insitu experiments of the excavation disturbed zone induced mechanical excavation in Neogene sedimentary rock at Tono mine, central Japan. Engineering Geology 56(1-2), 97-108.
- Sbar, M.L. and L.R. Sykes. 1973. Contemporary Compressive Stress and Seismicity in Eastern North America: An Example of Intra-Plate Tectonics. Geological Society of America Bulletin 84, 1861-1882.
- Schaetzl, R.J., S.A. Drzyzga, B.N. Weisenborn, K.A. Kincare, X.C. Lepczyk, K.A. Shein, C.M. Dowd and J. Linker. 2002. Measurement, Correlation, and Mapping of Glacial Lake Algonquin Shorelines in Northern Michigan. Annals of the Association of American Geographers 92, 399-415.
- Schandl, E. 2009. Petrography of DGR-1 and DGR-2 Core. GeoConsult Report TR-07-12 Rev.0. Toronto, Canada
- Scheidegger, A.E. 1977. Joints in Ontario. Revista Italiana di Geofisica e Scienze Affini 4, 1-10.
- Schloemer, S. and B.M. Krooss. 1997. Experimental characterization of the hydrocarbon sealing efficiency of cap rocks. Marine and Petroleum Geology 14, 565-580.
- Schloemer, S. and B.M. Krooss. 2004. Molecular transport of methane, ethane and nitrogen and the influence of diffusion on the chemical and isotopic composition of natural gas accumulations. Geofluids 4, 81-108.
- Schmidtke, R.H. and E.Z. Lajtai. 1985. The long-term strength of Lac du Bonnet Granite. International Journal of Rock Mechanics and Mining Sciences 22(6), 461-465.

- Senior Seismic Hazard Advisory Committee (SSHAC). 1997. Recommendations for Probabilistic Seismic Hazard Analysis. Guidance on Uncertainty and Use of Experts. U.S. Nuclear Regulatory Commission, NUREG/CR-6372.
- Shao, H., K. Schuster, J. Sönke and V. Bräuer. 2008. EDZ development in indurated clay formations—In situ borehole measurements and coupled HM modelling. *Physics and Chemistry of the Earth* 33, 388-395.
- Sharpe, D.R. and W.A.D. Edwards. 1979. Quaternary geology of the Chesley–Tiverton area, Southern Ontario. Ontario Geological Survey Preliminary Map 2314, 1.50.000.
- Shaw, J. 2002. The meltwater hypothesis for subglacial bedforms. *Quaternary International* 90, 5-22.
- Sherwood Lollar B., S.M. Weise, S.K. Frape and J.F. Barker. 1994. Isotopic constraints on the migration of hydrocarbon and helium gases of southwestern Ontario. *Bulletin of Canadian Petroleum Geology* 42, 283-295.
- Shouakar-Stash, O., S.V. Alexeev, S.K. Frape, L.P. Alexeeva and R.J. Drimmie. 2007. Geochemistry and stable isotopic signatures, including chlorine and bromine isotopes, of the deep groundwaters of the Siberian Platform, Russia. *Applied Geochemistry* 22, 589-605.
- Simon, M.A. and M.L. Brusseau. 2007. Analysis of a gas-phase partitioning tracer test conducted in an unsaturated fractured-clay formation. *Journal of Contaminant Hydrology* 90, 146–158.
- Singer, S.N., C.K. Cheng and M.G. Scafe. 2003. The hydrogeology of southern Ontario, Second Edition, Environmental Monitoring and Reporting Branch, Ontario Ministry of the Environment.
- Skowron, A. and E. Hoffman. 2009a. XRD Mineralogical Analysis of DGR-1 and DGR-2 Core. Intera Engineering Ltd. Report TR-08-01 Rev.0. Activation Laboratories, Ancaster. Ottawa, Canada.
- Skowron, A. and E. Hoffman. 2009b. Geochemical and SEM/EDS Analysis of DGR-1 and DGR-2 Core. Intera Engineering Ltd. Report TR-08-02 Rev.0. Ottawa, Canada.
- Slattery, S. 2011. Neotectonic Features and Landforms Assessment. Nuclear Waste Management Organization Report NWMO DGR-TR-2011-19 R000. Toronto, Canada.
- Slattery, S.R., P.J. Barnett and D.G.F. Long. 2007. Constraints on paleolake levels, spillways and glacial lake history, north-central Ontario, Canada. *Journal of Paleolimnology* 37, 331-348.
- Sloss, L.L. 1963. Sequences in the cratonic interior of North America. *Geological Society of America Bulletin* 74, 93-114.
- Sloss, L.L. 1982. The Michigan Basin: Selected structural basins of the Midcontinent, USA. *UMR Journal* 3, 25-29.
- Smith, L.B., Jr. 2006. Origin and reservoir characteristics of Upper Ordovician Trenton–Black River hydrothermal dolomite reservoirs in New York. *AAPG Bulletin* 90(11), 1691–1718

- Sofer, Z. 1978. Isotopic composition of water in gypsum. *Geochimica et Cosmochimica Acta* 42, 1141-1149.
- Souley, M., G. Armand, K. Su and Y. Wileveau. 2007. Modelling of the hydromechanical response of a shaft sinking in a deep claystone. In: Tenth international symposium of numerical models geomechanics (NUMOG X), 25–27 April 2007, Rhodes, Greece, 269-275.
- Sterling, S. 2010a. Bedrock Formations in DGR-1 and DGR-2. Intera Engineering Ltd. Report TR-07-05 Rev.3. Ottawa, Canada.
- Sterling, S. 2010b. Drilling Logging and Sampling of DGR-1 and DGR-2. Intera Engineering Ltd. Report TR-07-06 Rev.1. Ottawa, Canada.
- Sterling, S. and M. Melaney. 2010. Bedrock Formations in DGR-1 to DGR-6. Intera Engineering Ltd. Report TR-09-11 Rev.1. Ottawa, Canada.
- Sterling, S., R. E. Jackson, R. Walsh, D. Heagle and I. Clark. 2011. Assessment of Porosity Data and Gas Presence in DGR Cores. Intera Engineering Ltd. Report TR-08-34 Rev.0. Ottawa, Canada.
- Straw, A. 1968. Late Pleistocene glacial erosion along the Niagara Escarpment of Southern Ontario. *Geological Society of America Bulletin* 79, 889-910.
- Stroes-Gascoyne, S. and C.J. Hamon. 2008. Preliminary microbial analysis of limestone and shale rock samples. Nuclear Waste Management Organization Report NWMO TR-2008-09. Toronto, Canada.
- Sugden, D.E. 1976. A case against deep erosion of shields by ice sheets. *Geology* 4, 580-582.
- Sutter, J.F., N.M. Ratcliffe and S.B. Mukasa. 1985.  $^{40}\text{Ar}/^{39}\text{Ar}$  and K-Ar data bearing on the metamorphic and tectonic history of western New England. *Geological Society of America Bulletin* 96, 123-136.
- Sykes, E.A. 2007. Hydrogeologic modelling to assess conditions related to OPG's proposed Deep Geologic Repository in Tiverton, Ontario. Master's thesis, University of Waterloo.
- Sykes, J.F., S.D. Normani and Y. Yin. 2011. Hydrogeologic Modelling. Nuclear Waste Management Organization Report NWMO DGR-TR-2011-16 R000. Toronto, Canada.
- Tarasov, L. and W.R. Peltier. 2004. A geophysically constrained large ensemble analysis of the deglacial history of the North American ice-sheet complex. *Quaternary Science Reviews* 34(3-4), 359–388.
- Taylor, T.R. and D.F. Sibley. 1986. Petrographic and geochemical characteristics of dolomite types and the origin of ferroan dolomite in the Trenton Formation, Ordovician, Michigan Basin, U.S.A. *Sedimentology* 33, 61-86.
- Thomas, W.A. 2006. Tectonic inheritance at a continental margin. *GSA Today* 16(2), 4-11.
- Thurston, P.C.. 1991. Geology of Ontario: Introduction. In: Geology of Ontario, Ontario Geological Survey, Special Volume 4, Part 1, 3-26.

- Trotter, J.A., I.S. Williams, C.R. Barnes, C.L. Robert and S. Nicoll. 2008. Did Cooling Oceans Trigger Ordovician Biodiversification? Evidence from Conodont Thermometry. *Science* 321, 550-554.
- Tsang, C.F. and F. Bernier. 2004. Definitions of excavation disturbed zone and excavation damaged zone in Impact of the excavation disturbed or damaged zone (EDZ) on the performance of radioactive waste geological repositories. Proceedings of the European Commission Cluster Conference and Workshop held in Luxembourg, Davies, C., and F. Bernier (Eds.) 2003. EUR 21028 EN.
- Tsang, C.F., F. Bernier and C. Davies. 2005. Geohydromechanical processes in the Excavation Damaged Zone in crystalline rock, rock salt, and indurated and plastic clays – in the context of radioactive waste disposal. *International Journal of Rock Mechanics and Mining Sciences* 43(1), 109-125.
- Tushingham, A.M. 1992. Postglacial uplift predictions and historical water levels of the Great Lakes. *Journal of Great Lakes Research* 18, 440–455
- Uyeno, T.T., P.G. Telford and B.V. Sanford. 1982. Devonian conodonts and stratigraphy of southwestern Ontario. *Geological Survey of Canada, Bulletin* 332.
- Valley, B. and S. Maloney. 2010. Technical Report. Analysis of DGR-1, DGR-2, DGR-3 and DGR-4 Borehole Images for Stress Characterization, TR-08-35, Revision 1, January 28, MIRARCO/Geomechanics Research Centre, Laurentian University, Sudbury.
- van der Pluijm, B.A. and S. Marshak. 2004. *Earth Structure: An Introduction to Structural Geology & Tectonics*. 2nd Edition.
- van der Pluijm, B.A., J.P. Craddock, B.R. Graham and J.H. Harris. 1997. Paleostress in cratonic North America: implications for deformation of continental interiors. *Science* 277, 794-796.
- Van der Voo, R. 1982. Pre-mesozoic paleomagnetism and plate tectonics. *Annual Review of Earth and Planetary Sciences* 10, 191-220.
- van Genuchten, M. 1980. A closed-form equation for predicting hydraulic conductivity of unsaturated soils. *Soil Science Society of America Journal* 44, 892–898.
- Van Loon, L.R. 2010. Diffusion of <sup>125</sup>I in Limestone and Red Shale Samples from DGR-2. Intera Engineering Ltd. Report TR-07-22 Rev.0. Ottawa, Canada.
- Van Schmus, W.R. 1992. Tectonic setting of the Midcontinent Rift system. *Tectonophysics* 213, 1-15.
- Vasconcelos, C., J.A. McKenzie, R. Warthmann and S.M. Bernasconi. 2005. Calibration of the <sup>18</sup>O paleothermometer for dolomite precipitated in microbial cultures and natural environments. *Geology* 33, 317-320.
- Veizer, J. and F.T. MacKenzie. 2005. Evolution of sedimentary rocks. In: Mackenzie, F.T. (Ed.). *Sediments, Diagenesis, and Sedimentary Rocks. Treatise on Geochemistry* 7, p.369-407. Elsevier, New York, USA.

- Wallach, J.L., A.A. Mohajer and R.L. Thomas. 1998. Linear zones, seismicity, and the possibility of a major earthquake in the intraplate western Lake Ontario area of eastern North America. *Canadian Journal of Earth Sciences* 35(7), 762-786.
- Walsh, R. 2011. Compilation and Consolidation of Field and Laboratory Data for Hydrogeological Properties. Intera Engineering Ltd. Report TR-08-10 Rev.0. Ottawa, Canada.
- Waltham, A.C. 1981. Origin and development of limestone caves. *Progress in Physical Geography* 5, 242-256.
- Wang, H.F., K.D. Crowley and G.C. Nadon. 1994. Thermal History of the Michigan Basin from Apatite Fission-Track Analysis and Vitrinite Reflectance. In *Basin Compartments and Seals*, P. J. Ortoleva (Ed.), AAPG Memoir 61, 167-178.
- Watts, M., D. Schieck and M. Coniglio. 2009. 2D Seismic Survey of the Bruce Site. Intera Engineering Ltd. Report TR-07-15 Rev.0. Ottawa, Canada.
- Wheeler, R.L. 1995. Earthquakes and the cratonward limit of Iapetan faulting in eastern North America. *Geology* 23, 105-108.
- White, D.J., D.A. Forsyth, I. Asudeh, S.D. Carr, H. Wu, R.M. Easton and R.F. Mereu. 2000. A seismic-based cross-section of the Grenville Orogen in southern Ontario and western Quebec. *Canadian Journal of Earth Sciences* 37, 183-192.
- Whiticar, M.J. 1999. Carbon and hydrogen isotope systematics of bacterial formation and oxidation of methane. *Chemical Geology* 161, 291-314.
- Whitney, C. and R. Lee. 2010. Laboratory Petrophysical Testing of DGR-2 Core. Intera Engineering Ltd. Report TR-07-18 Rev.2. Core Laboratories, Houston, USA.
- Wigston, A. and D. Heagle. 2009. Bedrock Formations in DGR-1, DGR-2, DGR-3 and DGR-4. Intera Engineering Ltd. Report TR-08-12 Rev.1. Ottawa, Canada.
- Wigston, A. and R.E. Jackson. 2010a. Mineralogy and Geochemistry of DGR-3 Core. Intera Engineering Ltd. Report TR-08-23 Rev.0. Ottawa, Canada.
- Wigston, A. and R.E. Jackson. 2010b. Mineralogy and Geochemistry of DGR-4 Core. Intera Engineering Ltd. Report TR-08-24 Rev.0. Ottawa, Canada.
- Williams, H. and R.D. Hatcher. 1982. Suspect terranes and accretionary history of the Appalachian Orogen. *Geology* 10, 530-536.
- Wilson, T.P. and D.T. Long. 1993a. Geochemistry and isotope chemistry Ca-Na-Cl brines in Silurian strata, Michigan Basin, U.S.A. *Applied Geochemistry* 8, 507-524.
- Wilson, T.P. and D.T. Long. 1993b. Geochemistry and isotope chemistry of Michigan Basin brines: Devonian formations. *Applied Geochemistry* 8, 81-100.
- Winder, C.G. and B.V. Sanford. 1972. Stratigraphy and paleontology of the Paleozoic rocks of southern Ontario; Excursion A45-C45 (Guidebook), 24th Session, International Geology Conference, Montreal, Quebec.



- Winter, B.L., C.M. Johnson, J.A. Simo and J.W. Valley. 1995. Paleozoic Fluid History of the Michigan Basin: Evidence from Dolomite Geochemistry in the Middle Ordovician St. Peter Sandstone. *Journal of Sedimentary Research* A65(2), 306-320.
- Wood, J.R. and W.B. Harrison. 2002. Advanced characterization of fractured reservoirs in carbonate rocks: the Michigan Basin. Department of Energy (DOE) Report, DE-AC26-98BC15100.
- WORTHINGTON. 2011. Karst Assessment. Worthington Groundwater report for the Nuclear Waste Management Organization NWMO DGR-TR-2011-22 R000. Toronto, Canada.
- Xiang, Y.L., D. Cavé, D. Loomer and T. Al. 2009. Diffusive anisotropy in low-permeability Ordovician sedimentary rocks from the Michigan basin in southwest Ontario. 62<sup>nd</sup> Canadian Geotechnical Conference and 10th Joint CGS/ IAH-CNC Groundwater Specialty Conference. September 20-24.
- Youngs, R. 2009. Site Evaluation for the OPG New Nuclear at Darlington-Probabilistic Seismic Hazard Assessment. NK054-REP-01210-00014 R01.
- Zheng, Q. 1999. Carbonate Diagenesis and Porosity Evolution in the Guelph Formation, Southwestern Ontario. Ph.D. Thesis, University of Waterloo. Waterloo, Canada.
- Ziegler, A.M., C.R. Scotese, W.S. McKerrow, M.E. Johnson and R.K. Bambach. 1977. Paleozoic biogeography of continents bordering the Iapetus (pre-Caledonian) and Rheic (pre-Hercynian) oceans. *Contributions in Biology and Geology* 2, 1-22.
- Ziegler, K. and F.J. Longstaffe. 2000a. Multiple episodes of clay alteration at the Precambrian/Paleozoic unconformity, Appalachian Basin: Isotopic evidence for long-distance and local fluid migrations. *Clays and Clay Minerals* 48, 474-493.
- Ziegler, K. and F.J. Longstaffe. 2000b. Clay mineral authigenesis along a mid-continent scale fluid conduit in Palaeozoic sedimentary rocks from southern Ontario, Canada. *Clay Minerals* 35, 239-260.
- Zoback, M.L. and M.D. Zoback. 1989. Regional tectonic stress field of the continental U.S. Geophysical Framework of the Continental U.S. Pakiser, L. and W.D. Mooney (Eds.), Geological Society of America Memoir 172, 523-539.
- Zoback, M.L. 1992. Stress field constraints on intraplate seismicity in eastern North America. *Journal of Geophysical Research* 97, 11761-11782.
- Zwally, H., W. Abdalati, T. Herring, K. Larson, J. Saba, and K. Steffan. 2002. Surface-melt induced acceleration of Greenland ice-sheet flow. *Science* 297, 218-222.

**10. UNITS**

a	annum
C	Celsius
cm	centimetre
cm <sup>2</sup>	square centimetre
dm	decimetre
g	gram
Ga	billion years
GPa	gigapascal
ha	hectare
hr	hour
ka	thousand years
kg	kilogram
km	kilometre
km <sup>2</sup>	square kilometre
kPa	kilopascal
L	litre
m	metre
m <sup>2</sup>	square metre
m <sup>3</sup>	cubic metre
Ma	million years
MaBP	million years before present
mAGS	metres above ground surface
mASL	meters above sea-level
mBGS	metres below ground surface
mBSL	metres below sea level
Mg	megagram
µg	microgram

mg	milligram
min	minute
mLBGS	metres length along incline below ground surface
mm	millimetre
mmol/kgw	millimole per kilogram (water)
mol	mole
MPa	megapascal
Pa	Pascal
Pa·s	Pascal seconds
‰	parts per thousand
%g	percent of gravitational acceleration
°	degrees
s	second
wt%	mass percentage

**11. ABBREVIATIONS AND ACRONYMS**

3DGF	3D Geological Framework
AE	Acoustic emission
AECL	Atomic Energy of Canada Limited
AGCM	Atmospheric General Circulation Models
AMB	Akron Magnetic Boundary
ANDRA	Agence Nationale pour la Gestion des Déchets Radioactifs
A-OSS	Appalachian-Ouachita Stratigraphic System (includes rocks of the Michigan and Illinois Basins on the cratonward side of the Nashville Dome to Cincinnati to Findlay Arch to Algonquin Arch crustal upfold)
ArcGIS	WINDOWS® suite consisting of Geographic Information System software products generated by Esri
ATV	Acoustic Televiwer
BP	Before Present
CAI	Conodont (color) Alteration Index
CC	Central Craton
CD	Crack Damage
CENA	Central and Eastern North America
CI	Crack Initiation
CMBBZ	Central Metasedimentary Belt Boundary Zone
COCORP	Consortium for Continental Reflection Profiling
CPS	Counts per second
$C_{tz}$	Test-zone compressibility
D	Deuterium
$D_e$	Effective Diffusion Coefficient
DEM	Digital Elevation Model
DF	Dawn Fault
DGR	Deep Geologic Repository
DGSM	Descriptive Geosphere Site Model

E	Elastic Modulus
ECC	Extended Continental Crust
ED-B	EDZ evolution, mine-by test (Mont Terri, Switzerland)
EDS	Energy Dispersive Spectral
EdZ	Excavation Disturbed Zone
EDZ	Excavation Damaged Zone
EF	Electric Fault
FEP	Features, Events and Processes
FRAC3DVS-OPG	FRACtured 3D Variably Saturated-OPG
GBLZ	Georgian Bay Linear Zone
GFTZ	Grenville Front Tectonic Zone
GGM	Gas Generation Model
GIA	Glacial Isostatic Adjustment
GMH	Great Meteor Hotspot
GMWL	Global Meteoric Water Line
GSC	Geological Survey of Canada
GSCP	Geoscientific Site Characterization Plan
GSI	Geological Strength Index
HDZ	Highly Damaged Zone
HLEL	Hamilton – Lake Erie Lineament
HS Unit	Hydrostratigraphic Unit
HTD	Hydrothermal Dolomite
HTO	Tritiated Water
IRM	Iapetan Rifted Margin
K	Hydraulic Conductivity
k	Permeability
K-Ar	Potassium-argon
K <sub>H</sub>	Horizontal hydraulic conductivity

---

K <sub>v</sub>	Vertical hydraulic conductivity
L&ILW	Low and Intermediate Level Waste
LGM	Last Glacial Maximum
LIS	Laurentide Ice Sheet
LSD	Long-term Strength Degradation
M	Earthquake Magnitude
MLE	Mean Life Expectancy
MNR	Ministry of Natural Resources
MRS	Midcontinent Rift System
MS	Mechano-stratigraphic Unit
MSGs	Michigan State Geological Survey
MVT	Mississippi Valley Type
NAZ	Northern Appalachians
NBCC	National Building Code of Canada
NEA	Nuclear Energy Agency
NGR	Northern Grenville
NHF	Natural Hydraulic Fractures
NMR/He	Technique to determine total fluid saturation within rock core (Nuclear Magnetic Resonance for liquid saturation [water and oil]; Boyle's Law of gas expansion using He for gas saturation)
NOAA	National Oceanic and Atmospheric Administration
NPLZ	Niagara-Pickering Linear Zone
nSIGHTS	Computer code used for the analysis of hydraulic test data
NTS	National Topographic System
NWMO	Nuclear Waste Management Organisation
ODP	Ocean Drilling Project
OG	Ottawa Graben
OGS	Ontario Geological Survey
OGSR	Ontario Oil, Gas and Salt Resources Library

OPG	Ontario Power Generation
Pb-Zn	Lead-zinc
$P_c$	Capillary Pressure
$P_e$	Effective pressure
$P_i$	Ice pressure
$P_f$	Formation pressure
$P_w$	Water pressure
PL	Point Load
PSHA	Probabilistic Seismic Hazard Assessment
RLmz	Robertson Lake Mylonite Zone
$\rho$	Density
RQD	Rock Quality Designation, as specified by the ISRM (International Society of Rock Mechanics)
RSA	Regional Study Area
RSL	Relative Sea Level
SAR	Synthetic Aperture Radar
SDI	Slake Durability Index
SEM	Scanning Electron Microscope
SG	Southern Grenville
SI	Saturation Index
SKB	Swedish Nuclear Fuel and Waste Management Company
SMOW	Standard Mean Ocean Water
SRTM	Shuttle Radar Topography Mission
SSC	Seismic Source Characterization
SSHAC	Senior Seismic Hazard Advisory Committee
$\sigma$	Compressive stress
$\sigma_v$	Vertical compressive stress
$\sigma_H$	Maximum horizontal stress
$\sigma_h$	Minimum horizontal stress

TDS	Total Dissolved Solids
TIN	Triangulated Irregular Network
TOC	Total Organic Carbon
TR	Technical Report
UCS	Uniaxial Compressive Strength
UDEC	Universal Distinct Element Code
UMV	Upper Mississippi Valley
UofT GSM	University of Toronto Glacial Systems Model
URL	Underground Research Laboratory
UTM	Universal Transverse Mercator
V	Linear Groundwater Velocity
VSMOW	Vienna Standard Mean Ocean Water
WWMF	Western Waste Management Facility
XRD	X-Ray Diffraction